

**University of Maryland
Advanced Rotorcraft Code
(UMARC)**

Theory Manual

UM-AERO 94-18

University of Maryland Advanced Rotorcraft Code (UMARC)

Theory Manual

Gunjit Bir

Inderjit Chopra

Ranjan Ganguli
Edward C. Smith
Senthilvel Vellaichamy
James Wang
Ki C. Kim
Wai Yip Chan
Mark W. Nixon
Norman W. Kimata
Jodi A. Smith
Michael Torok
Khanh Nguyen

*Center for Rotorcraft Education and Research
University of Maryland
College Park, Maryland*

July 20, 1994



Contents

List of Symbols.....	xi
1. Introduction.....	1 - 1
1.1 Background of UMARC Development.....	1 - 3
1.2 Organization of The Theory Manual.....	1 - 9
1.3 Overview of UMARC Theory Basis.....	1 - 10
1.3.1 Structural Modeling.....	1 - 10
1.3.2 Aerodynamic Modeling.....	1 - 12
1.3.3 Analysis.....	1 - 16
References.....	1 - 21

Part 1. Modeling and Analysis Theory

2. Structural Modeling

Summary.....	2 - 1
---------------------	--------------

2.1 The Helicopter Model.....	2 - 2
2.1.1 Vehicle Kinematics and Coordinate Systems.....	2 - 2
2.1.2 Blade Deformation Kinematics Coordinate Systems.....	2 - 4
2.1.3 Nondimensionalization and Ordering Scheme.....	2 - 8
2.2 Formulation Using Hamilton's Principle.....	2 - 11
2.2.1 Energy Expressions for the Blade.....	2 - 13
2.2.1.1 Strain Energy, δU_b.....	2 - 14
2.2.1.2 Kinetic Energy, δT_b.....	2 - 18
2.2.1.3 Virtual Work, δW_b.....	2 - 34
2.2.2 Energy Expressions for the Fuselage.....	2 - 35

2.2.2.1 Strain Energy, δU_F	2 - 35
2.2.1.2 Kinetic Energy, δT_F	2 - 35
2.2.1.3 Virtual Work, δW_F	2 - 36
2.3 Blade Equations of Motion.....	2 - 37
2.3.1 Finite Element Discretization in Space.....	2 - 37
2.3.2. Finite Element Formulation in Space.....	2 - 42
2.3.3 Element Structural Matrices (and Load Vector).....	2 - 45
2.3.3.1 Blade Matrices (and Load Vector).....	2 - 45
2.3.3.2 Blade-Fuselage Coupled Matrices.....	2 - 50
2.3.3.3 Gaussian Integration.....	2 - 52
2.3.4 Assembly of Element Matrices (and Load Vector).....	2 - 52
2.3.5 Application of Blade Kinematic Boundary Conditions.....	2 - 55
2.4 Fuselage Equations of Motion.....	2 - 56
2.4.1 Finite Element Discretization of the Blade Dependent.....	2 - 56
Degrees of Freedom	
2.4.2 Fuselage Matrices.....	2 - 59
2.4.3 Fuselage-Blade Coupled Matrices.....	2 - 62
2.5 UMARC Implementation of Structural Modeling.....	2 - 65
2.5.1 Computation of Blade Matrices	
(SUBROUTINE STRUCT).....	2 - 65
2.5.1.1 Function of SUBROUTINE STRUCT.....	2 - 65
2.5.1.2 Calling of SUBROUTINE STRUCT.....	2 - 66
2.5.1.3 Input to SUBROUTINE STRUCT.....	2 - 68
2.5.1.4 Output from SUBROUTINE STRUCT.....	2 - 70
2.5.1.5 Performance and Specific Tasks of	
SUBROUTINE STRUCT.....	2 - 71
References.....	2 - 77

3. Aerodynamic Modeling.....	3 - 1
3.1 Quasi-Steady Aero Modeling.....	3 - 3
3.1.1 Derivation of Air Velocity.....	3 - 4
3.1.2 Quasisteady Airloads Expressions.....	3 - 16
3.1.3 Finite Element Discretization.....	3 - 26
3.1.4 Finite Element Discretization of Blade Equations.....	3 - 29
3.1.5 Finite Element Discretization of Fuselage Equations.....	3 - 31
3.1.6 Fuselage -Blade Matrices.....	3 - 35
3.1.7 Nonlinear Forces.....	3 - 37
3.1.8 Fuselage Aerodynamic Modeling.....	3 - 38
3.2 Implementation Scheme for Quasisteady Aerodynamic Modeling	
3.2.1 Implementation of Blade Velocity.....	3 - 41
3.2.2 Implementation of Linear Aerodynamics.....	3 - 49
3.2.3 Implementation of Nonlinear Aerodynamics.....	3 - 54
3.2.4 Virtual Work due to Blade Motion.....	3 - 58
3.2.5 Virtual Work due to Fuselage Motion.....	3 - 60
3.2.6 Description of SUBROUTINE AEROMX.....	3 - 67a
3.2.6.1 Function of SUBROUTINE AEROMX.....	3 - 67b
3.2.6.2 Calling of SUBROUTINE AEROMX.....	3 - 67d
3.2.6.3 Input to SUBROUTINE AEROMX.....	2 - 67e
3.2.6.4 Output from SUBROUTINE AEROMX.....	2 - 67g
3.3 Unsteady Aerodynamics.....	3 - 68
3.3.1 Attached Flow Formulation.....	3 - 69
3.3.2 Circulatory and Impulsive Lift Due to Angle of Attack Change	3 - 72
3.3.3 Circulatory and Impulsive Pitching Moment Due to Angle of Attack Change	3 - 73

3.3.4	Circulatory and Impulsive Lift Due to Pitch Rate	3 - 74
3.3.5	Circulatory and Impulsive Pitching Moment Due to Pitch Rate	3 - 75
3.3.6	Separated Flow Formulation.....	3 - 76
3.3.7	Dynamic Stall Formulation.....	3 - 79
3.4	Implementation of Unsteady Aerodynamics.....	3 - 83
3.4.1	Circulatory Lift Due to Plunge and Pitch Rate.....	3 - 83
3.4.2	Impulsive Lift Due to Plunge.....	3 - 91
3.4.3	Impulsive Lift Due to Pitch Rate.....	3 - 94
3.4.4	Unsteady Pitching Moment Due to Circulatory Plunge and Pitch Rate.....	3 - 96
3.4.5	Unsteady Pitching Moment Due to Impulsive Plunge.....	3 - 97
3.4.6	Unsteady Pitching Moment Due to Impulsive Pitch Rate....	3 - 97
3.4.7	Unsteady Drag.....	3 - 99
3.4.8	Modifying Quasi-Steady Airloads for Unsteady Effects.....	3 - 104
3.4.9	Implementation of Steady and Unsteady Flow Separation in UMARC.....	3 - 107
3.4.10	Implementing Quasi-steady Trailing Edge Separation Factor.....	3 - 107
3.4.11	Implementation of Unsteady Trailing Edge Separation Point.....	3 - 111
3.4.12	Dynamic Stall.....	3 - 119
3.5	Rotor Wake Modeling.....	3 - 124
3.5.1	Uniform and Linear Inflow Models.....	3 - 124
3.5.2	Prescribed and Free Wake Models.....	3 - 126
3.5.3	Rotor Wake Analysis.....	3 - 127
3.5.4	Rotor Wake Geometry.....	3 - 130

3.5.5	Equation of the Wake Geometry.....	3 - 130
3.5.6	Prescribed Wake Model.....	3 - 133
3.5.7	Free Wake Model.....	3 - 136
3.5.8	Calculation of Influence Coefficients.....	3 - 137
3.5.9	Induced Velocity Calculation.....	3 - 137
3.5.10	Improved Free Wake Model for High Speed Flight.....	3 - 138
3.6	Implementation of Wake Models.....	3 - 148
3.6.1	Flow Chart for Wake Analysis.....	3 - 149
3.6.2	Wake Subroutines.....	3 - 152
3.7	Dynamic Inflow Modeling.....	3 - 158
	References.....	3 - 168
4.	Trim Analysis.....	4 - 1
4.1	Introduction.....	4 - 1
4.2	Trim Equations.....	4 - 2
4.2.1	Vehicle Trim Equations.....	4 - 2
4.2.2	Wind Tunnel Trim.....	4 - 6
4.2.3	Blade Response Equations.....	4 - 6
4.2.4	Modal Reduction of the Blade Response Equations.....	4 - 7
4.3	Finite Element Discretization in Time.....	4 - 9
4.4	Coupled Trim Procedure.....	4 - 14
4.4.1	Initial Controls Estimate.....	4 - 15
4.4.2	Blade Steady State Periodic Response Using Finite Element in Time.....	4 - 18
4.4.3	Computation of Blade Loads and Spanwise Aerodynamic Circulation.....	4 - 18

4.4.3.1	Force Summation Method.....	4 - 19
4.4.3.2	Modal Summation Method.....	4 - 23
4.4.4	Computation of Hubloads and Harmonics.....	4 - 32
4.4.5	Computation of Vehicle Loads.....	4 - 34
4.4.6	Inflow Update.....	4 - 34
4.4.7	Computation of the Jacobian and Controls Update.....	4 - 35
4.4.8	Modified Trim Scheme.....	4 - 37
4.4.9	Converged Blade and Vehicle Response.....	4 - 39
4.5	Implementation of Trim Analysis in UMARC.....	4 - 42
4.6	Function of SUBROUTINE TRIM.....	4 - 42
4.6.1	Inputs to the Subroutine.....	4 - 42
4.6.2	Output	4 - 47
4.6.3	Performance.....	4 - 48
References.....		4 - 66
5.	Stability Analysis.....	5 - 1
5.1	Introduction.....	5 - 1
5.2	Linearized System Eigenanalysis.....	5 - 3
5.2.1	Rotor-Fuselage Equations.....	5 - 4
5.2.2	Linearization of Rotor-Fuselage Equations.....	5 - 6
5.2.3	Dynamic Inflow Equations.....	5 - 10
5.2.4	System Linearized Equations.....	5 - 12
5.2.4.1	Normal Mode Transformation.....	5 - 13
5.2.4.2	Transformation to First Order.....	5 - 14
5.2.4.3	Fixed Coordinate Transformation.....	5 - 15
5.2.5	Floquet Theory.....	5 - 21
5.2.6	Constant Coefficient Approximation.....	5 - 25

5.3	Transient Perturbation Methods.....	5 - 26
5.4	Implementation in UMARC.....	5 - 29
	References.....	5 - 50
6.	Advanced Geometry Rotors.....	6 - 1
6.1	Introduction.....	6 - 1
6.2	Blade Geometry.....	6 - 2
6.2.1	Undeformed Blade Geometry.....	6 - 3
6.2.2	Deformed Blade Geometry.....	6 - 9
6.3	Equations of Motion.....	6 - 17
6.3.1	Strain Energy, δU	6 - 17
6.3.2	Kinetic Energy, δT	6 - 19
6.3.3	Blade Virtual Work	6 - 25
6.4	Aerodynamic Modeling.....	6 - 26
6.4.1	Derivation of Blade Velocity.....	6 - 26
6.4.2	Aerodynamic Loads.....	6 - 30
6.5	Inertial Loads.....	6 - 32
6.6	Hub Loads.....	6 - 36
6.6	Implementation of Advanced-Tip Blade in UMARC.....	6 - 39
	References.....	6 - 46
7.	Bearingless Rotor Modeling.....	7 - 1
7.1	Introduction.....	7 - 1
7.2	Analytical Model.....	7 - 3
7.3	Bearingless Rotor Hub Kinematics.....	7 - 6

7.3.1	Kinematics Constraints due to Pitch Link and Lag Pin.....	7 - 6
7.3.2	Displacement Compatibility Conditions at the Clevis.....	7 - 14
7.4	Finite Element Analysis.....	7 - 15
7.4.1	Formulation Using Hamilton's Principle.....	7 - 15
7.4.2	Finite Element Modeling.....	7 - 19
7.4.3	Application of the Kinematic Constraints.....	7 - 22
7.4.4	Modeling of Snubber.....	7 - 28
7.5	Modification in the Solution Procedure.....	7 - 30
7.5.1	Centrifugal Force Computation	7 - 30
7.5.2	Trim Solution.....	7 - 31
7.6	Implementation in UMARC.....	7 - 36
	References.....	7 - 43
8.	Composite Blade Modeling.....	8 - 1
8.1	Structural Modeling.....	8 - 3
8.1.1	Laminated Composite Box-Beam Analysis.....	8 - 4
8.1.1.1	Formulation of Governing Equations.....	8 - 4
8.1.1.2	Special Forms of Governing Equations.....	8 - 17
8.1.2	The Helicopter Model.....	8 - 20
8.1.2.1	Blade Deformation Kinematics and Coordinate Systems.....	8 - 20
8.1.2.2	Nondimensionalization and Ordering Scheme.....	8 - 22
8.1.3	Formulation Using Hamilton's Principle.....	8 - 23
8.1.3.1	Blade Strain Energy, δU_b	8 - 24
8.1.3.2	Blade Kinetic Energy, δT_b	8 - 30
8.1.3.3	Blade Virtual Work, δW_b	8 - 36
8.1.4	Blade Equations of Motion.....	8 - 37

8.1.4.1	Finite Element Discretization in Space.....	8 - 37
8.1.4.2	Application of Blade Kinematic Boundary Conditions.....	8 - 42
8.1.5	Element Structural Matrices and Load Vector.....	8 - 42
8.1.5.1	Blade Matrices and Load Vector.....	8 - 42
8.1.6	Summary.....	8 - 48
8.2	Aerodynamic Modeling.....	8 - 49
8.2.1	Derivation of Resultant Air Velocity.....	8 - 49
8.2.2	Quasi-Steady Airloads Expressions.....	8 - 55
8.2.3	Finite Element Discretization.....	8 - 56
8.2.3.1	Discretization of Blade Equations.....	8 - 58
8.2.3.2	Discretization of Fuselage Equations.....	8 - 59
8.3	Vehicle Trim and Response Analysis.....	8 - 60
8.3.1	Initial Controls Estimate.....	8 - 61
8.3.2	Computation of Blade Loads.....	8 - 62
8.4	Composite Blade Model Implementation.....	8 - 66
	References.....	8 - 74
9.	Dissimilar Rotor Blades.....	9 - 1
9.1	Blade Response and Trim Analysis.....	9 - 2
9.2	Stability Analysis.....	9 - 6
9.3	Implementation.....	9 - 8
	<i>Part 2. User's Manual</i>	
I.	UMARC User's Guide.....	I - 1
I.1	Input Data File.....	I - 1

I.1.1	Description.....	I - 2
I.1.2	Dynamic Formatting.....	I - 3
I.1.3	Data Dictionary.....	I - 4
I.2	User Defined Routines.....	I - 4
I.3	Compilation and Execution of UMARC.....	I - 4
I.3.1	UMARC Source Code Files.....	I - 5
I.3.2	Compiling UMARC (IBM).....	I - 8
I.3.3	Executing UMARC (IBM).....	I - 9
I.3.4	Command Macros (IBM).....	I - 10
I.3.5	Compiling UMARC (Sun).....	I - 11
I.3.6	Executing UMARC (Sun).....	I - 12
I.4	Description of UMARC Input Routines.....	I - 12
I.4.1	Subroutine DINPUT.....	I - 13
I.4.2	Subroutine DATCHK.....	I - 14
I.4.3	Subroutine DATCHR.....	I - 14
I.4.4	Subroutine DATCHD.....	I - 15
I.4.5	Subroutine DATFLO.....	I - 15
I.4.6	Subroutine DATINT.....	I - 16
I.4.7	FORTRAN Implementation Details.....	I - 16
I.5	UMARC Structure Charts.....	I - 21
I.6	Input Data Files.....	I - 22
I.7	Output Data Files.....	I - 23
I.8	Data Dictionary.....	I - 24
I.9	Important Notes	I - 51
II.	Validation Studies.....	II - 1
II.1	Isolated Rotor Aeroelastic Stability.....	II - 2

II.1.1 Hingeless Model Rotor Aeroelastic Stability	
Correlation in Hover	II - 2
II.1.2 Validation of Aeroelastic Stability Analysis	
for a Bearingless Rotor	II - 7
II.2 Rotor-Fuselage Aeromechanical Stability.....	II - 12
II.2.1 Hingeless Model Rotor Correlation	
Under Simulated Vacuum Conditions	II - 12
II.2.2 Hingeless Model Rotor Correlation.....	II - 17
References	II - 22

List of symbols

a	Lift curve slope
a_s	Sonic velocity
\vec{a}	Blade acceleration vector relative to an inertial frame.
A_j	Coefficients of indicial response functions
\mathbf{A}	Stability matrix.
b_j	Exponents of indicial response functions
c	Blade chord.
c_0	Lift coefficient at zero angle of attack.
$c_{0_{ht}}$	Lift coefficient at zero angle of attack of horizontal tail.
c_1	Lift curve slope.
$c_{1_{ht}}$	Lift curve slope of horizontal tail.
$c_{1_{rt}}$	Lift Curve Slope of Tail Rotor Blades
C_c	Chord force coefficient
C_d	Drag coefficient
C_{d_0}	Zero lift (viscous) drag coefficient
C_l	Blade section lift coefficient.
C_m^v	Vortex induced pitching moment coefficient
$C_{m_{ac}}$	Blade section pitching moment coefficient about aerodynamic center.
C_{n_1}	Critical normal force coefficient delimiting attached flow
C_n^c	Circulatory normal force coefficient

C_n^i	non-circulatory (impulsive) normal force coefficient
C_m	Pitching moment coefficient about 1/4-chord
C_n^p	Normal force under potential flow conditions
C_n^v	Vortex induced normal force coefficient
C_{n_a}	Normal force (lift) curve slope, /rad
C_n	Normal force coefficient
C'_n	Lagged normal force coefficient
$C_{n_{max}}$	Maximum normal force coefficient
CP_v	Vortex induced center of pressure
C_p	Pressure coefficient
C_T	Rotor thrust coefficient
C_v	Vortex lift increment
\mathbf{C}_b	Blade damping matrix.
\mathbf{C}_{bF}	Blade-fuselage damping matrix
\mathbf{C}_{Fb}	Fuselage-Blade damping matrix
\mathbf{C}_{FF}	Fuselage damping matrix
$\bar{\mathbf{C}}_b$	Modal blade damping matrix, $\bar{\mathbf{C}}$ in trim analysis
D_f	Deficiency function for boundary layer lag
D_F	Fuselage drag.
D_p	Deficiency function for leading edge pressure lag
\mathbf{D}	Wake distortion vector.
e_a	Chordwise offset of tensile axis ahead of elastic axis.

e_d	Chordwise offset of aerodynamic center behind elastic axis.
e_g	Chordwise offset of blade center-of-mass ahead of elastic axis.
E	Young's modulus.
EA	Axial stiffness
EB_1, EB_2	Section stiffness constants
EC_1	Warping rigidity
EC_2	Section warping constant
EI_y, EI_z	Flap bending stiffness, lag bending stiffness.
f	Trailing edge separation point,
f	Nondimensional spanwise coordinate, $y + \mu \sin\psi$.
f_0, f_1	Pitching moment coefficient.
F_A	Blade axial force.
F_x, F_y, F_z	Resultant blade section shears in x, y, z directions, respectively.
F_x^H, F_y^H, F_z^H	Rotor hub shears in fixed frame in X, Y, Z directions, respectively.
\mathbf{F}^I	Distributed inertial force vector.
\mathbf{F}_b	Blade load vector.
$\bar{\mathbf{F}}_b$	Modal load vector, $\bar{\mathbf{F}}$ in trim analysis.
G	Shear modulus.
GJ	Torsional stiffness
\dot{h}	Plunging velocity
h	Vertical distance from helicopter center-of-gravity to hub center,

along Z axis.

\mathbf{H}_u	Axial shape function vector
\mathbf{H}	Bending shape function vector
$\mathbf{H}_{\hat{\phi}}$	Torsion shape function vector
\mathbf{H}_t	Shape function matrix for finite element in time.
$\hat{i}, \hat{j}, \hat{k}$	Unit vectors for the blade undeformed coordinate system.
$\hat{i}_2, \hat{j}_2, \hat{k}_2$	Unit vectors for the deformed tip coordinate system.
$\hat{i}_\epsilon, \hat{j}_\eta, \hat{k}_\zeta$	Unit vectors of coordinate system
$\hat{I}_2, \hat{J}_2, \hat{K}_2$	Unit vectors for the undeformed tip coordinate system.
I_{xp}	Effective fuselage mass moment of inertia about roll axis
I_y, I_z	Blade cross-sectional moment of inertia about y and z axis, respectively.
I_{yp}	Effective fuselage mass: moment of inertia about pitch axis
$\hat{I}, \hat{J}, \hat{K}$	Unit vectors for the hub fixed rotating coordinate system.
$\hat{I}_F, \hat{J}_F, \hat{K}_F$	Unit vectors of vehicle coordinate system
$\hat{I}_H, \hat{J}_H, \hat{K}_H$	Unit vectors of hub fixed nonrotating coordinate system
$\hat{I}_I, \hat{J}_I, \hat{K}_I$	Unit vectors of inertial coordinate system
k	Reduced frequency = $\omega c / 2U$
k_0, k_1, k_2	Coefficients representing pitching moment curve fit
k_A	Radius of gyration of the blade cross section
k_i	non-circulatory time constant multiplier
k_m	Blade cross-sectional mass radius of gyration.

k_{m_1}, k_{m_2}	Blade cross-sectional mass radius of gyration in the flap and lag directions, respectively.
K	Deficiency functions for non-circulatory components
\mathbf{K}_b	blade stiffness matrix
\mathbf{K}_{bF}	Blade-fuselage stiffness matrix
\mathbf{K}_{Fb}	Fuselage-Blade stiffness matrix
\mathbf{K}_{FF}	Fuselage stiffness matrix
\mathbf{K}_t^G	<i>Jacobian</i> for the generalized load vector \mathbf{Q}^G .
$\bar{\mathbf{K}}_b$	Modal blade stiffness matrix, $\bar{\mathbf{K}}$ in trim analysis
L	Blade section lift.
l_i	Length of the i th beam element.
L_u, L_v, L_w	Distributed blade airloads in the undeformed directions, respectively.
$\bar{L}_u, \bar{L}_v, \bar{L}_w$	Distributed blade airloads in the deformed coordinate system.
m	Blade section mass.
m_F	Effective fuselage mass
m_o	Reference blade section mass.
M	Mach number
M_x, M_y, M_z	Resultant blade bending moments in the x, y, z directions, respectively.
M_X^H, M_Y^H, M_Z^H	Rotor hub moment components in the X, Y, Z directions in the hub fixed frame, respectively.
M_ϕ	Blade sectional pitching moment about deformed elastic axis.

\mathbf{M}_b	blade mass matrix.
\mathbf{M}_{bF}	Blade-fuselage mass matrix
\mathbf{M}_{Fb}	Fuselage-Blade mass matrix
\mathbf{M}_{FF}	Fuselage mass matrix
$\bar{\mathbf{M}}_b$	Modal blade mass matrix, $\bar{\mathbf{M}}$ in trim analysis
n	Current time sample
N	Normal force
N_b	Total number of blades
N_{cc}	Number of points used to average the stability matrix to obtain constant coefficient stability matrix.
N_t	Number of time elements for one rotor revolution.
N_G	Number of degrees of freedom for beam model.
\mathbf{p}_b	Modal displacement vector.
q	Non-dimensional pitch rate = $\dot{\alpha}c/U$
\mathbf{q}_b	Global displacement vector.
\mathbf{Q}	Generalized load vector for trim analysis, Floquet Transition matrix in stability analysis
r	Radial blade station.
\vec{r}	Blade displacement vector in the rotating blade frame.
R	Blade radius.
R_{tr}	tail rotor radius
s	Local coordinate of time element or space element.

S	non-dimensional distance traveled by airfoil in semi-chords
S_1, S_2	Coefficients of separation point curve fit
St	Strouhal number
S_{ht}	Horizontal Tail Area
\mathbf{S}	modal matrix associated with the Floquet Transition matrix
t	Time.
T	Rotor thrust
T	Kinetic energy
T_i	non-circulatory time constant = c/a
T_p	Time constant for leading edge pressure lag (semi-chords)
T_f	Time constant for boundary layer lag (semi-chords)
T_v	Time constant for vortex decay (semi-chords)
T_{st}	Time constant for secondary vortex shedding (semi-chords)
T_{vl}	Vortex passage time constant
\mathbf{T}_2	Transformation matrix from tip undeformed frame to tip deformed frame.
\mathbf{T}_{DU}	Transformation matrix from blade undeformed frame to blade deformed frame.
\mathbf{T}_{HI}	Transformation matrix from inertial frame to hub fixed nonrotating frame.
\mathbf{T}_{RH}	Transformation matrix from hub fixed nonrotating frame to hub rotating frame.

\mathbf{T}_{UH}	Transformation matrix from hub fixed nonrotating frame to blade undeformed frame.
\mathbf{T}_{UR}	Transformation matrix from hub rotating frame to blade undeformed frame.
\mathbf{T}_A	Transformation matrix from blade undeformed system to tip undeformed system.
u	Blade displacement in the x direction.
U_P	blade element downwash velocity at 3/4 chord
U_{P_1}	blade element downwash velocity at 1/4 chord
U_T	blade element velocity tangential to blade chord
U	blade element velocity = $\sqrt{U_T^2 + U_P^2}$
U	Strain energy
v	Blade displacement in the y direction.
V	Helicopter forward speed.
V_x, V_y, V_z	x,y,z, components of \vec{V}
\vec{V}	Total velocity vector
\vec{V}_b	Velocity of the blade relative to the hub
$\vec{V}_{b_x}, \vec{V}_{b_y}, \vec{V}_{b_z}$	x,y,z, components of \vec{V}_b
\vec{V}_f	Fuselage (hub) motion induced velocity vector
$\vec{V}_{f_x}, \vec{V}_{f_y}, \vec{V}_{f_z}$	x,y,z, components of \vec{V}_f
w	Blade displacement in the z direction, downwash velocity
W	Fuselage weight minus fuselage aerodynamic lift.

W_b	Work Done
W_s	swashplate deflection
x	non-dimensional chord
x_{ac}	Aerodynamic center
x_{CG}, y_{CG}	Hub center position relative to helicopter center-of-gravity in the X and Y directions, respectively.
x_F	Fuselage motion in X_I direction
x, y, z	Undeformed blade coordinate system
X, Y	Circulatory deficiency functions
X_{ht}	horizontal tail position relative to center of gravity in X direction
X_{tr}	tail rotor position relative to center of gravity in X direction
Z_{tr}	tail rotor position relative to center of gravity in Z direction
X, Y, Z	Hub rotating coordinate system
X_F, Y_F, Z_F	Vehicle coordinate system
X_H, Y_H, Z_H	Hub coordinate system
X_I, Y_I, Z_I	Inertial coordinate system
\mathbf{x}_F	Fuselage degree of freedom vector
y_F	Fuselage motion in Y_I direction
Y_F	Fuselage side force.
\mathbf{y}_G	Modal state vector.
\mathbf{Y}	System state vector.
z_F	Fuselage motion in Z_I direction

α	Blade section angle of attack.
α_0	Zero lift angle of attack, <i>rad.</i>
α_d	Delayed angle of attack.
α_{ds}	Dynamic stall angle.
	Flow reattachment angle.
α_E	Effective angle of attack
α_f	Effective angle of attack, used in the calculation of f .
α_k	decrement ratio of the k 'th stability mode.
α_s	Longitudinal shaft tilt angle (positive nose down)
β	Prandtl-Glauert compressibility factor = $\sqrt{1 - M^2}$
β_p	Blade precone.
Γ	Vortex strength, Circulation
δT	Variation in kinetic energy
δU	Variation in strain energy
δW	Virtual work
$\delta(\cdot)$	Virtual variation.
$\Delta(\cdot)$	$(\cdot)_n - (\cdot)_{n-1}$, perturbation.
ϵ	Parameter having the order of w/R or v/R .
ϵ_{xx}	Axial strain
$\epsilon_{x\eta}, \epsilon_{x\zeta}$	Engineering shear strain
η	Chordwise force recovery factor
η_r	Distance from blade elastic axis to blade 3/4 chord

θ_o	Rigid pitch angle due to control pitch and pretwist
θ_1	Total pitch angle resulting from rigid pitch and elastic twist.
θ_{1c}, θ_{1s}	Lateral and longitudinal cyclic trim inputs, respectively.
θ_{FP}	Flight path angle.
$\theta_{.75}$	Collective blade pitch at 0.75 percent radius.
θ_{tw}	Blade linear pretwist.
θ_t	Tail rotor collective pitch.
θ	Rotor controls.
Θ	Matrix containing system stability eigenvalues.
κ_x, κ_y	Longitudinal and lateral tilts of linear inflow model.
λ	Rotor total inflow.
λ_i	Rotor induced inflow.
λ_T	Warping function
Λ_1	Tip sweep angle, positive for forward sweep.
Λ_2	Tip droop angle, negative for droop.
Λ_3	Tip pitch angle, positive for nose up pitch.
Λ	eigenvalue matrix in stability analysis.
μ	Rotor advance ratio.
ξ, η, ζ	Rotating deformed blade coordinate system.
$\dot{\xi}$	Temporal modal displacement vector for time element.
$\bar{\xi}$	Fixed frame coordinates.

ρ	Air density.
ρ_s	Blade structural density.
σ	Rotor solidity ratio.
σ_{tr}	Tail rotor solidity ratio.
σ_{zz}	Axial stress
$\sigma_{xz}, \sigma_{z\zeta}$	Shear stresses
τ_v	Non-dimensional vortex time
ϕ	Indicial response function, or wake age
$\hat{\phi}$	Elastic twist ($\hat{\phi} = \phi - \int_0^x w' v''$)
ϕ_s	Lateral shaft tilt (positive advancing side down)
Φ	Normal mode transformation matrix or Floquet transition matrix.
ω	Circular frequency, rad/s
ω	Blade natural frequency.
ω_f	Fuselage angular rotation rate about inertial axis
ω_k	Floquet stability frequency of the k 'th stability mode.
Ω	Rotor rotational speed.
ψ	Rotor azimuth angle.
ψ_0	Initial time (nondimensional).
$(\cdot)'$	$\partial(\cdot)/\partial x$
$(\cdot)''$	$\partial(\cdot)^2/\partial x^2$
$(\cdot)^\cdot$	$\partial(\cdot)/\partial t$

Subscripts and Superscripts

$(\cdot)^A$	Aerodynamic quantity.
$(\cdot)_{av}$	Average of (\cdot) .
$(\cdot)^C, (\cdot)_c, (\cdot)^c$	Circulatory origin.
$(\cdot)^f$	Loading component with trailing edge separation effects
$(\cdot)^I$	Inertial quantity.
$(\cdot)^I, (\cdot)_i, (\cdot)^i$	Impulsive or noncirculatory origin.
$(\cdot)_k$	flexbeam quantity
$(\cdot)^p$	Attached flow (potential) component
$(\cdot)_{pl}$	pitch link quantity
$(\cdot)^s$	Structural quantity.
$(\cdot)_t$	torque tube quantity
$[]^T$	Transpose of a matrix
$(\cdot)_0$	Trim condition
$(\cdot)_b$	Refers to the b 'th blade
$[\cdot]_{bF}$	Blade-fuselage quantity
$[\cdot]_{b\lambda}$	Blade-inflow coupled matrix
$(\cdot)_F$	Fuselage quantity
$[\cdot]_{Fb}$	Fuselage-blade quantity
$[\cdot]_{FR}$	Fuselage-rotor coupled matrix
$(\cdot)_h$	Angle of attack or plunge component
$(\cdot)_{LG}$	Landing gear

$(\cdot)_m$	Pitching moment component
$(\cdot)_q$	Pitch rate component
$(\cdot)_{qs}$	Quasi-steady component
$(\cdot)_r$	Reattachment component
$[\cdot]_{RR}, (\cdot)_R$	Refers to Rotor
$(\cdot)_{tr}$	tail rotor quantity
$[\cdot]^T$	Transpose of a matrix
$[\cdot]_{RF}$	Rotor-fuselage coupled matrix
$[\cdot]_{\lambda b}$	Inflow-blade coupled matrix
$(\cdot)_1$	Blade coordinate system origin.
$(\cdot)_2$	Tip coordinate system origin.
$(\cdot)_{nc}, (\cdot)_{ns}$	n th harmonics of cosine and sine components of (\cdot) , respectively.
$(\cdot)^A$	Aerodynamic quantity.
$(\cdot)^I$	Inertial quantity.
$(\cdot)^S$	Structural quantity.
$(\cdot)_1$	Blade coordinate system origin.
$(\cdot)_2$	Tip coordinate system origin.

Chapter 1

INTRODUCTION

Chapter 1

Introduction

The UMARC (University of Maryland Advanced Rotorcraft Code) is a comprehensive code, which is based on finite element methodology and readily adapts to existing as well as evolving advanced rotor designs, and offers a multitude of analysis options. In addition, the code provides a user-friendly interface and uses state-of-the-art techniques for rotor analysis. The modeling and analysis capabilities of UMARC are summarized in Tables 1-3.

Over the past few years, graduate students at the University of Maryland have developed several sophisticated rotor codes offering one or more of the following analysis options: nonlinear coupled aeroelastic trim, blade flap-lag-torsion stability in forward flight, air/ground resonance, blade and hub loads, three dimensional gust and vortex field response, circulation control aerodynamics, coupling with three dimensional CFD codes, composite rotors, higher harmonic control, and aeroelastic optimization. These codes, however, were developed by individual researchers with very specific objectives, and therefore lack user-friendliness, modularity, numerical robustness and flexibility for

further expansion.

The objective of the UMARC project was to extensively update various rotor analysis codes developed at the University of Maryland and synthesize them into a single comprehensive code. The integrated code offers a user friendly interface, robustness and computational efficiency of numerical schemes, clarity of programming logic, state-of-the-art modeling and analysis methods, and a rigorous theory basis.

Putting together a comprehensive analysis code in a consistent and balanced manner is a very involved task. For this reason, only a limited number of such codes are available today. References 1-3 review existing comprehensive codes. These references also offer a definition for the word “comprehensive” against which the scope of a comprehensive code can be judged.

One of the modern advanced comprehensive rotor codes is the CAMRAD (Comprehensive Analytical Model of Rotorcraft Aerodynamics and Dynamics) developed by Johnson [4]. It covers diverse technical disciplines in a consistent and balanced manner, and is widely used by the industry and the government. CAMRAD is a multidisciplinary code with analysis options for trim, performance, blade loads, vibration, noise, aeroelastic stability, gust response, flight dynamics and handling qualities. Other comprehensive codes, collectively referred to as the first generation comprehensive codes, had emerged in response to specialized modeling and/or analysis requirements, including the Rotorcraft Flight Simulation Code C81, developed by Bell Helicopter Textron, Rexor, de-

veloped by Lockheed, and C60 developed by Boeing Helicopter Company. Recently, more comprehensive codes have emerged, again with a focused scope in terms of applications. These include RDYNE of Sikorsky Aircraft, G400 of the United Technology Research Center, RACAP of McDonnell Douglas Helicopter, COPTER of Bell Helicopter Textron, and DYSCO of Kaman. These codes are very useful in solving complex design and analysis problems related to specific rotor designs. These codes, however, do not incorporate state-of-the art finite element methodology. Recognizing this shortcoming, the Army and its Aeroflightdynamics Directorate at Ames initiated the development of a Second Generation Comprehensive Helicopter Analysis System (2GCHAS) which will be extensively based on finite element methodology.

The present effort, the development of a comprehensive rotorcraft aeroelastic code UMARC, using modern analysis techniques and emerging finite element methodology, with consistent and balanced modeling of dynamic and aerodynamic phenomena, represents a significant step in the evolution of comprehensive codes.

1.1 Background of UMARC Development

The in-house rotor analysis codes developed over the last ten years at the University of Maryland by different graduate students evolved from the finite element formulation developed by Sivaneri and Chopra [5, 6] to study the coupled flap-lag-torsion stability of a bearingless rotor blade in hover. All these graduate

students worked on their dissertations under the supervision of Prof. Inderjit Chopra. The flexbeam and the torque tube were modeled using a 15-degree of freedom beam finite element. The coupled, nonlinear blade equations were obtained using the Hamilton approach [7]. Quasisteady aerodynamic strip theory, including noncirculatory effects and coupled with uniform induced inflow , was used to compute airloads. This finite element formulation [6] was the first investigation which showed the potential of finite element methodology in the analysis of rotors with complex hubs involving redundant load paths. It was shown that approximate modeling of bearingless rotors, such as the “equivalent beam approach” model, can lead to erroneous conclusions.

Hong [8, 9] enhanced the structural modeling capabilities to analyze composite blade stability in hover. The blade was modeled as a single-cell laminated shell beam composed of an arbitrary lay-up of composite plies. Important structural coupling, such as bending-torsion and extension-torsion, arising from nonisotropic ply orientations were identified and their effects on blade stability were investigated systematically. These couplings were shown to have substantial influence on blade aeroelastic stability. Recently, Smith [10] further refined the modeling of composite blades by including nonclassical structural effects, such as section warping and transverse shear, and also validated the analysis by correlating calculated results with experimental data [10, 11]. This refined composite modeling is incorporated in UMARC.

Panda [12] -[15] extended the formulation to the forward flight regime. This

involved the calculation of vehicle trim, rotor steady response, and stability of perturbation motion. Uncoupled trim was calculated from nonlinear vehicle equilibrium equations and the rotor steady periodic response was calculated using a finite element in time method. Blade stability was analyzed using Floquet transition matrix theory. The analysis was initially formulated for metal blades and later extended to include composite blades [14]. Results from this analysis showed the potential of aeroelastic tailoring of composite blades to reduce vibration and blades stresses and to improve rotor stability.

Bir [16, 17] developed a coupled rotor-fuselage math model and used it to study the helicopter response due to general three-dimensional gust fields. A dynamic inflow model was used to capture low-frequency aerodynamic effects. This inflow model was modified to include effects of hub motion and gust field. Force summation formulation was developed to compute blade stresses and hub loads. The analysis was also used [18] to investigate the transient response of a helicopter encountering the trailing vortices shed by a large fixed-wing airplane. In addition, Elliott [19] investigated the response of a hingeless rotor due to nondeterministic atmospheric turbulence for a simple rotor model.

Dull [20] extended the finite element formulation to examine the aeroelastic stability of an isolated bearingless rotor in hover and forward flight. A comparison of predicted and measured stability results for several bearingless rotors showed satisfactory correlation in both hover and forward flight. Further, Jang [21, 22] included body degrees of freedom in the analysis in order to calculate

ground and air resonance of bearingless rotors in hover and forward flight. To validate these analyses, several correlation studies were carried out for hingeless and bearingless rotors by comparing calculated results with model stability data obtained from both in-house and outside sources [23]-[25].

Lim [26]-[29] linked the rotor aeroelastic analysis with optimization algorithms to predict an optimum design which both minimized oscillatory hub loads and maintained aeroelastic stability in forward flight. Vehicle trim and rotor steady response were solved as a coupled solution using a modified Newton method. A direct analytical technique was developed to compute the sensitivity derivatives of blade response, rotor hub loads and stability roots with respect to the design variables used in the optimization process. Calculation of these gradients formed an integral part of the trim and stability analyses, and required only a fraction of the computation time as compared to the frequently used finite differences methods. The optimized solutions yielded a significant reduction in oscillatory hub loads.

These advancements resulted in analyses with state-of-the-art structural modeling capabilities. Continuing research efforts were then directed toward improvement of the aerodynamic modeling capabilities. Nguyen [30, 32] implemented a computationally-efficient nonlinear unsteady aerodynamic model [33]-[36] for calculation of blade airloads associated with attached flow, separated flow and dynamic stall. A free wake model adapted from CAMRAD [4] was incorporated in the code to compute the induced inflow distribution during

steady flight conditions. The trim analysis was extended to compute optimal higher harmonic control (HHC) pitch settings to minimize the vibratory hub loads and to study the effects of HHC on blade and control system fatigue loads, rotor performance, and actuation power requirements.

Torok [37]-[39] incorporated the nonlinear aerodynamic model and the CAM-RAD's free wake model into the rotor aeroelastic analysis to investigate the loads and stability of hingeless and articulated rotors. A correlation of predicted trim controls, blade aerodynamic loads, and blade bending moments with Gazelle flight test data was carried out to validate the rotor response analysis. The nonlinear aerodynamic model improved correlation in a high-speed, high-thrust flight condition, whereas the free wake modeling proved important for capturing the harmonics of loads at low advance ratios. The rotor stability analysis was correlated with model hingeless rotor data. At high advance ratios, the inclusion of unsteady aerodynamics significantly improved damping predictions. At high thrust flight conditions, dynamic stall was an important factor in stability prediction.

Kim [40, 43] coupled the rotor dynamic code with a finite-difference transonic aerodynamic code based on three-dimensional, small disturbance, unsteady aerodynamic theory. Three-dimensional aerodynamic effects on blade response and loads in steady flight were investigated, and calculated results were correlated with Gazelle flight test data. At high forward speeds, three-dimensional effects were shown to be important in the prediction of blade re-

sponse and loads.

Benquet [42] modified the finite element analysis to study the dynamic response and loads of an advanced tip rotor in forward flight. A special finite element was developed for the blade tip to analyze blades with sweep, anhedral and tapered planforms. It was shown that tip-sweep and tip-anhedral have a powerful influence on blade dynamics. Also, Kim [43] analyzed three dimensional aerodynamic effects on advanced tip rotors by coupling the finite difference code with the dynamic code. Three-dimensional aerodynamics showed a considerable effect on the torsional response of swept-tip and anhedral-tip blades.

Chopra [44, 45] included circulation control (CC) aerodynamics in the rotor aeroelastic analysis to investigate the stability of hingeless and bearingless rotors in forward flight. For CC airfoils, lift is a nonlinear function of jet momentum and the geometric angle of incidence. Accordingly, the aerodynamics for the CC rotor were reformulated to include the perturbation in blowing momentum due to inplane velocity and an optional table look-up for nonlinear characteristics. For CC rotors, geometric pitch is held fixed and cyclic control of lift is achieved through cyclic control of blowing. This required a revision of the trim procedure. It was shown that trailing edge blowing can have a major influence on blade stability and loads and must be considered in CC rotor design.

In summary, these investigations yielded a library of aerodynamic and dynamic modeling capabilities. These state-of-the-art modeling and analysis tech-

niques have been selectively synthesized into UMARC, keeping in view the programming efficiency, user friendliness and modularity.

1.2 Organization of the UMARC Manual

This manual is divided into four parts; Part I covers development of the mathematical model for the rotorcraft system, Part II describes the analysis procedures, which are broadly classified into trim and stability analyses, Part III covers specialized features of the UMARC, e.g. the bearingless rotor and the advance-tip rotor blade (This part will expand further as more features, e.g., higher harmonic control, aeroelastic optimization and composite rotor blade are integrated into UMARC), and Part IV addresses the user-interface issues and the details of code execution (This part will eventually develop into a stand-alone Users' Manual as more explanatory notes, particularly those related to the structuring of the UMARC code are added).

Each part of the manual is further subdivided into chapters. Each chapter takes up a major component of UMARC and provides a detailed discussion of its theory basis, mathematical formulation and implementation. It should be emphasized that the implementation details do not cover the software issues of the code, but point out the equivalence between the theory basis and the computer language and its intergration within the code. Each chapter is self-contained with its own list of figures and references. The authors have closely collaborated on the entire manual. The following section summarizes the UMARC

theory basis and points out sections in the manual where the pertinent details are covered.

1.3 Overview of UMARC Theory Basis

1.3.1 Structural Modeling

The rotorcraft structural model is a nonlinear representation of elastic rotor blades coupled to a rigid fuselage (Chapter 2). The key feature is the use of a finite element methodology which can accurately model the kinematic and elastic behavior of the rotating blade, and readily adapt to evolving advanced rotor configurations. The blade is modeled as a slender elastic beam undergoing flap bending, lag bending, elastic twist, and axial deflection (section 2.1.2). Nonlinear coupled differential equations, formulated for moderately large deflections, are used. These equations are adapted from the work of Hodges and Dowell [7]. Typically, these contain at least second order geometric terms in the flap, lag, axial and torsion equations. These nonlinear equations involve differentials in spatial (radial) and temporal coordinates.

A finite element approach, which is the basis of modern structural analysis, is used to eliminate the radial variables from the blade equations (section 2.3.1). This finite element method is based on Hamilton's principle (section 2.2). The blade is discretized into a number of beam elements, each consists of fifteen degrees of freedom. Between elements, continuity of displacement and slope for flap and lag bending deflections, and continuity of displacement for

elastic twist and axial deflections is maintained. Each element has three internal nodes, two for axial deflections and one for elastic twist. In the finite element formulation, the elastic twist is represented in the form of a quasi-coordinate (non-Euler) which implicitly includes spatial integral over the beam. Using this coordinate, the resulting equations do not contain any integro-differential terms and the global matrices are banded. In the earlier versions of the code from which UMARC has evolved, the axial degree of freedom was also a quasi-coordinate representing the resultant effect of elastic elongation and kinematic shortening due to beam flexure. In the current version of UMARC, the axial degree of freedom represents the physical elastic deflection. Though this necessitates computation of spatial integrals, numerical accuracy and stability, specially during trim analysis, are substantially enhanced.

The assembly of elemental energy terms, followed by the application of boundary constraints, yields the nonlinear blade equations in terms of nodal coordinates. This method is very adaptable to different blade boundary conditions since the boundary constraints are applied to the assembled finite element equations. Also, the effects of lag damping, pitch actuation, and blade articulation can be introduced by modifying the properties of the appropriate finite elements.

One of the distinguishing features of this analysis is the precise modeling of bearingless rotors (Chapter 7). These rotors involve redundant load paths and therefore, the finite element approach appears a natural choice for the analysis.

The flexbeam and torque tube are discretized into beam elements. Displacement compatibility conditions at the clevis (where the flexbeam, torque tube and main blade are joined) are introduced into the assembled matrices. The pitch link location and stiffness and other boundary constraints at the hub are introduced by appropriate modifications of the properties of the blade root element in the assembled global matrices.

In the current phase of the UMARC, the fuselage is modeled as a rigid body with five degrees of freedom : longitudinal, lateral, and vertical translations and pitch and roll rotations. Rotor dynamics coupling effects are included in the derivation of the fuselage equations (section 2.4). For the ground resonance analysis, the characteristics of landing gear, i.e., stiffness and damping, are also included in the body equations (section 2.2.2.1).

To analyze advanced tip rotors, a special element is developed for the tip portion of the blade (Chapter 6). Nonlinear transformation expressions valid for moderate rotations are used to assemble the outboard blade element and the tip element. Geometric angles between blade and tip segments at the junction are retained before and after bending (section 6.5). The analysis can incorporate tip sweep, anhedral and planform-taper.

1.3.2 Aerodynamic Modeling

The aerodynamic environment of a helicopter rotor in forward flight is extremely complex, involving transonic flow with shocks on advancing blades,

stalled and reversed flow on the retreating blades and swept flow on the fore and aft regions of the rotor disk. The blade is exposed to unsteady variations of angle of attack and freestream velocity, varying in both the radial and azimuthal directions. Because of the complexity of the flow, accurate modeling of the unsteady flow field on the blade requires a sophisticated analysis. Currently, many analyses use quasisteady aerodynamic model with uniform inflow distribution. There is now an increased emphasis on the refinement of aerodynamic modeling of rotor blades to enhance the predictive capability of rotor analyses.

The aerodynamic modeling of a rotor can be divided into two parts: a local blade-element model and a global wake model. It is important that the modeling of airloads for a comprehensive rotor analysis be sophisticated enough to allow accurate prediction of unsteady aerodynamic forces over all the possible flow regions ranging from attached flow to separated and dynamically stalled flow, and still be simple and computationally efficient.

Blade-Element Aerodynamic Model

The formulation of the blade element aerodynamic model is based on the work of Leishman and Beddoes [36]. It consists of three parts: a linear attached flow model (section 3.3.1), a separated flow model (section 3.3.6), and a dynamic stall model (section 3.3.7). An important feature of this model is that the compressibility effects are implicitly included. In addition, this model requires only a few empirical constants (most of which can be derived from static airfoil data).

Attached Flow: In the attached flow formulation, the unsteady lift, drag and pitching moment are assumed to consist of circulatory and impulsive (noncirculatory) components. These airloads are calculated using an indicial response representation implemented in the form of a finite-difference discretization of integral equations. This method determines the aerodynamic loadings due to a step change in the downwash at the three-quarter chord position. The circulatory loads include the effects of the near shed wake. The impulsive loads are due to the presence of propagating pressure waves.

Separated Flow: A Kirchhoff flow model is used to simulate the nonlinear aerodynamics associated with trailing edge flow separation. This model relates the nonlinear lift behavior to the location of the trailing edge separation point on the airfoil upper surface. Using Kirchhoff's model, the location of the separation point can be inferred from the static airfoil lift data at a given Mach number. Under steady conditions, the separation point is governed by the dynamics of the airfoil pressure distribution and the boundary layer response. To simulate both effects, a lag is introduced in the unsteady lift development. The unsteady drag and moment are also computed using the separation point concept.

Dynamic Stall: This is characterized by separation at the leading edge and the shedding of concentrated vorticity from the leading edge region. The vorticity is swept downstream chordwise and significantly affects the load distribution on the airfoil. The vortex convection rate is calculated using a nondimensional time parameter based on the distance traveled by the airfoil in terms of semi-

chord length. By monitoring the excess lift and the center of pressure movement, the vortex-induced pitching moment is computed. As the vortex reaches the trailing edge, the model assumes rapid decay of the incremental lift.

These unsteady aerodynamic models have been validated for various airfoils under flow conditions ranging from attached flow to deep stall regimes. Details of the implementation of these models in the rotor analysis can be found in Refs.[33]-[39].

In addition to the unsteady aerodynamic models described above, UMARC offers the option of using quasisteady aerodynamics (section 3.1). Airloads, in this method, are based on static airfoil characteristics and corrections for swept flow and reversed flow are introduced. Furthermore, there is an option to approximately capture the unsteady aerodynamic effects using a dynamic inflow model.

Rotor Wake Model

The inflow distribution over the rotor disk is computed using either a simple linear inflow model, a nonuniform prescribed wake model, or a free wake model (Chapter 3.5). For the simple linear-inflow model, Drees' model is used for moderate to high speed flight, and White and Blake's model is used for low forward speed. For non-uniform inflow calculations, prescribed and free wake models adapted from CAMRAD are implemented. Also, a newly developed free wake model [46], specially suited for high forward speed conditions, is implemented (section 3.5.10). The prescribed wake model is based on Landgrebe's wake ge-

ometry and the free wake model is based on Scully's work. The geometry of the free wake is partitioned into three parts: near wake, rolling-up wake, and far wake. The near wake is modeled by a series of radial panels with liner circulation distributions. The rolling-up wake model consists of an inboard linear circulation distribution panel and a tip panel which models the roll-up of the tip vortex. The far wake is modeled by one linear circulation panel and a concentrated tip vortex with strength proportional to the maximum bound circulation value on the rotor blade. The free wake model is completely coupled with the aeroelastic analysis. The coupling is achieved through iterative transference of blade bound circulation, blade motion and induced inflow distribution. In the free wake analysis, the shed wake effects are suppressed since they are included in blade element aerodynamic models.

1.3.3 Analysis

The equations governing the rotor-fuselage-inflow dynamics are inherently nonlinear and include time-dependent terms (section 2.2). Due to the complexity of these equations, the analyses are broken into three phases: vehicle trim, steady rotor response, and stability solution. These three phases are uncoupled and solved individually. Then, through an iterative process, a certain degree of coupling is achieved between different phases. In UMARC, vehicle trim and rotor steady response are solved as one coupled solution (section 4.4), and stability of the system is calculated from linearized equations (section 5.2).

Vehicle Trim

A vehicle trim solution involves the calculation of control positions and vehicle orientation. These are many forms of trim solutions. Broadly, these can be classified into two categories: free flight trim and wind tunnel trim. In UMARC, free flight trim implies propulsive trim, for which it is assumed that the main rotor supplies all the propulsive and thrust forces and the engine provides the power needed to maintain the specified flight condition. Trim is calculated from the satisfaction of three force (longitudinal, lateral, and vertical), and three moment (pitch, roll, and yaw) vehicle equilibrium equations (section 4.2). For a specified gross weight and a level flight speed, the solutions yield main rotor controls (collective, and longitudinal and lateral cyclic), vehicle orientation (longitudinal and lateral shaft tilt), and tail rotor collective pitch.

The wind tunnel trim solution simulates the test conditions in the wind tunnel. One frequently adopted procedure is to specify collective pitch, shaft tilt and forward speed, and then calculate the cyclic pitch angles to trim both the cyclic flap angles to zero (section 4.2.1).

Blade Steady Response

Blade response involves determination of the blade deflected positions for one complete rotor revolution for a specified set of trim controls (section 4.4.2). The blade equations in forward flight are coupled, nonlinear and periodic. For steady flight conditions, blade response is assumed periodic, with a time period of one rotor revolution. In UMARC, blade steady response is calculated using finite

element methods in both space and time. Spatial discretization transforms the blade partial differential equations into a set of differential equations with time as the independent variable. To reduce the computation time, these equations are transformed to a few equations (6 to 8) in the normal mode domain using the coupled rotating natural modes of the blade (section 4.2.3). These nonlinear periodic equations are then solved, using the finite-element method in time (section 4.4.2). The formulation is based on Hamilton's principle in weak form and results in a set of nonlinear algebraic equations. The time period of one rotor revolution is discretized into a number of time elements, and within each element a polynomial distribution for response (section 4.3) is assumed. Through the assembly of elemental properties, the periodicity of response is imposed by connecting the first and the last time elements. These equations are solved using a Newton-Raphson procedure. The time finite element method is very efficient and robust and the solution can accurately capture higher harmonic response. Blade and hub loads are obtained using either a modal summation method or a force summation method (section 4.4.3). Aerodynamic and inertial loads are integrated along the blade span to obtain blade loads at the root, and then summed over all the blades to obtain rotor hub loads (section 4.4.4).

In UMARC, vehicle trim and steady response are calculated iteratively as one coupled solution, using a modified Newton method (section 4.4). During the iteration process, pitch control settings and vehicle orientation are continually updated, which in turn influence the blade dynamic behavior. The converged

solution simultaneously satisfies the blade and the vehicle equilibrium equations. For computational efficiency and fast convergence, the computationally intensive parts of the analysis are taken out of the inner loop of calculations. The calculation of free wake geometry is computationally intensive and therefore is performed in the outer loop.

To start the inner loop analysis, a linear inflow model (section 3.5.1) is used until a near trimmed condition is achieved. Then, within the inner trim loop, the scheme to calculate bound circulation is activated and repeated after every few iterations. In the outer scheme, the wake geometry and the associated coefficients relating induced velocity distribution with blade bound circulation are calculated (section 3.5.9). Since the wake geometry is less sensitive to small changes in trim controls, the outer loop is repeated infrequently.

Stability

For the stability analysis, the perturbation equations of motion are linearized about the blade steady equilibrium positions and solved for stability roots (Chapter 5). To save computation time, the finite element equations of the blade are transformed into a few (6 to 8) normal mode equations using blade coupled rotating modes about their calculated mean deflected position. Two approaches are offered in UMARC to calculate the roots of these periodic equations, a Floquet approach (section 5.2.5) and a constant coefficient approach (section 5.2.6). In the first approach, the Floquet transition matrix is calculated numerically over one rotor revolution and stability roots are inferred

from its eigenvalues. In the second approach, the blade equations in the rotating frame are transformed to the fixed frame using a multi-blade coordinate transformation. The periodic terms are then averaged out over one revolution and the resulting constant coefficient equations are solved as an algebraic eigenvalue problem. This approach provides a good estimate of roots at low advance ratios (μ less than approximately 0.4).

If dynamic inflow (section 5.2.7) or fuselage motion is included in the stability analysis, then it is more convenient to calculate Floquet stability solution in the fixed reference frame. With the inclusion of linear unsteady aerodynamics, blade stability may be calculated using two approaches discussed above. However, if nonlinear unsteady aerodynamics is included in the blade analysis, it is not possible to calculate stability using these methods. In UMARC, a transient approach is used for this case (section 5.3). The blade is disturbed from its equilibrium position and the transient response is calculated using a time integration technique. Damping of a mode is estimated using the Moving-Block method [47], and is identical to the procedure followed to determine the stability of a model rotor in a wind tunnel.

For ground and air resonance stability, the fuselage degrees of freedom are also included. Body equations are coupled with rotor equations as well as inflow dynamics equations (section 5.2.1-5.2.4). Linearized rotor, body and inflow equations are solved for stability using either a Floquet approach or a constant coefficient approach.

Structural Modelling Options

Blade Modelling

- articulated/hinged with arbitrary hinge sequencing
- hingeless
- bearingless
- teetering/gimballed
- uniform/distributed structural properties
- droop, sweep, precone
- number and length of beam elements
- participating modes
- metallic/composite blades

Other Modelling Options

- fuselage with six degrees of freedom
- number of rotor blades
- pitch link/control stiffness
- pitch-lag, pitch-flap coupling
- composite blade lay-up parameters
- torque tube and flex beam properties for the bearingless rotors
- fuselage-support and hub-support stiffness values for the ground and/or air resonance analyses
- relative location of the subsystem components (e.g., fuselage, main rotor, tail rotor)

Table 1

Aerodynamic Modeling Options

- Quasisteady strip theory
 - with/without apparent mass effects
- Unsteady aerodynamics
 - linear (attached flow)
 - with/without apparent mass effects
 - with/without impulse affects
 - nonlinear (separated flow)
 - with/without dynamic stall
- Reverse flow
- Compressibility
- Drees inflow model
- Vortex ring model
- Prescribed wake
- Free wake
- Dynamic inflow
- Circulation control aerodynamics

Table 2

Analysis Options

- Rotating blade natural frequencing
and mode shapes
- Trim
 - propulsive trim
 - wind tunnel trim with choice
of trim variables
- Stability
 - aeroelastic stability
 - ground resonance
 - air resonance
- Aeroelastic response
 - steady state response
 - gust response
- HHC
- Aeroelastic optimazition
(not available yet)

Table 3

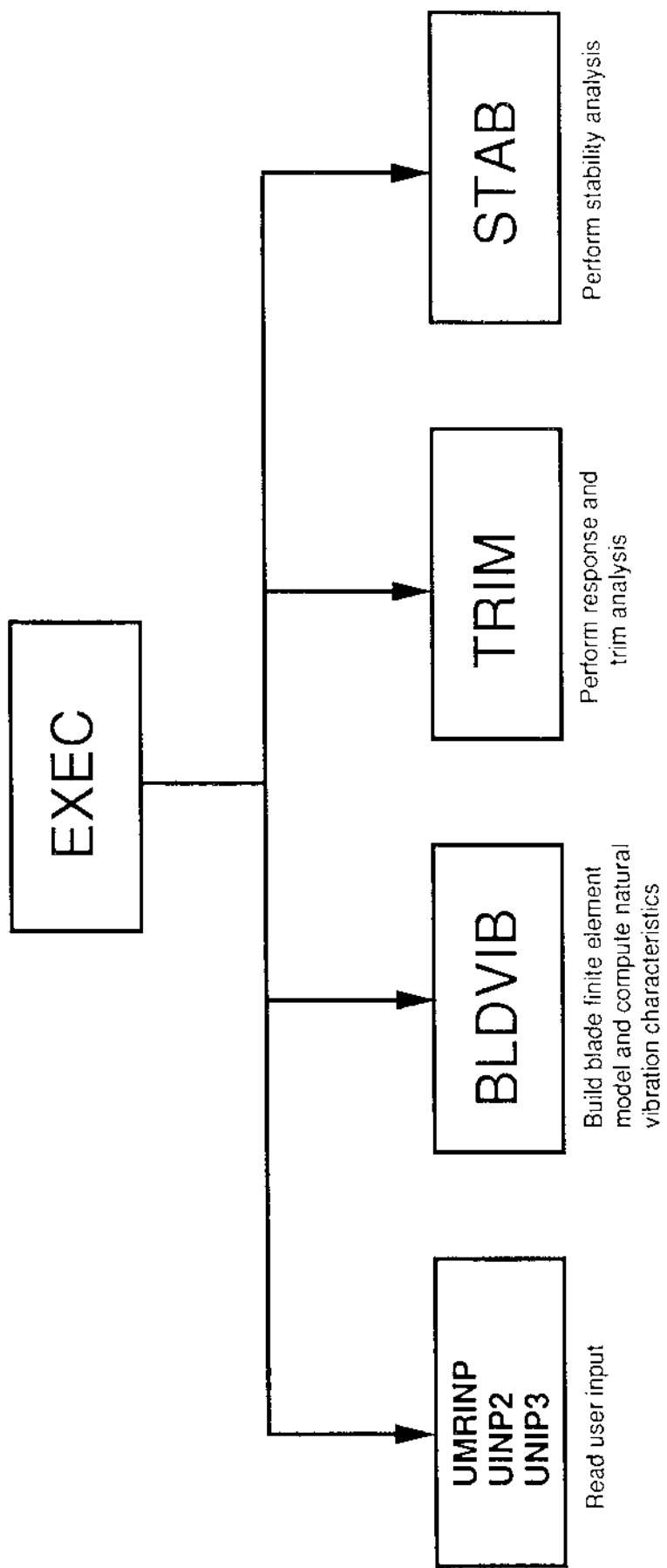


Fig. 1.1 Major Routines of the UMARC CODE

A review of the state-of-the-art blade modeling and analysis methodologies is provided in Ref. [48], in particular those adopted in UMARC.

Figure 1.1 presents the top-level modules of the UMARC computer code. The *EXEC* is the main module which checks for consistency of the user-input data and invokes other modules to build helicopter model and perform user-requested analyses. Modules *UMRINP*, *UNIP2* and *UNIP3* read the user-input data and translate this into appropriate Fortran variables and flags. Module *BLDVIB* builds up the rotor blade finite element model and computes its rotating natural frequencies and mode shapes. Module *TRIM* computes the blade response and vehicle trim. In accordance with the user request, the trim analysis is carried out either in the wind tunnel mode or propulsive mode. Module *STAB* performs rotor aeroelastic stability analysis and/or aeromechanical stability analysis. Detailed structure charts and functions of each module are provided in appropriate chapters of the theory manual.

Bibliography

- [1] Stephens, W.B., and Austin,E.E., "Comprehensive Rotor Analysis Methods", Proceedings of NASA/Army Rotorcraft Technology Conference, NASA Ames Research Center, Moffett Field, California, March 17-19,1987
- [2] Johnson, W., "Assessment of Aerodynamic and Dynamic Models in Comprehensive Analysis for Rotorcraft", *Computers and Mathematics with Applications*, Vol. 12A, No.1, January 1986, pp.11-28
- [3] Stephens, W.B., Rutkowski, M.J., Ormiston, R.A., and Tan, C.M., "Development of the Second Generation Comprehensive Helicopter Analysis System (2GCHAS)", *Proceedings of the National Specialists Meeting on Rotorcraft Dynamics*, Arlington; Texas, November 13-14,1989
- [4] Johnson,W., "A Comprehensive Analytical Model of Rotorcraft Aerodynamics and Dynamics, Part 1: Analysis Development," NASA TM 81182, June 1980.
- [5] Sivaneri, N.T. and Chopra, I., "Dynamic Stability of a Rotor Blade Using Finite Element Analysis", *AIAA Journal*, Vol.20, No.5, May 1982.

- [6] Sivaneri, N.T. and Chopra, I., "Finite Element Analysis for Bearingless Rotor Blade Aeroelasticity", *Journal of American Helicopter Society*, Vol.29, No.2, April 1984.
- [7] Hodges,D.H.and Dowell, E.H., "Nonlinear Equations of Motion for the Elastic Bending and Torsion of Twisted Nonuniform Rotor Blades" NASA TN D-7818, 1974.
- [8] Hong, C.H., and Chopra, I., "Aeroelastic Stability Analysis of Composite Rotor Blade", *Journal of the American Helicopter Society*, Vol.30, No.2, April 1985.
- [9] Hong, C.H., and Chopra, I., "Aeroelastic Stability Analysis of Composite Bearingless Rotor Blade", *Journal of the American Helicopter Society*, Vol.31, No.4, October 1986.
- [10] Smith,E., and Chopra,I., " Formulation and Evaluation of an Analytical Model for Composite Box-Beam", *Journal of the American Helicopter Society*, Vol.36, No.3, July 1991.
- [11] Chandra, R., Stemple, A.D., and Chopra,I., "Thin-Walled Composite Beams Under Bending, Torsional, and Extensional Loads ", *Journal of Aircraft*, Vol.27, No.7, , July, 1990.
- [12] Panda,B., and Chopra,I., "Flap-Lag-Torsion Stability in Forward Flight", *Journal of the American Helicopter Society*, Vol.30, No.4, October 1985.

- [13] Panda, B., and Chopra,I., " Dynamics Stability of Hingeless and Bearingless Rotor in Forward Flight", *Journal of Computers and Mathematics with Applications*, Vol.12A, No.1, January 1986.
- [14] Panda, B. and Chopra, I., "Dynamics of Composite Rotor Blades in Forward Flight", *Vertica*, Vol 11, No.1/2, Jan. 1987.
- [15] Panda,B., "Dynamic Stability of Hingeless and Bearingless Rotors in Forward Flight", PhD Dissertation, Department of Aerospace Engineering, University of Maryland, College Park, Maryland, August 1985.
- [16] Bir, G.S., and Chopra,I., " Gust Response of Hingeless Rotors", *Journal of the American Helicopter Society* , Vol.31, No.2, April 1986.
- [17] Bir, G.S., and Chopra,I., " Prediction of Blade Stresses Due to Gust Loading", *Vertica*, Vol.10, 1986.
- [18] Kim, K.C., Bir, G.S., and Chopra,I., " Helicopter Response to an Airplane's Vortex Wake", *Vertica*, Vol.12, 1988.
- [19] Elliott, A.S., and Chopra,I., "Helicopter Response to Atmospheric Turbulence in Forward Flight", *Journal of the American Helicopter Society* , Vol.35, No.2, April 1990.
- [20] Dull, A.L., and Chopra,I., "Aeroelastic Stability of Bearingless Rotors in Forward Flight", *Journal of the American Helicopter Society*, Vol.33, No.4, October, 1988.

- [21] Jang, J., and Chopra,I., "Ground and Air Resonance of an Advanced Bearingless Rotor in Hover", *Journal of the American Helicopter Society*, Vol.33, No.3, July 1988.
- [22] Jang, J., and Chopra,I., "Air Resonance of an Advanced Bearingless Rotor in Forward Flight", *Proceedings of Second International Conference on Rotorcraft Basic Research*, College Park, Maryland, February, 1988.
- [23] Wang, J., Jang J. and Chopra, I., "Air Resonance of Hingeless Rotor in Forward Flight", *Vertica*, Vol.14, No.2, May 1990.
- [24] Wang, J., Chopra, I., Samak, D.K., Green, M., and Graham, T., "Theoretical and Experimental Investigation of Aeroelastic Stability of an Advanced Bearingless Rotor in Hover and Forward Flight", *Proceedings of National Technical Specialists' Meeting on Rotorcraft Dynamics*, American Helicopter Society, Arlington, Texas, November 1989.
- [25] Wang, J., and Chopra, I., "Bearingless Rotor Aeromechanical Stability Measurements and Correlations Using Nonlinear Aerodynamics", *16th European Rotorcraft Forum*, Glasgow, Scotland, September 1990.
- [26] Lim,J.W., and Chopra, I., "Aeroelastic Optimization of a Helicopter Rotor", *Journal of the American Helicopter Society*, Vol.34, No.1, January 1989.

- [27] Lim,J.W., and Chopra, I., "Design Sensitivity Analysis for Aeroelastic Optimization of a Helicopter Rotor ", *AIAA Journal* , Vol.28, No.1, January 1990.
- [28] Lim,J.W., and Chopra, I., "Stability Sensitivity Analysis for Aeroclastic Optimization of a Helicopter Rotor ", *AIAA Journal* , Vol.28, No.3, March 1990.
- [29] Lim,J.W., and Chopra, I., "Aeroelastic Optimization of a Helicopter Rotor Using Efficient Sensitivity Analysis", *Journal of Aircraft*, Vol.28, No.1, January 1991.
- [30] Nguyen, K., and Chopra,I., "Application of Higher Harmonic Control to Rotors Operating at High Speed and Thrust", *Journal of the American Helicopter Society* , Vol.35, No.3, July 1990.
- [31] Nguyen, K., and Chopra,I., "Application of Higher Harmonic Control (HHC) to Hingeless Rotor Systems", *Proceedings of the 45th Annual Forum of the American Helicopter Society*, Boston, Massachusetts, May 1989; Also, *Vertica*, Vol. 14, No.4, October 1990.
- [32] Nguyen, K., and Chopra,I., "Effects of Higher Harmonic Control on Rotor Performance and Control Loads ", *Proccedings of the 31st AIAA/ASME/ASCE/ASC/AHS Structures, Structural Dynamics and Materials Conference*, Long Beach, California, April 1990; Also, accepted for publication in the *Journal of Aircraft*, 1992.

- [33] Beddoes, T.S., "Representation of Airfoil Behavior", *Vertica*, Vol.7, No.2, 1983
- [34] Leishman,J.G., "Validation of Approximate Indicial Aerodynamic Functions for Two-Dimensional Subsonic Flow," *Journal of Aircraft*, Vol. 25, No. 10, October 1988.
- [35] Leishman,J.G., "Two-Dimensional Model for Airfoil Unsteady Drag Below Stall," *Journal of Aircraft*, Vol. 25, No. 7, July 1988.
- [36] Leishman,J.G., and Beddoes,T.S., "A Semi-Empirical Model for Dynamic Stall", *Journal of the American Helicopter Society*, Vol. 34, No. 3, 1989.
- [37] Torok,M.S., and Chopra,I., "A Coupled Rotor Aeroelastic Analysis Utilizing Non-Linear Aerodynamics and Refined Wake Modeling", *Vertica*, Vol. 13, No. 2, 1989.
- [38] Torok,M.S., and Chopra,I., "Rotor Loads Prediction Utilizing a Coupled Aeroelastic Analysis with Refined Aerodynamic Modeling", *Journal of the American Helicopter Society* , Vol.36, No.1, January 1991.
- [39] Torok,M.S., and Chopra,I., "Hingeless Rotor Aeroelastic Stability with Refined Aerodynamic Modeling," *Journal of the American Helicopter Society* , Vol.36, No.4, October 1991.

- [40] Kim, K.C., Desopper, A. and Chopra, I., "Blade Response Calculations Using Three-Dimensional Aerodynamic Modeling", *Journal of the American Helicopter Society*, Vol.36, No.1, January 1991.
- [41] Kim,K.C., and Chopra,I., "Effects of Three-Dimensional Aerodynamics on Blade Response and Loads", *AIAA Journal*, Vol. 29, No.7, July 1991.
- [42] Benquet, P., and Chopra,I., "Calculated Dynamic Response and Loads for an Advanced Tip Rotor in Forward Flight", *Proceedings of the Fifteenth European Rotorcraft Forum*, Amsterdam, Netherlands, September 1989.
- [43] Kim, K.C., and Chopra, I., "Aeroelastic Analysis Stability of Helicopter Rotor Blades with Advanced Tip Shapes", *Proceedings of the 31st AIAA/ASME/ASCE/AHS/ASC Structures, Structural Dynamics and Materials Conference*, Long Beach, California, April 1990.
- [44] Chopra,I., "Aeroelastic Stability of Bearingless Circulation Control Rotor in Hover", *Journal of the American Helicopter Society*, Vol.30, No.4, October 1985.
- [45] Chopra,I., "Aeroelastic Stability of Bearingless Circulation Control Rotor in Forward Flight", *Journal of the American Helicopter Society*, Vol.33, No.3, July 1988.
- [46] Johnson,W., "Wake Model for Helicopter Rotors in High-Speed Flight", NASA Contractor Report, No. 177507, Nov. 1988.

- [47] Tasker,F.A. and Chopra,I., "Assessment of Transient Analysis Techniques for Rotor Stability", *Journal of the American Helicopter Society*, Vol.35, No.1, January 1990.
- [48] Chopra,I., "Perspectives in Aeromechanical Stability of Helicopter Rotors", *Vertica*, Vol. 14, No. 4, 1990, pp. 457-508.

Part 1

Modeling and Analysis Theory

Chapter 2

STRUCTURAL MODELING

Summary

The nonlinear governing equations of motion for the combined rotor and fuselage are discretized using the finite element method in space. In the present formulation, the rotor is assumed to be an elastic beam built out of isotropic materials. The fuselage is assumed to be rigid. The following section describes the formulation of the mass, damping, and stiffness matrices, as well as the load vector for the blade finite elements. The corresponding fuselage matrices and coupling matrices (blade-fuselage and fuselage-blade) are also described. In general, these matrices (and load vectors) contain contributions from: strain energy and kinetic energy of the isolated rotor blade, strain energy and kinetic energy associated with fuselage (hub) motion, and work done by aerodynamic loading (motion dependent and non-motion dependent). Contributions due to aerodynamic loading are discussed in Chapter 3. For analysis, the blade is discretized into a number of beam elements. Each beam element consists of fifteen degrees of freedom. The finite element formulation is based on Hamilton's principle.

The present formulation is applicable to hingeless rotors, articulated/gimballed rotors, as well as bearingless rotors. Special considerations dealing with bearingless rotor modeling are discussed in a separate chapter. Blades with advanced tip shapes such as the swept-tip, anhedral-tip, or tapered-tip require specially modified finite elements. Considerations for blade tip elements are also covered in a separate chapter.

2.1 The Helicopter Model

The helicopter is modeled as a rigid fuselage connected to a single main rotor with an arbitrary number, N_b , elastic blades. Each blade is assumed to be an elastic beam undergoing flap bending, lag bending, elastic twist and axial deflections. Deflections are considered to be of moderate magnitude while strains are assumed to be small. Nonuniform blades having pretwist, precone, and chordwise offsets of blade center of gravity and aerodynamic center from the elastic axis can be accommodated. The helicopter fuselage is modeled as a rigid body with five degrees of freedom. These degrees of freedom consist of three translations, plus pitch and roll rotations. The helicopter landing gear support is modeled as a combination of linear springs and viscous dampers.

2.1.1 Vehicle Kinematics and Coordinate Systems

Figure 2.1 shows the coordinate systems for describing the motion of the helicopter system. Rigid body motion of the vehicle is defined relative to a *ground-fixed inertial coordinate system* (X_I^G, Y_I^G, Z_I^G), with the corresponding unit vectors $\hat{I}_I^G, \hat{J}_I^G, \hat{K}_I^G$. The ground-fixed inertial coordinate system is fixed to the ground and by definition does not move with the helicopter. For convenience, the *inertial coordinate system* (X_I, Y_I, Z_I), with unit vectors $\hat{I}_I, \hat{J}_I, \hat{K}_I$ is defined parallel to the ground-fixed inertial system and located at the vehicle center of gravity. The vehicle is located in space by the position of the vehicle center of gravity. The term vehicle defines the combined system including both the fuselage and the rotor. The *vehicle coordinate system* (X_F, Y_F, Z_F), and corresponding unit vectors $\hat{I}_F, \hat{J}_F, \hat{K}_F$ are fixed to the vehicle center of gravity. The X_F axis is along the longitudinal axis of the fuselage, the Y_F axis is towards the advancing side of the rotor, and the Z_F axis points upwards parallel to the rotor hub. The rectangular coordinate system

(X_H, Y_H, Z_H) , and corresponding unit vectors $\hat{I}_H, \hat{J}_H, \hat{K}_H$ are fixed to the rotor hub (*hub-fixed nonrotating coordinate system*). The hub-fixed system, (X_H, Y_H, Z_H) , is defined parallel to the vehicle coordinate system, (X_F, Y_F, Z_F) . The transformation between the inertial system and the hub-fixed nonrotating system is defined as

$$\begin{Bmatrix} \hat{I}_H \\ \hat{J}_H \\ \hat{K}_H \end{Bmatrix} = \begin{bmatrix} 1 & 0 & \alpha_s \\ 0 & 1 & -\phi_s \\ -\alpha_s & \phi_s & 1 \end{bmatrix} \begin{Bmatrix} \hat{I}_I \\ \hat{J}_I \\ \hat{K}_I \end{Bmatrix} = \mathbf{T}_{HI} \begin{Bmatrix} \hat{I}_I \\ \hat{J}_I \\ \hat{K}_I \end{Bmatrix} = \begin{Bmatrix} \hat{I}_F \\ \hat{J}_F \\ \hat{K}_F \end{Bmatrix} \quad (2.1)$$

where α_s is the longitudinal shaft tilt angle (positive nose down), and ϕ_s is the lateral shaft tilt angle (positive advancing-side down). Note that these angles are assumed to be small.

The *hub-rotating coordinate system* (X, Y, Z) is rotating at constant angular velocity $\Omega \hat{K}$ with respect to the hub-fixed nonrotating frame (see Figure 2.2a). The transformation between the hub-fixed nonrotating and rotating systems is defined as

$$\begin{Bmatrix} \hat{i} \\ \hat{j} \\ \hat{k} \end{Bmatrix} = \begin{bmatrix} \cos\psi & \sin\psi & 0 \\ -\sin\psi & \cos\psi & 0 \\ 0 & 0 & 1 \end{bmatrix} \begin{Bmatrix} \hat{I}_H \\ \hat{J}_H \\ \hat{K}_H \end{Bmatrix} = \mathbf{T}_{RH} \begin{Bmatrix} \hat{I}_H \\ \hat{J}_H \\ \hat{K}_H \end{Bmatrix} \quad (2.2)$$

where the azimuth angle, ψ , equals Ωt .

The *undeformed blade coordinate system* (x, y, z) and the unit vectors $\hat{i}, \hat{j}, \hat{k}$ are attached to the undeformed blade. The undeformed blade is at a precone angle of β_p as shown in Figure 2.2a. The x axis is coincident with the elastic axis of the blade, and the y axis is in the plane of rotation pointed towards the leading edge of the blade. Precone effectively rotates the blade coordinate system about the (negative) y axis. The coordinate

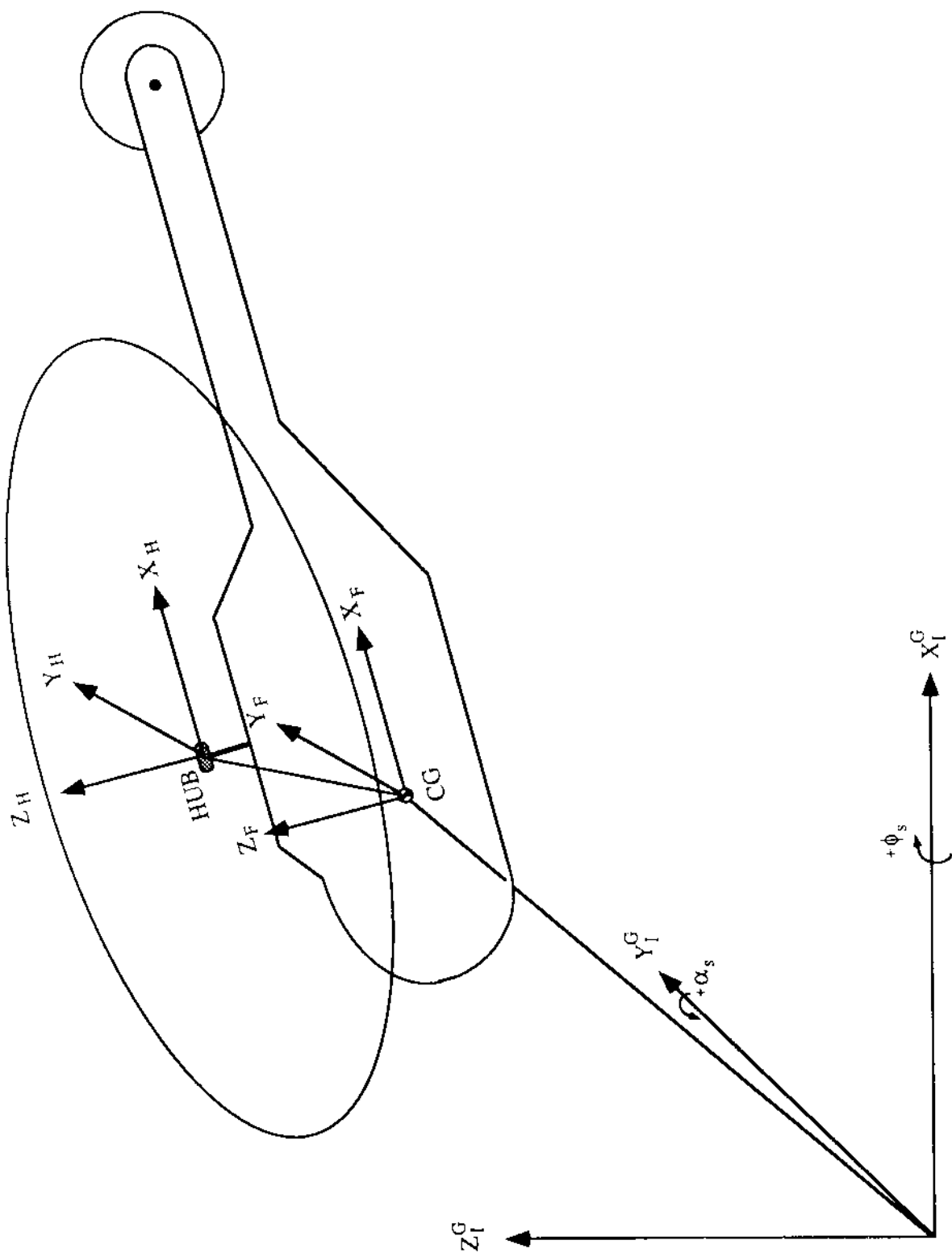


Figure 2.1 Inertial, Vehicle, and Hub Coordinate Systems

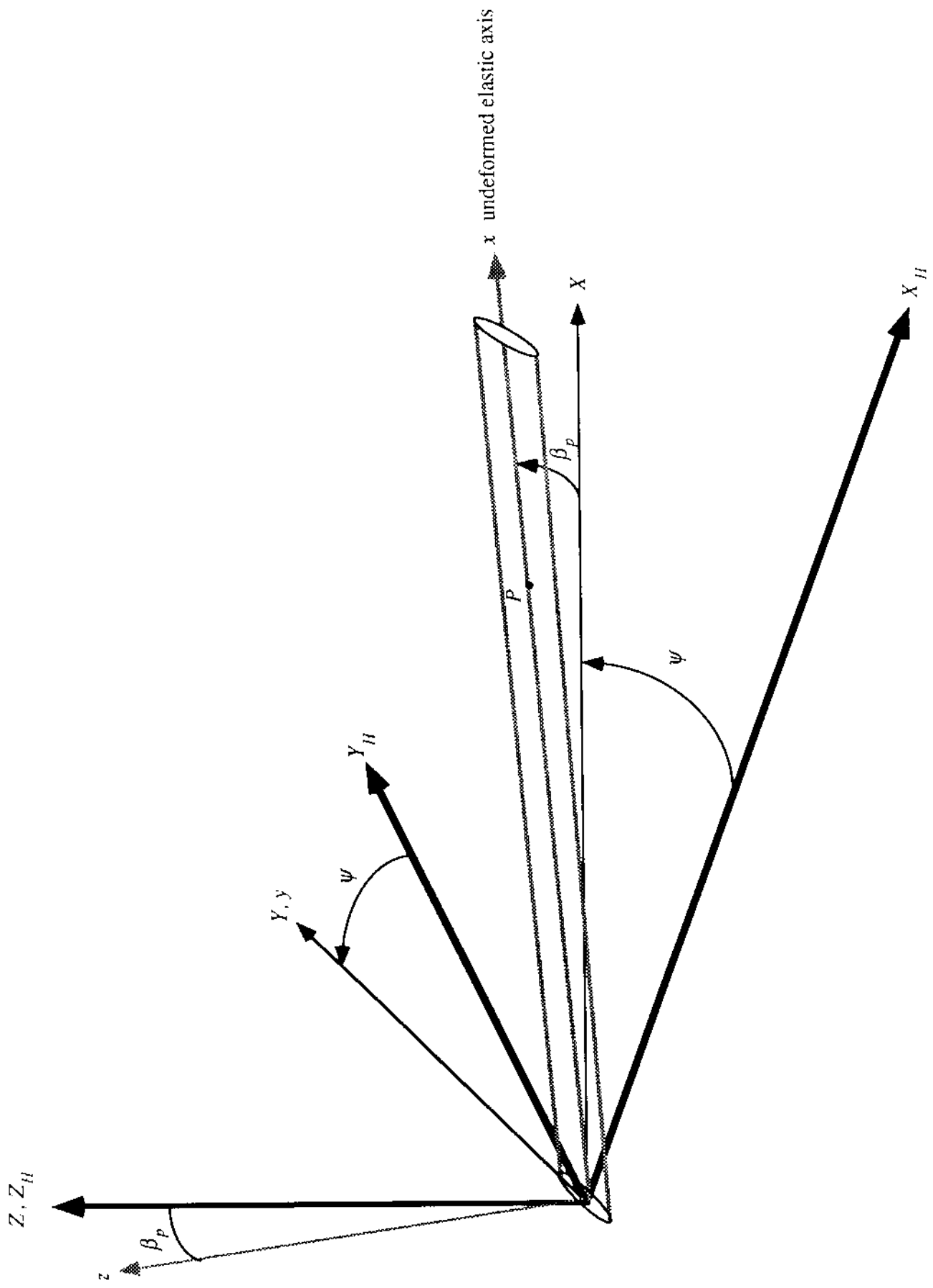


Figure 2.2a Undefomed Blade Coordinate Systems

transformation between the hub-fixed rotating coordinate system and the undeformed blade coordinate system is given by

$$\begin{Bmatrix} \hat{i} \\ \hat{j} \\ \hat{k} \end{Bmatrix} = \begin{bmatrix} \cos\beta_p & 0 & \sin\beta_p \\ 0 & 1 & 0 \\ -\sin\beta_p & 0 & \cos\beta_p \end{bmatrix} \begin{Bmatrix} \hat{I} \\ \hat{J} \\ \hat{K} \end{Bmatrix} = \mathbf{T}_{UR} \begin{Bmatrix} \hat{I} \\ \hat{J} \\ \hat{K} \end{Bmatrix} \quad (2.3)$$

Letting $\mathbf{T}_{UH} = \mathbf{T}_{UR}\mathbf{T}_{RH}$, the transformation between the hub-fixed nonrotating system and the undeformed blade system is written as

$$\begin{Bmatrix} \hat{i} \\ \hat{j} \\ \hat{k} \end{Bmatrix} = \begin{bmatrix} \cos\beta_p \cos\psi & \cos\beta_p \sin\psi & \sin\beta_p \\ -\sin\psi & \cos\psi & 0 \\ -\sin\beta_p \cos\psi & -\sin\beta_p \sin\psi & \cos\beta_p \end{bmatrix} \begin{Bmatrix} \hat{I}_H \\ \hat{J}_H \\ \hat{K}_H \end{Bmatrix} = \mathbf{T}_{UH} \begin{Bmatrix} \hat{I}_H \\ \hat{J}_H \\ \hat{K}_H \end{Bmatrix} \quad (2.4)$$

This transformation matrix is used to obtain blade velocities and accelerations for calculation of the variation in kinetic energy. The transformation is also used to obtain the blade velocity components required for aerodynamic loads.

2.1.2 Blade Deformation Kinematics and Coordinate Systems

Accurate modeling of elastic rotor blades requires that deflections be considered moderately large. Although deflections are assumed to be moderately large, strains are still assumed to be small. These assumptions result in a nonlinear strain-displacement relationship based on either the undeformed configuration (Lagrangian strain tensor) or on the deformed configuration (Eulerian strain tensor). The Lagrangian formulation is generally the more suitable for elasticity problems because the undeformed geometry is well known. Helicopter blades modeled as Bernoulli-Euler beams, however, are an exception to this

generality. Under the Bernoulli-Euler hypothesis, the cross section remains rigid and perpendicular to the elastic axis. The section properties of the rotor blade are defined about the principle axes of the blade cross section. Thus, the cross section geometry and section properties are well known even in the deformed state. The next step in the analytical procedure is to satisfy stress equilibrium which must be done in the final deformed state. Thus, it is advantageous to develop the stress-strain relationships in the deformed configuration. The strain-displacement relationships are developed based on the deformed configuration (Eulerian formulation) so that the same reference is used for both the stress and strain tensors. For most elasticity problems (based on Lagrangian formulation) the stress would have to be transformed from the deformed system to the undeformed system where the strains are defined. This difficulty is avoided in the present analysis as both strains and stresses may be referenced to the deformed configuration.

The deformed blade is characterized by the *deformed blade coordinate system* (ξ, η, ζ) and the corresponding unit vectors $\hat{i}_\xi, \hat{j}_\eta, \hat{k}_\zeta$ (see Figure 2.2b). As shown in Figure 2.3, η and ζ are aligned with the principle cross-section axis. A point P on the undeformed elastic axis undergoes deflection u, v, w in the x, y, z directions and moves to a point P' as shown in Figure 2.2b. Then the blade cross section containing P' undergoes a rotation θ_1 about the deformed elastic axis. The total blade pitch, θ_1 , is defined as

$$\theta_1 = \theta_0 + \hat{\phi} \quad (2.5)$$

where θ_0 is the rigid pitch angle due to control pitch and pretwist. In general, the pretwist can be an arbitrary function of radial location, i.e., $\theta_0 = \theta_0(r)$. For a blade with *linear pretwist*, the rigid pitch angle is given by

$$\theta_0 = \theta_{75} + \theta_{tw} \left(\frac{x}{R} - 0.75 \right) + \theta_{1c} \cos \psi + \theta_{1s} \sin \psi \quad (2.6)$$

In this case, θ_{75} is the blade pitch at 75% span (including collective pitch), θ_{lw} is the blade linear pretwist, and θ_{lc} and θ_{ls} are the cyclic pitch controls.

Total blade pitch, θ_1 , also includes elastic twist, $\hat{\phi}$. The elastic twist is defined as

$$\hat{\phi} = \phi - \int_0^x \frac{\partial w}{\partial x} \frac{\partial^2 v}{\partial x^2} dx \quad (2.7)$$

The ϕ is the elastic twist about the undeformed elastic axis, while the $\hat{\phi}$ can be viewed as the elastic twist about the deformed elastic axis. This is a nonlinear kinematic effect arising from moderate deflections. Further discussion dealing specifically with this kinematic effect can be found in Refs. [2.1] and [2.2]. In the derivation of strain energy and kinetic energy variations, the ordering scheme allows $\hat{\phi}$ to be simplified to ϕ . However, the aerodynamic forces are proportional to the elastic twist, $\hat{\phi}$, and these terms *do not drop out* with the application of the ordering scheme. In order to capture this effect, the degree of freedom, $\hat{\phi}$, is used throughout the formulation (see Ref. [2.3]). This technique implicitly captures the effect of the nonlinear kinematic twist. Expressions for strain energy and kinetic energy are derived in terms of ϕ and then transformed to $\hat{\phi}$. Details of this procedure will be discussed later in this chapter.

The coordinate transformation between the undeformed and deformed blade coordinate systems is given by

$$\begin{Bmatrix} \hat{i}_\xi \\ \hat{j}_\eta \\ \hat{k}_\zeta \end{Bmatrix} = \mathbf{T}_{DU} \begin{Bmatrix} \hat{i} \\ \hat{j} \\ \hat{k} \end{Bmatrix} \quad (2.8)$$

The origin of the transformation matrix, \mathbf{T}_{DU} , is now described. Blade deformation can be described by a series of Euler angles as shown in Figure 2.4. In terms of these Euler angles, the transformation matrix between the deformed and undeformed blade coordinate systems is given by

$$\mathbf{T}_{DU} = \begin{bmatrix} \cos\bar{\beta}\cos\bar{\zeta} & \cos\bar{\beta}\sin\bar{\zeta} & \sin\bar{\beta} \\ -\sin\bar{\theta}\sin\bar{\beta}\cos\bar{\zeta} & \cos\bar{\theta}\cos\bar{\zeta} & \cos\bar{\beta}\sin\bar{\theta} \\ -\cos\bar{\theta}\sin\bar{\zeta} & -\sin\bar{\zeta}\sin\bar{\beta}\sin\bar{\theta} & \cos\bar{\beta}\cos\bar{\theta} \\ -\cos\bar{\theta}\sin\bar{\beta}\cos\bar{\zeta} & -\sin\bar{\theta}\cos\bar{\zeta} & \cos\bar{\beta}\cos\bar{\theta} \\ +\sin\bar{\theta}\sin\bar{\zeta} & -\sin\bar{\zeta}\sin\bar{\beta}\cos\bar{\theta} & \end{bmatrix} \quad (2.9)$$

The Euler angles, $\bar{\zeta}$, $\bar{\beta}$, and $\bar{\theta}$ can be written in terms of blade deformations as

$$\cos\bar{\zeta} = \frac{\sqrt{1-v'^2-w'^2}}{\sqrt{1-w'^2}} \quad \sin\bar{\zeta} = \frac{v'}{\sqrt{1-w'^2}} \quad (2.10)$$

$$\cos\bar{\beta} = \sqrt{1-w'^2} \quad \sin\bar{\beta} = w'$$

$$\bar{\theta} = \theta_1$$

Substituting the above relations and simplifying to second order terms yields the transformation between deformed and undeformed blade positions

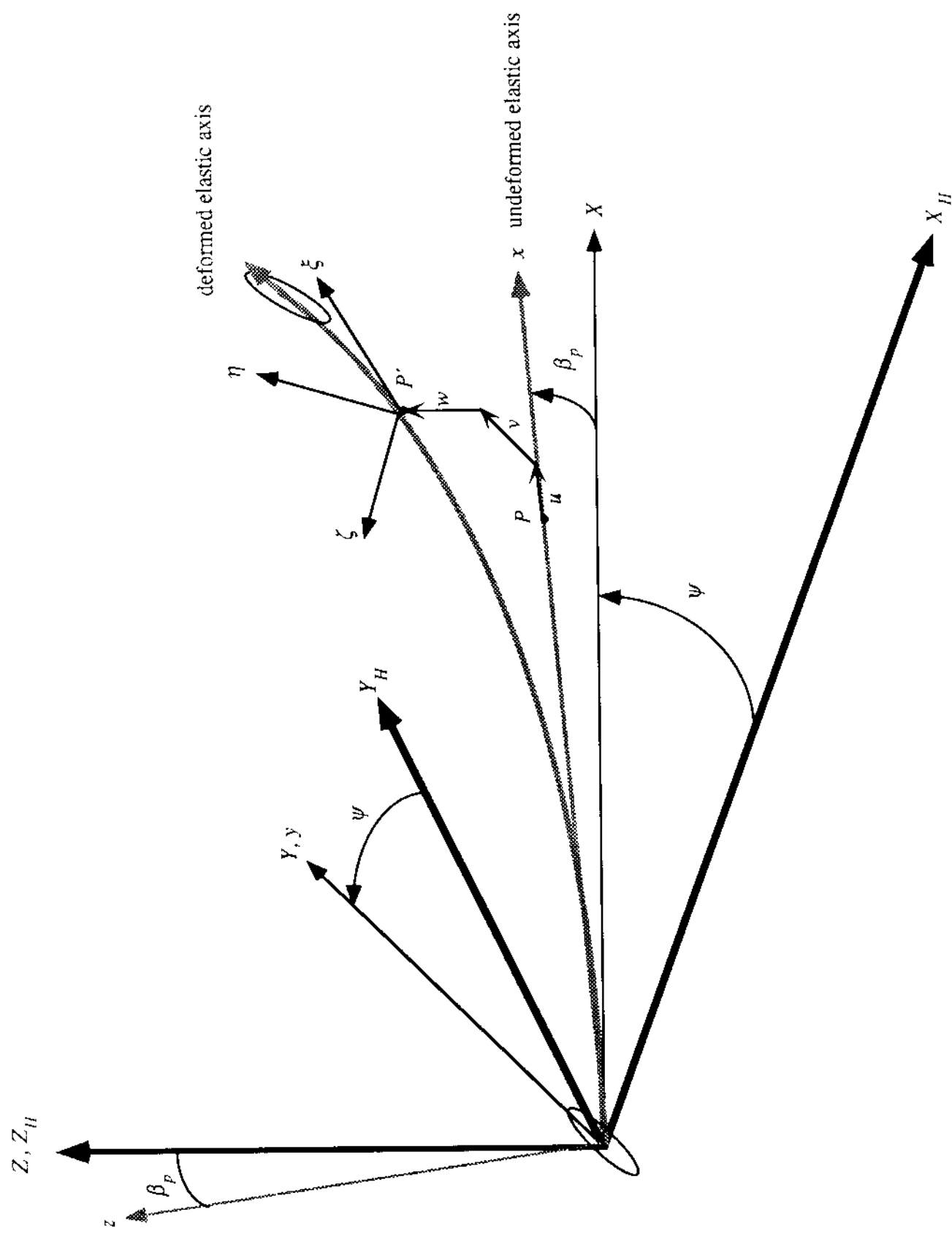


Figure 2.2b Blade Coordinate Systems and Deflections

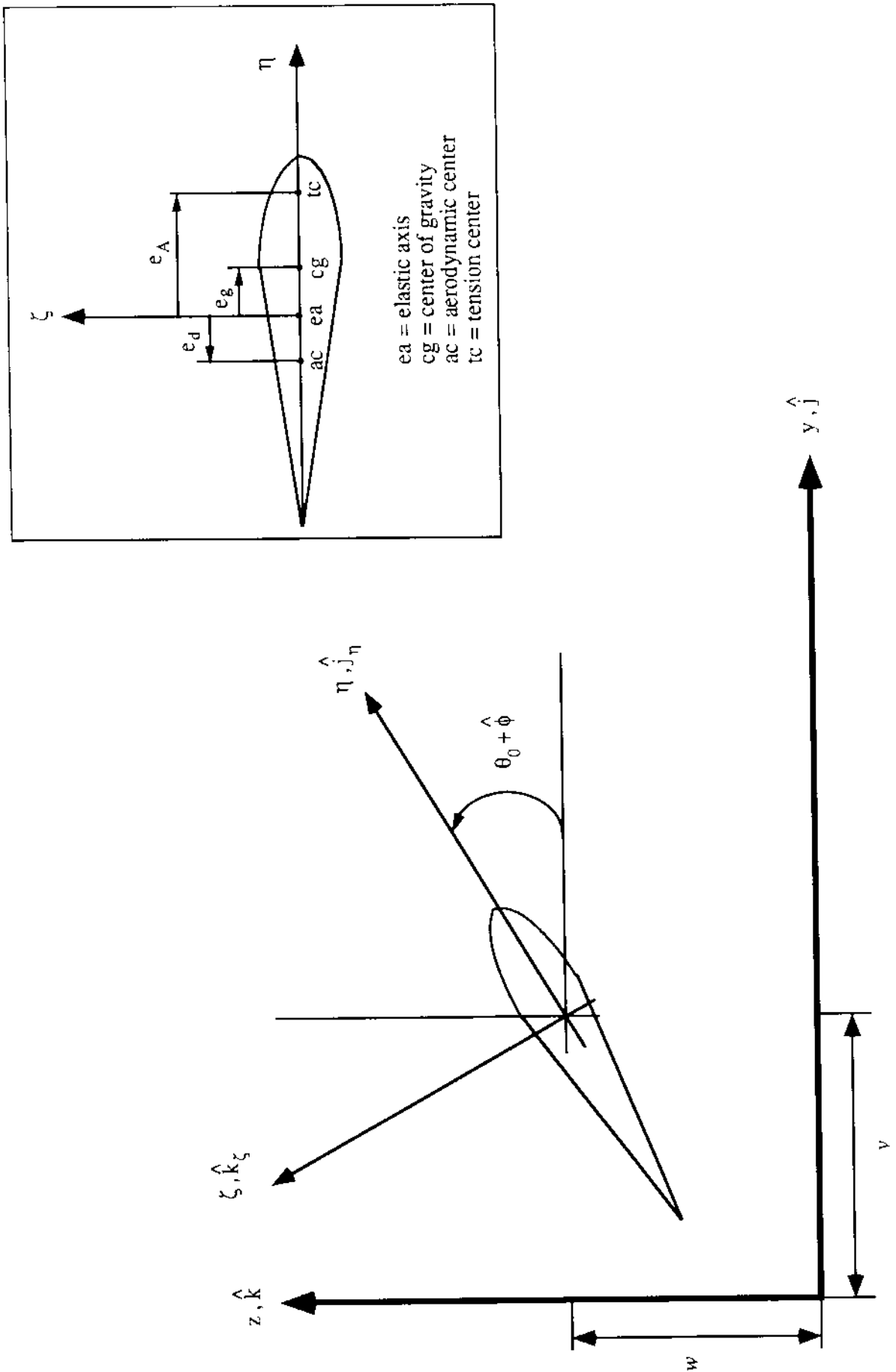


Figure 2.3 Cross-Section Coordinates

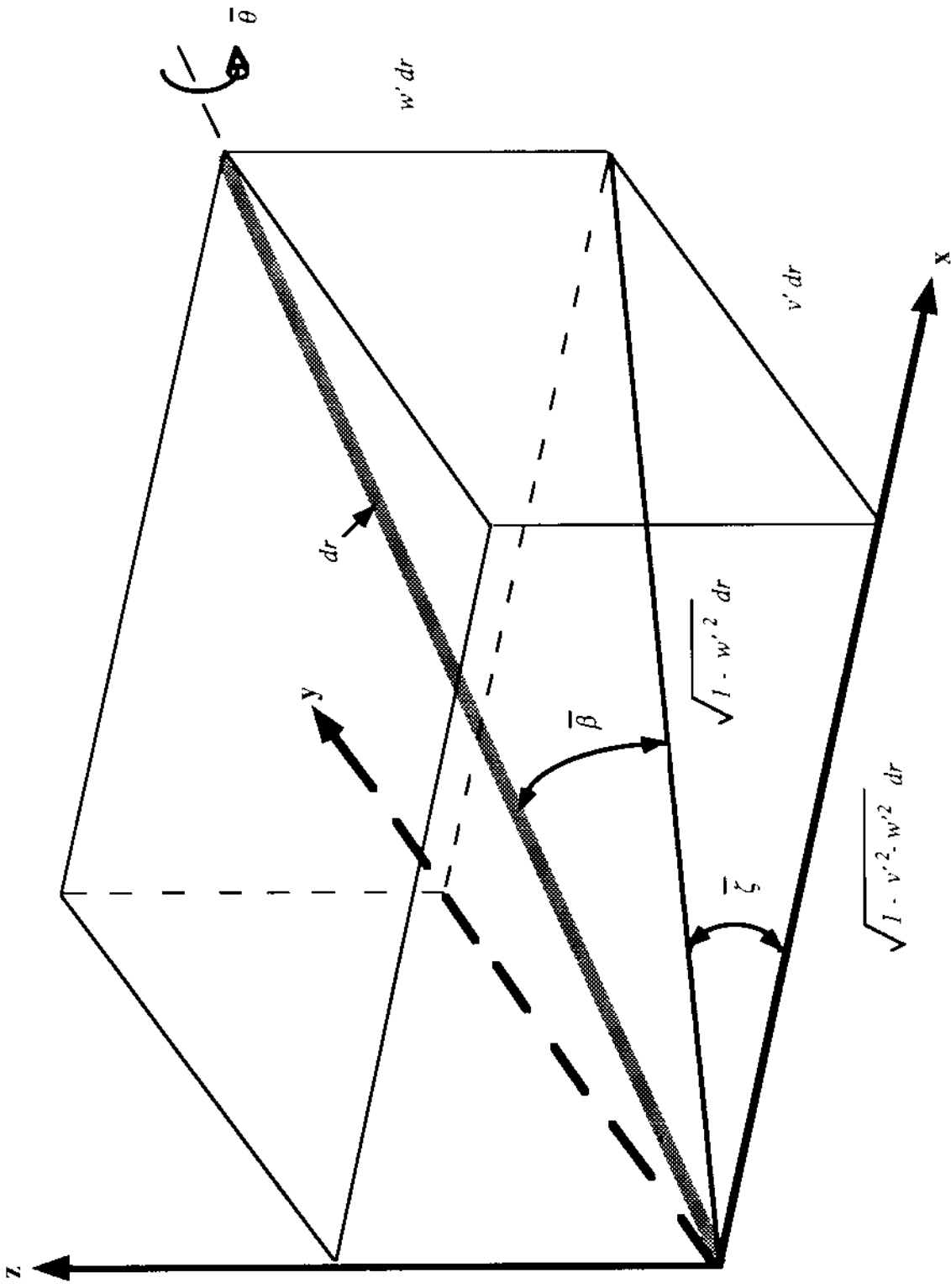


Figure 2.4 Deformation in Terms of Euler Angles

$$\mathbf{T}_{DU} = \begin{bmatrix} 1 - \frac{v'^2}{2} - \frac{w'^2}{2} & v' & w' \\ -v'\cos\theta_1 - w'\sin\theta_1 & (1 - \frac{v'^2}{2})\cos\theta_1 - v'w'\sin\theta_1 & (1 - \frac{w'^2}{2})\sin\theta_1 \\ v'\sin\theta_1 - w'\cos\theta_1 & -(1 - \frac{v'^2}{2})\sin\theta_1 - v'w'\cos\theta_1 & (1 - \frac{w'^2}{2})\cos\theta_1 \end{bmatrix} \quad (2.11)$$

This transformation matrix is similar to that which is derived in Ref [2.1].

All of the above transformation matrices arise from transformations between orthogonal coordinate systems. This results in the convenient equality of the transpose and inverse matrices

$$\mathbf{T}^T = \mathbf{T}^{-1} \quad (2.12)$$

where \mathbf{T} can be either \mathbf{T}_{HI} , \mathbf{T}_{RH} , \mathbf{T}_{UR} , \mathbf{T}_{UH} , or \mathbf{T}_{DU} .

Rotors with advanced tips (e.g. swept-tip, tapered-tip, anhedral-tip) require additional transformations. These transformations enable the aeroelastic behavior of the tip element to be consistently incorporated into the finite element model of the entire rotor. For description of these transformations, see Chapter 6.

2.1.3 Nondimensionalization and Ordering Scheme

The entire formulation and all ensuing computations are carried out in nondimensional form. In addition to increasing the generality of the analysis, working with nondimensional quantities (when computing results) can help avoid scaling problems. In

developing the analysis, the following physical quantities are nondimensionalized by the given reference parameters.

<u>Physical Quantity</u>	<u>Reference Parameter</u>
Length	R
Time	$1 / \Omega$
Mass / Length	m_0
Velocity	ΩR
Acceleration	$\Omega^2 R$
Force	$m_0 \Omega^2 R^2$
Moment	$m_0 \Omega^2 R^3$
Energy or Work	$m_0 \Omega^2 R^3$

Based on the above relations, only nondimensional quantities are used in the subsequent analysis.

In formulating Hamilton's principle, it is important to neglect higher order terms to simplify the analysis. Terms up to second order are retained in the analysis by introducing the nondimensional quantity ϵ , such that $\epsilon \ll 1$. Some third order terms related to elastic torsion are also retained in the energy expressions. The order of magnitude of the nondimensional quantities is defined as follows:

$$\frac{EA}{m_0 \Omega^2 R^2} = O(\epsilon^{-2}) \quad (2.13)$$

$$\frac{M_{xF}}{m_0 R}, \frac{M_{yF}}{m_0 R}, \frac{M_{zF}}{m_0 R} = O(\epsilon^{-1})$$

$$\frac{x}{R}, \frac{h}{R}, \frac{x_{CG}}{R}, \frac{y_{CG}}{R}, \frac{m}{m_0}, \frac{\partial}{\partial \psi}, \frac{\partial}{\partial x} = O(1)$$

$$\mu, \cos\psi, \sin\psi, \theta_0, \theta_{tw}, \theta_{75}, \theta_{lc}, \theta_{ls}, \frac{c_1}{a}, \frac{d_2}{a} = O(1)$$

$$\frac{EI_y}{m_0\Omega^2R^4}, \frac{EI_z}{m_0\Omega^2R^4}, \frac{GJ}{m_0\Omega^2R^4} = O(1)$$

$$\frac{I_{xF}}{m_0R^3}, \frac{I_{yF}}{m_0R^3} = O(1)$$

$$\frac{v}{R}, \frac{w}{R}, \phi, \beta_p, \frac{k_A}{R}, \frac{k_{m1}}{R}, \frac{k_{m2}}{R} = O(\epsilon)$$

$$\alpha_s, \phi_s = O(\epsilon)$$

$$\lambda, \frac{\eta_c}{R}, \frac{c_0}{a}, \frac{d_1}{a}, \frac{f_0}{a} = O(\epsilon)$$

$$\frac{EB_2}{m_0\Omega^2R^5}, \frac{EC_2}{m_0\Omega^2R^5} = O(\epsilon)$$

$$\frac{e_d}{R}, \frac{e_g}{R}, \frac{e_A}{R} = O(\epsilon^{3/2})$$

$$\dot{x}_F, \dot{y}_F, \dot{z}_F, \dot{\alpha}_s, \dot{\phi}_s = O(\epsilon^{3/2})$$

$$\lambda_T, \frac{EB_1}{m_0\Omega^2R^6}, \frac{EC_1}{m_0\Omega^2R^6} = O(\epsilon^2)$$

$$\frac{u}{R}, \frac{d_0}{a}, \frac{f_1}{a} = O(\epsilon^2)$$

where a is the lift curve slope and m_0 is a reference mass per unit length. For this analysis, the reference mass per unit length, m_0 , is defined as the mass per unit length of an equivalent *uniform* blade which has the same flap inertia as the actual (*i.e. nonuniform*) blade. Using this definition, m_0 can be written as

$$m_0 = \frac{3I_\beta}{R^3} = \frac{3 \int_0^R mr^2 dr}{R^3} \quad (2.14)$$

When nondimensionalizing the energy expressions, care must be taken to insure that the physics of the system is not violated. Symmetry in the structural stiffness matrix and mass matrix should be retained, and the antisymmetric damping matrix should reflect the gyroscopic couplings associated with Coriolis effects.

Azimuth angle can be considered as nondimensional time; therefore, throughout this section time derivatives are written as

$$\dot{(\)} = \frac{\partial(\)}{\partial t} = \frac{\partial(\)}{\partial \psi} \frac{\partial \psi}{\partial t} = \Omega \frac{\partial(\)}{\partial \psi} \quad (2.15)$$

$$\ddot{(\)} = \frac{\partial^2(\)}{\partial t^2} = \frac{\partial^2(\)}{\partial \psi^2} \frac{\partial^2 \psi}{\partial t^2} = \Omega^2 \frac{\partial^2(\)}{\partial \psi^2}$$

2.2 Formulation Using Hamilton's Principle

Hamilton's variational principle is used to derive the system equations of motion. For a conservative system, Hamilton's principle states that the true motion of a system, between prescribed initial conditions at time t_1 and final conditions at time t_2 , is that particular motion for which the time integral of the difference between the potential and kinetic energies is a minimum [2.4]. For an aeroelastic system, e.g., the rotor, there are nonconservative forces which are not derivable from a potential function. The generalized Hamilton's principle, applicable to nonconservative systems, is expressed as

$$\delta\Pi = \int_{t_1}^{t_2} (\delta U - \delta T - \delta W) dt = 0 \quad (2.16)$$

where δU is the virtual variation of strain energy and δT is the virtual variation of kinetic energy. The δW is the virtual work done by external forces. These virtual variations have contributions from both the rotor and the fuselage. The contributions from the rotor can be expressed as the sum of contributions from each blade. The variations can be written as

$$\delta U = \delta U_R + \delta U_F = \left(\sum_{b=1}^{N_b} \delta U_b \right) + \delta U_F \quad (2.17)$$

$$\delta T = \delta T_R + \delta T_F = \left(\sum_{b=1}^{N_b} \delta T_b \right) + \delta T_F \quad (2.18)$$

$$\delta W = \delta W_R + \delta W_F = \left(\sum_{b=1}^{N_b} \delta W_b \right) + \delta W_F \quad (2.19)$$

where the subscript R denotes contribution from the rotor, the subscript F denotes contribution from the fuselage, and N_b is the total number of rotor blades. It should be noted that the strain energy variation for the b th blade, δU_b , also includes the contribution from the b th pitch link if it is elastic. Since the fuselage is considered rigid in the current version of UMARC, contributions to δU_F come solely from the landing gear elasticity. The following sections describe the derivations of the expressions for δU_b , δU_F , δT_b , and δT_F . Expressions for the virtual work of the blade, δW_b , and the fuselage, δW_F are discussed in the chapter on Aerodynamic Modeling.

2.2.1 Energy Expressions for the Blade

Energy is stored in the blade in the form of strain energy and kinetic energy. Strain energy is stored when the blade undergoes elastic deformation. Strain energy can also be stored in a flexible pitch-link or hub spring. Kinetic energy is stored when the blade moves with some velocity. The velocity can either be caused by blade motion, fuselage (hub) motion, or a combination of both blade and fuselage (hub) motions.

2.2.1.1 Strain Energy, δU_b

Each rotor blade is considered to be a long slender isotropic beam. For such a structure, the uniaxial stress assumption ($\sigma_{yy} = \sigma_{yz} = \sigma_{zz} = 0$) is valid. The corresponding relationship between stresses and classical engineering strains is given by

$$\sigma_{xx} = E\epsilon_{xx} \quad (2.20)$$

$$\sigma_{x\eta} = G\epsilon_{x\eta} \quad (2.21)$$

$$\sigma_{x\zeta} = G\epsilon_{x\zeta} \quad (2.22)$$

where ϵ_{xx} is axial strain, and $\epsilon_{x\eta}$ and $\epsilon_{x\zeta}$ are engineering shear strains.

Under these assumptions, the expression for strain energy of the b th blade, is given by

$$U_b = \frac{1}{2} \int_0^R \iint_A (\sigma_{xx}\epsilon_{xx} + \sigma_{x\eta}\epsilon_{x\eta} + \sigma_{x\zeta}\epsilon_{x\zeta}) d\eta d\zeta dx \quad (2.23)$$

The expression for the variation of strain energy is given by

$$\delta U_b = \int_0^R \iint_A (\sigma_{xx} \delta \varepsilon_{xx} + \sigma_{x\eta} \delta \varepsilon_{x\eta} + \sigma_{x\zeta} \delta \varepsilon_{x\zeta}) d\eta d\zeta dx \quad (2.24)$$

Substituting the stress-strain relations into the variation of strain energy yields

$$\delta U_b = \int_0^R \iint_A (E \varepsilon_{xx} \delta \varepsilon_{xx} + G \varepsilon_{x\eta} \delta \varepsilon_{x\eta} + G \varepsilon_{x\zeta} \delta \varepsilon_{x\zeta}) d\eta d\zeta dx \quad (2.25)$$

The explicit expressions for the strain components are described in detail in Ref. [2.1]. These strains reflect the nonlinearities due to moderate deflections of the beam. Additional terms are also visible due to blade pitch, θ_0 . This pitch is generally due to combinations of elastic torsion, pretwist, and pitch control inputs.

$$\begin{aligned} \varepsilon_{xx} = \varepsilon_{11} &= u' + \frac{v'^2}{2} + \frac{w'^2}{2} - \lambda_T \phi'' + (\eta^2 + \zeta^2) (\theta'_0 \phi' + \frac{\phi'^2}{2}) \\ &- v'' [\eta \cos(\theta_0 + \hat{\phi}) - \zeta \sin(\theta_0 + \hat{\phi})] \\ &- w'' [\eta \sin(\theta_0 + \hat{\phi}) + \zeta \cos(\theta_0 + \hat{\phi})] \end{aligned} \quad (2.26)$$

$$\varepsilon_{x\eta} = 2\varepsilon_{12} = -\left(\zeta + \frac{\partial \lambda_T}{\partial \eta}\right) \phi' = -\hat{\zeta} \phi' \quad (2.27)$$

$$\varepsilon_{x\zeta} = 2\varepsilon_{13} = \left(\eta - \frac{\partial \lambda_T}{\partial \zeta}\right) \phi' = \hat{\eta} \phi' \quad (2.28)$$

where ε_{12} and ε_{13} are tensorial shear strains and $\varepsilon_{x\eta}$ and $\varepsilon_{x\zeta}$ are engineering shear strains. The λ_T is the cross-sectional warping function.

The variations in strains are given by

$$\begin{aligned}\delta\epsilon_{xx} = & \delta u' + v' \delta v' + w' \delta w' + (\eta^2 + \zeta^2)(\theta'_0 + \phi') \delta \phi' - \lambda_T \delta \phi'' \\ & - [\eta \cos(\theta_0 + \hat{\phi}) - \zeta \sin(\theta_0 + \hat{\phi})](\delta v'' + w'' \delta \phi) \\ & - [\eta \sin(\theta_0 + \hat{\phi}) + \zeta \cos(\theta_0 + \hat{\phi})](\delta w'' + v'' \delta \phi)\end{aligned}\quad (2.29)$$

$$\delta\epsilon_{x\eta} = -\zeta \delta \phi' \quad (2.30)$$

$$\delta\epsilon_{x\zeta} = \hat{\eta} \delta \phi' \quad (2.31)$$

Variation of strain energy is determined using the stress-strain relations and strain-displacement relations given above. For small angles $\hat{\phi}$, the following trigonometric expansion can be used

$$\sin(\theta_0 + \hat{\phi}) = \sin \theta_0 \cos \hat{\phi} + \sin \hat{\phi} \cos \theta_0 \approx \sin \theta_0 + \hat{\phi} \cos \theta_0 \quad (2.32)$$

$$\cos(\theta_0 + \hat{\phi}) = \cos \theta_0 \cos \hat{\phi} - \sin \hat{\phi} \sin \theta_0 \approx \cos \theta_0 - \hat{\phi} \sin \theta_0 \quad (2.33)$$

The expression for variation of strain energy in nondimensional form is obtained retaining terms up to the second order in basic governing equations. In addition, some third order terms are also retained in the torsion equations. The strain energy variation can be written in terms of the variable $\hat{\phi}'$ using the following relations (see Eqn. (2.7))

$$\hat{\phi}' = \phi' - w' v'' \quad (2.34a)$$

$$\delta \hat{\phi}' = \delta \phi' - w' \delta v'' - v'' \delta w' \quad (2.34b)$$

The axial deflection, u , is represented by two separate components; an elastic axial deflection, u_e , and a kinematic axial deflection due to foreshortening, u_F . Using this representation (see Ref. 2.5), the following relations are substituted into the strain energy expression.

$$u = u_e - \frac{1}{2} \int_0^x (v'^2 + w'^2) dx \quad (2.35a)$$

$$u' = u'_e - \frac{1}{2} (v'^2 + w'^2) \quad (2.35b)$$

$$\dot{u} = \dot{u}'_e - \int_0^x (v' \dot{v}' + w' \dot{w}') dx \quad (2.35c)$$

$$\delta u = \delta u'_e - \int_0^x (v' \delta v' + w' \delta w') dx \quad (2.35d)$$

$$\delta u' = \delta u'_e - v' \delta v' - w' \delta w' \quad (2.35e)$$

For the *bth* blade, the resulting expression is given by

$$\frac{\delta U_b}{m_0 \Omega^2 R^3} = \int_0^1 (U_{u'_e} \delta u'_e + U_{v'} \delta v' + U_{w'} \delta w' + U_{v''} \delta v'' + U_{w''} \delta w'' + U_{\hat{\phi}} \delta \hat{\phi} + U_{\hat{\phi}'} \delta \hat{\phi}' + U_{\hat{\phi}''} \delta \hat{\phi}'') dx \quad (2.36)$$

where

$$U_{u'_e} = EA \left[u'_e + k_A^2 \theta'_0 (\hat{\phi}' + w' v'') + k_A^2 \frac{\hat{\phi}'^2}{2} \right] - EA e_A [v'' (\cos \theta_0 - \hat{\phi} \sin \theta_0) + w'' (\sin \theta_0 + \hat{\phi} \cos \theta_0)] \quad (2.37)$$

$$U_{v''} = v''(EI_z \cos^2 \theta_0 + EI_y \sin^2 \theta_0) + w''(EI_z - EI_y) \cos \theta_0 \sin \theta_0$$

$$- EAe_A u'_e (\cos \theta_0 - \hat{\phi} \sin \theta_0) - \hat{\phi}' EB_2 \theta'_0 \cos \theta_0$$

$$+ w'' \hat{\phi} (EI_z - EI_y) \cos 2\theta_0 - v'' \hat{\phi} (EI_z - EI_y) \sin 2\theta_0$$

$$+ (GJ + EB_1 \theta'_0)^2 \hat{\phi}' w' + EAk_A^2 \theta'_0 w' u'_e$$

$$U_{w'} = (GJ + EB_1 \theta'_0)^2 \hat{\phi}' v'' + EAk_A^2 \theta'_0 v'' u'_e$$

$$U_{w''} = w''(EI_y \cos^2 \theta_0 + EI_z \sin^2 \theta_0) + v''(EI_z - EI_y) \cos \theta_0 \sin \theta_0$$

$$- EAe_A u'_e (\sin \theta_0 + \hat{\phi} \cos \theta_0) - \hat{\phi}' EB_2 \theta'_0 \sin \theta_0$$

$$+ w'' \hat{\phi} (EI_z - EI_y) \sin 2\theta_0 + v'' \hat{\phi} (EI_z - EI_y) \cos 2\theta_0$$

$$U_{\hat{\phi}} = w''^2 (EI_z - EI_y) \sin \theta_0 \cos \theta_0 + v''^2 (EI_z - EI_y) \cos 2\theta_0$$

$$- v''^2 (EI_z - EI_y) \sin \theta_0 \cos \theta_0$$

$$U_{\hat{\phi}'} = GJ (\hat{\phi}' + w' v'') + EB_1 \theta'_0 \hat{\phi}' + EAk_A^2 (\theta'_0 + \hat{\phi}') u'_e$$

$$- EB_2 \theta' (v'' \cos \theta_0 + w'' \sin \theta_0)$$

$$U_{\hat{\phi}''} = EC_1 \hat{\phi}'' + EC_2 (w'' \cos \theta_0 - v'' \sin \theta_0)$$

The section properties are defined as follows:

$EA = \iint_A E d\eta d\zeta$	$EAe_A = \iint_A E \eta d\eta d\zeta$	(2.38)
$EI_y = \iint_A E \zeta^2 d\eta d\zeta$	$EI_z = \iint_A E \eta^2 d\eta d\zeta$	
$GJ = \iint_A G(\hat{\eta}^2 + \hat{\zeta}^2) d\eta d\zeta$	$EAk_A^2 = \iint_A E(\eta^2 + \zeta^2) d\eta d\zeta$	
$EB_1 = \iint_A E(\eta^2 + \zeta^2)^2 d\eta d\zeta$	$EB_2 = \iint_A E\eta(\eta^2 + \zeta^2)^2 d\eta d\zeta$	
$EC_1 = \iint_A E\lambda_T^2 d\eta d\zeta$	$EC_2 = \iint_A E\zeta\lambda_T d\eta d\zeta$	

where E and G are nondimensionalized with respect to the quantity $m_0\Omega^2$. The axial (extensional) stiffness of the blade is EA . The tensile axis offset from the elastic axis is e_A (positive forward). The EI_y and EI_z are, respectively, the flap and lag bending stiffnesses, and GJ is the torsional stiffness. Tilde(\wedge) in the GJ expression implies the inclusion of the effect of cross-sectional warping. An antisymmetric warping function, λ_T , is assumed ($\lambda_T \propto \eta\zeta$). The warping function specifies the distribution of the axial warping displacements around the cross section. The EC_1 is the warping rigidity and EC_2 is another constant related to the warping of the beam section. Both EC_1 and EC_2 are related to the restraint of warping displacements; therefore, they are generally more important for open section beams. The k_A is the radius of gyration of the blade cross section, and EB_1 and EB_2 are other sectional constants which appear due to blade pitch. Because of the assumed symmetry of the blade cross section about the η axis, the following relationships hold:

$$\begin{aligned}\iint_A E\zeta d\eta d\zeta &= 0 \\ \iint_A E\eta\zeta d\eta d\zeta &= 0 \\ \iint_A E\zeta(\eta^2 + \zeta^2) d\eta d\zeta &= 0\end{aligned}\tag{2.39}$$

2.2.1.2 Kinetic Energy, δT_b

The kinetic energy of the b th blade, δT_b , depends on the blade velocity. This velocity is generally due to: (1) blade motion relative to the hub, as well as (2) the motion of the hub itself. This relationship is expressed mathematically as

$$\vec{V} = \vec{V}_b + \vec{V}_f\tag{2.40}$$

where \vec{V}_b is the velocity of the blade relative to the hub and \vec{V}_f is the velocity (at the blade) induced by the motion of the fuselage. In the present analysis, the hub is assumed to be rigidly attached to the fuselage.

Blade Motion Induced Velocity, \vec{V}_b

A point $P(x,0,0)$ on the undeformed elastic axis moves to $P'(x+u,v,w)$ after deformation, and then the blade section undergoes a rotation θ_1 about the deformed elastic axis (see Figure 2.2b). The position vector, \vec{r} , of an arbitrary point on the blade after deformation can be written as (x_1,y_1,z_1) in the undeformed blade coordinate system (Refs. [2.1,2.2])

$$\vec{r} = x_1 \hat{i} + y_1 \hat{j} + z_1 \hat{k} \quad (2.41)$$

where

$$x_1 = x + u - \lambda_T \phi' - v'(y_1 - v) - w'(z_1 - w) \quad (2.42)$$

$$y_1 = v + (y_1 - v)$$

$$z_1 = w + (z_1 - w)$$

The terms $(y_1 - v)$ and $(z_1 - w)$ are defined as

$$(y_1 - v) = \eta \cos(\theta_0 + \hat{\phi}) - \zeta \sin(\theta_0 + \hat{\phi}) = \eta \cos\theta_1 - \zeta \sin\theta_1 \quad (2.43)$$

$$(z_1 - w) = \eta \sin(\theta_0 + \hat{\phi}) + \zeta \cos(\theta_0 + \hat{\phi}) = \eta \sin\theta_1 + \zeta \cos\theta_1$$

The quantities $(y_1 - v)$ and $(z_1 - w)$ denote the position of an arbitrary point in the blade section from the elastic axis, and $v'(y_1 - v)$ and $w'(z_1 - w)$ are radial shortenings due to lagwise and flapwise deflections, respectively. By differentiating the position vector with respect to the hub-fixed nonrotating system, the velocity of a point on the blade is obtained

$$\frac{d\vec{r}}{dt} = [\dot{x}_1, \dot{y}_1, \dot{z}_1] \begin{Bmatrix} \hat{i} \\ \hat{j} \\ \hat{k} \end{Bmatrix} + [x_1, y_1, z_1] \frac{d}{dt} \begin{Bmatrix} \hat{i} \\ \hat{j} \\ \hat{k} \end{Bmatrix} \quad (2.44)$$

Recalling the relationship of transformation between the undeformed blade and hub-fixed nonrotating coordinate systems in Eqn. (2.3), it may be understood that the unit vectors $\hat{i}, \hat{j}, \hat{k}$ depend on time, while the vectors $\hat{I}_H, \hat{J}_H, \hat{K}_H$ are unchanged with respect to time for a steady flight condition. Therefore, the time derivative of the unit vectors in the undeformed blade frame are expressed in terms of the transformation matrix, \mathbf{T}_{UH} , as

$$\frac{d}{dt} \begin{Bmatrix} \hat{i} \\ \hat{j} \\ \hat{k} \end{Bmatrix} = \dot{\mathbf{T}}_{UH} \begin{Bmatrix} \hat{I}_H \\ \hat{J}_H \\ \hat{K}_H \end{Bmatrix} = \dot{\mathbf{T}}_{UH} \mathbf{T}_{UH}^T \begin{Bmatrix} \hat{i} \\ \hat{j} \\ \hat{k} \end{Bmatrix} \quad (2.45)$$

After performing the necessary algebraic manipulations, the following expression for the velocity of an arbitrary point on the blade, *relative to the hub*, is obtained:

$$\vec{V}_b = \frac{\partial \vec{r}}{\partial t} = V_{bx}\hat{i} + V_{by}\hat{j} + V_{bz}\hat{k} \quad (2.46)$$

where

$$V_{bx} = \dot{x}_1 - \Omega y_1 \cos \beta_p \quad (2.47)$$

$$V_{by} = \dot{y}_1 + \Omega x_1 \cos \beta_p - \Omega z_1 \sin \beta_p$$

$$V_{bz} = \dot{z}_1 + \Omega y_1 \sin \beta_p$$

The blade velocity can also be determined using the expression

$$\vec{V}_b = \dot{x}_1\hat{i} + \dot{y}_1\hat{j} + \dot{z}_1\hat{k} + \Omega \hat{K}_H \times (x_1\hat{i} + y_1\hat{j} + z_1\hat{k}) \quad (2.48)$$

Expanding the above vector equation yields the same result as Eqn. (2.46).

For small precone angles,

$$\sin\beta_p \approx \beta_p \quad (2.49)$$

$$\cos\beta_p \approx 1$$

The derivatives of the arbitrary point on the blade with respect to time are given as

$$\dot{x}_1 = \dot{u} - \lambda_T \dot{\phi}' - (\dot{v}' + w' \dot{\theta}_1)(y_1 - v) - (\dot{w}' - v' \dot{\theta}_1)(z_1 - w) \quad (2.50)$$

$$\dot{y}_1 = \dot{v} - \dot{\theta}_1(z_1 - w)$$

$$\dot{z}_1 = \dot{w} + \dot{\theta}_1(y_1 - v)$$

$$\ddot{x}_1 = \ddot{u} - \lambda_T \ddot{\phi}' - (\ddot{v}' + w' \ddot{\theta}_1 + 2\dot{\theta}_1 \dot{w}')(y_1 - v) \quad (2.51)$$

$$-(\ddot{w}' - v' \ddot{\theta}_1 - 2\dot{\theta}_1 \dot{v}')(z_1 - w)$$

$$\ddot{y}_1 = \ddot{v} - \ddot{\theta}_1(z_1 - w)$$

$$\ddot{z}_1 = \ddot{w} + \ddot{\theta}_1(y_1 - v)$$

These expressions are approximated with terms up to second order kept using the ordering scheme in a consistent manner. The first derivatives appear in the expression for blade velocity, whereas the second derivatives will be required for determining the variation in kinetic energy, δT . The preceding derivation of δT is similar to that presented in Ref. [2.1], however, the procedure has been extended to the case of time varying rigid pitch angle (see Ref. [2.6]). This extension is necessary due to the application of cyclic pitch controls in the forward flight condition.

Fuselage Motion Induced Velocity

Hamilton's principle requires the formulation of the total kinetic energy of the coupled rotor-fuselage system. The initial step in this procedure is the derivation of the velocity of a point P on the blade as seen by an observer on the ground. Recall the definitions of the triads associated with the coordinate systems: the undeformed system $(\hat{i}, \hat{j}, \hat{k})$, the hub-fixed system $(\hat{I}_H, \hat{J}_H, \hat{K}_H)$, the fuselage system $(\hat{I}_F, \hat{J}_F, \hat{K}_F)$, the inertial system fixed to the helicopter center of gravity $(\hat{I}_I, \hat{J}_I, \hat{K}_I)$ and the inertial system fixed to the ground $(\hat{I}_I^G, \hat{J}_I^G, \hat{K}_I^G)$. The transformation matrices relating these coordinate systems are given in section 2.1.1. The triad $(\hat{I}_I, \hat{J}_I, \hat{K}_I)$ translates with respect to $(\hat{I}_I^G, \hat{J}_I^G, \hat{K}_I^G)$ and has a translation vector defined by

$$\vec{r}_3^I = x_F \hat{I}_I^G + y_F \hat{J}_I^G + z_F \hat{K}_I^G \quad (2.52)$$

The vector from the origin of the fuselage system (vehicle center of gravity) to the hub-fixed system is

$$\vec{r}_2^I = x_{CG} \hat{I}_F + y_{CG} \hat{J}_F + z_{CG} \hat{K}_F \quad (2.53)$$

The vector from the hub-fixed system to the undeformed blade system is defined as

$$\vec{r}_1^I = x_1 \hat{i} + y_1 \hat{j} + z_1 \hat{k} \quad (2.54)$$

where x_1 , y_1 , and z_1 are defined in section 2.1.1.2. The velocity at point P on the blade is then given by

$$\vec{V}_f = \dot{\vec{r}}_1^I + \dot{\vec{r}}_2^I + \dot{\vec{r}}_3^I \quad (2.55)$$

where

$$\dot{\vec{r}}_1^I = \dot{x}_1 \hat{i} + \dot{y}_1 \hat{j} + \dot{z}_1 \hat{k} + x_1 \dot{\hat{i}} + y_1 \dot{\hat{j}} + z_1 \dot{\hat{k}} \quad (2.56a)$$

$$\dot{\vec{r}}_2^I = x_{CG} \dot{\hat{i}}_F + y_{CG} \dot{\hat{j}}_F + z_{CG} \dot{\hat{k}}_F \quad (2.56b)$$

$$\dot{\vec{r}}_3^I = \dot{x}_F \hat{i}_F^G + \dot{y}_F \hat{j}_F^G + \dot{z}_F \hat{k}_F^G \quad (2.56c)$$

The assumption that the triad fixed to the ground-based inertial system $(\hat{i}_I^G, \hat{j}_I^G, \hat{k}_I^G)$ has a zero time derivative is made during this differentiation. The unit vectors associated with the other coordinate systems have non-zero time derivatives (i.e. their orientation with respect to the ground inertial system is time dependent). The following transformations are used to express all unit vectors in Eq. (2.56a-c) in the ground-fixed inertial system

$$\mathbf{e}_i = \mathbf{T}_{UH} \mathbf{T}_{HI} \mathbf{e}_{I_I^G} \quad (2.57)$$

$$\dot{\mathbf{e}}_i = (\dot{\mathbf{T}}_{UH} \mathbf{T}_{HI} + \mathbf{T}_{UH} \dot{\mathbf{T}}_{HI}) \mathbf{e}_{I_I^G} \quad (2.58)$$

$$\mathbf{e}_{I_F} = \mathbf{T}_{HI} \mathbf{e}_{I_I^G} \quad (2.59)$$

$$\dot{\mathbf{e}}_{I_F} = \dot{\mathbf{T}}_{HI} \mathbf{e}_{I_I^G} \quad (2.60)$$

where \mathbf{e} are triads indicated by their respective subscripts. The final expression for the velocity at point P is given by

$$\vec{V}_f = V_{fx} \hat{i}_I^G + V_{fy} \hat{j}_I^G + V_{fz} \hat{k}_I^G \quad (2.61)$$

where

$$\begin{aligned} V_x &= -\dot{\alpha}_s h + \dot{x}_F - \alpha_s \dot{z}_1 + \alpha_s \phi_s x_1 \cos \psi \\ &\quad + \dot{x}_1 \cos \psi - y_1 \cos \psi - \beta_p \dot{z}_1 \cos \psi \\ &\quad - x_1 \sin \psi - \dot{y}_1 \sin \psi + \beta_p z_1 \sin \psi \end{aligned}$$

$$\begin{aligned}
V_y &= h\dot{\phi}_s + \dot{y}_F + \phi_s\dot{z}_1 + x_1\cos\psi + \dot{y}_1\cos\psi \\
&\quad - \beta_p z_1\cos\psi + \dot{x}_1\sin\psi - y_1\sin\psi - \beta_p \dot{z}_1\sin\psi \\
V_z &= \dot{\alpha}_s x_{CG} - \dot{\phi}_s y_{CG} + \dot{z}_F + \dot{\alpha}_s x_1\cos\psi \\
&\quad - \phi_s x_1\cos\psi - \alpha_s y_1\cos\psi - \phi_s \dot{y}_1\cos\psi - \alpha_s x_1\sin\psi \\
&\quad - \dot{\phi}_s x_1\sin\psi + \phi_s y_1\sin\psi - \alpha_s \dot{y}_1\sin\psi + \dot{z}_1
\end{aligned}
\tag{2.62}$$

In accordance with the ordering scheme, all terms of order greater than ε^2 have been dropped from the above relations. The virtual variation of the velocity is given by

$$\delta\vec{V} = \delta V_x \hat{I}_I^G + \delta V_y \hat{J}_I^G + \delta V_z \hat{K}_I^G \tag{2.63}$$

where

$$\begin{aligned}
\delta V_x &= (-\dot{\alpha}_s x_{CG} - \dot{z}_1 - \dot{\alpha}_s x_1\cos\psi + \phi_s x_1\cos\psi + \alpha_s y_1\cos\psi \\
&\quad + \phi_s \dot{y}_1\cos\psi + \alpha_s x_1\sin\psi - \phi_s y_1\sin\psi + \alpha_s \dot{y}_1\sin\psi) \delta\alpha_s \\
&\quad + (\phi_s y_{CG} - h - \beta_p x_1 - \alpha_s x_{CG} - z_1 - \alpha_s x_1\cos\psi + \phi_s x_1\sin\psi) \delta\dot{\alpha}_s \\
&\quad + (\dot{\alpha}_s y_{CG} + \alpha_s x_1\cos\psi + \alpha_s \dot{y}_1\cos\psi + \dot{\alpha}_s x_1\sin\psi - \alpha_s y_1\sin\psi) \delta\phi_s \\
&\quad + (\alpha_s \phi_s \cos\psi - \sin\psi) \delta x_1 + (\cos\psi - \alpha_s \beta_p + \alpha_s \phi_s \sin\psi) \delta \dot{x}_1 \\
&\quad - (\cos\psi + \alpha_s \phi_s \sin\psi) \delta y_1 + (\alpha_s \phi_s \cos\psi - \sin\psi) \delta \dot{y}_1 \\
&\quad - (\dot{\alpha}_s - \beta_p \sin\psi) \delta z_1 - (\alpha_s + \beta_p \cos\psi) \delta \dot{z}_1 + \delta \dot{x}_F \\
\delta V_y &= (\dot{\phi}_s x_{CG} + \dot{\phi}_s x_1\cos\psi) \delta\alpha_s + (\dot{z}_1 - \dot{\phi}_s y_{CG} - \phi_s x_1\cos\psi \\
&\quad - \phi_s \dot{y}_1\cos\psi + \dot{\phi}_s x_1\sin\psi + \phi_s y_1\sin\psi) \delta\phi_s + (h + \beta_p x_1 + \alpha_s x_{CG} - \phi_s y_{CG} \\
&\quad + z_1 - \alpha_s x_1\cos\psi - \phi_s x_1\sin\psi) \delta\dot{\phi}_s + \cos\psi \delta x_1 + (\beta_p \phi_s + \sin\psi) \delta \dot{x}_1 \\
&\quad + \cos\psi \delta y_1 + (\dot{\phi}_s - \beta_p \cos\psi) \delta z_1 - \sin\psi \delta y_1 + (\phi_s - \beta_p \sin\psi) \delta \dot{z}_1 + \delta \dot{y}_F
\end{aligned}$$

$$\begin{aligned}
\delta V_z = & (-\dot{\alpha}_s h - \alpha_s \dot{z}_1 + \alpha_s \phi_s x_1 \cos \psi + \dot{x}_1 \cos \psi - y_1 \cos \psi \\
& - \beta_p \dot{z}_1 \cos \psi - x_1 \sin \psi - \dot{y}_1 \sin \psi + \beta_p z_1 \sin \psi) \delta \alpha_s \\
& + (x_{CG} - \alpha_s h + x_1 \cos \psi - y_1 \sin \psi) \delta \dot{\alpha}_s \\
& + (y_1 \sin \psi - h \dot{\phi}_s - \phi_s \dot{z}_1 - x_1 \cos \psi - \dot{y}_1 \cos \psi + \beta_p z_1 \cos \psi \\
& - \dot{x}_1 \sin \psi + \beta_p \dot{z}_1 \sin \psi) \delta \phi_s - (h \dot{\phi}_s + y_{CG} + y_1 \cos \psi + x_1 \sin \psi) \delta \dot{\phi}_s \\
& + (\dot{\alpha}_s \cos \psi - \phi_s \cos \psi - \alpha_s \sin \psi - \dot{\phi}_s \sin \psi) \delta x_1 \\
& + (\beta_p + \alpha_s \cos \psi - \phi_s \sin \psi) \delta \dot{x}_1 \\
& + (-\alpha_s \cos \psi - \dot{\phi}_s \cos \psi - \dot{\alpha}_s \sin \psi + \phi_s \sin \psi) \delta y_1 \\
& - (\phi_s \cos \psi + \alpha_s \sin \psi) \delta \dot{y}_1 + (\beta_p \phi_s \cos \psi + \alpha_s \beta_p \sin \psi) \delta z_1 \\
& + (1 - \alpha_s \beta_p \cos \psi + \beta_p \phi_s \sin \psi) \delta \dot{z}_1 + \delta \ddot{z}_F
\end{aligned} \tag{2.64}$$

The variation of the velocity components is taken before the ordering scheme is applied to the velocity components. The ordering scheme is then applied to the variational velocity expressions and all terms of order greater than ε^2 are dropped.

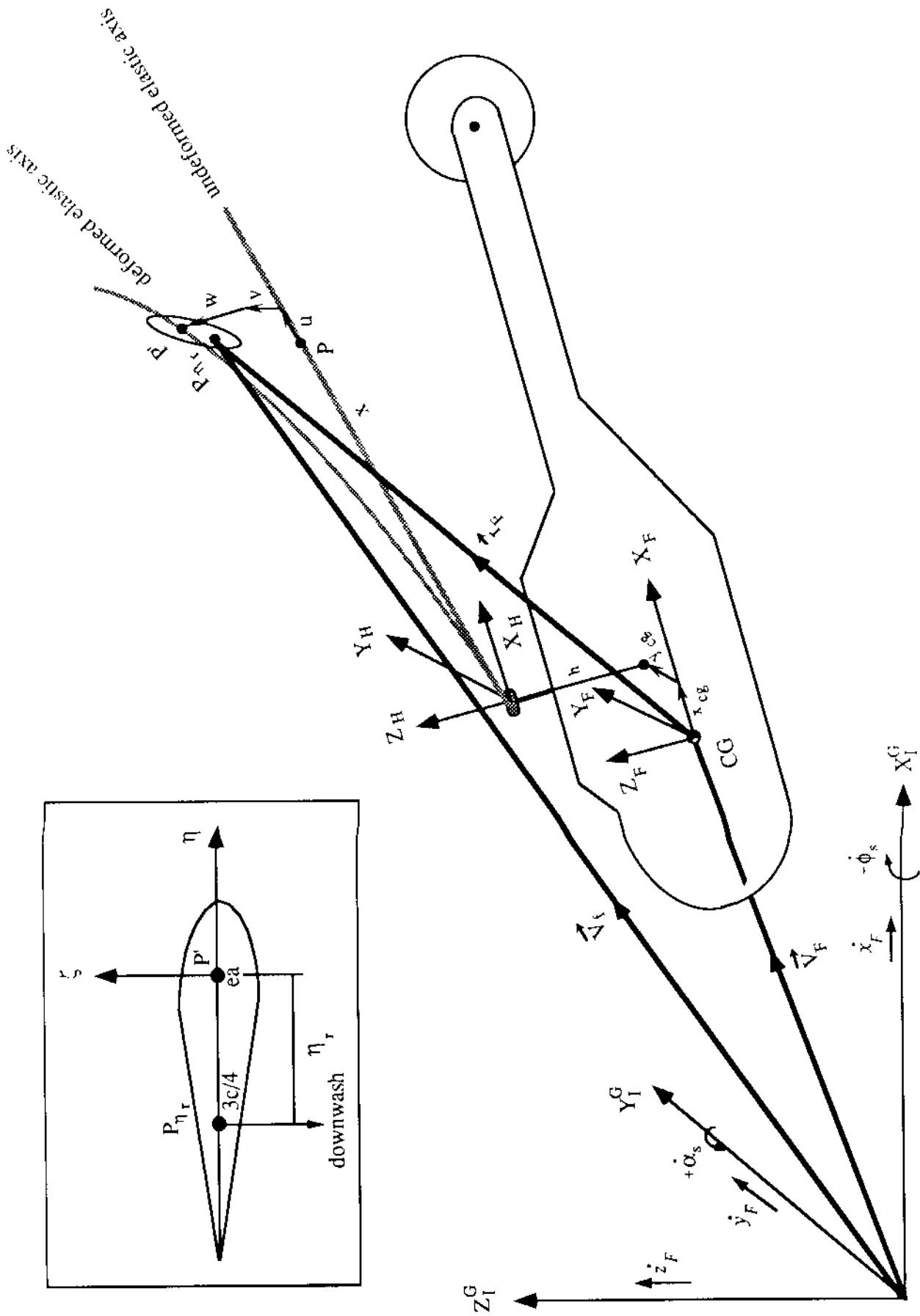


Figure 2.5 Blade Velocities at $3c/4$ Due to Fuselage Motion, $\vec{V}_f = \vec{V}_F + \vec{\omega}_f \times \vec{r}_F$

Variation in Kinetic Energy Without Fuselage (Hub) Motion

The kinetic energy of the *bth* blade is given by

$$T_b = \frac{1}{2} \int_0^R \iint_A \rho_s \vec{V} \cdot \vec{V} d\eta d\zeta dx \quad (2.65)$$

where \vec{V} is the total blade velocity and ρ_s is the mass density of the blade.

The variation of kinetic energy is given by

$$\delta T_b = \int_0^R \iint_A \rho_s \vec{V} \cdot \delta \vec{V} d\eta d\zeta dx \quad (2.66)$$

Without the contribution of fuselage motion induced velocity components, the total blade velocity, \vec{V} , equals only the velocity of the blade relative to the hub, \vec{V}_b (given by Eqn. (2.46)). For this type of analysis, the variation in kinetic energy reduces to a significantly simpler form. Substituting the velocity expression given in Eqn.(2.46) and then integrating by parts results in the following nondimensional equation:

$$\frac{\delta T_b}{m_0 \Omega^2 R^3} = \int_0^1 \iint_A \rho_s (T_{x1} \delta x_1 + T_{y1} \delta y_1 + T_{z1} \delta z_1) d\eta d\zeta dx \quad (2.67)$$

where

$$T_{x1} = -\ddot{x}_1 + 2\dot{y}_1 + x_1 - z_1 \beta_p \quad (2.68)$$

$$T_{y1} = y_1 - \ddot{y}_1 - 2\dot{x}_1 + 2\dot{z}_1 \beta_p$$

$$T_{z1} = -x_1 \beta_p + z_1 \beta_p^2 - 2\dot{y}_1 \beta_p - \ddot{z}_1$$

Using Eqns. (2.34), 2.35), (2.50), and (2.51), the nondimensional kinetic energy variation can be rewritten retaining terms up to second order in governing equations. In some instances, important third order terms are kept in the axial and torsional equations. Using Eqns. (2.35a-e), the kinetic energy is also recast in terms of the axial elastic deflection, u_e .

For the *bth* blade, the resulting kinetic energy expression is given by

$$\frac{\delta T_b}{m_0 \Omega^2 R^3} = \int_0^1 m (T_{u_e} \delta u_e + T_v \delta v + T_w \delta w + T_{v'} \delta v' + T_{w'} \delta w' + T_\phi \delta \phi + T_F) dx \quad (2.69)$$

where

$$T_{u_e} = x + u_e + 2\dot{v} - \ddot{u}_e \quad (2.70)$$

$$\begin{aligned} T_v &= e_g (\cos \theta_0 + \ddot{\theta}_0 \sin \theta_0) + v - \dot{\phi} e_g \sin \theta_0 \\ &\quad + 2\dot{w} \beta_p + 2\dot{v}' e_g \cos \theta_0 + 2\dot{w}' e_g \sin \theta_0 - \ddot{v} + \dot{\phi} e_g \sin \theta_0 \\ &\quad - 2\dot{u}_e + 2 \int_0^x (v' \dot{v}' + w' \dot{w}') d\xi \end{aligned}$$

$$T_{v'} = -e_g (x \cos \theta_0 - \dot{\phi} x \sin \theta_0 + 2\dot{v} \cos \theta_0)$$

$$T_w = -x \beta_p - \ddot{\theta}_0 e_g \cos \theta_0 - 2\dot{v} \beta_p - \ddot{w} - \dot{\phi} e_g \cos \theta_0$$

$$T_{w'} = -e_g (x \sin \theta_0 + \dot{\phi} x \cos \theta_0 + 2\dot{v} \sin \theta_0)$$

$$\begin{aligned} T_\phi &= -k_m^2 \dot{\phi} - (k_{m2}^2 - k_{m1}^2) \cos \theta_0 \sin \theta_0 - x \beta_p e_g \cos \theta_0 \\ &\quad - v e_g \sin \theta_0 + v' x e_g \sin \theta_0 - w' x e_g \cos \theta_0 + \ddot{v} e_g \sin \theta_0 \\ &\quad - \dot{\phi} (k_{m2}^2 - k_{m1}^2) \cos 2\theta_0 - \ddot{w} e_g \cos \theta_0 - k_m^2 \ddot{\theta}_0 \end{aligned}$$

$$T_F = -(x + 2\dot{v}) \int_0^x (v' \delta v' + w' \delta w') d\xi$$

and the blade sectional integrals are defined as

$$\begin{aligned} m &= \iint_A \rho_s d\eta d\zeta & mk_{m1}^2 &= \iint_A \rho_s \zeta^2 d\eta d\zeta \\ me_g &= \iint_A \rho_s \eta d\eta d\zeta & mk_{m2}^2 &= \iint_A \rho_s \eta^2 d\eta d\zeta \\ && mk_m^2 &= mk_{m1}^2 + mk_{m2}^2 \end{aligned} \quad (2.71)$$

The blade mass per unit length, m , is nondimensionalized with respect to reference mass m_0 . The e_g is the blade center of gravity offset from the elastic axis (positive forward). The k_{m1}^2 and k_{m2}^2 are the flapwise and chordwise mass moments of inertia per unit blade length, respectively. Note that these are moments of inertia about the *elastic axis*. Since it is assumed that there is no offset in the thickness direction of the airfoil, additional blade sectional integrals related to the blade center of gravity offset can be defined as,

$$\begin{aligned} \iint_A \rho_s (y_1 - v) d\eta d\zeta &= me_g \cos(\theta_0 + \hat{\phi}) \\ \iint_A \rho_s (z_1 - w) d\eta d\zeta &= me_g \sin(\theta_0 + \hat{\phi}) \end{aligned} \quad (2.72a)$$

and the relationships hold:

$$\begin{aligned} \iint_A \rho_s \zeta d\eta d\zeta &= 0 \\ \iint_A \rho_s \eta \zeta d\eta d\zeta &= 0 \end{aligned} \quad (2.72b)$$

As indicated by the foreshortening term, T_F (see Eqn. 2.70), the variation of kinetic energy, δT_b , results in the following *double integral* expression

$$-\int_0^1 mT_F dx = \int_0^1 m(x + 2\dot{v}) \left[\int_0^x (v' \delta v' + w' \delta w') d\xi \right] dx \quad (2.73a)$$

Integrating the above expression by parts yields the more convenient form,

$$\begin{aligned} -\int_0^1 mT_F dx &= \int_0^1 (v' \delta v' + w' \delta w') \left[\int_x^1 m(x + 2\dot{v}) d\xi \right] dx \\ &= \int_0^1 F_A (v' \delta v' + w' \delta w') dx + \int_0^1 (v' \delta v' + w' \delta w') \left[\int_x^1 2m\dot{v} d\xi \right] dx \end{aligned} \quad (2.73b)$$

with the axial centrifugal force, F_A , defined as,

$$F_A(x) = \int_x^1 mx d\xi$$

The above expression reflects the "centrifugal stiffening" effect on the flap and lag equations, as well as the non-linear Coriolis damping effect. The anti-symmetric counterparts to the Coriolis damping terms are visible in the expression for T_v in Eqn. (2.70).

Variation in Kinetic Energy Including Fuselage Motion

The velocity and virtual velocity expressions including the fuselage motion are used to formulate the variation in kinetic energy for the *bth* blade as

$$\delta T_b = \int_0^R (T_{u_s} \delta u + T_v \delta v + T_w \delta w + T_{\dot{\phi}} \delta \dot{\phi} + T_{v'} \delta v' + T_{w'} \delta w' + T_{x_F} \delta x_F + T_{y_F} \delta y_F + T_{z_F} \delta z_F + T_{\alpha_s} \delta \alpha_s + T_{\phi_s} \delta \phi_s) dx \quad (2.74)$$

where

$$T_{u_s} = m(x + 2\dot{v} - \ddot{u} - \ddot{x}_F \cos \psi - \ddot{y}_F \sin \psi + h\ddot{\alpha}_s \cos \psi - h\ddot{\phi}_s \sin \psi)$$

$$\begin{aligned} T_v &= m((v + e_g \cos \theta_0) + 2(\beta_p \dot{w} - \dot{u}) \\ &\quad + 2e_g(\dot{v}' \cos \theta_0 + \dot{w}' \sin \theta_0) - \ddot{v} + e_g(\ddot{\phi} + \ddot{\theta}_0) \sin \theta_0 \\ &\quad + \ddot{x}_F \sin \psi - \ddot{y}_F \cos \psi - h\ddot{\alpha}_s \sin \psi - h\ddot{\phi}_s \cos \psi) \end{aligned}$$

$$\begin{aligned} T_w &= m(-(\beta_p (x + 2\dot{v}) + \ddot{w} + e_g(\ddot{\phi} + \ddot{\theta}_0) \cos \theta_0 \\ &\quad - \ddot{z}_F - x\ddot{\alpha}_s \cos \psi + x\ddot{\phi}_s \sin \psi + 2x\dot{\alpha}_s \sin \psi + 2x\dot{\phi}_s \cos \psi \\ &\quad - x_{CG}\ddot{\alpha}_s + y_{CG}\ddot{\phi}_s) \end{aligned}$$

$$\begin{aligned} T_{\dot{\phi}} &= m((k_m^2 \ddot{\phi} + (k_{m_2}^2 - k_{m_1}^2) \cos \theta_0 \sin \theta_0 \\ &\quad + \dot{\phi}((k_{m_2}^2 - k_{m_1}^2) \cos \theta_0 \sin \theta_0 + k_m^2 \ddot{\theta}_0 \\ &\quad + e_g x(w' \cos \theta_0 - v' \sin \theta_0) + e_g v \sin \theta_0 \\ &\quad + e_g \beta_p x \cos \theta_0 - e_g(\ddot{v} \sin \theta_0 - \ddot{w} \cos \theta_0) \\ &\quad - e_g(\ddot{x}_F \sin \psi \sin \theta_0 - \ddot{y}_F \cos \psi \sin \theta_0 + \ddot{z}_F \cos \theta_0 \\ &\quad + (x \cos \psi \cos \theta_0 - h \sin \theta_0 \sin \psi) \ddot{\alpha}_s \\ &\quad + (-x \sin \psi \cos \theta_0 - h \sin \theta_0 \cos \psi) \ddot{\phi}_s) \\ &\quad - e_g \ddot{\alpha}_s x_{CG} \cos \theta_0 + e_g \ddot{\phi}_s y_{CG} \cos \theta_0) \end{aligned}$$

$$T_{v'} = -me_g x \hat{\phi} \sin \theta_0 + me_g \cos \theta_0 (x + 2\dot{v} + \ddot{x}_F \cos \psi \\ + \ddot{y}_F \sin \psi + \ddot{z}_F \beta_p - h \ddot{\alpha}_s \cos \psi + h \ddot{\phi}_s \sin \psi)$$

$$T_{w'} = me_g x \hat{\phi} \cos \theta_0 + me_g \sin \theta_0 (x + 2\dot{v} + \ddot{x}_F \cos \psi + \ddot{y}_F \sin \psi \\ + \ddot{z}_F \beta_p - h \ddot{\alpha}_s \cos \psi + h \ddot{\phi}_s \sin \psi)$$

$$T_{x_F} = m(\ddot{v} \sin \psi + 2\dot{v} \cos \psi - v \sin \psi - \ddot{x}_F + h \ddot{\alpha}_s)$$

$$T_{y_F} = m(-\ddot{v} \cos \psi + 2\dot{v} \sin \psi + v \cos \psi - \ddot{y}_F - h \ddot{\phi}_s)$$

$$T_{z_F} = m(-\ddot{w} - \ddot{z}_F - \ddot{\alpha}_s x \cos \psi + \ddot{\phi}_s x \sin \psi - x_{CG} \ddot{\alpha}_s + y_{CG} \ddot{\phi}_s \\ + 2\dot{\alpha}_s x \sin \psi + 2\dot{\phi}_s x \cos \psi + \alpha_s x \cos \psi - \phi_s x \sin \psi)$$

$$T_{\alpha_s} = m(-h^2 \ddot{\alpha}_s - x_{CG}^2 \ddot{\alpha}_s + h \ddot{x}_F + \ddot{\phi}_s x_{CG} y_{CG} \\ - x_{CG} \ddot{w} - x_{CG} \ddot{z}_F - h x \cos \psi - \beta_p x^2 \cos \psi \\ + h \ddot{v} \cos \psi - 2\dot{\alpha}_s x x_{CG} \cos \psi + 2\dot{\phi}_s x x_{CG} \cos \psi \\ - 2h \dot{v} \cos \psi + \phi_s x y_{CG} \cos \psi + \ddot{\phi}_s x y_{CG} \cos \psi - x w \cos \psi \\ - x \ddot{w} \cos \psi - x \ddot{z}_F \cos \psi - \ddot{\alpha}_s x^2 \cos^2 \psi + 2\dot{\phi}_s x^2 \cos^2 \psi \\ - 2h \dot{u} \sin \psi + 2\dot{\alpha}_s x x_{CG} \sin \psi - \phi_s x x_{CG} \sin \psi \\ + \ddot{\phi}_s x x_{CG} \sin \psi + h v \sin \psi \\ - h \ddot{v} \sin \psi + 2\dot{\alpha}_s x^2 \cos \psi \sin \psi + \ddot{\phi}_s x^2 \cos \psi \sin \psi)$$

$$\begin{aligned}
T_{\phi_s} = & m(-h^2 \ddot{\phi}_s + \ddot{\alpha}_s x_{CG} y_{CG} - \ddot{\phi}_s y_{CG}^2 - h \ddot{y}_F + y_{CG} \ddot{w} \\
& + y_{CG} \ddot{z}_F - 2h \dot{u} \cos \psi + h v \cos \psi - h \dot{v} \cos \psi - x^2 \ddot{\phi}_s \sin^2 \psi \\
& + \ddot{\alpha}_s x y_{CG} \cos \psi - 2 \dot{\phi}_s x y_{CG} \cos \psi + h x \sin \psi \\
& + \beta_p x^2 \sin \psi - h u \sin \psi + \ddot{\alpha}_s x x_{CG} \sin \psi + 2 h v \sin \psi \\
& - 2 \dot{\alpha}_s x y_{CG} \sin \psi - 2 \ddot{\phi}_s x y_{CG} \sin \psi + x w \sin \psi \\
& + x \ddot{w} \sin \psi + x \ddot{z}_F \sin \psi + \ddot{\alpha}_s x^2 \cos \psi \sin \psi \\
& - 2 \dot{\phi}_s x^2 \cos \psi \sin \psi - 2 \dot{\alpha}_s x^2 \sin^2 \psi)
\end{aligned} \tag{2.75}$$

2.2.1.3 Virtual Work, δW_b

External aerodynamic forces on the rotor contribute to the virtual work of the system. For each degree of freedom there is a corresponding external force (or moment) due to aerodynamic loading. The general expression for δW_b is given by

$$\delta W_b = \int_0^R (L_u^A \delta u + L_v^A \delta v + L_w^A \delta w + M_{\phi}^A \delta \hat{\phi}) dx \quad (2.76)$$

where L_u^A , L_v^A , and L_w^A are the distributed airloads in the x , y , z directions respectively, and M_{ϕ}^A is the aerodynamic pitching moment about the undeformed elastic axis. Many of the aerodynamic terms are motion dependent and thereby contribute to the element stiffness, damping, and mass matrices. The method in which the aerodynamic forces and moments are computed is discussed in detail in Chapter 3.

2.2.2 Energy Expressions for the Fuselage

2.2.2.1 Strain Energy, δU_F

$$U_{LG} = \frac{1}{2} [K_x x_F^2 + K_y y_F^2 + K_z z_F^2 + K_\alpha \alpha_s^2 + K_\phi \phi_s^2] \quad (2.77)$$

$$\delta U_{LG} = [K_x x_F \delta x_F + K_y y_F \delta y_F + K_z z_F \delta z_F + K_\alpha \alpha_s \delta \alpha_s + K_\phi \phi_s \delta \phi_s] \quad (2.78)$$

2.2.1.2 Kinetic Energy, δT_F

In addition to the contribution of the fuselage motion terms to the blade kinetic energy expression, the kinetic energy of the fuselage also contributes to the total system kinetic energy. The total system kinetic energy is expressed as the sum of the blade kinetic energy, T_b , and the fuselage kinetic energy, T_F , as shown below

$$T = \left(\sum_{b=1}^{N_b} T_b \right) + T_F \quad (2.79)$$

The fuselage kinetic energy is given by

$$T_F = \frac{1}{2} [m_F x_F^2 + m_F y_F^2 + m_F z_F^2 + I_{\alpha_s} \alpha_s^2 + I_{\phi_s} \phi_s^2] \quad (2.80)$$

where m_F is the effective fuselage mass, I_{ϕ_s} is the effective roll mass moment of inertia about the vehicle center of gravity, and I_{α_s} is the effective pitch mass moment of inertia about the vehicle center of gravity. The variational form of the fuselage kinetic energy is given by

$$\delta T_F = [m_F \dot{x}_F \delta \dot{x}_F + m_F \dot{y}_F \delta \dot{y}_F + m_F \dot{z}_F \delta \dot{z}_F + I_{\alpha_s} \dot{\alpha}_s \delta \dot{\alpha}_s + I_{\phi_s} \dot{\phi}_s \delta \dot{\phi}_s] \quad (2.81)$$

After integrating by parts, the variational fuselage kinetic energy expression is

$$\delta T_F = [m_F \ddot{x}_F \delta x_F + m_F \ddot{y}_F \delta y_F + m_F \ddot{z}_F \delta z_F + I_{\alpha_s} \ddot{\alpha}_s \delta \alpha_s + I_{\phi_s} \ddot{\phi}_s \delta \phi_s] \quad (2.82)$$

2.2.1.3 Virtual Work, δW_F

Aerodynamic forces on the fuselage contribute to the external virtual work of the system. The formulation of the virtual work expressions is contained in Chapter 3 on Aerodynamic Modeling.

2.3 Blade Equations of Motion

For the b th blade, the virtual energy expression in Eqn.(2.16) is written in the discretized form such that

$$\delta\Pi_b = \int_{\psi_i}^{\psi_f} \left[\sum_{i=1}^N (\delta U_i - \delta T_i - \delta W_i) \right]_b d\psi = 0 \quad (2.83)$$

Using the notation,

$$\Delta_i = \delta U_i - \delta T_i - \delta W_i \quad (2.84)$$

the virtual energy expression can also be written as

$$\delta\Pi_b = \int_{\psi_i}^{\psi_f} \left[\sum_{i=1}^N \Delta_i \right]_b d\psi = 0 \quad (2.85)$$

where the subscript i denotes the i th beam element and the N is the total number of spatial finite elements in the blade. Applying the finite element method in space domain for this virtual energy expression yields the discretized equations of motion for the b th blade.

2.3.1 Finite Element Discretization in Space

The blade is discretized into a number of beam elements (see Figure 2.6). Each beam element consists of fifteen degrees of freedom (Ref. [2.3]). These degrees of freedom are distributed over five element nodes (2 boundary nodes and 3 interior nodes). There are six degrees of freedom at each element boundary node. These six degrees of freedom

correspond to u, v, v', w, w' , and $\hat{\phi}$. There are two internal nodes for axial (elastic) deflection u (the subscript "e" on the axial elastic deflection is dropped for notational convenience), and one internal node for elastic twist $\hat{\phi}$. Between elements there is continuity of displacement and slope for flap and lag bending deflections, and continuity of displacement for elastic twist and axial deflections. This element insures physically consistent linear variations of bending moments and torsional moment, and quadratic variation of axial force within each element. Using the interpolating polynomials, the distribution of deflections over a beam element is expressed in terms of the elemental nodal displacements \mathbf{q}_i . For the i th beam element, one would obtain the blade deflections as follows:

$$\mathbf{u}(s) = \begin{Bmatrix} u(s) \\ v(s) \\ w(s) \\ \hat{\phi}(s) \end{Bmatrix} = \begin{bmatrix} \mathbf{H}_u & 0 & 0 & 0 \\ 0 & \mathbf{H} & 0 & 0 \\ 0 & 0 & \mathbf{H} & 0 \\ 0 & 0 & 0 & \mathbf{H}_{\hat{\phi}} \end{bmatrix} \mathbf{q}_i \quad (2.86)$$

where the elemental nodal displacement vector is defined as

$$\mathbf{q}_i^T = [u_1, u_2, u_3, u_4, v_1, v'_1, v_2, v'_2, w_1, w'_1, w_2, w'_2, \hat{\phi}_1, \hat{\phi}_2, \hat{\phi}_3] \quad (2.87)$$

The interpolating polynomials for the shape functions in Eqn.(2.86) are given as

$$\mathbf{H}_u^T = \begin{Bmatrix} H_{u1} \\ H_{u2} \\ H_{u3} \\ H_{u4} \end{Bmatrix} = \begin{Bmatrix} -4.5s^3 + 9s^2 - 5.5s + 1 \\ 13.5s^3 - 22.5s^2 + 9s \\ -13.5s^3 + 18s^2 - 4.5s \\ 4.5s^3 - 4.5s^2 + s \end{Bmatrix} \quad (2.88)$$

$$H^T = \begin{Bmatrix} H_1 \\ H_2 \\ H_3 \\ H_4 \end{Bmatrix} = \begin{Bmatrix} 2s^3 - 3s^2 + 1 \\ l_i(s^3 - 2s^2 + s) \\ -2s^3 + 3s^2 \\ l_i(s^3 - s^2) \end{Bmatrix} \quad (2.89)$$

$$H_{\dot{\phi}}^T = \begin{Bmatrix} H_{\dot{\phi}1} \\ H_{\dot{\phi}2} \\ H_{\dot{\phi}3} \end{Bmatrix} = \begin{Bmatrix} 2s^2 - 3s + 1 \\ -4s^2 + 4s \\ 2s^2 - s \end{Bmatrix} \quad (2.90)$$

where $s = x_i / l_i$ and l_i is the length of the i th beam element.

For lag and flap bending deflections, the interpolating polynomial is chosen from the family of Hermite polynomials, which allow continuity of displacement and slope. Derivation of these interpolating polynomials, or shape functions, is straight forward.

As an example, consider flap bending deflection only. As shown in Figure 2.6, each element has two bending nodes. At each node, the deflection and slope are degrees of freedom; therefore, each element has four bending degrees of freedom for flap bending. The flap bending deflection, w , is given by the cubic polynomial

$$w = \alpha_1 + \alpha_2 x + \alpha_3 x^2 + \alpha_4 x^3 \quad (2.91)$$

where x is the local element distance from $x=0$ to $x=l_i$. Writing deflections and slopes as functions of element degrees of freedom (see Figure 2.6) at both element nodes yields

$$w(x=0) = \alpha_1 = w_1 \quad (2.92)$$

$$w'(x=0) = \alpha_2 = w'_1$$

$$w(x=l) = \alpha_1 + \alpha_2 l + \alpha_3 l^2 + \alpha_4 l^3 = w_2$$

$$w'(x = l) = \alpha_2 + 2\alpha_3l + 3\alpha_4l^2 = w'_2$$

These can be written in matrix form as

$$\begin{Bmatrix} w_1 \\ w'_1 \\ w_2 \\ w'_2 \end{Bmatrix} = \begin{bmatrix} 1 & 0 & 0 & 0 \\ 0 & 1 & 0 & 0 \\ 1 & l & l^2 & l^3 \\ 0 & 1 & 2l & 3l^2 \end{bmatrix} \begin{Bmatrix} \alpha_1 \\ \alpha_2 \\ \alpha_3 \\ \alpha_4 \end{Bmatrix} \quad (2.93)$$

Inverting the above matrix yields

$$\begin{Bmatrix} \alpha_1 \\ \alpha_2 \\ \alpha_3 \\ \alpha_4 \end{Bmatrix} = \begin{bmatrix} 1 & 0 & 0 & 0 \\ 0 & 1 & 0 & 0 \\ -3/l^2 & -2/l & 3/l^2 & -1/l \\ 2/l^3 & 1/l^2 & -2/l^3 & 1/l^2 \end{bmatrix} \begin{Bmatrix} w_1 \\ w'_1 \\ w_2 \\ w'_2 \end{Bmatrix} \quad (2.94)$$

The deflection can now be expanded to give the form

$$\begin{aligned} w = & (2s^3 - 3s^2 + 1)w_1 + (l_i(s^3 - 2s^2 + s))w'_1 \\ & + (-2s^3 + 3s^2)w_2 + (l_i(s^3 - s))w'_2 \end{aligned} \quad (2.95)$$

In terms of shape functions, the deflection w can be written as

$$w = H_1 w_1 + H_2 w'_1 + H_3 w_2 + H_4 w'_2 \quad (2.96)$$

with nondimensional local element distance, $s = x / l_i$. Comparing the above equations for w , the Hermite polynomial shape functions for flap bending are derived. By replacing w

with v in the above procedure, the lag bending shape functions can also be derived. These functions are identical to the flap bending shape functions.

For elastic twist and axial deflections, Lagrangian polynomials are used, since these give a continuity of displacement. Derivation of these functions is carried out in a similar manner to that described for bending shape functions. Each element has three torsion nodes. Each torsion node has only one degree of freedom. The elastic twist can be written as

$$\hat{\phi} = \alpha_1 + \alpha_2 s + \alpha_3 s^2 \quad (2.97)$$

Note the initial use of nondimensional element distance, s . Writing twist as a function of element degrees of freedom (see Figure 2.6) at all three element nodes yields

$$\hat{\phi}(s=0) = \alpha_1 = \hat{\phi}_1 \quad (2.98)$$

$$\begin{aligned}\hat{\phi}(s=1) &= \alpha_1 + \alpha_2 + \alpha_3 = \hat{\phi}_2 \\ \hat{\phi}(s=\frac{1}{2}) &= \alpha_1 + \frac{\alpha_2}{2} + \frac{\alpha_3}{4} = \hat{\phi}_3\end{aligned}$$

This can be written in matrix form as

$$\begin{Bmatrix} \hat{\phi}_1 \\ \hat{\phi}_2 \\ \hat{\phi}_3 \end{Bmatrix} = \begin{bmatrix} 1 & 0 & 0 \\ 1 & 1 & 1 \\ 1 & \frac{1}{2} & \frac{1}{4} \end{bmatrix} \begin{Bmatrix} \alpha_1 \\ \alpha_2 \\ \alpha_3 \end{Bmatrix} \quad (2.99)$$

Inverting the above matrix yields

$$\begin{Bmatrix} \alpha_1 \\ \alpha_2 \\ \alpha_3 \end{Bmatrix} = \begin{bmatrix} 1 & 0 & 0 \\ -3 & -1 & 4 \\ 2 & 2 & -4 \end{bmatrix} \begin{Bmatrix} \hat{\phi}_1 \\ \hat{\phi}_2 \\ \hat{\phi}_3 \end{Bmatrix} \quad (2.100)$$

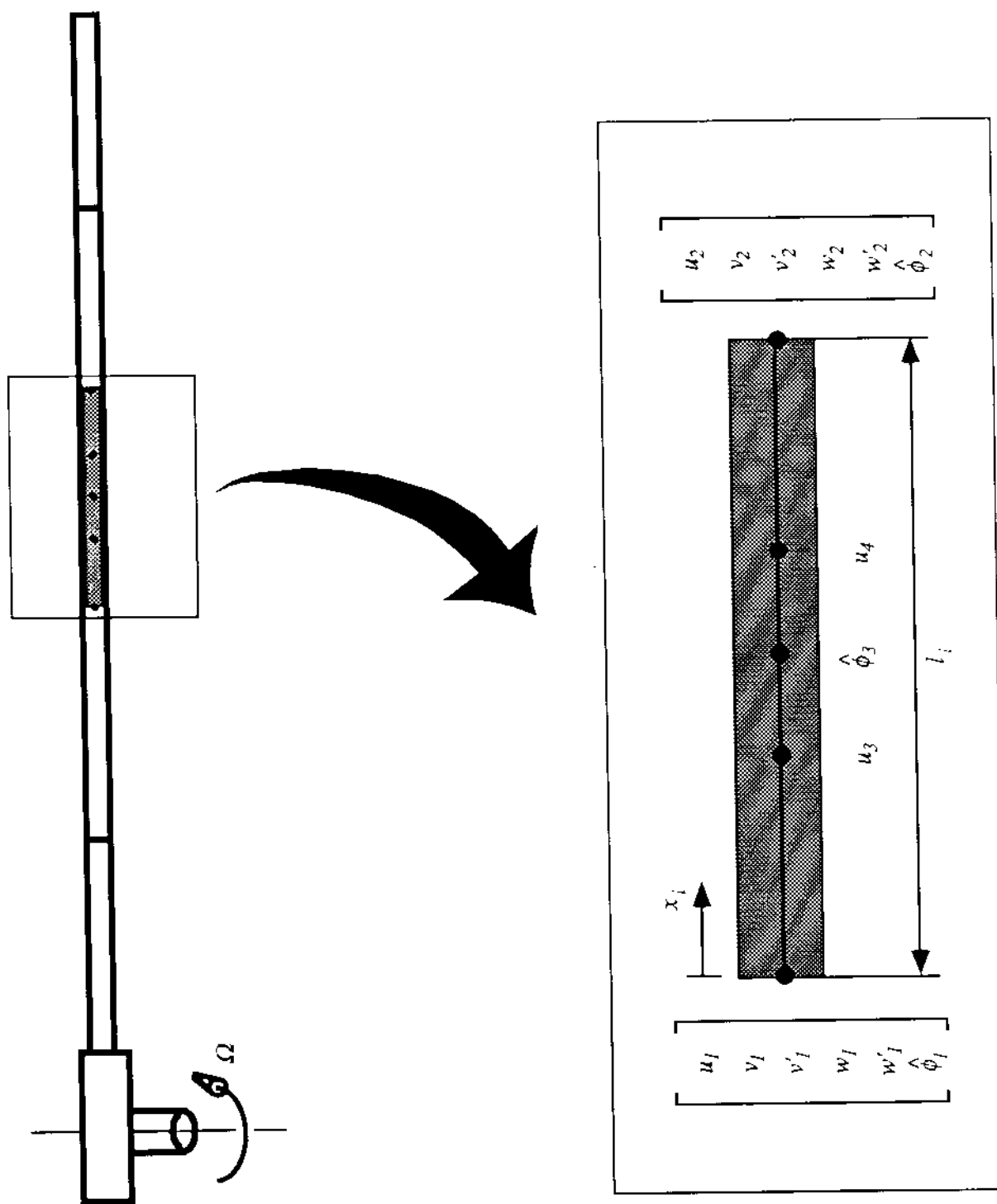


Figure 2.6 Beam Finite Element Used for Rotor Blade

The twist can now be expanded to give the form

$$\hat{\phi} = (2s^2 - 3s + 1)\hat{\phi}_1 + (-4s^2 + 4s)\hat{\phi}_2 + (2s^2 - s)\hat{\phi}_3 \quad (2.101)$$

In terms of shape functions, the elastic twist, $\hat{\phi}$, can be written as

$$\hat{\phi} = H_{\hat{\phi}1}\hat{\phi}_1 + H_{\hat{\phi}2}\hat{\phi}_2 + H_{\hat{\phi}3}\hat{\phi}_3 \quad (2.102)$$

Comparing the above equations for $\hat{\phi}$, the Lagrangian polynomial shape functions for elastic twist are derived. Derivation of Lagrangian polynomial shape functions for axial elastic deflection is almost identical to the derivation of twist shape functions. The only difference is the use of two internal axial nodes compared to the one internal node for torsion.

2.3.2. Finite Element Formulation in Space

The discretized equations governing the motion of the fuselage are derived by considering the variation in the discretized virtual energy expression due to a variation in the blade motion, δq_i .

The discretized virtual energy expression given in Eqn. (2.83), can be written in terms of the blade element nodal quantities and fuselage degrees of freedom in the space domain. Recalling from Eqn. (2.83), for the *i*th element of the *b*th blade,

$$\Delta_i = \delta U_i - \delta T_i - \delta W_i \quad (2.103)$$

where δU is the virtual variation of strain energy due to a variation in blade motion, $\delta \mathbf{q}_i$, and δT is the virtual variation of kinetic energy due to a variation in blade motion, $\delta \mathbf{q}_i$. The δW is the virtual work done by external forces due to a variation in blade motion, $\delta \mathbf{q}_i$. For the equations governing the *motion of the blade*, there is no variation of the fuselage degrees of freedom (i.e. $\delta \mathbf{x}_F = 0$). Since there is no variation in fuselage degrees of freedom, the kinetic energy of the *bth* blade given in Eqn. (2.74) simplifies to

$$\delta T_b = \int_0^R (T_u \delta u + T_v \delta v + T_w \delta w + T_{v'} \delta v' + T_{w'} \delta w' + T_{\phi} \delta \dot{\phi}) dx \quad (2.104)$$

The dependence of the blade energy variation on the blade motion, \mathbf{q}_i , fuselage motion, \mathbf{x}_F , control settings θ_i , inflow, λ , and azimuth position, ψ , is shown below.

$$\begin{aligned} (\delta U_i)_b &= \delta U_i(\delta \mathbf{q}_i, \theta_i, \psi, \mathbf{q}_i, \mathbf{q}_i^2)_b \\ (\delta T_i)_b &= \delta T_i(\delta \mathbf{q}_i, \theta_i, \psi, \mathbf{q}_i, \dot{\mathbf{q}}_i, \dot{\mathbf{x}}_F, \ddot{\mathbf{x}}_F, \mathbf{q}_i \dot{\mathbf{x}}_F, \mathbf{q}_i \ddot{\mathbf{x}}_F)_b \\ (\delta W_i)_b &= \delta W_i(\delta \mathbf{q}_i, \theta_i, \psi, \mathbf{q}_i, \dot{\mathbf{q}}_i, \mathbf{q}_i^2, \mathbf{q}_i \dot{\mathbf{q}}_i, \mathbf{x}_F, \dot{\mathbf{x}}_F, \ddot{\mathbf{q}}_i, \lambda)_b \end{aligned} \quad (2.105)$$

Regarding the notation used in the above expressions: \mathbf{q}_i^2 indicates second order nonlinearity in blade motion terms, and $\mathbf{q}_i \dot{\mathbf{x}}_F$ indicates second order bilinear terms involving one term from blade motion and one term from fuselage velocity. Other dependencies in Eqn. (2.105) are defined in a similar manner.

The fuselage contributions to the total energy variation are not dependent on the blade motion. These energies depend only on the motion of the fuselage as will be discussed in section 2.4.1 - Fuselage Equations of Motion.

The expressions for δU and δW contain nonlinear terms. The variation in kinetic energy, δT , does not contain any nonlinear terms. Note that δT does contain second order bilinear terms if fuselage (hub) motion is included in the analysis.

Using appropriate shape functions, the elemental variation in energy, Δ_i , can be written in the following matrix form as

$$\Delta_i = \delta \mathbf{q}_i^T (\mathbf{M}_b \ddot{\mathbf{q}} + \mathbf{C}_b \dot{\mathbf{q}} + \mathbf{K}_b \mathbf{q} + \mathbf{M}_{bF} \ddot{\mathbf{x}}_F + \mathbf{C}_{bF} \dot{\mathbf{x}}_F + \mathbf{K}_{bF} \mathbf{x}_F - \mathbf{F}_b)_i \quad (2.106)$$

where $(\mathbf{M}_b)_i$, $(\mathbf{C}_b)_i$, $(\mathbf{K}_b)_i$, and $(\mathbf{F}_b)_i$ are (blade) elemental mass, damping, stiffness, and load matrices, respectively, and $(\mathbf{M}_{bF})_i$, $(\mathbf{C}_{bF})_i$, and $(\mathbf{K}_{bF})_i$ are the blade-fuselage elemental mass, damping, and stiffness matrices, respectively.

The matrices $(\mathbf{M}_b)_i$, $(\mathbf{C}_b)_i$, and $(\mathbf{K}_b)_i$ are obtained from *linear terms only*. The nonlinear terms in the energy expressions are all brought to the right side of the energy equation (force terms) and then linearized using a first order Taylor series approximation. In this manner, all nonlinear terms are included in $(\mathbf{F}_b)_i$. The force vector, $(\mathbf{F}_b)_i$ can be written as

$$\mathbf{F}_i = (\mathbf{F}_0)_i + (\mathbf{F}_{NL})_i \quad (2.107)$$

where $(\mathbf{F}_0)_i$ is the constant part of the element force vector and $(\mathbf{F}_{NL})_i$ is the nonlinear part of the element force vector. The nonlinear part of the force vector is expanded using a first order Taylor series as

$$(\mathbf{F}_{NL})_i = (\mathbf{F}_{NL})_i|_{(\mathbf{q}_0)_i} + \frac{\partial (\mathbf{F}_{NL})_i}{\partial \mathbf{q}_i} \mathbf{q}_i \quad (2.108)$$

$$(\mathbf{F}_{NL})_i \Big|_{(\mathbf{q}_0)_i} \rightarrow (\mathbf{F}_0)_i \quad (2.109)$$

In the above equations, the subscript b has been dropped for convenience.

As indicated in Eqn. (2.109), the constant part of the Taylor expansion is combined with $(\mathbf{F}_0)_i$. The linearized (derivative) part of the nonlinear force is derived analytically by differentiating the nonlinear force vector terms with respect to each term in the element displacement vector \mathbf{q}_i . This results in a displacement Jacobian matrix.

The finite element matrices are functions of radial position (space), and can also be functions of azimuthal location (time). In other words, $\mathbf{M}_i = \mathbf{M}_i(r)$, $\mathbf{C}_i = \mathbf{C}_i(r, \psi)$, $\mathbf{K}_i = \mathbf{K}_i(r, \psi)$, and $\mathbf{F}_i = \mathbf{F}_i(r, \psi)$. The radial variation is due to the rotation of the rotor blade, while the azimuthal variation is due to application of cyclic pitch control and aerodynamic forces in forward flight. This necessitates computation of *element matrices for each radial and azimuthal position over the rotor disk*. This is particularly important for calculating rotor dynamic response.

2.3.3 Element Structural Matrices and Load Vector

2.3.3.1 Blade Matrices and Load Vector

The element mass, stiffness, and damping matrices can be partitioned to indicate contributions from axial deflection, flap bending, lag bending, and elastic torsion. The *linear* mass, stiffness, and damping matrices can then be written as

$$[\mathbf{M}_b]_i = \begin{bmatrix} [\mathbf{M}_{uu}] & [\mathbf{M}_{uv}] & [\mathbf{M}_{uw}] & [\mathbf{M}_{u\phi}] \\ [\mathbf{M}_{vu}] & [\mathbf{M}_{vv}] & [\mathbf{M}_{vw}] & [\mathbf{M}_{v\phi}] \\ [\mathbf{M}_{wu}] & [\mathbf{M}_{wv}] & [\mathbf{M}_{ww}] & [\mathbf{M}_{w\phi}] \\ [\mathbf{M}_{\phi u}] & [\mathbf{M}_{\phi v}] & [\mathbf{M}_{\phi w}] & [\mathbf{M}_{\phi\phi}] \end{bmatrix} \quad (2.110)$$

$$[\mathbf{K}_b]_i = \begin{bmatrix} [\mathbf{K}_{uu}] & [\mathbf{K}_{uv}] & [\mathbf{K}_{uw}] & [\mathbf{K}_{u\phi}] \\ [\mathbf{K}_{vu}] & [\mathbf{K}_{vv}] & [\mathbf{K}_{vw}] & [\mathbf{K}_{v\phi}] \\ [\mathbf{K}_{wu}] & [\mathbf{K}_{wv}] & [\mathbf{K}_{ww}] & [\mathbf{K}_{w\phi}] \\ [\mathbf{K}_{\phi u}] & [\mathbf{K}_{\phi v}] & [\mathbf{K}_{\phi w}] & [\mathbf{K}_{\phi\phi}] \end{bmatrix} \quad (2.111)$$

$$[\mathbf{C}_b]_i = \begin{bmatrix} [\mathbf{C}_{uu}] & [\mathbf{C}_{uv}] & [\mathbf{C}_{uw}] & [\mathbf{C}_{u\phi}] \\ [\mathbf{C}_{vu}] & [\mathbf{C}_{vv}] & [\mathbf{C}_{vw}] & [\mathbf{C}_{v\phi}] \\ [\mathbf{C}_{wu}] & [\mathbf{C}_{wv}] & [\mathbf{C}_{ww}] & [\mathbf{C}_{w\phi}] \\ [\mathbf{C}_{\phi u}] & [\mathbf{C}_{\phi v}] & [\mathbf{C}_{\phi w}] & [\mathbf{C}_{\phi\phi}] \end{bmatrix} \quad (2.112)$$

The element structural stiffness and mass matrices are symmetric (e.g. $[\mathbf{K}_{uu}] = [\mathbf{K}_{vu}]$, etc.).

The linear mass matrix terms are defined as

$$\begin{aligned} [\mathbf{M}_{uu}] &= \int_0^1 m \mathbf{H}_u^T \mathbf{H}_u \, ds & (2.113) \\ [\mathbf{M}_{vv}] &= \int_0^1 m \mathbf{H}^T \mathbf{H} \, ds \\ [\mathbf{M}_{ww}] &= \int_0^1 m \mathbf{H}^T \mathbf{H} \, ds \\ [\mathbf{M}_{\phi\phi}] &= \int_0^1 m k_m^2 \mathbf{H}_{\dot{\phi}}^T \mathbf{H}_{\dot{\phi}} \, ds \\ [\mathbf{M}_{v\phi}] &= - \int_0^1 m e_g \sin \theta_0 \mathbf{H}^T \mathbf{H}_{\dot{\phi}} \, ds \\ [\mathbf{M}_{w\phi}] &= \int_0^1 m e_g \cos \theta_0 \mathbf{H}^T \mathbf{H}_{\dot{\phi}} \, ds \\ [\mathbf{M}_{uv}] &= 0 \\ [\mathbf{M}_{uw}] &= 0 \\ [\mathbf{M}_{vw}] &= 0 \end{aligned}$$

The linear stiffness matrix terms are defined as

$$\begin{aligned}
[\mathbf{K}_{uu}] &= \int_0^1 EA \mathbf{H}'^T \mathbf{H}'_u ds & (2.114) \\
[\mathbf{K}_{vv}] &= \int_0^1 F_A \mathbf{H}'^T \mathbf{H}' ds + \int_0^1 (EI_y \sin^2 \theta_0 + EI_z \cos^2 \theta_0) \mathbf{H}''^T \mathbf{H}'' ds - \int_0^1 m\Omega^2 \mathbf{H}^T \mathbf{H} ds \\
[\mathbf{K}_{ww}] &= \int_0^1 F_A \mathbf{H}'^T \mathbf{H}' ds + \int_0^1 (EI_z \sin^2 \theta_0 + EI_y \cos^2 \theta_0) \mathbf{H}''^T \mathbf{H}'' ds \\
[\mathbf{K}_{\phi\phi}] &= \int_0^1 m\Omega^2 (k_{m2}^2 - k_{m1}^2) \cos 2\theta_0 \mathbf{H}_\phi'^T \mathbf{H}_\phi' ds + \int_0^1 (GJ + EB_1 \theta_0'^2) \mathbf{H}_\phi'^T \mathbf{H}_\phi' ds \\
&\quad + \int_0^1 EC_1 \mathbf{H}_\phi''^T \mathbf{H}_\phi'' ds \\
[\mathbf{K}_{uv}] &= - \int_0^1 EA e_A \cos \theta_0 \mathbf{H}'_u^T \mathbf{H}'' ds \\
[\mathbf{K}_{uw}] &= - \int_0^1 EA e_A \sin \theta_0 \mathbf{H}'_u^T \mathbf{H}'' ds \\
[\mathbf{K}_{u\phi}] &= \int_0^1 EA k_A^2 \theta_0' \mathbf{H}'_u^T \mathbf{H}_\phi' ds \\
[\mathbf{K}_{vw}] &= \int_0^1 (EI_z - EI_y) \sin \theta_0 \cos \theta_0 \mathbf{H}''^T \mathbf{H}'' ds \\
[\mathbf{K}_{v\phi}] &= \int_0^1 m\Omega^2 e_g \sin \theta_0 \mathbf{H}^T \mathbf{H}_\phi' ds - \int_0^1 xm\Omega^2 e_g \sin \theta_0 \mathbf{H}'^T \mathbf{H}_\phi' ds \\
&\quad - \int_0^1 EB_2 \theta_0' \cos \theta_0 \mathbf{H}''^T \mathbf{H}_\phi' ds - \int_0^1 EC_2 \sin \theta_0 \mathbf{H}''^T \mathbf{H}_\phi'' ds \\
[\mathbf{K}_{w\phi}] &= \int_0^1 xm\Omega^2 e_g \cos \theta_0 \mathbf{H}'^T \mathbf{H}_\phi' ds - \int_0^1 EB_2 \theta_0' \sin \theta_0 \mathbf{H}''^T \mathbf{H}_\phi' ds \\
&\quad + \int_0^1 EC_2 \cos \theta_0 \mathbf{H}''^T \mathbf{H}_\phi'' ds
\end{aligned}$$

The linear damping matrix terms are defined as

$$\begin{aligned}
[\mathbf{C}_{uv}] &= - \int_0^1 2m\Omega \mathbf{H}'_u^T \mathbf{H} ds & (2.115) \\
[\mathbf{C}_{vv}] &= \int_0^1 2me_g \Omega \cos \theta_0 \mathbf{H}'^T \mathbf{H} ds - \int_0^1 2me_g \Omega \cos \theta_0 \mathbf{H}^T \mathbf{H}' ds \\
[\mathbf{C}_{vw}] &= - \int_0^1 2m\Omega \beta_p \mathbf{H}^T \mathbf{H} ds - \int_0^1 2me_g \Omega \sin \theta_0 \mathbf{H}^T \mathbf{H}' ds \\
[\mathbf{C}_{vu}] &= -[\mathbf{C}_{uv}] \\
[\mathbf{C}_{ww}] &= -[\mathbf{C}_{vv}] \\
[\mathbf{C}_{uu}] &= 0 \\
[\mathbf{C}_{u\phi}] &= [\mathbf{C}_{\phi u}] = 0 \\
[\mathbf{C}_{v\phi}] &= [\mathbf{C}_{\phi v}] = 0 \\
[\mathbf{C}_{w\phi}] &= 0
\end{aligned}$$

$$\begin{aligned} [C_{w\phi}] &= [C_{\phi w}] = 0 \\ [C_{\phi\phi}] &= 0 \end{aligned}$$

The element force vector, \mathbf{F}_i , consists of contributions from the external virtual work, δW , as well as contributions from the variation in kinetic energy, δT . The force terms from the kinetic energy arise due to inertial forces on the blade (e.g. centrifugal force). This vector, like the element matrices, also contains linear and nonlinear terms. Recalling Eqn. (2.107), the elemental force vector can be written as

$$\mathbf{F}_i = (\mathbf{F}_0)_i + (\mathbf{F}_{NL})_i \quad (2.116)$$

The constant force vector terms are given below as

$$\{\mathbf{F}_u\}_0 = \int_0^1 m\Omega^2 x \mathbf{H}_u^T ds \quad (2.117)$$

$$\{\mathbf{F}_v\}_0 = \int_0^1 m(\Omega^2 e_g \cos\theta_0 + \ddot{\theta}_0 e_g \sin\theta_0) \mathbf{H}^T ds - \int_0^1 m\Omega^2 e_g \cos\theta_0 x \mathbf{H}'^T ds$$

$$\{\mathbf{F}_w\}_0 = -\int_0^1 m\Omega^2 (\beta_{pc} x + \ddot{\theta}_0 e_g \sin\theta_0) \mathbf{H}^T ds - \int_0^1 m\Omega^2 e_g \sin\theta_0 x \mathbf{H}'^T ds$$

$$\{\mathbf{F}_\phi\}_0 = -\int_0^1 m k_m^2 \ddot{\theta}_0 + m\Omega^2 (k_{m2}^2 - k_{m1}^2) \sin\theta_0 \cos\theta_0 \mathbf{H}_\phi^T ds$$

$$-\int_0^1 m\Omega^2 \beta_{pc} e_g \cos\theta_0 x \mathbf{H}_\phi^T ds$$

The nonlinear force vector terms are given below as

$$\{\mathbf{F}_u\}_{NL} = -\int_0^1 EA \left(e_A (v'' \hat{\phi} \sin\theta_0 - w'' \hat{\phi} \cos\theta_0) + k_A^2 \frac{\hat{\phi}^{'2}}{2} + k_A^2 \theta'_0 w' v'' \right) \mathbf{H}'_u^T ds \quad (2.118)$$

$$\{\mathbf{F}_v\}_{NL} = \int_0^1 \left((EI_z - EI_y) v'' \hat{\phi} \sin 2\theta_0 - (EI_z - EI_y) w'' \hat{\phi} \cos 2\theta_0 \right) \mathbf{H}''^T ds$$

$$\begin{aligned}
& - \int_0^1 EA e_A u'_e \hat{\phi}' \sin \theta_0 \mathbf{H}''^T ds - \int_0^1 (GJ \hat{\phi}' w' + EA k_A^2 \theta'_0 w' u'_e) \mathbf{H}''^T ds \\
& + \int_0^1 \left(2m \int_x^x (v' \dot{v}' + w' \dot{w}') d\xi \right) \mathbf{H}^T ds - \int_0^1 \left(2v' \int_x^1 m \dot{v} d\xi \right) \mathbf{H}'^T ds \\
\{F_w\}_{NL} &= - \int_0^1 \left((EI_z - EI_y) \cos 2\theta_0 v'' \hat{\phi} + (EI_z - EI_y) \sin 2\theta_0 w'' \hat{\phi} \right) \mathbf{H}''^T ds \\
& + \int_0^1 EA e_A u'_e \hat{\phi}' \cos \theta_0 \mathbf{H}''^T ds - \int_0^1 (GJ \hat{\phi}' v'' + EA k_A^2 \theta'_0 v'' u'_e) \mathbf{H}'^T ds \\
& - \int_0^1 \left(2w' \int_x^1 m \dot{v} d\xi \right) \mathbf{H}'^T ds \\
\{F_{\phi}\}_{NL} &= - \int_0^1 \left((EI_z - EI_y) w''^2 \sin \theta_0 \cos \theta_0 + (EI_z - EI_y) v'' w'' \cos 2\theta_0 \right) \mathbf{H}_{\hat{\phi}}^T ds \\
& + \int_0^1 (EI_z - EI_y) v''^2 \sin \theta_0 \cos \theta_0 \mathbf{H}_{\hat{\phi}}^T ds - \int_0^1 (EA k_A^2 \hat{\phi}' u'_e + GJ w' v'') \mathbf{H}'_{\hat{\phi}}^T ds
\end{aligned}$$

When evaluated at reference position, \mathbf{q}_0 , the nonlinear terms above are combined with the constant force terms, \mathbf{F}_0 (see Eqn. (2.109)). The partial derivative terms in the Taylor series approximation result in the displacement Jacobian matrix.

2.3.3.2 Blade-Fuselage Coupled Matrices

This hub motion induces (kinetic) energy at the blade (see Eqn.2.74) and thereby influences the blade dynamics. Element shape functions can be substituted into the energy expressions (Eqns.2.75) to yield the following blade-hub coupled matrices.

The blade-fuselage mass matrix is

$$[\mathbf{M}_{bf}] = \begin{bmatrix} \mathbf{M}_{ux_F} & \mathbf{M}_{uy_F} & \mathbf{M}_{uz_F} & \mathbf{M}_{v\alpha_s} & \mathbf{M}_{u\phi_s} \\ \mathbf{M}_{vx_F} & \mathbf{M}_{vy_F} & \mathbf{M}_{vz_F} & \mathbf{M}_{v\alpha_s} & \mathbf{M}_{v\phi_s} \\ \mathbf{M}_{w\alpha_s} & \mathbf{M}_{wy_F} & \mathbf{M}_{wz_F} & \mathbf{M}_{w\alpha_s} & \mathbf{M}_{w\phi_s} \\ \mathbf{M}_{\dot{\phi}x_F} & \mathbf{M}_{\dot{\phi}y_F} & \mathbf{M}_{\dot{\phi}z_F} & \mathbf{M}_{\dot{\phi}\alpha_s} & \mathbf{M}_{\dot{\phi}\phi_s} \end{bmatrix} \quad (2.119)$$

where

$$\begin{aligned} \mathbf{M}_{ux_F} &= \int_0^1 m \cos \psi \mathbf{H}_u^T dx \\ \mathbf{M}_{uy_F} &= \int_0^1 m \sin \psi \mathbf{H}_u^T dx \\ \mathbf{M}_{uz_F} &= 0 \\ \mathbf{M}_{v\alpha_s} &= - \int_0^1 mh \cos \psi \mathbf{H}_u^T dx \\ \mathbf{M}_{u\phi_s} &= \int_0^1 mh \sin \psi \mathbf{H}_u^T dx \\ \mathbf{M}_{v\alpha_s} &= - \int_0^1 m(\sin \psi \mathbf{H}^T + \epsilon_g \cos \theta_o \cos \psi \mathbf{H}'^T) dx \\ \mathbf{M}_{vy_F} &= \int_0^1 m(\cos \psi \mathbf{H}^T - \epsilon_g \cos \theta_o \sin \psi \mathbf{H}'^T) dx \\ \mathbf{M}_{vz_F} &= - \int_0^1 m \beta_o \epsilon_g \cos \theta_o \mathbf{H}'^T dx \\ \mathbf{M}_{w\alpha_s} &= \int_0^1 m(h \sin \psi \mathbf{H}^T + \epsilon_g h \cos \theta_o \cos \psi \mathbf{H}'^T) dx \end{aligned}$$

$$\begin{aligned}
\mathbf{M}_{v\phi_s} &= \int_0^1 m(h \cos \psi \mathbf{H}^T - \epsilon_g h \cos \theta_o \sin \psi \mathbf{H}'^T) dx \\
\mathbf{M}_{wx_F} &= - \int_0^1 m \epsilon_g \sin \theta_o \cos \psi \mathbf{H}'^T dx \\
\mathbf{M}_{wy_F} &= - \int_0^1 m \epsilon_g \sin \theta_o \sin \psi \mathbf{H}'^T dx \\
\mathbf{M}_{wz_F} &= \int_0^1 m \mathbf{H}^T dx + \int_0^1 m \beta_p \epsilon_g \sin \theta_o \mathbf{H}'^T dx \\
\mathbf{M}_{w\alpha_s} &= \int_0^1 m((x \cos \psi + x_{CG}) \mathbf{H}^T + h \epsilon_g \sin \theta_o \cos \psi \mathbf{H}'^T) dx \\
\mathbf{M}_{w\phi_s} &= - \int_0^1 m((x \sin \psi + y_{CG}) \mathbf{H}^T + h \epsilon_g \sin \theta_o \sin \psi \mathbf{H}'^T) dx \\
\mathbf{M}_{\dot{\phi}x_F} &= \int_0^1 m \epsilon_g \sin \psi \sin \theta_o \mathbf{H}_\phi^T dx \\
\mathbf{M}_{\dot{\phi}y_F} &= - \int_0^1 m \epsilon_g \cos \psi \sin \theta_o \mathbf{H}_\phi^T dx \\
\mathbf{M}_{\dot{\phi}\alpha_s} &= - \int_0^1 m \epsilon_g (h \sin \theta_o \sin \psi + x_{CG} \cos \theta_o - x \cos \psi \cos \theta_o) \mathbf{H}_\phi^T dx \\
\mathbf{M}_{\dot{\phi}\phi_s} &= - \int_0^1 m \epsilon_g (h \sin \theta_o \cos \psi + y_{CG} \cos \theta_o \\
&\quad + x \sin \psi \cos \theta_o) \mathbf{H}_\phi^T dx
\end{aligned} \tag{2.120}$$

The blade-fuselage damping matrix is

$$[\mathbf{C}_{bf}] = \begin{bmatrix} 0 & 0 & 0 & 0 & 0 \\ 0 & 0 & 0 & 0 & 0 \\ 0 & 0 & 0 & \mathbf{C}_{w\alpha_s} & \mathbf{C}_{w\phi_s} \\ 0 & 0 & 0 & 0 & 0 \end{bmatrix} \tag{2.121}$$

where

$$\begin{aligned}
\mathbf{C}_{w\alpha_s} &= - \int_0^1 2m x \sin \psi \mathbf{H}^T dx \\
\mathbf{C}_{w\phi_s} &= - \int_0^1 2m x \cos \psi \mathbf{H}^T dx
\end{aligned} \tag{2.122}$$

The blade-fuselage stiffness matrix is $[\mathbf{K}_{bf}] = 0$

2.3.3.3 Gaussian Integration

Calculation of the element matrices and load vector requires integration over the nondimensional local element length, ds ($0 \leq s \leq 1$). These integrals are evaluated numerically using a Gauss quadrature procedure. This procedure transforms the integral into a summation as shown below

$$\int_0^1 F(s) ds = \sum_{j=1}^{\text{NGAUSS}} F(s_j) w_j \quad (2.123)$$

where s_j is the local element position of the j th quadrature point and w_j is the weighting factor for the j th quadrature point. NGAUSS is the total number of quadrature points used for the interval $0 \leq s \leq 1$. In general, if more quadrature points are used, a higher degree function can be integrated without error. Typically, for evaluation of all integrals in the structural matrices, six quadrature points are used (i.e., NGAUSS = 6).

2.3.4 Assembly of Element Matrices (and Load Vector)

Assembling these elemental matrices gives the global nonlinear equations of motion in terms of nodal displacements. Assembly must insure compatibility between degrees of freedom at adjoining element nodes.

By assembling elemental matrices over N spatial beam elements, the following expression for the variation of total energy is obtained:

$$\delta\Pi = \int_{\psi_f}^{\psi_i} \delta\mathbf{q}^T (\mathbf{M}_b \ddot{\mathbf{q}} + \mathbf{C}_b \dot{\mathbf{q}} + \mathbf{K}_b \mathbf{q} + \mathbf{M}_{bF} \ddot{\mathbf{x}}_F + \mathbf{C}_{bF} \dot{\mathbf{x}}_F + \mathbf{K}_{bF} \mathbf{x}_F - \mathbf{F}_b) d\psi = 0 \quad (2.124)$$

where the global nodal displacement vector \mathbf{q} , and global blade matrices in space domain \mathbf{M}_b , \mathbf{C}_b , \mathbf{K}_b , and \mathbf{F}_b are defined as follows:

$$\mathbf{q} = \sum_{i=1}^N \mathbf{q}_i \quad (2.125)$$

$$\mathbf{M}_b = \sum_{i=1}^N (\mathbf{M}_b)_i \quad (2.126)$$

$$\mathbf{C}_b = \sum_{i=1}^N (\mathbf{C}_b)_i \quad (2.127)$$

$$\mathbf{K}_b = \sum_{i=1}^N (\mathbf{K}_b)_i \quad (2.128)$$

$$\mathbf{F}_b = \sum_{i=1}^N (\mathbf{F}_b)_i \quad (2.129)$$

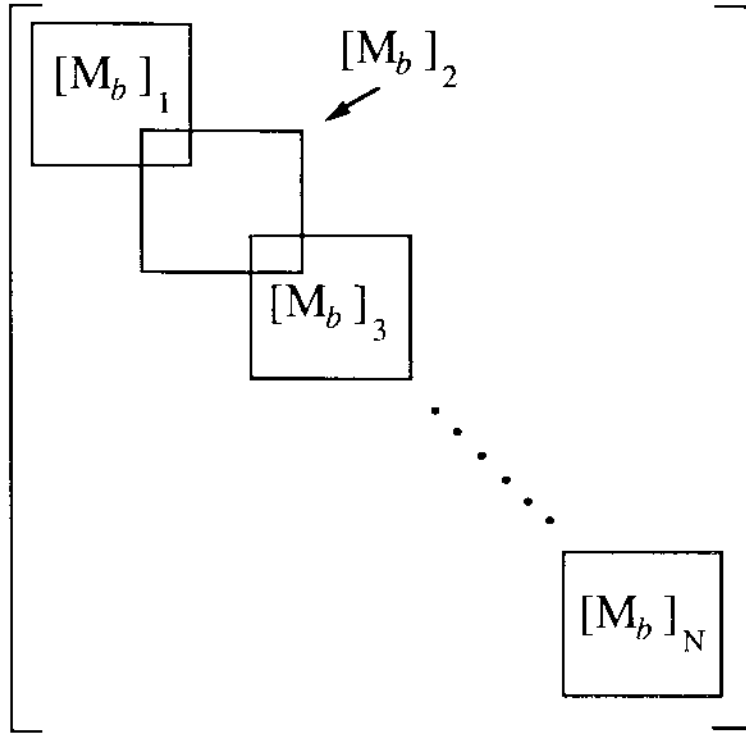
Global blade-fuselage matrices in the space domain \mathbf{M}_{bF} , \mathbf{C}_{bF} , and \mathbf{K}_{bF} , are defined as follows:

$$\mathbf{M}_{bF} = \sum_{i=1}^N (\mathbf{M}_{bF})_i \quad (2.130)$$

$$\mathbf{C}_{bF} = \sum_{i=1}^N (\mathbf{C}_{bF})_i \quad (2.131)$$

$$\mathbf{K}_{bF} = \sum_{i=1}^N (\mathbf{K}_{bF})_i \quad (2.132)$$

In the relations given above, the summations symbolically represent the assembly procedure. This procedure is shown pictorially for the blade mass matrix, \mathbf{M}_b , as



where N is the total number of finite elements used in the rotor blade, and $[\mathbf{M}_b]_i$ is the blade mass matrix for the i th element. The presence of any *double integral* terms, related to axial foreshortening, (see Eqn. (2.73a-b)) destroys the banded structure of the global damping and stiffness matrices.

Since the virtual displacements, $\delta\mathbf{q}$, are arbitrary, the integrand in Eqn.(2.124) must vanish. This gives finite element equations of motion for the blade as follows:

$$\mathbf{M}_b \ddot{\mathbf{q}} + \mathbf{C}_b \dot{\mathbf{q}} + \mathbf{K}_b \mathbf{q} + \mathbf{M}_{bF} \ddot{\mathbf{x}}_F + \mathbf{C}_{bF} \dot{\mathbf{x}}_F + \mathbf{K}_{bF} \mathbf{x}_F = \mathbf{F}_b \quad (2.133)$$

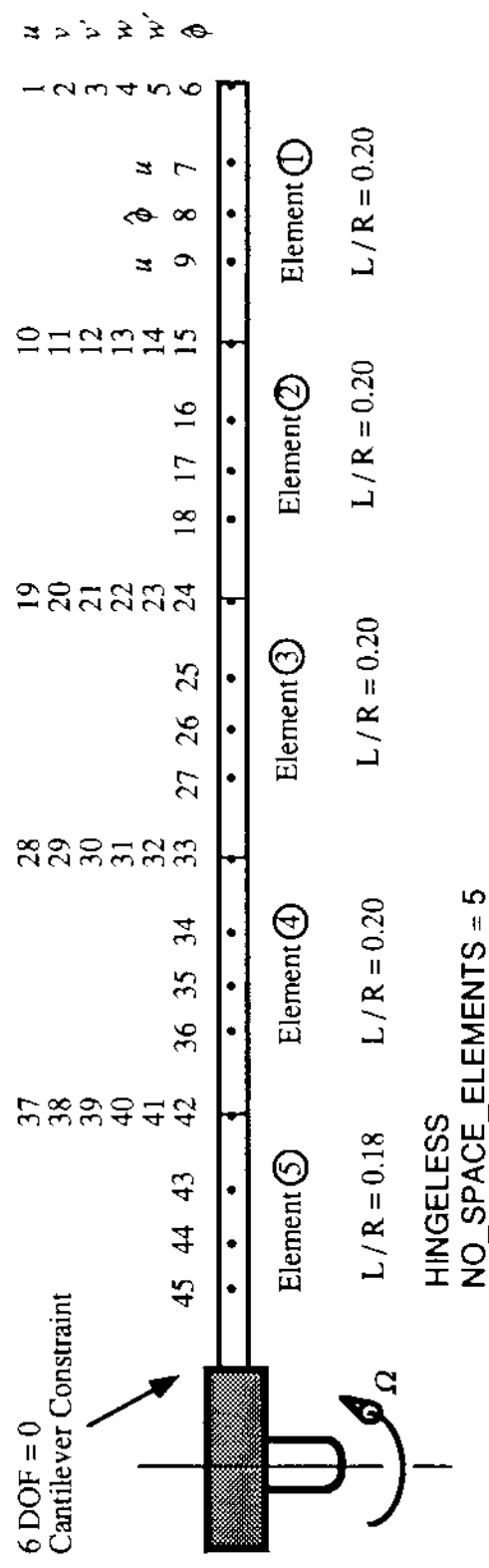
2.3.5 Application of Blade Kinematic Boundary Conditions

Figure 2.8 shows the numbering scheme used for blade finite elements and global degrees of freedom. Element local degrees of freedom are described in Figure 2.6 and Section 2.5. Figure 2.8 also illustrates how the kinematic boundary conditions are applied for hingeless and articulated rotor configurations.

For a hingeless rotor blade, the blade is assumed to be cantilevered at the blade root. This assumption implies that the response quantities u , v , v' , w , w' , and $\hat{\phi}$ to be zero at the root. For an articulated rotor, the constraint on v' is relaxed at the lag hinge, and the constraint on w' is relaxed at the flap hinge. Geometric boundary conditions are enforced during the assembly of the element matrices.

The bearingless rotor boundary conditions are dependent on the particular configuration and design of the rotor. Bearingless rotor boundary conditions can be identical to hingeless rotor conditions, or they can be very complicated. The more complex designs involve various combinations of kinematic constraints. Boundary conditions for bearingless rotors will be discussed in more detail in a section specifically devoted to bearingless rotors.

Hingeless Rotor with blade starting at 2% radial location



Articulated Rotor with flap hinge at 2% radial location and no lag hinge

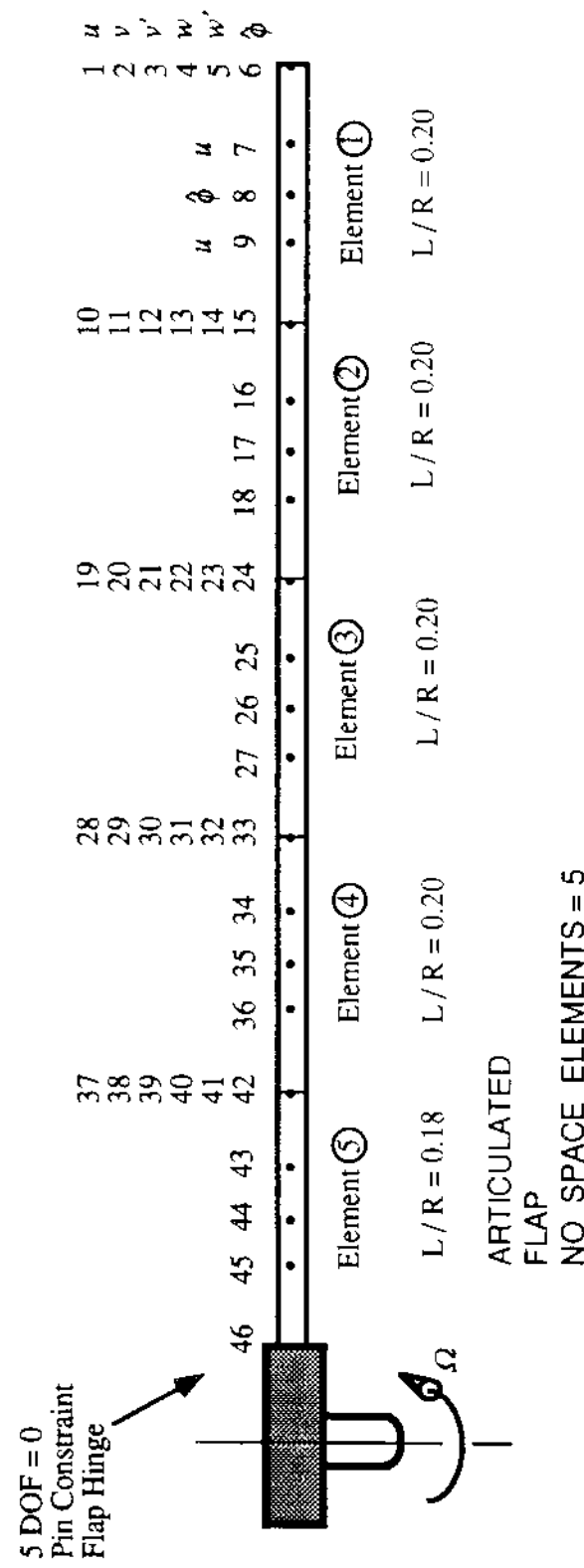
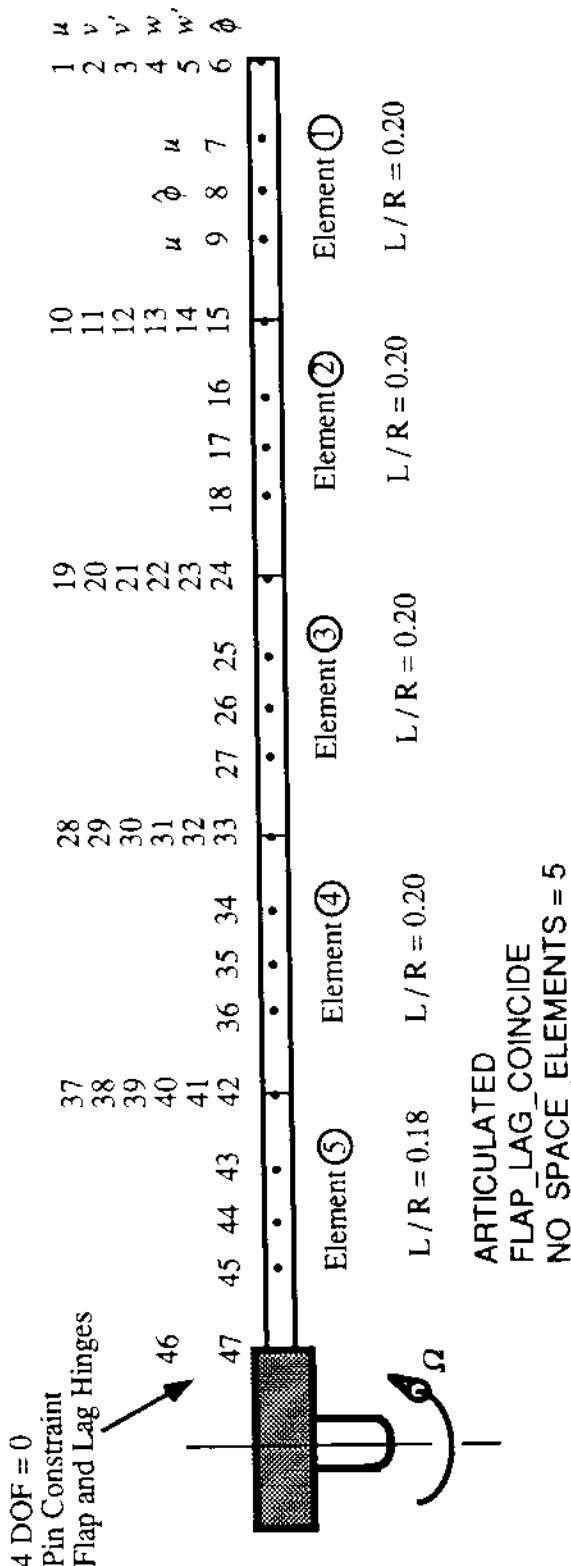


Figure 2.8 Global Degrees of Freedom and Finite Element Model Descriptions

Articulated Rotor with coincident flap and lag hinges at 2% radial location



Articulated Rotor with flap hinge at 2% and lag hinge at 5% radial location

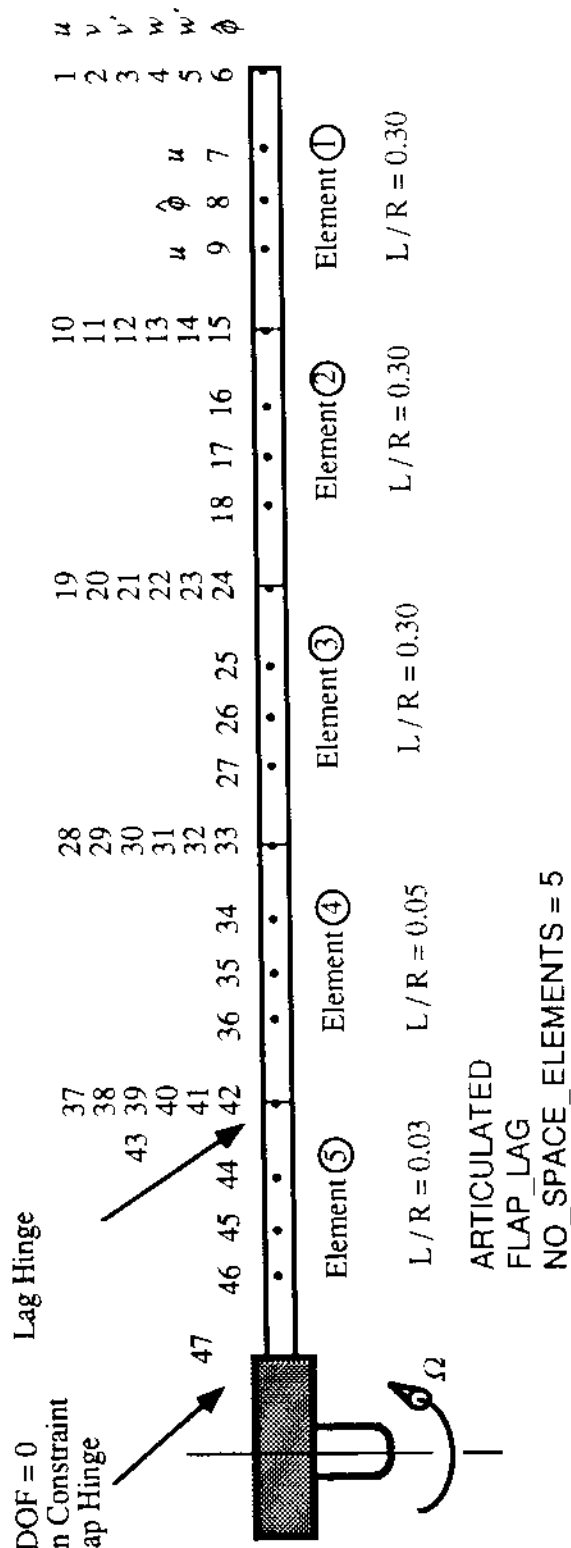


Figure 2.8 (continued) Global Degrees of Freedom and Finite Element Model Descriptions

2.4 Fuselage Equations of Motion

2.4.1 Finite Element Discretization of the Blade Dependent Degrees of Freedom

Motion of the fuselage is described by five degrees of freedom as

$$\mathbf{x}_F^T = [x_F, y_F, z_F, \alpha_s, \phi_s] \quad (2.134)$$

where x_F , y_F , and z_F are fuselage motions along the inertial axis X_I , Y_I , and Z_I respectively, α_s is the fuselage rotation about the X_I axis (positive nose-down), and ϕ_s is the rotation about the X_I axis (positive advancing-side down). The discretized equations governing the motion of the fuselage are derived by considering the variation in the discretized virtual energy expressions due to a variation in the fuselage motion, $\delta\mathbf{x}_F$.

The discretized virtual energy expression (for the blade) given in Eqn. (2.83), can be written in terms of the blade element nodal quantities and fuselage degrees of freedom in the space domain. Recalling from Eqn. (2.84), for the i th element of the b th blade,

$$\Delta_i = \delta U_i - \delta T_i - \delta W_i \quad (2.135)$$

where δU is the virtual strain energy due to a virtual displacement in fuselage motion, $\delta\mathbf{x}_F$, and δT is the virtual kinetic energy due to a virtual displacement in fuselage motion, $\delta\mathbf{x}_F$. The δW is the virtual work done by external forces due to a virtual displacement in fuselage motion, $\delta\mathbf{x}_F$. For the equations governing the *motion of the fuselage*, there is no variation of the blade motion (i.e. $\delta\mathbf{q}_i = 0$). Since there is no variation in blade motion, the kinetic energy of the b th blade given in Eqn. (2.74) simplifies to

$$\delta T_b = \int_0^R (T_{x_F} \delta x_F + T_{y_F} \delta y_F + T_{z_F} \delta z_F + T_{\alpha_s} \delta \alpha_s + T_{\phi_s} \delta \phi_s) dx \quad (2.136)$$

The dependence of the blade energy variation on the blade motion, \mathbf{q}_i , fuselage motion, \mathbf{x}_F , control settings θ_i , inflow, λ , and azimuth position, ψ , is shown below.

$$(\delta T_i)_b = \delta T_i(\delta \mathbf{x}_F, \theta_i, \psi, \mathbf{q}_i, \dot{\mathbf{q}}_i, \ddot{\mathbf{x}}_F, \mathbf{q}_i \dot{\mathbf{x}}_F, \mathbf{q}_i \ddot{\mathbf{x}}_F)_b \quad (2.137)$$

$$(\delta W_i)_b = \delta W_i(\delta \mathbf{x}_F, \theta_i, \psi, \mathbf{q}_i, \dot{\mathbf{q}}_i, \mathbf{q}_i^2, \mathbf{q}_i \dot{\mathbf{q}}_i, \mathbf{x}_F, \dot{\mathbf{x}}_F, \ddot{\mathbf{q}}_i, \lambda)_b$$

Note that the strain energy of the blade does not depend on fuselage motion (see Eqn. (2.105)).

The dependence of the fuselage energy variation on the blade motion, \mathbf{q}_i , fuselage motion, \mathbf{x}_F , control settings θ_i , inflow, λ , and azimuth position, ψ , is shown below.

$$\delta U_F = \delta U_F(\delta \mathbf{x}_F, \mathbf{x}_F) \quad (2.138)$$

$$\delta T_F = \delta T_F(\delta \mathbf{x}_F, \dot{\mathbf{x}}_F, \dot{\mathbf{x}}_F^2)$$

$$\delta W_F = \delta W_F(\delta \mathbf{x}_F, \mathbf{x}_F, \dot{\mathbf{x}}_F)$$

Note that the fuselage energies depend only on fuselage motions.

Regarding the notation used in the above expressions: \mathbf{q}_i^2 indicates second order nonlinearity in blade motion terms, and $\mathbf{q}_i \dot{\mathbf{x}}_F$ indicates second order bilinear terms involving blade deflection and fuselage velocity. Other dependencies in Eqns. (2.137) and (2.138) are defined in a similar manner.

The variational energy expressions given above yield the uncoupled fuselage mass, damping and stiffness matrices \mathbf{M}_{FF} , \mathbf{C}_{FF} , and \mathbf{K}_{FF} respectively. Substitution of element shape functions into the variational energy expressions yields the coupled fuselage-blade element matrices, $(\mathbf{M}_{Fb})_i$, $(\mathbf{C}_{Fb})_i$, and $(\mathbf{K}_{Fb})_i$. These matrices arise from the contributions to blade energy due to fuselage motion (see Eqn. (2.75)).

After assembling the fuselage-blade coupling matrices over N spatial finite elements in the blade (see section 2.3.4), the variation in total energy due to variation in fuselage motion is given by

$$\delta\Pi = \int_{\psi_i}^{\psi_f} \delta\mathbf{x}_F^\top (\mathbf{M}_{Fb}\ddot{\mathbf{q}} + \mathbf{C}_{Fb}\dot{\mathbf{q}} + \mathbf{K}_{Fb}\mathbf{q} + \mathbf{M}_{FF}\ddot{\mathbf{x}}_F + \mathbf{C}_{FF}\dot{\mathbf{x}}_F + \mathbf{K}_{FF}\mathbf{x}_F - \mathbf{F}_F) d\psi = 0 \quad (2.139)$$

where \mathbf{M}_{Fb} , \mathbf{C}_{Fb} , and \mathbf{K}_{Fb} are the global fuselage-blade coupling matrices, and \mathbf{M}_{FF} , \mathbf{C}_{FF} , and \mathbf{K}_{FF} are the global fuselage matrices. The global fuselage force vector, \mathbf{F}_F , is due to aerodynamic forces on the fuselage (e.g. drag). The aerodynamic force vector is derived in Chapter 3. Since the virtual displacements, $\delta\mathbf{x}_F$, are arbitrary, the integrand in Eqn. (2.139) must vanish. This gives finite element equations of motion for the fuselage as

$$\mathbf{M}_{Fb}\ddot{\mathbf{q}} + \mathbf{C}_{Fb}\dot{\mathbf{q}} + \mathbf{K}_{Fb}\mathbf{q} + \mathbf{M}_{FF}\ddot{\mathbf{x}}_F + \mathbf{C}_{FF}\dot{\mathbf{x}}_F + \mathbf{K}_{FF}\mathbf{x}_F = \mathbf{F}_F \quad (2.140)$$

The following sections describe in detail the fuselage-blade element matrices, as well as, the uncoupled fuselage matrices.

2.4.2 Fuselage Matrices

The fuselage mass matrix is

$$[\mathbf{M}_{FF}] = \begin{bmatrix} \mathbf{M}_{x_F x_F} & 0 & 0 & \mathbf{M}_{x_F \alpha_s} & 0 \\ 0 & \mathbf{M}_{y_F y_F} & 0 & 0 & \mathbf{M}_{y_F \phi_s} \\ 0 & 0 & \mathbf{M}_{z_F z_F} & \mathbf{M}_{z_F \phi_s} & \mathbf{M}_{z_F \phi_s} \\ \mathbf{M}_{\alpha_s x_F} & 0 & \mathbf{M}_{\alpha_s z_F} & \mathbf{M}_{\alpha_s \phi_s} & \mathbf{M}_{\alpha_s \phi_s} \\ 0 & \mathbf{M}_{\phi_s y_F} & \mathbf{M}_{\phi_s z_F} & \mathbf{M}_{\phi_s \phi_s} & \mathbf{M}_{\phi_s \phi_s} \end{bmatrix} \quad (2.141)$$

where

$$\begin{aligned} \mathbf{M}_{x_F x_F} &= m_F + \int_0^1 m \, dx \\ \mathbf{M}_{x_F \alpha_s} &= - \int_0^1 m h \, dx \\ \mathbf{M}_{y_F y_F} &= m_F + \int_0^1 m \, dx \\ \mathbf{M}_{y_F \phi_s} &= \int_0^1 m h \, dx \\ \mathbf{M}_{z_F z_F} &= m_F + \int_0^1 m \, dx \\ \mathbf{M}_{z_F \phi_s} &= \int_0^1 m(x \cos \psi + x_{CG}) \, dx \\ \mathbf{M}_{x_F \phi_s} &= - \int_0^1 m(x \sin \psi + y_{CG}) \, dx \\ \mathbf{M}_{\alpha_s x_F} &= - \int_0^1 m h \, dx \\ \mathbf{M}_{\alpha_s z_F} &= \int_0^1 m(x \cos \psi + x_{CG}) \, dx \\ \mathbf{M}_{\alpha_s \phi_s} &= I_{\alpha_s} + \int_0^1 m(x^2 \cos^2 \psi + h^2 + x_{CG}^2 + 2x x_{CG} \cos \psi) \, dx \\ \mathbf{M}_{\phi_s y_F} &= - \int_0^1 m(x^2 \sin \psi \cos \psi + x y_{CG} \cos \psi + x_{CG} y_{CG} + x x_{CG} \sin \psi) \, dx \\ \mathbf{M}_{\phi_s z_F} &= \int_0^1 m h \, dx \\ \mathbf{M}_{\phi_s \phi_s} &= - \int_0^1 m(x \sin \psi + y_{CG}) \, dx \end{aligned}$$

$$\begin{aligned}\mathbf{M}_{\phi_s \phi_s} &= - \int_0^1 m(x^2 \cos \psi \sin \psi + x_{CG} y_{CG} + x y_{CG} \cos \psi + x x_{CG} \sin \psi) dx \\ \mathbf{M}_{\phi_s \phi_s} &= I_{\phi_s} + \int_0^1 m(x^2 \sin^2 \psi + h^2 + y_{CG}^2 + 2x y_{CG} \sin \psi) dx\end{aligned}\quad (2.142)$$

The fuselage damping matrix is

$$[\mathbf{C}_{FF}] = \begin{bmatrix} 0 & 0 & 0 & 0 & 0 \\ 0 & 0 & 0 & 0 & 0 \\ 0 & 0 & 0 & \mathbf{C}_{z_F \alpha_s} & \mathbf{C}_{z_F \phi_s} \\ 0 & 0 & 0 & \mathbf{C}_{\alpha_s \alpha_s} & \mathbf{C}_{\alpha_s \phi_s} \\ 0 & 0 & 0 & \mathbf{C}_{\phi_s \alpha_s} & \mathbf{C}_{\phi_s \phi_s} \end{bmatrix} \quad (2.143)$$

where

$$\begin{aligned}\mathbf{C}_{z_F \alpha_s} &= - \int_0^1 2mx \sin \psi dx \\ \mathbf{C}_{z_F \phi_s} &= - \int_0^1 2mx \cos \psi dx \\ \mathbf{C}_{\alpha_s \alpha_s} &= \int_0^1 2m(x^2 \sin \psi \cos \psi + x x_{CG} \sin \psi) dx \\ \mathbf{C}_{\alpha_s \phi_s} &= \int_0^1 2m(x^2 \cos^2 \psi + x x_{CG} \cos \psi) dx \\ \mathbf{C}_{\phi_s \alpha_s} &= \int_0^1 m(2x^2 \sin^2 \psi + 2x y_{CG} \sin \psi) dx \\ \mathbf{C}_{\phi_s \phi_s} &= \int_0^1 2m(x^2 \cos \psi \sin \psi + x y_{CG} \cos \psi) dx\end{aligned}\quad (2.144)$$

The fuselage stiffness matrix is

$$[\mathbf{K}_{FF}] = \begin{bmatrix} \mathbf{K}_{x_F} & 0 & 0 & 0 & 0 \\ 0 & \mathbf{K}_{y_F} & 0 & 0 & 0 \\ 0 & 0 & \mathbf{K}_{z_F} & 0 & 0 \\ 0 & 0 & 0 & \mathbf{K}_{\alpha_s} & 0 \\ 0 & 0 & 0 & 0 & \mathbf{K}_{\phi_s} \end{bmatrix} \quad (2.145)$$

where

$$\mathbf{K}_{x_F x_F} = K_x$$

$$\mathbf{K}_{x_F y_F} = K_y$$

$$\mathbf{K}_{x_F z_F} = K_z$$

$$\begin{aligned}\mathbf{K}_{x_F x_F} &= K_\alpha \\ \mathbf{K}_{x_F x_I} &= K_\phi\end{aligned}\tag{2.146}$$

2.4.3 Fuselage-Blade Coupled Matrices

The fuselage-blade mass matrix is

$$[\mathbf{M}_{Fb}] = \begin{bmatrix} \mathbf{M}_{x_F u} & \mathbf{M}_{x_F v} & \mathbf{M}_{x_F w} & \mathbf{M}_{x_F \dot{\phi}} \\ \mathbf{M}_{y_F u} & \mathbf{M}_{y_F v} & \mathbf{M}_{y_F w} & \mathbf{M}_{y_F \dot{\phi}} \\ \mathbf{M}_{z_F u} & \mathbf{M}_{z_F v} & \mathbf{M}_{z_F w} & \mathbf{M}_{z_F \dot{\phi}} \\ \mathbf{M}_{\alpha_s u} & \mathbf{M}_{\alpha_s v} & \mathbf{M}_{\alpha_s w} & \mathbf{M}_{\alpha_s \dot{\phi}} \\ \mathbf{M}_{\varphi_s u} & \mathbf{M}_{\varphi_s v} & \mathbf{M}_{\varphi_s w} & \mathbf{M}_{\varphi_s \dot{\phi}} \end{bmatrix} \quad (2.147)$$

where

$$\mathbf{M}_{x_F u} = 0$$

$$\mathbf{M}_{x_F v} = - \int_0^1 m \sin \psi \mathbf{H}^T dx$$

$$\mathbf{M}_{x_F w} = 0$$

$$\mathbf{M}_{x_F \dot{\phi}} = 0$$

$$\mathbf{M}_{y_F u} = 0$$

$$\mathbf{M}_{y_F v} = \int_0^1 m \cos \psi \mathbf{H}^T dx$$

$$\mathbf{M}_{y_F w} = 0$$

$$\mathbf{M}_{y_F \dot{\phi}} = 0$$

$$\mathbf{M}_{z_F u} = 0$$

$$\mathbf{M}_{z_F v} = 0$$

$$\mathbf{M}_{z_F w} = \int_0^1 m \mathbf{H}^T dx$$

$$\mathbf{M}_{z_F \dot{\phi}} = 0$$

$$\mathbf{M}_{\alpha_s u} = - \int_0^1 h \cos \psi \mathbf{H}_u^T dx$$

$$\begin{aligned}
\mathbf{M}_{\alpha, u} &= \int_0^1 m h \sin \psi \mathbf{H}^T dx \\
\mathbf{M}_{\alpha, w} &= \int_0^1 m(x \cos \psi + x_{CG}) \mathbf{H}^T dx \\
\mathbf{M}_{\alpha, \dot{\phi}} &= 0 \\
\mathbf{M}_{\phi, u} &= \int_0^1 m h \sin \psi \mathbf{H}_u^T dx \\
\mathbf{M}_{\phi, v} &= \int_0^1 m h \cos \psi \mathbf{H}^T dx \\
\mathbf{M}_{\phi, w} &= - \int_0^1 m(x \sin \psi + y_{CG}) \mathbf{H}^T dx \\
\mathbf{M}_{\phi, \dot{\phi}} &= 0
\end{aligned} \tag{2.148}$$

The fuselage blade damping matrix $[\mathbf{T}\mathbf{C}] = [\mathbf{C}_{FB}]$ consists of

$$[\mathbf{C}_{FB}] = \begin{bmatrix} 0 & \mathbf{C}_{x_F v} & 0 & 0 \\ 0 & \mathbf{C}_{y_F v} & 0 & 0 \\ 0 & 0 & 0 & 0 \\ 0 & \mathbf{C}_{\dot{\phi}, v} & 0 & 0 \\ 0 & \mathbf{C}_{\phi, v} & 0 & 0 \end{bmatrix} \tag{2.149}$$

where

$$\begin{aligned}
\mathbf{C}_{x_F v} &= - \int_0^1 2m \cos \psi \mathbf{H}^T dx \\
\mathbf{C}_{y_F v} &= - \int_0^1 2m \sin \psi \mathbf{H}^T dx \\
\mathbf{C}_{\alpha, u} &= \int_0^1 2mh \sin \psi \mathbf{H}_u^T dx \\
\mathbf{C}_{\alpha, v} &= \int_0^1 2mh \cos \psi \mathbf{H}^T dx \\
\mathbf{C}_{\phi, u} &= \int_0^1 2mh \cos \psi \mathbf{H}_u^T dx \\
\mathbf{C}_{\phi, v} &= - \int_0^1 2mh \sin \psi \mathbf{H}^T dx
\end{aligned} \tag{2.150}$$

The fuselage-blade stiffness matrix is

$$[\mathbf{K}_{Fb}] = \begin{bmatrix} 0 & \mathbf{K}_{x_Fv} & \mathbf{K}_{x_Fw} & 0 \\ 0 & \mathbf{K}_{y_Fv} & \mathbf{K}_{y_Fw} & 0 \\ 0 & 0 & 0 & 0 \\ 0 & \mathbf{K}_{\alpha_sv} & \mathbf{K}_{\alpha_sw} & 0 \\ 0 & \mathbf{K}_{\phi_sv} & \mathbf{K}_{\phi_sw} & 0 \end{bmatrix} \quad (2.151)$$

where

$$\begin{aligned} \mathbf{K}_{x_Fv} &= \int_0^1 m \sin \psi \mathbf{H}^T dx \\ \mathbf{K}_{y_Fv} &= - \int_0^1 m \cos \psi \mathbf{H}^T dx \\ \mathbf{K}_{\alpha_sv} &= \int_0^1 mh \sin \psi \mathbf{H}^T dx \\ \mathbf{K}_{\alpha_sw} &= \int_0^1 mx \cos \psi \mathbf{H}^T dx \\ \mathbf{K}_{\phi_sv} &= - \int_0^1 mh \cos \psi \mathbf{H}^T dx \\ \mathbf{K}_{\phi_sw} &= \int_0^1 mx \sin \psi \mathbf{H}^T dx \end{aligned} \quad (2.152)$$

2.5 UMARC Implementation of Structural Modeling

2.5.1 Computation of Blade Matrices (SUBROUTINE STRUCT)

The structures formulation presented in the preceding section describes the theoretical development of the element mass matrix, stiffness matrix, damping matrix, and load vector. The structural contribution to the load vector arises from inertial forces such as the centrifugal force. These matrices are then assembled to yield the global discretized equations of motion. In UMARC, calculation of the structural contributions to the element matrices and load vector is carried out in the SUBROUTINE STRUCT. The following section will describe:

- function of SUBROUTINE STRUCT (general tasks)
- when and where SUBROUTINE STRUCT is called
- input to and output from SUBROUTINE STRUCT
(see Figures 2.8a and 2.8b)
- performance and specific tasks of SUBROUTINE STRUCT

2.5.1.1 Function of SUBROUTINE STRUCT

This subroutine calculates the structural blade contributions to the element load vector, $\{EQ\}$ (due to inertial forces), element mass matrix, element stiffness matrix, and element damping matrix. This subroutine also calculates the structural (rotor) contributions to the blade-fuselage, fuselage-blade and fuselage matrices used in aeromechanical stability analysis. Both the linear and nonlinear terms are calculated within SUBROUTINE STRUCT. Structural nonlinearities present in the variation of strain energy, δU , are evaluated by computing the displacement Jacobian matrix.

2.5.1.2 Calling of SUBROUTINE STRUCT

In all cases, SUBROUTINE STRUCT is called within a loop over the number of spatial elements. During response calculations, SUBROUTINE STRUCT is called within a loop over the number of time elements also.

SUBROUTINE STRUCT is called from 4 locations within UMARC:

1) From SUBROUTINE BLDVIB

Flag: INDRNS = -1

Function: Calculate element mass matrix, [EM], and stiffness matrix, [EK], about the undeflected blade position ($\{EU\} = \{0\}$).

These matrices are used in calculating rotating vacuum frequencies and mode shapes about the initial undeflected blade position. These frequencies and mode shapes are required for forming the normal mode equations for steady response calculations.

2) From SUBROUTINE ASBGBM (within SUBROUTINE TRIM)

Flag: INDRNS = 1

Function: Calculate element mass matrix, [EM], damping matrix, [EC], stiffness matrix, [EK], displacement Jacobian matrix, [DFX], and load vector, [EQ], about the deflected blade position ($\{EU\} \neq \{0\}$).

These matrices (and vector) are used in calculating steady response during the iterative coupled trim procedure. This procedure uses both the finite element method in time and the finite element method in space to determine converged steady periodic response $\{EU\}_{trim}$.

3) From SUBROUTINE STAB

Flag: INDRNS = -2

Function: Calculate element mass matrix, [EM], and stiffness matrix, [EK], about the trim deflected blade position ($\{EU\} = \{EU\}_{trim}$).

These matrices are used in calculating vacuum frequencies and mode shapes about the trim deflected blade position. These frequencies and mode shapes are required for stability analysis using normal modes.

4) From SUBROUTINE ASBGM2 (within SUBROUTINE STAB)

Flag: INDRNS = 2

Function: Calculate element mass matrix, [EM], damping matrix, [EC], stiffness matrix, [EK], and displacement Jacobian matrix, [DFX], about the trim deflected blade position ($\{EU\} = \{EU\}_{trim}$).

These matrices are used in calculating linearized stability. Note that for linearized stability analysis, the load vector, [EQ], is not used.

Note: Blade-Fuselage, Fuselage-Blade, and Fuselage matrices are also calculated when INDRNS = 2 and INDFUS = 1
(Aeromechanical Stability Analysis)

2.5.1.3 Input to SUBROUTINE STRUCT

Input through Argument List

GQP	=	Gauss quadrature sampling points (local element axis)
GQW	=	Gauss quadrature weighting factors
EU	=	element displacement vector $\{EU\}^T = \mathbf{q}_i^T = [u_1, u_2, u_3, u_4, v_1, v'_1, v_2, v'_2, w_1, w'_1, w_2, w'_2, \hat{\phi}_1, \hat{\phi}_2, \hat{\phi}_3]$
SHI	=	Azimuth angle, ψ
NGAUSS	=	number of spatial gaussian integration points
NEDOF	=	number of spatial element degrees of freedom
XBI	=	x coordinate of left node of element
EL	=	element length, l
L	=	element number (1 = tip element)
AXFI	=	total axial force at right node of element
INDRNS	:	-1 for vacuum frequencies and mode shapes (undeflected position) -2 for vacuum frequencies and mode shapes (about trim position) 1 for response calculation 2 for stability analysis
INDNL	:	0 for neglecting all nonlinearities 1 for including all nonlinearities
IFLAG	:	(not used)
TLAM	=	Transformation matrix for special finite element for advanced tip
GU	=	Global displacement vector
GUD	=	Global velocity vector
INDEG	=	Connectivity matrix
ELV	=	Array containing all element lengths

Input through Common Blocks

Common block COMMON /STRUC/ :	All elastic and inertial properties for each element (i.e., EIY , EIZ , GJ)
Common block COMMON /AEROD/ :	Precone angle, $BTP = \beta_p$
Common block COMMON /RADSHR/ :	Parameters for radial shortening effect
Common block COMMON /TRIMV/ :	Cyclic pitch control inputs TH1C and TH1S
Common block COMMON /CFUNC/ :	Collective pitch control input TH75, and linear twist slope, THTW
Common block COMMON /PBRNG/ :	Parameters for " δ_3 effect", articulated rotor
Common block COMMON /PERT/ :	Flags to indicate stability analysis, IPERT
Common block COMMON /RINPUT/	Fuselage CG offsets, HBAR, XCG, YCG
Common block COMMON /FUSE/	Flags to indicate if hub motion is used, INDFUS

2.5.1.4 Output from SUBROUTINE STRUCT

Output through Argument List

EK	=	element stiffness matrix, $(\mathbf{K}_b)_i$
EC	=	element damping matrix, $(\mathbf{C}_b)_i$
EM	=	element mass matrix, $(\mathbf{M}_b)_i$
EQ	=	element load vector, $(\mathbf{F}_b)_i$
DFX	=	element displacement Jacobian matrix

$$[\text{DFX}] = \frac{\partial(\mathbf{F}_{NL})_i}{\partial q_i}$$

EMAS	=	coupled blade-fuselage mass matrix $(\mathbf{M}_{bF})_i$
ECAS	=	coupled blade-fuselage damping matrix $(\mathbf{C}_{bF})_i$
TMS	=	coupled fuselage-blade mass matrix $(\mathbf{M}_{Fb})_i$
TCS	=	coupled fuselage-blade damping matrix $(\mathbf{C}_{Fb})_i$
TKS	=	coupled fuselage-blade stiffness matrix $(\mathbf{K}_{Fb})_i$
TPS	=	fuselage damping matrix \mathbf{C}_{FF}
UMS	=	fuselage mass matrix \mathbf{M}_{FF}
DFXC	=	Nonlinear "double integral" stiffness matrix (all elements)
DFXCD	=	Nonlinear "double integral" damping matrix (all elements)
TCSD	=	Nonlinear "double integral" coupled fuselage-blade damping matrix
TKSD	=	Nonlinear "double integral" coupled fuselage-blade stiffness matrix

2.5.1.5 Performance and Specific Tasks of SUBROUTINE STRUCT

- 1) Initialize matrices and load vector.
- 2) If response or stability, INDRNS = 1 or 2, calculate $\sin\psi$ and $\cos\psi$ for input azimuth angle ψ .
- 3) Calculate rigid pitch inertia, $\ddot{\theta}_0$
- 4) Calculate combinations of elastic constants.
- 5) Calculate square of right node location for the element.
- 6) Set sweep connectivity parameters (see Chapter 6)

If response or stability, INDRNS = 1 or 2, and nonlinear terms included, INDNL = 1:
Calculate and store the required terms for nonlinear double integrals related to axial foreshortening. (Eqn. 2.118)

If 1st element ($L = 1$) and number of elements (MSEL T) > 1:
Calculate and store the required terms for nonlinear double integrals (Eqn. 2.118)

- 7) Initialize matrices required for foreshortening terms.

Enter loop over the number of spatial finite elements.

DO 1300 N = I, MSEL T

- 8) Get elemental displacement and velocity vectors.

Enter loop over the number of spatial gaussian integration points.

DO 5731 N = 1, NGAUSS

- 9) Compute shape functions at elemental gauss point.
- 10) Compute deflections at gauss point.
- 11) Compute required products for double integral expressions (Eqn. 2.118)

5731 CONTINUE

1300 CONTINUE

Compute nonlinear foreshortening terms required for current (Lth) element.

- 12) Initialized nonlinear matrices.

Enter loop over the number of spatial gaussian integration points for current element (L).

DO 5832 N = 1, NGAUSS

- 13) Define reduced length of "partial element" (based on location of Nth Gauss Point).

Enter loop over the number of spatial gaussian integration points for "partial element".

DO 5833 N1 = 1, NGAUSS

- 14) Compute shape functions at elemental gauss point.
- 15) Compute deflections at gauss point.
- 16) Compute required products for double integral expressions (Eqn. 2.118)

5833 CONTINUE

5832 CONTINUE

End preliminary calculations for foreshortening terms.

Begin calculations for matrices and load vector for "Lth" element.

Enter loop over the number of spatial gaussian integration points.

DO 5000 N = 1, NGAUSS

- 17) Calculate location of Gauss point within the element, and along the blade.
- 18) Evaluate all necessary shape functions at Gauss point location (Eqns. 2.88-2.90)
- 19) Calculate deflections for nonlinear terms
- 20) Evaluate rigid twist at Gauss point
 - If linear twist, evaluate twist explicitly (Eqn. 2.6)
 - If Gazelle, evaluate twist via user defined subroutine (SUBROUTINE GZTWST)
 - If ITR-BMR, evaluate twist via user defined subroutine (SUBROUTINE TWISTX)
 - If articulated with δ_3 effect, evaluate twist including couplings
- 21) Calculate trigonometric functions involving rigid twist
- 22) Calculate functions involving trigonometric functions and elastic coefficients
- 23) Calculate products of nonlinear terms
- 24) Calculate total axial force, F_A , and axial slope, u' , at Gauss point. Add contributions to axial force from centrifugal force, radial aerodynamic force, and Coriolis force (Eqn. 2.37).
- 25) If no axial modes used (for stability analysis), calculate radial shortening terms.
This is required to properly capture Coriolis damping forces.

Linear load vector and matrices:

Enter loop over element axial and bending degrees of freedom (rows)

DO 600 I = 1, 4

- 26) If response calculations, calculate load vector (axial and bending terms,
Eqn. 2.117)

Enter loop over element axial and bending degrees of freedom (columns)

DO 800 J = 1, 4

- 27) Calculate stiffness matrix (axial and bending terms, Eqn. 2.114)
28) If response calculation or stability analysis, calculate damping matrix (axial and
bending terms, Eqn. 2.115)
29) Calculate mass matrix (axial and bending terms, Eqn. 2.113)

800 CONTINUE

Enter loop over element torsion degrees of freedom (columns)

DO 600 J = 1, 3

- 30) Calculate stiffness matrix (coupled axial-torsion and bending-torsion terms,
Eqn. 2.114)
31) Calculate mass matrix (coupled axial-torsion and bending-torsion terms,
Eqn. 2.113)

600 CONTINUE

Enter loop over element torsion degrees of freedom (rows)

DO 1200 I = 1, 3

- 32) If response calculation, calculate load vector (torsion terms, Eqn. 2.117)

DO 1200 J = 1, 3

Enter loop over element torsion degrees of freedom (columns)

- 33) Calculate stiffness matrix (torsion terms, Eqn. 2.114)

- 34) Calculate mass matrix (torsion terms, Eqn. 2.113)

1200 CONTINUE

Nonlinear load vector and matrices (if not neglected, INDNL ≠ 0, and not vacuum frequencies and mode shapes about initial undeflected position, INDRNS ≠ -1) :

- 35) Calculate nonlinear terms in δU and δT for use in nonlinear part of load vector

Enter loop over element axial, bending, and torsion degrees of freedom (rows)

DO 2000 I = 1, 4

- 36) If response calculation, calculate nonlinear load vector (axial, bending, and torsion terms, Eqn. 2.118)

2000 CONTINUE

- 37) Calculate nonlinear terms for "displacement Jacobian matrix, [DFX]"

See Eqn. 2.108, and recall, $[DFX] = \frac{\partial(F_{NL})_i}{\partial q_i}$

Enter loop over element axial and bending degrees of freedom (rows)

DO 2200 I = 1, 4

Enter loop over element axial and bending degrees of freedom (columns)

DO 2100 J = 1, 4

- 38) Calculate "displacement Jacobian matrix, [DFX]" (axial and bending terms)

2100 CONTINUE

Enter loop over element torsion degrees of freedom (columns)

DO 2200 J = 1, 3

- 39) Calculate "displacement Jacobian matrix, [DFX]" (coupled axial-torsion and bending-torsion terms)

2200 CONTINUE

- 40) If stability analysis (INDRNS = 2) and fuselage motion included (INDFUS = 1), then calculate blade-fuselage (Eqns 2.119-2.122), fuselage-blade (Eqns 2.147-2.152), and fuselage matrices (Eqns 2.141-2.146).

5000 CONTINUE

Return and End Subroutine

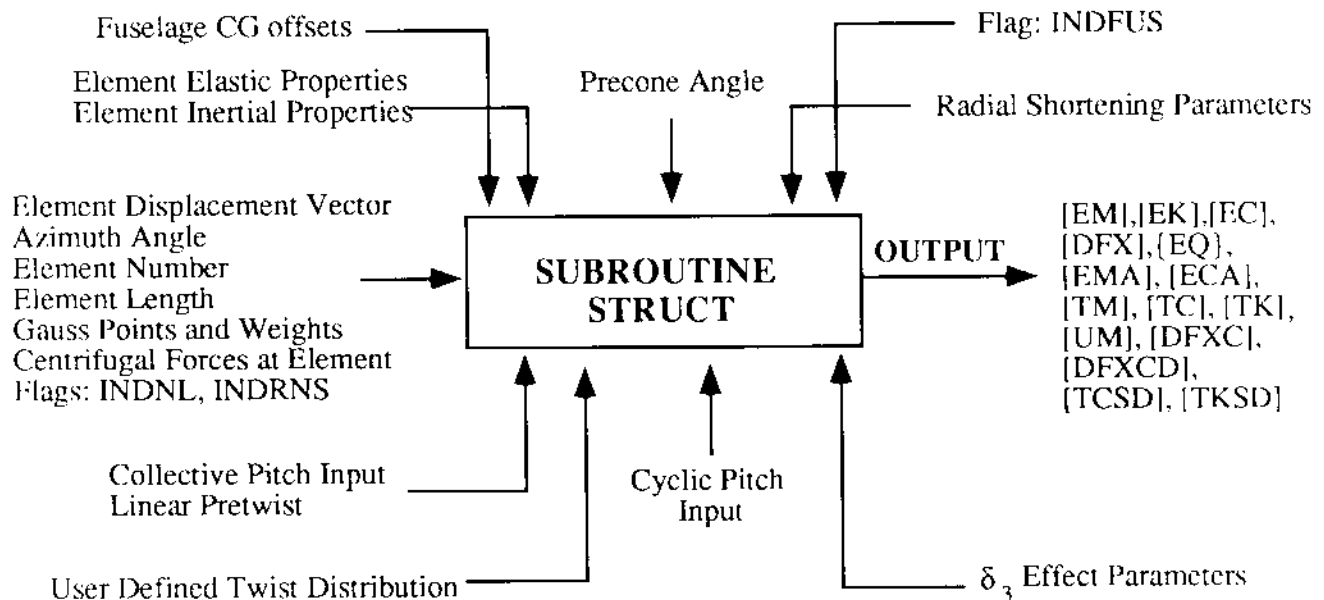


Figure 2.7a INPUT and OUTPUT for SUBROUTINE STRUCT - Physical Variables

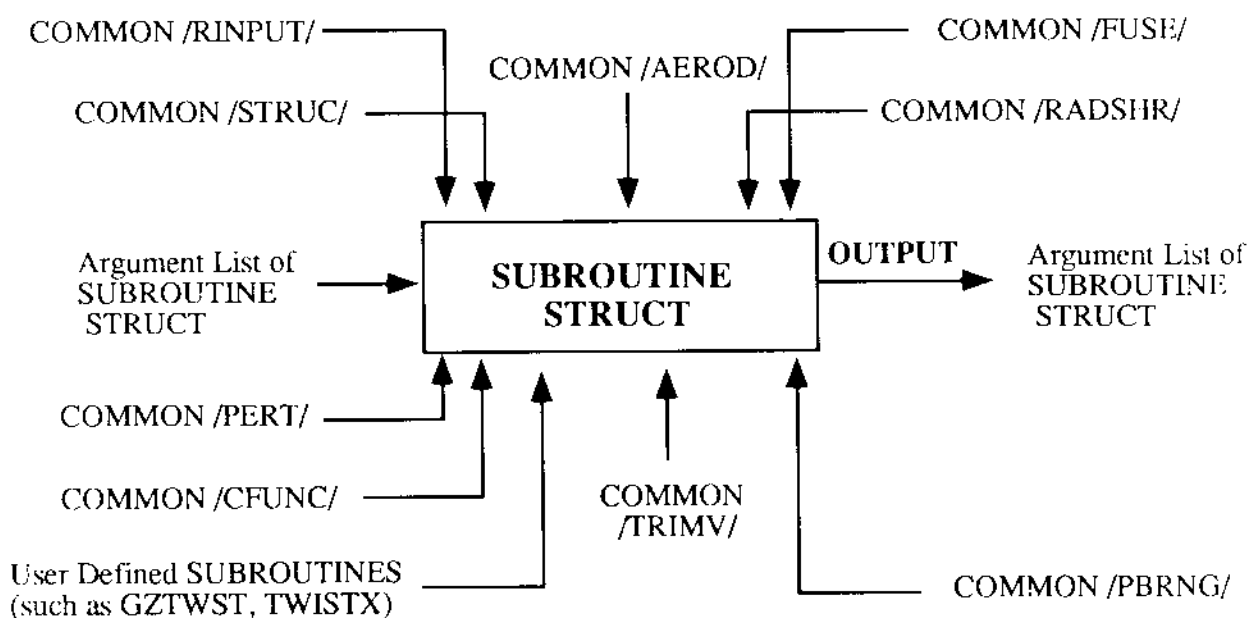


Figure 2.7b INPUT and OUTPUT for SUBROUTINE STRUCT - Paths of Dataflow

References

- [2.1] Hedges, D.H. and Dowell, E.H., "Nonlinear Equations of Motion for the Elastic Bending and Torsion of Twisted Nonuniform Blades," NASA TND-7818, Dec 1974.
- [2.2] Hedges, D.H., Ormiston, R.A., and Peters, D.A., "On the Nonlinear Geometry of Euler-Bernoulli Beams," NASA TP 1566, April 1980.
- [2.3] Chopra, I. and Sivaneri, N.T., "Aeroelastic Stability of Rotor Blades Using Finite Element Analysis," NASA CR 166389, August 1982.
- [2.4] Lanczos, C., *The Variational Principles of Mechanics*, Dover Publications, Inc., New York, NY, 1970.
- [2.5] Kaza, K.R., and Kvaternik, R.G., "Nonlinear Aeroelastic Equations for Combined Flapwise Bending, Chordwise Bending, Torsion, and Extension of Twisted, Nonuniform Rotor Blades in Forward Flight," NASA TM 74059, August 1977.
- [2.6] Lim, J.W., "Aeroelastic Optimization of a Helicopter Rotor," UMAERO Report No. 88-6, Also, Doctoral Dissertation. Department of Aerospace Engineering, University of Maryland, 1988.
- [2.7] Bir, G.S., "Gust Response of Helicopters," Doctoral Dissertation. Department of Aerospace Engineering, University of Maryland, 1985.
- [2.8] Jang, J., "Ground and Air Resonance of Bearingless Rotors in Hover and Forward Flight," UMAERO Report No. 88-30, Also, Doctoral Dissertation. Department of Aerospace Engineering, University of Maryland, 1988.

Chapter 3

AERODYNAMIC MODELING

Chapter 3

AERODYNAMIC MODELING

The rotor response is directly dependent on the aerodynamic forces on the individual blades. Therefore, to meet the growing demand to better predict the dynamic characteristics of rotorcraft, an accurate modeling of the rotor aerodynamics is required. The UMARC goal is to provide comprehensive analyses that can predict rotor loads, response, and stability with sufficient accuracy and aid design of rotorcraft of the next generation. The analysis must be efficient with minimal computational cost. In recent years, several theoretical and semi-empirical aerodynamic models have evolved to predict the complex aerodynamic environment inherent in rotary-wing flight. These analyses range from linear quasi-static analyses to full Navier-Stokes computational fluid dynamics (CFD) analyses. In addition, several models have evolved to capture the complex three-dimensional transient nature of rotor wake structures; these range from linear inflow models to iterative free wake models. These new analyses also have some disadvantages. The increased complexities cause penalties in efficiency, computational cost, and usability.

One objective of UMARC is to integrate advanced aerodynamic models with dynamic analysis schemes such that predictive capabilities are improved without resorting to usage of super computers.

Blade-element aerodynamic models used in the code include quasi-steady model, linear attached flow model, and non-linear separated flow and dynamic stall models developed by Leishman and Beddoes [1]. Wake modeling includes Drees inflow [2], prescribed and free wake models used in CAMRAD [3], and a newly developed free wake model developed by Johnson [4].

The aerodynamic analysis formulation used in UMARC can be broken down into the following parts: quasi-steady aerodynamics, attached linear unsteady aerodynamics, nonlinear flow separation, dynamic stall and wake modeling. Section 3.1 presents the formulation of a quasi-steady aerodynamic model. The implementation of the quasi-steady model in the UMARC is discussed in Section 3.2. The details of the subroutine which performs all the aerodynamic calculations (AEROMX) is discussed in Section 3.3. Section 3.4 details the refined unsteady aerodynamic model, non-linear flow separation, and dynamic stall model used in UMARC. Section 3.5 discusses the wake models used in the UMARC.

3.1 Quasi-Steady Aerodynamic Modeling

Quasi-steady aerodynamic analysis assumes that the blade airloads are solely a function of the instantaneous blade section angle of attack. Further, the lift, drag, and pitching moment data, for a specific airfoil section, is strictly based on static data.

The quasi-steady aerodynamic analysis results in the finite element mass, damping and stiffness matrices, and the load vector associated with the aerodynamic loading acting on the blade and fuselage. The calculation of these matrices requires the calculation of the incident air velocity on the blade in the deformed frame.

The air velocity in the deformed plane is derived in Section 3.1.1. The derivation of the aerodynamic loads is presented in Section 3.1.2. The application of the Hamilton's principle to obtain the discretized finite element equations for the blade, fuselage and dynamic inflow degrees of freedom is presented in Section 3.1.3. The finite element discretization to obtain the blade aerodynamic matrices is carried out in Section 3.1.4. The finite element discretization of the fuselage equations is explained in Section 3.1.5. The fuselage matrices due to aerodynamic loading are derived in Section 3.1.6. The contribution of the nonlinear aerodynamic terms is explained in section 3.1.7.

The formulation of the blade governing equations is based on Hamilton's principle. To apply the Hamilton's principle, the external virtual work is defined as a function of the external forces on the system. These external forces are

the aerodynamic loads on the blade. The blade airloads are function of the magnitude and direction of the incident airflow at each blade section.

3.1.1 Derivation of Air Velocity

The incident velocity at a particular blade station consists of three components; the wind velocity, the blade velocity and the velocity induced by fuselage motion. The general expression for the resultant blade velocity at a radial station x in the rotating undeformed frame is

$$\vec{V} = -\vec{V}_w + \vec{V}_b + \vec{V}_f \quad (3.1)$$

where \vec{V}_w is the wind velocity with contributions from the vehicle forward speed and the rotor inflow, \vec{V}_b is the blade velocity relative to the hub fixed frame resulting from blade rotation and blade motions and \vec{V}_f is the blade velocity due to fuselage motion.

Wind Velocity

The expression for the wind velocity is given by (see Fig. 3.1)

$$\vec{V}_w = (\mu\Omega R)\hat{I}_H - (\lambda\Omega R)\hat{K}_H \quad (3.2)$$

where $\mu = V \cos \alpha_s / \Omega R$ is the rotor advance ratio; V is the vehicle forward speed; α_s is the rotor shaft tilt, positive forward; λ is the rotor non-dimensional inflow; and ΩR is the rotor tip speed. The unit vectors $(\hat{I}_H, \hat{J}_H, \hat{K}_H)$ are the

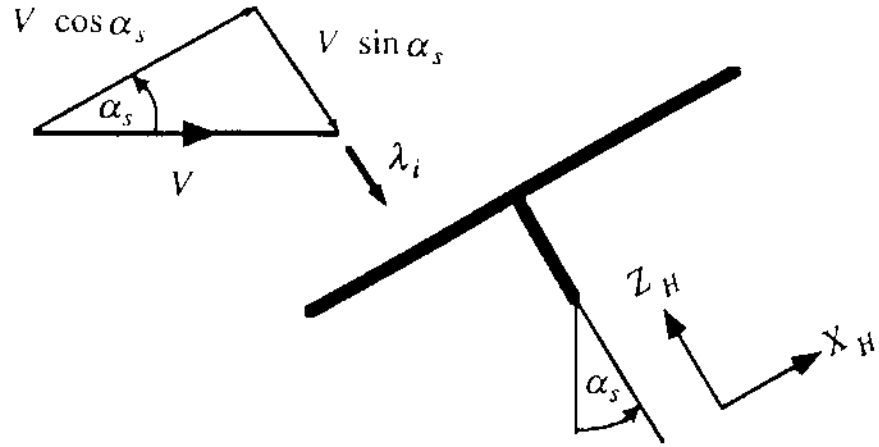


Figure 3.1: The horizontal and vertical components of the wind velocity.

unit vectors for the nonrotating hub fixed coordinate system. The rotor inflow, λ_i , consists of two components and is expressed as

$$\lambda_i = \mu \tan \alpha_s + \lambda_r \quad (3.3)$$

For small longitudinal shaft tilt angles,

$$\lambda_i \approx \mu \alpha_s + \lambda_r \quad (3.4)$$

where $\mu \tan \alpha_s$ is the component of the forward flight velocity perpendicular to the hub plane and λ_r is the nondimensional rotor *induced* inflow associated with the lift on the rotor. The velocity components which appear in Eq. 3.2 are expressed in the nonrotating system. Two transformations are required to reference these to the rotating undeformed frame (See Fig 2.2b). The first transformation, from the hub fixed nonrotating frame to the rotating frame, is given by

$$\begin{Bmatrix} \hat{I} \\ \hat{J} \\ \hat{K} \end{Bmatrix} = T_{RH} \begin{Bmatrix} \hat{I}_H \\ \hat{J}_H \\ \hat{K}_H \end{Bmatrix} \quad (3.5)$$

where

$$\mathbf{T}_{RH} = \begin{bmatrix} \cos \psi & \sin \psi & 0 \\ -\sin \psi & \cos \psi & 0 \\ 0 & 0 & 1 \end{bmatrix} \quad (3.6)$$

The second transformation relates the rotating coordinate system with no precone to that at a precone angle β_p (undeformed frame) and is expressed as

$$\begin{Bmatrix} \hat{i} \\ \hat{j} \\ \hat{k} \end{Bmatrix} = \mathbf{T}_{UR} \begin{Bmatrix} \hat{I} \\ \hat{J} \\ \hat{K} \end{Bmatrix} \quad (3.7)$$

where

$$\mathbf{T}_{UR} = \begin{bmatrix} \cos \beta_p & 0 & \sin \beta_p \\ 0 & 1 & 0 \\ -\sin \beta_p & 0 & \cos \beta_p \end{bmatrix} \quad (3.8)$$

Substitution of Eq. 3.5 and Eq. 3.7 in Eq. 3.2 results in the wind velocity expression

$$\vec{V}_w = V_{w_x} \hat{i} + V_{w_y} \hat{j} + V_{w_z} \hat{k} \quad (3.9)$$

where V_{w_x} , V_{w_y} , and V_{w_z} are the components of the wind velocity

$$V_{w_x} = \mu \Omega R \cos \psi \cos \beta_p - \lambda \Omega R \sin \beta_p \quad (3.10)$$

$$V_{w_y} = -\mu \Omega R \sin \psi \quad (3.11)$$

$$V_{w_z} = -\mu \Omega R \cos \psi \sin \beta_p - \lambda \Omega R \cos \beta_p \quad (3.12)$$

The precone angle is assumed to be small. Therefore,

$$\sin \beta_p \approx \beta_p \quad (3.13)$$

$$\cos \beta_p \approx 1 \quad (3.14)$$

Substituting Eq. 3.13 and Eq. 3.14 in Eqs. 3.10, 3.11 and 3.12 gives the final expression of the wind velocity in the blade undeformed coordinate system as

$$V_{w_x} = \mu\Omega R \cos \psi - \lambda\Omega R \beta_p \quad (3.15)$$

$$V_{w_y} = -\mu\Omega R \sin \psi \quad (3.16)$$

$$V_{w_z} = -\mu\Omega R \cos \psi \beta_p - \lambda\Omega R \quad (3.17)$$

Blade Velocity

The general expression for the blade velocity with respect to the rotating undeformed frame can be written as

$$\vec{V}_b = \dot{\vec{r}} + \vec{\Omega} \times \vec{r} \quad (3.18)$$

where,

$$\vec{r} = x_1 \hat{i} + y_1 \hat{j} + z_1 \hat{k} \quad (3.19)$$

$$\dot{\vec{r}} = \dot{x}_1 \hat{i} + \dot{y}_1 \hat{j} + \dot{z}_1 \hat{k} \quad (3.20)$$

$$\vec{\Omega} = \Omega \hat{K} \quad (3.21)$$

and $x_1, y_1, z_1, \dot{x}_1, \dot{y}_1, \dot{z}_1$ are defined in Section 2.2.1.2. The position vector from the center of the hub to a point (ξ, η, ζ) on the rotating deformed blade is \vec{r} . The velocity with which the point moves relative to the undeformed position is $\dot{\vec{r}}$. The expressions for \vec{r} and $\dot{\vec{r}}$ consist of the blade motion terms and are calculated at an arbitrary position (η, ζ) of the blade cross-section (see Section

2.2.1.2 for derivation of $\dot{\hat{i}}$, $\dot{\hat{j}}$ and $\dot{\hat{k}}$ terms). $\vec{\Omega}$, is the angular velocity of the rotating coordinate system and is expressed in the undeformed blade coordinate system using the transformation

$$\begin{Bmatrix} \dot{\hat{i}} \\ \dot{\hat{j}} \\ \dot{\hat{k}} \end{Bmatrix} = \mathbf{T}_{UR} \begin{Bmatrix} \dot{I} \\ \dot{J} \\ \dot{K} \end{Bmatrix} \quad (3.22)$$

Substitution of Eq 3.22 in Eq 3.21 yields

$$\vec{\Omega} = \Omega \sin \beta_p \hat{i} + \Omega \cos \beta_p \hat{k} \quad (3.23)$$

Substituting Eq 3.19, 3.20 and 3.23 in Eq 3.18 yields

$$\vec{V}_b = V_{b_x} \hat{i} + V_{b_y} \hat{j} + V_{b_z} \hat{k} \quad (3.24)$$

where

$$V_{b_x} = \dot{x}_1 - \Omega y_1 \cos \beta_p$$

$$V_{b_y} = \dot{y}_1 + \Omega x_1 \cos \beta_p - \Omega z_1 \sin \beta_p$$

$$V_{b_z} = \dot{z}_1 + \Omega y_1 \sin \beta_p$$

After substituting for x_1 , y_1 , z_1 , \dot{x}_1 , \dot{y}_1 and \dot{z}_1 (defined in Section 2.2.1.2), the components of the blade velocity become

$$V_{b_x} = [\dot{u} - \lambda_T \dot{\phi}' - (\dot{v}' + w' \dot{\theta}_1)(\eta \cos \theta_1 - \zeta \sin \theta_1)$$

$$\begin{aligned}
&= (\dot{w}' - v'\dot{\theta}_1)(\eta \sin \theta_1 + \zeta \cos \theta_1) \\
&= \Omega(v + \eta \cos \theta_1 - \zeta \sin \theta_1) \cos \beta_p
\end{aligned}$$

$$\begin{aligned}
V_{b_y} &= \dot{v} - \dot{\theta}_1(\eta \sin \theta_1 + \zeta \cos \theta_1) \\
&+ \Omega[x + u - \lambda_T \dot{\phi}' - v'(\eta \cos \theta_1 - \zeta \sin \theta_1) - w'(\eta \sin \theta_1 + \zeta \cos \theta_1) \cos \beta_p]
\end{aligned}$$

$$- \Omega(w + \eta \sin \theta_1 + \zeta \cos \theta_1) \sin \beta_p$$

$$V_{b_x} = \dot{w} + \dot{\theta}_1(\eta \cos \theta_1 - \zeta \sin \theta_1) + \Omega(v + \eta \cos \theta_1 - \zeta \sin \theta_1) \sin \beta_p \quad (3.25)$$

where

$$\begin{aligned}
\theta_1 &= \theta_o + \hat{\phi} \\
\dot{u} &= \dot{u}_e - \frac{1}{2} \int_0^x (v' \dot{v}' + w' \dot{w}') d\xi
\end{aligned} \quad (3.26)$$

For quasi-steady aerodynamics, rotor blade aerodynamic loads are calculated using a blade section “strip” analysis based on the angle of attack at the three-quarter chord location. This requires calculation of the velocity components at the three-quarter chord location ($\eta = \eta_r$ and $\zeta = 0$), and Eq. 3.25 simplifies to

$$\begin{aligned}
V_{b_x} &= \dot{u} - (v' + w'\dot{\theta}_1)\eta_r \cos \theta_1 \\
&- (\dot{w}' - v'\dot{\theta}_1)\eta_r \sin \theta_1 - \Omega(v + \eta_r \cos \theta_1)
\end{aligned}$$

$$\begin{aligned}
V_{b_y} &= \dot{v} - \dot{\theta}_1 \eta_r \sin \theta_1 + \Omega [(x + u - v' \eta_r \cos \theta_1 \\
&\quad - w' \eta_r \sin \theta_1 - (w + \eta_r \sin \theta_1) \beta_p] \\
V_{b_z} &= \dot{w} + \dot{\theta}_1 \eta_r \cos \theta_1 + \Omega \beta_p (v + \eta_r \cos \theta_1)
\end{aligned} \tag{3.27}$$

The small angle assumptions in Eq. 3.13 and Eq. 3.14 have been made in deriving Eq. 3.27.

Velocity of the Blade due to Fuselage Motion

UMARC has the option of including rigid body fuselage motion for aeromechanical stability analysis. Fuselage motion induces additional velocities on the blade. In the current version of UMARc, the rotor shaft is considered rigid. The rigid body fuselage motion results in blade velocity (at point P_{η_r} at three quarter chord on the rotating deformed blade) given by

$$\vec{V}_f = \vec{V}_F + w_f \times \vec{r}_F \tag{3.28}$$

The location of this point relative to the vehicle's center of gravity is described by a position vector \vec{r}_F (See Fig. 2.5). \vec{V}_F is the velocity with which the fuselage center of gravity is moving in the inertial frame and w_f is the angular rate with which the fuselage axis is rotating in the inertial frame. The components of the velocity \vec{V}_f in Eq. 3.28 are written as

$$\vec{r}_F = (x_{CG} \hat{i}_F + y_{CG} \hat{j}_F + z_{CG} \hat{k}_F) + ((x + u) \hat{i} + v \hat{j} + w \hat{k} + \eta_r \hat{j}_\eta) \tag{3.29}$$

$$\vec{V}_F = \dot{x}_F \hat{i}_I + \dot{y}_F \hat{j}_I + \dot{z}_F \hat{k}_I \tag{3.30}$$

$$w_f = -\dot{\phi}_s \hat{I}_I - \dot{\alpha}_s \hat{J}_I \quad (3.31)$$

Substituting Eq. 3.29, Eq. 3.30, and Eq. 3.31 in Eq. 3.28 yields

$$\begin{aligned} \vec{V}_f = & (\dot{x}_F \hat{I}_I + \dot{y}_F \hat{J}_I + \dot{z}_F \hat{K}_I) \\ & + (-\dot{\phi}_s \hat{I}_I - \dot{\alpha}_s \hat{J}_I) \times [(x+u)\hat{i} + v\hat{j} + w\hat{k} + \eta_r \hat{j}_\eta \\ & + x_{CG} \hat{I}_F + y_{CG} \hat{J}_F + h \hat{K}_F] \end{aligned} \quad (3.32)$$

The fuselage induced velocity given by Eq. 3.32 can be expressed in the blade undeformed rotating axis (\hat{i} , \hat{j} , \hat{k}) system using the following transformation matrices [Section 2.1.2]

$$\begin{Bmatrix} \hat{i} \\ \hat{j} \\ \hat{k} \end{Bmatrix} = \mathbf{T}_{UR} \mathbf{T}_{RH} \mathbf{T}_{HI} \begin{Bmatrix} \hat{I}_I \\ \hat{J}_I \\ \hat{K}_I \end{Bmatrix} \quad (3.33)$$

$$\begin{Bmatrix} \hat{i} \\ \hat{j} \\ \hat{k} \end{Bmatrix} = \mathbf{T}_{UR} \mathbf{T}_{RH} \begin{Bmatrix} \hat{I}_F \\ \hat{J}_F \\ \hat{K}_F \end{Bmatrix} \quad (3.34)$$

$$\begin{Bmatrix} \hat{i} \\ \hat{j} \\ \hat{k} \end{Bmatrix} = \mathbf{T}_{DU} \begin{Bmatrix} \hat{i}_\xi \\ \hat{j}_\eta \\ \hat{k}_\zeta \end{Bmatrix} \quad (3.35)$$

After applying the transformation, all terms of order higher than ϵ^2 are dropped in accordance with the ordering scheme defined in Section 2.1.3. The precone angle is assumed to be small ($\sin \beta_p \approx \beta_p$, $\cos \beta_p \approx 1$). Using Eqs. 3.33-3.35 in Eq. 3.32 yields:

$$\vec{V}_f = V_{fx} \hat{i} + V_{fy} \hat{j} + V_{fz} \hat{k} \quad (3.36)$$

where

$$\begin{aligned}
 V_{fx} &= (\dot{x}_F - h\dot{\alpha}_s) \cos \psi + (\dot{y}_F + h\dot{\phi}_s) \sin \psi \\
 V_{fy} &= -(\dot{x}_F - h\dot{\alpha}_s) \sin \psi + (\dot{y}_F + h\dot{\phi}_s) \cos \psi \\
 V_{fz} &= \dot{z}_F - \dot{\phi}_s x \sin \psi + \dot{\alpha}_s x \cos \psi + x_{cg} \dot{\alpha}_s - y_{cg} \dot{\phi}_s
 \end{aligned}$$

Resultant Velocity

The resultant blade velocity at a radial station x given by Eq. 3.1 can be written in terms of the unit vectors of the rotating undeformed coordinate system as

$$\begin{aligned}
 \vec{V} &= U_x \hat{i} + U_y \hat{j} + U_z \hat{k} \\
 &= (V_{bx} - V_{wx} + V_{fx}) \hat{i} + (V_{by} - V_{wy} + V_{fy}) \hat{j} \\
 &\quad + (V_{bz} - V_{wz} + V_{fz}) \hat{k}
 \end{aligned} \tag{3.37}$$

where,

$$\begin{aligned}
 U_x &= \underline{\dot{u} - (\dot{v}' + w'\dot{\theta}_1)\eta_r \cos \theta_1 - (\dot{w}' - v'\dot{\theta}_1)\eta_r \sin \theta_1 - \Omega(v + \eta_r \cos \theta_1)} \\
 &\quad \underline{- \mu \Omega R \cos \psi + \lambda \Omega R \beta_p} \\
 &\quad + (\dot{x}_F - h\dot{\alpha}_s) \cos \psi \cos \beta_p + (\dot{y}_F + h\dot{\phi}_s) \sin \psi \cos \beta_p \\
 U_y &= \underline{\dot{v} - \dot{\theta}_1 \eta_r \sin \theta_1 + \Omega((x + u - v'\eta_r \cos \theta_1 - w'\eta_r \sin \theta_1 - (w + \eta_r \sin \theta_1)\beta_p)}
 \end{aligned}$$

$$\begin{aligned}
& + \underline{\mu \Omega R \sin \psi} \\
& - (\dot{x}_F - h \dot{\alpha}_s) \sin \psi + (\dot{y}_F + h \dot{\phi}_s) \cos \psi
\end{aligned}$$

$$\begin{aligned}
U_x &= \underline{\dot{w} + \dot{\theta}_1 \eta_r \cos \theta_1 + \Omega \beta_p (v + \eta_r \cos \theta_1)} \\
& + \underline{\mu \Omega R \beta_p \cos \psi + \lambda \Omega R} \\
& + \dot{z}_F - \dot{\phi}_s x \sin \psi + \dot{\alpha}_s x \cos \psi + x_{cg} \dot{\alpha}_s - y_{cg} \dot{\phi}_s
\end{aligned}$$

The underlined terms are due to the blade and wind velocities relative to the hub, (\vec{V}_b and \vec{V}_w). All other terms are due to motion of the fuselage.

The blade section loads are calculated using the resultant velocity and aerodynamic angle of attack in the deformed blde. Therefore, the velocity components in the undeformed frame (U_x, U_y, U_z) need to be transformed to the deformed frame:

$$\begin{Bmatrix} U_R \\ U_T \\ U_P \end{Bmatrix} = \mathbf{T}_{DU} \begin{Bmatrix} U_x \\ U_y \\ U_z \end{Bmatrix} \quad (3.38)$$

where,

$$\mathbf{T}_{DU} = \begin{bmatrix} 1 - \frac{v'^2}{2} - \frac{w'^2}{2} & v' & w' \\ -(v' \cos \theta_1 + w' \sin \theta_1) & (1 - \frac{v'^2}{2}) \cos \theta_1 - v' w' \sin \theta_1 & \sin \theta_1 (1 - \frac{w'^2}{2}) \\ v' \sin \theta_1 - w' \cos \theta_1 & -(1 - \frac{v'^2}{2}) \sin \theta_1 - v' w' \cos \theta_1 & \cos \theta_1 (1 - \frac{w'^2}{2}) \end{bmatrix}$$

In the above matrix, θ_1 is the total pitch angle given by

$$\theta_1 = \theta_0 + \hat{\phi} \quad (3.39)$$

where θ_0 is the rigid pitch (including blade pretwist, collective input, and cyclic input) and $\hat{\phi}$ is the elastic twist. Expanding $\cos \theta_1$ and $\sin \theta_1$, and assuming $\hat{\phi}$ is a small angle,

$$\begin{aligned}
\cos \theta_1 &= \cos(\theta_0 + \hat{\phi}) \\
&= \cos \theta_0 \cos \hat{\phi} - \sin \theta_0 \sin \hat{\phi} \\
&\approx \cos \theta_0 - \hat{\phi} \sin \theta_0 \\
\sin \theta_1 &= \sin(\theta_0 + \hat{\phi}) \\
&= \sin \theta_0 \cos \hat{\phi} + \cos \theta_0 \sin \hat{\phi} \\
&\approx \sin \theta_0 + \hat{\phi} \cos \theta_0
\end{aligned} \tag{3.40}$$

Substitution of Eq. 3.40 into the transformation matrix \mathbf{T}_{DU} yields

$$\mathbf{T}_{DU} = \begin{bmatrix} 1 - \frac{v'^2}{2} - \frac{w'^2}{2} & v' & w' \\ -(v' \cos \theta_0 + w' \sin \theta_0) & (1 - \frac{v'^2}{2})(\cos \theta_0 - \hat{\phi} \sin \theta_0) & \sin \theta_0(1 - \frac{w'^2}{2}) \\ +\hat{\phi}(v' \sin \theta_0 - w' \cos \theta_0) & -v' w' \sin \theta_0 & +\hat{\phi} \cos \theta_0 \\ v' \sin \theta_0 - w' \cos \theta_0 & -(1 - \frac{v'^2}{2}) \sin \theta_0 - v' w' \cos \theta_0 & \cos \theta_0(1 - \frac{w'^2}{2}) \\ +\hat{\phi}(v' \cos \theta_0 + w' \sin \theta_0) & -\hat{\phi} \cos \theta_0 & -\hat{\phi} \sin \theta_0 \end{bmatrix}$$

Using the ordering scheme defined in Section 2.1.3, only terms up to second order (ϵ^2) are retained in \mathbf{T}_{DU} .

After transformation to the deformed plane using Eq. 3.38, the resultant blade velocity in the rotating deformed frame is expressed as,

$$\vec{V} = U_R \hat{i}_\xi + U_T \hat{j}_\eta + U_P \hat{k}_\zeta \tag{3.41}$$

where

$$\begin{aligned}
\frac{U_R}{\Omega R} = & \frac{\dot{u} - v + v'(x + \mu \sin \psi) - \mu \cos \psi(1 - \beta_p w') + \lambda(\beta_p + w')}{\eta_r \cos \theta_0(1 + \dot{v}') + \eta_r \sin \theta_0(\hat{\phi} - \dot{w}')} \\
& + \frac{v' \dot{v} + w' \dot{w} + \frac{1}{2} \mu \cos \psi(v'^2 + w'^2)}{(x_F - \dot{\alpha}_s h) \cos \psi + (\dot{y}_F + \dot{\psi}_s h) \sin \psi} \\
& + \sin \theta_0(\dot{w} + \lambda + v(\beta_p + w') - \hat{\phi} \dot{v}) \\
& - (x + \mu \sin \psi)(v' w' + \hat{\phi}) + \mu \cos \psi(w' + \beta_p - \hat{\phi} v') \\
& - (\dot{x}_F - \dot{\alpha}_s h) \sin \psi \cos \theta_0 + (\dot{y}_F + \dot{\phi}_s h) \cos \psi \cos \theta_0 \\
& + \sin \theta_0(\dot{z}_F - \dot{\phi}_s x \sin \psi + \dot{\alpha}_s x \cos \psi + x_{cg} \dot{\alpha}_s - y_{cg} \dot{\phi}_s)
\end{aligned} \tag{3.42}$$

$$\begin{aligned}
\frac{U_T}{\Omega R} = & \frac{\cos \theta_0(\dot{v} + u - w \beta_p + \hat{\phi}(\lambda + \dot{w}) + v' v)}{(x + \mu \sin \psi)(1 - \frac{v'^2}{2}) + \mu \cos \psi(v' + \hat{\phi}(\beta_p + w'))} \\
& + \frac{\sin \theta_0(\dot{w} + \lambda + v(\beta_p + w') - \hat{\phi} \dot{v})}{(x + \mu \sin \psi)(v' w' + \hat{\phi}) + \mu \cos \psi(w' + \beta_p - \hat{\phi} v')} \\
& - (\dot{x}_F - \dot{\alpha}_s h) \sin \psi \cos \theta_0 + (\dot{y}_F + \dot{\phi}_s h) \cos \psi \cos \theta_0 \\
& + \sin \theta_0(\dot{z}_F - \dot{\phi}_s x \sin \psi + \dot{\alpha}_s x \cos \psi + x_{cg} \dot{\alpha}_s - y_{cg} \dot{\phi}_s)
\end{aligned} \tag{3.43}$$

$$\begin{aligned}
\frac{U_P}{\Omega R} = & \frac{\cos \theta_0(\dot{w} + \lambda + \beta_p v + v w' + \mu \cos \psi(\beta_p + w' - \hat{\phi} v')}{(x + \mu \sin \psi)(v' w' + \hat{\phi}) + \sin \theta_0(-(\dot{v} + u) - v v' + w \beta_p)} \\
& - \frac{\hat{\phi}(\dot{w} + \lambda) - \mu \cos \psi(v' + \hat{\phi}(\beta_p + w')) - (x + \mu \sin \psi)(1 - \frac{v'^2}{2})}{(\dot{x}_F - \dot{\alpha}_s h) \sin \psi - (\dot{y}_F + \dot{\phi}_s h) \cos \psi} \\
& + \frac{\eta_r(\dot{\theta}_0 + \dot{\phi} + w' + \beta_p)}{\cos \theta_0(\dot{z}_F - \dot{\phi}_s x \sin \psi + x \dot{\alpha}_s \cos \psi + x_{cg} \dot{\alpha}_s - y_{cg} \dot{\phi}_s)}
\end{aligned} \tag{3.44}$$

Once again, the underlined terms are due to blade and wind velocities relative to the hub, (\vec{V}_b and \vec{V}_w). All other terms are due to motion of the fuselage.

3.1.2 Quasi-Steady Airloads Expressions

Once the air velocity in the blade deformed plane is calculated, two dimensional strip theory is used to determine the aerodynamic loads on the blade.

The blade airloads in the rotating deformed frame can be directly written as;

$$(\bar{L})_C = \frac{1}{2}\rho V^2 c C_l \quad (3.45)$$

$$(\bar{D})_C = \frac{1}{2}\rho V^2 c C_d \quad (3.46)$$

$$(\bar{M})_C = \frac{1}{2}\rho V^2 c^2 C_m \quad (3.47)$$

where the bar identifies forces and moments in the deformed plane, the subscript C identifies forces of circulatory origin (the noncirculatory forces derived later use subscript NC), V is the incident velocity, and C_l , C_d , C_m are the section lift, drag, and pitching moment coefficients, respectively. The aerodynamic coefficients are expressed as

$$C_l = c_0 + c_1\alpha \quad (3.48)$$

$$C_d = d_0 + d_1|\alpha| + d_2\alpha^2 \quad (3.49)$$

$$C_m = f_0 + f_1\alpha = c_{m_{ac}} + f_1\alpha \quad (3.50)$$

where c_0 is the zero angle lift coefficient, c_1 is the lift curve slope, d_0 is the viscous drag coefficient, f_0 or $c_{m_{ac}}$ is the zero angle pitching moment coefficient about the aerodynamic center, and d_1 , d_2 , and f_1 are the additional drag and moment coefficients. These relations are restricted to incompressible attached flow conditions. Compressibility effects are accounted for by modifying the lift curve slope as

$$c_1 = \frac{c_{1M=0}}{\beta} \quad (3.51)$$

where β is the Prandtl-Glauert factor:

$$\beta = \sqrt{1 - M^2} \quad (3.52)$$

The Prandtl-Glauert correction factor is applicable only at low Mach numbers ($M \leq 0.9$), characteristic of a rotor blade [5].

The normal force, chord force, axial force, and moment about the elastic axis are (See Fig. 3.2):

$$(\bar{L}_w)_C = (\bar{L})_C \cos \alpha + (\bar{D})_C \sin \alpha \quad (3.53)$$

$$(\bar{L}_v)_C = (\bar{L})_C \sin \alpha - (\bar{D})_C \cos \alpha \quad (3.54)$$

$$(\bar{L}_u)_C = -(\bar{D})_C \sin \Lambda \quad (3.55)$$

$$(\bar{M}_{\dot{\phi}})_C = (\bar{M}_{ac})_C - e_d (\bar{L}_w)_C \quad (3.56)$$

the $(\bar{L}_u)_C$, $(\bar{L}_v)_C$, and $(\bar{L}_w)_C$ are the external loads along the deformed axes (ξ, η, ζ) , $(\bar{M}_{\dot{\phi}})_C$ is the moment about the deformed elastic axis, Λ is the axial

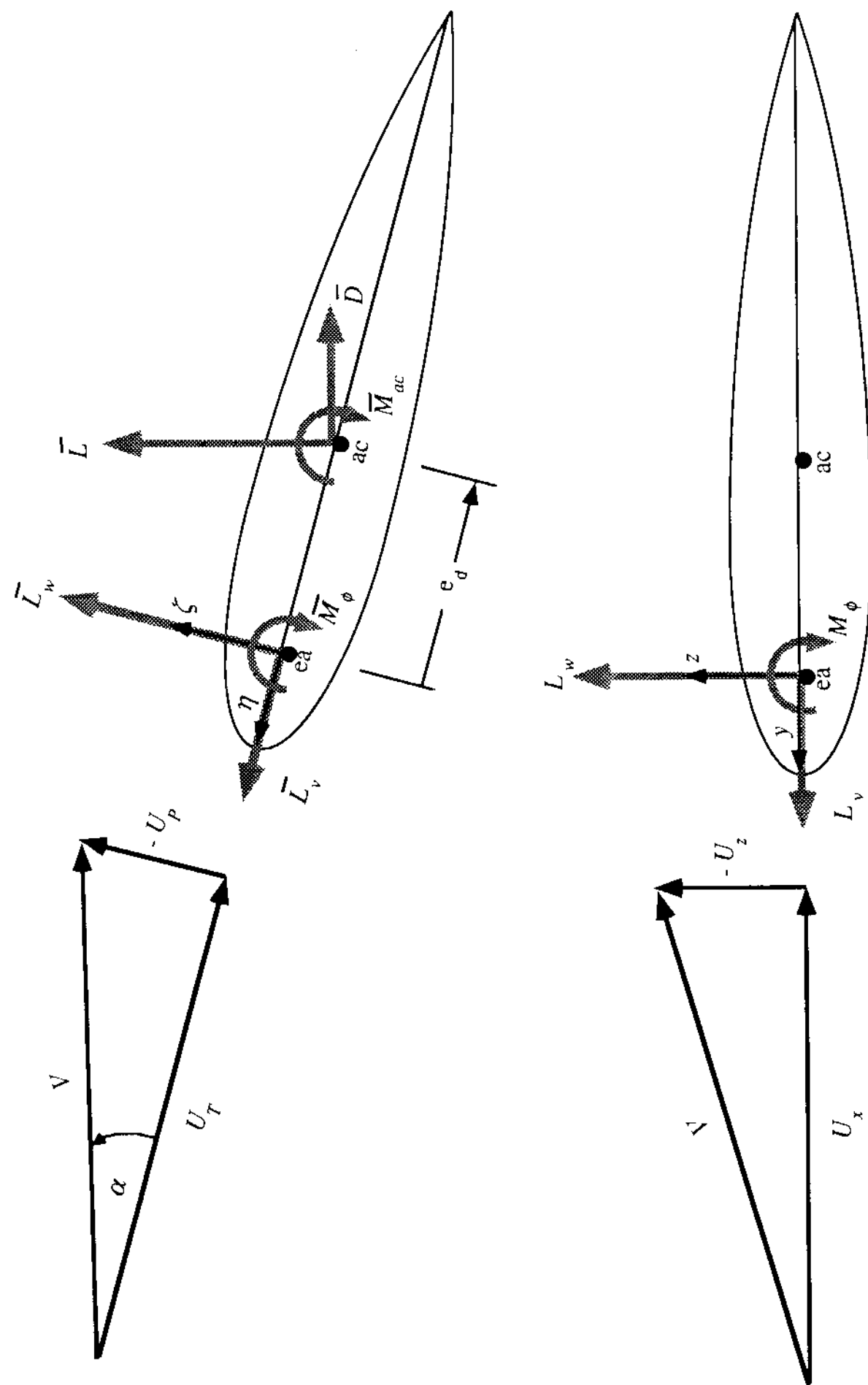


Figure 3.2 Blade Element Aerodynamics - Deformed (Top) and Undeformed (Bottom) Frames

skew angle due to the radial component of velocity, U_R , acting on the blade, and e_d is the chordwise offset of the aerodynamic center behind elastic axis.

All forces, moments, and velocities are nondimensionalized using the scheme described in Chapter 2.1.3. The 2-D section lift and drag forces, \bar{L} and \bar{D} , are nondimensionalized by dividing by $m_0\Omega^2 R$. The 2-D section moment \bar{M} is divided by $m_0\Omega^2 R^2$. The nondimensional resultant velocity, \bar{V} , is obtained by dividing the resultant velocity, V , by tip speed ΩR . Introducing the Lock number, $\gamma = \frac{\rho acR^4}{I_b}$, and flap inertia, $I_b = \frac{m_0 R^3}{3}$, \bar{L} , \bar{D} and \bar{M} from Eqs. 3.45- 3.47, are written in the nondimensional form as:

$$(\bar{L})_C = \frac{\gamma \bar{V}^2}{6a} C_l \quad (3.57)$$

$$(\bar{D})_C = \frac{\gamma \bar{V}^2}{6a} C_d \quad (3.58)$$

$$(\bar{M}_{ac})_C = \frac{\gamma \bar{V}^2 c}{6aR} C_m \quad (3.59)$$

Similarly, the nondimensionalized forces and moment in the deformed frame are obtained as

$$(\bar{L}_w)_C = \frac{\gamma \bar{V}^2}{6a} (C_l \cos \alpha + C_d \sin \alpha) \quad (3.60)$$

$$(\bar{L}_v)_C = \frac{\gamma \bar{V}^2}{6a} (C_l \sin \alpha - C_d \cos \alpha) \quad (3.61)$$

$$(\bar{L}_u)_C = \frac{\gamma \bar{V}^2}{6a} (-C_d \sin \Lambda) \quad (3.62)$$

$$(\bar{M}_\phi)_C = \frac{\gamma \bar{V}^2}{6a} \left(\frac{c}{R} C_m \right) - (e_d (\bar{L}_w)_C) \quad (3.63)$$

Substituting the expressions for C_d , C_l and C_m from Eqs. 3.48- 3.50 into Eqs. 3.57- 3.63, and using the approximations

$$\sin \alpha \approx \alpha \quad (3.64)$$

$$\cos \alpha \approx 1 \quad (3.65)$$

$$\bar{V} \approx U_T \quad (3.66)$$

$$\alpha \approx -U_P/U_T \quad (3.67)$$

$$\sin \Lambda \approx U_R/U_T \quad (3.68)$$

yields

$$(\bar{L}_w)_C = \frac{\gamma}{6a}(c_0 U_T^2 - (c_1 + d_0)U_T U_P + d_1|U_P|U_P) \quad (3.69)$$

$$(\bar{L}_v)_C = \frac{\gamma}{6a}(-d_0 U_T^2 - (c_0 U_P - d_1|U_P|)U_T + (c_1 - d_2)U_P^2) \quad (3.70)$$

$$(\bar{L}_u)_C = \frac{\gamma}{6a}(-d_0 U_R U_T) \quad (3.71)$$

$$(\bar{M}_{\dot{\phi}})_C = \frac{\gamma}{6a}\left(\frac{c}{R}(c_{m_{ac}}(U_T^2 + U_P^2) - f_1 U_T U_P)\right) - (e_d (\bar{L}_w)_C) \quad (3.72)$$

The aerodynamic forces in the underformed frame are obtained by using the orthogonal coordinate transformation ($\mathbf{T}_{DU}^{-1} = \mathbf{T}_{DU}^T$),

$$\left\{ \begin{array}{l} (L_u^A)_C \\ (L_v^A)_C \\ (L_w^A)_C \end{array} \right\} = (\mathbf{T}_{DU})^T \left\{ \begin{array}{l} (\bar{L}_u)_C \\ (\bar{L}_v)_C \\ (\bar{L}_w)_C \end{array} \right\} \quad (3.73)$$

$$(M_{\phi}^A)_C \approx (\overline{M}_{\phi})_C \quad (3.74)$$

The equations derived above for the circulatory lift and pitching moments require modifications when reverse flow effects and Mach number perturbations are considered. These modifications are described below.

Reverse Flow

The inboard sections of the retreating rotor blade experience reverse flow conditions in forward flight. The reverse flow is due to the forward speed component of the velocity U_T becoming larger than the component due to the rotational speed. The reverse flow causes the aerodynamic center of the airfoil to shift from x_{ac} to $\frac{c}{R} - x_{ac}$. The equations previously derived are applicable for reverse flow condition ($U_T < 0$) with the following changes:

$$e_d^R = e_d + \frac{\frac{c}{R}}{2} \quad (3.75)$$

$$\eta_r^R = x_{ac} - \frac{\frac{c}{R}}{4} - e_d \quad (3.76)$$

where the superscript R refers to the reverse flow condition. It should be noted that U_T is negative in the reverse flow region.

Mach Number Perturbations

The lift acting on the blade is a function of the angle of attack of the airfoil and the local Mach number:

$$C_l = C_l(\alpha, M) \quad (3.77)$$

The perturbation in the lift can be written as

$$\Delta C_l = \frac{\partial C_l}{\partial \alpha} \Delta \alpha + \frac{\partial C_l}{\partial M} \Delta M \quad (3.78)$$

where

$$\alpha = -\frac{U_p}{U_T} \quad (3.79)$$

$$\Delta \alpha = \frac{U_p \Delta U_T - U_T \Delta U_p}{U_T^2} \quad (3.80)$$

$$M = \frac{M_{tip}}{V_{tip}} V \approx M_{tip} \frac{U_T}{\Omega R} \quad (3.81)$$

$$\Delta M = M_{tip} \frac{\Delta V}{\Omega R} \approx M_{tip} \frac{\Delta U_T}{\Omega R} \quad (3.82)$$

The symbol Δ is an operator, analogous to the derivative, which gives the perturbation values of the quantities on which it operates. Assuming Prandtl-Glauert model given in Eq. 3.51, and differentiating C_l with respect to α and M gives

$$\frac{\partial C_l}{\partial \alpha} = \frac{c_1|_{M=0}}{\sqrt{1-M^2}} \quad (3.83)$$

$$\frac{\partial C_l}{\partial M} = -\frac{1}{2} c_1|_{M=0} \alpha \sqrt{1-M^2} \quad (3.84)$$

Using the above equations to derive the lift and moment expressions gives a modified form of Eq. 3.69 and 3.70 as

$$\begin{aligned}
(\bar{L}_w)_C &= \frac{\gamma}{6a} (c_0 U_T^2 - (c_1 + d_0) U_T U_P + d_1 U_P^2 \\
&\quad + \underline{c_2 M_{tip} U_T (U_T^2 + U_P^2)})
\end{aligned} \tag{3.85}$$

$$\begin{aligned}
(\bar{L}_v)_C &= \frac{\gamma}{6a} (-d_0 U_T^2 - (c_0 - d_1) U_T U_P + (c_1 - d_2) U_P^2 \\
&\quad - \underline{c_2 M_{tip} U_P (U_T^2 + U_P^2)})
\end{aligned} \tag{3.86}$$

where,

$$c_2 = -\frac{1}{2} \alpha \sqrt{1 - M^2} c_1|_{M=0} \tag{3.87}$$

The underlined terms in the above equations show the effect of the Mach number perturbation. The Mach number perturbation effects blade forces $(\bar{L}_v)_C$ and $(\bar{L}_w)_C$ because these terms are directly dependent on the lift (C_l). There is no change in $(\bar{L}_u)_C$ since it is not dependent on lift. The pitching moment, $(\bar{M}_\delta)_C$ changes indirectly due to its dependence on $(\bar{L}_w)_C$.

If the variation of the lift coefficient of an airfoil with Mach number is known from experimental data and is available in the form of a table, then $\frac{\partial C_l}{\partial M}$ can be directly calculated using finite difference approximation and a table lookup scheme.

Noncirculatory airloads

The airloads acting on the rotor blade can be classified into two categories: circulatory and noncirculatory. The previous sections focussed on the derivation

of the circulatory loads. The noncirculatory loads(also called apparent or virtual forces) will now be derived.

For a airfoil section undergoing plunge motion, \tilde{h} , and pitch motion, α , the noncirculatory lift and pitching moment are given by [6],

$$(L_w^A)_{NC} = \rho\pi b^2(\tilde{h} - a_h b \ddot{\alpha}) + \rho\pi b^2 U \dot{\alpha} \quad (3.88)$$

$$\begin{aligned} &= L_2 + L_3 \\ (M_\phi^A)_{NC} &= a_h b L_2 - \left(\frac{1}{2} - a_h\right) b L_3 - \frac{\rho\pi b^4}{8} \ddot{\alpha} \end{aligned} \quad (3.89)$$

where

$$U = \Omega R(x + \mu \sin \psi) \quad (3.90)$$

$$a_h b = e_d + \frac{c}{4} \quad (3.91)$$

$$\tilde{h} = -\ddot{w} \quad (3.92)$$

$$\ddot{\alpha} = \ddot{\theta}_1 = \ddot{\theta}_0 + \ddot{\phi} \quad (3.93)$$

$$\dot{\alpha} = \dot{\theta}_1 = \dot{\theta}_0 + \dot{\phi} \quad (3.94)$$

$$b = \frac{c}{2} \quad (3.95)$$

Note that U is the free stream tangential velocity, $a_h b$ is the distance from mid-chord to the elastic axis(positive aft), \tilde{h} is the plunge acceleration (positive down), $\ddot{\alpha}$ is the pitch acceleration (positive nose up), $\dot{\alpha}$ is the pitch angular velocity and b is the airfoil semi-chord. The L_2 component of the noncirculatory lift acts at the mid-chord and the L_3 component acts at the third-quarter chord point. Also note that the noncirculatory airloads are assumed to act directly on the blade deformed section.

Substitution of Eq. 3.90-3.95 in Eq. 3.88 and Eq. 3.89 yields

$$(L_w^A)_{NC} = \frac{1}{4}\rho\pi c^2(-\ddot{w} + (\frac{c}{4} + e_d)\ddot{\theta}_1 + \Omega R(x + \mu \sin \psi)\dot{\theta}_1) \quad (3.96)$$

$$\begin{aligned} (M_{\dot{\phi}}^A)_{NC} &= \frac{1}{4}\rho\pi c^2((\frac{c}{4} + e_d)\ddot{w} - (\frac{c}{4} + e_d)^2\ddot{\theta}_1 \\ &\quad - \Omega R(\frac{c}{2} + e_d)(x + \mu \sin \psi)\dot{\theta} - \frac{c^2\ddot{\theta}_1}{32}) \end{aligned} \quad (3.97)$$

The noncirculatory airloads are then nondimensionalized to yield

$$\frac{(L_w^A)_{NC}}{m_0\Omega^2 R} = \frac{\gamma\pi\frac{c}{R}}{12a}(-\frac{\ddot{w}}{R} + \frac{\frac{c}{4} + e_d}{R}\ddot{\theta}_1 + (x + \mu \sin \psi)\dot{\theta}_1) \quad (3.98)$$

$$\begin{aligned} \frac{(M_{\dot{\phi}}^A)_{NC}}{m_0\Omega^2 R^2} &= \frac{\gamma\pi\frac{c}{R}}{12a}(\frac{\frac{c}{4} + e_d}{R}\frac{\ddot{w}}{R} - (\frac{\frac{c}{4} + e_d}{R})^2\ddot{\theta}_1 \\ &\quad - \frac{\frac{c}{2} + e_d}{R}(x + \mu \sin \psi)\dot{\theta}_1 - \frac{c^2}{R^2}\frac{1}{32}\ddot{\theta}_1) \end{aligned} \quad (3.99)$$

These airloads are added to the circulatory airloads to give the total loads acting on the blade section

$$L_w^A = (L_w^A)_C + (L_w^A)_{NC} \quad (3.100)$$

$$L_v^A = (L_v^A)_C \quad (3.101)$$

$$L_u^A = (L_u^A)_C \quad (3.102)$$

$$BM_{\dot{\phi}}^A = (M_{\dot{\phi}}^A)_C + M_{\dot{\phi}}^A)_{NC} \quad (3.103)$$

These airloads depend on blade motion, fuselage motion, pitch controls, induced inflow λ_i , and forward speed μ .

3.1.3 Finite Element Discretization

The finite element formulation using Hamilton's principle requires an expression for the virtual work done by the aerodynamic forces. For a rotor-fuselage model of the helicopter the virtual work is given by

$$\delta W = \sum_{m=1}^{N_b} \delta W_b + \delta W_F \quad (3.104)$$

where δW_b represents the work done on the b th blade and δW_F represents the work done on the fuselage.

The external work done on the b th blade is given by

$$\delta W_b = \int_0^R (L_u^A \delta u + L_v^A \delta v + L_w^A \delta w + M_\phi^A \delta \hat{\phi}) dx \quad (3.105)$$

where L_u^A , L_v^A and L_w^A are the distributed airloads in the blade undeformed frame and M_ϕ^A is the sectional aerodynamic pitching moment about the undeformed elastic axis. The superscript A denotes aerodynamic loading and is used to distinguish from the inertial loading (superscript I) used in Chapter 4.

The external work done on the fuselage is given by

$$\begin{aligned} \delta W_F = & \int_0^R (F_x^A \delta x_F + F_y^A \delta y_F + F_z^A \delta z_F \\ & - M_{\alpha_s}^A \delta \alpha_s - M_{\phi_s}^A \delta \phi_s) dx \end{aligned} \quad (3.106)$$

where F_x^A , F_y^A , F_z^A are the fuselage aerodynamic forces and $M_{\alpha_s}^A$ and $M_{\phi_s}^A$ are the aerodynamic pitch and roll moments (about the vehicle center of gravity). The negative sign before the moment terms is now explained. The sign convention

in UMARC defines α_s and ϕ_s as positive nose down and advancing side down respectively. The cross products taken to calculate the moments define positive α_s and ϕ_s in the opposite direction, in accordance with the right hand rule of vector multiplication.

In general, aerodynamic forces on the fuselage arise from two sources. The first source is the main rotor. Aerodynamic forces acting on the blades of the main rotor can be transmitted to the fuselage through the rotor hub. Aerodynamic forces which are generated directly by the fuselage also contribute to the work on the fuselage. For example, direct fuselage aerodynamic forces include fuselage drag, fuselage lift and lift on the horizontal tail. In the current version of UMARC, the influence of the direct fuselage aerodynamic forces on system dynamics is neglected. However, for trim analysis, all the external forces are retained. The description of the trim analysis in Chapter 4 includes the effects of direct fuselage aerodynamic forces.

In order to simplify the description of the finite element discretization, the following vector notation is defined

$$\mathbf{L}^A = [L_u^A \ L_v^A \ L_w^A \ L_{\hat{\phi}}^A]^T \quad (3.107)$$

$$\mathbf{u} = [u \ v \ w \ \hat{\phi}]^T \quad (3.108)$$

$$\mathbf{F}_F^A = [F_x^A \ F_y^A \ F_z^A \ M_{\alpha_s}^A \ M_{\phi_s}^A]^T \quad (3.109)$$

$$\mathbf{x}_F = [x_F \ y_F \ z_F \ \alpha_s \ \phi_s]^T \quad (3.110)$$

$$\boldsymbol{\lambda} = [\lambda_0 \ \lambda_{1c} \ \lambda_{1s}]^T \quad (3.111)$$

where \mathbf{L}^A and \mathbf{F}_F^A are the aerodynamic forces acting on the blade and fuselage and \mathbf{u} , \mathbf{x}_F and $\boldsymbol{\lambda}$ are the blade, fuselage and inflow degrees of freedom respectively.

The virtual work on the blade and the virtual work on the fuselage, given by Eq. 3.105 and Eq. 3.106, can be written in symbolic form using Eq. 3.107-Eq. 3.110 as:

$$\delta W_b = \int_0^R \delta \mathbf{u}^T \mathbf{L}^A dr \quad (3.112)$$

$$\delta W_F = \int_0^R \delta \mathbf{x}_F^T \mathbf{F}_F^A dr \quad (3.113)$$

The aerodynamic forces can be expressed as

$$\begin{aligned} \mathbf{L}^A &= \frac{\gamma}{6} [(\mathbf{L}^A)_0 + (\mathbf{L}^A)_q + (\mathbf{L}^A)_{x_F} + (\mathbf{L}^A)_\lambda \\ &\quad + (\mathbf{L}^A)_{q^2} + (\mathbf{L}^A)_{qx_F}] \end{aligned} \quad (3.114)$$

$$\mathbf{F}_F^A = \mathbf{F}_{Fb}^A + \mathbf{F}_{FF}^A \quad (3.115)$$

The subscripts 0, q, x_F , λ , q^2 and qx_F refer to constant terms, linear blade terms, linear fuselage terms, linear inflow terms, nonlinear blade terms and bilinear blade-fuselage terms respectively. The fuselage load \mathbf{F}_{Fb}^A represents the contribution of the blade aerodynamic loads to the total fuselage load. The fuselage load \mathbf{F}_{FF}^A is the contribution of the direct fuselage aerodynamic loads to the total fuselage load and is neglected in the present version of UMARC.

3.1.4 Finite Element Discretization of the Blade Equations

The linear terms in Eq. 3.114 can be written as:

$$\begin{aligned} (\mathbf{L}^A)_q + (\mathbf{L}^A)_{x_F} + (\mathbf{L}^A)_\lambda &= \mathbf{A}_u \mathbf{u} + \mathbf{A}_{u'} \mathbf{u}' + \mathbf{A}_{\dot{u}} \dot{\mathbf{u}} + \mathbf{A}_{\ddot{u}} \ddot{\mathbf{u}} \\ &\quad + \mathbf{A}_{x_F} \mathbf{x}_F + \mathbf{A}_{\dot{x}_F} \dot{\mathbf{x}}_F + \mathbf{A}_\lambda \boldsymbol{\lambda} \end{aligned} \quad (3.116)$$

The displacement vector, \mathbf{u} , is discretized in terms of spatial shape functions, \mathbf{H}_s , and nodal degrees of freedom, \mathbf{q} . This discretization yields

$$\mathbf{u} = \mathbf{H}_s \mathbf{q} \quad (3.117)$$

$$\mathbf{u}' = \mathbf{H}_s' \mathbf{q} \quad (3.118)$$

$$\dot{\mathbf{u}} = \mathbf{H}_s \dot{\mathbf{q}} \quad (3.119)$$

where the spatial shape function matrix is defined by

$$\mathbf{H}_s = \begin{bmatrix} \mathbf{H}_u & 0 & 0 & 0 \\ 0 & \mathbf{H} & 0 & 0 \\ 0 & 0 & \mathbf{H} & 0 \\ 0 & 0 & 0 & \mathbf{H}_\phi \end{bmatrix} \quad (3.120)$$

and the nodal degree of freedom vector is defined by

$$\mathbf{q}^T = [u_1 \ u_2 \ u_3 \ u_4 \ v_1 \ v'_1 \ v_2 \ v'_2 \ w_1 \ w'_1 \ w_2 \ w'_2 \ \hat{\phi}_1 \ \hat{\phi}_2 \ \hat{\phi}_3] \quad (3.121)$$

The specific polynomials used in the spatial shape functions are defined in Chapter 2.3.1.

The discretized expression for the blade virtual work can now be obtained. The virtual work is first discretized using

$$\delta W_b = \sum_{i=1}^{N_e} [\delta W_b]_i \quad (3.122)$$

The next step is to derive the virtual work at the element level. First, substitute Eqs. 3.117- 3.119 into Eq. 3.116. Second, substitute Eq. 3.116 into Eq. 3.114. Third, substitute Eq. 3.114 into Eq. 3.112. These three sequential steps yield the discretized blade virtual work for the i th element.

$$\begin{aligned} [\delta W_b]_i &= \delta \mathbf{q}^T ([\mathbf{M}_b^A]_i \ddot{\mathbf{q}} + [\mathbf{C}_b^A]_i \dot{\mathbf{q}} + [\mathbf{K}_b^A]_i \mathbf{q} + [\mathbf{C}_{bF}^A]_i \dot{\mathbf{x}}_F + [\mathbf{K}_{bF}^A]_i \mathbf{x}_F \\ &\quad + [\mathbf{K}_{b\lambda}^A]_i \boldsymbol{\lambda} + [(\mathbf{Q}_b^A)_{0i}]_i \\ &\quad + [(\mathbf{Q}_b^A)_{q^2}]_i + [(\mathbf{Q}_{bF}^A)_{qx_F}]_i) ds \end{aligned} \quad (3.123)$$

where,

$$[\mathbf{M}_b^A]_i = \frac{\gamma}{6} l_i \int_0^1 \mathbf{H}_s^T \mathbf{A}_{\ddot{\mathbf{u}}} \mathbf{H}_s ds \quad (3.124)$$

$$[\mathbf{C}_b^A]_i = \frac{\gamma}{6} l_i \int_0^1 \mathbf{H}_s^T \mathbf{A}_{\dot{\mathbf{u}}} \mathbf{H}_s ds \quad (3.125)$$

$$[\mathbf{K}_b^A]_i = \frac{\gamma}{6} l_i \int_0^1 (\mathbf{H}_s^T \mathbf{A}_u \mathbf{H}_s + \mathbf{H}_s^T \mathbf{A}_{u'} \mathbf{H}'_s) ds \quad (3.126)$$

$$[\mathbf{C}_{bF}^A]_i = \frac{\gamma}{6} l_i \int_0^1 \mathbf{H}_s^T \mathbf{A}_{\dot{\mathbf{x}}_F} ds \quad (3.127)$$

$$[\mathbf{K}_{bF}^A]_i = \frac{\gamma}{6} l_i \int_0^1 \mathbf{H}_s^T \mathbf{A}_{x_F} ds \quad (3.128)$$

$$[\mathbf{K}_{b\lambda}^A]_i = \frac{\gamma}{6} l_i \int_0^1 \mathbf{H}_s^T \mathbf{A}_{\lambda} ds \quad (3.129)$$

$$[(\mathbf{Q}_b^A)_0]_i = \frac{\gamma}{6} l_i \int_0^1 \mathbf{H}_s^T (\mathbf{L}^A)_0 ds \quad (3.130)$$

$$[(\mathbf{Q}_b^A)_{q^2}]_i = \frac{\gamma}{6} l_i \int_0^1 \mathbf{H}_s^T (\mathbf{L}^A)_{q^2} ds \quad (3.131)$$

$$[(\mathbf{Q}_{bF}^A)_{qx_F}]_i = \frac{\gamma}{6} l_i \int_0^1 \mathbf{H}_s^T (\mathbf{L}^A)_{qx_F} ds \quad (3.132)$$

In the above equations, γ is the Lock number and l_i is the length of the i th element. The constant load vector $[(\mathbf{Q}_b^A)_0]_i$ is used in the response analysis. The nonlinear force vectors $[(\mathbf{Q}_b^A)_{q^2}]_i$ and $[(\mathbf{Q}_{bF}^A)_{qx_F}]_i$ are linearized about the trim position (Section 3.2) and contribute to the stiffness and damping terms.

3.1.5 Finite Element Discretization of the Fuselage Equations

As discussed previously in this section, blade aerodynamic forces can be transmitted to the fuselage through the main rotor hub. The contribution of the blade force, \mathbf{L}^A , to the fuselage aerodynamic force is expressed as

$$\begin{Bmatrix} F_x^A \\ F_y^A \\ F_z^A \\ M_{\alpha_s}^A \\ M_{\phi_s}^A \end{Bmatrix} = \mathbf{T}_{FL} \begin{Bmatrix} L_u^A \\ L_v^A \\ L_w^A \\ M_{\alpha_s}^A \\ M_{\phi_s}^A \end{Bmatrix} \quad (3.133)$$

which can be written in symbolic form as

$$\mathbf{F}_F^A = \mathbf{T}_{FL} \mathbf{L}^A \quad (3.134)$$

where,

$$(\mathbf{T}_{FL}) = \begin{bmatrix} \cos \psi - \beta_p \alpha_s & -\sin \psi & -\beta_p \cos \psi - \alpha_s & 0 \\ \sin \psi + \beta_p \phi_s & \cos \psi & -\beta_p \sin \psi + \phi_s & 0 \\ \beta_p + \alpha_s \cos \psi - \phi_s \sin \psi & -\alpha_s \sin \psi - \phi_s \cos \psi & 1 - \alpha_s \beta_p \cos \psi + \phi_s \beta_p \sin \psi & 0 \\ -x_{cg} \beta_p & (-w - h) \sin \psi & v \sin \psi - (x + u) \cos \psi & (1 - \beta_p w') \sin \psi \\ (w + h) \cos \psi + v \beta_p \sin \psi & -(x + u) \beta_p \sin \psi & -h \beta_p \cos \psi - x_{cg} & +v' \cos \psi \\ \beta_p \cos \psi v + \beta_p v_{cg} & (-w - h) \cos \psi & v \cos \psi + v_{cg} & (1 - \beta_p w') \cos \psi \\ -(h + w) \sin \psi & -(u + x) \beta_p & +(u + x - \beta_p h) \sin \psi & -v' \sin \psi \end{bmatrix}$$

is the fuselage blade transformation matrix and represents the effect of the blade forces on the fuselage.

Derivation of the \mathbf{T}_{FL} matrix

The blade forces in the undeformed blade rotating coordinate system are

$$L_u^A \hat{i} + L_v^A \hat{j} + L_w^A \hat{k} \quad (3.135)$$

Using Eq. 3.34, the components of the blade forces in Eq. 3.135 can be expressed in the hub fixed coordinate system as:

$$\begin{Bmatrix} F_x^A \\ F_y^A \\ F_z^A \end{Bmatrix} = \mathbf{T}_{UH}^T \begin{Bmatrix} L_u^A \\ L_v^A \\ L_w^A \end{Bmatrix} \quad (3.136)$$

The forces induced on the fuselage due to the blade motion can be written in the fuselage axes system using the transformation in Eq. 3.136 as

$$\begin{aligned} F_x^A{}_F &= L_u^A \cos \psi - L_v^A \sin \psi - \beta_p L_w^A \cos \psi \\ F_y^A{}_F &= L_u^A \sin \psi + L_v^A \cos \psi - \beta_p L_w^A \sin \psi \\ F_z^A{}_F &= L_u^A \beta_p + L_w^A \end{aligned} \quad (3.137)$$

The subscript F identify that the equations are in the fuselage axes system. These equations are next transformed to the inertial axes system. It should be noted that the stability analysis is performed in the inertial coordinate system and, therefore, all derivations relating to stability analysis must finally lead to expressions in the inertial axes. The transformation matrix T_{HI} defined in Section 2.1.1 is used to obtain the fuselage forces in the inertial frame as

$$\begin{aligned} F_x^A_I &= L_u^A \cos \psi - L_v^A \sin \psi - \beta_p L_w^A \cos \psi - \underline{(\beta_p L_u + L_w)} \alpha_s \\ F_y^A_I &= L_u^A \sin \psi + L_v^A \cos \psi - \beta_p L_w^A \sin \psi + \underline{(\beta_p L_u + L_w)} \phi_s \\ F_z^A_I &= L_u^A \beta_p + L_w^A + \underline{(L_u^A \cos \psi - L_v^A \sin \psi - \beta_p L_w^A \cos \psi)} \alpha_s \\ &\quad - \underline{(L_u^A \sin \psi + L_v^A \cos \psi - \beta_p L_w^A \sin \psi)} \phi_s \end{aligned} \quad (3.138)$$

The underlined terms in the Eq. 3.138 come from the transformation from the fuselage axes system to the inertial axes system. The subscript I indicates that the fuselage forces are in inertial axes. This subscript is dropped in future reference for notational convenience.

The moment in the blade rotating deformed frame is

$$\bar{M}_{\dot{\phi}}^A \hat{i}_\xi \quad (3.139)$$

The moment in Eq. 3.139 is transformed to the deformed frame using Eq. 3.35 to yield

$$\left\{ \begin{array}{c} M_{\dot{\phi}u}^A \\ M_{\dot{\phi}v}^A \\ M_{\dot{\phi}w}^A \end{array} \right\} = T_{DU} \left\{ \begin{array}{c} \bar{M}_{\dot{\phi}}^A \\ 0 \\ 0 \end{array} \right\} = \left\{ \begin{array}{c} \bar{M}_{\dot{\phi}}^A \\ v' \bar{M}_{\dot{\phi}}^A \\ w' \bar{M}_{\dot{\phi}}^A \end{array} \right\} \quad (3.140)$$

The position vector from the helicopter center of gravity to the point on the blade where the blade forces are acting is given by

$$\begin{aligned}\vec{r}_F &= (x + u) \hat{i} + v \hat{j} + w \hat{k} \\ &+ x_{cg} \hat{I}_H + y_{cg} \hat{J}_H + h \hat{K}_H\end{aligned}\quad (3.141)$$

The moment induced on the fuselage comes from two sources: the blade moment and the moment induced by the blade forces L_u^A , L_v^A and L_w^A due to the moment arm \vec{r}_F from the helicopter center of gravity to the point P on the blade where the forces act (Fig. 2.5). This total moment can be written as

$$M_{\phi u}^A \hat{i} + M_{\phi v}^A \hat{j} + M_{\phi w}^A \hat{k} + \vec{r}_F \times (L_u^A \hat{i} + L_v^A \hat{j} + L_w^A \hat{k}) \quad (3.142)$$

Substituting Eq. 3.140 and 3.141 in Eq. 3.142 and using the transformations defined in Eq. 3.34 gives the fuselage moments as

$$M_{\phi s}^A \hat{I}_H + M_{\alpha s}^A \hat{J}_H \quad (3.143)$$

where

$$\begin{aligned}M_{\phi s}^A &= [(-w - h) \sin \psi + \beta_p \cos \psi v + y_{cg} \beta_p] L_u^A \\ &+ [(-w - h) \cos \psi - (u + x) \beta_p \cos \psi] L_v^A \\ &+ [v \cos \psi + (u + x - \beta_p h) \sin \psi + y_{cg}] L_w^A \\ &+ [(1 - \beta_p w') \cos \psi - v' \sin \psi] M_{\phi}^A\end{aligned}\quad (3.144)$$

$$\begin{aligned}M_{\alpha s}^A &= [(w + h) \cos \psi + v \beta_p \sin \psi - x_{cg} \beta_p] L_u^A \\ &+ [(-w - h - (x + u) \beta_p) \sin \psi] L_v^A \\ &+ [v \sin \psi - (x + u + h \beta_p) \cos \psi - x_{cg}] L_w^A\end{aligned}$$

$$+[v' \cos \psi + (1 - \beta_p w') \sin \psi] M_{\phi}^A \quad (3.145)$$

The fuselage moments in Eq. 3.145 are in the fuselage axes system. The transformation to the inertial axes system is not undertaken for the moments because the yawing moment (the \hat{K}_H component) is small and is neglected throughout the analysis. The corresponding force component ($L_w \hat{K}_H$) is large and the transformation for the forces is necessary. Writing Eqs. 3.138, 3.144 and 3.145 in a matrix form gives the \mathbf{T}_{FL} matrix defined in Eq. 3.133.

3.1.6 Fuselage Blade Matrices

The matrix \mathbf{T}_{FL} contains constant terms, linear blade terms and linear fuselage terms.

$$\mathbf{T}_{FL} = (\mathbf{T}_{FL})_0 + (\mathbf{T}_{FL})_q + (\mathbf{T}_{FL})_{x_F} \quad (3.146)$$

Substituting Eq. 3.114 and Eq. 3.146 in Eq. 3.134 gives

$$\begin{aligned} \mathbf{F}_{Fb}^A &= (\mathbf{F}_{Fb}^A)_0 + (\mathbf{F}_{Fb}^A)_q + (\mathbf{F}_{Fb}^A)_{x_F} \\ &\quad + (\mathbf{F}_{Fb}^A)_\lambda + (\mathbf{F}_{Fb}^A)_{q^2} + (\mathbf{F}_{Fb}^A)_{qx_F} \end{aligned} \quad (3.147)$$

$$\mathbf{F}_{FF}^A = (\mathbf{F}_{FF}^A)_0 \quad (3.148)$$

where

$$(\mathbf{F}_{Fb}^A)_0 = (\mathbf{T}_{FL})_0 (\mathbf{L}^A)_0 \quad (3.149)$$

$$(\mathbf{F}_{Fb}^A)_q = (\mathbf{T}_{FL})_0 (\mathbf{L}^A)_q + (\mathbf{T}_{FL})_q (\mathbf{L}^A)_0 \quad (3.150)$$

$$(\mathbf{F}_{Fb}^A)_{q^2} = (\mathbf{T}_{FL})_0 (\mathbf{L}^A)_{q^2} + (\mathbf{T}_{FL})_q (\mathbf{L}^A)_q \quad (3.151)$$

$$(\mathbf{F}_{Fb}^A)_{qx_F} = (\mathbf{T}_{FL})_q (\mathbf{L}^A)_{x_F} + (\mathbf{T}_{FL})_0 (\mathbf{L}^A)_{qx_F} \quad (3.152)$$

$$(\mathbf{F}_{Fb}^A)_{x_F} = (\mathbf{T}_{FL})_0 \cdot (\mathbf{L}^A)_{x_F} + (\mathbf{T}_{FL})_{x_F} \cdot (\mathbf{L}^A)_0 \quad (3.153)$$

$$(\mathbf{F}_{Fb}^A)_\lambda = (\mathbf{T}_{FL})_0 \cdot (\mathbf{L}^A)_\lambda \quad (3.154)$$

The linear term, $(\mathbf{F}_{Fb}^A)_q$ can be written as (Section 3.2)

$$(\mathbf{F}_{Fb}^A)_q = \mathbf{B}_u \mathbf{u} + \mathbf{B}_{\dot{u}} \dot{\mathbf{u}} + \mathbf{B}_{u'} u' + \mathbf{B}_\lambda \lambda + \mathbf{B}_{x_F} \mathbf{x}_F + \mathbf{B}_{\dot{x}_F} \dot{\mathbf{x}}_F \quad (3.155)$$

Substituting Eq. 3.147 in Eq. 3.113 and discretizing the fuselage virtual work gives:

$$\delta W_F = \sum_{i=1}^{N_e} [\delta W_F]_i \quad (3.156)$$

where

$$\begin{aligned} [\delta W_F]_i &= \delta \mathbf{x}_F^T ([\mathbf{C}_{Fb}^A]_i \dot{\mathbf{q}} + [\mathbf{K}_{Fb}^A]_i \mathbf{q} + [\mathbf{K}_{F\lambda}^A]_i \lambda + [\mathbf{C}_{FF}^A]_i \dot{\mathbf{x}}_F \\ &\quad + [\mathbf{K}_{FF}^A]_i \mathbf{x}_F + [(\mathbf{Q}_{Fb}^A)_0]_i \\ &\quad + [(\mathbf{Q}_{Fb}^A)_0]_{q^2} + [(\mathbf{Q}_{Fb}^A)_{qx_F}]_i) \end{aligned} \quad (3.157)$$

and

$$[\mathbf{C}_{Fb}^A]_i = \frac{\gamma}{6} l_i \int_0^1 \mathbf{B}_{\dot{u}} \mathbf{H}_s \, ds \quad (3.158)$$

$$[\mathbf{K}_{Fb}^A]_i = \frac{\gamma}{6} l_i \int_0^1 (\mathbf{B}_u \mathbf{H}_s + \mathbf{B}_{u'} \mathbf{H}'_s) \, ds \quad (3.159)$$

$$[\mathbf{C}_{FF}^A]_i = \frac{\gamma}{6} l_i \int_0^1 \mathbf{B}_{\dot{x}_F} \, ds \quad (3.160)$$

$$[\mathbf{K}_{FF}^A]_i = \frac{\gamma}{6} l_i \int_0^1 \mathbf{B}_{x_F} \, ds \quad (3.161)$$

$$[\mathbf{K}_{F\lambda}^A]_i = \frac{\gamma}{6} l_i \int_0^1 \mathbf{B}_\lambda \, ds \quad (3.162)$$

$$[(\mathbf{Q}_{Fb}^A)_0]_i = \frac{\gamma}{6} l_i \int_0^1 (\mathbf{F}_{Fb}^A)_0 \, ds \quad (3.163)$$

$$[(\mathbf{Q}_{Fb}^A)_{q^2}]_i = \frac{\gamma}{6} l_i \int_0^1 (\mathbf{F}_{Fb}^A)_{q^2} \, ds \quad (3.164)$$

$$[(\mathbf{Q}_{Fb}^A)_{qx_F}]_i = \frac{\gamma}{6} l_i \int_0^1 (\mathbf{F}_{Fb}^A)_{qx_F} \, ds \quad (3.165)$$

It should be noted that fuselage degrees of freedom are only considered in stability analysis. Also, stability analysis deals exclusively with perturbations about the trimmed mean position of the helicopter. Therefore, the constant load vector $[(\mathbf{Q}_{Fb}^A)_0]_i$ is neglected. The nonlinear force vectors $[(\mathbf{Q}_{Fb}^A)_{q^2}]_i$ and $[(\mathbf{Q}_{Fb}^A)_{qx_F}]_i$ are linearized about the trim position and contribute to the stiffness and damping terms (Section 3.2)

3.1.7 Nonlinear Forces

The mass, stiffness and damping matrices are obtained by considering linear terms only. The force vector \mathbf{Q} can be written for the i element as

$$[\mathbf{Q}]_i = [\mathbf{Q}_0]_i + [\mathbf{Q}_{NL}]_i \quad (3.166)$$

where \mathbf{Q}_0 and \mathbf{Q}_{NL} are the constant and nonlinear part of the element force vector respectively. The nonlinear aerodynamic terms are linearized using a first order Taylor series expansion. Therefore,

$$\begin{aligned} [\mathbf{Q}_{NL}]_i &= [\mathbf{Q}_{NL}]_i|_{q_0} + \frac{\partial [\mathbf{Q}_{NL}]_i}{\partial \mathbf{q}} \dot{\mathbf{q}} + \frac{\partial [\mathbf{Q}_{NL}]_i}{\partial \mathbf{x}_F} \dot{\mathbf{x}}_F \\ &\quad + \frac{\partial [\mathbf{Q}_{NL}]_i}{\partial \dot{\mathbf{q}}} \ddot{\mathbf{q}} + \frac{\partial [\mathbf{Q}_{NL}]_i}{\partial \dot{\mathbf{x}}_F} \ddot{\mathbf{x}}_F \end{aligned} \quad (3.167)$$

The linearization is performed about the trimmed response of the helicopter.

The nonlinear stiffness and damping matrices are provided in Section 3.2.

3.1.8 Fuselage Aerodynamic Modeling

In addition to the contributions from the main rotor, aerodynamic forces and moments on the vehicle are generated by the tail rotor, horizontal and vertical tail surfaces, and the fuselage body (i.e. fuselage drag and pitching moment).

The following section describes the way in which these additional forces are modeled in UMARC.

The tail rotor is modeled using blade element theory. Cyclic flapping is neglected and only collective pitch input is considered. The resulting expression relates tail rotor collective pitch to the thrust of the tail rotor. The tail rotor blades are assumed to be rigid, linearly twisted isotropic blades with symmetric airfoils.

Under these assumptions, the tail rotor thrust coefficient is given by

$$C_{T_{tr}} = \frac{\sigma_{tr} a_{tr}}{2} \left[\frac{\theta_{75tr}}{3} (1 + \mu^2) - \frac{\theta_{twtr}}{8} \mu^2 - \frac{\lambda_{tr}}{2} \right] \quad (3.168)$$

Uniform inflow is used for the tail rotor. The inflow is given by the expression

$$\lambda_{tr} = \frac{C_{T_{tr}}}{\sqrt{\mu^2 + \lambda_{tr}^2}} \quad (3.169)$$

In forward flight, a Newton-Raphson procedure is used to iteratively calculate the tail rotor inflow and thrust. Given the tail rotor thrust coefficient, the

nondimensional tail rotor thrust can be calculated as

$$\frac{T_{tr}}{m_0 \Omega^2 R^2} = C_{T_{tr}} \left(\frac{\Omega_{tr}}{\Omega} \right)^2 \left(\frac{\gamma}{3a} \right) \left(\frac{N_b}{\sigma} \right) \left(\frac{R_{tr}}{R} \right)^4 \quad (3.170)$$

During the coupled trim procedure, the above expression is then used to calculate the side force, yaw moment, and roll moment generated by the tail rotor (see Chapter 4).

The horizontal tail surface can have an important role in determining the trim condition of the helicopter in forward flight. For aeromechanical stability, the horizontal tail can influence the longitudinal fuselage modes of the helicopter. In UMARC, the horizontal tail is modeled as a lifting surface with a cambered inverted airfoil. The lift force on the horizontal tail (positive download) is given by

$$L_{ht} = \frac{1}{2} \rho V^2 S_{ht} (c_{0ht} + c_{1ht} \alpha_{ht}) \quad (3.171)$$

The nondimensional form of the horizontal tail lift is expressed as

$$\frac{L_{ht}}{m_0 \Omega^2 R^2} = \frac{\gamma}{6a} \mu^2 \left(\frac{S_{ht}}{\pi R^2} \right) \left(\frac{N_b}{\sigma} \right) (c_{0ht} + c_{1ht} \alpha_{ht}) \quad (3.172)$$

It is assumed that the horizontal tail is mounted parallel to the longitudinal axis of the fuselage; therefore, the horizontal tail angle of attack, α_{ht} , is given by

$$\alpha_{ht} = \alpha_s + \frac{\dot{z}_F}{\mu \Omega R} + \frac{l_{ht} \dot{\alpha}_s}{\mu \Omega R} \quad (3.173)$$

The horizontal tail is located a distance l_{ht} behind the vehicle center of gravity.

The resulting pitching moment (positive nose-up) is given by

$$M_{ht} = l_{ht} L_{ht} \quad (3.171)$$

The lift force (and resulting pitching moment about the fuselage center of gravity) contribute to the virtual work on the fuselage. Drag force and aerodynamic pitching moment on the horizontal tail are neglected. The effects of the vertical tail are also not considered.

The pressure distribution over the body of the fuselage generally results in fuselage drag, pitching moment, rolling moment, and side force. These effects are modeled in UMARC using the relations below

$$D_F = \frac{1}{2} \rho V^2 f \quad (3.174a)$$

$$Y_F = \frac{1}{2} \rho V^2 \pi R^2 C_{yF} \quad (3.174b)$$

$$M_{xF} = \frac{1}{2} \rho V^2 \pi R^3 C_{mxF} \quad (3.174c)$$

$$M_{yF} = \frac{1}{2} \rho V^2 \pi R^3 C_{myF} \quad (3.174d)$$

In nondimensional form, the above relations are given by

$$\frac{D_F}{m_0 \Omega^2 R^2} = \left(\frac{\gamma N_b}{3\sigma a} \right) \left(\frac{f}{\pi R^2} \right) \left(\frac{\mu^2}{2} \right) \quad (3.174e)$$

$$\frac{Y_F}{m_0 \Omega^2 R^2} = \left(\frac{\gamma N_b}{3\sigma a} \right) \left(\frac{\mu^2}{2} \right) C_{yF} \quad (3.174f)$$

$$\frac{M_{xF}}{m_0 \Omega^2 R^3} = \left(\frac{\gamma N_b}{3\sigma a} \right) \left(\frac{\mu^2}{2} \right) C_{mxF} \quad (3.174g)$$

$$\frac{M_{yF}}{m_0 \Omega^2 R^3} = \left(\frac{\gamma N_b}{3\sigma a} \right) \left(\frac{\mu^2}{2} \right) C_{myF} \quad (3.174h)$$

3.2 Implementation Scheme for Quasi-Steady Aerodynamic Modeling

As evident in the previous section, even the simple quasi-steady aerodynamics for the blade can lead to complex expressions. Rotor blade motions (flap, lag, torsion and axial) and fuselage motions introduce complex nonlinear motion dependent forces in the dynamic system. In UMARC, an efficient procedure is developed to address these complexities.

The quasi-steady aerodynamics is coded in the subroutine "AEROMX" of UMARC. This subroutine calculates the aerodynamic mass, damping and stiffness matrices as well as the load vector. Section 3.3 provides a detailed explanation of the routine AEROMX. The implementation sections described below run parallel to those described in the theory sections to show how theory is translated into coding.

3.2.1 Implementation of the blade velocity

In the code, the nondimensional velocity components, $\frac{U_R}{\Omega R}$, $\frac{U_T}{\Omega R}$, $\frac{U_P}{\Omega R}$ are simply referred as UR , UT , UP . Long mathematical expressions for these velocities are not directly coded in AEROMX; rather, these are broken into constant, linear and nonlinear terms for easier manipulation. The linear terms are grouped according to their dependence on the blade displacement (q), the fuselage displacement (x_F) and the inflow (λ). The nonlinear terms are due to blade motion (q^2), fuselage motion (x_F^2), inflow terms (λ^2), blade-fuselage terms (qx_F), and blade-inflow terms ($q\lambda$).

As explained in the theory section, the blade, fuselage and inflow degrees of freedom are as follows.

$$\mathbf{q}_e^T = [u_1 \ u_2 \ u_3 \ u_4 \ v_1 \ v'_1 \ v_2 \ v'_2 \ w_1 \ w'_1 \ w_2 \ w'_2 \ \hat{\phi}_1 \ \hat{\phi}_2 \ \hat{\phi}_3]^T \quad (3.175)$$

$$\mathbf{x}_F = [x_F \ y_F \ z_F \ \alpha_s \ \phi_s]^T \quad (3.176)$$

$$\boldsymbol{\lambda} = [\lambda_o \ \lambda_{1c} \ \lambda_{1s}]^T \quad (3.177)$$

As mentioned earlier, the blade velocities U_T , U_P and U_R can be written as a combination of constant, linear and nonlinear terms. For example, consider the typical velocity term, U_T ; it can be written as

$$U_T = TC + (TU \ u + TV \ v + \dots + TLS \ \lambda_{1s}) + (TN1 \ vw' + \dots + TNL3 \ \lambda_{1s} \ \hat{\phi}),$$

where TC is the constant term; TU, TV,, TLS are the coefficients associated with the linear displacement terms; and TN1, ..., TNL3 are the coefficients associated with the nonlinear displacement terms.

The Table on the next page provides UMARC Fortran symbols for the various coefficients appearing in the velocity expressions for U_T , U_P and U_R .

Table. Associated Coefficients in Velocity Expressions

Term	U_T	U_P	U_R
Constant	TC	PC	RC
<u>Linear Terms</u>			
u	TU	PU	RU
v	TV	PV	RV
w	TW	PW	RW
$\hat{\phi}$	TP	PP	RP
v'	TVP	PVP	RVP
w'	TWP	PWP	RWP
\dot{v}	TVD	PVD	RVD
\dot{w}	TWD	PWD	RWD
$\ddot{\phi}$	TPD	PPD	RPD
\dot{v}'	TVDP	PVDP	RVDP
\dot{w}'	TWDP	PWDP	RWDP
α_s	TAS	PAS	RAS
x_F	TXFD	PXFD	RXFD
y_F	TYFD	PYFD	RYFD
z_F	TZFD	PZFD	RZFD
$\dot{\alpha}_s$	TASD	PASD	RASD
$\dot{\phi}_s$	TPSD	PPSD	RPSD
λ_o	TLO	PLO	RLO
λ_{1c}	TLC	PLC	RLC
λ_{1s}	TLS	PLS	RLS
<u>Non-linear terms</u>			
vw'	TN1	PN1	0
$\dot{v}\hat{\phi}$	TN2	PN2	0
vv'	TN3	PN3	0
$\dot{w}\hat{\phi}$	TN4	PN4	0
$v'\hat{\phi}$	TN5	PN5	0
$w'\hat{\phi}$	TN6	PN6	0
$v'v'$	TN7	PN7	0
$v'w'$	TN8	PN8	0
$\alpha_s\hat{\phi}$	TNF1	PNF1	0
$\lambda_o\hat{\phi}$	TNL1	PNL1	0
$\lambda_{1c}\hat{\phi}$	TNL2	PNL2	0
$\lambda_{1s}\hat{\phi}$	TNL3	PNL3	0

The coefficients shown in the above table are derived from Eq. 3.44 and are listed below.

Coefficients appearing in U_T :

Constant Term

$$TC = (\lambda_i + \mu\beta_p \cos \psi) \sin \theta + (x + \mu \sin \psi) \cos \theta$$

Linear Terms

TU	=	$\cos \theta$
TU	=	$\cos \theta$
TV	=	$\beta_p \sin \theta$
TW	=	$-\beta_p \cos \theta$
TP	=	$-(x + \mu \sin \psi) \sin \theta + (\lambda_i + \mu\beta_p \cos \psi) \cos \theta$
TVP	=	$\mu \cos \psi \cos \theta$
TWP	=	$\mu \cos \psi \sin \theta$
TVD	=	$\cos \theta$
TWD	=	$\sin \theta$
TPD	=	0
TVDP	=	0
TWDP	=	0
TAS	=	$\mu \sin \theta$
TXFD	=	$-\sin \psi \cos \theta$
TYFD	=	$\cos \psi \cos \theta$
TZFD	=	$\sin \theta$
TASD	=	$h \cos \theta \sin \psi + x \cos \psi \sin \theta + X_{CG} \sin \theta$
TPSD	=	$h \cos \theta \cos \psi - x \sin \psi \sin \theta - Y_{CG} \sin \theta$
TLO	=	$\sin \theta$
TLC	=	$x \sin \theta \cos \psi$
TLS	=	$x \sin \theta \sin \psi$

Nonlinear Terms

TN1	=	$\sin \theta$
TN2	=	$-\sin \theta$
TN3	=	$\cos \theta$
TN4	=	$\cos \theta$
TN5	=	$-\mu \cos \psi \sin \theta$
TN6	=	$\mu \cos \psi \cos \theta$
TN7	=	$-\frac{1}{2}(x + \mu \sin \psi) \cos \theta$
TN8	=	$-(x + \mu \sin \psi) \sin \theta$
TNF1	=	$\mu \cos \theta$
TNL1	=	$\cos \theta$
TNL2	=	$x \cos \theta \cos \psi$
TNL3	=	$x \cos \theta \sin \psi$

Coefficients appearing in U_P :

Constant Term

$$PC = (\lambda_i + \mu\beta_p \cos \psi) \cos \theta - (x + \mu \sin \psi) \sin \theta + \eta_r(\dot{\theta} + \beta_p + \mu \cos \psi \theta_{tw})$$

Linear Terms

PU	=	$-\sin \theta$
PV	=	$\beta_p \cos \theta$
PW	=	$\beta_p \sin \theta$
PP	=	$-(x + \mu \sin \psi) \cos \theta - (\lambda_i + \mu \beta_p \cos \psi) \sin \theta$
PVP	=	$-\mu \cos \psi \sin \theta$
PWP	=	$\mu \cos \psi \cos \theta + \eta_r$
PVD	=	$-\sin \theta$
PWD	=	$\cos \theta$
PPD	=	η_r
PVDP	=	0
PWD _P	=	0
PAS	=	$\mu \cos \theta$
PXFD	=	$\sin \theta \sin \psi$
PYFD	=	$-\sin \theta \cos \psi$
PZFD	=	$\cos \theta$
PASD	=	$-h \sin \theta \sin \psi + x \cos \psi \cos \theta + X_{CG} \cos \theta$
PPSD	=	$-h \sin \theta \cos \psi - x \sin \psi \cos \theta - Y_{CG} \cos \theta$
PLO	=	$\cos \theta$
PLC	=	$x \cos \theta \cos \psi$
PLS	=	$x \cos \theta \sin \psi$

Nonlinear Terms

PN1	=	$\cos \theta$
PN2	=	$-\cos \theta$
PN3	=	$-\sin \theta$
PN4	=	$-\sin \theta$
PN5	=	$-\mu \cos \psi \cos \theta$
PN6	=	$-\mu \cos \psi \sin \theta$
PN7	=	$\frac{1}{2}(x + \mu \sin \psi) \sin \theta$
PN8	=	$-(x + \mu \sin \psi) \cos \theta$
PNF1	=	$-\mu \sin \theta$
PNL1	=	$-\sin \theta$
PNL2	=	$-x \sin \theta \cos \psi$
PNL3	=	$-x \sin \theta \sin \psi$

Coefficients appearing in U_R

Constant Term

$$RC = -\mu \cos \psi + \lambda_i \beta_p - \eta_r \cos \theta$$

Linear Terms

RU	=	0
RV	=	-1
RW	=	0
RP	=	$\eta_r \sin \theta$
RVP	=	$x + \mu \sin \psi$
RWP	=	$\mu \beta_p \cos \psi + \lambda_i$
RVD	=	0
RWD	=	0
RPD	=	0
RVIDP	=	$-\eta_r \cos \theta$
RWDP	=	$-\eta_r \sin \theta$
RLO	=	β_p
RLC	=	$\beta_p x \cos \psi$
RLS	=	$\beta_p x \sin \psi$

Nonlinear terms in U_R are neglected. The blade velocities and their products are written as a sum of constant, linear and nonlinear terms:

$$U_T = TC + [LIN_{TB} + LIN_{TF} + LIN_{TL}]$$

$$+[NL_{TB} + NL_{TBF} + NL_{TBL}]$$

$$U_P = PC + [LIN_{PB} + LIN_{PF} + LIN_{PL}]$$

$$+[NL_{PB} + NL_{PBF} + NL_{PBL}]$$

$$U_R = RC + [LIN_{RB} + LIN_{RF} + LIN_{RL}] \quad (3.178)$$

In the code, the linear and nonlinear trim values of blade motion are defined as follows:

$$LIN_{TB} = SUMT$$

$$\begin{aligned}
NL_{TB} &= SUMTN \\
LIN_{PB} &= SUMP \\
NL_{PB} &= SUMPN \\
LIN_{RB} &= SUMR
\end{aligned} \tag{3.179}$$

where 'LIN' and 'NL' represent linear and nonlinear terms. Among the subscripts, the first letter identifies the direction of the velocity vector and other letters identify whether it is blade term (B), blade-fuselage term (BF), or blade-inflow term (BL). For example LIN_{TB} = linear terms (LIN) in U_T (T) due to blade motion (B).

Velocity Products for Load Calculations :

The aerodynamic loads in Eq. 3.69- 3.72 require the calculation of the velocity product terms. Using the earlier expressions for U_T , U_P and U_R , this is done as follows (the ordering scheme given in Chapter 2 is used here. All terms having order higher than ϵ^2 are neglected):

$$\begin{aligned}
U_T^2 &= \text{constant} + \text{linear} + \text{nonlinear} \\
&= TC^2 + 2TC[LIN_{TB} + LIN_{TF} + LIN_{TL}] \\
&\quad + 2TC[NL_{TB} + NL_{TBF} + NL_{TBL}] + LIN_{TB}^2 + (LIN_{TF})_{\epsilon^2} + LIN_{TL}^2 \\
&\quad + 2[LIN_{TB}(LIN_{TF})_{\epsilon} + LIN_{TB}LIN_{TL} + (LIN_{TF})_{\epsilon}LIN_{TL}] \\
&= TT0 + TT1 u + TT2 v + TT3 w + TT4 \hat{\phi} + \dots \text{etc....(IN CODE).}
\end{aligned}$$

(3.180)

$$\begin{aligned}
U_P^2 &= \text{constant} + \text{linear} + \text{nonlinear} \\
&= PC^2 + 2PC[LIN_{PB} + LIN_{PF} + LIN_{PL}] \\
&\quad + 2PC[NL_{PB} + NL_{PBF} + NL_{PBL}] + LIN_{PB}^2 + (LIN_{PF})_{\epsilon 2} + LIN_{PL}^2 \\
&\quad + 2[LIN_{PB}(LIN_{PF})_{\epsilon} + LIN_{PB}LIN_{PL} + (LIN_{PF})_{\epsilon}LIN_{PL}] \\
&= PP0 + PP1 u + PP2 v + PP3 w + PP4 \dot{\phi} + \dots \text{etc.} \dots (\text{IN CODE}). \\
&
\end{aligned} \tag{3.181}$$

$$\begin{aligned}
U_T U_P &= \text{constant} + \text{linear} + \text{nonlinear} \\
&= PC.TC + PC[LIN_{TB} + LIN_{TF} + LIN_{TL}] \\
&\quad + TC[LIN_{PB} + LIN_{PF} + LIN_{PL}] \\
&\quad + PC[NL_{TB} + NL_{TBF} + NL_{TBL}] + TC[NL_{PB} + NL_{PBF} + NL_{PBL}] \\
&\quad + [LIN_{TB} + (LIN_{TF})_{\epsilon} + LIN_{TL}] \times \\
&\quad [LIN_{PB} + (LIN_{PF})_{\epsilon} + LIN_{PL}] \\
&= TP0 + TP1 u + TP2 v + TP3 w + TP4 \dot{\phi} + \dots \text{etc.} \dots (\text{IN CODE}). \\
&
\end{aligned} \tag{3.182}$$

$$\begin{aligned}
U_R U_T &= \text{constant} + \text{linear} + \text{nonlinear} \\
&= RC.TC + RC[LIN_{TB} + LIN_{TF} + LIN_{TL}] \\
&\quad + TC[LIN_{RB} + LIN_{RF} + LIN_{RL}] \\
&\quad + RC[NL_{TB} + NL_{TBF} + NL_{TBL}]
\end{aligned}$$

$$\begin{aligned}
& + [LIN_{TB} + (LIN_{TF})_\epsilon + LIN_{TL}] \times \\
& [LIN_{RB} + (LIN_{RF})_\epsilon + LIN_{PL}] \\
= & RT0 + RT1 u + RT2 v + RT3 w + RT4 \hat{\phi} + \dots \text{etc.} \dots (\text{IN CODE}).
\end{aligned} \tag{3.183}$$

In the expressions for product of velocities, subscripts ϵ and ϵ^2 indicate that terms up to that order only are retained.

3.2.2 Implementation of Linear Aerodynamics

The linear aerodynamic matrices arise due to blade motion (q), fuselage motion (x_F) and inflow (λ) terms.

Constant and Linear Aerodynamic Forces in Undeformed Frame :

Using Eq. 3.69- 3.72, the constant and linear aerodynamic force terms are obtained in the deformed frame. These forces are transformed to the undeformed frame by the following transformation.

$$\begin{aligned} \left\{ \begin{array}{c} L_u^A \\ L_v^A \\ L_w^A \end{array} \right\} &= \mathbf{T}_{DU}^{-1} \left\{ \begin{array}{c} \bar{L}_u \\ \bar{L}_v \\ \bar{L}_w \end{array} \right\} = \mathbf{T}_{DU}^T \left\{ \begin{array}{c} \bar{L}_u \\ \bar{L}_v \\ \bar{L}_w \end{array} \right\} \\ M_{\dot{\phi}}^A &= \bar{M}_{\dot{\phi}} \quad (3.184) \end{aligned}$$

The transformation matrix \mathbf{T}_{DU}^T , derived in Chapter 2, can be written as a summation of constant, linear and nonlinear terms in the following manner.

$$\mathbf{T}_{DU}^T = \left(\mathbf{T}_{DU}^T \right)_o + \left(\mathbf{T}_{DU}^T \right)_q + \left(\mathbf{T}_{DU}^T \right)_{q^2} \quad (3.185)$$

where,

$$(\mathbf{T}_{DU})_o^T = \begin{bmatrix} 1 & 0 & 0 \\ 0 & \cos \theta & -\sin \theta \\ 0 & \sin \theta & \cos \theta \end{bmatrix}$$

$$(\mathbf{T}_{DU})_q^T = \begin{bmatrix} 0 & -v' \cos \theta - w' \sin \theta & v' \sin \theta - w' \cos \theta \\ v' & -\hat{\phi} \sin \theta & -\hat{\phi} \cos \theta \\ w' & \hat{\phi} \cos \theta & -\hat{\phi} \sin \theta \end{bmatrix}$$

$$(\mathbf{T}_{DU})_{q^2}^T = \begin{bmatrix} -\frac{1}{2}(v'^2 + w'^2) & \hat{\phi}(v' \sin \theta - w' \cos \theta) & \hat{\phi}(v' \cos \theta + w' \sin \theta) \\ 0 & -\frac{1}{2}v'^2 \cos \theta - v'w' \sin \theta & \frac{1}{2}v'^2 \sin \theta - v'w' \cos \theta \\ 0 & -\frac{1}{2}w'^2 \sin \theta & \frac{1}{2}w'^2 \cos \theta \end{bmatrix}$$

Constant Forces and Moment :

The blade forces in Eq. 3.184 have constant, linear and nonlinear components.

The constant part of the blade forces is given by :

$$\begin{aligned} \left\{ \begin{array}{c} L_u^A \\ L_v^A \\ L_w^A \end{array} \right\}_o &= (\mathbf{T}_{DU}^T)_o \left\{ \begin{array}{c} \bar{L}_u \\ \bar{L}_v \\ \bar{L}_w \end{array} \right\}_o \\ (M_{\hat{\phi}}^A)_o &= (\bar{M}_{\hat{\phi}})_o \end{aligned} \quad (3.186)$$

Linear Forces and Moment :

The linear forces and moments are due to blade, fuselage and inflow terms.

Due to Blade Motion :

$$\begin{aligned} \left\{ \begin{array}{c} L_u^A \\ L_v^A \\ L_w^A \end{array} \right\}_q &= (\mathbf{T}_{DU}^T)_o \left\{ \begin{array}{c} \bar{L}_u \\ \bar{L}_v \\ \bar{L}_w \end{array} \right\}_q + (\mathbf{T}_{DU}^T)_q \left\{ \begin{array}{c} \bar{L}_u \\ \bar{L}_v \\ \bar{L}_w \end{array} \right\}_o \\ (M_{\hat{\phi}}^A)_q &= (\bar{M}_{\hat{\phi}})_q \end{aligned} \quad (3.187)$$

This can be written in matrix notations as

$$(\mathbf{L}^A)_q = \frac{\gamma}{6} (\mathbf{A}_u \mathbf{u} + \mathbf{A}_{u'} \mathbf{u}' + \mathbf{A}_{\dot{u}} \dot{\mathbf{u}} + \mathbf{A}_{\ddot{u}} \ddot{\mathbf{u}}) \quad (3.188)$$

where

$$\begin{aligned} \mathbf{u} &= [u \ v \ w \ \dot{\phi}]^T \\ \mathbf{u}' &= [u' \ v' \ w' \ \dot{\phi}']^T \\ \dot{\mathbf{u}} &= [\dot{u} \ \dot{v} \ \dot{w} \ \ddot{\phi}]^T \\ \ddot{\mathbf{u}} &= [\ddot{u} \ \ddot{v} \ \ddot{w} \ \ddot{\dot{\phi}}]^T \end{aligned} \quad (3.189)$$

In the above equation, $\mathbf{A}_{\ddot{u}}$ is due to noncirculatory terms.

Due to Fuselage Motion :

$$\begin{aligned} \left\{ \begin{array}{c} L_u^A \\ L_v^A \\ L_w^A \end{array} \right\}_{x_F} &= (\mathbf{T}_{DU}^T)_{\circ} \left\{ \begin{array}{c} \bar{L}_u \\ \bar{L}_v \\ \bar{L}_w \end{array} \right\}_{x_F} \\ (M_{\dot{\phi}}^A)_{x_F} &= (\bar{M}_{\dot{\phi}})_{x_F} \end{aligned} \quad (3.190)$$

This can be written in matrix notations as

$$(\mathbf{L}^A)_{x_F} = \frac{\gamma}{6} (\mathbf{A}_{x_F} \mathbf{x}_F + \mathbf{A}_{\dot{x}_F} \dot{\mathbf{x}}_F) \quad (3.191)$$

where

$$\mathbf{x}_F = [x_F \ y_F \ z_F \ \alpha_s \ \phi_s]^T \quad (3.192)$$

Due to Inflow :

$$\begin{aligned} \left\{ \begin{array}{c} L_u^A \\ L_v^A \\ L_w^A \end{array} \right\}_\lambda &= (\mathbf{T}_{DU}^T)_o \left\{ \begin{array}{c} \bar{L}_u \\ \bar{L}_v \\ \bar{L}_w \end{array} \right\}_\lambda \\ (M_\phi^A)_\lambda &= (\bar{M}_\phi)_\lambda \end{aligned} \quad (3.193)$$

This can be written in matrix notations as

$$(\mathbf{L}^A)_\lambda = \frac{\gamma}{6} \mathbf{A}_\lambda \boldsymbol{\lambda} \quad (3.194)$$

where

$$\boldsymbol{\lambda} = [\lambda_o \quad \lambda_{1c} \quad \lambda_{1s}]^T \quad (3.195)$$

In the above three equations, the subscripts q , x_F , and λ represent linear terms due to blade, fuselage and inflow respectively and the force vector \mathbf{L}^A is defined as :

$$(\mathbf{L}^A) = \left\{ \begin{array}{c} L_u^A \\ L_v^A \\ L_w^A \\ M_\phi^A \end{array} \right\} \quad (3.196)$$

All the linear forces can now be combined as follows.

$$\begin{aligned} (\mathbf{L}^A)_L &= (\mathbf{L}^A)_q + (\mathbf{L}^A)_{x_F} + (\mathbf{L}^A)_\lambda \\ &= \frac{\gamma}{6} (\mathbf{A}_u \mathbf{u} + \mathbf{A}_{u'} \mathbf{u}' + \mathbf{A}_{\dot{u}} \dot{\mathbf{u}} + \mathbf{A}_{\ddot{u}} \ddot{\mathbf{u}} \\ &\quad + \mathbf{A}_{x_F} \mathbf{x}_F + \mathbf{A}_{\dot{x}_F} \dot{\mathbf{x}}_F + \mathbf{A}_\lambda \boldsymbol{\lambda}) \end{aligned} \quad (3.197)$$

In UMARC, the linear aerodynamic matrices are defined as :

$$\mathbf{A}_u = \begin{bmatrix} U1 & U2 & U4 & U6 \\ V1 & V2 & V4 & V6 \\ W1 & W2 & W4 & W6 \\ AM1 & AM2 & AM4 & AM6 \end{bmatrix} \quad (3.198)$$

$$\mathbf{A}_{u'} = \begin{bmatrix} 0 & U3 & U5 & 0 \\ 0 & V3 & V5 & 0 \\ 0 & W3 & W5 & 0 \\ 0 & AM3 & AM5 & 0 \end{bmatrix} \quad (3.199)$$

$$\mathbf{A}_{\dot{u}} = \begin{bmatrix} 0 & U8 & U10 & U12 \\ 0 & V8 & V10 & V12 \\ 0 & W8 & W10 & W12 \\ 0 & AM8 & AM10 & AM12 \end{bmatrix} \quad (3.200)$$

$$\mathbf{A}_{\ddot{u}} = \begin{bmatrix} 0 & 0 & 0 & 0 \\ 0 & 0 & 0 & 0 \\ 0 & 0 & -CARG & CARGE \\ 0 & 0 & CARGE & -CARGE \end{bmatrix} \quad (3.201)$$

$$\mathbf{A}_{x_F} = \begin{bmatrix} 0 & 0 & 0 & UF4 & 0 \\ 0 & 0 & 0 & VF4 & 0 \\ 0 & 0 & 0 & WF4 & 0 \\ 0 & 0 & 0 & AMF4 & 0 \end{bmatrix} \quad (3.202)$$

$$\mathbf{A}_{\dot{x}_F} = \begin{bmatrix} UF6 & UF7 & UF8 & UF9 & UF10 \\ VF6 & VF7 & VF8 & VF9 & VF10 \\ WF6 & WF7 & WF8 & WF9 & WF10 \\ AMF6 & AMF7 & AMF8 & AMF9 & AMF10 \end{bmatrix} \quad (3.203)$$

$$\mathbf{A}_\lambda = \begin{bmatrix} UL1 & UL2 & UL3 \\ VL1 & VL2 & VL3 \\ WL1 & WL2 & WL3 \\ AML1 & AML2 & AML3 \end{bmatrix} \quad (3.204)$$

The shape function matrices corresponding to \mathbf{u} and \mathbf{u}' are as follows (the individual terms are given in Chapter 2):

$$\mathbf{H}_s = \begin{bmatrix} \mathbf{H}_u(s) & 0 & 0 & 0 \\ 0 & \mathbf{H}(s) & 0 & 0 \\ 0 & 0 & \mathbf{H}(s) & 0 \\ 0 & 0 & 0 & \mathbf{H}_{\dot{\phi}}(s) \end{bmatrix} \quad (3.205)$$

$$\mathbf{H}'_s = \begin{bmatrix} \mathbf{H}'_u(s) & 0 & 0 & 0 \\ 0 & \mathbf{H}'(s) & 0 & 0 \\ 0 & 0 & \mathbf{H}'(s) & 0 \\ 0 & 0 & 0 & \mathbf{H}'_{\dot{\phi}}(s) \end{bmatrix} \quad (3.206)$$

$$\mathbf{u} = \mathbf{H}_s \mathbf{q}$$

$$\mathbf{u}' = \mathbf{H}'_s \mathbf{q}$$

$$\dot{\mathbf{u}} = \mathbf{H}_s \dot{\mathbf{q}} \quad (3.207)$$

Using the shape functions, the linear aerodynamic load vector can be expressed as

$$\begin{aligned} (\mathbf{L}^A)_L = \frac{\gamma}{6} & (\mathbf{A}_u \mathbf{H}_s \mathbf{q} + \mathbf{A}_{u'} \mathbf{H}'_s \mathbf{q} + \mathbf{A}_{\dot{u}} \mathbf{H}_s \dot{\mathbf{q}} + \mathbf{A}_{\ddot{u}} \mathbf{H}_s \ddot{\mathbf{q}} \\ & + \mathbf{A}_{x_F} \mathbf{x}_F + \mathbf{A}_{\dot{x}_F} \dot{\mathbf{x}}_F + \mathbf{A}_\lambda \boldsymbol{\lambda}) \end{aligned} \quad (3.208)$$

In the code, the linear element matrices are calculated first. Then the nonlinear matrices are added as a user-specified option.

3.2.3 Implementation of Nonlinear Aerodynamics

The nonlinear aerodynamic matrices come from the blade-blade terms (q^2), fuselage-blade terms (qx_F) and inflow-blade terms (λq) in the virtual work expression.

Nonlinear Forces :

The nonlinear forces are due to blade, fuselage and inflow terms.

$$(\mathbf{L}^A)_{NL} = (\mathbf{L}^A)_{q^2} + (\mathbf{L}^A)_{x_F^2} + (\mathbf{L}^A)_{\lambda^2} + (\mathbf{L}^A)_{qx_F} + (\mathbf{L}^A)_{q\lambda} \quad (3.209)$$

Nonlinear Forces due to Blade

$$\begin{aligned} \left\{ \begin{array}{c} L_u^A \\ L_v^A \\ L_w^A \end{array} \right\}_{q^2} &= \left(\mathbf{T}_{DU}^T \right)_o \left\{ \begin{array}{c} \bar{L}_u \\ \bar{L}_v \\ \bar{L}_w \end{array} \right\}_{q^2} + \left(\mathbf{T}_{DU}^T \right)_q \left\{ \begin{array}{c} \bar{L}_u \\ \bar{L}_v \\ \bar{L}_w \end{array} \right\}_q + \left(\mathbf{T}_{DU}^T \right)_{q^2} \left\{ \begin{array}{c} \bar{L}_u \\ \bar{L}_v \\ \bar{L}_w \end{array} \right\}_o \\ (M_{\dot{\phi}}^A)_{q^2} &= (\bar{M}_{\dot{\phi}})_{q^2} \end{aligned} \quad (3.210)$$

Nonlinear Forces due to Fuselage Terms

$$\begin{aligned} \left\{ \begin{array}{c} L_u^A \\ L_v^A \\ L_w^A \end{array} \right\}_{x_F^2} &= \left(\mathbf{T}_{DU}^T \right)_o \left\{ \begin{array}{c} \bar{L}_u \\ \bar{L}_v \\ \bar{L}_w \end{array} \right\}_{x_F^2} \\ (M_{\dot{\phi}}^A)_{x_F^2} &= (\bar{M}_{\dot{\phi}})_{x_F^2} \end{aligned} \quad (3.211)$$

Nonlinear Forces due to Inflow Terms

$$\begin{aligned} \left\{ \begin{array}{c} L_u^A \\ L_v^A \\ L_w^A \end{array} \right\}_{\lambda^2} &= \left(\mathbf{T}_{DU}^T \right)_o \left\{ \begin{array}{c} \bar{L}_u \\ \bar{L}_v \\ \bar{L}_w \end{array} \right\}_{\lambda^2} \\ (M_{\dot{\phi}}^A)_{\lambda^2} &= (\bar{M}_{\dot{\phi}})_{\lambda^2} \end{aligned} \quad (3.212)$$

Nonlinear Forces due to Bilinear Terms : The bilinear terms come from coupled blade-inflow ($q\lambda$) and blade-fuselage terms (qx_F).

$$\begin{aligned} \left\{ \begin{array}{c} L_u^A \\ L_v^A \\ L_w^A \end{array} \right\}_{qx_F} &= \left(\mathbf{T}_{DU}^T \right)_o \left\{ \begin{array}{c} \bar{L}_u \\ \bar{L}_v \\ \bar{L}_w \end{array} \right\}_{qx_F} + \left(\mathbf{T}_{DU}^T \right)_q \left\{ \begin{array}{c} \bar{L}_u \\ \bar{L}_v \\ \bar{L}_w \end{array} \right\}_{x_F} \\ (M_{\dot{\phi}}^A)_{qx_F} &= (\bar{M}_{\dot{\phi}})_{qx_F} \end{aligned} \quad (3.213)$$

$$\begin{aligned} \left\{ \begin{array}{c} L_u^A \\ L_v^A \\ L_w^A \end{array} \right\}_{q\lambda} &= \left(\mathbf{T}_{DU}^T \right)_o \left\{ \begin{array}{c} \bar{L}_u \\ \bar{L}_v \\ \bar{L}_w \end{array} \right\}_{q\lambda} + \left(\mathbf{T}_{DU}^T \right)_q \left\{ \begin{array}{c} \bar{L}_u \\ \bar{L}_v \\ \bar{L}_w \end{array} \right\}_{\lambda} \\ (M_{\dot{\phi}}^A)_{q\lambda} &= (\bar{M}_{\dot{\phi}})_{q\lambda} \end{aligned}$$

Linearization of Nonlinear Forces: The nonlinear forces are linearized using first order Taylor's series expansion.

$$\begin{aligned} (\mathbf{L}^A)_{NL} &= (\mathbf{L}^A)_{NL}|_o + \frac{\partial}{\partial \mathbf{q}_e} (\mathbf{L}^A)_{NL} \Delta \mathbf{q} + \frac{\partial}{\partial \dot{\mathbf{q}}_e} (\mathbf{L}^A)_{NL} \Delta \dot{\mathbf{q}} \\ &\quad + \frac{\partial}{\partial \mathbf{x}_F} (\mathbf{L}^A)_{NL} \Delta \mathbf{x}_F + \frac{\partial}{\partial \dot{\mathbf{x}}_F} (\mathbf{L}^A)_{NL} \Delta \dot{\mathbf{x}}_F \\ &\quad + \frac{\partial}{\partial \boldsymbol{\lambda}} (\mathbf{L}^A)_{NL} \Delta \boldsymbol{\lambda} \\ &= (\mathbf{L}^A)_{NL}|_o + (\mathbf{A}_u)_{NL} \mathbf{u} + (\mathbf{A}_{u'})_{NL} \mathbf{u}' + (\mathbf{A}_{\dot{u}})_{NL} \dot{\mathbf{u}} \\ &\quad + (\mathbf{A}_{x_F})_{NL} \mathbf{x}_F + (\mathbf{A}_{\dot{x}_F})_{NL} \dot{\mathbf{x}}_F \\ &\quad + (\mathbf{A}_{\lambda})_{NL} \boldsymbol{\lambda} \\ &= (\mathbf{L}^A)_{NL}|_o + (\mathbf{A}_u)_{NL} \mathbf{H}_s \mathbf{q} + (\mathbf{A}_{u'})_{NL} \mathbf{H}'_s \mathbf{q} + (\mathbf{A}_{\dot{u}})_{NL} \mathbf{H}_s \dot{\mathbf{q}} \\ &\quad + (\mathbf{A}_{x_F})_{NL} \mathbf{x}_F + (\mathbf{A}_{\dot{x}_F})_{NL} \dot{\mathbf{x}}_F \\ &\quad + (\mathbf{A}_{\lambda})_{NL} \boldsymbol{\lambda} \end{aligned} \quad (3.214)$$

In the code, the trim nonlinear forces are coded as follows.

$$(\mathbf{L}^A)_{NL}|_o = \begin{Bmatrix} XANLU \\ XANLV \\ XANLW \\ AXNLM \end{Bmatrix} \quad (3.215)$$

The nonlinear aerodynamic matrices $(\mathbf{A}_u)_{NL}$, $(\mathbf{A}_{u'})_{NL}$ and $(\mathbf{A}_{\dot{u}})_{NL}$ are written in the following manner.

$$\begin{aligned} (\mathbf{A}_u)_{NL} &= \left[\frac{\partial}{\partial u}(\mathbf{L}^A)_{q^2} \quad \frac{\partial}{\partial v}(\mathbf{L}^A)_{q^2} \quad \frac{\partial}{\partial w}(\mathbf{L}^A)_{q^2} \quad \frac{\partial}{\partial \phi}(\mathbf{L}^A)_{q^2} \right] \\ &= \begin{bmatrix} DFU1 & DFU2 & DFU4 & DFU6 \\ DFV1 & DFV2 & DFV4 & DFV6 \\ DFW1 & DFW2 & DFW4 & DFW6 \\ DFM1 & DFM2 & DFM4 & DFM6 \end{bmatrix} \end{aligned} \quad (3.216)$$

$$\begin{aligned} (\mathbf{A}_{u'})_{NL} &= \left[\frac{\partial}{\partial u'}(\mathbf{L}^A)_{q^2} \quad \frac{\partial}{\partial v'}(\mathbf{L}^A)_{q^2} \quad \frac{\partial}{\partial w'}(\mathbf{L}^A)_{q^2} \quad \frac{\partial}{\partial \phi'}(\mathbf{L}^A)_{q^2} \right] \\ &= \begin{bmatrix} 0 & DFU3 & DFU5 & 0 \\ 0 & DFV3 & DFV5 & 0 \\ 0 & DFW3 & DFW5 & 0 \\ 0 & DFM3 & DFM5 & 0 \end{bmatrix} \end{aligned} \quad (3.217)$$

$$\begin{aligned} (\mathbf{A}_{\dot{u}})_{NL} &= \left[\frac{\partial}{\partial \dot{v}}(\mathbf{L}^A)_{q^2} \quad \frac{\partial}{\partial \dot{v}}(\mathbf{L}^A)_{q^2} \quad \frac{\partial}{\partial \dot{w}}(\mathbf{L}^A)_{q^2} \quad \frac{\partial}{\partial \dot{\phi}}(\mathbf{L}^A)_{q^2} \right] \\ &= \begin{bmatrix} 0 & DFU8 & DFU10 & DFU12 \\ 0 & DFV8 & DFV10 & DFV12 \\ 0 & DFW8 & DFW10 & DFW12 \\ 0 & DFM8 & DFM10 & DFM12 \end{bmatrix} \end{aligned} \quad (3.218)$$

In the code, DFX and DFXD matrices are as follows.

$$DFX = \mathbf{H}_s^T (\mathbf{A}_u)_{NL} \mathbf{H}_s + \mathbf{H}_s^T (\mathbf{A}_{u'})_{NL} \mathbf{H}'_s$$

$$DFXD = \mathbf{H}_s^T (\mathbf{A}_u)_{NL} \mathbf{H}_s$$

(3.219)

Total Aerodynamic Forces :

The total aerodynamic forces are the summation of the constant, linear and nonlinear forces.

$$\begin{aligned}
(\mathbf{L}^A) &= (\mathbf{L}^A)_o + (\mathbf{L}^A)_L + (\mathbf{L}^A)_{NL} \\
&= (\mathbf{L}^A)_o + (\mathbf{L}^A)_{NL}|_o \\
&\quad + \{\mathbf{A}_u \mathbf{H}_s + \mathbf{A}_{u'} \mathbf{H}'_s + (\mathbf{A}_u)_{NL} \mathbf{H}_s + (\mathbf{A}_{u'})_{NL} \mathbf{H}'_s\} \mathbf{q} \\
&\quad + \{\mathbf{A}_{\dot{u}} \mathbf{H}_s + (\mathbf{A}_{\dot{u}})_{NL} \mathbf{H}_s\} \dot{\mathbf{q}} \\
&\quad + \mathbf{A}_{\ddot{u}} \mathbf{H}_s \ddot{\mathbf{q}} \\
&\quad + \{\mathbf{A}_{x_F} + (\mathbf{A}_{x_F})_{NL}\} \mathbf{x}_F \\
&\quad + \{\mathbf{A}_{\dot{x}_F} + (\mathbf{A}_{\dot{x}_F})_{NL}\} \dot{\mathbf{x}}_F \\
&\quad + \{\mathbf{A}_{\lambda} + (\mathbf{A}_{\lambda})_{NL}\} \boldsymbol{\lambda}
\end{aligned} \tag{3.220}$$

3.2.4 Virtual Work due to Blade Motion

The virtual work done on the blade due to aerodynamic forces is given by

$$\delta W_b = \int_0^R \delta \mathbf{u}^T \mathbf{L}^A dr \tag{3.221}$$

Substituting the total aerodynamic force vector for \mathbf{L}^A , we obtain the following aerodynamic matrices.

Blade Aerodynamic Matrices

$$\begin{aligned}
 (\mathbf{M}_b^A)^i &= -\frac{\gamma}{6} l_i \int_0^1 \mathbf{H}_s^T \mathbf{A}_{\bar{u}} \mathbf{H}_s ds \\
 (\mathbf{K}_b^A)^i &= -\frac{\gamma}{6} l_i \int_0^1 \mathbf{H}_s^T \{ \mathbf{A}_u \mathbf{H}_s + \mathbf{A}_{u'} \mathbf{H}'_s + (\mathbf{A}_u)_{NL} \mathbf{H}_s + (\mathbf{A}_{u'})_{NL} \mathbf{H}'_s \} ds \\
 (\mathbf{C}_b^A)^i &= -\frac{\gamma}{6} l_i \int_0^1 \mathbf{H}_s^T \{ \mathbf{A}_{\dot{u}} \mathbf{H}_s + (\mathbf{A}_{\dot{u}})_{NL} \mathbf{H}_s \} ds
 \end{aligned} \tag{3.222}$$

Blade Fuselage Matrices

$$\begin{aligned}
 (\mathbf{K}_{bF}^A)^i &= -\frac{\gamma}{6} l_i \int_0^1 \mathbf{H}_s^T \{ \mathbf{A}_{x_F} + (\mathbf{A}_{x_F})_{NL} \} ds \\
 (\mathbf{C}_{bF}^A)^i &= -\frac{\gamma}{6} l_i \int_0^1 \mathbf{H}_s^T \{ \mathbf{A}_{\dot{x}_F} + (\mathbf{A}_{\dot{x}_F})_{NL} \} ds
 \end{aligned} \tag{3.223}$$

Blade Inflow Matrices

$$(\mathbf{K}_{b\lambda}^A)^i = -\frac{\gamma}{6} l_i \int_0^1 \mathbf{H}_s^T \{ \mathbf{A}_\lambda + (\mathbf{A}_\lambda)_{NL} \} ds \tag{3.224}$$

Load Vector

$$(\mathbf{Q}_{b\lambda}^A)^i = \frac{\gamma}{6} l_i \int_0^1 \mathbf{H}_s^T \{ (\mathbf{L}^A)_o + (\mathbf{L}^A)_{NL}|_o \} ds \tag{3.225}$$

3.2.5 Virtual Work due to Fuselage Motion

$$\delta W_{Fb} = \int_0^R \delta \mathbf{x}_F^T \mathbf{F}_F^A dr \quad (3.226)$$

The blade load vector, (\mathbf{L}^A) , is transferred to the fixed frame fuselage forces and moments (\mathbf{F}_F^A) using the transformation matrix \mathbf{T}_{FL} . The derivation of this matrix is provided in section 3.2.2.

$$\mathbf{F}_F^A = \mathbf{T}_{FL} \mathbf{L}^A \quad (3.227)$$

The blade element force vector \mathbf{L}^A is a summation of constant, linear and second order nonlinear terms due to blade, fuselage and inflow terms. The transformation matrix \mathbf{T}_{FL} is a summation of only the constant and linear terms.

$$\begin{aligned} \mathbf{L}^A &= (\mathbf{L}^A)_o + (\mathbf{L}^A)_q + (\mathbf{L}^A)_{q^2} \\ &\quad + (\mathbf{L}^A)_{x_F} + (\mathbf{L}^A)_{x_F^2} \\ &\quad + (\mathbf{L}^A)_\lambda + (\mathbf{L}^A)_{\lambda^2} \\ &\quad + (\mathbf{L}^A)_{qx_F} + (\mathbf{L}^A)_{q\lambda} \\ \mathbf{T}_{FL} &= (\mathbf{T}_{FL})_o + (\mathbf{T}_{FL})_q + (\mathbf{T}_{FL})_{x_F} \end{aligned} \quad (3.228)$$

Constant Force and Moment:

$$(\mathbf{F}_F^A)_o = (\mathbf{T}_{FL})_o (\mathbf{L}^A)_o \quad (3.229)$$

Linear Forces and Moment :

$$(\mathbf{F}_F^A)_L = (\mathbf{T}_{FL})_q (\mathbf{L}^A)_o + (\mathbf{T}_{FL})_{x_F} (\mathbf{L}^A)_0 + (\mathbf{T}_{FL})_o (\mathbf{L}^A)_L \quad (3.230)$$

where,

$$(\mathbf{T}_{FL})_o = \begin{bmatrix} \cos \psi & -\sin \psi & -\beta_p \cos \psi & 0 \\ \sin \psi & \cos \psi & -\beta_p \sin \psi & 0 \\ \beta_p & 0 & 1 & 0 \\ h \cos \psi - \beta_p X_{CG} & -(h + x\beta_p) \sin \psi & -(x + h\beta_p) \cos \psi - X_{CG} & \sin \psi \\ -h \sin \psi + \beta_p Y_{CG} & -(h + x\beta_p) \cos \psi & (x + h\beta_p) \sin \psi + Y_{CG} & \cos \psi \end{bmatrix}$$

$$(\mathbf{T}_{FL})_q = \begin{bmatrix} 0 & 0 & 0 & 0 \\ 0 & 0 & 0 & 0 \\ 0 & 0 & 0 & 0 \\ v\beta_p \sin \psi + w \cos \psi & -w \sin \psi & -u \cos \psi + v \sin \psi & -w' \beta_p \sin \psi + v' \cos \psi \\ v\beta_p \cos \psi - w \sin \psi & -w \cos \psi & v \cos \psi + u \sin \psi & -w' \beta_p \cos \psi - v' \sin \psi \end{bmatrix}$$

$$(\mathbf{T}_{FL})_{xF} = \begin{bmatrix} -\beta_p \alpha_s & 0 & -\alpha_s & 0 \\ \beta_p \phi_s & 0 & \phi_s & 0 \\ \alpha_s \cos \psi - \phi_s \sin \psi & -\alpha_s \sin \psi - \phi_s \cos \psi & -\alpha_s \beta_p \cos \psi + \phi_s \beta_p \sin \psi & 0 \\ 0 & 0 & 0 & 0 \\ 0 & 0 & 0 & 0 \end{bmatrix}$$

In the code the following symbols are used to designate the matrices.

$$(\mathbf{T}_{FL})_o = TFL0$$

$$(\mathbf{T}_{FL})_q = TFLQ$$

$$(\mathbf{T}_{FL})_{xF} = TFLXF$$

The first term $(\mathbf{T}_{FL})_q (\mathbf{L}^A)_o$, on the right hand side of Eq. 3.230 is expressed as

$$(\mathbf{T}_{FL})_q (\mathbf{L}^A)_o = (\mathbf{T}_{FL})_o^u \mathbf{u} + (\mathbf{T}_{FL})_o^{u'} \mathbf{u}' \quad (3.231)$$

where

$$(\mathbf{T}_{FL})_o^u = \begin{bmatrix} 0 & 0 & 0 & 0 \\ 0 & 0 & 0 & 0 \\ 0 & 0 & 0 & 0 \\ (L_v^A)_o \sin \psi & (L_w^A)_o \beta_p \cos \psi + (L_u^A)_o \cos \psi & -(L_u^A)_o \sin \psi - (L_v^A)_o \cos \psi & 0 \\ -(L_v^A)_o \beta_p \sin \psi - (L_w^A)_o \cos \psi & (L_u^A)_o \beta_p \sin \psi + (L_w^A)_o \sin \psi & (L_u^A)_o \cos \psi - (L_v^A)_o \sin \psi & 0 \end{bmatrix}$$

and

$$(\mathbf{T}_{FL})_o^{u'} = \begin{bmatrix} 0 & 0 & 0 & 0 \\ 0 & 0 & 0 & 0 \\ 0 & 0 & 0 & 0 \\ 0 & (M_{\phi}^A)_o \cos \psi & -(M_{\phi}^A)_o \beta_p \sin \psi & 0 \\ 0 & -(M_{\phi}^A)_o \sin \psi & -(M_{\phi}^A)_o \beta_p \cos \psi & 0 \end{bmatrix}$$

The $(L_u^A)_o$, $(L_v^A)_o$, $(L_w^A)_o$, and $(M_{\phi}^A)_o$ are constant parts of the aerodynamic forces arising from constant parts of velocity and fuselage terms.

In a similar manner, the second term $(\mathbf{T}_{FL})_{x_F} (\mathbf{L}^A)_o$ in Eq. 3.230 is written as :

$$(\mathbf{T}_{FL})_{x_F} (\mathbf{L}^A)_o = (\mathbf{T}_{FL})_o^{x_F} \mathbf{x}_F \quad (3.232)$$

where

$$(\mathbf{T}_{FL})_o^{x_F} = \begin{bmatrix} 0 & 0 & 0 & -\beta_p (L_u^A)_o - (L_w^A)_o & 0 \\ 0 & 0 & 0 & 0 & \beta_p (L_u^A)_o + (L_w^A)_o \\ 0 & 0 & 0 & t1 & t2 \\ 0 & 0 & 0 & 0 & 0 \\ 0 & 0 & 0 & 0 & 0 \end{bmatrix}$$

$$t1 = (L_u^A)_o \cos \psi - (L_v^A)_o \sin \psi - \beta_p \cos \psi (L_w^A)_o$$

$$t2 = -(L_u^A)_o \sin \psi - (L_v^A)_o \cos \psi + \beta_p \sin \psi (L_w^A)_o$$

The above matrix is not directly coded; it is added to the fuselage-fuselage stiffness matrix at the appropriate locations.

We have already obtained the expressions for $(\mathbf{L}^A)_L$ in terms of blade, fuselage and inflow degrees of freedom. The linear part of fuselage forces can be written as follows.

$$(\mathbf{F}_F^A)_L = (\mathbf{T}_{FL})_o^u \mathbf{u} + (\mathbf{T}_{FL})_o^{u'} \mathbf{u}' + (\mathbf{T}_{FL})_o^{x_F} \mathbf{x}_F + (\mathbf{T}_{FL})_o (\mathbf{L}^A)_L \quad (3.233)$$

Non-linear Forces :

The \mathbf{T}_{FL} matrix has only linear and constant terms. Therefore, the nonlinear forces and moments along the fuselage degrees of freedom are :

$$(\mathbf{L}^A)_{NL} = (\mathbf{T}_{FL})_o (\mathbf{L}^A)_{NL} + (\mathbf{T}_{FL})_L (\mathbf{L}^A)_L \quad (3.234)$$

where

$$(\mathbf{T}_{FL})_L = (\mathbf{T}_{FL})_q + (\mathbf{T}_{FL})_{x_F} \quad (3.235)$$

For linearizing the above equation, the nonlinear forces, $(\mathbf{L}^A)_{NL}$, derived earlier are used directly. Now only the last term $(\mathbf{T}_{FL})_L (\mathbf{L}^A)_L$ needs to be linearized as shown below.

$$\begin{aligned} (\mathbf{T}_{FL})_L (\mathbf{L}^A)_L &= (\mathbf{T}_{FL})_o (\mathbf{L}^A)_L|_o + \Delta(\mathbf{T}_{FL})_L (\mathbf{L}^A)_L \\ &\quad + (\mathbf{T}_{FL})_L \Delta (\mathbf{L}^A)_L \\ &= (\mathbf{T}_{FL})_o (\mathbf{L}^A)_L|_o + (\mathbf{A}_u^f)_{NL} \mathbf{u} + (\mathbf{A}_{u'}^f)_{NL} \mathbf{u}' + (\mathbf{A}_{\dot{u}}^f)_{NL} \dot{\mathbf{u}} \\ &\quad + (\mathbf{A}_{x_F}^f)_{NL} \mathbf{x}_F + (\mathbf{A}_{\dot{x}_F}^f)_{NL} \dot{\mathbf{x}}_F + (\mathbf{A}_{\lambda}^f)_{NL} \boldsymbol{\lambda} \end{aligned} \quad (3.236)$$

where

$$\begin{aligned} (\mathbf{A}_u^f)_{NL} &= \left[\frac{\partial}{\partial u} (\mathbf{T}_{FL})_L (\mathbf{L}^A)_L \quad \frac{\partial}{\partial v} (\mathbf{T}_{FL})_L (\mathbf{L}^A)_L \quad \frac{\partial}{\partial w} (\mathbf{T}_{FL})_L (\mathbf{L}^A)_L \quad \mathbf{0} \right] \\ &\quad + \left[(\mathbf{T}_{FL})_L \frac{\partial}{\partial u} (\mathbf{L}^A)_L \quad (\mathbf{T}_{FL})_L \frac{\partial}{\partial v} (\mathbf{L}^A)_L \quad (\mathbf{T}_{FL})_L \frac{\partial}{\partial w} (\mathbf{L}^A)_L \quad (\mathbf{T}_{FL})_L \frac{\partial}{\partial \phi} (\mathbf{L}^A)_L \right] \end{aligned}$$

$$\begin{aligned}
(\mathbf{A}_{u'}^f)_{NL} = & \left[\mathbf{0} \quad \frac{\partial}{\partial v'} (\mathbf{T}_{FL})_L (\mathbf{L}^A)_L \quad \frac{\partial}{\partial w'} (\mathbf{T}_{FL})_L (\mathbf{L}^A)_L \quad \mathbf{0} \right] \\
& + \left[\mathbf{0} \quad (\mathbf{T}_{FL})_L \frac{\partial}{\partial v'} (\mathbf{L}^A)_L \quad (\mathbf{T}_{FL})_L \frac{\partial}{\partial w'} (\mathbf{L}^A)_L \quad (\mathbf{T}_{FL})_L \frac{\partial}{\partial \phi'} (\mathbf{L}^A)_L \right]
\end{aligned}$$

$$(\mathbf{A}_u^f)_{NL} = \left[\mathbf{0} \quad (\mathbf{T}_{FL})_L \frac{\partial}{\partial v} (\mathbf{L}^A)_L \quad (\mathbf{T}_{FL})_L \frac{\partial}{\partial w} (\mathbf{L}^A)_L \quad (\mathbf{T}_{FL})_L \frac{\partial}{\partial \phi} (\mathbf{L}^A)_L \right]$$

$$\begin{aligned}
(\mathbf{A}_{x_F})_{NL}^f = & \left[\mathbf{0} \quad \mathbf{0} \quad \mathbf{0} \quad \frac{\partial}{\partial \alpha_s} (\mathbf{T}_{FL})_L (\mathbf{L}^A)_L \quad \frac{\partial}{\partial \phi_s} (\mathbf{T}_{FL})_L (\mathbf{L}^A)_L \right] \\
& + \left[(\mathbf{T}_{FL})_L \frac{\partial}{\partial x_F} (\mathbf{L}^A)_L \quad \dots \quad \dots \quad (\mathbf{T}_{FL})_L \frac{\partial}{\partial \alpha_s} (\mathbf{L}^A)_L \quad (\mathbf{T}_{FL})_L \frac{\partial}{\partial \phi_s} (\mathbf{L}^A)_L \right]
\end{aligned}$$

$$(\mathbf{A}_{\dot{x}_F})_{NL}^f = \left[(\mathbf{T}_{FL})_L \frac{\partial}{\partial \dot{x}_F} (\mathbf{L}^A)_L \quad \dots \quad \dots \quad (\mathbf{T}_{FL})_L \frac{\partial}{\partial \dot{\alpha}_s} (\mathbf{L}^A)_L \quad (\mathbf{T}_{FL})_L \frac{\partial}{\partial \dot{\phi}_s} (\mathbf{L}^A)_L \right]$$

$$(\mathbf{A}_\lambda)_NL^f = \left[(\mathbf{T}_{FL})_L \frac{\partial}{\partial \lambda_o} (\mathbf{L}^A)_L \quad (\mathbf{T}_{FL})_L \frac{\partial}{\partial \lambda_{1c}} (\mathbf{L}^A)_L \quad (\mathbf{T}_{FL})_L \frac{\partial}{\partial \lambda_{1s}} (\mathbf{L}^A)_L \right]$$

Derivatives of the \mathbf{T}_{FL} matrix.

$$\frac{\partial}{\partial u} (\mathbf{T}_{FL})_L = \begin{bmatrix} 0 & 0 & 0 & 0 \\ 0 & 0 & 0 & 0 \\ 0 & 0 & 0 & 0 \\ 0 & 0 & \sin \psi & 0 \\ 0 & \beta_p \sin \psi & -\cos \psi & 0 \end{bmatrix} \quad . \quad (3.237)$$

$$\frac{\partial}{\partial v}(\mathbf{T}_{FL})_L = \begin{bmatrix} 0 & 0 & 0 & 0 \\ 0 & 0 & 0 & 0 \\ 0 & 0 & 0 & 0 \\ \beta_p \cos \psi & 0 & \cos \psi & 0 \\ \beta_p \sin \psi & 0 & \sin \psi & 0 \end{bmatrix} \quad (3.238)$$

$$\frac{\partial}{\partial w}(\mathbf{T}_{FL})_L = \begin{bmatrix} 0 & 0 & 0 & 0 \\ 0 & 0 & 0 & 0 \\ 0 & 0 & 0 & 0 \\ -\sin \psi & -\cos \psi & 0 & 0 \\ \cos \psi & -\sin \psi & 0 & 0 \end{bmatrix} \quad (3.239)$$

$$\frac{\partial}{\partial v'}(\mathbf{T}_{FL})_L = \begin{bmatrix} 0 & 0 & 0 & 0 \\ 0 & 0 & 0 & 0 \\ 0 & 0 & 0 & 0 \\ 0 & 0 & 0 & -\sin \psi \\ 0 & 0 & 0 & \cos \psi \end{bmatrix} \quad (3.240)$$

$$\frac{\partial}{\partial w'}(\mathbf{T}_{FL})_L = \begin{bmatrix} 0 & 0 & 0 & 0 \\ 0 & 0 & 0 & 0 \\ 0 & 0 & 0 & 0 \\ 0 & 0 & 0 & -\beta_p \cos \psi \\ 0 & 0 & 0 & -\beta_p \sin \psi \end{bmatrix} \quad (3.241)$$

$$\frac{\partial}{\partial \alpha_s}(\mathbf{T}_{FL})_{x_F} = \begin{bmatrix} -\beta_p & 0 & -1 & 0 \\ 0 & 0 & 0 & 0 \\ \cos \psi & -\sin \psi & -\beta_p \cos \psi & 0 \\ 0 & 0 & 0 & 0 \\ 0 & 0 & 0 & 0 \end{bmatrix}$$

$$\frac{\partial}{\partial \phi_s} (\mathbf{T}_{FL})_{x_F} = \begin{bmatrix} 0 & 0 & 0 & 0 \\ \beta_p & 0 & 1 & 0 \\ -\sin \psi & -\cos \psi & \beta_p \sin \psi & 0 \\ 0 & 0 & 0 & 0 \\ 0 & 0 & 0 & 0 \end{bmatrix}.$$

Total Blade Forces and Moments Along Fuselage Degrees of Freedom:

$$\begin{aligned} \mathbf{F}_F^A &= (\mathbf{F}_F^A)_o + (\mathbf{F}_F^A)_L + (\mathbf{F}_F^A)_{NL} \\ &= (\mathbf{F}_F^A)_o + [(\mathbf{T}_{FL})_o^u \mathbf{u} + (\mathbf{T}_{FL})_o^{u'} \mathbf{u}' + (\mathbf{T}_{FL})_o (\mathbf{L}^A)_L] \\ &\quad + [(\mathbf{T}_{FL})_o (\mathbf{L}^A)_{NL} + (\mathbf{T}_{FL})_L (\mathbf{L}^A)_L] \end{aligned}$$

Using the explicit expressions for $(\mathbf{L}^A)_L$, $(\mathbf{L}^A)_{NL}$ and $(\mathbf{T}_{FL})_L (\mathbf{L}^A)_L$, we can calculate the load vector, and the fuselage-blade, fuselage-fuselage and fuselage-inflow matrices.

Load Vector

$$(\mathbf{Q}_{Fb})_o^i = l_i \int_0^1 \{(\mathbf{F}_F^A)_o + (\mathbf{F}_F^A)_{NL}|_o\} ds \quad (3.242)$$

Fuselage-Blade Aerodynamic Matrices

$$\begin{aligned} (\mathbf{K}_{Fb}^A)_o^i &= -l_i \int_0^1 \{(\mathbf{T}_{FL})_o^u \mathbf{H}_s + (\mathbf{T}_{FL})_o^{u'} \mathbf{H}'_s \\ &\quad + \frac{\gamma}{6} (\mathbf{T}_{FL})_o \mathbf{A}_u \mathbf{H}_s + \frac{\gamma}{6} (\mathbf{T}_{FL})_o \mathbf{A}_{u'} \mathbf{H}'_s \\ &\quad + \frac{\gamma}{6} (\mathbf{T}_{FL})_o (\mathbf{A}_u)_{NL} \mathbf{H}_s + \frac{\gamma}{6} (\mathbf{T}_{FL})_o (\mathbf{A}_{u'})_{NL} \mathbf{H}'_s \\ &\quad + \frac{\gamma}{6} (\mathbf{A}_u^f)_{NL} \mathbf{H}_s + \frac{\gamma}{6} (\mathbf{A}_{u'}^f)_{NL} \mathbf{H}'_s\} ds \quad (3.243) \\ (\mathbf{C}_{Fb}^A)_o^i &= -\frac{\gamma}{6} l_i \int_0^1 \{(\mathbf{T}_{FL})_o \mathbf{A}_{\dot{u}} \mathbf{H}_s + \frac{\gamma}{6} (\mathbf{T}_{FL})_o (\mathbf{A}_{\dot{u}})_{NL} \mathbf{H}_s \end{aligned}$$

$$+ \frac{\gamma}{6} (\mathbf{A}_{\dot{u}}^f)_{NL} \mathbf{H}_s \} ds \quad (3.244)$$

Fuselage-Fuselage Matrices due to Blade Forces

$$\begin{aligned} (\mathbf{K}_{FF}^A)^i &= -\frac{\gamma}{6} l_i \int_0^1 \{ (\mathbf{T}_{FL})_o^{x_F} + (\mathbf{T}_{FL})_o \mathbf{A}_{x_F} + \frac{\gamma}{6} (\mathbf{T}_{FL})_o (\mathbf{A}_{x_F})_{NL} + \frac{\gamma}{6} (\mathbf{A}_{x_F}^f)_{NL} \} ds \\ (\mathbf{C}_{FF}^A)^i &= -\frac{\gamma}{6} l_i \int_0^1 \{ (\mathbf{T}_{FL})_o \mathbf{A}_{\dot{x}_F} + \frac{\gamma}{6} (\mathbf{T}_{FL})_o (\mathbf{A}_{\dot{x}_F})_{NL} \\ &\quad + \frac{\gamma}{6} (\mathbf{A}_{\dot{x}_F}^f)_{NL} \} ds \end{aligned} \quad (3.245)$$

Fuselage-Inflow Matrices due to Blade Forces

$$(\mathbf{K}_{F\lambda}^A)^i = -\frac{\gamma}{6} l_i \int_0^1 \{ (\mathbf{T}_{FL})_o \mathbf{A}_\lambda + \frac{\gamma}{6} (\mathbf{T}_{FL})_o (\mathbf{A}_\lambda)_{NL} + \frac{\gamma}{6} (\mathbf{A}_\lambda^f)_{NL} \} ds \quad (3.246)$$

3.2.6 Description of SUBROUTINE AEROMX

The quasi-steady aerodynamics formulation presented in the preceding section provides the theory basis for generating the aerodynamic element mass, stiffness, and damping matrices, and the element load vector. These matrices, together with their structural counterparts, are assembled to yield the global discretized equations of motion for the blade. As described in the previous sections, inclusion of fuselage motion for stability analysis generates additional element matrices. Additional matrices are also required for stability analysis using dynamic inflow. All of the aerodynamic element matrices required for the rotorcraft system, including blade, fuselage, and dynamic inflow, are calculated in SUBROUTINE AEROMX.

The subroutine AEROMX also contains calculations of unsteady aerodynamic contributions to the element matrices and load vectors. The unsteady calculations will be described in a later section.

The following section will describe (pertaining to quasi-steady aerodynamics only):

- function of SUBROUTINE AEROMX
- Interface of SUBROUTINE AEROMX with the rest of UMARC
- Input/output associated with SUBROUTINE AEROMX
(see Figures 3.3a and 3.3b)
- performance of SUBROUTINE AEROMX

3.2.6.1 Function of SUBROUTINE AEROMX

The function of this subroutine is to:

- Calculate aerodynamic contribution to element *blade* matrices and load vector

blade element load vector	{EQ}	\mathbf{Q}_b^A
blade element mass matrix	[EM]	\mathbf{M}_b^A
blade element damping matrix	[EC]	\mathbf{C}_b^A
blade element stiffness matrix	[EK]	\mathbf{K}_b^A
blade displacement Jacobian matrix	[DFX]	$\frac{\partial(\mathbf{Q}_b^A)_{NL}}{\partial \mathbf{q}}$
blade velocity Jacobian matrix	[DFXD]	$\frac{\partial(\mathbf{Q}_b^A)_{NL}}{\partial \dot{\mathbf{q}}}$

- Calculate aerodynamic contribution to element *blade-fuselage* (*bF*) matrices

blade-fuselage element damping matrix	[ECA]	\mathbf{C}_{bF}^A
blade-fuselage element stiffness matrix	[EKA]	\mathbf{K}_{bF}^A

- Calculate aerodynamic contribution to element *fuselage-blade* (*Fb*) matrices

fuselage-blade element damping matrix	[TM]	\mathbf{M}_{Fb}^A
fuselage-blade element damping matrix	[TC]	\mathbf{C}_{Fb}^A
fuselage-blade element stiffness matrix	[TK]	\mathbf{K}_{Fb}^A

- Calculate aerodynamic contribution to *fuselage-fuselage* (FF) matrices

fuselage-fuselage damping matrix	[TP]	\mathbf{C}_{FF}^A
fuselage-fuselage stiffness matrix	[TK]	\mathbf{K}_{FF}^A

- Calculate aerodynamic contribution to element *blade-inflow* ($b\lambda$) matrices

blade-inflow element damping matrix	[ECBL]	$\mathbf{C}_{b\lambda}$
blade-inflow element stiffness matrix	[EKBL]	$\mathbf{K}_{b\lambda}$

- Calculate aerodynamic contribution to element *fuselage-inflow* ($F\lambda$) matrices

fuselage-inflow element stiffness matrix	[EKFL]	$\mathbf{K}_{F\lambda}$
--	--------	-------------------------

- Calculate aerodynamic contribution to element *inflow-blade* (λb) matrices

inflow-blade element damping matrix	[ECLB]	$\mathbf{C}_{\lambda b}$
inflow-blade element stiffness matrix	[EKLB]	$\mathbf{K}_{\lambda b}$

- Calculate aerodynamic contribution to *inflow-fuselage* (λF) matrices

inflow-fuselage element damping matrix	[ECLF]	$\mathbf{C}_{\lambda F}$
inflow-fuselage element stiffness matrix	[EKLF]	$\mathbf{K}_{\lambda F}$

- Calculate aerodynamic contribution to element *inflow* ($\lambda\lambda$) matrices

inflow element stiffness matrix	[EKLL]	$\mathbf{K}_{\lambda\lambda}$
---------------------------------	--------	-------------------------------

3.2.6.2 Calling of SUBROUTINE AEROMX

In all cases, SUBROUTINE AEROMX is called within a loop over the number of spatial elements. During response calculations, SUBROUTINE AEROMX is called within a loop over the number of time elements also.

SUBROUTINE AEROMX is called from two (2) locations within UMARC:

1) From SUBROUTINE ASBGBM

Flag: INDRNS = 1

Function: Calculate element mass matrix, [EM], damping matrix, [EC], stiffness matrix, [EK], displacement Jacobian matrix, [DFX], and velocity Jacobian matrix, [DFXD], and load vector, [EQ], about the deflected blade position ($\{EU\} \neq \{0\}$).

These matrices (and vector) are used in calculating steady response during the iterative coupled trim procedure. This procedure uses both the finite element method in time and the finite element method in space to determine converged steady periodic response $\{EU\}_{trim}$.

2) From SUBROUTINE ASBGM2

Flag: INDRNS = 2

Function: Calculate element mass matrix, [EM], damping matrix, [EC], stiffness matrix, [EK], displacement Jacobian matrix, [DFX], and velocity Jacobian matrix, [DFXD] about the trim deflected blade position ($\{EU\} = \{EU\}_{trim}$).

Also calculate fuselage related matrices if fuselage motion included.

Also calculate dynamic inflow related matrices if dynamic inflow is included. These matrices are used in calculating linearized stability. Note that for linearized stability analysis, the load vector, [EQ], is not used.

3.2.6.3 Input to SUBROUTINE AEROMX

Input to the routine AEROMX is provided through the argument list and the common blocks.

Input through Argument List:

GQP	=	Gauss quadrature sampling points (local element axis)
GQW	=	Gauss quadrature weighting factors
EU	=	element displacement vector $\{EU\}^T = \mathbf{q}_i^T = [u_1, u_2, u_3, u_4, v_1, v'_1, v_2, v'_2, w_1, w'_1, w_2, w'_2, \dot{\phi}_1, \dot{\phi}_2, \dot{\phi}_3]$
EUD	=	element velocity vector $\{EUD\}^T = \dot{\mathbf{q}}_i^T = [\dot{u}_1, \dot{u}_2, \dot{u}_3, \dot{u}_4, \dot{v}_1, \dot{v}'_1, \dot{v}_2, \dot{v}'_2, \dot{w}_1, \dot{w}'_1, \dot{w}_2, \dot{w}'_2, \ddot{\phi}_1, \ddot{\phi}_2, \ddot{\phi}_3]$
SII	=	Azimuth angle, ψ
NGAUSS	=	number of spatial gaussian integration points
NEDOF	=	number of spatial element degrees of freedom
XBI	=	x coordinate of left node of element
EL	=	element length, l
L	=	element number (1 = tip element)

INDRNS : -1 for vacuum frequencies and mode shapes (undeflected position)
 -2 for vacuum frequencies and mode shapes (about trim position)
 1 for response calculation
 2 for stability analysis

 INDNL : 0 for neglecting all nonlinearities
 1 for including all nonlinearities

 IFLAG : Utility flag (unused)

 NSELT : number of total spatial elements

 IVHJAC : Flag used in calculation of vehicle Jacobian matrix

 TLAM : Linear transformation matrix for modified tip element

Input through Common Blocks:

COMMON /STRUC/ :	Chord length of element, c
COMMON /AEROD/ :	Lock Number, GAMA = γ
	Precone angle, BTP = β_p
	Airfoil coefficients, C0, C1, D0, D1, D2, CMAC,F1
	Reference lift curve slope, a = SLC
	Chordwise offsets ED = e_d , and η_r = ETR
COMMON /RADSHR/ :	Parameters for radial shortening effect
COMMON /TRIMV/ :	Cyclic pitch control inputs TH1C and TH1S
COMMON /CFUNC/ :	Collective pitch control input TH75, and linear twist slope, THTW
COMMON /PBRNG/ :	Parameters for " δ_3 effect", articulated rotor
COMMON /PERT/ :	Flags to indicate stability analysis, IPERT

COMMON /REVF/ :	Flag to indicate use of reverse flow corrections, IREVF
COMMON /UNSTDY/ :	Parameters for use in unsteady aerodynamics
COMMON /DYSTAL/ :	Flags for dynamic stall calculations
COMMON /FREEWK/ :	Parameters for free wake calculations
COMMON /TRNUNS/ :	Parameters for unsteady aerodynamics
COMMON /INPUT/ :	Solidity ratio, SIGMA
	Reference lift curve slope, SLCA
	Lock number, GAMMA = γ
	Fuselage C.G. offsets
COMMON /FUSE/ :	Flag to indicate fuselage motion, INDFUS
	Number of fuselage degrees of freedom, NHUB
	Flag to indicate dynamic inflow, IDYN
COMMON /CONF/ :	Flag for use in BMR rotor, NCONF
COMMON /FIXED/ :	Number of blades, NBLADE
COMMON /SWEPT/ :	Element rotation flag indicator, IELROT
	Sweep angle, SWRAD
	Droop Angle, DRRAD
	Element where tip begins, NETIP

3.2.6.4 Output from SUBROUTINE AEROMX

Output through the Argument List :

EK = element aerodynamic blade stiffness matrix, $(\mathbf{K}_b^A)_i$

EC	=	element aerodynamic blade damping matrix, $(\mathbf{C}_b^A)_i$
EM	=	element aerodynamic blade mass matrix, $(\mathbf{M}_b^A)_i$
EQ	=	element aerodynamic blade load vector, $(\mathbf{Q}_b^A)_i$
DFX	=	element aerodynamic blade displacement Jacobian matrix

$$[\text{DFX}] = \frac{\partial(\mathbf{Q}_{NL})_i}{\partial \mathbf{q}_i}$$

DFXD	=	element aerodynamic blade velocity Jacobian matrix
------	---	--

$$[\text{DFXD}] = \frac{\partial(\mathbf{Q}_{NL})_i}{\partial \dot{\mathbf{q}}_i}$$

ECA	=	element aerodynamic blade-fuselage damping matrix, \mathbf{C}_{bf}^A
EKA	=	element aerodynamic blade-fuselage stiffness matrix, \mathbf{K}_{bf}^A
EMFB	=	element aerodynamic fuselage-blade mass matrix, \mathbf{M}_{Fb}^A
ECFB	=	element aerodynamic fuselage-blade damping matrix, \mathbf{C}_{Fb}^A
EKFB	=	element aerodynamic fuselage-blade stiffness matrix, \mathbf{K}_{Fb}^A
ECFF	=	element aerodynamic fuselage damping matrix, \mathbf{C}_{FF}^A
EKFF	=	element aerodynamic fuselage stiffness matrix, \mathbf{K}_{FF}^A
EKBL	=	element aerodynamic blade-inflow stiffness matrix, $\mathbf{K}_{b\lambda}$
EKFL	=	element aerodynamic fuselage-inflow stiffness matrix, $\mathbf{K}_{F\lambda}$
EKLB	=	element aerodynamic inflow-blade stiffness matrix, $\mathbf{K}_{\lambda b}$
ECLB	=	element aerodynamic inflow-blade damping matrix, $\mathbf{C}_{\lambda b}$
EKLF	=	element aerodynamic inflow-fuselage stiffness matrix, $\mathbf{K}_{\lambda F}$
ECLF	=	element aerodynamic inflow-fuselage damping matrix, $\mathbf{C}_{\lambda F}$
EKLL	=	element aerodynamic inflow stiffness matrix, $\mathbf{K}_{\lambda\lambda}$

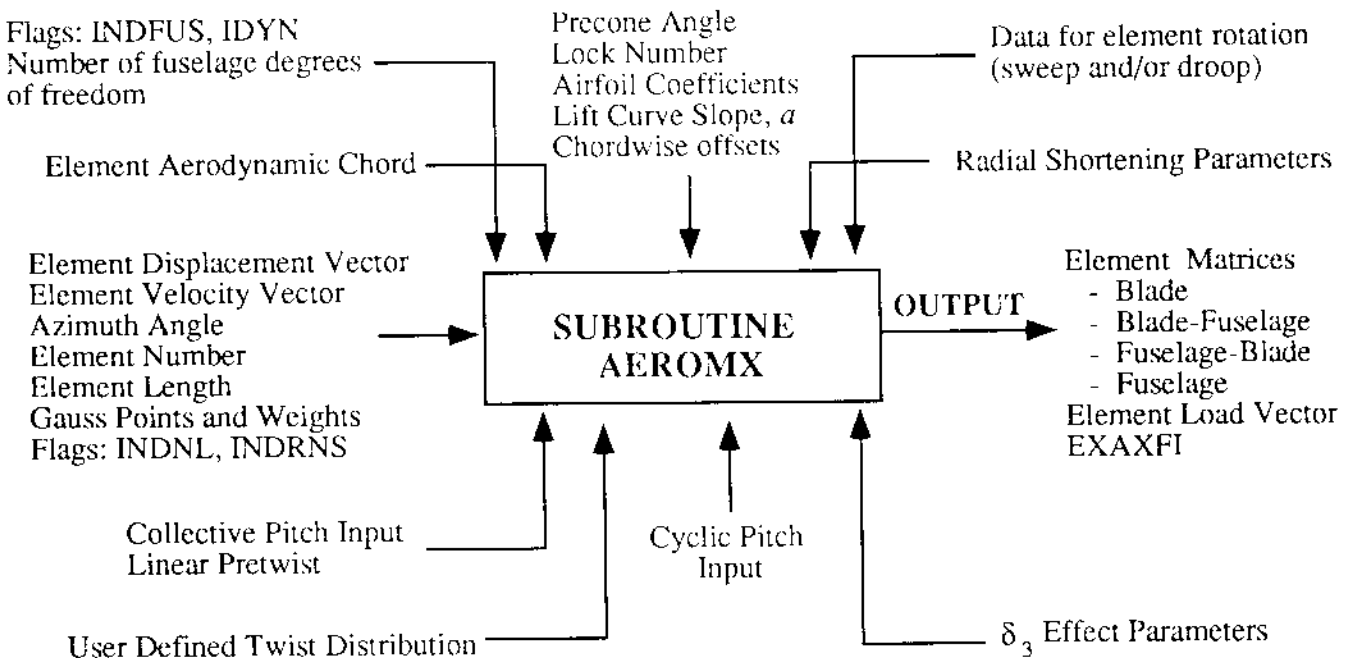


Figure 3.3a INPUT and OUTPUT for SUBROUTINE AEROMX - Physical Variables

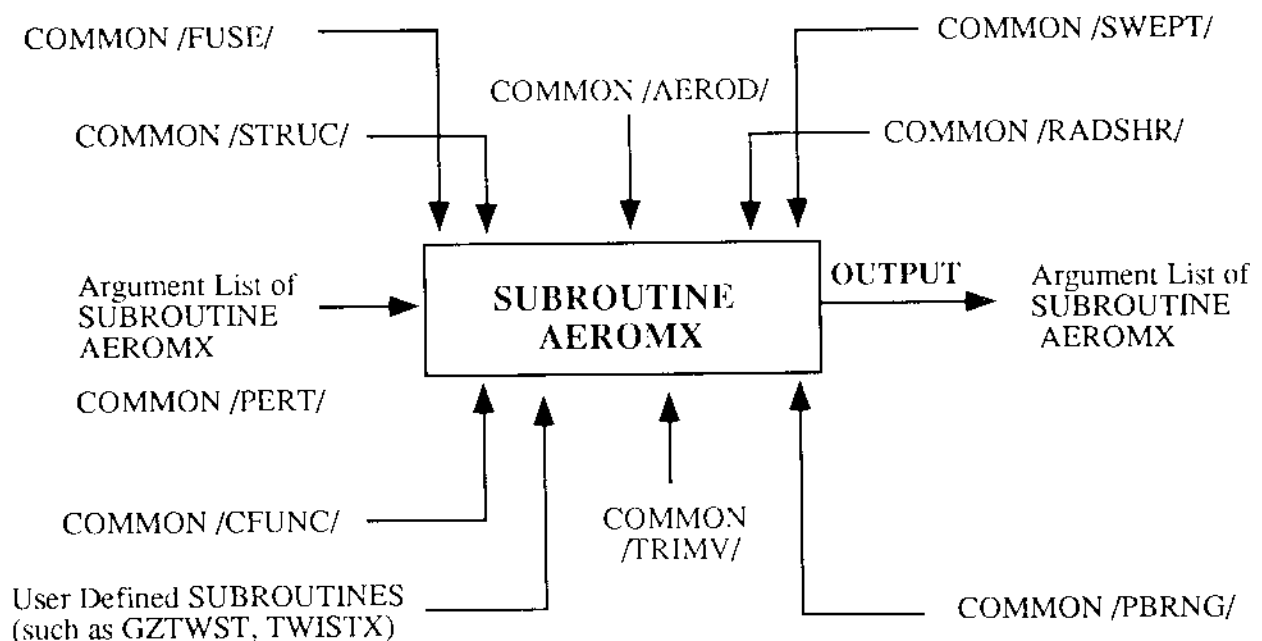


Figure 3.3b INPUT and OUTPUT for SUBROUTINE AEROMX - Paths of Dataflow

3.3 Unsteady Aerodynamics

The aerodynamic environment of a rotor is highly complex and unsteady, with regions of transonic flow, separated flow and dynamic stall. As such, application of the quasi-steady model discussed in the previous section, is quite restricted; it yields reasonably accurate results only for moderate flight conditions. At extreme flight conditions, it cannot adequately model the unsteady phenomena, and the non-linear effects associated with flow separation and dynamic stall. A refined aerodynamic model is required that can accurately model flow separation, dynamic stall, and transonic compressibility effects. The model must also be computationally efficient and compatible with rotor dynamic analysis. One such model was proposed by Leishman and Beddoes [1]. This aerodynamic model consists of three distinct parts: 1) an attached potential flow formulation for linear unsteady airloads, 2) a separated flow formulation for nonlinear unsteady airloads, and 3) a dynamic stall formulation for vortex induced airloads. These parts are arranged sequentially such that output from a subsystem forms the input to the next subsystem.

The attached flow formulation is based on the indicial response method in which response is computed from a finite difference approximation to Duhamel's integral. The indicial response function consists of two parts: one part for response due to circulatory loading accounting for shed vorticity, and the other part due to noncirculatory loading. Compressibility effects are implicitly included in the indicial response functions.

Nonlinear aerodynamic formulation for separated flow is based on Kirchhoff theory which relates air loads to angle of attack and the trailing edge separation point location. For unsteady conditions, a simple open loop procedure is used to compute the time-dependent effective separation point. This part receives its input from the attached flow formulation discussed earlier.

The dynamic stall formulation accounts for the vortex induced aerodynamic loads. The formulation models the separation of the concentrated leading edge vortex, its passage over the airfoil chord, and its eventual dissipation into the airfoil wake. The dynamic stall is assumed to initiate when an effective leading edge pressure parameter reaches a Mach number dependent critical value, indicative of leading edge or shock induced separation. This part receives its input from both the attached flow and the separated flow algorithms.

3.3.1 Attached Flow Formulation

The attached flow solution predicts airloads in a linear attached potential flow regime, under unsteady conditions. In conjunction with the quasi-steady model, this model provides incremental correction factors to the section load parameters. It predicts circulatory, and non-circulatory or impulsive loads separately, and then sums them to attain the final solution.

Using the indicial function formulation, the component of circulatory lift can be expressed as

$$L_w^c(S) = -\frac{1}{2}\rho c C_1 U_T \left[\phi_c(S) U_P(0) + \int_0^S \phi_c(S - \sigma) \frac{dU_P(\sigma)}{d\sigma} d\sigma \right] \quad (3.247)$$

The circulatory indicial response $\phi_c(s)$ is given by [7],

$$\phi_c(S) = 1 - (A_1 \exp(-b_1 \beta^2 S) + A_2 \exp(-b_2 \beta^2 S)) \quad (3.248)$$

where the terms in bracket represent the lift deficiency due to vortices shed downstream in the airfoil wake. Without the Mach scaling parameter β^2 , this indicial function is quite similar to the classical Kussner function; it differs only in the values of the coefficient A_1 and A_2 . For this indicial function, $A_1 = 0.3$; $A_2 = 0.7$; $b_1 = 0.14$; $b_2 = 0.53$, while the coefficients for the Kussner function are: $A_1 = A_2 = 0.5$; $b_1 = 0.13$; $b_2 = 1.0$ [8]. The variable s represents the distance an airfoil travels in terms of semi-chord, and it can be expressed in terms of incident free stream velocity as,

$$S = \frac{2}{\Omega c} \int_0^\Psi U_T(\Psi) d\Psi \quad (3.249)$$

In general, the indicial normal force and pitching moment response due to step changes in angle of attack (from a step change in α or plunge velocity \dot{h}) and in the pitch rate, $q (= \dot{\alpha}c/U)$, can be represented by the equations

	impulsive	circulatory	
$\frac{C_{n,h}(S,M)}{\alpha}$	$\frac{4}{M} \phi_h^i(S, M)$	$+\frac{2\pi}{\beta} \phi_h^c(S, M)$	plunge
$\frac{C_{m,h}(S,M)}{\alpha}$	$-\frac{1}{M} \phi_{h_m}^i(S, M)$	$+\frac{2\pi}{\beta} \phi_h^c(S, M)(0.25 - x_{ac})$	plunge
$\frac{C_{n,q}(S,M)}{q}$	$\frac{1}{M} \phi_q^i(S, M)$	$+\frac{\pi}{\beta} \phi_q^c(S, M)$	pitch rate
$\frac{C_{m,q}(S,M)}{q}$	$-\frac{7}{12M} \phi_{q_m}^i(S, M)$	$-\frac{\pi}{8\beta} \phi_{q_m}^c(S, M)$	pitch rate

where the superscript $(.)^i$ refers to the non-circulatory (impulsive) part of the response, and the superscript $(.)^c$ refers to the circulatory part. The subscript $(.)_h$ refers to changes in angle of attack due to plunge. The subscript $(.)_q$ refers

to pitch rate. The β term is the classical Prandtl-Glauert compressibility factor, $\sqrt{1 - M^2}$. The pitching moment is computed about the quarter-chord point.

In the above equations, the coefficients associated with the impulsive indicial functions represent the initial response values derivable directly from the piston theory, i.e.,

$$\frac{C_{n_h}(0)}{\alpha} = \frac{4}{M} \quad (3.251)$$

$$\frac{C_{m_h}(0)}{\alpha} = -\frac{1}{M} \quad (3.252)$$

$$\frac{C_{n_q}(0)}{q} = \frac{1}{M} \quad (3.253)$$

$$\frac{C_{m_q}(0)}{q} = -\frac{7}{12M} \quad (3.254)$$

The coefficients associated with the circulatory indicial functions represent the final values as given by the quasisteady theory, i.e.,

$$\frac{C_{n_h}(\infty)}{\alpha} = \frac{2\pi}{\beta} \quad (3.255)$$

$$\frac{C_{m_h}(\infty)}{\alpha} = \frac{2\pi}{\beta} (0.25 - x_{ac}) \quad (3.256)$$

$$\frac{C_{n_q}(\infty)}{q} = \frac{\pi}{\beta} \quad (3.257)$$

$$\frac{C_{m_q}(\infty)}{q} = -\frac{\pi}{8\beta} \quad (3.258)$$

The indicial response functions ϕ represent the time-dependent behavior of the lift and pitching moment between $S = 0$ and $S = \infty$.

If the airfoil static data are available, the linearized value of the lift curve slope, $2\pi/\beta$, may be replaced by the experimental value at the appropriate Mach

number, which is generally denoted by $C_{n_a}(M)$ or $C_1(M)$. Additionally, the second term in Eq. 3.250 represents the contribution to the pitching moment due to a Mach number dependent offset of the aerodynamic center from the airfoil 1/4-chord axis. The value of the aerodynamic center, x_{ac} , can also be obtained from static airfoil measurements at the appropriate Mach number. Note that the second terms of Eq. 3.250 represents the induced camber pitching moment due to pitch rate motion, as given by the thin airfoil theory.

3.3.2 Circulatory and Impulsive Lift due to Angle of Attack Change

The normal force response to a “unit step” change in angle of attack, α , can be expressed as the sum of a non-circulatory part $C_{n_h}^i$ and a circulatory part $C_{n_h}^c$, viz

$$\frac{C_{n_h}(S)}{\alpha} = C_{n_h}(S) = C_{n_h}^i(S, M) + C_{n_h}^c(S, M) \quad (3.259)$$

or in terms of the indicial functions

$$\frac{C_{n_h}(S)}{\alpha} = C_{n_h}(S) = \frac{4}{M} \phi_h^i(S, M) + \frac{2\pi}{\beta} \phi_h^c(S, M) \quad (3.260)$$

The circulatory lift response can be expressed quite adequately in terms of a two-term exponential function which scales directly with Mach number,

$$\phi_h^c(S, M) = 1 - A_1 \exp(-b_1 \beta^2 S) - A_2 \exp(-b_2 \beta^2 S) \quad (3.261)$$

where $A_1 = 0.3$, $A_2 = 0.7$, $b_1 = 0.14$, and $b_2 = 0.53$ and $\beta = \sqrt{1 - M^2}$ is the Prandtl-Glauert compressibility factor. Values of the particular coefficients for

this indicial response function have been selected to match extensive experimental and analytical results. It should be noted that the above coefficients may be considered as independent of airfoil shape.

For the non-circulatory part, the indicial response is approximated by a single exponential function as follows

$$C_{n_h}^i(S) = \frac{4}{M} \phi_h^i(S, M) = \frac{4}{M} \exp\left(\frac{-S}{T'_h}\right) \quad (3.262)$$

The circulatory part of T'_h is defined, and the exact results for the total indicial response for the short time period between $0 \leq S \leq 2M/(M + 1)$ are known. Substituting (3.18) and (3.19) in (3.17) and matching the resulting indicial response function with the exact result yields

$$T'_h(M) = \frac{4M}{2(1 - M) + 2\pi\beta M^2(A_1 b_1 + A_2 b_2)} \quad (3.263)$$

3.3.3 Circulatory and Impulsive Pitching Moment due to Angle of Attack Change

A matching process similar to that in the previous section can be used to find approximations for the other indicial response functions. For the indicial pitching moment response due to a “step change” in angle of attack (from α or plunge h) can also be written as the sum of a non-circulatory part $C_{m_h}^i$ and a circulatory part $C_{m_h}^c$, i.e.,

$$\frac{C_{m_h}}{\alpha} = C_{m_h}(S) = C_{m_h}^i(S, M) + C_{m_h}^c(S, M) \quad (3.264)$$

or in terms of the indicial functions

$$\frac{C_{m_h}}{\alpha} = C_{m_h}(S) = \frac{-1}{M} \phi_{m_h}^i(S, M) + \frac{2\pi}{\beta} (0.25 - x_{ac}) \phi_{n_h}^c(S, M) \quad (3.265)$$

For the non-circulatory part, a convenient expression for the indicial function is of the form

$$\phi_{m_h}^i(S) = A_3 \exp\left(\frac{-S}{b_3 T'_{m_h}}\right) + A_4 \exp\left(\frac{-S}{b_4 T'_{m_h}}\right) \quad (3.266)$$

A good approximation to this function can be made using the values $A_3 = 1.5$, $A_4 = -0.5$, $b_3 = 0.25$ and $b_4 = 0.1$. The time constant is given by [1]

$$T'_{m_h} = \left[\frac{A_3 b_4 + A_4 b_3}{b_3 b_4 (1 - M)} \right] \quad (3.267)$$

3.3.4 Circulatory and Impulsive Lift due to Pitch Rate

The indicial lift response to a “step change” in pitch rate, q , can be written as the sum of a non-circulatory part $C_{n_q}^i$ and a circulatory part $C_{n_q}^c$. (Note that q is the nondimensionalized pitch rate $q = \dot{\alpha}_c / U$; $\dot{\alpha}$ is the angular velocity about the 1/4-chord.)

$$\frac{C_{n_q}}{q} = C_{n_q} = C_{n_q}^i + C_{n_q}^c \quad (3.268)$$

Or, in terms of the indicial functions

$$\frac{C_{n_q}}{q} = C_{n_q} = \frac{1}{M} \phi_{n_q}^i + \frac{\pi}{\beta} \phi_{n_q}^c \quad (3.269)$$

By virtue of the thin airfoil result, the circulatory part of the lift can be written as

$$C_{n_q}^c = \frac{\pi}{\beta} \left[1 - A_1 \exp(-b_1 \beta^2 S) - A_2 \exp(-b_2 \beta^2 S) \right] \quad (3.270)$$

The non-circulatory function is assumed to be of the form

$$C_{nq}^i = \frac{1}{M} \phi_{nq}^i(S) = \frac{1}{M} \exp\left(\frac{-S}{T'_q}\right) \quad (3.271)$$

The time constant derived in [1] is given by

$$T'_q = \frac{2M}{[(1 - M) + 2\pi\beta M^2(A_1 b_1 + A_2 b_2)]} \quad (3.272)$$

3.3.5 Circulatory and Impulsive Pitching Moment due to Pitch Rate

The indicial moment response due to a “step change” in pitch rate q about the 1/4-chord can be written as the sum of a non-circulatory part $C_{m_q}^i$ and a circulatory part $C_{m_q}^c$,

$$\frac{C_{m_q}}{q} = C_{m_q} = C_{m_q}^i + C_{m_q}^c \quad (3.273)$$

or, in terms of the indicial functions

$$\frac{C_{m_q}}{q} = C_{m_q} = \frac{-7}{12M} \phi_{m_q}^i + \frac{-\pi}{8\beta} \phi_{m_q}^c \quad (3.274)$$

The circulatory part is assumed to be of the form

$$C_{m_q}^c = \frac{-\pi}{8\beta} \phi_{m_q}^c = \frac{-\pi}{8\beta} [1 - A_5 \exp(-b_5 \beta^2 S)] \quad (3.275)$$

where $A_5 = 1.0$ and $b_5 = 0.5$. For the non-circulatory part we use

$$C_{m_q}^i = \frac{-7}{12M} \phi_{m_q}^i = \frac{-7}{12M} \exp\left(\frac{-S}{T'_{m_q}}\right) \quad (3.276)$$

Following the same procedure as before, the non-circulatory time constant is obtained as

$$T'_{m_q} = \left[\frac{2M \cdot 7}{15(1 - M) + 3\pi\beta M^2 A_5 b_5} \right] \quad (3.277)$$

3.3.6 Separated Flow Formulation

At sufficiently large angles of attack, the flow on the airfoil separates from the surface causing a non-linear alleviation of lift, and a non-linear increase of drag and moment. Kirchoff formulated a quasi-static model which relates the separated flow loads to the trailing edge separation point (see Fig. 3.3).

The normal force coefficient, C_N , and the chordwise force coefficient, C_C , are given by

$$C_N = C_1 \left(\frac{1 + \sqrt{f}}{2} \right)^2 \alpha \quad (3.278)$$

$$C_C = \eta_a C_1 \sqrt{f} \alpha^2 \quad (3.279)$$

the value of f varies from unity for attached flow to zero for completely detached flow. No expression for the pitching moment is given; thus an empirical relation is derived [1]:

$$C_M = (k_0 + k_1(1 - f) + k_2 \sin \pi f^2) C_N \quad (3.280)$$

where k_0 is the offset of the airfoil aerodynamic center from the quarter chord, and k_1 and k_2 are empirical coefficients which are functions of airfoil shape and Mach number.

For a given airfoil, the effective separation point, f , can be computed from measurements of static C_N with respect to α . The variation is expressed empirically using the curve fits:

$$f = \begin{cases} 1 - 0.3 \exp \left(\frac{\alpha - \alpha_1}{S_1} \right) & \text{for } \alpha \leq \alpha_1 \\ 0.04 + 0.66 \exp \left(\frac{\alpha_1 - \alpha}{S_2} \right) & \text{for } \alpha > \alpha_1 \end{cases} \quad (3.281)$$

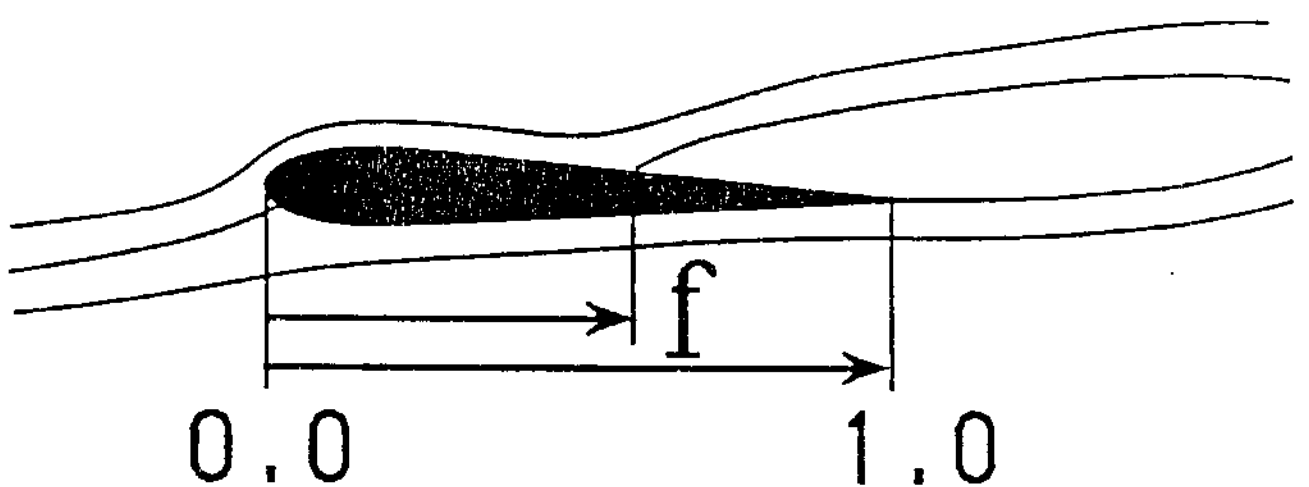


Figure 3.3: Blade Section Separation Point.

where parameters α_1, S_1, S_2 are functions of airfoil shape and Mach number.

The quasi-static separation point is thus solely a function of angle of attack.

For unsteady flow, two physical phenomena governing behavior of the separation point have been identified [1]. The first is the lag effect on the pressure response, and the second is the lag of the unsteady boundary layer. To account for the unsteady pressure lag, the angle of attack is modified as follows

$$\alpha_f = \frac{C'_N}{C_1} \quad (3.282)$$

where,

$$C'_N = C_{N_n} - D_{p_n} \quad (3.283)$$

$$D_{p_n} = D_{p_{n-1}} \exp(-\Delta s/T_p) + (C_{N_n} - C_{N_{n-1}}) \exp(-\Delta s/2T_p) \quad (3.284)$$

The value, α_f , is used to yield a pressure-corrected separation point, f' . To correct for boundary layer effects, f' is modified as follows

$$f'' = f' - D_{f_n} \quad (3.285)$$

where

$$D_{f_n} = D_{f_{n-1}} \exp(-\Delta s/T_f) + (f'_n - f'_{n-1}) \exp(-\Delta s/2T_f) \quad (3.286)$$

The time constants T_p , and T_f are Mach dependent but are fairly insensitive to airfoil shape. The value, f'' , is the effective unsteady separation point parameter and is used to determine the resultant separated flow loads. In the present

analysis, normal force and chord force corrections are made to the lift curve slope during the appropriate calculations as

$$C_1 ==> C_1 \left(\frac{1 + \sqrt{f}}{2} \right)^2 \quad \text{for } \bar{L}_w \text{ and} \quad (3.287)$$

$$C_1 ==> C_1 \sqrt{f} \quad \text{for } \bar{L}_v \quad (3.288)$$

The separated pitching moment increment is added directly to the attached flow value of \bar{M}_ϕ .

In the event of gross separation, the drag force, \bar{L}_v , is further modified as [9],

$$C_1 ==> C_1 \sqrt{f} \Phi \quad (3.289)$$

where,

$$\Phi = f'' \exp(K_f(C'_N - C_N^1)/2) \quad (3.290)$$

and K_f is an empirical Mach dependent parameter. C_N^1 is a Mach dependent stall boundary parameter, and is roughly equal to the static maximum normal force coefficient. The gross separation factor, Φ , is employed only if the value of f'' is less than 0.7, and the value of C'_N exceeds C_N^1 . This condition defines "gross" separation.

3.3.7 Dynamic Stall Formulation

The third and final part of the unsteady blade-element aerodynamic model is dynamic stall formulation. This requires accurate representation of several

physical phenomenon, e.g., the magnitude of the vortex induced lift, the conditions upon which it separates from the leading edge, and the time history of the vortex as it traverses the chord and dissipates into the wake. Experimental data [1] suggests that the excess vortex lift is related to the difference between the attached flow lift and the separated flow lift. The model allows this excess lift to decay exponentially, with provision for simultaneous increments at each time step. Numerically, this is expressed as

$$C_{N_{v_n}} = C_{N_{v_{n-1}}} \exp(-\Delta s/T_v) + (C_V - C_{V_{n-1}}) \exp(-\Delta s/2T_v) \quad (3.291)$$

and

$$C_V = C_N^C \left[1 - \left(\frac{1 + \sqrt{f}}{2} \right)^2 \right] \quad (3.292)$$

where C_{N_v} is the incremental lift due to time history effect of the dynamic stall, and C_V is the instantaneous excess lift due to the vortex. The T_v is a Mach dependent parameter and is insensitive to airfoil shape. The criterion for vortex separation from the leading edge is a function of the leading edge pressure gradient and the airfoil characteristics. A leading edge pressure parameter is calculated based on lag of the pressure with respect to the airfoil normal force, C'_n . For an airfoil, a limit value of this parameter, C_n^1 , can be determined. The vortex separates from the leading edge when C'_n exceeds C_n^1 . The final effect that needs to be modeled is the rate of vortex travel across the chord. This rate has been shown experimentally to be approximately one-half to one-third of the free stream velocity [1]. This rate is also Mach dependent. As the vortex reaches

the airfoil trailing edge and passes into the wake, its effect on the airloads is rapidly reduced. Monitoring of the magnitude of the vortex induced lift, and its passage on the airfoil chord, yields an accurate representation of the airfoil lift behavior under dynamically stalled conditions.

As a direct result of this dynamic stall process, the pitching moment characteristics of the airfoil also change. This variation is modeled by representing the variation of the airfoil center of pressure, aft of the quarter-chord, as

$$CP_V = \frac{1}{4} \left[1 + \sin \left\{ \pi \left(\frac{\tau_V}{T_{VL}} - 0.5 \right) \right\} \right] \quad (3.293)$$

where τ_V is the non-dimensional time elapsed after the shedding of the vortex, and T_{VL} is the total time for the vortex to traverse the chord. The incremental pitching moment is then simply the vortex induced lift times the offset of the center of pressure from the quarter-chord position, i.e.,

$$C_{M_V} = -CP_V C_{N_V} \quad (3.294)$$

The incremental vortex normal force and pitching moment are normalized and added to the separated flow values to yield the final values for the deformed blade frame external loads. As in the quasi-steady analysis, these terms are transformed to the undeformed frame and included in the virtual work expression based on Hamilton's principle.

The last three sections have referred to several parameters that are required to utilize this model. These parameters are primarily a function of static airfoil loads data. Values for these parameters, for a NACA 0012 airfoil, are provided

in subroutines AIRFLS and INITAF. The parameters T_p , T_f , T_v , and T_{VL} have been shown to be fairly insensitive to airfoil shape, and thus the NACA0012 values may be used for other airfoils.

A number of modifications to the model are made to account for "interactional" effects among the individual parts of the model. These modifications are principally carried out through modifying just two time constants, T_f and T_v , the former associated with trailing edge separation, and the later associated with vortex lift. These changes include the effects of separation suppression due to moderate pitch rates, and the acceleration of trailing edge separation due to either vortex separation at the leading edge or a change in pitch direction during vortex passage down the airfoil chord. Flow reattachment is modeled by monitoring the leading edge pressure, C'_n . Reattachment is initiated when C'_n becomes less than C_N^1 . Appropriate logic for these phenomena is incorporated into the algorithm [1].

3.4 Implementation of Unsteady Aerodynamics

3.4.1 Circulatory Lift (due to Plunge and Pitch Rate)

One of the most important aspects of the unsteady airloads calculation is the development of numerical algorithms for arbitrary forcing. Computational requirements for a rotor analysis dictate that the selected algorithms be easy to implement, computationally efficient, accurate and relatively insensitive to azimuth (time) step size.

For unsteady linearized compressible flow, the circulatory component of the normal force can be written in the time domain as

$$N_n^c(t) = \frac{1}{2} \rho U^2(t) C_{n\alpha}(M) \alpha_E(t) c \quad (3.295)$$

where n is the current time sample corresponding to the n th azimuth location. For a constant (or low frequency blade motion) the blade element velocity, the unsteady lift and the moment can be simplified in terms of the effective angle of attack at the 3/4-chord of the blade section. This is justified for the helicopter rotor environment and permits a considerable simplification in the model through elimination of a considerable number of deficiency functions. The effective angle of attack α_E at the 3/4 chord can be rewritten in terms of the downwash velocity at the 3/4 chord, U_P :

$$\alpha_E(t) = \arcsin \frac{-U_P(t)}{U(t)} = \arctan \frac{-U_P(t)}{U_T(t)} \approx \frac{-U_P(t)}{U_T(t)} \quad (3.296)$$

$$N_n^c(t) \approx \frac{-1}{2} \rho U(t) C_{n\alpha} U_P(t) c \quad (3.297)$$

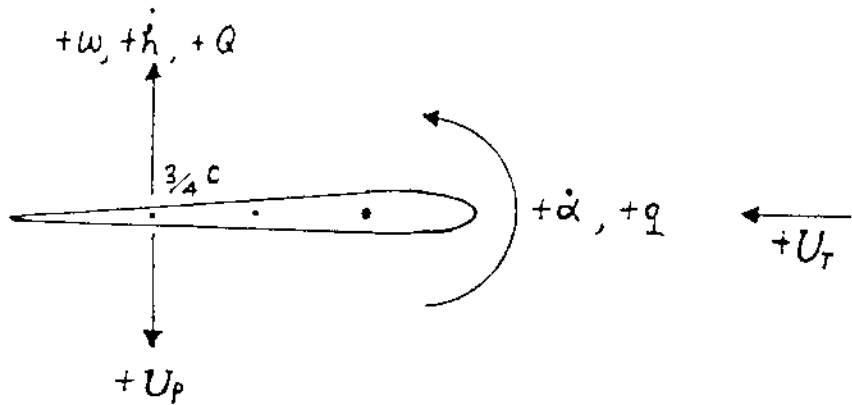


Figure 3.4: Flow Velocities on the Airfoil

U_P represents the effective time-dependent downwash at the 3/4-chord accounting for the effects of the shed wake. Note that U_P must be negative valued for α_E to be positive valued. For an airfoil undergoing arbitrary plunge (h), pitch (α) and pitch rate q about an axis at the 1/4 chord, the instantaneous quasi-steady downwash at the 3/4-chord is given by w .

$$w = \alpha U + Q + h \quad (3.298)$$

$$U_P = -w \quad (3.299)$$

where $Q = -\dot{\alpha}\frac{c}{2}$ (ft/sec). Since $q = \dot{\alpha}c/U$, therefore, $Q = -q\frac{U}{2}$. The directions of q, Q, h, w and U_P are defined in Fig. 3.4. To compute the time-history effect of the shed wake on w , Duhamel's superposition integral can be used, i.e.

$$w(S) = w(0)\phi_h^c(S, M) + \int_0^S \frac{dw(\sigma)}{d\sigma} \phi_h^c(S - \sigma, M) d\sigma \quad (3.300)$$

$$-U_P(S) = -U_P(0)\phi_h^c(S, M) + \int_0^S \frac{-dU_P(\sigma)}{d\sigma} \phi_h^c(S - \sigma, M) d\sigma \quad (3.301)$$

where σ is a dummy time variable and ϕ_h^c is the circulatory indicial lift response function. The variable S represents the distance traveled by the airfoil in semi-chords, and is proportional to the area under the velocity time curve, i.e.

$$S = \frac{\int_0^t U(t)dt}{c/2} \quad (3.302)$$

where U is the resultant 2-D velocity at the blade section. It should be noted that we may write S in terms of nondimensionalized time ψ , viz

$$S = \frac{\int_0^\psi U(\psi)d\psi}{\Omega c/2} \approx \frac{\int_0^\psi U_T(\psi)d\psi}{\Omega c/2} \quad (3.303)$$

where Ω is the rotor rotational speed.

After substituting for the downwash in Duhamel's integral in Eq. 3.301, a zero-order hold finite-difference approximation to the resulting integrals is made. Denoting the current sample by n , then

$$\omega_n = \sum_{i=0}^n U_i \Delta \alpha_i - X_n^{(1)} - Y_n^{(1)} + \sum_{i=0}^n \alpha_i \Delta U_i - X_n^{(2)} - Y_n^{(2)} \quad (3.304)$$

$$+ \sum_{i=0}^n \Delta Q_i - X_n^{(3)} - Y_n^{(3)} \quad (3.305)$$

$$+ \sum_{i=0}^n \Delta \dot{h}_i - X_n^{(4)} - Y_n^{(4)}$$

where the $X^{(j)}$ and $Y^{(j)}$, $j = 1, 2, 3, 4$ terms are called "deficiency" functions; they represent the deficiency in the corresponding quasi-steady values due to the presence of the unsteady shed wake.

It will be shown in the next section that the deficiency functions can be written as one-step recursive relations of the form

$$X_n^{(j)} = X_{n-1}^{(j)} \exp(-b_1 \beta^2 \Delta S) + A_1 \Delta^{(j)} \quad (3.306)$$

$$Y_n^{(j)} = Y_{n-1}^{(j)} \exp(-b_2 \beta^2 \Delta S) + A_2 \Delta^{(j)} \quad (3.307)$$

where the $\Delta^{(j)}$ terms are given by

$$\Delta^{(1)} = U_n \Delta \alpha_n \quad \text{and} \quad \Delta^{(2)} = \alpha_n \Delta U_n$$

$$\Delta^{(3)} = \Delta Q_n \quad \text{and} \quad \Delta^{(4)} = \Delta \dot{h}_n$$

The increment in distance traveled ΔS over the sample period is given by

$$\Delta S = \frac{\int_t^{t+\Delta t} U dt}{c/2} \quad (3.308)$$

If the integral is evaluated using the trapezoidal rule, we have

$$\Delta S = (U_n + U_{n-1}) \Delta t / c \quad (3.309)$$

If U_n is assumed to change only a little between each time step, then $\Delta U_n \approx 0$.

Equation 3.304 can be rewritten as

$$-U_{P_n} = \sum_{i=0}^n U_i \Delta \alpha_i - X_n^{(1)} - Y_n^{(1)} \quad (3.310)$$

$$+ \sum_{i=0}^n \Delta q_i - X_n^{(3)} - Y_n^{(3)} \quad (3.311)$$

$$+ \sum_{i=0}^n \Delta \dot{h}_i - X_n^{(4)} - Y_n^{(4)}$$

The circulatory normal force, due to an accumulating series of step inputs in angle of attack (which will typically include a plunge velocity) and pitch rate about the quarter-chord is

$$C_{n_n}^c = C_{n_a}(M) \frac{(-U_P)}{U_T} \quad \beta \quad \zeta \quad (3.312)$$

where n is the current sample time. The value of the normal lift curve slope, $C_{n_a}(M)$, is obtained from tables. Finally, the circulatory normal force at the n th sample time is written as

$$N_n^c = \frac{1}{2} \rho U_n C_{n_a} (-U_{P_n} - X_n - Y_n) \quad (3.313)$$

$$C_n^c = C_{n_a} (-U_{P_n} - X_n - Y_n) \quad (3.314)$$

$$X_n = X_{n-1} \exp(-b_1 \beta^2 \Delta S) + A_1 \Delta U_{P_n} \exp\left(\frac{-b_1 \beta^2 \Delta S}{2}\right) \quad (3.315)$$

The corresponding change in downwash velocity at 3/4 chord from previous time step to the next is given by

$$\Delta U_{P_n} = U_{P_n} - U_{P_{n-1}} \quad (3.316)$$

Since we have replaced α_{E_n} by U_{P_n} , the deficiency function in Eq. 3.315 represents the “deficiency” in the induced downwash velocity at 3/4 chord due to unsteady aerodynamic effects, and contains all the information about the time history of the shed wake effects.

Thus, the total response to an arbitrary time-varying forcing (α, q, h, U) is obtained by simply updating the deficiency functions X_n and Y_n at each sample. A similar approach is adopted to derive numerical algorithms for the pitching moment terms.

Derivation of X_n and Y_n :

$$C_n = C_{n_a} \alpha_E \quad (3.317)$$

$$\alpha_E \approx \frac{-U_P}{U_T} \quad (3.318)$$

$$-U_P = \phi(s)(-U_P(0)) + \int_0^S \phi(S-\sigma) \frac{-dU_P}{d\sigma} d\sigma \quad (3.319)$$

$$\approx \sum_{m=1}^n \phi(S_n - S_m)(-U_{P_m} - -U_{P_{m-1}}) \quad (3.320)$$

where

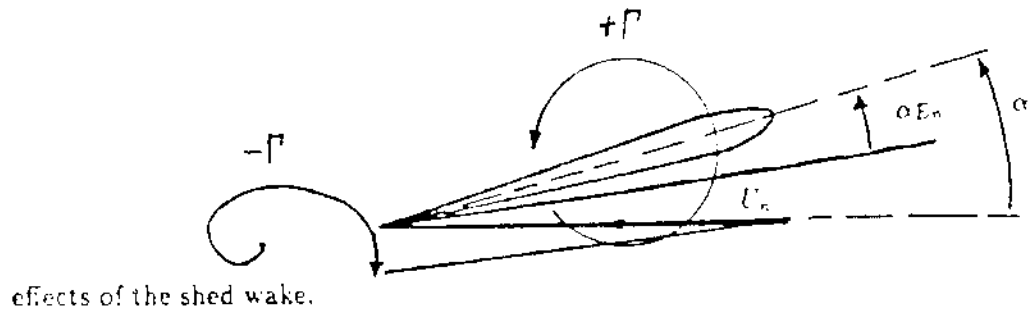
$$\phi(S_n - S_m) = 1 - A_1 \exp(-b_1 \beta^2 (S_n - S_m)) - A_2 \exp(-b_2 \beta^2 (S_n - S_m))$$

$$\begin{aligned} \sum_{m=1}^n \phi(S_n - S_m)(-U_{P_m} + U_{P_{m-1}}) &= \sum_{m=1}^n (-U_{P_m} + U_{P_{m-1}}) \\ &- A_1 \sum_{m=1}^n (-U_{P_m} + U_{P_{m-1}}) \exp(-b_1 \beta^2 (S_n - S_m)) \\ &- A_2 \sum_{m=1}^n (-U_{P_m} + U_{P_{m-1}}) \exp(-b_2 \beta^2 (S_n - S_m)) \\ &= (-U_p - X_n - Y_n) \end{aligned} \quad (3.321)$$

U_p is the quasi-steady downwash velocity at 3/4 chord. X_n and Y_n are called the **deficiency functions**, these physically represent the reduction in U_p , at the instant $t = n$, due to the shed vorticity. Figure 3.5 shows the effect of shed wake on U_p . Figure 3.6 illustrate the “deficiency” concept.

From Eq. 3.321, we define X_n and Y_n as:

$$X_n = A_1 \sum_{m=1}^n -(U_{P_m} - U_{P_{m-1}}) \exp(-b_1 \beta^2 (S_n - S_m))$$



effects of the shed wake.

Figure 3.5: The induced velocity from the shed wake reduces the downwash U_P and therefore effective angle of attack.

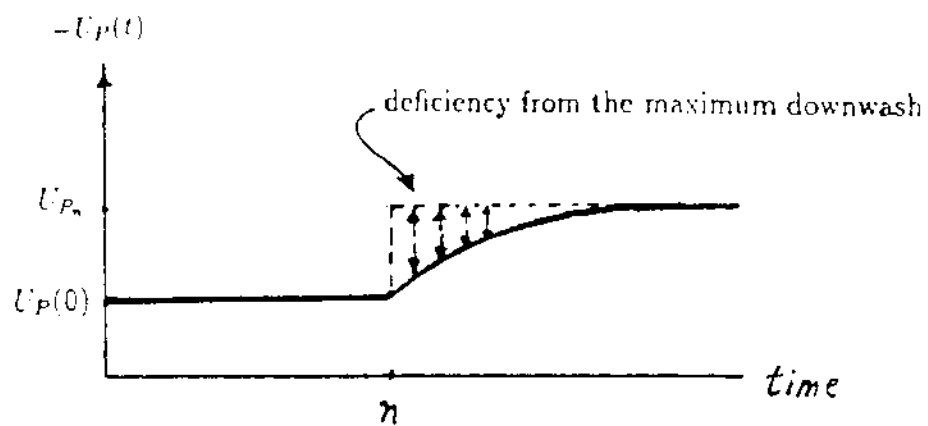


Figure 3.6: Physical concept of lift deficiency. $U_P(0)$ is the baseline downwash velocity before time step n , and $U_P(n)$ is the maximum achievable downwash at time n . X_n and Y_n represent the deficiency from the maximum downwash due to the "feedback" effect from the shed wake.

$$Y_n = A_2 \sum_{m=1}^n -(-U_{P_m} - U_{P_{m-1}}) \exp(-b_2 \beta^2 (S_n - S_m))$$

Isolating the last term in the summation expression for X_n yields

$$\begin{aligned} X_n &= A_1 \sum_{m=1}^{n-1} -(U_{P_m} - U_{P_{m-1}}) e^{(-b_1 \beta^2 (S_n - S_m))} + A_1 [-(U_{P_n} - U_{P_{n-1}})] e^{(-b_1 \beta^2 (S_n - S_n))} \\ &= A_1 \sum_{m=1}^{n-1} -(U_{P_m} - U_{P_{m-1}}) e^{(-b_1 \beta^2 (S_n - S_{n-1} + S_{n-1} - S_m))} + A_1 [-(U_{P_n} - U_{P_{n-1}})] \\ &= A_1 \sum_{m=1}^{n-1} -\Delta U_{P_m} e^{(-b_1 \beta^2 \Delta S)} e^{(-b_1 \beta^2 (S_{n-1} - S_m))} + A_1 (-\Delta U_{P_n}) \\ &= X_{n-1} e^{(-b_1 \beta^2 \Delta S)} + A_1 (-\Delta U_{P_n}) \end{aligned} \quad (3.322)$$

Introducing half-step numerical factor,

$$X_n = X_{n-1} \exp(-b_1 \beta^2 \Delta S) + A_1 (-\Delta U_P) \exp(-b_1 \beta^2 \frac{\Delta S}{2}) \quad (3.323)$$

The expression for Y_n is obtained in the same manner.

Implementation of the Lift Deficiency X_n and Y_n inside the Finite Element in Time

To apply the finite element in time technique, the rotor is divided into NTEL T number of time elements (Fig. 3.7). Within a time element, the blade displacements are calculated at each of the NGAUSS number of Gaussian integration point. At each time Gaussian location, the velocities U_P , U_T and Q are evaluated at all the “spatial” Gaussian integration points along the blade span. The velocities at the spatial Gaussian points are called U_{P_n} , where the subscript n denotes at the n th azimuth location. After the velocities have been calculated

at time step n , they are stored as $U_{P_{n-1}}$, then the numerical scheme marches onto the azimuth location for next time Gaussian point. (In the subroutine AEROMX, $U_{P_{n-1}}$ are called UPMAT(L,M). where L is the number of spatial elements, and M is the number of spatial Gaussian integration points. In the subroutine, all the velocities at $n - 1$ location have the suffix MAT in the name to signify “matrix” and only the velocities at time $n - 1$ need to be saved.) The velocities which are essential for attached unsteady aerodynamics computations are:

$$U_{P_n} = \frac{U_{P_n}}{\Omega R} \text{ the downwash at } 1/4 \text{ chord}$$

$$U_{P_{1n}} = \frac{U_{P_{1n}}}{\Omega R} \text{ the downwash at } 3/4 \text{ chord}$$

$$U_{T_n} = \frac{U_{T_n}}{\Omega R} \text{ the tangential velocity at } 1/4 \text{ chord}$$

$$Q_n = -\dot{\alpha}_2^c = -q \frac{U}{2} \text{ the downwash at } 3/4 \text{ chord due to pitch rate q}$$

3.4.2 Impulsive Lift (due to Plunge)

In a way similar to that associated in the preceding section, the non-circulatory (impulsive) normal force coefficient can be obtained using a first-order hold numerical scheme. The normal force coefficient due to changes in angle of attack is written as

$$\begin{aligned} C_n^i &= \frac{4}{M} \alpha_E \approx \frac{-4}{M} \frac{U_P}{U_T} = \frac{-4U_P a_s}{U_T^2} \\ -U_P &= \phi_h^i(s)(-U_P(0)) + \int_0^S \phi_h^i(S - \sigma) \frac{-dU_P}{d\sigma} d\sigma \\ \int_0^S d\sigma &= \sum_{m=1}^n \phi_h^i(S_n - S_m)(-U_{P_m} + U_{P_{m-1}}) \end{aligned} \quad (3.324)$$

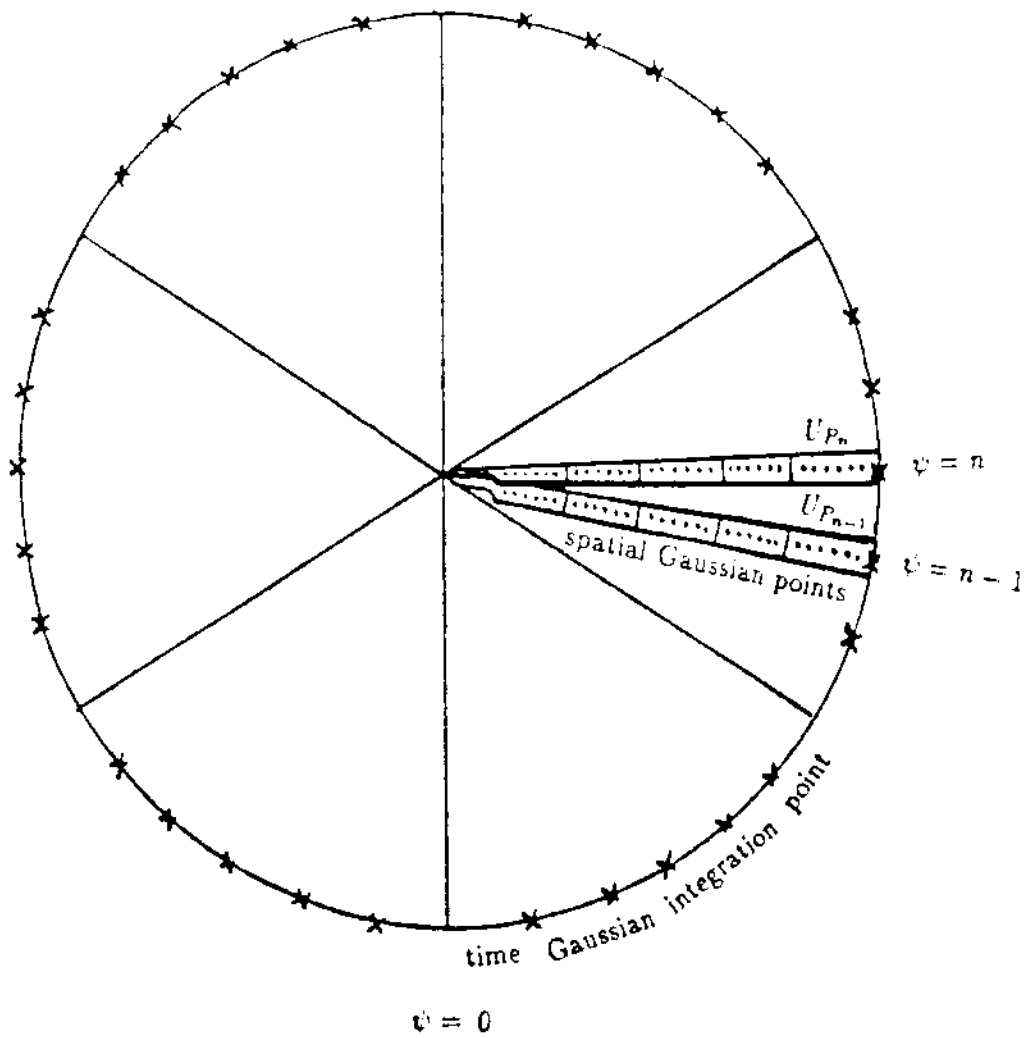


Figure 3.7: The velocities U_P , U_T , and q are evaluated at all the spanwise Gaussian point along the blade at $\psi = n$.

C_n Normal Lift Force Coef.

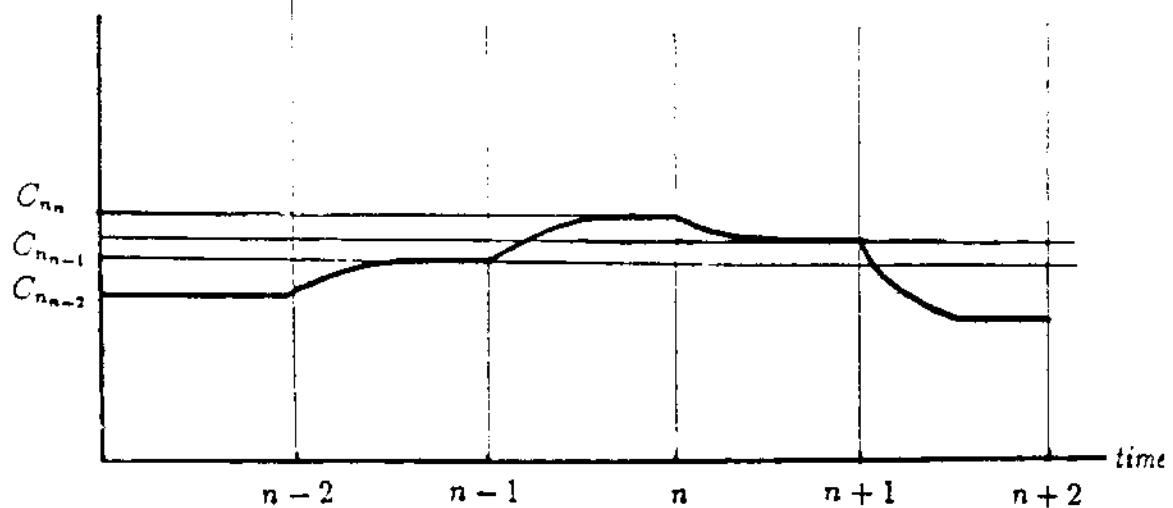


Figure 3.8: The deficiency functions X_n, Y_n and D'_n 's represent the shed-vorticity induced deficiency in the blade quasi-steady lift at the n th time step.

$$\phi_h^i(S_n - S_m) = \exp\left(\frac{-(S_n - S_m)}{2Mk_h}\right)$$

$$C_{n_n}^i = \frac{4k_h T_I}{M} \left(\frac{-\Delta \hat{U}_{P_n} - D_n}{U_{T_n}} \right) = \frac{4k_h \bar{c}}{U_{T_n}^2} (-\Delta \hat{U}_{P_n} - D_n) \quad (3.325)$$

where

$$\Delta \hat{U}_{P_n} = \frac{U_{P_n} - U_{P_{n-1}}}{\Delta \psi} \quad (3.326)$$

and the deficiency function D_n is given by

$$D_n = D_{n-1} \exp\left(\frac{-\Delta t}{k_h T_I}\right) + [(-\Delta \hat{U}_{P_n}) - (-\Delta \hat{U}_{P_{n-1}})] \exp\left(\frac{-\Delta t}{2k_h T_I}\right) \quad (3.327)$$

$$= D_{n-1} \exp\left(\frac{-\Delta \psi R}{k_h M_{tip} c}\right) + [(-\Delta \hat{U}_P) - (-\Delta \hat{U}_{P_{n-1}})] \exp\left(\frac{-\Delta \psi R}{2k_h M_{tip} c}\right) \quad (3.328)$$

Where $\psi = \Omega t$ and $M_{tip} = \Omega R$.

3.4.3 Impulsive Lift (due to Pitch Rate)

The normal force coefficient due to changes in pitch rate is written as

$$C_{n_q}^i = \frac{1}{M} = \frac{qa_s}{U_T} \quad (3.329)$$

where

$$\begin{aligned} q &= \phi_q^i(s)q(0) + \int_0^S \phi_q^i(S - \sigma) \frac{q}{d\sigma} d\sigma \\ &\quad \int_0^S \dots d\sigma = \sum_{m=1}^n \phi_q^i(S_n - S_m)(q_m - q_{m-1}) \\ \phi_q^i(S_n - S_m) &= \exp\left(\frac{-(S_n - S_m)}{2Mk_q}\right) \end{aligned}$$

$$C_{n_n}^i = \frac{k_q T_I}{M} (\Delta \dot{q}_n - D_n^3) = \frac{k_q \bar{c}}{U_{T_n}^2} (\Delta \dot{q}_n - D_n^3) \quad (3.330)$$

where

$$\Delta \hat{q}_n = \left(\frac{q_n - q_{n-1}}{\Delta \psi} \right) \quad (3.331)$$

and the deficiency function D_n^3 is given by

$$D_n^3 = D_{n-1}^3 \exp \left(\frac{-\Delta t}{k_q T_I} \right) + (\Delta \hat{q}_n - \Delta \hat{q}_{n-1}) \exp \left(\frac{-\Delta t}{2k_q T_I} \right) \quad (3.332)$$

$$= D_{n-1}^3 \exp \left(\frac{-\Delta \psi R}{k_q M_{tip} c} \right) + (\Delta \hat{q}_n - \Delta \hat{q}_{n-1}) \exp \left(\frac{-\Delta \psi R}{2k_q M_{tip} c} \right) \quad (3.333)$$

The non-circulatory deficiency functions in Eqs. 3.328 and 3.333 account for time-history effects on the airloads due to the accumulation of wave-like pressure disturbances.

The non-circulatory time constant governing the decay of the loads due to the propagation of pressure disturbances is given by $T_I = c/a$. The factors k_h and k_q are associated with a particular loading component and its mode of forcing and are derived in Ref.[1]. After imposing 25% reductions in these time constants, based on experimental data, they are expressed as

$$k_h = \frac{0.75}{(1 - M) + \pi \beta M^2 (A_1 b_1 + A_2 b_2)} \quad (3.334)$$

and

$$k_q = \frac{0.75}{(1 - M) + 2\pi \beta M^2 (A_1 b_1 + A_2 b_2)} \quad (3.335)$$

The total normal force coefficient under attached (potential) flow conditions, C_n , is given by the sum of circulatory and non-circulatory components, viz

$$\begin{aligned}
C_{n_n} &= C_{n_n}^i + C_{q_n}^i + C_{n_n}^c \\
&\text{normal} = \text{impulsive} \quad \text{impulsive} \quad \text{circulatory} \\
&\text{coeff.} \quad \text{plunge} \quad \text{pitch rate} \quad \text{plunge and pitch rate} \quad (3.336)
\end{aligned}$$

3.4.4 Unsteady Pitching Moment (due to Circulatory Plunge and Pitch Rate)

The circulatory component of the pitching moment about the quarter-chord due to an accumulating series of step inputs in angle of attack is obtained as

$$C_{m_n}^c = C_{m_0} + (0.25 - x_{ac}) C_{n_n}^c - \frac{\pi}{8\beta} (q_n - X^{(5)}) \frac{c}{U} \quad (3.337)$$

which may also be written as

$$C_{m_n}^c = C_{m_0} + k_0 C_{n_n}^c - \frac{\pi}{8\beta} (q_n - X^{(5)}) \frac{c}{U} \quad (3.338)$$

where C_{m_0} is the zero lift moment. The second term in Eq. 3.338 represents the component of the pitching moment due to an offset of the aerodynamic center from the quarter-chord axis. The value of $k_0 (= 0.25 - x_{ac})$ is obtained from a look-up table and is provided in subroutine AIRFLS. Since k_0 for all the airfoils is usually less than .02, the second term is neglected in UMARC. The third term represents the pitching moment due to the instantaneously effective induced camber and the deficiency function $X^{(5)}$ is computed recursively:

$$X_n^{(5)} = X_{n-1}^{(5)} \exp(-b_5 \beta^2 \Delta S) + A_5 \Delta q_n \exp\left(\frac{-b_5 \beta^2 \Delta S}{2}\right) \quad (3.339)$$

ΔS is the incremental distance traveled by the airfoil (in semi-chords) over the sample interval, as given by Eq. 3.309. Furthermore, Δq_n is given by

$$\Delta q_n = q_n - q_{n-1} \quad (3.340)$$

3.4.5 Unsteady Pitching Moment (Due to Impulsive Plunge)

The non-circulatory pitching moment components is also obtained using a first-order hold numerical scheme. The non-circulatory pitching moment coefficient due to changes in angle of attack are written as

$$C_{m_n}^i = \frac{-k_{m_h} T_l}{M} \left\{ A_3 b_3 (-\Delta \hat{U}_p - D_n^4) + A_4 b_4 (-\Delta \hat{U}_P - D_n^5) \right\} \quad (3.341)$$

$$C_{m_n}^i = \frac{-k_{m_h} \bar{c}}{U_T} \left\{ A_3 b_3 (-\Delta \hat{U}_p - D_n^4) + A_4 b_4 (-\Delta \hat{U}_P - D_n^5) \right\} \quad (3.342)$$

where the deficiency functions D_n^4 and D_n^5 are given by

$$\begin{aligned} D_n^4 &= D_{n-1}^4 \exp \left(\frac{-\Delta \psi R}{b_3 k_{m_h} M_{tip} c} \right) - (\Delta \hat{U}_{P_n} - \Delta \hat{U}_{P_{n-1}}) \exp \left(\frac{-\Delta \psi R}{2b_3 k_{m_h} M_{tip} c} \right) \\ D_n^5 &= D_{n-1}^5 \exp \left(\frac{-\Delta \psi R}{b_4 k_{m_h} M_{tip} c} \right) \\ &\quad - (\Delta \hat{U}_{P_n} - \Delta \hat{U}_{P_{n-1}}) \exp \left(\frac{-\Delta \psi R}{2b_4 k_{m_h} M_{tip} c} \right) \end{aligned} \quad (3.343)$$

3.4.6 Unsteady Pitching Moment (Due to Impulsive Pitch Rate)

The pitching moment coefficient due to changes in pitch rate is written as

$$\begin{aligned} C_{m_{q_n}}^i &= \frac{-7k_q T_I}{12M} (\Delta \hat{q}_n - D_n^6) \\ &= \frac{-7k_q \bar{c}}{12U_{T_n}} (\Delta \hat{q}_n - D_n^6) \end{aligned} \quad (3.344)$$

where

$$\Delta \hat{q}_n = \left(\frac{\Delta q_n - \Delta q_{n-1}}{\Delta \psi} \right) \quad (3.345)$$

and where the deficiency function D_n^6 is given by

$$D_n^6 = D_{n-1}^6 \exp \left(\frac{-\Delta \psi R}{k_{m_h} M_{tip} c} \right) + (\Delta \hat{q}_n - \Delta \hat{q}_{n-1}) \exp \left(\frac{-\Delta \psi R}{2k_{m_q} M_{tip} c} \right) \quad (3.346)$$

As in the case of the lift response, the basic non-circulatory time constant governing the decay of the loads due to the propagation of pressure disturbances is given by $T_I = c/a_s$. The factors k_{m_h} and k_{m_q} are associated with the particular loading component and its mode of forcing. In summary, these non-circulatory time constants are written in terms of Mach number as

$$k_{m_h} = \frac{0.8(A_3 b_4 + A_4 b_3)}{b_3 b_4 (1 - M)} \quad (3.347)$$

and

$$k_{m_q} = \frac{5.6}{15(1 - M) + 3\pi\beta M^2 A_5 b_5} \quad (3.348)$$

where both k_{m_h} and k_{m_q} have been adjusted to reflect a 20% reduction in the values given by Eqs. 3.267 and 3.275 respectively [1].

The total pitching moment coefficient under attached flow conditions, C_m , is given by the sum of circulatory and non-circulatory components:

$$\begin{aligned}
C_{m_n} &= C_{m_n}^i + C_{m_{qn}}^i + C_{m_n}^c \\
\text{moment} &= \text{impulsive} \quad \text{impulsive} \quad \text{circulatory} \\
\text{coef.} &\quad \text{plunge} \quad \text{pitch rate} \quad \text{plunge}
\end{aligned} \tag{3.349}$$

3.4.7 Unsteady Drag

A rotor blade has a much lower stiffness and effective damping than a fixed wing aircraft for the in-plane (lead-lag) degree-of-freedom. While the flap and torsion degrees-of-freedom are primarily influenced by the lift and pitching moment respectively, the lead-lag degree-of-freedom is strongly influenced by the drag. Also, the blade lead-lag motion may couple with the flap or torsion degrees-of-freedom and may lead to an aeroelastic instability of the blades. These coupling effects are due to both the Coriolis forces and the aerodynamic loads. Thus, for a comprehensive model of the rotor system it is necessary to include aerodynamic loads for all the three degrees-of-freedom.

For steady flow conditions, the pressure drag coefficient, C_{d_p} , may be computed by resolving the normal force and chord force (sometimes known as the leading edge suction force) coefficients through the angle of attack α using

$$C_{d_p} = C_n \sin \alpha - C_c \cos \alpha \tag{3.350}$$

Now for a steady potential flow, the pressure drag, C_{d_p} , is identically zero, viz

$$C_{d_p} = C_n \sin \alpha - C_c \cos \alpha = 0 \tag{3.351}$$

For a real flow, however, there is a net pressure drag on the airfoil due to viscous effects on the chordwise pressure distribution. The inability of the airfoil to attain 100% leading edge suction is modeled using the recovery factor η , viz

$$C_c = \eta C_n \tan \alpha \quad (3.352)$$

where the value of η may be adjusted as necessary to give the best fit with the static chord force and/or drag test data. Typically, for rotor airfoils, the value of η is approximately 0.95 to 0.97.

The viscous (shear stress) drag is represented by the term C_{d_0} , and is a function of Mach number. However, its value is nominally constant for the angle of attack range below stall. Thus, the total drag in steady flow is given by the sum of the pressure and viscous shear components

$$C_d = C_{d_0} + C_{d_p} = C_{d_0} + (C_n \sin \alpha - C_c \cos \alpha) \quad (3.353)$$

where the values of η and C_{d_0} are obtainable from a look-up table and are provided in subroutine AIRFLS.

The above expression for C_d is usually written as

$$C_d = C_{d_0} + d_1 \alpha + d_2 \alpha^2 \quad (3.354)$$

where d_1 and d_2 are now written in terms of η and C_0 and C_1 .

$$C_c = \eta C_n \tan \alpha \approx \eta C_n \alpha \quad (3.355)$$

$$\begin{aligned}
C_d &= C_{d_0} + C_n \sin \alpha - C_c \cos \alpha \\
&\approx C_{d_0} + C_n \alpha - \eta C_n \alpha \\
&= C_{d_0} + (1 - \eta) C_n \alpha \\
&= C_{d_0} + (1 - \eta)(C_0 + C_1 \alpha) \alpha \\
&= C_{d_0} + (1 - \eta) C_0 \alpha + (1 - \eta) C_1 \alpha^2
\end{aligned} \tag{3.356}$$

From above, it is clear that

$$d_1 = (1 - \eta) C_0 \tag{3.357}$$

$$d_2 = (1 - \eta) C_1 \tag{3.358}$$

Since C_1 is corrected for variations due to Mach number through the Prandtl-Glauert correction factor β , d_1 and d_2 are automatically corrected for changes due to Mach number.

The unsteady chord force coefficient, $C_c(t)$ depends only on the circulatory component of the loading. There is no non-circulatory chord force. This is proved by considering the chordwise form of the circulatory and non-circulatory pressure loadings. The circulatory form is given by the standard thin airfoil theory, namely

$$\Delta C_p^c(x) = 4\alpha_E \sqrt{\frac{1 - x/c}{x/c}} \tag{3.359}$$

Where α_E is the effective angle of attack at 3/4 chord due to circulatory downwash from plunge and pitch rate. The circulatory form has a leading edge pressure singularity, and this form of pressure distribution is obtained no matter what the value of the effective angle of attack. The non-circulatory form (at time zero) is given by the piston theory result

$$\Delta C_p^i(x) = \frac{4}{M} \alpha \quad (3.360)$$

While this initial loading changes with time as pressure waves propagate from the airfoil, no leading edge singularity exists for any time. Thus, if we consider the general expression for the leading edge suction force,

$$C_c = \frac{\pi}{8} \lim_{x/c \rightarrow 0} \left\{ \Delta C_p^2 \frac{x}{c} \right\} \quad (3.361)$$

and insert the circulatory loading (which has a leading edge singularity) we get

$$C_c = \frac{\pi}{8} \lim_{x/c \rightarrow 0} \left\{ 16(\alpha_E)^2 \left(1 - \frac{x}{c} \right) \right\} = 2\pi(\alpha_E)^2 \quad (3.362)$$

The unsteady chord force may be obtained directly from the steady result by replacing α by the instantaneously effective angle of attack α_E ,

$$C_c(t) = \eta C_n(t) \tan(\alpha_E) \approx \eta C_{n_0}(\alpha_E)^2 \quad (3.363)$$

Note that the non-circulatory loading does not appear in this expression. The unsteady pressure drag is obtained by resolving the total normal force and chord force coefficients through the angle of attack α to yield

$$C_d(t) = C_{d_0} + (C_n(t) \sin \alpha - C_c(t) \cos \alpha) \quad (3.364)$$

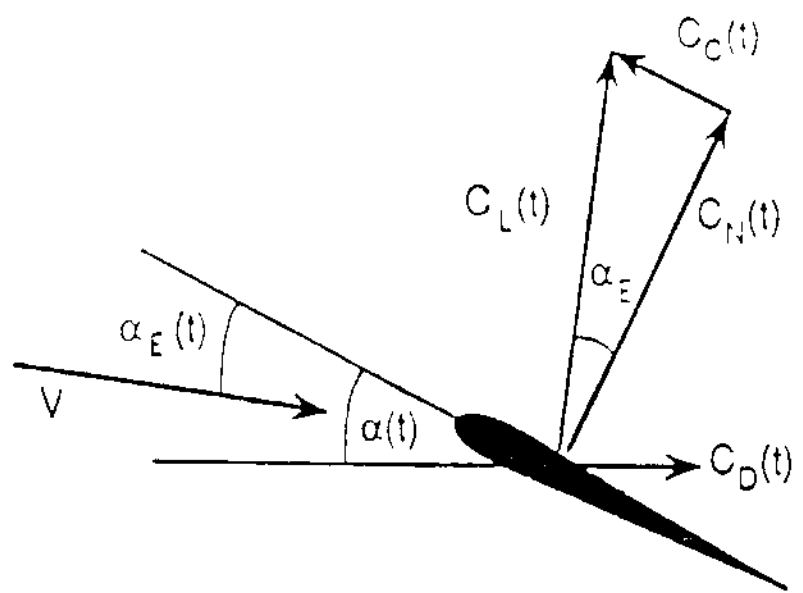


Figure 3.9: Unsteady Pressure Drag

as shown in Fig. 3.9.

It should be noted that unsteady normal force $C_n(t)$ includes *both* a circulatory and a non-circulatory component. As a consequence of this, and because of the phasing between the build up of the normal force and the chord force component, the instantaneous pressure drag may actually become negative under unsteady (potential flow) conditions [9].

3.4.8 Modifying Quasi-Steady $\bar{L}_w, \bar{L}_v, M_{\dot{\phi}}$ for Unsteady Effects

The deficiency functions X_n, Y_n , and D'_n 's modify the deformed rotating frame aerodynamic loadings \bar{L}_w and \bar{L}_v , and the pitching moment $M_{\dot{\phi}}$. The total circulatory lift force \bar{L}_w at ψ_n is the quasi-steady lift minus the lift deficiency:

$$\begin{aligned}\bar{L}_w &= \frac{\gamma}{6a} U_T^2 C_{n_a} \alpha_E \\ &= \frac{\gamma}{6a} U_T C_{n_a} (-U_P) \\ \bar{L}_{w_n} &= \frac{\gamma}{6a} U_T C_{n_a} (-U_P - X_n - Y_n) \\ &= \frac{\gamma}{6} \left[\frac{-U_T}{a} C_{n_a} U_P - \frac{U_T}{a} C_{n_a} (X_n + Y_n) \right] \quad (3.365)\end{aligned}$$

$$Total \ WB0 = \frac{\gamma}{6} [Q.S. \ WB0 - deficiencies \ to \ WB0] \quad (3.366)$$

Therefore,

$$WB0 = WB0 - (X_n + Y_n) \frac{U_T C_{n_a}}{a} \quad (3.367)$$

WB0 is a constant at ψ location; but as explained in the quasi-steady aerodynamics section, WB0 is multiplied by constant, linear, and ϵ^2 nonlinear dis-

placement terms in the transformation matrix T_3^{-1} .

The product of WB0 times the constant term in T_3^{-1} goes to the linear force vector EQ.

The product of WB0 times the linear term in T_3^{-1} goes to the stiffness matrix K.

The product of WB0 times the ϵ^2 term in T_3^{-1} will go to the nonlinear EQ vector.

The total circulatory lift \bar{L}_w is also reduced by the deficiencies due to impulsive plunge D_n and impulsive pitch rate D_n^3 .

$$WB0 = WB0 + (\Delta \dot{U}_{P1n} - D_n) \frac{4k_h \bar{c}}{c_1} \quad (plunge) \\ + (\Delta \dot{q}_n - D_n^3) \frac{k_q \bar{c}}{c_1} \quad (pitch\ rate) \quad (3.368)$$

Where c_1 is the lift curve slope, and $\bar{c} = \frac{c}{R}$ is the chord nondimensionalized by the radius. The velocity U_T in the denominators of Eq. 3.325 and 3.330 are cancelled by the U_T in the numerator of Eq. 3.382.

As shown earlier, the chordwise force \bar{L}_v is reduced only by unsteady circulatory plunge loadings, and not by the impulsive loadings.

$$VB0 = VB0 - (C_0 - d_1) U_T (X_n + Y_n) \quad (plunge) \\ + (C_1 - d_2) [2U_P (X_n + Y_n) + (X_n + Y_n)^2] \quad (plunge) \quad (3.369)$$

Like WB0, unsteady VB0 affects the the linear EQ vector, stiffness matrix K,

and the nonlinear EQ vector.

The pitching moment is modified by the unsteady circulatory pitching moment deficiencies from plunge and pitch rate as follows

$$AM0 = AM0 - f_1(X_n + Y_n) \quad (\text{plunge}) \\ + \frac{\pi U_T X_n^5}{8a\beta} \quad (\text{pitch rate}) \quad (3.370)$$

The pitching moment is also modified by the unsteady impulsive pitching moment deficiencies from plunge and pitch rate:

$$AM0 = AM0 - \frac{c}{aR} k_{m_h} A_3 b_3 (\Delta U_P - D_n^4) \quad (\text{plunge}) \\ + \frac{c}{aR} k_{m_h} A_4 b_4 (\Delta U_P - D_n^5) \quad (\text{plunge}) \\ + \frac{7c}{12aR} k_{m_q} (\Delta q_n - D_n^6) \quad (\text{pitch rate}) \quad (3.371)$$

Again, the unsteady AM0 affects the the linear EQ vector , stiffness matrix K, and the nonlinear EQ vector.

3.4.9 Implementation of Steady and Unsteady Flow Separation in UMARC

The nonlinear flow separation modeling is implemented in the subroutine AEROMX.

The algorithms have been designed such that the user may specify four levels of aerodynamic modeling:

1. Fully attached aerodynamics, quasi-steady or unsteady (ITESEP=2)
2. Nonlinear aerodynamics with only static trailing edge separation effects (ITESEP=0)
3. Nonlinear aerodynamics with unsteady flow separation off the trailing edge (ITESEP=1)
4. Nonlinear aerodynamics with unsteady trailing edge separation and dynamic stall (ITESEP=1, and IVORTEX=1).

This allows the user to independently study the effect of nonlinear aerodynamics and dynamic stall on the rotor loads or blade response. However, the second and third options, dealing with trailing edge separation effects only, are physically unrealistic options and should be used with caution. Normally, only the first or the fourth option should be used.

3.4.10 Implementing Quasi-steady Trailing Edge Separation Factor

Option (2) represents the easiest way to include nonlinear airfoil aerodynamic effect: flow separation off the trailing edge under an assumed quasi-steady flow

condition. In hover at high C_T/σ , this option may be fine, but it is not realistic in modeling the retreating blade stall in high speed forward flight. This simple stall modeling is based on Kirchhoff theory wherein the normal force coefficient, C_n , is approximated by the equation

$$C_n = C_1(M) \left(\frac{1 + \sqrt{f}}{2} \right)^2 \alpha \quad (3.372)$$

where $C_1(M)$ is the normal force curve slope, f is the trailing edge separation point (non-dimensionalized with respect to chord), and α is the angle of attack. Thus, if the separation point can be determined, it is straight forward to compute the normal force coefficient. The α is measured relative to the zero lift angle; $\alpha = \alpha - \alpha_0$.

To implement this procedure, the relationship between the separation point, f , and the angle of attack, α , must be obtained. The effective separation point, f , can be deduced from the experimental measurements of the static C_n variation with α by rearranging Eq. 3.372 to solve directly for f , i.e.

$$f = \left(2 \sqrt{\frac{C_n}{C_{n\alpha}(\alpha - \alpha_0)}} - 1 \right)^2 \quad (3.373)$$

Because of the similar empirical relationship between α and f at each Mach number, the variations are generalized in a fairly simple manner using curve-fits Fig. 3.10

$$f = \begin{cases} 1 - 0.3 \exp \{((\alpha - \alpha_0) - \alpha_1)/S_1\} & \text{if } \alpha \leq \alpha_1 \\ 0.04 + 0.66 \exp \{(\alpha_1 - (\alpha - \alpha_0))/S_2\} & \text{if } \alpha > \alpha_1 \end{cases} \quad (3.374)$$

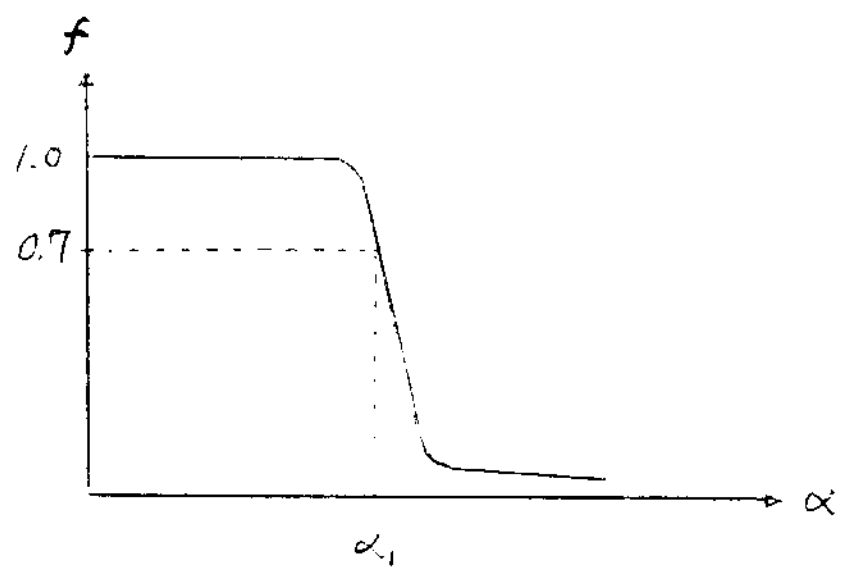


Figure 3.10: Generalization of separation point versus angle of attack relationship

The coefficients S_1 and S_2 define the static stall characteristic, and determine whether the stall occurs progressively or abruptly. The α_1 defines the break point corresponding to $f = 0.7$. This point is defined only as a matter of convenience; $f \approx 0.7$ closely corresponds to the static stall angle of attack for most airfoil sections. The parameters S_1 , S_2 and α_1 are determined for different Mach numbers from the static lift data. Their values are inputs to the aerodynamic model and stored in subroutines AIRFLS and INITAF.

An expression for the chord force C_c may also be deduced from the Kirchhoff solution to the trailing edge stall problem. From Kirchhoff theory, the chord force at small angles of attack can be written as

$$C_c = C_{n_\alpha} (\alpha_f)^2 \sqrt{f} \quad (3.375)$$

where the factor \sqrt{f} accounts for the influence of trailing edge separation. The expression in Eq. 3.375 is further modified to take account of viscous effects via the parameter η , i.e.

$$C_c = \eta C_{n_\alpha} (\alpha_f)^2 \sqrt{f} \quad (3.376)$$

The factor η must be included, since even with no separation on the airfoil the airfoil does not realize 100% of the chord force which would be attained in potential flow. In UMARC, $\eta = 0.97$ is used for the NACA 0012 airfoil, and this value is good for most rotor airfoils in use.

In AEROMX, the effect of Kirchhoff flow separation on chord force C_c is implemented by modifying the coefficients C1MD2=($C_1 - d_2$). The derivation of

how \sqrt{f} affects C_c , and hence $(C_1 - d_2)$, is shown below.

From Eq. 3.358

$$d_2 = (1 - \eta)C_1 \quad (3.377)$$

or,

$$C_1 - d_2 = \eta C_1 \quad (3.378)$$

$$(C_1 - d_2)\alpha^2 = \eta C_1 \alpha^2 = C_c \quad (3.379)$$

Therefore, the effect of flow separation on chord force, C_c , is modeled simply by multiplying $(C_1 - d_2)$ by \sqrt{f} in AEROMX.

$$(C_1 - d_2)\alpha^2 \sqrt{f} = \eta C_1 \alpha^2 \sqrt{f} = C_c \quad (3.380)$$

$$(C_1 - d_2)\sqrt{f} = \eta C_1 \sqrt{f} \quad (3.381)$$

3.4.11 Determine Unsteady Trailing Edge Separation Point

Unsteady Leading edge Pressure

For unsteady conditions, there is a lag in $C_n(t)$ with respect to changes in angle of attack; however there is also a lag in the leading edge pressure response with respect to $C_n(t)$. The lag in the pressure response can be significant, particularly as the frequency increases. Thus, for an increasing angle of attack the lag in the leading edge pressure response results in the critical pressure conditions being

achieved at a larger value of C_n , and hence at a higher angle of attack than the quasi-steady case. This is true for both subcritical and supercritical flows. This mechanism contributes to an overall delay in the onset of dynamic stall and must be modeled appropriately.

To implement the critical pressure criterion under unsteady conditions, a first order lag may be applied to $C_n(t)$ to produce a substitute value $C'_n(t)$ with the presumption that whatever modifications apply to the pressure must also apply to $C'_n(t)$. For a discretely sampled system the modification to $C_n(t)$ may be written in numerical form as

$$C'_{n_n} = (C_{n_n} - D_{p_n}) \quad (3.382)$$

where the lag applies only to the circulatory part of the normal lift coefficient C_n . For unsteady flow, C_{n_n} is modified from the static flow condition by using the unsteady $U_{P_{UN}}$ velocity instead of the quasi-steady U_P . The unsteady flow C_{n_n} and $U_{P_{UN}}$ are defined in AEROMX as

$$U_{P_{UN_n}} = U_{P_n} + X_n + Y_n \quad (3.383)$$

$$C_{n_n} = d_1 U_{P_{UN_n}}^2 + C_0 U_{T_n}^2 - (C_1 + d_0) U_{T_n} U_{P_{UN_n}} \quad (3.384)$$

The deficiency function D_p in Eq. 3.382 in the discrete time domain is given by

$$D_{p_n} = D_{p_{n-1}} \exp\left(\frac{-\Delta S}{T_p}\right) + (C_{n_n}^c - C_{n_{n-1}}^c) \exp\left(\frac{-\Delta S}{2T_p}\right) \quad (3.385)$$

This deficiency function has the familiar first order lag form that we have derived for X_n and Y_n in Section 3.4.1. The time constant T_p is given in terms of semi-chords of airfoil travel.

The onset of leading edge/shock induced separation under dynamic conditions is initiated when $C'_n(t)$ exceeds the critical $C_{n_1}(M)$ value. This means that the onset of leading edge separation is delayed to higher angles of attack for increasing reduced frequency (or increasing pitch rate), a fact observed experimentally.

The aforementioned lag applied to the leading edge pressure models a physical effect, namely that the pressure on the airfoil lags with respect to both the lift force and the airfoil motion. The lagged value of the lift is monitored, and attainment of a critical value is used to initiate the onset of leading edge or shock induced stall.

It should be noted that the time constant T_p is a function of Mach number and must be determined empirically from unsteady data for a particular airfoil. Generally, this is done by plotting the measured value of the unsteady pressure near the leading edge versus the measured value of unsteady lift for a case where the airfoil is unstalled. Appropriate values for T_p over a range of Mach numbers are provided for the NACA 0012 airfoil in subroutine AIRFLS. Recent studies indicate that the value of T_p is quite independent of airfoil shape. Similar conclusion is drawn from similar analysis on various rotor airfoils under oscillatory pitch conditions. Thus, in the absence of any unsteady data for a given airfoil section, value of T_p for the NACA 0012 airfoil may be used.

Determination of Pressure Lagged Separation Point

To determine the unsteady trailing edge separation point, first the airfoil unsteady leading edge pressure response, via Eq. 3.382 is used to define an effective angle of attack, α_f , which yields the same unsteady leading edge pressure conditions as the quasi-steady case,

$$\alpha_f(t) = \frac{C'_n(t)}{C_{n_a} SLC} \frac{180}{\pi} \quad (3.386)$$

Where SLC is the reference lift curve slope, usually set equal to C_1 . α_f is measured with respect to the zero lift angle α_0 . Therefore,

$$\alpha_f(t) = \alpha_f(t) - \alpha_0 \quad (3.387)$$

This value of α_f is then used to determine the effective separation point, f' . The f versus α equations from the Kirchhoff static flow separation principle can be used again simply by substituting f' for f , and α_f for α .

$$f' = \begin{cases} 1 - 0.3 \exp \{(|\alpha_f| - \alpha_1)/S_1\} & \text{if } \alpha_f \leq \alpha_1 \text{ and } \alpha_f \geq -\alpha_1 \text{ no stall} \\ 0.04 + 0.66 \exp \{(\alpha_1 - |\alpha_f|)/S_2\} & \text{if } \alpha_f > \alpha_1 \text{ and } \alpha_f < -\alpha_1 \text{ lift stall} \\ 0.04 & \text{if } \alpha_f > + \text{ or } - 60 \text{ degrees} \end{cases} \quad (3.388)$$

Similarly, the value of α_f is used to determine the effective separation point, f'_m , for the moment stall. The f' versus α_f equations are used again simply by substituting f'_m for f' .

$$f'_m = \begin{cases} 1 - 0.3 \exp \{(|\alpha_f| - \alpha_{1_m})/S_1\} & \text{if } \alpha_f \leq \alpha_{1_m} \text{ and } \alpha_f \geq -\alpha_{1_m} \text{ no stall} \\ 0.04 + 0.66 \exp \{(\alpha_{1_m} - |\alpha_f|)/S_2\} & \text{if } \alpha_f > \alpha_{1_m} \text{ and } \alpha_f < -\alpha_{1_m} \text{ moment stall} \\ 0.04 & \text{if } \alpha_f > + \text{ or } - 60 \text{ degrees} \end{cases} \quad (3.389)$$

where α_{1_m} equals approximately the static moment stall angle.

Non-linear Trailing Edge Separation Correction

The above procedure assumes that the instantaneously effective pressure distribution on the airfoil drives the boundary layer response. Although this procedure results in a hysteresis in the separation point location as a function of angle of attack, it does not account for the additional unsteady effects on the boundary layer response.

Prandtl suggested a very simple spring/mass/damper analogy to the Navier-Stokes equations for a viscous fluid Ref.[8]. In the limiting case when the mass of this system becomes very small (which is equivalent to a large Reynolds number), a solution to the governing differential equation can be obtained in terms of matched asymptotic expansions. In this approach the outer expansion represents the behavior of the outer (potential) flow, and the inner expansion represents the counterpart of the boundary layer solution which is determined by the presence of viscosity. Thus, according to Prandtl's analogy, the boundary layer equations take on the form of a first order system.

If we assume the input to this system is the location of the separation point from the preceding analysis, f' , then the additional lag in the boundary layer response to unsteady effects may be represented for a discretely sampled system as

$$f_n'' = f_n' - D_{f_n} \quad (3.390)$$

$$f_{m_n}'' = f_{m_n}' - D_{f_n} \quad (3.391)$$

where the deficiency function is

$$D_{f_n} = D_{f_{n-1}} \exp\left(\frac{\Delta S}{T_f}\right) + \left(f'_n - f'_{n-1}\right) \exp\left(\frac{\Delta S}{2T_f}\right) \quad (3.392)$$

As in the case of T_p , T_f is a Mach number/Reynolds number dependent time constant, although experience shows that this dependence is much weaker variation for T_f . Studies have also shown that the values of T_f is quite independent of airfoil shape. Thus, in the absence of any unsteady data for a given airfoil section, values of T_f for the NACA 0012 airfoil may be used.

Finally, the effects of unsteady flow separation is to reduce the quasi-steady 2-D lift coefficient, the chord force, and introduce additional pitching moment.

Effect of Unsteady T.E. Separation on Lift Coefficient C_1

Unsteady flow separation reduces the quasi-steady 2-D lift coefficient $C1M$, $C_1(M)$. In the code, the coefficient $C1PD0$, ($C_1 + d_0$), becomes

$$(C_1 + d_0) = C_1(M) * \frac{(1 + \sqrt{f_n''})^2}{4} + d_0 \quad (3.393)$$

Light or Gross Separation Drag Correction

The effect of flow separation on the chord force C_c has been explained in the section on static separation and the expression for the chord force has been found to be adequate for cases when the separation is moderate. For gross flow separation, i.e. when $f < 0.7$, the Kirchhoff expression has been found inaccurate when compared with experimental data. In deep stall conditions, it appears that the chord force correlates more with f itself as opposed to \sqrt{f} .

In view of this, the chord force in the deep stall regime is computed according to the expressions

$$C_c = \begin{cases} \eta C_{n_a}(\alpha_f)^2 \sqrt{f''} & \text{if } C'_n \leq C_{n_1} \\ \eta C_{n_a}(\alpha_f)^2 f'' & \text{if } C'_n > C_{n_1} \end{cases} \quad (3.394)$$

To prevent a discontinuity in the chord force in Eq. 3.394, when switching from one equation to the next, the chord force is calculated using the scheme

$$C_c = \eta C_{n_a} \alpha^2 \sqrt{f''} \text{ CTFAC T} \quad (3.395)$$

where $\sqrt{f''}$ is now modified by the factor CTFAC T.

$$(C_1 - d_2) = \eta C_1 \sqrt{f''} \text{ CTFAC T} \quad (3.396)$$

The parameter CTFAC T is evaluated using

$$\text{CTFACT} = f^{(\frac{\text{GRDGCK}}{2})} \quad (3.397)$$

where GRDGCK is

$$\text{GRDGCK} = \text{UNKF}(C'_n - C_{n_1}) \quad \text{where } 0 \leq \text{GRDGCK} \leq 1 \quad (3.398)$$

The value of UNKF is a constant obtained empirically from the static chord force (or drag) data for a given airfoil at a given Mach number. UNKF is stored in subroutine AIRFLS. Additionally, GRDGCK is constrained so that its maximum value is unity. The previous equations thus ensure that the variation in the chord force is fairly continuous and causes no sudden discontinuities. Also, these equations are adequate under both steady and unsteady conditions.

Under steady conditions, C'_n in Eq. 3.398 is equal to the steady potential value of the normal force, $C_{n_a} \alpha$.

Pitching Moment Variation with Trailing edge Separation

A general expression for the pitching moment behavior cannot be obtained analytically from Kirchhoff theory, and an alternative empirical relation is used.

Using the airfoil static data, the center of pressure at an angle of attack may be determined from the ratio C_m/C_n (allowing for the zero lift moment C_{m_0}). The variation is plotted versus the corresponding value of the separation point and curve fitted using a low order polynomial. One suitable curve fit is to use the form

$$\frac{C_m}{C_n} = k_0 + k_1(1 - f_m'') + k_2 \sin(\pi f_m''^2) \quad (3.399)$$

where $k_0 = (0.25 - x_{ac})$ is the aerodynamic center offset from the 1/4-chord. The constant k_1 accounts for the center of pressure variation due to the growth of the separated flow region, and the constant k_2 determines the shape of the moment break at stall. The values of k_0 , k_1 , k_2 and m can be obtained using a least squares curve fit (or other procedure), and can be adjusted for different airfoils, as necessary, to give the best moment curve reconstruction.

In subroutine AEROMX, the pitching moment change due to unsteady flow separation is implemented by modifying the term $AM0$. As explained in the quasi-steady aerodynamics section of the manual, $AM0$ is the steady bias term in pitching moment expression. Now, $AM0$ is simply modified as

$$AM0 = AM0 + C_n \frac{(1 + \sqrt{f_m''})^2 [K_1(1 - f_m'') + K_2 \sin(\pi f_m''^2)]}{4 SLC} U_T^2 \quad (3.400)$$

3.4.12 Dynamic Stall

Calculation of Vortex Normal Force Parameter

The effects of dynamic stall are to modify (1) airfoil lift, and (2) the pitching moment characteristics. In this section it is shown how the the vortex induced lift is incorporated by considering the vortex lift contribution as an excess accumulation of circulation retained in the vicinity of the airfoil until some critical condition is reached. This critical condition is the onset of leading edge or shock induced separation, as discussed previously.

For a discretely sampled system, the vortex lift coefficient C_v^v is represented by assuming, that for a given sample period, the increment in vortex lift C_v depends on the difference between the instantaneous linearized value of the unsteady circulatory lift and the corresponding unsteady non-linear lift as given by the Kirchhoff approximation, i.e.

$$C_{v_n} = C_{v_n}^c \left(1 - \frac{(1 + \sqrt{f_n''})^2}{4} \right) \quad (3.401)$$

At the same time, the total accumulated vortex lift C_v^v is allowed to decay exponentially with time to model the viscous diffusion as well as the lessening influence of the vortex as it is swept downstream. However, as long as the angle of attack (and lift) is changing with time, the accumulated vortex lift is updated by a new increment. Following a approach similar to that used in Section 3.4.11, this “vortex lift” may be expressed in discrete time form as

$$C_{v_n}^v = C_{v_{n-1}}^v \exp \left(\frac{-\Delta S}{T_v TVFACT} \right) + (C_{v_n} - C_{v_{n-1}}) \exp \left(\frac{-\Delta S}{2T_v TVFACT} \right) \quad (3.402)$$

When the rate of change of lift is low, the vortex lift dissipates as fast as it accumulates, and in the limit, as the rate of change of angle of attack tends to zero, the airfoil characteristics revert smoothly back to the static (non-linear) behavior.

Abrupt airloading changes occur when the critical conditions for leading edge or shock induced separation effects are satisfied, i.e. $(C'_n(t) > C_{n_1})$. At this point, the accumulated vortex lift starts convecting over the airfoil chord. The rate at which this convection occurs has been determined from experimental tests to be somewhere between one-third and one-half of the free-stream velocity, with a weak dependence on Mach number. The results from recent measurements of the vortex convection suggest that the convection speed is closer to one-third of the free-stream velocity.

During the vortex convection process, the vortex lift is assumed to continue via Eqs. 3.401 and 3.402; however, the accumulation is terminated when the vortex reaches the airfoil trailing edge and is shed into the wake. To track the position of the vortex, a non-dimensional vortex time parameter τ_v (in semi-chords) is used such that $\tau_v = 0$ at the onset of separation conditions, and $\tau_v = T_{vl}$ when the vortex reaches the trailing edge.

The center of pressure location on the airfoil varies with the chordwise position of the vortex and attains a maximum value when the vortex reaches the trailing edge. Based on experimental data involving dynamic stall over a wide range of Mach numbers, a fairly general empirical representation of the center

of pressure behavior (aft of 1/4-chord) has been suggested, i.e.,

$$CP_v = 0.25 \left(1 - \cos \left(\frac{\pi \tau_v}{T_{vl}} \right) \right) \quad (3.403)$$

Since $\sin(A - \frac{\pi}{2}) = -\cos A$,

$$CP_v = 0.25 \left(1 + \sin \left(\frac{\pi \tau_v}{T_{vl}} - \frac{\pi}{2} \right) \right) \quad (3.404)$$

The increment in the 1/4-chord pitching moment due to the aft-moving center of pressure is given by

$$C_m^v = -CP_v C_n^v \quad (3.405)$$

The extra lift due to the vortex rolling over the top of the airfoil surface is treated as an extra bias term, similar to C_0 , and is added to the constant $WB0$ term in the expression for the normal lift, $\overline{L_w}$:

$$WB0 = WB0 + \frac{C_{n_n}^v}{SLC} U_T^2 \quad (3.406)$$

The extra pitching moment due to the vortex rolling past the 1/4 chord over the top of the airfoil surface is treated as an extra bias term, similar to C_{m_0} . This extra pitching moment due to dynamic stall is added to the constant $AM0$ term in the expression for the pitching moment, M .

$$AM0 = AM0 + \frac{C_{m_n}^v}{SLC} U_T^2 \quad (3.407)$$

Derivation of Time Constants T_v and T_{vl}

Both the vortex decay time constant, T_v , and the time for the vortex to traverse the chord, T_{vl} , can be determined empirically from unsteady test data. Values for the NACA 0012 airfoil are stored in subroutine AIRFLS.

Experimental data suggest that both T_v and T_{vl} are relatively independent of Mach number. However, no formal conclusion can be made regarding the variability of these parameters with airfoil shape. Dynamic stall experiments performed by a variety of investigators have indicated that while there is a significant effect of airfoil shape under light stall conditions, all airfoils behave very similarly under strong dynamic stall conditions. Thus, it can be tentatively concluded that the parameters T_v and T_{vl} should be relatively insensitive to airfoil shape.

The value of T_v depends on the instantaneous chordwise location of the rolled up vortex. In AEROMX, T_v is multiplied by the factor TVFACT. TVFACT has value of 0.5 or 1.0.

$$f^{qs} = \begin{cases} 1.0 & \text{if } 0 < \tau_v \leq T_{vl} \\ 0.5 & \text{if } T_{vl} < \tau_v \leq 2T_{vl} \end{cases} \quad (3.408)$$

Logic Flags for Vortex Shedding Model

In the algorithms, the flags IVF1MX and IVF2MX indicate whether or not the vortex is convecting over the chord. When IVF1MX=IVF2MX=0, the vortex is not present in the vicinity of the airfoil. When IVF1MX=1, the vortex is within T_{vl} semi-chords of the airfoil, which also means that the vortex has not convected

pass the trailing edge. When IVF2MX=1, the vortex is within $2T_{vl}$ semi-chords of the airfoil, which means the vortex has convected pass the trailing edge, but still within two chord lengths from the leading edge. These flags are used to signal when to modify the time constants, T_f and T_v , by assigning numerical values to the factors TFFACT and TVFACT.

3.5 Rotor Wake Modeling

The wake behind the rotor disk determines the induced inflow distribution over the disk and plays an important role in the prediction of blade response, blade loads, acoustic signature, and rotor performance. An accurate modeling of the induced inflow on the rotor disk is essential for rotor analysis, more so at low speed flight condition. At low speed, the wake stays close to the disk and has a dominating influence on blade airloads.

Calculation of the complex wake structure is still one of the most difficult problems for rotary-wing aerodynamicists. There are many wake models available with varying levels of complexity and accuracy. These range from simple uniform inflow distributions to elaborate vortex-lattice free wake models. This section describes the three rotor wake models presently available in UMARC: the linear inflow model, the prescribed wake model, and the free wake model.

3.5.1 Uniform and Linear Inflow Models

The simplest model assumes a uniform inflow distribution over the rotor disk and is frequently referred as Glauert model. In this model, the rotor induced inflow is expressed in terms of the rotor thrust coefficient, advance ratio, and rotor shaft tilt.

$$\lambda = \mu \tan \alpha_s + \lambda_i$$

$$= \mu \tan \alpha_s + \frac{C_T/2}{\sqrt{\lambda^2 + \mu^2}} \quad (3.409)$$

where λ is total inflow ratio, λ_i is induced inflow ratio and α_s is forward tilt of rotor disk plane.

For an improved simple inflow model, the rotor induced inflow is assumed to vary linearly across the rotor disk

$$\lambda_i = \frac{C_T/2}{\sqrt{\lambda^2 + \mu^2}} (1 + \kappa_x x \cos \psi + \kappa_y x \sin \psi) \quad (3.410)$$

There are many forms of this model available in literature. One form is called Drees model [2], where κ_x and κ_y are defined as:

$$\begin{aligned} \kappa_x &= \frac{4}{3} \left[(1 - 1.8\mu^2) \sqrt{1 + \left(\frac{\lambda}{\mu}\right)^2} - \frac{\lambda}{\mu} \right] \\ \kappa_y &= -2\mu \end{aligned} \quad (3.411)$$

For low speed flight conditions ($\mu < .2$), the Blake and White model can also be used:

$$\begin{aligned} \kappa_x &= \sqrt{2} \\ \kappa_y &= 0 \end{aligned} \quad (3.412)$$

These simple inflow models may capture the global effects of rotor wake and are usually satisfactory for high speed flight condition, more so for rotor performance and stability predictions. The influence of the near wake becomes less

severe at high speed because large portions of the wake are swept away by a high incoming velocity. Linear wake model becomes less accurate at low speed and hovering flight conditions when the inflow distribution becomes highly nonuniform over the rotor disk.

3.5.2 Prescribed and Free Wake Models

The assumption of a linear distribution of inflow can capture the influence of the wake in a global manner, but it ignores the detailed inflow distribution caused by the complex wake structure. A rotor wake is primarily generated by gradients of circulation, spatially and temporally. Conservation of vorticity dictates the formation of trailed vorticity with magnitude proportional to the radial gradient of circulation along the blade span. Since the magnitude of the circulation is concentrated near the tip, falling off to zero at the blade tip, the resulting steep gradient results in strong trailed vortices in this region. These trailed vorticity components quickly roll-up into a discrete trailed-tip vortex. Trailed vorticity inboard of the circulation peak yields vorticity of an opposite sign, which is comparatively weak since the radial gradient is generally small.

In addition to the trailed vorticity, temporal gradients of the bound circulation, around the rotor disk, generate shed vorticity in the wake. This vorticity is proportional to the temporal circulation gradient, and can be of either sign, depending on whether the circulation increases or decreases around the rotor azimuth. In addition, conservation of vorticity for a three-dimensional wing

requires that the bound circulation itself be trailed into the wake at both the blade tip and the blade root. Combination of trailed and shed vorticity creates a vortex sheet, skewed further by rotor blade motion and vortex interactions, and free stream velocity components.

In the UMARC, prescribed wake and free wake models, as used in CAM-RAD [3], are adapted and implemented. Also, a recently developed free wake model by Johnson [4], which can model the dual-peak span loading condition at high speed, is implemented. The underlying theory of the models is briefly discussed here, and then a description of the implementation is presented.

3.5.3 Rotor Wake Analysis

Calculation of the inflow at an arbitrary point on a blade must take into consideration the motion of the blade, the free stream velocity, and the distribution of vorticity in the wake structure. The first two components are relatively straightforward and are discussed in the earlier section. The effects of the wake vorticity are function of both the vortex strengths, and their geometric distances from the point of interest. The vortex strengths, as mentioned earlier, can be computed easily from the circulation gradients. A major step in rotor wake analysis is to determine the wake geometry.

The present wake model is based on a vortex lattice (straight line segment) approximation. As mentioned earlier, the dominant feature of the wake is the tip vortex, and is therefore modeled separately. The effect of the inboard trailed

vorticity is less significant; therefore, is modeled approximately by a small number of large-core vortices. The resulting model offers computational efficiency while still capturing the important effects of the inboard trailed vorticity.

The wake is divided into three distinct regions; near wake, rolling-up wake, and far wake (Fig. 3.11). The near wake is of prime importance to its generating blade because of its proximity. The trailed vorticity is modeled as a finite number of vortex panels along the blade span. In the rolling-up wake region, the panel number is reduced to two: one for the inboard vorticity sheet or filament, and one for the rolling up of the tip vortex. The magnitude of the rolling-up vortex filament is a prescribed fraction of the maximum bound circulation along the blade span. The far wake model consists of just one vortex panel inboard, and a discrete concentrated tip vortex of strength equal to the maximum value of bound circulation along the blade.

Some other important features of the modeling concern with the strength of vortex filaments. The model assumes either a uniform, or a linear variation of vorticity within a filament, the latter being used in this analysis. The other feature concerns with a vortex encountering the following blade. A blade-vortex interaction results in rapid variations of induced loading, which the lifting line theory cannot predict accurately. To improve this prediction, the lifting surface correction is utilized.

This is based on an infinite aspect-ratio, non-rotating wing encountering a straight infinite, constant-strength vortex. Following such an interaction, the

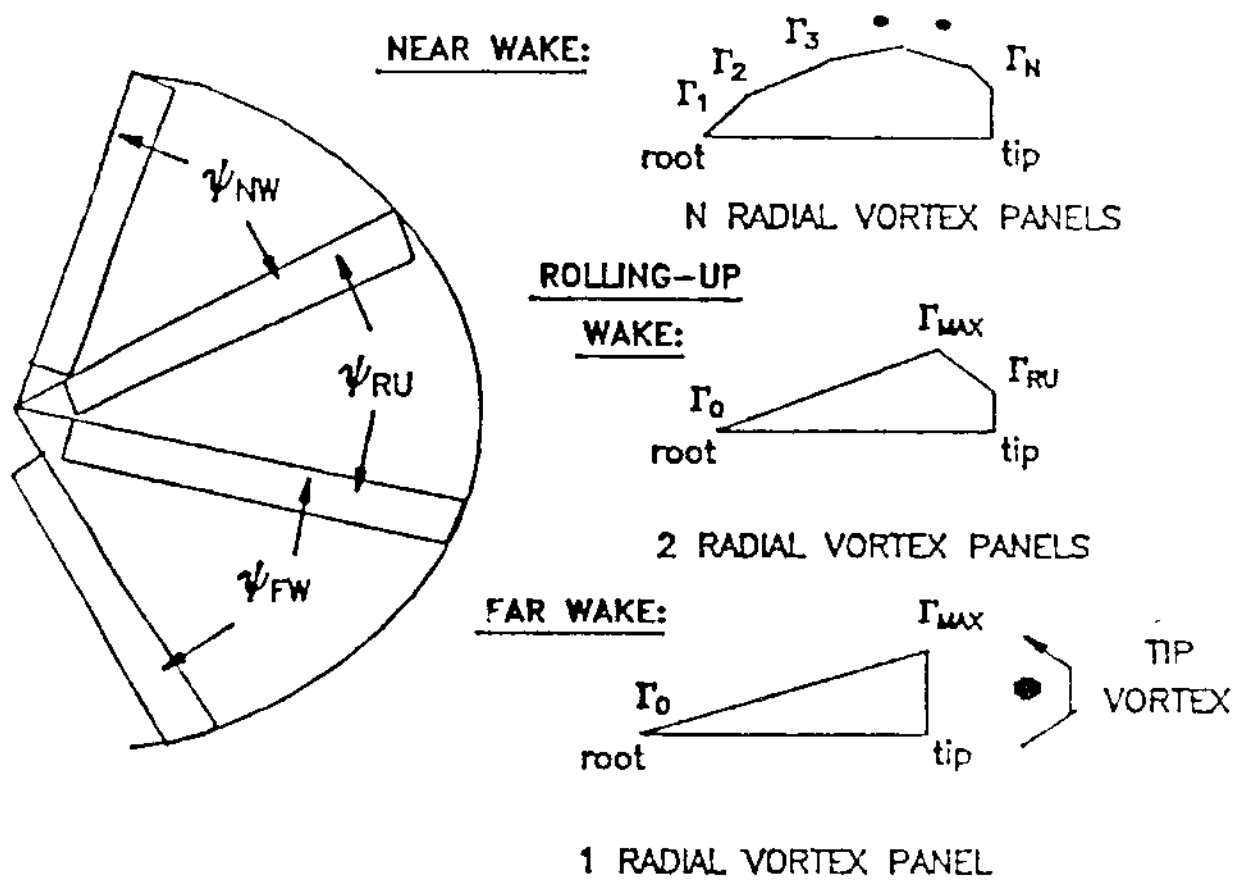


Figure 3.11: Wake model for nonuniform induced velocity calculation (Ref. 3)

effects of the vortex are reduced, and these are done by increasing, or “bursting” the vortex core. The physics of this phenomena is though speculative, yet the increase in vortex core size captures observed results.

Another important assumption pertains to the prescribed magnitude of the vortex cores. Since this is an inviscid model, the mathematical representation of a vortex leads to a numerical singularity at the vortex center. To avoid this problem, and to better represent the viscous nature of a “real” vortex, a vortex core radius is prescribed, and a finite velocity distribution is assumed within the core. The magnitude of the core radius, typically five to twenty percent of blade chord for the tip vortices, and larger inboard, is prescribed and can have a significant effect on the resultant blade airloads.

3.5.4 Rotor Wake Geometry

The most difficult part of the wake analysis is to calculate the wake geometry. In the present wake model, the wake is modeled as a finite number of vortex filaments, trailed and shed into the wake. These filaments are convected with the local flow velocity, which consists of the free stream velocity and the wake self-induced velocity. Since the self-induced velocity is, in turn, a function of the wake geometry, the analysis is of a highly non-linear in nature. In this respect, the two wake models, prescribed and free wake models, differ from each other. The prescribed wake model assumes a fixed wake geometry. On the other hand, the free wake model calculates the wake geometry, accounting for effects of both

free stream and self-induced velocities.

The geometry of the vortex behind the reference blade is described by the position vector $\mathbf{r}_w(\Psi, \phi)$, where Ψ is the current azimuth position of the generating blade and ϕ is the age of the vortex element (Fig. 3.12). The wake age, ϕ , determines whether the panel considered is part of the near wake, the rolling up wake, or the far wake models. The near wake model is used only behind the reference blade.

The wake geometry is computed at the discrete azimuth positions $\Psi_l = l\Delta\Psi$ ($\Delta\Psi = 2\pi/J$) and wake ages $\phi_k = k\Delta\phi$ ($\Delta\phi = 5^\circ - 15^\circ$). l determines the current azimuthal position of the blade and ranges from 1 to J , and k determines the number of the wake panel to be used for induced velocity calculation and ranges from zero to the specified number, depending on whether the panel considered is part of the near wake ($k = k_{NW}$), the rolling up wake ($k = k_{RW}$), or the far wake ($k = k_{FW}$) models. The wake geometry behind the other blades can be obtained for \mathbf{r}_w at the appropriate blade azimuth angle.

3.5.5 Equation of the Wake Geometry

The tip vortex elements are created at the blade tip, convected with the free stream velocity, and distorted by the self-induced velocity in the wake. The rotation of the blade together with convection by the free stream velocity produces the basic helical geometry of the rotor wake. However, the actual position of the wake elements, determined by the integral of the local convec-

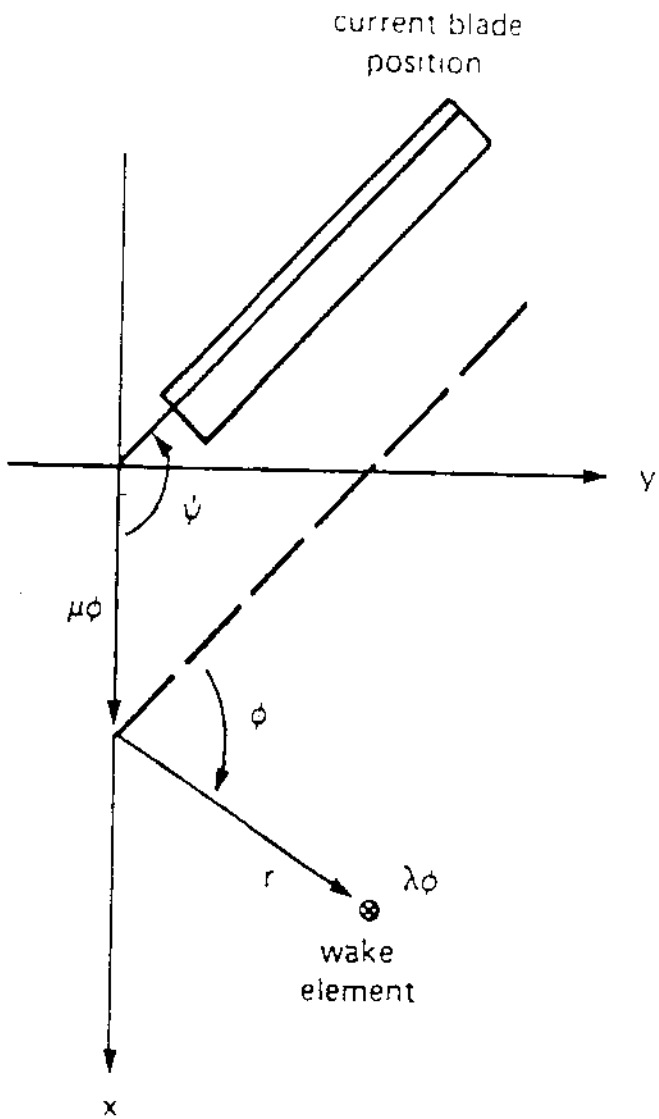


Figure 3.12: Rotor wake geometry (Ref. 3)

tion velocity, is highly distorted from the basic helical geometry. The resulting wake geometry is

$$\mathbf{r}_w(\Psi, \phi) = \mathbf{r}_b(\Psi - \phi) + \phi\boldsymbol{\mu} + \mathbf{D}(\Psi, \phi) \quad (3.413)$$

where \mathbf{r}_b is a position vector of the blade at radial station r ($r = 1$ for blade tip), and $\boldsymbol{\mu}$ is free stream velocity vector. The first and second terms in Eq. 3.413 represent the equation of the basic helical geometry ($\mathbf{r}_b(\Psi - \phi)$ due to blade rotation and $\phi\boldsymbol{\mu}$ due to free stream convection), and $\mathbf{D}(\Psi, \phi)$ represents the distortion due to the wake self-induced velocity.

Similarly, the geometry of the inboard wake sheet is defined at the root and tip edges, trailing from the blade \mathbf{r}_b , at radial station $r = r_{ROOT}$ and $r = 1$, respectively. In general, the distortion \mathbf{D} is different for the tip vortex and the inboard sheet. Because of the dominant role due to tip vortices, the most important information in the wake geometry is the tip vortex position, and a less accurate modeling of the inboard sheet is often acceptable.

3.5.6 Prescribed Wake Model

The prescribed wake assumes a fixed wake geometry (not calculated iteratively), based on parameters like advance ratio, thrust, etc.. This simplifies the wake analysis and saves computation time.

A simplified prescribed wake (a rigid wake) assumes that all elements in the wake are convected downward by the mean induced velocity at the rotor disk,

giving

$$\mathbf{D} = \begin{bmatrix} 0 \\ 0 \\ D_Z \end{bmatrix} \quad (3.414)$$

where

$$D_Z = -\phi \lambda_i \quad (3.415)$$

It should be noted that the distortion is independent of the azimuth angle Ψ . The convection velocity λ_i is the mean induced velocity at the rotor disk. Sometimes, this model can be generalized to a two stage-convection:

$$\begin{aligned} D_Z &= -K_1 \phi & \phi \leq 2\pi/N \\ &= -K_1 2\pi/N - K_2(\phi - 2\pi/N) & \phi > 2\pi/N \end{aligned} \quad (3.416)$$

If one includes the wake contraction in Eq. 3.414, it gives

$$\mathbf{D} = \begin{bmatrix} D_r \cos(\Psi - \phi) \\ D_r \sin(\Psi - \phi) \\ D_Z \end{bmatrix} \quad (3.417)$$

where the radial displacement (also independent of Ψ) is expressed as:

$$D_r = -(1 - e^{-K_3 \phi})(1 - K_4) r_i \quad (3.418)$$

where $r_i = 1$ is used for the tip vortex and the outside edge of the inboard sheet, and $r_i = r_{ROOT}$ for the inside edge. There are many forms of the prescribed models, which differ in their definition of K_1, K_2, K_3 and K_4 parameters. One of the widely-used wake models is the Landgrebe's model [10].

Landgrebe's Prescribed Wake Model

Landgrebe developed a prescribed wake geometry from flow visualization results of a model rotor.

I. For tip vortex,

$$K_1 = .25(C_T/\sigma + .001\theta_{tw}) \quad (3.419)$$

$$K_2 = (1 + .01\theta_{tw})\sqrt{C_T} \quad (3.420)$$

II. For outside edge of vortex sheet,

$$K_1 = 1.55\sqrt{C_T} \quad (3.421)$$

$$K_2 = 1.9\sqrt{C_T} \quad (3.422)$$

III. For inside edge of vortex sheet,

$$K_1 = 0 \quad (3.423)$$

$$K_2 = -(.0025\theta_{tw}^2 + .099\theta_{tw})\sqrt{C_T} \quad (3.424)$$

IV. For radial contraction,

$$K_3 = .145 + 27C_T \quad (3.425)$$

$$K_4 = .78 \quad (3.426)$$

where θ_{tw} is the blade linear twist in degrees.

3.5.7 Free Wake Model

The free wake model iteratively solves for the wake geometry, accounting for both free stream and self-induced velocity fields. This iteration allows convection of vortex filaments in different spatial directions, and convergence of solution is not achieved until the geometry has attained a steady-state condition. This model yields increased accuracy over the prescribed wake model when complex wake geometries evolve, such as occurs in transitional flight regimes.

In the present free wake model, only the distorted geometry of the tip vortex is calculated. Rigid or prescribed geometry is used for the inboard vorticity. This is done because of the dominant role of tip vortices as compared to inboard vortices.

The procedure for calculating the wake geometry consists of integrating the induced velocity at each wake element [11]. The outer loop in the calculation is an iteration on the wake age ϕ . The induced velocity $\hat{\mathbf{q}}(\Psi)$ is calculated at all wake elements for a given age ϕ , and all azimuth angle Ψ . Then the increment in the distortion as the wake age increase by $\Delta\Psi$ is:

$$\mathbf{D}(\Psi, \phi) = \mathbf{D}(\Psi, \phi - \Delta\Psi) + \Delta\Psi\hat{\mathbf{q}} \quad (3.427)$$

Using this procedure, the distorted geometry of tip vortex, $\mathbf{D}(\Psi, \phi)$ is obtained.

3.5.8 Calculation of Influence Coefficients

The next step is to obtain a set of influence coefficients for each point in the flow field at which the induced velocity is calculated, at points distributed radially and azimuthally over the rotor disk. At this stage, the geometry of the wake is already known to us by using either prescribed wake or free wake model. Influence coefficients are calculated using the Biot-Savart law, and combines the influence of all vortex elements and wake systems.

The induced velocity due to the vortex line elements is expressed as:

$$\Delta \vec{v} = -\frac{1}{4\pi} \int \frac{\Gamma \vec{r} \times d\vec{\sigma}}{r^3} \quad (3.428)$$

where \vec{r} is the vector from the element $d\vec{\sigma}$ on the line segment, to the point P and $r = |\vec{r}|$.

For the vortex sheet element, it is expressed as:

$$\Delta \vec{v} = -\frac{1}{4\pi} \oint \frac{\vec{r} \times \vec{\omega}}{r^3} d\mathbf{A} \quad (3.429)$$

where $\vec{\omega}$ is the vorticity of the sheet element.

3.5.9 Induced Velocity Calculation

The final stage of the wake analysis is to calculate the induced velocity at the discrete points on the rotor disk, $\lambda_i(r_i, \Psi_j)$.

Summing the contributions from all vortex elements in the wake gives the induced velocity as the product of the blade bound circulation and influence

coefficients:

$$\lambda_i = \sum_{j=1}^J \Gamma_j \vec{C}_j + \sum_{j=l-k_{NW}}^l \sum_{i=1}^M \Gamma_{ij} \vec{C}_{ij} \quad (3.430)$$

where Γ_{ij} is the circulation of i th radial and j th azimuthal station, Γ_j is the maximum circulation values at each azimuthal station, and \vec{C}_{ij} and \vec{C}_j are accompanying influence coefficients due to all the vortex filaments. The second term in Eq. 3.430 is due to the near wake (extending from $\phi = 0$ to $\phi = k_{NW}\Delta\Psi$) behind the reference blade at azimuth angle $\Psi = l\Delta\Psi$.

3.5.10 Improved Free Wake Model for High Speed Flight

It is common for rotors in high speed flight to encounter negative lift on the advancing tips, particularly in the second quadrant of the rotor disk. In forward flight, the lifting capability on the retreating side is limited by the combination of low dynamic pressure and airfoil stall. As a result, the lift on the advancing side must be small in order to maintain roll moment balance. At sufficiently high speed, the lift on the advancing tip can become negative. In such cases, the bound circulation is still positive along the entire blade length for most of the rotor disk, but in the second quadrant there is a negative maximum near the tip and positive maximum inboard. Therefore, in this region the tip vortex rolls up with negative strength (opposite sign form normal roll-up), with a region of positive vorticity trailed between the positive and negative circulation peaks.

The new wake model concerns the cases with negative loading on the blade advancing tip. Hence the capability was introduced to model the wake created

by dual-peak span loading. In addition, new alternative methods are introduced for improving the wing model for blade-vortex interaction: a second order lifting line theory, and a lifting surface theory correction.

Dual-Peak Wake Model

The old wake [3] model assumes that Γ has the same sign (positive or negative) along the entire blade length. If we consider the application of this model to a case where $\Gamma(r)$ changes sign, we will obtain a tip vortex of the wrong sign and of large magnitude. This will result in erroneous estimation.

In the new model, the bound circulation are now represented by two peaks of opposite sign (negative and positive peaks of $\Gamma(r)$) to accommodate more complex loading conditions. The outboard peak is represented as Γ_O and the inboard is Γ_I , at r_{GO} and r_{GI} respectively. The following options are now available for the new wake model (Fig. 3.13).

- (a) A single-peak model, using Γ_{max} . This is the old model.
- (b) A single-peak model, using Γ_O . This model gives correct sign and magnitude for tip vortex, which is usually the first priority.
- (c) A dual-peak model, using Γ_O and Γ_I .
- (d) A dual-peak model, with a rolled-up inboard trailede wake.

In summary, two wake models, single-peak and dual-peak are now possible for both far wake and rolling up wake. For the single-peak model, either Γ_{max}

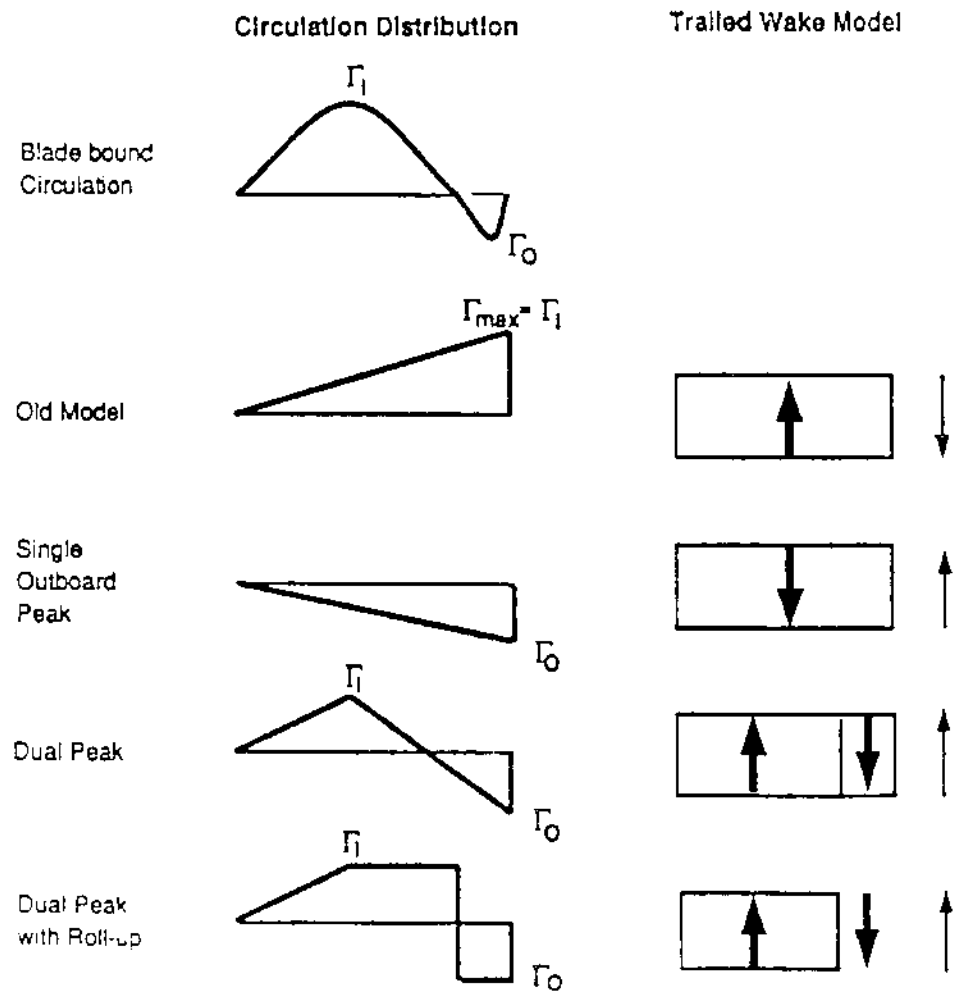


Figure 3.13: Wake models for dual-peak loading condition (Ref. 4)

or Γ_O can be used (with the same influence coefficients). For the dual-peak model, the inboard trailed vorticity can also be rolled up if necessary.

For the new wake model, the expression for the induced velocity are modified as:

$$\lambda_i = \sum_{j=1}^J \Gamma_{Oj} \vec{C}_{Oj} + \sum_{j=1}^J \Gamma_{Ij} \vec{C}_{Ij} + \sum_{j=l-k_{NW}}^l \sum_{i=1}^M \Gamma_{ij} \vec{C}_{ij} \quad (3.431)$$

The following three options are considered:

- (a) for the single-peak model using Γ_{max} , Γ_{max} replaces Γ_O in the first term, and the second term is absent.
- (b) for the single-peak model using Γ_O , second term is absent.
- (c) for the dual-peak model, all three terms are used.

The wake geometry, either prescribed or free, is based on Γ_{max} for option (a) and Γ_O for option (b) and (c).

Blade-Vortex Interaction

A tip vortex encountering the following blade induces a large aerodynamic loading on that blade. In view of the fact that such vortex-induced loading is a principal source of rotor higher harmonic loads and vibration, its calculation is an important part of rotary wing analysis.

The new wake model introduces two alternative methods for improving the wake model for blade-vortex interaction: a second order lifting line theory, and

a lifting surface correction. The intent is to improve the calculation of the airloads without actually resorting to methods such as lifting surface theory, which require more computation time.

Second Order Lifting Line Theory

Formal lifting line theory is the solution of the three-dimensional wing loading problem. Based on the assumption of large wing aspect ratio, the problem is divided into two separate outer wake and inner wake problems, which are solved individually and then combined through a matching procedure. For a rotor in forward flight, it is necessary to consider a swept and yawed flow, and also, unsteady, compressible, and viscous flow. The lowest order fixed wing solution is Prandtl's theory (steady and no sweep). For higher order lifting line theory, Weissinger suggested intuitive methods, and Van Dyke proposed singular perturbation methods.

The lifting line theories generally available in the literature, including unsteady, transonic, and swept flow, offer analytical methods (they offer analytical solutions for both the inner and outer problems). For the rotary wing, it is however necessary to include stall in the inner solution, and the helical, distorted, rolled-up wake geometry in the outer solution. Hence for the rotor problem, the objective is to obtain from lifting line theory a separate formulation of the inner wake and outer wake problems that will be the basis for an iterative solution.

Second Order Lifting Line Formulation for New Wake Model

The outer problem is an incompressible vortex wake behind a lifting-line, with distorted geometry and roll-up. The lifting line (bound vortex) is at the quarter-chord. The trailed wake begins at the bound vortex, while shed wake is created at a quarter-chord aft of the collocation point on the wing (the lifting-line approximation for unsteady loading). Three components of wake-induced velocity are evaluated at the collocation points, excluding the contribution of the bound vortex. The collocation points are at the three-quarter-chord in the direction of the local flow (the approximation for linearly varying induced velocity, from the second order wake).

The inner problem consists of unsteady, compressible, viscous flow about an infinite aspect-ratio wing; in a uniform flow consisting of the yawed free stream and three components of induced velocity. This problem is split into several parts: two-dimensional, steady, compressible, viscous (2D airfoil tables); plus correction for unsteady flow (small angle noncirculatory loads, but without any shed wake), dynamic stall, and yawed flow (equivalence assumption for a swept wing).

This formulation is generally of second order (in $AR = c/R$) in accuracy for lift, including the effects of sweep and yaw. If one places the collocation points at the quarter-chord, it gives a first order lifting-line theory.

Lifting Surface Theory Correction

This section describes the second method for improving the wing model for blade-vortex interactions: a lifting surface correction. It should be noted that the lifting surface correction is an alternative to second order lifting line theory described in the preceding section; the two methods should not be used simultaneously. It should also be noted that the old wake model does include the lifting surface theory correction for the vortex-induced loads. However, the new wake model incorporates the revised version of the lifting surface theory correction.

The basis for the lifting surface theory correction is the model problem in Fig. 3.14: an infinite wing encountering a straight infinite vortex with intersection angle Λ . The wing and vortex line in parallel planes with separation h . The wing semichord is b . The intersection angle Λ is 90 degree for a perpendicular encounter and 180 degree for a parallel encounter (angles between 0 and 90 degree are treated by symmetry considerations). The wing spanwise variable r is measured from the intersection with the vortex: so $(r \sin \Lambda)$ is the distance to vortex line.

For the velocity induced along the wing span by a vortex strength Γ :

$$w = \frac{\Gamma}{2\pi b} \frac{-r \sin \Lambda}{(r \sin \Lambda)^2 + h^2} \quad (3.432)$$

where r and h are here divided by the wing semichord b . The approximate lifting surface solution for the section lift is:

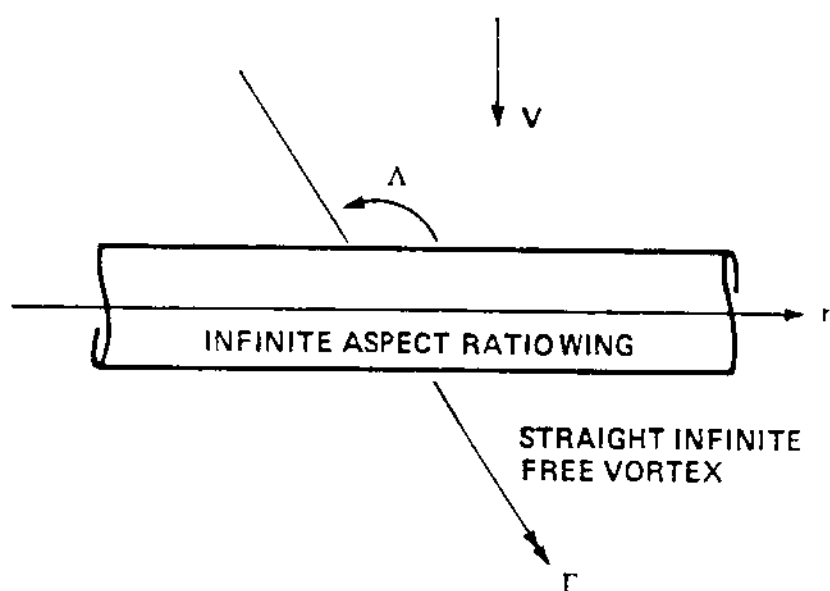


Figure 3.14: Lifting surface theory for vortex-induced loads

$$\begin{aligned}
L_{ls} &= \rho V \Gamma \left\{ \frac{r \sin \Lambda}{(r \sin \Lambda)^2 + (h + c_0)^2} \right. \\
&- \frac{a'_0 \frac{b_0(-(r \sin \Lambda)^2 + (h + c'_0)^2 + b_0^2)}{(-(r \sin \Lambda)^2 + (h + c'_0)^2 + b_0^2)^2 + 4(r \sin \Lambda)^2(h + c'_0)^2} \\
&\left. - \sum_{n=1}^2 a_n \left(\frac{d}{dr \sin \Lambda} \right)^{2n} \left[\frac{-(r \sin \Lambda + b_2) \cos b_2 + (h + c_n) \sin b_2}{(r \sin \Lambda + b_2)^2 + (h + c_n)^2} \right] \right\} (3.433)
\end{aligned}$$

For the incompressible case, the coefficients in this expression are functions of the Λ :

$$b_0 = 8.88 - 1.88(\Lambda/90)$$

$$b_1 = -0.5 \cos \Lambda$$

$$b_2 = 0$$

$$a'_0 = 0.75(.544(-\cos \Lambda) + .07 \sin 2\Lambda)$$

$$a_1 = (1.25 + .5 \sin \Lambda)(-.434 - 1.09(1 - \sin \Lambda)^{.94} + .607(1 - \sin \Lambda)^{2.46})$$

$$a_2 = (2.5 + \sin \Lambda)(.0084 + .0069(-\cos \Lambda)^{1.8})$$

$$c'_0 = 5.9$$

$$c_0 = 1.571$$

$$c_1 = 1.417 + .366(1 - \sin \Lambda)^{.84} - .392(1 - \sin \Lambda)^{2.0}$$

$$c_2 = .91 + .93(1 - \sin \Lambda)^{1.0} - 1.025(1 - \sin \Lambda)^{1.45}$$

The corresponding lifting line theory solution for the vortex induced loading is

$$\begin{aligned}
 L_{ll} &= \rho V \Gamma \left\{ \frac{r \sin \Lambda}{(r \sin \Lambda)^2 + (h + c_0)^2} \right. \\
 &\quad \left. - a_1 \left(\frac{d}{dr \sin \Lambda} \right)^2 \left[\frac{-r \sin \Lambda}{(r \sin \Lambda)^2 + (h + c_1)^2} \right] \right\} \quad (3.434)
 \end{aligned}$$

where $a_1 = -0.662$, $c_1 = 1.296$ and $c_0 = \pi/2$.

In the new wake model, the lifting surface theory corrections are used in the following manner. For each line segment of the tip vortex, it will be determined whether it is close enough to the blade for lifting surface effects to be important. If so, the induced velocity of each line segment of the tip vortex is multiplied by the factor L_{ls}/L_{ll} . By this means, the lifting line calculation of the vortex-induced loads would give the lifting surface theory results.

It should be noted that the shed wake part of present wake model is suppressed when Leishman's unsteady aerodynamic model is utilized, as described in section 3.3.

3.6 Implementation of Wake Models

The ultimate requirement of an inflow or wake model is to predict inflow velocity, $\lambda_i(r_i, \Psi_j)$, at arbitrary radial and azimuthal locations. Uniform and linear inflow models directly calculate this value from known flight parameters. The prescribed and free wake models require additional information to solve for inflow velocity. Blade bending mode shapes and modal responses are required. In addition, vortex strengths are related to circulation distributions, thus bound circulation magnitudes must be determined. Finally a temporal and spatial grid is defined to map out locations for circulation (input) and inflow velocity (output) calculations.

The present wake model utilizes a harmonic solution scheme, thus the blade modal response must be transformed, via Fourier analysis, into harmonic coefficients. In addition, the wake models utilize only flap and lag bending modes to define blade motion, and therefore, torsional and axial mode shapes must be filtered out from the system modal shape vector. The analysis utilizes radial gaussian integration to determine distributed blade loading. Radial grid points can be selected at any point on the blade. A maximum of thirty radial grid points are allowed in the analysis, though six to ten points would suffice for most analyses. The temporal grid selection is a uniform stepping distance around the azimuth, to a maximum of 24 steps, one point every fifteen degrees. The radial and temporal grids used in the wake analysis do not have to correspond to the grids used in the calculation of the rotor loads. The circulation

is calculated at each of these points, and the temporal and spatial gradients are determined utilizing finite difference schemes. Since the bound circulation varies more rapidly near the blade tip, the radial grid points are concentrated in this region.

The output of the model is the resultant inflow at each of the grid locations. Since inflow velocity is required at additional locations, linear interpolation approximation is used. The inflow values derived from these wake analyses must be added to the free stream velocity component to yield the final inflow result.

$$\lambda = \mu \tan \alpha_s + \lambda_i$$

In UMARC, a user can optionally select the wake models (either old or new) by changing the input data set.

3.6.1 Procedure for Wake Analysis

An interface between main routines in UMARC and wake subroutines are performed using the following procedure.

- (1) A linear inflow model is used in the rotor analysis until the iteration number reaches the iteration number at which the wake has been switched on.
- (2) Γ_{ij} , Γ_j are calculated and passed to the routine WAKEMD (WAKEM2 for new wake option). Γ_{ij} represent the circulations of i th radial and j th azimuthal

station, where the nonuniform inflow velocity λ_{ij} are calculated in the wake routine. The subscript i ranges from 1 to MRA (number of radial locations, usually $MRA = 6$ to 10) and j ranges from 1 to $MPSI$ (number of azimuthal location, usually $MPSI = 24$), resulting in an azimuthal interval of 15 degrees ($\Delta\Psi = 2\pi/MPSI = 15$ deg). Γ_j represent the maximum circulation values at each azimuthal location: $\Gamma_j = \Gamma_{max}$. The role of WAKEMD (WAKEM2) is to interface main routines and wake subroutines. It calls the other wake subroutines, and sets up various parameters used in wake analysis. This routine reconfigures the input and output to and from the other wake routines to account for the difference in topology between the trim subroutine and the other wake subroutines.

(3) WAKEMD (WAKEM2) calls WAKEC1 (WAKECN). The circulations and wake parameters are passed WAKEC1 (WAKECN). WAKEC1 (WAKECN) is the main wake analysis routine. It calculates the wake geometry (prescribed or free) and resulting nonuniform wake-induced coefficients (influence coefficients). Output are either C_j and $C_{ij,NW}$ (for old wake option) or C_{Oj} , C_{Ij} and $C_{ij,NW}$ (for new wake option).

(4) WAKEMD (WAKEM2) calls WAKEN1 (WAKENN) to calculate the nonuniform induced velocity using either Eq. (3.430) or (3.431).

(5) Final output from WAKEMD (WAKEM2) is

$$\lambda_i(r_i, \Psi_j) = -VIND(3, r_i, \Psi_j) \quad (3.435)$$

Note that WAKEMD or WAKEM2 gives only $\lambda_i(30, 24)$ from the wake analysis. Therefore, an interpolation routine, GETFWI(x,SHIFW,ZLAM) is utilized in the main routines to obtain λ_i at additional locations. For input sets of x (radial location, r_i) and SHIFW(azimuthal location, Ψ_j), one can obtain ZLAM, $\lambda_i(r_i, \Psi_j)$.

(6) The above calculated nonuniform induced velocity is used in the analysis and Γ_{ij} , Γ_j are reevaluated. Steps (2)-(6) are repeated until convergence is achieved.

3.6.2 Wake Subroutines

This section describes each wake subroutine used in the wake analysis. The structure of wake subroutines are composed of two sector: ‘WAKEC1 and its calling routines’, and ‘WAKEN1’.

WAKEC1 (level)

WAKEC1 (level)

THIS IS A MAJOR SUBROUTINE FOR WAKE ANALYSIS.

Called by WAKEMD.

Calculates influence coefficients, C_{Oj} , C_{Ij} , C_{ij} (Eq. 3.431) or C_j , C_{ij} (Eq. 3.430), to be used in λ_i calculation (WAKEN1).

level : 0 for uniform inflow (not used).

level : 1 for prescribed wake.

level : 2 for free wake.

WAKEC1 calls following subroutines.

GEOMR1 (Calculates distorted geometry, \mathbf{D}).

GEOME1 (Calculates wake geometry, \mathbf{r}_w).

WAKEB1 (Calculates blade position, \mathbf{r}_b).

VTXL (Calculates vortex-line segment)

VTXS (Calculates vortex-sheet segment)

GEOMR1 (level)

Called by WAKEC1.

Calculates distorted geometry, **D**.

First, GEOMR1 calls WAKEB1 to evaluate the blade position, \mathbf{r}_b within the Ψ loop. Then, it calculates a prescribed wake geometry (default value OPRWG= 5, Landgrebe's model). If the free wake option (level=2) is used, it calls GEOMF1 for free wake distorted geometry, **D** (*DFWG*).

GEOMF1 (FREE WAKE ANALYSIS ROUTINE)

Called by GEOMR1, when *level* = 2.

Calculates free wake distorted geometry **D**.

Calls WGAM and DCALC.

GEOMF1 first calls WGAM for initial guess for **D**, and then calls DCALC for iterative solution for **D**.

Output from this routine is **D** (DFWG(3,2304), stored in common block WG1CM).

WGAM (FREE WAKE ANALYSIS ROUTINE)

Called by GEOMF1.

Calculates a rigid wake geometry using Eq. (3.414), as an initial guess for free wake geometry.

DCALC (FREE WAKE ANALYSIS ROUTINE)

Called by GEOMF1.

Calculates **D** iteratively.

Calls NWCAL.

NWCAL (FREE WAKE ANALYSIS ROUTINE)

Called by DCALC.

Calls WQCAL.

WQCAL (FREE WAKE ANALYSIS ROUTINE)

Called by NWCAL.

Computes velocity due to vortex filaments to be used in NWCAL.

Calls QVS, QSVL, QCVL, VSCAL.

VSCAL (FREE WAKE ANALYSIS ROUTINE)

Called by WQCAL.

It is a routine for the vortex sheet wake model.

Calls QVS, QSVL, QCVL.

QVS (FREE WAKE ANALYSIS ROUTINE)

Calculates induced velocity due to vortex sheet.

QSVL (FREE WAKE ANALYSIS ROUTINE)

Calculates induced velocity due to straight vortex line segment.

QCVL (FREE WAKE ANALYSIS ROUTINE)

Calculates induced velocity due to curved vortex line segment.

GEOME1 (*k,l,level,RWT,RWSI,RSWO*)

Called by WAKEC1.

Calculates wake geometry \mathbf{r}_w .

Inputs are k and l , where $\Psi_l = l\Delta\Psi$ and $\phi_k = k\Delta\phi$, and outputs are.

RWT(3) : \mathbf{r}_w at tip vortex.

RWSO(3) : \mathbf{r}_w at outside edge of vortex sheet.

RWSI(3) : \mathbf{r}_w at inside edge of vortex sheet.

At this stage, we already know the distorted geometry \mathbf{D} from either prescribed or free wake model.

WAKEB1 (Ψ ,option,rbr,rbt,rb)

Calculates the blade position vector, \mathbf{r}_b , at the specified azimuthal position, Ψ .

option 1 gives rbr and rbt.

option 2 and 3 gives rb.

rbr : \mathbf{r}_b at r_{ROOR} .

rbt : \mathbf{r}_b at r_{TIP} .

rb : \mathbf{r}_b at circulation station (MRA).

The blade position vector, \mathbf{r}_b , is used to calculate the wake geometry, \mathbf{r}_w in Eq. 3.413.

Note that \mathbf{r}_b contains the information of blade bending modes, which are calculated and passed by main routine.

ETA: bending mode at r_i , $i = 1$ to MRA.

ETAR : bending mode at r_{ROOT} .

ETAT : bending mode at r_{TIP} .

VTXL

Calculates induced velocity of vortex line segment using the Biot-Savart law.

VTXS

Calculates induced velocity of vortex sheet segment using the Biot-Savart law.

----- END OF WAKEC1 (level) -----

WAKEN1 (level)

Called by WAKEMD.

Calculates non-uniform induced velocity (Eq. 3.430 or Eq. 3.431) using in-

fluence coefficients obtained from WAKEC1 C_{Oj} , C_{Ij} , C_{ij} (new wake option) or C_j , C_{ij} (old wake option), and blade circulations Γ 's, which were calculated in the main routine (HUBLDS) and passed via the common block FREEWK.

3.7 Dynamic Inflow Modeling

The induced flow field associated with a lifting rotor responds in a dynamic fashion to changes in blade loads. This is called dynamic inflow. The unsteady effects with the dynamic inflow can have an important influence on the rotor dynamics. The dynamic inflow components are related to the unsteady rotor loads (thrust, roll and pitch moments). These relations are complex and are still a subject of research. For computational efficiency, it is important to obtain these relations in a simplified form. One possible way to apply the unsteady actuator disk theory, which yields the following relation.

$$[\mathbf{m}]\Delta\boldsymbol{\lambda} + [\mathbf{l}]^{-1}\Delta\boldsymbol{\lambda} = \Delta\mathbf{C}_F \quad (3.436)$$

where

$$\begin{aligned} \Delta\boldsymbol{\lambda} &= [\Delta\lambda_o \quad \Delta\lambda_{1s} \quad \Delta\lambda_{1c}]^T \\ \Delta\mathbf{C}_F &= [\Delta C_T \quad -\Delta C_{M_{x_h}} \quad \Delta C_{M_{y_h}}]^T \end{aligned} \quad (3.437)$$

The basic assumption here is that the rotor forces vary slowly enough for the actuator theory to be valid. Equation 3.436 is in nondimensional form (independent of rotational speed).

The matrices \mathbf{m} and \mathbf{l} are given by

$$[\mathbf{l}] = \frac{1}{v} \begin{bmatrix} 0.5 & 0 & \frac{15\pi}{64} \sqrt{\frac{1-\sin\alpha}{1+\sin\alpha}} \\ 0 & \frac{-4}{1+\sin\alpha} & 0 \\ \frac{15\pi}{64} \sqrt{\frac{1-\sin\alpha}{1+\sin\alpha}} & 0 & \frac{-4\sin\alpha}{1+\sin\alpha} \end{bmatrix} \quad (3.438)$$

$$[\mathbf{m}] = \begin{bmatrix} \frac{128}{75\pi} & 0 & 0 \\ 0 & \frac{-16}{45\pi} & 0 \\ 0 & 0 & \frac{-16}{45\pi} \end{bmatrix} \quad (3.439)$$

where v is a mass flow parameter given by

$$v = \frac{\mu^2 + \lambda(\lambda + \lambda_i)}{\sqrt{\mu^2 + \lambda^2}} \quad (3.440)$$

and α is defined as

$$\alpha = \arctan \frac{\lambda}{\mu} \quad (3.441)$$

(Note : α is not the shaft tilt)

In UMARC, the inflow velocities are referred to the hub plane. The perturbation forces on the right hand side of the inflow equations result from blade forces. In section 3.1, the blade forces in the deformed frame are transformed to the fuselage frame. Setting $\alpha_s = 0, \phi_s = 0, X_{CG} = 0, Y_{CG} = 0$ and $h = 0.0$ in Eq.3.133, we obtain forces in the hub plane. The inflow equation requires only the thrust, the pitching and rolling moments. Equation 3.133 is written as

$$\mathbf{F}_H^A = \mathbf{T}_{HL} (\mathbf{L}^A) \quad (3.442)$$

where \mathbf{F}_H^A are the forces in the hub plane, (\mathbf{L}^A) are the blade forces in undeformed frame and \mathbf{T}_{HL} is the transformation matrix.

$$\begin{aligned} \mathbf{F}_H^A &= [F_z^A \quad -M_x^A \quad M_y^A]^T \\ (\mathbf{L}^A) &= [L_u^A \quad L_v^A \quad L_w^A \quad M_\phi^A]^T \\ \mathbf{T}_{HL} &= \begin{bmatrix} \beta_p & 0 & 1 & 0 \\ -v\beta_p \cos \psi & w \cos \psi & -v \cos \psi & (-1 + \beta_p w') \cos \psi \\ +w \sin \psi & +(u + x)\beta_p \cos \psi & -(u + x) \sin \psi & +v' \sin \psi \\ u \cos \psi + v\beta_p \sin \psi & -w \sin \psi & v \sin \psi - (x + u) \cos \psi & (1 - \beta_p w') \sin \psi \\ & -(x + u)\beta_p \sin \psi & & +v' \cos \psi \end{bmatrix} \end{aligned} \quad (3.443)$$

For stability analysis, we need perturbation forces in the hub plane. These are obtained as follows.

$$\begin{aligned}\Delta \mathbf{F}_H^A &= \Delta(\mathbf{T}_{HL}(\mathbf{L}^A)) \\ &= (\Delta \mathbf{T}_{HL})(\mathbf{L}^A) + \mathbf{T}_{HL}(\Delta(\mathbf{L}^A))\end{aligned}\quad (3.444)$$

Note that \mathbf{T}_{HL} is a function of u, v, w, v' and w' .

First Term

The first term $\Delta(\mathbf{T}_{HL})(\mathbf{L}^A)$ in Eq. 3.444 can be written as

$$\begin{aligned}(\Delta \mathbf{T}_{HL})(\mathbf{L}^A) &= \left(\frac{\partial}{\partial u} \mathbf{T}_{HL} \right)(\mathbf{L}^A) \Delta u + \left(\frac{\partial}{\partial v} \mathbf{T}_{HL} \right)(\mathbf{L}^A) \Delta v + \left(\frac{\partial}{\partial w} \mathbf{T}_{HL} \right)(\mathbf{L}^A) \Delta w \\ &\quad + \left(\frac{\partial}{\partial v'} \mathbf{T}_{HL} \right)(\mathbf{L}^A) \Delta v' + \left(\frac{\partial}{\partial w'} \mathbf{T}_{HL} \right)(\mathbf{L}^A) \Delta w' \\ &= [\mathbf{DTQU}] \begin{Bmatrix} \Delta u \\ \Delta v \\ \Delta w \\ \Delta \dot{\phi} \end{Bmatrix} + [\mathbf{DTQUP}] \begin{Bmatrix} \Delta u' \\ \Delta v' \\ \Delta w' \\ \Delta \dot{\phi}' \end{Bmatrix}\end{aligned}\quad (3.445)$$

where

$$[\mathbf{DTQU}] = \begin{bmatrix} 0 & 0 & 0 & 0 \\ \beta_p \cos \psi L_v^A - \sin \psi L_w^A & -(\beta_p L_u^A + L_w^A) \cos \psi & \sin \psi L_u^A + \cos \psi L_v^A & 0 \\ -\beta_p \sin \psi L_v^A + \cos \psi L_w^A & (\beta_p L_u^A + L_w^A) \sin \psi & \cos \psi L_u^A - \sin \psi L_v^A & 0 \end{bmatrix} \quad (3.446)$$

$$[\mathbf{DTQUP}] = \begin{bmatrix} 0 & 0 & 0 & 0 \\ 0 & \sin \psi M_\phi^A & \beta_p \cos \psi M_\phi^A & 0 \\ 0 & \cos \psi M_\phi^A & -\beta_p \sin \psi M_\phi^A & 0 \end{bmatrix} \quad (3.447)$$

L_u^A, L_v^A, L_w^A and M_ϕ^A in the above two matrices are the trim values.

Second Term

The perturbation force vector in undeformed frame are written as

$$\begin{aligned}\Delta(\mathbf{L}^A) &= \Delta(\mathbf{T}_{DU}^T \bar{\mathbf{L}}) \\ &= (\Delta\mathbf{T}_{DU}^T) \bar{\mathbf{L}} + \mathbf{T}_{DU}^T (\Delta\bar{\mathbf{L}})\end{aligned}\quad (3.448)$$

where $\bar{\mathbf{L}}$ are the blade forces in deformed frame, and $(\mathbf{T}_{DU})^T$ is the transformation matrix from deformed frame to undeformed frame which is given by (Ref: Chapter 2)

$$(\mathbf{T}_{DU})^T = \begin{bmatrix} 1 - \frac{1}{2}(v'^2 + w'^2) & \hat{\phi}(v' \sin \theta - w' \cos \theta) & \hat{\phi}(v' \cos \theta + w' \sin \theta) & 0 \\ v' & -v' \cos \theta - w' \sin \theta & +v' \sin \theta - w' \cos \theta & 0 \\ w' & -\frac{1}{2}v'^2 \cos \theta - v'w' \sin \theta & \frac{1}{2}v'^2 \sin \theta - v'w' \cos \theta & 0 \\ 0 & +\cos \theta - \hat{\phi} \sin \theta & -\sin \theta - \hat{\phi} \cos \theta & 0 \\ 0 & -\frac{1}{2}w'^2 \sin \theta & \frac{1}{2}w'^2 \cos \theta & 0 \\ 0 & +\sin \theta + \hat{\phi} \cos \theta & +\cos \theta - \hat{\phi} \sin \theta & 0 \\ 0 & 0 & 0 & 1 \end{bmatrix} \quad (3.449)$$

Note \mathbf{T}_{DU}^T is a matrix of order 4×4 here, contrary to 3×3 in Chapter 2. This facilitates easy algebraic manipulation. It is a function of $\hat{\phi}$, v' and w' (θ is a constant).

The term $(\Delta\mathbf{T}_{DU}^T)\bar{\mathbf{L}}$ in Eq. 3.448 is written as

$$\begin{aligned}\Delta(\mathbf{T}_{DU}^T)\bar{\mathbf{L}} &= \left(\frac{\partial}{\partial \hat{\phi}} \mathbf{T}_{DU}^T\right) \bar{\mathbf{L}} \Delta\hat{\phi} + \left(\frac{\partial}{\partial v'} \mathbf{T}_{DU}^T\right) \bar{\mathbf{L}} \Delta v' + \left(\frac{\partial}{\partial w'} \mathbf{T}_{DU}^T\right) \bar{\mathbf{L}} \Delta w' \\ &= [\mathbf{DTDU}] \begin{Bmatrix} \Delta u \\ \Delta v \\ \Delta w \\ \Delta \hat{\phi} \end{Bmatrix} + [\mathbf{DTDUP}] \begin{Bmatrix} \Delta u' \\ \Delta v' \\ \Delta w' \\ \Delta \hat{\phi}' \end{Bmatrix}\end{aligned}\quad (3.450)$$

where

$$[\mathbf{DTDU}] = \begin{bmatrix} 0 & 0 & 0 & \left(\frac{\partial}{\partial \hat{\phi}} \mathbf{T}_{DU}^T\right) \bar{\mathbf{L}} \end{bmatrix} \quad (3.451)$$

$$[\mathbf{DTDUP}] = \begin{bmatrix} \mathbf{0} & (\frac{\partial}{\partial v'} \mathbf{T}_{DU}^T) \mathbf{L} & (\frac{\partial}{\partial w'} \mathbf{T}_{DU}^T) \bar{\mathbf{L}} & \mathbf{0} \end{bmatrix} \quad (3.452)$$

$(\Delta \bar{\mathbf{L}})$ in the second term of Eq. 3.448 is written as

$$\Delta \mathbf{L} = \Delta \begin{Bmatrix} L_u \\ L_v \\ \bar{L}_w \\ \bar{M}_{\dot{\phi}} \end{Bmatrix} \quad (3.453)$$

where \bar{L}_u , \bar{L}_v , \bar{L}_w and $\bar{M}_{\dot{\phi}}$ are the blade forces in deformed frame.

In section 3.1, we had obtained the blade forces in deformed frame as follows (Eq.3.68 - Eq.3.71).

$$\begin{aligned} L_u &= \frac{\gamma}{6}(-d_o U_R U_T) \\ \bar{L}_v &= \frac{\gamma}{6}(-d_o U_T^2 - (c_o - d_1) U_T U_P + (c_1 - d_2) U_P^2) \\ \bar{L}_w &= \frac{\gamma}{6}(c_o U_T^2 - (c_1 + d_o) U_T U_P + d_1 U_P^2) \\ \bar{M}_{\dot{\phi}} &= \frac{\gamma c}{6 R} \{c_{mac}(U_T^2 + U_P^2) - f_1 U_T U_P\} - e_d L_w \end{aligned} \quad (3.454)$$

Perturbations are given by

$$\begin{aligned} \Delta L_u &= \frac{\gamma}{6}(UUT \times \Delta U_T + UUR \times \Delta U_R) \\ \Delta L_v &= \frac{\gamma}{6}(VUT \times \Delta U_T + VUP \times \Delta U_P) \\ \Delta \bar{L}_w &= \frac{\gamma}{6}(WUT \times \Delta U_T + WUP \times \Delta U_P) \\ \Delta \bar{M}_{\dot{\phi}} &= \frac{\gamma}{6}(AMUT \times \Delta U_T + AMUP \times \Delta U_P) \end{aligned} \quad (3.455)$$

where

$$UUT = -d_o(U_R)$$

$$UUR = -d_o(U_T)$$

$$\begin{aligned}
VUT &= -2d_o U_T - (c_o - d_1) U_P \\
VUP &= -(c_o - d_1) U_T + 2(c_1 - d_2) U_P \\
WUT &= 2c_o U_T - (c_1 + d_o) U_P \\
WUP &= -(c_1 + d_o) U_T + 2d_1 U_P \\
AMUT &= \frac{c}{R} (2c_{mac} U_T - f_1 U_P) - e_d \times WUT \\
AMUP &= \frac{c}{R} (2c_{mac} U_P - f_1 U_T) - e_d \times WUP
\end{aligned} \tag{3.456}$$

The perturbation velocities are written as

$$\begin{aligned}
\Delta U_T &= [TU \ TV \ TW \ TP] \begin{Bmatrix} \Delta u \\ \Delta v \\ \Delta w \\ \Delta \dot{\phi} \end{Bmatrix} + [0 \ TVP \ TWP \ 0] \begin{Bmatrix} \Delta u' \\ \Delta v' \\ \Delta w' \\ \Delta \hat{\phi}' \end{Bmatrix} \\
&\quad + [0 \ TVD \ TWD \ TPD] \begin{Bmatrix} \Delta \dot{u} \\ \Delta \dot{v} \\ \Delta \dot{w} \\ \Delta \dot{\hat{\phi}} \end{Bmatrix} + [0 \ 0 \ 0 \ TAS \ 0] \begin{Bmatrix} \Delta x_F \\ \Delta y_F \\ \Delta z_F \\ \Delta \alpha_s \\ \Delta \phi_s \end{Bmatrix} \\
&\quad + [Txfd \ Tyfd \ Tzfd \ TASD \ TPSD] \begin{Bmatrix} \Delta \dot{x}_F \\ \Delta \dot{y}_F \\ \Delta \dot{z}_F \\ \Delta \dot{\alpha}_s \\ \Delta \dot{\phi}_s \end{Bmatrix} \\
&\quad + [TLO \ TLS \ TLC] \begin{Bmatrix} \Delta \lambda_o \\ \Delta \lambda_{1s} \\ \Delta \lambda_{1c} \end{Bmatrix}
\end{aligned} \tag{3.457}$$

$$\begin{aligned}
\Delta U_P &= [PU \ PV \ PW \ PP] \begin{Bmatrix} \Delta u \\ \Delta v \\ \Delta w \\ \Delta \dot{\phi} \end{Bmatrix} + [0 \ PVP \ PWP \ 0] \begin{Bmatrix} \Delta u' \\ \Delta v' \\ \Delta w' \\ \Delta \hat{\phi}' \end{Bmatrix} \\
&\quad + [0 \ PVD \ PWD \ PPD] \begin{Bmatrix} \Delta \dot{u} \\ \Delta \dot{v} \\ \Delta \dot{w} \\ \Delta \dot{\hat{\phi}} \end{Bmatrix} + [0 \ 0 \ 0 \ PAS \ 0] \begin{Bmatrix} \Delta x_F \\ \Delta y_F \\ \Delta z_F \\ \Delta \alpha_s \\ \Delta \phi_s \end{Bmatrix}
\end{aligned}$$

$$\begin{aligned}
& + [PXFD \ PYFD \ PZFD \ PASD \ PPSD] \begin{Bmatrix} \Delta \dot{x}_F \\ \Delta \dot{y}_F \\ \Delta \dot{z}_F \\ \Delta \dot{\alpha}_s \\ \Delta \dot{\phi}_s \end{Bmatrix} \\
& + [PLO \ PLS \ PLC] \begin{Bmatrix} \Delta \lambda_o \\ \Delta \lambda_{1s} \\ \Delta \lambda_{1c} \end{Bmatrix} \quad (3.458)
\end{aligned}$$

$$\begin{aligned}
\Delta U_R = & [RU \ RV \ RW \ RP] \begin{Bmatrix} \Delta u \\ \Delta v \\ \Delta w \\ \Delta \dot{\phi} \end{Bmatrix} + [0 \ RVP \ RWP \ 0] \begin{Bmatrix} \Delta u' \\ \Delta v' \\ \Delta w' \\ \Delta \dot{\phi}' \end{Bmatrix} \\
& + [0 \ RVD \ RWD \ RPD] \begin{Bmatrix} \Delta \dot{u} \\ \Delta \dot{v} \\ \Delta \dot{w} \\ \Delta \ddot{\phi} \end{Bmatrix} + [0 \ 0 \ 0 \ RAS \ 0] \begin{Bmatrix} \Delta x_F \\ \Delta y_F \\ \Delta z_F \\ \Delta \dot{\alpha}_s \\ \Delta \dot{\phi}_s \end{Bmatrix} \\
& + [RXFD \ RYFD \ RZFD \ RASD \ RPSD] \begin{Bmatrix} \Delta \dot{x}_F \\ \Delta \dot{y}_F \\ \Delta \dot{z}_F \\ \Delta \dot{\alpha}_s \\ \Delta \dot{\phi}_s \end{Bmatrix} \\
& + [RLO \ RLS \ RLC] \begin{Bmatrix} \Delta \lambda_o \\ \Delta \lambda_{1s} \\ \Delta \lambda_{1c} \end{Bmatrix} \quad (3.459)
\end{aligned}$$

Using Eq. 3.457, Eq. 3.458 and Eq. 3.459 in Eq. 3.455, we get perturbation blade forces in undeformed frame :

$$\Delta \dot{\mathbf{L}} = \frac{\gamma}{6} (\mathbf{D}_u \Delta \mathbf{u} + \mathbf{D}_{u'} \Delta \mathbf{u}' + \mathbf{D}_{\dot{u}} \Delta \dot{\mathbf{u}} + \mathbf{D}_{x_F} \Delta \mathbf{x}_F + \mathbf{D}_{\dot{x}_F} \Delta \dot{\mathbf{x}}_F + \mathbf{D}_{\lambda} \Delta \boldsymbol{\lambda}) \quad (3.460)$$

where

$$\mathbf{D}_u = \begin{bmatrix} UUT \times TU + UUR \times RU & \dots & \dots & UUT \times TP + UUR \times RP \\ VUT \times TU + VUP \times PU & \dots & \dots & VUT \times TP + VUP \times PP \\ WUT \times TU + WUP \times PU & \dots & \dots & WUT \times TP + WUP \times PP \\ AMUT \times TU + AMUP \times PU & \dots & \dots & AMUT \times TP + AMUP \times PP \end{bmatrix} \quad (3.461)$$

$$\mathbf{D}_{u'} = \begin{bmatrix} UUT \times TUP + UUR \times RUP & \dots & \dots & UUT \times TPP + UUR \times RPP \\ VUT \times TUP + VUP \times PUP & \dots & \dots & VUT \times TPP + VUP \times PPP \\ WUT \times TUP + WUP \times PUP & \dots & \dots & WUT \times TPP + WUP \times PPP \\ AMUT \times TUP + AMUP \times PUP & \dots & \dots & AMUT \times TPP + AMUP \times PPP \end{bmatrix} \quad (3.462)$$

$$\mathbf{D}_{\dot{\mathbf{u}}} = \begin{bmatrix} UUT \times TUD + UUR \times RUD & \dots & \dots & UUT \times TPD + UUR \times RPD \\ VUT \times TUD + VUP \times PUD & \dots & \dots & VUT \times TPD + VUP \times PPD \\ WUT \times TUD + WUP \times PUD & \dots & \dots & WUT \times TPD + WUP \times PPD \\ AMUT \times TUD + AMUP \times PUD & \dots & \dots & AMUT \times TPD + AMUP \times PPD \end{bmatrix} \quad (3.463)$$

$$\mathbf{D}_{\mathbf{x}_F} = \begin{bmatrix} 0 & 0 & 0 & UUT \times TAS + UUP \times PAS & 0 \\ 0 & 0 & 0 & VUT \times TAS + VUP \times PAS & 0 \\ 0 & 0 & 0 & WUT \times TAS + WUP \times PAS & 0 \\ 0 & 0 & 0 & AMUT \times TAS + AMUP \times PAS & 0 \end{bmatrix} \quad (3.464)$$

$$\mathbf{D}_{\dot{\mathbf{x}}_F} = \begin{bmatrix} UUT \times TXFD + UUR \times RXFD & \dots & \dots & UUT \times PSD + UUR \times RPSD \\ VUT \times TXFD + VUR \times PXFD & \dots & \dots & VUT \times PSD + VUP \times PPSD \\ WUT \times TXFD + WUP \times PXFD & \dots & \dots & WUT \times PSD + WUP \times PPSD \\ AMUT \times TXFD + AMUP \times PXFD & \dots & \dots & AMUT \times PSD + AMUP \times PPSD \end{bmatrix} \quad (3.465)$$

$$\mathbf{D}_{\lambda} = \begin{bmatrix} UUT \times TL0 + UUR \times RL0 & UUT \times TLS + UUR \times RLS & UUT \times TLC + UUR \times RLC \\ VUT \times TL0 + VUR \times PL0 & VUT \times TLS + VUR \times PLS & VUT \times TLC + VUR \times PLC \\ AMUT \times TL0 + AMUP \times PL0 & AMUT \times TLS + AMUP \times PLS & AMUT \times TLC + AMUP \times PLC \end{bmatrix} \quad (3.466)$$

Using Eqs. 3.445, 3.450 and 3.460 in Eq. 3.444 we get

$$\begin{aligned} \Delta \mathbf{F}_H^A &= (\Delta \mathbf{T}_{HL}) (\mathbf{L}^A) + \mathbf{T}_{HL} (\Delta (\mathbf{L}^A)) \\ &= [\mathbf{DTQU}] \Delta \mathbf{u} + [\mathbf{DTQUP}] \Delta \mathbf{u}' \\ &\quad + \mathbf{T}_{HL} \{ [\mathbf{DTDU}] \Delta \mathbf{u} + [\mathbf{TDUP}] \Delta \mathbf{u}' \\ &\quad + (\mathbf{T}_{DU}^T) \mathbf{D}_u \Delta \mathbf{u} + (\mathbf{T}_{DU}^T) \mathbf{D}_{u'} \Delta \mathbf{u}' + (\mathbf{T}_{DU}^T) \mathbf{D}_{\dot{\mathbf{u}}} \Delta \dot{\mathbf{u}} \\ &\quad + (\mathbf{T}_{DU}^T) \mathbf{D}_{x_F} \Delta \mathbf{x}_F + (\mathbf{T}_{DU}^T) \mathbf{D}_{\dot{x}_F} \Delta \dot{x}_F \\ &\quad + (\mathbf{T}_{DU}^T) \mathbf{D}_{\lambda} \Delta \lambda \} \end{aligned} \quad (3.467)$$

The perturbation displacement vectors $\Delta \mathbf{u}$, $\Delta \mathbf{u}'$ and $\Delta \dot{\mathbf{u}}$ can be written in terms of shape functions as follows.

$$\Delta \mathbf{u} = \mathbf{H}_s \Delta \mathbf{q}$$

$$\Delta \mathbf{u}' = \mathbf{H}'_s \Delta \mathbf{q}$$

$$\Delta \dot{\mathbf{u}} = \mathbf{H}_s \Delta \dot{\mathbf{q}}$$

Eq. 3.467 gives the forces in hub plane due to blade forces along one radial location. To find the forces due to an element on the blade, the blade section force is integrated over the element length of l_i .

The following element matrices are obtained from Eq. 3.467.

Inflow-Blade Stiffness Matrix

$$\begin{aligned}
 [\mathbf{EKLB}] = & -l_i \int_0^1 \{ [\mathbf{DTQU}]\mathbf{H}_s + [\mathbf{DTQUP}]\mathbf{H}'_s, \\
 & + \mathbf{T}_{HL}[\mathbf{DTQU}]\mathbf{H}_s + \mathbf{T}_{HL}[\mathbf{DTQUP}]\mathbf{H}'_s, \\
 & + \mathbf{T}_{HL}(\mathbf{T}_{DU}^T)\mathbf{D}_u\mathbf{H}_s + \mathbf{T}_{HL}(\mathbf{T}_{DU}^T)\mathbf{D}_{u'}\mathbf{H}'_s \} \ ds
 \end{aligned} \quad (3.468)$$

Inflow-Blade Damping Matrix

$$[\mathbf{ECLB}] = -l_i \int_0^1 \mathbf{T}_{HL}(\mathbf{T}_{DU}^T)\mathbf{D}_{\dot{u}}\mathbf{H}_s \ ds \quad (3.469)$$

Inflow-Fuselage Stiffness Matrix

$$[\mathbf{EKLF}] = -l_i \int_0^1 \mathbf{T}_{HL}(\mathbf{T}_{DU}^T)\mathbf{D}_{x_F} \ ds \quad (3.470)$$

Inflow-Fuselage Damping Matrix

$$[\mathbf{ECLF}] = -l_i \int_0^1 \mathbf{T}_{HL}(\mathbf{T}_{DU}^T)\mathbf{D}_{\dot{x}_F} \ ds \quad (3.471)$$

Inflow-Inflow Stiffness Matrix

$$[\mathbf{EKLL}] = -l_i \int_0^1 \mathbf{T}_{HL}(\mathbf{T}_{DU}^T)\mathbf{D}_{\lambda} \ ds \quad (3.472)$$

Implementation

The matrices $[\mathbf{l}]$ and $[\mathbf{m}]$ are calculated in the subroutine DMODEL. The matrices EKLB, ECLB, EKLF, ECLF and EKLL are calculated in the subroutine AEROMX (these are element matrices). The blade-inflow and fuselage-inflow

matrices are derived in section 3.2. To calculate the thrust, the pitching and the rolling moments, the contributions from all the elements along each blade are summed up (see Eqn. 5.26 in Chapter 5 on Stability Analysis).

Bibliography

- [1] Leishman,J.G., Beddoes,T.S., "A Semi-Empirical Model for Dynamic Stall", *Journal of the American Helicopter Society*, Vol. 34, No. 3, 1989.
- [2] Drees,J.M., "A Theory of Airflow Through Rotors and its Application to Some Helicopter Problems," *Journal of the Helicopter Association of Great Britain*, Vol. 3, 1949.
- [3] Johnson,W., "A Comprehensive Analytical Model of Rotorcraft Aerodynamics and Dynamics, Part 1: Analysis Development," NASA TM 81182, June 1980.
- [4] Johnson,W., "Wake Model for Helicopter Rotor in High Speed Flight", NASA Contractor Report, No. 177507, Nov. 1988.
- [5] Anderson,J.D.,Jr., *Modern Compressible Flow, with Historical Perspective*, McGraw-Hill Book Co., 1982.
- [6] Fung,Y.C., *An Introduction to the Theory of Aeroelasticity*, Dover Publications Inc., N.Y., 1960.

- [7] Leishman,J.G., "Validation of Approximate Indicial Aerodynamic Functions for Two-Dimensional Subsonic Flow," *Journal of Aircraft*, Vol. 25, No. 10, 1988.
- [8] Bisplinghoff,R.L., Ashley,H., Halfman,R.L., *Aeroelasticity*, Addison-Wesley Publishers, 1955.
- [9] Leishman,J.G., "Two-Dimensional Model for Airfoil Unsteady Drag Below Stall," *Journal of Aircraft*, Vol. 25, No. 7, 1988.
- [10] Landgrebe,A.J., "An Analytical Method for Predicting Rotor Wake Geometry", *Journal of the American Helicopter Society*, Vol. 14, No. 4, 1969.
- [11] Scully,M.P., "Computation of Helicopter Rotor Wake Geometry and its Influence on Rotor Harmonic Airloads," Massachusetts Institute of Technology, ASRL TR 178-1, 1975.

- [12] Pitt,D.M., Peters,D.A., "Theoretical Prediction Of Dynamic Inflow Derivatives", *Vertica*, Vol. 5, 1981.
- [13] Gaonkar,G.H., Peters,D.A., "Effectiveness of Current Dynamic Inflow Models in Hover and Forward Flight," *Journal of the American Helicopter Society*, Vol. 31, No. 2, 1986.

Chapter 5

STABILITY ANALYSIS

Chapter 5

STABILITY ANALYSIS

5.1 Introduction

Designing a rotorcraft with satisfactory stability characteristics (which may imply blade aeroelastic stability, ground or air resonance) remains a major concern in the development of new helicopters. The rotorcraft stability phenomenon is characterized by periodic differential equations. Ref [1] provides a comprehensive review on aeromechanical stability of hingeless, articulated and bearingless rotor configurations. Majority of the analysis methods to determine rotor-vehicle stability fall under two broad categories: *linearized eigenanalysis* and *transient response analysis*.

The linearized eigenanalysis utilizes methods of the linear system theory, e.g., the Floquet transition matrix method and the constant coefficient approximation analysis. Linear differential equations are derived for the perturbed motion of the rotorcraft system about the trimmed state. Stability is then

determined from an eigenanalysis of these homogeneous equations. In this approach, considerable effort is required to derive the stability equations of motion. However, efficient techniques of the linear system theory can be used to advantage. Damping of the higher frequency modes can be estimated with sufficient accuracy, an advantage not offered by transient response techniques. If the entire helicopter is modeled, the aeroelastic stability analysis includes the rigid body motion, and therefore the stability results include the flight dynamics as well as the aeromechanical stability characteristics of the entire vehicle.

For the linearized stability analysis, it is necessary to either approximate or neglect altogether the nonlinear effects such as flow separation, dynamic stall, etc. On the other hand, the transient response analysis can directly capture the nonlinearities inherent in the system. It utilizes direct time integration to get the transient response. A damping estimation method, such as the Moving Block technique, is then used to extract the damping values of the stability modes. A major disadvantage of this technique is that a considerable amount of computation time is required to obtain the transient response. Also, damping estimation of the higher frequency modes is extremely difficult and sometimes even impossible. Further, due to nonlinearities in the system, the transient response can be quite sensitive to amplitudes of the control perturbations.

5.2 Linearized System Eigenanalysis

The first step involves derivation of the linearized system matrices. The next step is to apply either the Floquet theory or the constant coefficient approximation approach to compute the system eigenvalues. Let us first get familiar with a few terms which will be frequently used in this chapter. The term *rotor* will refer to all the blades collectively, and the term *vehicle* or *rotor-fuselage* will imply rotor and fuselage coupled together. The term *system* will imply either the isolated blade, or the rotor, or the whole vehicle, depending on the type of stability analysis being carried out. The dynamic inflow model becomes part of the *system* if unsteady wake effects are included in the stability analysis. The following table shows different types of stability analyses available in UMARC. Inclusion of dynamic inflow is optional.

Table 1

User-Requested Stability Analysis	System Definition
Isolated blade stability	Blade + [Dynamic Inflow]
Rotor aeroelastic stability	Rotor + [Dynamic Inflow]
Ground/Air Resonance, Vehicle aeroelastic stability	Rotor + Fuselage + [Dynamic Inflow]

The stability analysis can be carried out either in the rotating frame or in the fixed frame. It is expedient to use the rotating frame if the system is comprised of an isolated blade. If either the fuselage or the dynamic inflow model is included, the stability analysis is most conveniently carried out in fixed frame (UMARC automatically selects the fixed frame).

In the following formulation, the system will be assumed to be in its most general form consisting of the rotor, the fuselage and the dynamic inflow. However, it is understood that UMARC uses only those components of the system which are requested by the user.

5.2.1 Rotor-Fuselage Equations

Hamilton's variational principle offers a scalar (energy) method to derive equations of motion of a dynamic system. The generalized Hamilton's principle, viz.

$$\int_{t_1}^{t_2} (\delta\mathcal{U} - \delta T - \delta W) dt = 0 \quad (5.1)$$

is applicable to nonconservative systems. The δU and δT are respectively the virtual variations of strain and kinetic energies, and δW is the virtual work done by the external forces. These virtual variations have contributions from the rotor and the fuselage (if included in the system). Contributions from the rotor can in turn be expressed as a sum of contributions from each blade. Therefore,

$$\delta\mathcal{U} = \delta\mathcal{U}_R + \delta\mathcal{U}_F = \sum_{b=1}^{N_b} \delta\mathcal{U}_b + \delta\mathcal{U}_F$$

$$\begin{aligned}\delta T &= \delta T_R + \delta T_F = \sum_{b=1}^{N_b} \delta T_b + \delta T_F \\ \delta W &= \delta W_R + \delta W_F = \sum_{b=1}^{N_b} \delta W_b + \delta W_F\end{aligned}\quad (5.2)$$

If the pitch link associated with the b^{th} blade is elastic, its contribution to the strain energy is included in δU_b . The fuselage is considered rigid in the current version of UMARC, therefore contribution to δU_F comes solely from the landing gear springs. Expressions for δU_b , δU_F , δT_b , and δT_F are derived in Chapter 2 (structural modeling), and the expression for δW is provided in Chapter 3 (aerodynamic modeling). Consistent with the ordering scheme described in Section 2.1.3, the dependence of these expressions on the blade motion \mathbf{q}_b , the fuselage motion \mathbf{x}_F , the inflow $\boldsymbol{\lambda}$, the control settings θ , and the azimuth location, ψ , can be expressed as

$$\begin{aligned}\delta U_b &= \delta U_b(\delta \mathbf{q}_b, \theta, \psi, \mathbf{q}_b, \mathbf{q}_b^2) \\ \delta T_b &= \delta T_b(\delta \mathbf{q}_b, \delta \mathbf{x}_F, \theta, \psi, \mathbf{q}_b, \dot{\mathbf{q}}_b, \dot{\mathbf{x}}_F, \ddot{\mathbf{x}}_F, \mathbf{q}_b \dot{\mathbf{x}}_F, \mathbf{q}_b \ddot{\mathbf{x}}_F) \\ \delta W_b &= \delta W_b(\delta \mathbf{q}_b, \delta \mathbf{x}_F, \theta, \psi, \mathbf{q}_b, \dot{\mathbf{q}}_b, \mathbf{q}_b^2, \mathbf{q}_b \dot{\mathbf{q}}_b, \mathbf{x}_F, \dot{\mathbf{x}}_F, \ddot{\mathbf{x}}_F, \boldsymbol{\lambda}) \\ \delta U_F &= \delta U_F(\delta \mathbf{x}_F, \mathbf{x}_F) \\ \delta T_F &= \delta T_F(\delta \mathbf{x}_F, \dot{\mathbf{x}}_F, \dot{\mathbf{x}}_F^2) \\ \delta W_F &= \delta W_F(\delta \mathbf{x}_F, \mathbf{x}_F, \dot{\mathbf{x}}_F)\end{aligned}\quad (5.3)$$

A few words on the notation used in eqn. (5.3). The vector \mathbf{q}_b^2 denotes the vector of second order nonlinear terms in blade displacements. The vector $\mathbf{q}_b \mathbf{x}_F$

represents second order bilinear terms, i.e., each entry in the vector $\mathbf{q}_b \mathbf{x}_F$ is a product of a blade displacement term and a fuselage displacement term.

5.2.2 Linearization of the Rotor-Fuselage Equations

For stability analysis, we assume that the state variables $\mathbf{q}_b, \mathbf{x}_F$ and $\boldsymbol{\lambda}$ are small perturbations about the trimmed values, i.e.,

$$\begin{aligned}\mathbf{q}_b &= \mathbf{q}_{b_0} + \Delta \mathbf{q}_b; \quad b = 1, 2, \dots, N_b \\ \mathbf{x}_F &= \mathbf{x}_{F_0} + \Delta \mathbf{x}_F \\ \boldsymbol{\lambda} &= \boldsymbol{\lambda}_0 + \Delta \boldsymbol{\lambda}\end{aligned}\tag{5.4}$$

Therefore

$$\begin{aligned}\delta \mathbf{q}_b &= \delta \mathbf{q}_{b_0} + \delta \Delta \mathbf{q}_b; \quad b = 1, 2, \dots, N_b \\ \delta \mathbf{x}_F &= \delta \mathbf{x}_{F_0} + \delta \Delta \mathbf{x}_F \\ \delta \boldsymbol{\lambda} &= \delta \boldsymbol{\lambda}_0 + \delta \Delta \boldsymbol{\lambda}\end{aligned}\tag{5.5}$$

Since $\mathbf{q}_{b_0}, \mathbf{x}_{F_0}, \boldsymbol{\lambda}_0$ are known, we must have (by definition of the virtual displacement)

$$\delta \mathbf{q}_{b_0} = 0, \delta \mathbf{x}_{F_0} = 0, \delta \boldsymbol{\lambda}_0 = 0\tag{5.6}$$

Eqns (5.5) are thus simply

$$\begin{aligned}\delta \mathbf{q}_b &= \delta \Delta \mathbf{q}_b \\ \delta \mathbf{x}_F &= \delta \Delta \mathbf{x}_F \\ \delta \boldsymbol{\lambda} &= \delta \Delta \boldsymbol{\lambda}\end{aligned}\tag{5.7}$$

Note that δ refers to virtual variation, whereas Δ refers to the perturbation values. Substitution of relations (5.4) and (5.7) in (5.3) yields

$$\begin{aligned}
 \delta\mathcal{U}_b &= \delta\mathcal{U}_{b_o}(\Delta\mathbf{q}_b, \theta_o, \psi, \mathbf{q}_{b_o}, \mathbf{q}_{b_o}^2) \\
 &\quad + \delta\Delta\mathcal{U}_b(\delta\Delta\mathbf{q}_b, \theta_o, \psi, \mathbf{q}_{b_o}, \Delta\mathbf{q}_b) \\
 \delta\mathcal{T}_b &= \delta\mathcal{T}_{b_o} + \delta\Delta\mathcal{T}_b \\
 &\vdots \\
 \delta\mathcal{W}_F &= \delta\mathcal{W}_{F_o} + \delta\Delta\mathcal{W}_F
 \end{aligned} \tag{5.8}$$

Substituting Eqns (5.8) in (5.2) and finally in (5.1) yields

$$\begin{aligned}
 \int_{t_1}^{t_2} (\delta\mathcal{U}_o - \delta\mathcal{T}_o - \delta\mathcal{W}_o) dt + \int_{t_1}^{t_2} \sum_{b=1}^{N_b} \{(\delta\Delta\mathcal{U}_b - \delta\Delta\mathcal{T}_b - \delta\Delta\mathcal{W}_b) \\
 + (\delta\Delta\mathcal{U}_F - \delta\Delta\mathcal{T}_F - \delta\Delta\mathcal{W}_F)\} dt = 0
 \end{aligned} \tag{5.9}$$

The trim solution satisfies the equation

$$\int_{t_1}^{t_2} (\delta\mathcal{U}_o - \delta\mathcal{T}_o - \delta\mathcal{W}_o) dt = 0 \tag{5.10}$$

Eqn (5.9) therefore reduces to the form

$$\begin{aligned}
 \int_{t_1}^{t_2} \sum_{b=1}^{N_b} (\delta\Delta\mathcal{U}_b - \delta\Delta\mathcal{T}_b - \delta\Delta\mathcal{W}_b) \\
 + (\delta\Delta\mathcal{U}_F - \delta\Delta\mathcal{T}_F - \delta\Delta\mathcal{W}_F) dt = 0
 \end{aligned} \tag{5.11}$$

Let

$$\begin{aligned}
 \delta\Delta\mathcal{U}_b - \delta\Delta\mathcal{T}_b - \delta\Delta\mathcal{W}_b &= \delta\Delta\Pi_b; \quad m = 1, 2, \dots, N_b \\
 \delta\Delta\mathcal{U}_F - \delta\Delta\mathcal{T}_F - \delta\Delta\mathcal{W}_F &= \delta\Delta\Pi_F
 \end{aligned} \tag{5.12}$$

Equation (5.11) can then be symbolically expressed as

$$\begin{aligned} & \int_{t_1}^{t_2} \sum_{b=1}^{N_b} \delta \Delta \Pi_b(\delta \Delta \mathbf{q}_b, \delta \Delta \mathbf{x}_F, \delta \Delta \boldsymbol{\lambda}, \psi, \theta_o, \mathbf{q}_{b_o}, \mathbf{x}_{F_o}, \boldsymbol{\lambda}_o, \delta \boldsymbol{\lambda}, \dot{\mathbf{q}}_{b_o}, \\ & \quad \dot{\mathbf{x}}_{F_o}, \Delta \mathbf{x}_F, \Delta \mathbf{q}_b, \Delta \dot{\mathbf{x}}_{F_o}, \Delta \dot{\mathbf{q}}_b, \Delta \ddot{\mathbf{x}}_F, \Delta \ddot{\mathbf{q}}_b) \\ & \quad + \delta \Delta \Pi_F(\delta \Delta \mathbf{x}_F, \mathbf{x}_{F_o}, \Delta \mathbf{x}_{F_o}, \Delta \dot{\mathbf{x}}_{F_o}) dt = 0 \end{aligned} \quad (5.13)$$

Following the space finite element discretization procedure of Section 2.3.1, the assembly process of Section 2.3.4, and applying the blade kinematic boundary conditions, Eqn (5.13) is transformed to the matrix form

$$\begin{aligned} & \left\{ \begin{array}{c} \delta \mathbf{q}_1 \\ \delta \mathbf{q}_2 \\ \vdots \\ \delta \mathbf{q}_{N_b} \\ \delta \mathbf{x}_F \end{array} \right\}^T \left(\begin{bmatrix} \mathbf{M}_1 & 0 & \dots & 0 & \mathbf{M}_{1F}(\mathbf{q}_{1_o}) \\ 0 & \mathbf{M}_2 & \dots & 0 & \mathbf{M}_{2F}(\mathbf{q}_{2_o}) \\ \vdots & & \ddots & & \vdots \\ 0 & 0 & \dots & \mathbf{M}_{N_b} & \mathbf{M}_{N_b F}(\mathbf{q}_{N_b o}) \\ \mathbf{M}_{F1} & \mathbf{M}_{F2} & \dots & \mathbf{M}_{FN_b} & \mathbf{M}_{FF} \end{bmatrix} \right) \left\{ \begin{array}{c} \Delta \dot{\mathbf{q}}_1 \\ \Delta \dot{\mathbf{q}}_2 \\ \vdots \\ \Delta \dot{\mathbf{q}}_{N_b} \\ \Delta \dot{\mathbf{x}}_F \end{array} \right\} \\ & + \left[\begin{array}{ccccc} \mathbf{C}_1 & 0 & \dots & 0 & \mathbf{C}_{1F}(\mathbf{q}_{1_o}) \\ 0 & \mathbf{C}_2 & \dots & 0 & \mathbf{C}_{2F}(\mathbf{q}_{2_o}) \\ \vdots & & \ddots & & \vdots \\ 0 & 0 & \dots & \mathbf{C}_{N_b} & \mathbf{C}_{N_b F}(\mathbf{q}_{N_b o}) \\ \mathbf{C}_{F1} & \mathbf{C}_{F2} & \dots & \mathbf{C}_{FN_b} & \mathbf{C}_{FF} \end{array} \right] \left\{ \begin{array}{c} \Delta \dot{\mathbf{q}}_1 \\ \Delta \dot{\mathbf{q}}_2 \\ \vdots \\ \Delta \dot{\mathbf{q}}_{N_b} \\ \Delta \dot{\mathbf{x}}_F \end{array} \right\} \\ & + \left[\begin{array}{ccccc} \mathbf{K}_1 & 0 & \dots & 0 & \mathbf{K}_{1F} & \mathbf{K}_{1\lambda} \\ 0 & \mathbf{K}_2 & \dots & 0 & \mathbf{K}_{2F} & \mathbf{K}_{2\lambda} \\ \vdots & & \ddots & & \vdots & \vdots \\ 0 & 0 & \dots & \mathbf{K}_{N_b} & \mathbf{K}_{N_b F} & \mathbf{K}_{N_b \lambda} \\ \mathbf{K}_{F1} & \mathbf{K}_{F2} & \dots & \mathbf{K}_{FN_b} & \mathbf{K}_{FF} & 0 \end{array} \right] \left\{ \begin{array}{c} \Delta \mathbf{q}_1 \\ \Delta \mathbf{q}_2 \\ \vdots \\ \Delta \mathbf{q}_{N_b} \\ \Delta \mathbf{x}_F \\ \Delta \boldsymbol{\lambda} \end{array} \right\} \\ & = \left[\begin{array}{c} \Delta \mathbf{F}_1(\mathbf{q}_o \Delta \mathbf{q}_1, \mathbf{q}_o \Delta \dot{\mathbf{q}}_1, \dot{\mathbf{q}}_o \Delta \mathbf{q}_1) \\ \Delta \mathbf{F}_2(\mathbf{q}_o \Delta \mathbf{q}_2, \mathbf{q}_o \Delta \dot{\mathbf{q}}_2, \dot{\mathbf{q}}_o \Delta \mathbf{q}_2) \\ \vdots \\ \Delta \mathbf{F}_{N_b}(\mathbf{q}_o \Delta \mathbf{q}_{N_b}, \mathbf{q}_o \Delta \dot{\mathbf{q}}_{N_b}, \dot{\mathbf{q}}_o \Delta \mathbf{q}_{N_b}) \\ \Delta \mathbf{F}_F \end{array} \right] \end{aligned} \quad (5.14)$$

where $\mathbf{q}_1, \mathbf{q}_2, \dots, \mathbf{q}_{N_b}$ are the displacement vectors for blades $1, 2, \dots, N_b$, re-

spectively (\mathbf{q}_b refers to the displacement vector for the b th blade). Matrices \mathbf{M}_b , \mathbf{C}_b , and \mathbf{K}_b denote respectively the mass, damping, and stiffness matrices for the b th blade. \mathbf{M}_{bF} is the blade-fuselage coupled mass matrix which accounts for the effect of fuselage-induced inertia forces on the b th blade. Similarly, \mathbf{M}_{Fb} is the fuselage-blade coupled mass matrix which accounts for the effect of blade-induced inertia forces on the fuselage. The coupled damping matrices \mathbf{C}_{bF} , \mathbf{C}_{Fb} and the coupled stiffness matrices \mathbf{K}_{bF} , \mathbf{K}_{Fb} can be similarly interpreted. The matrices \mathbf{M}_{FF} , \mathbf{C}_{FF} and \mathbf{K}_{FF} refer to the fuselage.

The perturbation force, $\Delta\mathbf{F}_b$, can be approximated by Taylor's Series as

$$\Delta\mathbf{F}_b = \frac{\partial\mathbf{F}}{\partial\mathbf{q}_b}\Delta\mathbf{q}_b + \frac{\partial\mathbf{F}}{\partial\dot{\mathbf{q}}_b}\Delta\dot{\mathbf{q}}_b; \quad b = 1, 2, \dots, N_b \quad (5.15)$$

After substituting relation (5.15) in (5.14) and noting that the virtual variations $\delta\mathbf{q}_1, \dots, \delta\mathbf{q}_{N_b}, \delta\mathbf{x}_F$, and $\delta\lambda$ are arbitrary, the resulting equations can be expressed as

$$\begin{bmatrix} \mathbf{M}_{RR} & \mathbf{M}_{RF} \\ \mathbf{M}_{FR} & \mathbf{M}_{FF} \end{bmatrix} \begin{Bmatrix} \Delta\ddot{\mathbf{q}}_R \\ \Delta\ddot{\mathbf{x}}_F \end{Bmatrix} + \begin{bmatrix} \mathbf{C}_{RR} & \mathbf{C}_{RF} \\ \mathbf{C}_{FR} & \mathbf{C}_{FF} \end{bmatrix} \begin{Bmatrix} \Delta\dot{\mathbf{q}}_R \\ \Delta\dot{\mathbf{x}}_F \end{Bmatrix} + \begin{bmatrix} \mathbf{K}_{RR} & \mathbf{K}_{RF} & \mathbf{K}_{R\lambda} \\ \mathbf{K}_{FR} & \mathbf{K}_{FF} & 0 \end{bmatrix} \begin{Bmatrix} \Delta\mathbf{q}_R \\ \Delta\mathbf{x}_F \\ \Delta\lambda \end{Bmatrix} = \mathbf{0} \quad (5.16)$$

where

$$\mathbf{M}_{RR} = \begin{bmatrix} \mathbf{M}_1 & 0 & 0 & 0 \\ 0 & \mathbf{M}_2 & 0 & 0 \\ 0 & 0 & \ddots & 0 \\ 0 & 0 & 0 & \mathbf{M}_{N_b} \end{bmatrix} \quad (5.17)$$

$$\mathbf{C}_{RR} = \begin{bmatrix} (\mathbf{C}_1 - \frac{\partial \mathbf{F}}{\partial \dot{\mathbf{q}}_1}) & 0 & 0 & 0 \\ 0 & (\mathbf{C}_2 - \frac{\partial \mathbf{F}}{\partial \dot{\mathbf{q}}_2}) & 0 & 0 \\ 0 & 0 & \ddots & 0 \\ 0 & 0 & 0 & (\mathbf{C}_{N_b} - \frac{\partial \mathbf{F}}{\partial \dot{\mathbf{q}}_{N_b}}) \end{bmatrix} \quad (5.18)$$

$$\mathbf{K}_{RR} = \begin{bmatrix} (\mathbf{K}_1 - \frac{\partial \mathbf{F}}{\partial \mathbf{q}_1}) & 0 & 0 & 0 \\ 0 & (\mathbf{K}_2 - \frac{\partial \mathbf{F}}{\partial \mathbf{q}_2}) & 0 & 0 \\ 0 & 0 & \ddots & 0 \\ 0 & 0 & 0 & (\mathbf{K}_{N_b} - \frac{\partial \mathbf{F}}{\partial \mathbf{q}_{N_b}}) \end{bmatrix} \quad (5.19)$$

$$\Delta \mathbf{q}_R = [\Delta \mathbf{q}_1^T, \Delta \mathbf{q}_2^T, \dots, \Delta \mathbf{q}_{N_b}^T]^T \quad (5.20)$$

Note that Eqn (5.16) cannot be solved yet since the equations governing the inflow perturbations, $\Delta \boldsymbol{\lambda}$, are not yet available. The dynamic inflow model discussed next provides the required equations.

5.2.3 Dynamic Inflow Equations

Dynamic inflow modeling allows inclusion of low-frequency unsteady wake effects in the system dynamics. The model is based on the actuator disk theory, and relates the rotor inflow perturbations to perturbations of the rotor aerodynamic thrust, pitching and rolling moments [2]

$$\mathbf{m} \Delta \dot{\boldsymbol{\lambda}} + \mathbf{l}^{-1} \Delta \boldsymbol{\lambda} = \Delta \mathbf{C}_F \quad (5.21)$$

where

$$\Delta \boldsymbol{\lambda} = [\Delta \lambda_o, \Delta \lambda_{1s}, \Delta \lambda_{1c}]^T \quad (5.22)$$

$$\Delta \mathbf{C}_F = [\Delta C_T, -\Delta C_{m_x}, \Delta C_{m_y}]^T \quad (5.23)$$

Nonzero elements of the matrices \mathbf{m} and \mathbf{l} are given by [2]

$$\begin{aligned}
m_{11} &= \frac{128}{75\pi} \\
m_{22} &= m_{33} = \frac{-16}{45\pi} \\
l_{11} &= \frac{1}{2v} \\
l_{22} &= \frac{-4}{v(1 + \sin \alpha)} \\
l_{33} &= l_{22} \sin \alpha \\
l_{13} &= l_{31} = \frac{15\pi}{64v} \sqrt{\frac{1 - \sin \alpha}{1 + \sin \alpha}}
\end{aligned} \tag{5.24}$$

where

$$\begin{aligned}
\alpha &= \tan^{-1} \frac{\lambda}{\mu} \\
v &= \sqrt{\mu^2 + \lambda^2} + \frac{\lambda \lambda_i}{\sqrt{\mu^2 + \lambda^2}}
\end{aligned} \tag{5.25}$$

λ_i is the induced inflow, and λ is the total inflow velocity. Note that the dynamic inflow equations are in the first order form.

The rotor aerodynamic perturbations loads can be expressed as

$$\begin{aligned}
\Delta C_T &= \frac{3a\sigma}{\gamma N_b} \sum_{b=1}^{N_b} \int_0^1 \Delta L_w^b(\Delta \mathbf{q}_b, \Delta \dot{\mathbf{q}}_b, \psi_b, \Delta \boldsymbol{\lambda}, \Delta \mathbf{x}_F, \Delta \dot{\mathbf{x}}_F) dx \\
\Delta C_{m_{x_H}} &= \frac{3a\sigma}{\gamma N_b} \sum_{b=1}^{N_b} \int_0^1 \Delta L_w^b(\Delta \mathbf{q}_b, \Delta \dot{\mathbf{q}}_b, \psi_b, \Delta \boldsymbol{\lambda}, \Delta \mathbf{x}_F, \Delta \dot{\mathbf{x}}_F) x \sin \psi_b dx \\
\Delta C_{m_{y_H}} &= \frac{-3a\sigma}{\gamma N_b} \sum_{b=1}^{N_b} \int_0^1 \Delta L_w^b(\Delta \mathbf{q}_b, \Delta \dot{\mathbf{q}}_b, \psi_b, \Delta \boldsymbol{\lambda}, \Delta \mathbf{x}_F, \Delta \dot{\mathbf{x}}_F) x \cos \psi_b dx
\end{aligned} \tag{5.26}$$

where L_w^b is the blade section lift for the b^{th} blade and is derived in Chapter 3.1. Substituting this expression into eqns (5.26) and then substituting for the

perturbation airloads in equation (5.21), one obtains the dynamic equations in the form

$$[\mathbf{C}_{\lambda 1}, \mathbf{C}_{\lambda 2}, \dots, \mathbf{C}_{\lambda N_b}, \mathbf{m}] \begin{Bmatrix} \Delta \dot{\mathbf{q}}_1 \\ \Delta \dot{\mathbf{q}}_2 \\ \vdots \\ \Delta \dot{\mathbf{q}}_{N_b} \\ \Delta \boldsymbol{\lambda} \end{Bmatrix} + [\mathbf{K}_{\lambda 1}, \dots, \mathbf{K}_{\lambda N_b}, \mathbf{K}_{\lambda \lambda}] \begin{Bmatrix} \Delta \mathbf{q}_1 \\ \Delta \mathbf{q}_2 \\ \vdots \\ \Delta \mathbf{q}_{N_b} \\ \Delta \boldsymbol{\lambda} \end{Bmatrix} = 0$$

or ,

$$[\mathbf{C}_{\lambda R}, \mathbf{m}] \begin{Bmatrix} \Delta \dot{\mathbf{q}}_R \\ \Delta \boldsymbol{\lambda} \end{Bmatrix} + [\mathbf{K}_{\lambda R}, \mathbf{K}_{\lambda \lambda}] \begin{Bmatrix} \Delta \mathbf{q}_R \\ \Delta \boldsymbol{\lambda} \end{Bmatrix} = 0 \quad (5.27)$$

5.2.4 Linearized System Equations

Rotor-fuselage eqns (5.16) and the dynamic inflow eqns (5.27) together provide the complete set of linearized system equations,

$$\begin{aligned} & \begin{bmatrix} \mathbf{M}_{RR} & \mathbf{M}_{RF} & 0 \\ \mathbf{M}_{FR} & \mathbf{M}_{FF} & 0 \\ 0 & 0 & 0 \end{bmatrix} \begin{Bmatrix} \Delta \ddot{\mathbf{q}}_R \\ \Delta \ddot{\mathbf{x}}_F \\ \Delta \boldsymbol{\lambda} \end{Bmatrix} + \begin{bmatrix} \mathbf{C}_{RR} & \mathbf{C}_{RF} & 0 \\ \mathbf{C}_{FR} & \mathbf{C}_{FF} & 0 \\ \mathbf{C}_{\lambda R} & 0 & \mathbf{C}_{\lambda \lambda} \end{bmatrix} \begin{Bmatrix} \Delta \dot{\mathbf{q}}_R \\ \Delta \dot{\mathbf{x}}_F \\ \Delta \boldsymbol{\lambda} \end{Bmatrix} \\ & + \begin{bmatrix} \mathbf{K}_{RR} & \mathbf{K}_{RF} & \mathbf{K}_{R\lambda} \\ \mathbf{K}_{FR} & \mathbf{K}_{FF} & 0 \\ \mathbf{K}_{\lambda R} & 0 & \mathbf{K}_{\lambda \lambda} \end{bmatrix} \begin{Bmatrix} \Delta \mathbf{q}_R \\ \Delta \mathbf{x}_F \\ \Delta \boldsymbol{\lambda} \end{Bmatrix} = 0 \quad (5.28) \end{aligned}$$

5.2.4.1 Normal Mode Transformation

The b^{th} -blade degrees of freedom, \mathbf{q}_b , can be transformed to normal mode space using the transformation (section 4.2.3)

$$\Delta \mathbf{q}_b(\psi) = \Phi \Delta \mathbf{p}_b(\psi) \quad (5.29)$$

where Φ is the modal matrix, comprised of coupled modes obtained about the mean trimmed response position, and $\Delta\mathbf{p}_b$ is the vector of modal (generalized) coordinates for the b^{th} blade. The rotor degrees of freedom, $\Delta\mathbf{q}_R$, can thus be expressed as

$$\begin{aligned}\Delta\mathbf{q}_R(\psi) &= \left\{ \begin{array}{c} \Delta\mathbf{q}_1 \\ \Delta\mathbf{q}_2 \\ \vdots \\ \Delta\mathbf{q}_{N_b} \end{array} \right\} = \left[\begin{array}{cccc} \Phi & & & \\ & \Phi & & \\ & & \ddots & \\ & & & \Phi \end{array} \right] \left\{ \begin{array}{c} \Delta\mathbf{p}_1 \\ \Delta\mathbf{p}_2 \\ \vdots \\ \Delta\mathbf{p}_{N_b} \end{array} \right\} \\ &= \left[\begin{array}{cccc} \Phi & & & \\ & \Phi & & \\ & & \ddots & \\ & & & \Phi \end{array} \right] \Delta\mathbf{p}_R(\psi)\end{aligned}\quad (5.30)$$

where

$$\Delta\mathbf{p}_R(\psi) = [\Delta\mathbf{p}_1, \Delta\mathbf{p}_2, \dots, \Delta\mathbf{p}_{N_b}]^T \quad (5.31)$$

Using relation (5.30), system eqns (5.28) are transformed to the blades normal mode space. The resulting equations can be expressed as

$$\begin{aligned}\left[\begin{array}{ccc} \bar{\mathbf{M}}_{RR} & \bar{\mathbf{M}}_{RF} & 0 \\ \bar{\mathbf{M}}_{FR} & \bar{\mathbf{M}}_{FF} & 0 \\ 0 & 0 & 0 \end{array} \right] \left\{ \begin{array}{c} \Delta\tilde{\mathbf{p}}_R \\ \Delta\tilde{\mathbf{x}}_F \\ \Delta\lambda \end{array} \right\} + \left[\begin{array}{ccc} \bar{\mathbf{C}}_{RR} & \bar{\mathbf{C}}_{RF} & 0 \\ \bar{\mathbf{C}}_{FR} & \bar{\mathbf{C}}_{FF} & 0 \\ \bar{\mathbf{C}}_{\lambda b} & 0 & \mathbf{C}_{\lambda\lambda} \end{array} \right] \left\{ \begin{array}{c} \Delta\dot{\mathbf{p}}_R \\ \Delta\dot{\mathbf{x}}_F \\ \Delta\dot{\lambda} \end{array} \right\} \\ + \left[\begin{array}{ccc} \bar{\mathbf{K}}_{RR} & \bar{\mathbf{K}}_{RF} & \bar{\mathbf{K}}_{R\lambda} \\ \bar{\mathbf{K}}_{FR} & \bar{\mathbf{K}}_{FF} & 0 \\ \bar{\mathbf{K}}_{\lambda R} & 0 & \mathbf{K}_{\lambda\lambda} \end{array} \right] \left\{ \begin{array}{c} \Delta\mathbf{q}_R \\ \Delta\mathbf{x}_F \\ \Delta\lambda \end{array} \right\} = \mathbf{0}\end{aligned}\quad (5.32)$$

5.2.4.2 Transformation to First order – System Matrix

Define the state vector \mathbf{Y} as follows:

$$\mathbf{Y} = \begin{Bmatrix} \Delta \dot{\mathbf{p}}_R \\ \Delta \dot{\mathbf{x}}_F \\ \Delta \mathbf{p}_R \\ \Delta \mathbf{x}_F \\ \Delta \boldsymbol{\lambda} \end{Bmatrix} \quad (5.33)$$

System eqns (5.32) can then be rewritten as

$$\begin{bmatrix} \bar{\mathbf{M}}_{RR} & \bar{\mathbf{M}}_{RF} & 0 & 0 & 0 \\ \bar{\mathbf{M}}_{FR} & \bar{\mathbf{M}}_{FF} & 0 & 0 & 0 \\ 0 & 0 & \mathbf{I} & 0 & 0 \\ 0 & 0 & 0 & \mathbf{I} & 0 \\ 0 & 0 & 0 & 0 & \mathbf{C}_{\lambda\lambda} \end{bmatrix} \dot{\mathbf{Y}} + \begin{bmatrix} \bar{\mathbf{C}}_{RR} & \bar{\mathbf{C}}_{RF} & \bar{\mathbf{K}}_{RR} & \bar{\mathbf{K}}_{RF} & \bar{\mathbf{K}}_{R\lambda} \\ \bar{\mathbf{C}}_{FR} & \bar{\mathbf{C}}_{FF} & \bar{\mathbf{K}}_{FR} & \bar{\mathbf{K}}_{FF} & 0 \\ \mathbf{I} & 0 & 0 & 0 & 0 \\ 0 & \mathbf{I} & 0 & 0 & 0 \\ \mathbf{C}_{\lambda R} & 0 & \bar{\mathbf{K}}_{\lambda R} & 0 & \mathbf{K}_{\lambda\lambda} \end{bmatrix} \mathbf{Y} = \mathbf{0} \quad (5.34)$$

Premultiplication of Eqn (5.34) by the matrix

$$\begin{bmatrix} [\bar{\mathbf{M}}_{RR} \quad \bar{\mathbf{M}}_{RF}]^{-1} & 0 & 0 & 0 \\ \bar{\mathbf{M}}_{FR} & \bar{\mathbf{M}}_{FF} & 0 & 0 \\ 0 & & \mathbf{I} & 0 & 0 \\ 0 & & 0 & \mathbf{I} & 0 \\ 0 & & 0 & 0 & \mathbf{C}_{\lambda\lambda}^{-1} \end{bmatrix} \quad (5.35)$$

results in system perturbation equations in the standard first order form:

$$\dot{\mathbf{Y}} = \mathbf{A}(\psi, \mathbf{Y}_0) \mathbf{Y} \quad (5.36)$$

Note that the stability matrix, \mathbf{A} , is a function of time ψ and the trim solution vector \mathbf{Y}_0 . Eqns (5.36) are in the rotating frame. As mentioned earlier, if the system consists of only an isolated blade, it is time-saving to solve the

eigenproblem (5.36) in the rotating frame. However, if the system includes either the fuselage or the dynamic inflow models, it is more convenient to seek the eigensolution in the fixed frame.

5.2.4.3 Fixed Coordinate Transformation

The system equations consist of three sets of equations: the blade equations, the fuselage equations, and the dynamic inflow equations. Fixed coordinate transformation (FCT) of each set of equations will now be discussed.

Blade Equations

Consider equation of motion for the bth blade in the rotating frame:

$$\begin{aligned} \bar{\mathbf{M}}_b \Delta \ddot{\mathbf{p}}_b + \bar{\mathbf{C}}_b \Delta \dot{\mathbf{p}}_b + \bar{\mathbf{K}}_b \Delta \mathbf{p}_b + \bar{\mathbf{M}}_{bF} \Delta \ddot{\mathbf{x}}_F + \bar{\mathbf{C}}_{bF} \Delta \dot{\mathbf{x}}_F \\ + \bar{\mathbf{K}}_{bF} \Delta \mathbf{x}_F + \bar{\mathbf{K}}_{b\lambda} \Delta \lambda = \mathbf{0} \end{aligned} \quad (5.37)$$

Fixed coordinate transformation of blade equations involves two steps: transformation of the rotating coordinates to the fixed system coordinates, and transformation of the rotating frame equations to the fixed frame.

Step 1: Transforming coordinates

The rotating frame coordinates, $\Delta \mathbf{p}_b$, are related to the fixed frame coordinates, $\Delta \xi$, as follows:

$$\Delta \mathbf{p}_b = \mathbf{A}_b \Delta \xi \quad (5.38)$$

where

$$\Delta \bar{\xi} = \begin{Bmatrix} \Delta \bar{\xi}^{(1)} \\ \Delta \bar{\xi}^{(2)} \\ \vdots \\ \Delta \bar{\xi}^{(m)} \end{Bmatrix}_{mN_b \times 1} \quad (5.39)$$

The m is the number of modes used to represent the blade response and N_b is the number of blades. The element $\Delta \bar{\xi}^{(k)}$ in the column vector above represents the vector of fixed coordinates for the k^{th} modal displacement of the blade:

$$\Delta \bar{\xi}^{(k)} = \begin{Bmatrix} \Delta \bar{\xi}_o \\ \Delta \bar{\xi}_{1c} \\ \Delta \bar{\xi}_{2c} \\ \vdots \\ \Delta \bar{\xi}_{ns} \\ \Delta \bar{\xi}_{n/2} \end{Bmatrix}_{N_b \times 1}^{(k)} \quad (5.40)$$

$$\mathbf{A}_b = \begin{bmatrix} \mathbf{a}_b & 0 & 0 & \dots & 0 \\ 0 & \mathbf{a}_b & 0 & \dots & 0 \\ 0 & 0 & \mathbf{a}_b & \dots & 0 \\ 0 & 0 & 0 & \ddots & 0 \\ 0 & 0 & 0 & 0 & \mathbf{a}_b \end{bmatrix}_{(m \times mN_b)} \quad (5.41)$$

where

$$\begin{aligned} \mathbf{a}_b &= \begin{cases} [1, c\psi_b, c2\psi_b, \dots, cn\psi_b, s\psi_b, \dots, sn\psi_b, (-1)^b] & \text{if } N_b \text{ even} \\ [1, c\psi_b, c2\psi_b, \dots, cn\psi_b, s\psi_b, \dots, sn\psi_b] & \text{if } N_b \text{ odd} \end{cases} \\ n &= \frac{N_b - 2}{2} \text{ for } N_b \text{ even} \\ n &= \frac{N_b - 1}{2} \text{ for } N_b \text{ odd} \\ cn\psi_b &= \cos(n\psi_b), \quad sn\psi_b = \sin(n\psi_b) \end{aligned} \quad (5.42)$$

Differentiating eqn (5.38) with respect to time,

$$\begin{aligned} \Delta \dot{\mathbf{p}}_b &= \mathbf{A}_b \Delta \dot{\bar{\xi}} + \dot{\mathbf{A}}_b \Delta \bar{\xi} = \mathbf{A}_b \Delta \dot{\bar{\xi}} + \mathbf{B}_b \Delta \bar{\xi} \\ \Delta \ddot{\mathbf{p}}_b &= \mathbf{A}_b \Delta \ddot{\bar{\xi}} + 2\dot{\mathbf{A}}_b \Delta \dot{\bar{\xi}} + \ddot{\mathbf{A}}_b \Delta \bar{\xi} = \mathbf{A}_b \Delta \ddot{\bar{\xi}} + 2\mathbf{B}_b \Delta \dot{\bar{\xi}} + \mathbf{C}_b \Delta \bar{\xi} \end{aligned} \quad (5.43)$$

where

$$\mathbf{B}_b = \dot{\mathbf{A}}_b \quad \text{and} \quad \mathbf{C}_b = \ddot{\mathbf{A}}_b \quad (5.44)$$

Substituting eqns (5.38) and (5.43) into the blade eqn (5.37), we obtain

$$\begin{aligned} \bar{\mathbf{M}}_{FX_b} \Delta \ddot{\boldsymbol{\xi}} + \bar{\mathbf{C}}_{FX_b} \Delta \dot{\boldsymbol{\xi}} + \bar{\mathbf{K}}_{FX_b} \Delta \boldsymbol{\xi} + \bar{\mathbf{M}}_{bF} \Delta \ddot{\mathbf{x}}_F + \bar{\mathbf{C}}_{bF} \Delta \dot{\mathbf{x}}_F \\ + \bar{\mathbf{K}}_{bF} \Delta \mathbf{x}_F + \bar{\mathbf{K}}_{b\lambda} \Delta \lambda = \mathbf{0} \end{aligned} \quad (5.45)$$

where

$$\begin{aligned} \mathbf{M}_{FX_b} &= \bar{\mathbf{M}}_b \mathbf{A}_b \\ \mathbf{C}_{FX_b} &= 2\bar{\mathbf{M}}_b \mathbf{B}_b + \bar{\mathbf{C}}_b \mathbf{A}_b \\ \bar{\mathbf{K}}_{FX_b} &= \bar{\mathbf{M}}_b \mathbf{C}_b + \bar{\mathbf{C}}_b \mathbf{B}_b + \bar{\mathbf{K}}_b \mathbf{A}_b \end{aligned} \quad (5.46)$$

Step 2 : Transforming equations

Though the degrees of freedom, $\Delta \mathbf{p}_b$, have been transformed to the fixed coordinates, $\Delta \boldsymbol{\xi}$, the b^{th} blade eqn (5.45) is still in the rotating frame. To transform the differential eqns (5.45) to the fixed frame, the following summation operators are applied:

$$\frac{1}{N_b} \sum_{b=1}^{N_b} (d.eqns) \quad (5.47)$$

$$\frac{2}{N_b} \sum_{b=1}^{N_b} (d.eqns) \cos l\psi_b; \quad l = 1, 2, \dots, N_b \quad (5.48)$$

$$\frac{2}{N_b} \sum_{b=1}^{N_b} (d.eqns) \sin l\psi_b; \quad l = 1, 2, \dots, N_b \quad (5.49)$$

$$\frac{1}{N_b} \sum_{b=1}^{N_b} (d.eqns) (-1)^b \quad (5.50)$$

where *d.eqns* refers to the blade differential eqns (5.45) in the rotating frame. The last operation is applicable only if the number of blades, N_b , is even. Note that eqn (5.45) represents m equations, corresponding to the m modal degrees of freedom of the blade. Operation (5.47) therefore results in m equations corresponding to the m collective modes in the fixed frame. Equations (5.48) and (5.49) result in $2nm$ cyclic modes, and operation (5.50) yields m differential modes. The total number of degree of freedom in the fixed frame, therefore, equals $m + 2nm + m = (2n + 2)m = N_b m$, i.e., the number of blades times the modal degrees of freedom.

Summation operations (5.47–5.50) result in the following hub fixed frame differential equations

$$\begin{aligned} \mathbf{M}_H \ddot{\xi} + \mathbf{C}_H \dot{\xi} + \mathbf{K}_H \xi + \mathbf{M}_{HF} \Delta \ddot{\mathbf{x}}_F + \mathbf{C}_{HF} \Delta \dot{\mathbf{x}}_F \\ + \mathbf{K}_{HF} \Delta \mathbf{x}_F + \mathbf{K}_{H\lambda} \Delta \lambda = \mathbf{0} \end{aligned} \quad (5.51)$$

where

$$\begin{aligned} \mathbf{M}_H &= \frac{1}{N_b} \sum_{b=1}^{N_b} \mathbf{H}_b \bar{\mathbf{M}}_b \mathbf{A}_b \\ \mathbf{C}_H &= \frac{1}{N_b} \sum_{b=1}^{N_b} \mathbf{H}_b (2\bar{\mathbf{M}}_b \mathbf{B}_b + \bar{\mathbf{C}}_b \mathbf{A}_b) \\ \mathbf{K}_H &= \frac{1}{N_b} \sum_{b=1}^{N_b} \mathbf{H}_b (\bar{\mathbf{M}}_b \mathbf{C}_b + \bar{\mathbf{C}}_b \mathbf{B}_b + \bar{\mathbf{K}}_b \mathbf{A}_b) \\ \mathbf{M}_{HF} &= \frac{1}{N_b} \sum_{b=1}^{N_b} \mathbf{H}_b \bar{\mathbf{M}}_{bF} \\ \mathbf{C}_{HF} &= \frac{1}{N_b} \sum_{b=1}^{N_b} \mathbf{H}_b \bar{\mathbf{C}}_{bF} \\ \mathbf{K}_{HF} &= \frac{1}{N_b} \sum_{b=1}^{N_b} \mathbf{H}_b \bar{\mathbf{K}}_{bF} \end{aligned}$$

$$\mathbf{K}_{H\lambda} = \frac{1}{N_b} \sum_{b=1}^{N_b} \mathbf{H}_b \bar{\mathbf{K}}_{b\lambda} \quad (5.52)$$

where

$$\mathbf{H}_b = \begin{bmatrix} \mathbf{h}_b & & \\ & \ddots & \\ & & \mathbf{h}_b \end{bmatrix}_{(mN_b \times m)} \quad (5.53)$$

and

$$\mathbf{h}_b = \begin{Bmatrix} 1 \\ 2c\psi_b \\ 2c2\psi_b \\ \vdots \\ 2cn\psi_b \\ 2s\psi_b \\ 2s2\psi_b \\ \vdots \\ 2sn\psi_b \\ (-1)^b \end{Bmatrix}_{(N_b \times 1)} \quad (5.54)$$

Fuselage Equations

As seen from equations (5.14), the fuselage equations can be expressed as

$$\begin{aligned} & (\bar{\mathbf{M}}_{F1}\Delta\ddot{\mathbf{p}}_1 + \dots + \bar{\mathbf{M}}_{FN_b}\Delta\ddot{\mathbf{p}}_{N_b}) + \mathbf{M}_{FF}\Delta\ddot{\mathbf{x}}_F \\ & + (\bar{\mathbf{C}}_{F1}\Delta\dot{\mathbf{p}}_1 + \dots + \bar{\mathbf{C}}_{FN_b}\Delta\dot{\mathbf{p}}_{N_b}) + \mathbf{C}_{FF}\Delta\dot{\mathbf{x}}_F \\ & + (\bar{\mathbf{K}}_{F1}\Delta\mathbf{p}_1 + \dots + \bar{\mathbf{K}}_{FN_b}\Delta\mathbf{p}_{N_b}) + \mathbf{K}_{FF}\Delta\mathbf{x}_F = \mathbf{0} \end{aligned} \quad (5.55)$$

The fuselage equations are already in the fixed frame; only the blade modal degrees of freedom, $\Delta\mathbf{p}_b$, are in the rotating frame. Therefore, only one transformation is required, i.e., transformation of the blade rotating degrees of freedom to the fixed coordinates. Application of transformation relation (5.38) to the fuselage eqns (5.55) results in

$$\sum_{b=1}^{N_b} \mathbf{M}_{Fb}(\mathbf{A}_b\Delta\ddot{\boldsymbol{\xi}} + 2\mathbf{B}_b\Delta\dot{\boldsymbol{\xi}}_b + \mathbf{C}_b\Delta\boldsymbol{\xi}) + \mathbf{M}_{FF}\Delta\ddot{\mathbf{x}}_F$$

$$\begin{aligned}
& \sum_{b=1}^{N_b} \bar{\mathbf{C}}_{Fb} (\mathbf{A}_b \Delta \bar{\boldsymbol{\xi}} + \mathbf{B}_b \Delta \boldsymbol{\xi}) + \mathbf{C}_{FF} \Delta \dot{\mathbf{x}}_F \\
& + \sum_{b=1}^{N_b} \bar{\mathbf{K}}_{Fb} \mathbf{A}_b \Delta \bar{\boldsymbol{\xi}} + \mathbf{K}_{FF} \Delta \mathbf{x}_F = \mathbf{0}
\end{aligned} \tag{5.56}$$

or

$$\begin{aligned}
& \mathbf{M}_{FH} \Delta \bar{\boldsymbol{\xi}} + \mathbf{C}_{FH} \Delta \bar{\boldsymbol{\xi}} + \mathbf{K}_{FH} \Delta \bar{\boldsymbol{\xi}} + \mathbf{M}_{FF} \Delta \dot{\mathbf{x}}_F + \mathbf{C}_{FF} \Delta \dot{\mathbf{x}}_F \\
& + \mathbf{K}_{FF} \Delta \mathbf{x}_F = \mathbf{0}
\end{aligned} \tag{5.57}$$

where

$$\begin{aligned}
\mathbf{M}_{FH} &= \sum_{b=1}^{N_b} \bar{\mathbf{M}}_{Fb} \mathbf{A}_b \\
\mathbf{C}_{FH} &= \sum_{b=1}^{N_b} 2\bar{\mathbf{M}}_{Fb} \mathbf{B}_b + \bar{\mathbf{C}}_{Fb} \mathbf{A}_b \\
\mathbf{K}_{FH} &= \sum_{b=1}^{N_b} \bar{\mathbf{M}}_{Fb} \mathbf{C}_b + \bar{\mathbf{C}}_{Fb} \mathbf{B}_b + \bar{\mathbf{K}}_{Fb} \mathbf{A}_b
\end{aligned} \tag{5.58}$$

Dynamic Inflow Equations

As suggested by eqn (5.27), the dynamic inflow equations can be expressed as

$$\sum_{b=1}^{N_b} \bar{\mathbf{C}}_{\lambda b} \Delta \dot{\mathbf{p}}_b + \mathbf{C}_{\lambda\lambda} \Delta \dot{\boldsymbol{\lambda}} + \sum_{b=1}^{N_b} \bar{\mathbf{K}}_{\lambda b} \Delta \mathbf{p}_b + \mathbf{K}_{\lambda\lambda} \Delta \boldsymbol{\lambda} = \mathbf{0} \tag{5.59}$$

Like the fuselage equations, the inflow equations are already in the fixed frame. Arguments pertaining to the fuselage equations therefore apply, and the dynamic inflow equations in terms of the fixed coordinates are obtained as

$$\mathbf{C}_{\lambda H} \Delta \bar{\boldsymbol{\xi}} + \mathbf{C}_{\lambda\lambda} \Delta \dot{\boldsymbol{\lambda}} + \mathbf{K}_{\lambda H} \Delta \bar{\boldsymbol{\xi}} + \mathbf{K}_{\lambda\lambda} \Delta \boldsymbol{\lambda} = \mathbf{0} \tag{5.60}$$

where

$$\begin{aligned}\mathbf{C}_{\lambda H} &= \frac{1}{N_b} \sum_{b=1}^{N_b} \bar{\mathbf{C}}_{\lambda b} \mathbf{A}_b \\ \mathbf{K}_{\lambda H} &= \frac{1}{N_b} \sum_{b=1}^{N_b} \bar{\mathbf{C}}_{\lambda b} \mathbf{B}_b + \bar{\mathbf{K}}_{\lambda b} \mathbf{A}_b\end{aligned}\quad (5.61)$$

Rotor-Fuselage-Inflow Equations

Putting together eqns (5.53), (5.57) and (5.60), the coupled rotor-fuselage-inflow equations in the fixed frame are given by

$$\begin{aligned}\begin{bmatrix} \mathbf{M}_H & \mathbf{M}_{HF} & 0 \\ \mathbf{M}_{FH} & \mathbf{M}_{FF} & 0 \\ 0 & 0 & 0 \end{bmatrix} \begin{Bmatrix} \Delta \dot{\boldsymbol{\xi}} \\ \Delta \ddot{\mathbf{x}}_F \\ \Delta \dot{\lambda} \end{Bmatrix} + \begin{bmatrix} \mathbf{C}_H & \mathbf{C}_{HF} & 0 \\ \mathbf{C}_{FH} & \mathbf{C}_{FF} & 0 \\ \mathbf{C}_{\lambda H} & 0 & \mathbf{C}_{\lambda \lambda} \end{bmatrix} \begin{Bmatrix} \Delta \dot{\boldsymbol{\xi}} \\ \Delta \dot{\mathbf{x}}_F \\ \Delta \lambda \end{Bmatrix} \\ + \begin{bmatrix} \mathbf{K}_H & \mathbf{K}_{HF} & 0 \\ \mathbf{K}_{FH} & \mathbf{K}_{FF} & 0 \\ \mathbf{K}_{\lambda H} & 0 & \mathbf{K}_{\lambda \lambda} \end{bmatrix} \begin{Bmatrix} \Delta \dot{\boldsymbol{\xi}} \\ \Delta \mathbf{x}_F \\ \Delta \lambda \end{Bmatrix} = \mathbf{0}\end{aligned}\quad (5.62)$$

These equations have the same form as the rotating frame equations. Following the procedure of section 5.2.4.2, these equations can be transformed to the first order form

$$\dot{\mathbf{Y}}_{FX} = \mathbf{A}_{FX}(\psi) \mathbf{Y}_{FX} \quad (5.63)$$

where

$$\mathbf{Y}_{FX} = \begin{Bmatrix} \Delta \dot{\boldsymbol{\xi}} \\ \Delta \dot{\mathbf{x}}_F \\ \Delta \dot{\boldsymbol{\xi}} \\ \Delta \mathbf{x}_F \\ \Delta \lambda \end{Bmatrix} \quad (5.64)$$

5.2.5 Floquet Theory

The linearized homogeneous eqns (5.36) with periodic coefficients govern the system stability characteristics. The periodic coefficients arise as a result of the

aerodynamic forces in forward flight. The determination of stability of a linear, periodic system is carried out using Floquet theory [3]. The solution of the linear system of equations

$$\dot{\mathbf{Y}} = \mathbf{A}\mathbf{Y} \quad (5.65)$$

must be expressible as a linear combination of the state variables at time ψ_0 , i.e.,

$$\mathbf{Y}(\psi) = \Phi(\psi, \psi_0)\mathbf{Y}(\psi_0) \quad (5.66)$$

The matrix $\Phi(\psi, \psi_0)$ is called the state transition matrix. By definition,

$$\Phi(\psi_0, \psi_0) = \mathbf{I} \quad (5.67)$$

where \mathbf{I} is the identity matrix. By substituting (5.66) into (5.65), we obtain

$$\dot{\Phi} = \mathbf{A}\Phi \quad (5.68)$$

Since the rotorcraft equations are periodic with a period 2π , the stability matrix satisfies the relation

$$\mathbf{A}(\psi + 2\pi) = \mathbf{A}(\psi) \quad (5.69)$$

As discussed in Ref [3], for a periodic system, the transition matrix can be expressed as

$$\Phi(\psi, \psi_0) = \mathbf{P}(\psi)e^{\mathbf{B}(\psi - \psi_0)} \quad (5.70)$$

where \mathbf{P} is a periodic matrix of period 2π , and $\mathbf{P}(\psi_0) = \mathbf{I}$. The above equation suggests that the exponential decay or growth of the system solution depends on the matrix \mathbf{B} . Define the discrete transition matrix as

$$\mathbf{Q} = \Phi(\psi_0 + 2\pi, \psi_0) \quad (5.71)$$

Using Eqn (5.70), the transition matrix can be written as

$$\mathbf{Q} = e^{2\pi\mathbf{B}} \quad (5.72)$$

Let $\mathbf{\Lambda}$ be the eigenvalue matrix (Jordan form) of \mathbf{B} , and \mathbf{S} be the corresponding modal matrix. Then $\mathbf{B} = \mathbf{S}\mathbf{\Lambda}\mathbf{S}^{-1}$, and

$$e^{\mathbf{B}T} = \mathbf{S}e^{2\pi\mathbf{\Lambda}}\mathbf{S}^{-1} \quad (5.73)$$

Eqns (5.72) and (5.73) yield

$$\mathbf{Q} = \mathbf{S}e^{2\pi\mathbf{\Lambda}}\mathbf{S}^{-1} \quad (5.74)$$

The above equation shows that the \mathbf{S} matrix is also the modal matrix of \mathbf{Q} . The eigenvalue matrix associated with the Floquet transition matrix, \mathbf{Q} , is

$$\mathbf{\Theta} = e^{2\pi\mathbf{\Lambda}} \quad (5.75)$$

Therefore,

$$\mathbf{\Lambda} = \frac{1}{2\pi} \ln \mathbf{\Theta} \quad (5.76)$$

The system is unstable if the real part of any eigenvalue, $Re(\Lambda_i) > 0$.

The Floquet transition matrix \mathbf{Q} can be computed by integrating eqns (5.68) over one time period (2π) starting with the initial conditions given by eqn (5.67). This implies that the k^{th} column of the transition matrix, \mathbf{Q} is obtained by integrating eqns (5.68) over time period 2π with the following initial conditions:

$$\left\{ \begin{array}{c} 0 \\ \vdots \\ 1 \\ \vdots \\ 0 \end{array} \right\} \leftarrow \text{only the } k^{th} \text{ element is unity} \quad (5.77)$$

Either the Gear variable-order method or the Runge-Kutta method can be used for time integration.

Let the k^{th} eigenvalue of the Floquet transition matrix be

$$\theta_k = Re(\theta_k) + iIm(\theta_k) = e^{(\alpha_k+i\omega_k)2\pi} \quad (5.78)$$

The eigenvalues of \mathbf{B} , which define the system stability are, in view of eqn (5.76), given by

$$\alpha_k = \frac{1}{2\pi} \ln \sqrt{(Re(\theta_k))^2 + (Im(\theta_k))^2} \quad (5.79)$$

$$\omega_k = \frac{1}{2\pi} \tan^{-1} \left(\frac{Im(\theta_k)}{Re(\theta_k)} \right) \pm \Omega n; \quad n = 0, 1, 2, \dots \quad (5.80)$$

where α_k , and ω_k are respectively the decay rate and Floquet stability frequency of the k^{th} mode. Note that the frequency given by (5.80) is multivalued; it consists of the principal part, $\frac{1}{2\pi} \tan^{-1} \left(\frac{Im(\theta_k)}{Re(\theta_k)} \right)$, and a multiple of the fundamental frequency (rotor rotational speed). Determining the multiple n , which results in the right stability frequency, requires additional effort. One way is to use the constant coefficient approach, discussed in the next section. It provides a

reasonably accurate estimate of the frequency of the desired mode. Another approach may be to interpret the modes associated with the Floquet transition matrix. The k th mode is unstable if $\alpha_k > 0$, and the percent damping of the k th mode is simply

$$(\%damping)_{k\text{th mode}} = \frac{-\alpha_k}{\omega_k} \quad (5.81)$$

It should be noted that the Floquet method is applicable to the system equations, $\dot{\mathbf{Y}} = \mathbf{AY}$, whether these are in the rotating frame or the fixed frame. However, using this method in the fixed frame increases the size of the state vector by a factor of N_b (since all the blades need to be considered simultaneously in the fixed frame).

5.2.6 Constant Coefficient Approximation

The Floquet transition method provides the decrement ratio and the frequency of the stability modes as discussed in the previous section. However, due to the nature of the Floquet solution, the frequencies do not directly represent the physical frequencies of the stability modes. To aid in the identification of the actual frequencies, and also to get a quick estimate of the system stability characteristics, a constant coefficient approximation can be used. This simply requires averaging the fixed-frame system stability matrix over the time period of the system, i.e.,

$$\mathbf{A}_{CC} = \frac{1}{2\pi} \int_0^{2\pi} \mathbf{A}(\psi)_{FX} d\psi \approx \frac{1}{N_{CC}} \sum_{i=1}^{N_{CC}} \mathbf{A}_{FX}(\psi_i) \quad (5.82)$$

The matrix \mathbf{A}_{CC} cannot capture the full periodic behavior of the system; it can only approximate it. To better represent the system, the constant coefficient approximation must be introduced in the fixed frame [3]. If the rotating frame is used, the mean values of the aerodynamic coefficients associated with the advance ratio, μ , would disappear. On the other hand, the mean values of the aerodynamic coefficients in the fixed frame retain some of the higher harmonics of the aerodynamic coefficients in the rotating frame. For advance ratios below 0.3, constant coefficient approximation appears adequate.

The real part of an eigenvalue of the the constant coefficient matrix, \mathbf{A}_{CC} , provides the modal decrement ratio (identical to the Floquet decrement ratio). However, unlike its Floquet counterpart, the imaginary part of the eigenvalue of \mathbf{A}_{CC} directly represents the actual stability mode frequency in the fixed frame.

Floquet theory is a general method for linear, periodic equations and is independent of the reference frame. The rotor equations of motion are generally expressed in the fixed frame, and analyzed using Floquet theory. Transforming the equations to the fixed frame is useful when fuselage motion and/or dynamic inflow are included in the formulation.

5.3 Transient Perturbation Methods

The above method for determining the blade stability requires linearization of equations about a steady-state solution. It approximates the nonlinear forces, and therefore cannot adequately represent flow separation and dynamic stall effects. The use of a transient technique allows the inclusion of the nonlinear

aerodynamic models without any approximation or linearization. The complete nonlinear rotor normal mode equations are expressed as

$$\mathbf{M}(\psi)\ddot{\mathbf{p}} + \mathbf{C}(\psi)\dot{\mathbf{p}} + \mathbf{K}(\psi)\mathbf{p} = \mathbf{F}(\psi) \quad (5.83)$$

where \mathbf{F} contains constant and non-linear forcing, including non-linear unsteady aerodynamic contributions. This equation is transformed into first order form as,

$$\dot{\mathbf{X}} = \mathbf{T}\mathbf{X} + \mathbf{H} \quad (5.84)$$

where

$$\mathbf{X} = [\mathbf{p} \quad \dot{\mathbf{p}}]^T \quad (5.85)$$

$$\mathbf{T} = \begin{bmatrix} \mathbf{0} & \mathbf{I} \\ -\mathbf{M}^{-1}\mathbf{K} & -\mathbf{M}^{-1}\mathbf{C} \end{bmatrix} \quad (5.86)$$

$$\mathbf{H} = [\mathbf{0} \quad \mathbf{F}]^T \quad (5.87)$$

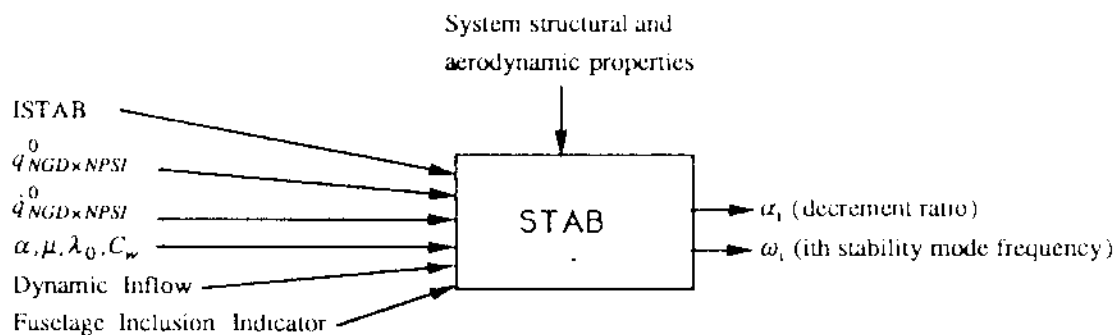
These are numerically integrated in time as an initial value problem. If the system is unperturbed, this method regenerates the trimmed modal response, equivalent to the temporal finite element solution. To determine modal damping values, the system controls are perturbed, and the resulting transient response is analyzed using a Moving-Block analysis [4] or some other modal identification technique [5]. The controls are perturbed using a sinusoidal forcing function at the frequency of the mode of interest. The magnitude of this perturbation is prescribed (typically 0.3 to 0.7 degrees). After several rotor revolutions, the

perturbation is set to zero, and the resulting transient response is analyzed [6]. The magnitude of the perturbation is kept small so that the transient accurately represents the damping at the prescribed flight condition. For a linear system, the magnitude of the perturbation is not important. However, for a system with nonlinearities, the magnitude of the perturbation could have an effect on the resulting damping values. The analysis can be used with any of the aerodynamic and wake models in the formulation; i.e. quasi-steady aerodynamics, linear unsteady aerodynamics, or non-linear unsteady aerodynamics; linear inflow, prescribed wake, or free wake, in any combination. One final note, the inflow field is taken from converged value of the coupled trim-response analysis, is assumed to be fixed throughout the perturbation and the transient response. Since the perturbation is kept small, this should not have a significant effect on the results. Since computationally feasible, transient, time-domain wake models are not yet available, this limitation is unavoidable.

5.4 Implementation in UMARC

The Stability chart shown in Fig.5.1 identifies the routines involved in the stability analysis. Each routine is called by its parent routine to perform a specialized subtask. Detailed performance of each routine is now discussed.

SUBROUTINE STAB



Function:

- Update the rotating blade natural modes.
- Interpret the user-supplied flags ISTAB and IROT to identify the type of stability analysis and assign the system degrees of freedom.

ISTAB = 1 : quasi-steady Floquet stability in rotating frame (for isolated blade in rotating frame)

= 3 : quasi-steady constant coefficient (rotor and/or fuselage and/or dynamic inflow)

= 4 : quasi-steady Floquet stability (rotor and/or fuselage)

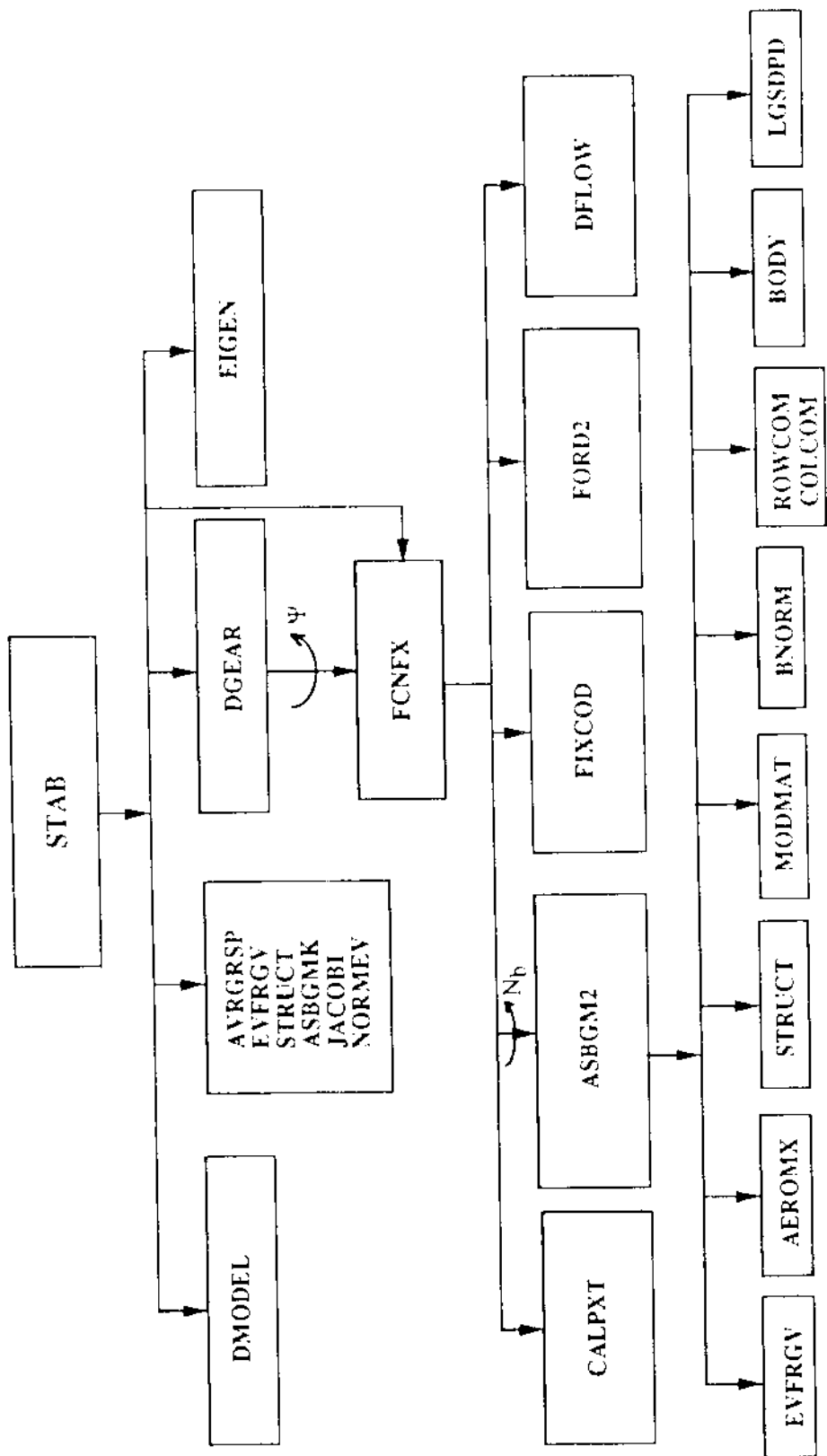


Fig. 5.1 Stability Analysis Structure Chart

- and/or dynamic inflow) in fixed or rotating frame
 = 5 : linear unsteady Floquet stability in rotating frame (for
 isolated blade in rotating frame)
 = 6 : transient stability analysis; linear unsteady aerodynamics
 = 7 : transient stability analysis; nonlinear unsteady aerodynamics
 IROT = 1 : stability analysis in rotating frame
 = 0 : stability analysis in fixed frame
- c) If linearized system analysis is required, obtain the stability matrix, \mathbf{A} .
 - d) If Floquet method is requested, obtain the transition matrix, \mathbf{Q} ,
and compute its eigenvalues.
 - e) If constant coefficient approximation is requested,
average the stability matrix over one rotor revolution and
compute the eigenvalues of the averaged matrix, \mathbf{A}_{cc} .
 - f) If transition perturbation method is requested, specify rotor control
history, $\boldsymbol{\theta}(t)$, compute the transient response.

Inputs:

- a) ISTAB = flag indicating stability analysis type
- b) IROT = flag indicating reference frame for stability
analysis (used only if ISTAB=4)
- c) INDFUS = 1: include fuselage degrees of freedom
=0: do not include fuselage degrees of freedom

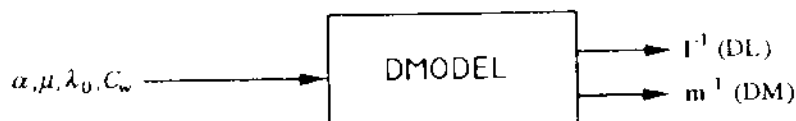
- d) BODYS = Vector defining the body modes to be used in stability analysis
- e) IDYNF = 1; include dynamic inflow model
=0; do not include dynamic inflow model
- f) AKS(NGD,NPSI) = trimmed blade displacements, q_0
- g) ACS(NGD,NPSI) = trimmed blade velocities, \dot{q}_0
- h) Blade properties, fuselage properties, aerodynamic properties.

Outputs:

- a) ALPHAR = decrement ratio for the i^{th} mode
- b) FREQ = frequency per rev of the i^{th} mode
- c) I = i^{th} stability mode.

Performance:

- 1) Compute I and m if dynamic inflow model is requested (IDYN=1).



- 2) Set unsteady aerodynamic flags:

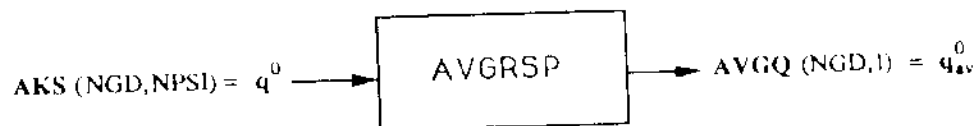
- If linearized system analysis requested (ISTAB =4), switch off the unsteady aero flags (IUNCIR, IUNIMP, IUNDRC, IUNMOM, ITESEP, IVORTX = 0).
- If ISTAB=5 (linear unsteady aero, Floquet method in rotating frame),

turn on the linear perturbation aero flag ILUPRT to 1.

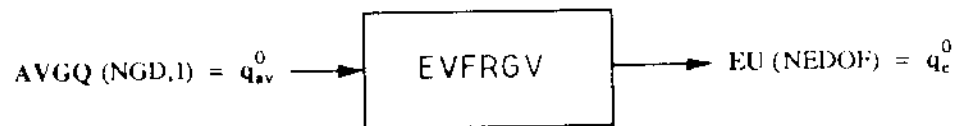
- If ISTAB=6 (transient perturbation method using linear unsteady aero),
turn off the nonlinear unsteady aero flags (ITSESEP, IVORTX=0).

3) Update blade natural modes about the trimmed state deflections:

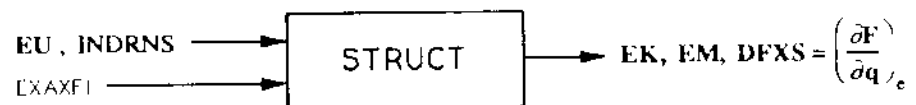
- Call AVGRSP to compute blade averaged response over one cycle,



- Set flag INDRNS=2 to indicate to routine STRUCT that only **GM** and **GK** (blade global mass and stiffness matrices) are to be updated.
Initialize **GM(NGD,NGD)** and **GK(NGD,NGD)**.
- Enter the element loop (I=1,NSELT).
- Call EVFRGV to obtain elemental displacement vector from the global displacement vector.

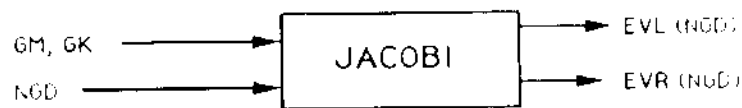


- Call STRUCT to compute the elemental mass and stiffness matrices:



$$[EK] = [EK] \cdot [DFXS]$$

- If BMR blade is selected, modify the torque tube boundary element to accommodate the boundary conditions. If the pitch link is soft (LSFT=1), include its stiffness in the blade stiffness matrix.
- Call ASBGMK to assemble the elemental EM and EK matrices.
- End blade element loop.
- For articulated blade configuration (IARTIC= 2 or 3), include lag spring stiffness.
- Call JACOBI to compute the blade eigenvalues and eigenvectors:



- Call NORMEV to normalize the mode shapes.
- 4) If Floquet method is requested (ISTAB = 1 or 4), compute the state transition matrix, TM :

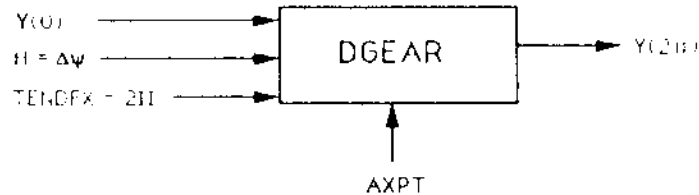
- Form a column vector \mathbf{Y}^0 as $\mathbf{Y}^0 = \begin{Bmatrix} \mathbf{e}_1 \\ \mathbf{e}_2 \\ \vdots \\ \mathbf{e}_{NFXD} \end{Bmatrix}$

$$\text{where } \mathbf{e}_i = \begin{Bmatrix} 0 \\ \vdots \\ 1 \\ \vdots \\ 0 \end{Bmatrix} \leftarrow \text{only the } i^{\text{th}} \text{ element is unity}$$

- Call the integration routine DGEAR to integrate the system

equations $\dot{\mathbf{Y}} = [\mathbf{AXPT}]\mathbf{Y}$ with initial conditions, \mathbf{Y}^0 .

Note that DGEAR calls the external routine FCNFX to compute the stability matrix $\mathbf{AXPT}(\phi)$.



- Form the state transition matrix,

$$\mathbf{Y}(2\pi) \Rightarrow \text{TMFX}(NFXD, NFXD)$$

- Call EIGEN to compute eigenvalues of the transition matrix:



- Compute ALPHAR = $\sigma = \frac{1}{4\pi} \ln |\lambda_Q|^2 = \frac{1}{2\pi} \ln |\lambda_Q|$

$$\text{FREQ} = \omega = \frac{1}{2\pi} \tan^{-1} \left(\frac{\text{Im}(\theta_k)}{\text{Re}(\theta_k)} \right)$$

Print ALPHAR and FREQ

5) If ISTAB=3, (Const coeff approximation, quasisteady aero, fixed frame):

- Set flag INDRNS=2

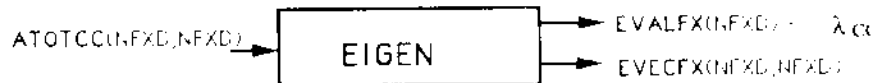
(i.e., flag to compute EM, EC, EK matrices for stability).

Initialize $\text{ATOTCC}(\text{NFXD}, \text{NFXD}) = \mathbf{A}_{cc} = \mathbf{0}$.

- Set the ψ -loop over NPSICC points. For each ψ_i , call FCNFX to compute $\text{AMATCC}(\psi_i)$, $i = 1, NPSICC$.
- Compute the constant coefficient matrix, \mathbf{A}_{cc} :

$$\begin{aligned}\mathbf{A}_{cc} &= \text{ATOTCC} = \frac{1}{2\pi} \int_0^{2\pi} \text{AMATCC}(\psi) d\psi \\ &\approx \frac{1}{NPSICC} \sum_{i=1}^{NPSICC} \text{AMATCC}(\psi_i)\end{aligned}$$

- Call EIGEN to compute eigenvalues of the constant coefficient matrix, ATOTCC .



- Compute $\alpha = ALPHAR = Re(\lambda_{cc})$

$$\omega = FREQ = Im(\lambda_{cc})$$

Print α, ω .

- If ISTAB=5, compute the Floquet transition matrix for isolated blade in the rotating frame (use linear unsteady aerodynamics).
- If ISTAB=6, compute the blade transient response using linear unsteady aerodynamics.
- If ISTAB=7, compute the blade transient response using nonlinear unsteady aerodynamics.

- Return to the parent routine, EXEC.

SUBROUTINE DGEAR

Function:

- Integrate $\dot{\mathbf{Y}} = \mathbf{A}\mathbf{Y}$ to output $\mathbf{Y}(2\pi)$, given $\mathbf{Y}(0) = \{\mathbf{I}\}$



Inputs:

- NFDX2 = (NFDX)²
- PSI0FX = $\psi(0) = 0$
- H = $\Delta\psi$ = time step
- TOL, METH, MITER, INDEX (see **DGEAR** coding)
- $\mathbf{Y}(0) = \{\mathbf{I}\}$
- FCNFX** = name of the external routine that computes $\dot{\mathbf{Y}} = \mathbf{A}\mathbf{Y}$

Output :

- $\mathbf{Y} = \{\mathbf{Y}(2\pi)\}$

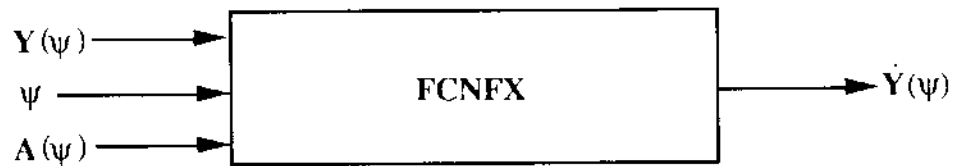
Performance:

- Solve the differential equation $\dot{\mathbf{Y}} = \mathbf{A}\mathbf{Y}$, provided by the routine **FCNFX**, using the variable-step Gears method.

SUBROUTINE FCNFX

Function:

- Obtain the stability matrix, $\mathbf{A}(\psi)$
- Compute $\dot{\mathbf{Y}} = \mathbf{A}\mathbf{Y}$



Inputs:

- a) $N = \text{size of the } \{Y\} \text{ vector} = (\text{system dof})^2$
- b) $\text{PSI} = \psi$
- c) $\mathbf{Y} = \{Y(\psi)\}$

Outputs:

$$\bullet \mathbf{Y} = \dot{\mathbf{Y}}(\psi)$$

Performance:

- a) Restrict ψ within $(0, 2\pi)$ range, i.e., if $\psi > 2\pi$, $\psi = \psi - 2\pi$.

Initialize matrices.

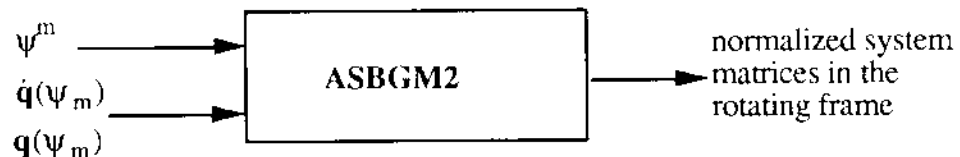
- b) Start blade loop.

- i) Call **CALXPT** to extract the blade global physical displacement vector, \mathbf{q} , and the global velocity vector, $\dot{\mathbf{q}}$, from the saved trimmed values.



In the block diagram above, m refers to the m^{th} blade.

- ii) Call **ASBGM2**



to obtain the system normalized mass, damping and stiffness matrices (see Eqn. (5.32), Theory Manual).

Code	Theory Manual
$\begin{bmatrix} \mathbf{PM} & \mathbf{PMA} & \mathbf{0} \\ \mathbf{PTM} & \mathbf{PMH} + \mathbf{PUM} & \mathbf{0} \\ \mathbf{0} & \mathbf{0} & \mathbf{0} \end{bmatrix}$	$= \begin{bmatrix} \overline{\mathbf{M}}_{bb} & \overline{\mathbf{M}}_{bf} & \mathbf{0} \\ \overline{\mathbf{M}}_{fb} & \mathbf{M}_{ff} & \mathbf{0} \\ \mathbf{0} & \mathbf{0} & \mathbf{0} \end{bmatrix}$
$\begin{bmatrix} \mathbf{PC} & \mathbf{PCA} & \mathbf{0} \\ \mathbf{PTC} & \mathbf{PCH} + \mathbf{PTP} & \mathbf{0} \\ \mathbf{PC1} & \mathbf{PC2} & \mathbf{0} \end{bmatrix}$	$= \begin{bmatrix} \overline{\mathbf{C}}_{bb} & \overline{\mathbf{C}}_{bf} & \mathbf{0} \\ \overline{\mathbf{C}}_{fb} & \mathbf{C}_{ff} & \mathbf{0} \\ \overline{\mathbf{C}}_{lb} & \mathbf{0} & \mathbf{C}_{ll} \end{bmatrix}$
$\begin{bmatrix} \mathbf{PK} & \mathbf{PKA} & \mathbf{PK2} \\ \mathbf{PTK} & \mathbf{PKH} & \mathbf{PKK} \\ \mathbf{PK1} & \mathbf{0} & \mathbf{PKK} \end{bmatrix}$	$= \begin{bmatrix} \overline{\mathbf{K}}_{bb} & \overline{\mathbf{K}}_{bf} & \overline{\mathbf{K}}_{bl} \\ \overline{\mathbf{K}}_{fb} & \mathbf{K}_{ff} & \mathbf{0} \\ \overline{\mathbf{K}}_{lb} & \mathbf{0} & \mathbf{K}_{ll} \end{bmatrix}$

iii) If stability analysis is required in the rotating frame, call **FIXCOD** to transform the system matrices from the rotating frame to the fixed frame. Fixed-frame mass, damping and stiffness matrices, as they appear in **UMARC**, are shown in the left hand column below.

$\begin{bmatrix} \mathbf{AMS} & \mathbf{PMAF} & \mathbf{0} \\ \mathbf{PTMF} & \mathbf{PMHS} & \mathbf{0} \\ \mathbf{0} & \mathbf{0} & \mathbf{0} \end{bmatrix}$	\leftarrow mass matrix \rightarrow	$\begin{bmatrix} & & \\ & & \\ & & \end{bmatrix}$
$\begin{bmatrix} \mathbf{ACS} & \mathbf{PCAF} & \mathbf{0} \\ \mathbf{PTCF} & \mathbf{PCMS} & \mathbf{0} \\ \mathbf{PC1F} & \mathbf{PC2F} & \mathbf{0} \end{bmatrix}$	\leftarrow damping matrix \rightarrow	$\begin{bmatrix} & & \\ & & \\ & & \end{bmatrix}$
$\begin{bmatrix} \mathbf{AKS} & \mathbf{PKAF} & \mathbf{PK2F} \\ \mathbf{PTKF} & \mathbf{PKHS} & \mathbf{PKKF} \\ \mathbf{PK1F} & \mathbf{0} & \mathbf{PKKF} \end{bmatrix}$	\leftarrow stiffness matrix \rightarrow	$\begin{bmatrix} & & \\ & & \\ & & \end{bmatrix}$

iv) Compute ψ for the next blade and return to the blade loop if $m \geq N_b$. If $m > N_b$, exit the blade loop.

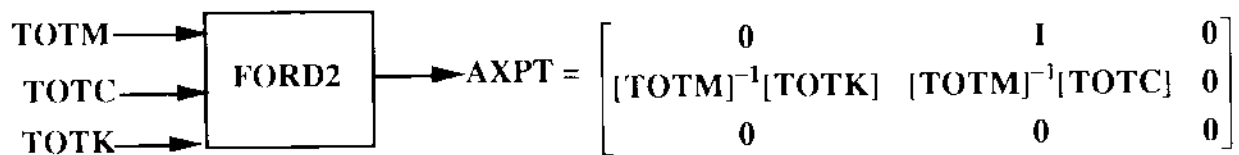
c) Assign rotor-fuselage equations to matrices **TOTM**, **TOTC**, and **TOTK**.

$$\begin{bmatrix} \text{AMS} & \text{PMAF} \\ \text{PTMF} & \text{PMHS} \end{bmatrix} \Rightarrow [\text{TOTM}]$$

$$\begin{bmatrix} \text{ACS} & \text{PCAF} \\ \text{PTCF} & \text{PCHS} \end{bmatrix} \Rightarrow [\text{TOTC}]$$

$$\begin{bmatrix} \text{AKS} & \text{PKAF} \\ \text{PTKF} & \text{PKHS} \end{bmatrix} \Rightarrow [\text{TOTK}]$$

d) Call **FORD2** to compute $[\text{TOTM}]^{-1}[\text{TOTC}]$, $[\text{TOTM}]^{-1}[\text{TOTK}]$ and store these in matrix **[AXPT]**, which will later become the first-order system matrix.



The size of the **AXPT** matrix is (NFXD, NFXD).

e) Call **DFLOW** to get additional dynamic inflow dependent terms and store them in **[AXPT]**, the system stability matrix.

f) If constant coefficient approximation is required (**ISTAB** = 3), assign **[AXPT]** to extended column vector, **{Y}**.

$$[\text{AXPT}(\text{NFXD}, \text{NFXD})] \rightarrow \{Y\}_{\text{NFXD}^2 \times 1}$$

g) If Floquet stability analysis is required (**ISTAB** = 4), compute
 $\dot{Y} = [\text{AXPT}]Y$

h) Return to the calling routine **DGEAR** (if **ISTAB** = 4) or **STAB**(if **ISTAB** = 3).

SUBROUTINE CALXPT

Function :

- Extract $\mathbf{q}^0(\psi^m)$ and $\dot{\mathbf{q}}^0(\psi^m)$ for the m^{th} blade from the saved trimmed blade response values.

Inputs:

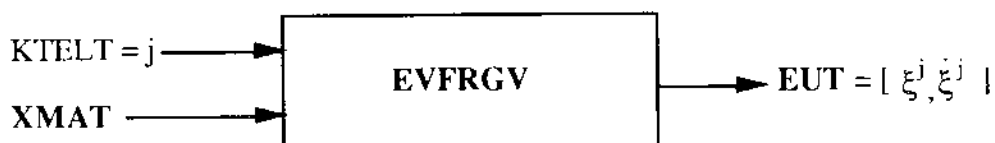
- $\mathbf{XMAT} = [\xi^G, \dot{\xi}^G]$ = vector of blade normalized trimmed displacements and velocities saved at the global time nodes.
- Ψ^m = azimuthal location of the m^{th} blade.

Outputs:

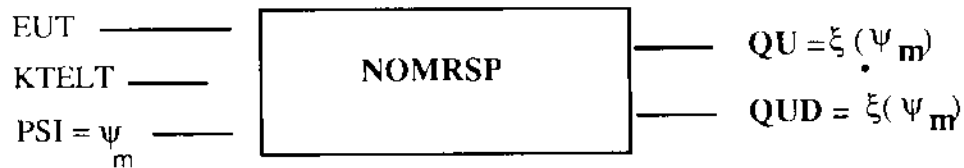
- $\mathbf{GU(NGD)} = \mathbf{q}(\psi^m)$ = blade geometric displacements at ψ^m .
- $\mathbf{GUD(NGD)} = \dot{\mathbf{q}}(\psi^m)$ = blade velocities at ψ^m .

Performance:

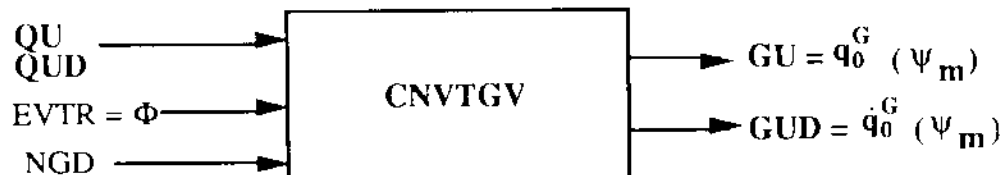
- Determine the time element number, j (=KTELT), which encloses the azimuth location ψ^m .
- Call **EVFRGV** to extract the blade modal (i.e., normalized) displacements at the time nodes of the j^{th} time element.



- Call **NOMRSP** to extract the blade modal displacements, ξ , and modal velocities, $\dot{\xi}$, at time ψ_m .



d) Call **CNVTGV** to extract the blade modal displacements and velocities (physical).

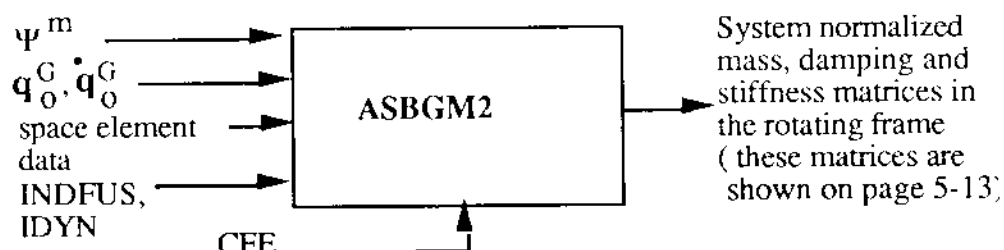


Note that the suffix ()₀ refers to the trimmed state.

SUBROUTINE ASBGM2

Functions :

- a) For a blade located at azimuth, Ψ^m , obtain the system normalized mass, damping and stiffness matrices.



Inputs :

- a) $\text{PSI} = \Psi^m$
- b) $\text{GU}, \text{GUD} = q_0^G, \dot{q}_0^G$
- c) INDFUS
- d) IDYN

- e) CFE : column vector of size NSELT; i^{th} entry in this vector represents centrifugal force acting on the left side of the blade element i (see fig 2.6)
- f) Space finite element data.

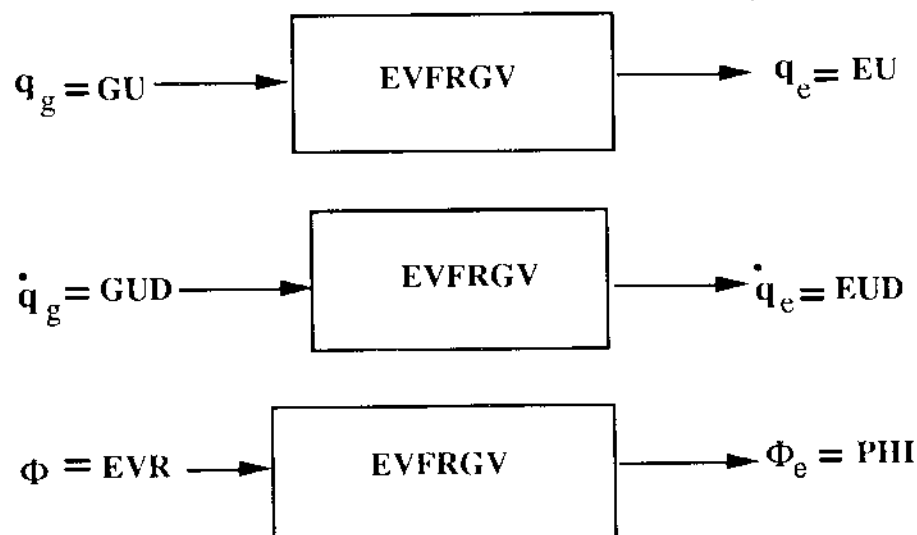
Outputs :

- a) Normalized mass, damping and stiffness matrices (see Eqn. 5.32)

Performance :

- a) Enter the space element loop ($i = 1, \text{NSELT}$)

i) Call **EVFRGV** thrice : to obtain the i element displacement vector, \mathbf{q}_e ; element velocity vector, $\dot{\mathbf{q}}_e$; and the element model matrix , Φ_e (NDOF, NMODES).

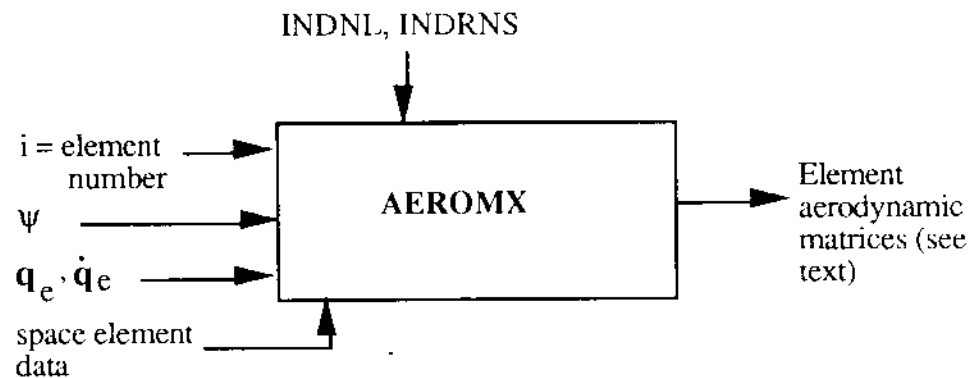


- ii) Call **AEROMX** to compute the following aerodynamic matrices for the i -th element ;
- EK = blade linear stiffness matrix
 - EC = blade linear damping matrix
 - EM = blade linear mass matrix
 - ECAA = blade-fuselage damping matrix
 - EKAA = blade-fuselage stiffness matrix
 - EMFB = fuselage-blade mass matrix

ECFB = fuselage-blade damping matrix
 EKFB = fuselage-blade stiffness matrix
 ECAA = blade-fuselage damping matrix
 ECFF = fuselage damping matrix
 EKFF = fuselage stiffness matrix
 DK2 = blade-inflow stiffness matrix
 DC1 = inflow-blade damping matrix
 DK1 = inflow-blade stiffness matrix
 DC2 = inflow-fuselage damping matrix
 ECCL = inflow-fuselage damping matrix

$$DFX = \left(\frac{\partial F}{\partial q} \right)_e = \text{blade nonlinear stiffness matrix}$$

$$DFXD = \left(\frac{\partial F}{\partial \dot{q}} \right)_e = \text{blade nonlinear damping matrix}$$



iii) Call STRUCT to compute the following structural matrices for the i th element :

EKP = blade linear stiffness matrix martix
 ECP = blade linear damping matrix
 EMP = blade linear mass matrix

$$DFXS = \left(\frac{\partial F}{\partial q} \right)_e = \text{blade nonlinear stiffness matrix}$$

EMAS = blade-fuselage mass matrix

ECAS = blade-fuselage damping matrix

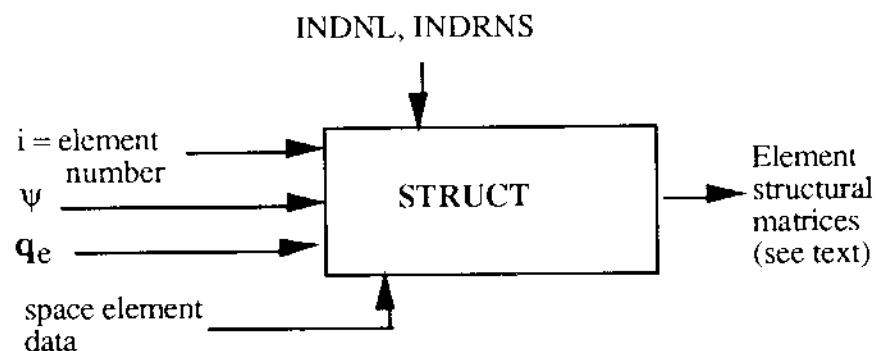
TMS = fuselage-blade mass matrix

TCS = fuselage-blade damping matrix

TKS = fuselage-blade stiffness matrix

TPS = fuselage damping matrix (from rotor)

UMS = fuselage mass matrix (from rotor)



iv) Add aerodynamic and structural matrices.

EMA = EMAS

ECA = ECAA + ECAS

EKA = EKAA

TM = TMS + EMFB

TC = TCS + ECFB

TK = TKS + EKFB

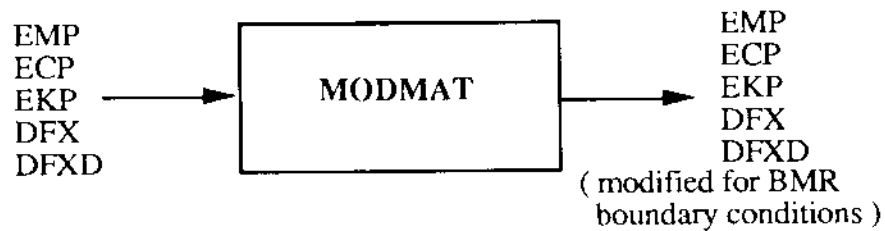
UM = UMS

TP = TPS + ECFF

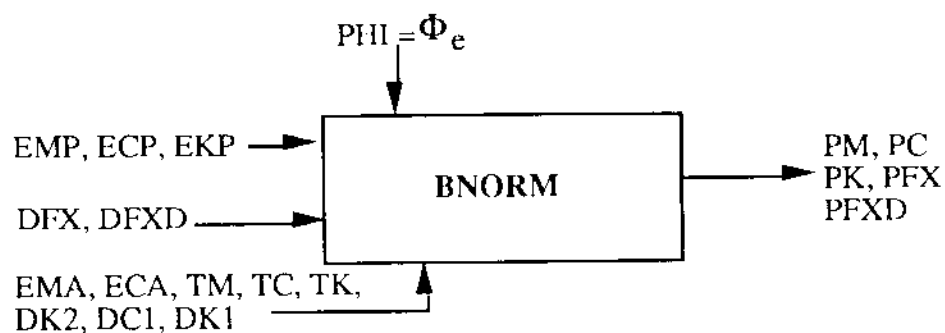
UK = EKFF

v) If BMR blade is requested and ith element is the torque tube element

(i.e. the last element), call BMRMOD to modify the elemental matrices in accordance with the boundary conditions at the torque tube end.



vi) Call BNORM to normalize the elemental matrices and assemble them into modal matrices :



vii) If pitch link is flexible (LSFT = 1), modify the element stiffness matrix.

viii) If INDFUS =1, normalize the balde-fuelage matrices (EM, ECA) and the fuselage martices (TM, TC, TK) :

$$\begin{aligned}
 [PMA] &= [\Phi^i]^T [EMA] \\
 [PCA] &= [\Phi^i]^T [ECA] \\
 [PTM] &= [TM] [\Phi^i] \\
 [PTC] &= [TC] [\Phi^i]
 \end{aligned}$$

$$[PTK] = [TK][\Phi^i]$$

ix) If IDYN = 1, normalize the blade-inflow matrix (DK2) and the inflow-blade matrices (DC1, DK1) :

$$[PK2] = [\Phi^i]^T [DK2]$$

$$[PC1] = [DC1][\Phi^i]$$

$$[PK1] = [DK1][\Phi^i]$$

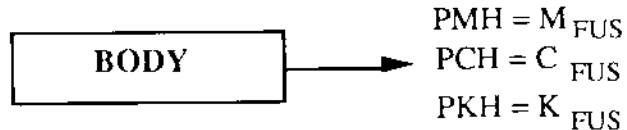
x) Assign the matrices TP, UK and UM to the fuselage damping and mass matrices PTP, PUM, respectively.

The coupled rotor - fuselage - inflow matrices (in normalized form) are listed below along with their names as they appear in the UMARC code and in the theory manual.

Nature of Matrix	Matrix name in the code	Matrix name in Theory Manual
Rotor - Fuselage (mass) (damping)	PMA	M_{bF}
	PCA	C_{bF}
Rotor - Inflow (stiffness)	PK2	$K_{b\lambda}$
Fuselage - Rotor (mass) (damping) (stiffness)	PTM	M_{Fb}
	PTC	C_{Fb}
	PTK	K_{Fb}
Fuselage - Rotor (stiffness)	PKK (upper part)	$K_{F\lambda}$
Fuselage (mass) (damping) (stiffness)	PMH * + PUM	M_F
	PCH * + PTP	C_F
	PKH	K_F
	*	F
Inflow - Rotor (damping) (stiffness)	PC1	$C_{\lambda b}$
	PK1	$K_{\lambda b}$
Inflow (damping) (stiffness)	—	$C_{\lambda\lambda}$
	PKK (lower part)	$K_{\lambda\lambda}$
Inflow - fuselage damping)	PC2	$K_{\lambda f}$

* The matrices PMH,PCH,PHK are computed in steps (b) and (c) which follow.

- xii) Exit the blade element loop.
- b) If INDFUS = 1 (fuselage dof are requested) call BODY to compute **PMH** and **PKH**.



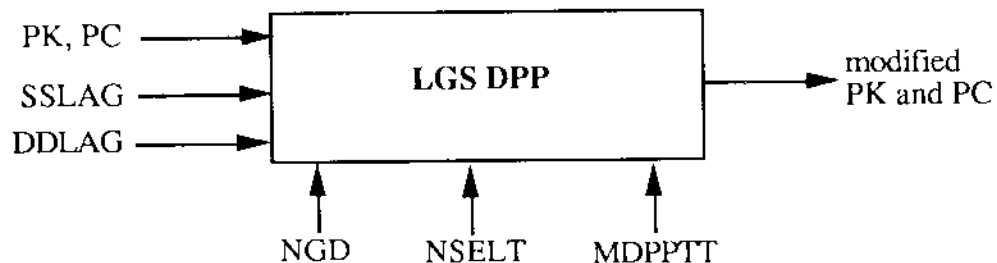
$PCH (NHUB, NHUB) = \text{fuselage structural damping matrix}$
 $= PMH * BDAMP$

where

$$PMH = MFUS = \begin{bmatrix} m_{Fus} & & & \\ & m_{Fus} & & \\ & & m_{Fus} & \\ & & & I_{xx} \\ & & & & I_{yy} \\ & & & & & I_{zz} \end{bmatrix}$$

and BDAMP is the vector of structural damping coefficient.

- c) If the blade is articulated and there is a lag hinge (IARTIC = 2 or 3), call LGSDPP to add lag stiffness and lag damping to the normalized stiffness matrix PK and the normalized damping matrix PC respectively.



In the figure above, SSLAG and DDLAG are respectively the stiffness and damping of the lag damper. MDPPTT = indicators identifying the blade modes used in the perturbation analysis.

- d) Modify the blade normalized stiffness and damping as follows :

$$PK = PK - PFX$$

$$PC = PC - PFXD$$

where PFX and PFXD were obtained in step a(vi).

Bibliography

- [1] Chopra,I., "Perspectives in Aeromechanical Stability of Helicopter Rotors", *Vertica*, Vol. 14, No. 4, 1990, pp. 457-508.
- [2] Pitt,D.M., Peters,D.A., "Theoretical Prediction of Dynamic Inflow Derivatives", *Vertica*, Vol. 5, No. 5, 1981.
- [3] Johnson,W., *Helicopter Theory*, Princeton University Press, 1980.
- [4] Hammond,C.E., Dogget,R., "Demonstration of Subcritical Damping by Moving Block/Randomdec Applications," NASA SP-415, October 1975.
- [5] Tasker,F.A. and Chopra,I., "Assessment of Transient Testing Techniques for Rotor Stability Testing," *Journal of the American Helicopter Society*, Vol. 35, No.1, January 1990.
- [6] Tork,M.S., Chopra,I., "Hingeless Rotor Aeroelastic Stability with Refined Aerodynamic Modeling," *Journal of the American Helicopter Society*, Vol. 36, No.4, October, 1991.

Chapter 6

ADVANCED GEOMETRY ROTORS

Chapter 6

Advanced Geometry Rotor

6.1 Introduction

An improved aeroelastic formulation for advanced geometry blades, involving variable sweep, droop, pretwist and planform, is presented in this chapter. Each blade is composed of an arbitrary number of Euler-Bernoulli-beam type straight segments with different sweep, droop, pretwist and planform taper. The only restriction on blade geometry is that the elastic axis of the undeformed segments form piecewise continuous straight lines. The formulation also covers offsets of blade section tension center, center of mass and aerodynamic center from the elastic axis. Each blade segment is modeled using one or more finite elements and intersegment compatibility relations are satisfied using nonlinear transformations. Hamilton's principle is used in the derivation of the nonlinear blade equations of motion. Quasi-steady strip theory is used for the aerodynamic modeling and the blade loads are calculated using a force summation

method.

This formulation for the advanced geometry blade [1] represents considerable refinements over previous work [2], [3]. These earlier analyses were limited to tip geometry only; the new formulation is applicable to blades with varying sweep, droop and pretwist along the blade-span. Other new features of the analysis include the way time-varying blade pitch control is translated into the flap, lag and pitch motions of the inclined segments as well as a more rigorous derivation of axial degree of freedom and Coriolis forces.

This chapter presents the derivation of expressions for the blade kinetic energy, strain energy, virtual work and the aerodynamic and inertial loads. The equations derived in this chapter are used in Chapter 5 for formulating the analytical sensitivity analysis. The blade geometry is discussed in Section 2.1, the equations of motion for the advanced geometry rotor are derived in Section 2.2, and the aerodynamic and inertial loads are derived in Sections 2.3 and 2.4 respectively. Finally, the hub loads are derived in Section 2.5.

6.2 Blade Geometry

Before equations governing blade dynamics can be derived, blade geometry both in the deformed and undeformed states must be specified. The coordinate systems defining the blade geometry are shown in Fig. 6.1. The nonrotating system attached to the hub has coordinate axes X_{NR} , Y_{NR} and Z_{NR} and the unit vectors along these axes are I_{NR} , J_{NR} and K_{NR} , respectively. The rotat-

ing system attached to the hub has axes X , Y and Z and unit vectors along these axes denoted by I , J and K , respectively. The undeformed main blade coordinate system is attached to the inboard segment and has axes x , y and z and unit vectors i , j and k , respectively. Any k th segment of the blade has a coordinate system x_k , y_k and z_k attached to it and unit vectors are i_k , j_k and k_k , respectively. When the blade undergoes deformation, any arbitrary point P on the elastic axis of the undeformed k th segment is transformed to point P_1 on the elastic axis of the deformed k th segment. The unit vectors along the k th deformed segment are \hat{i}_k , \hat{j}_k and \hat{k}_k , respectively.

6.2.1 Undeformed Blade Geometry

Each segment is assigned a segment coordinate system to describe its orientation with respect to the main blade coordinate system. At the k th intersegment junction, the inboard segment is called segment 1 and the outboard segment is called segment 2 (see Fig. 6.2). Note that both segments 1 and 2 can be arbitrarily configured in space with respect to the undeformed main blade coordinate system. The undeformed main blade reference triad is denoted by $(\hat{i}, \hat{j}, \hat{k})$, the undeformed segment 1 triad is denoted by $(\hat{i}_1, \hat{j}_1, \hat{k}_1)$ and the undeformed segment 2 triad is denoted by $(\hat{i}_2, \hat{j}_2, \hat{k}_2)$. These triads are related through a sequence of transformations involving the sweep, droop, pretwist and pitch-control angles. The transformations defined below are given for both segment 1 and segment 2.

Sweep Transformation

A blade with spanwise variation of sweep only is shown in Fig. 6.3. The undeformed segment 1 and segment 2 have a sweep of Λ_1^1 and Λ_1^2 , respectively, with respect to the main blade. The coordinate transformation from the undeformed main blade coordinate system to the undeformed segment 2 coordinate system with a forward sweep (Λ_1^2 rotation about the \hat{k} -axis) alone is given by:

$$\begin{Bmatrix} \hat{i}_2 \\ \hat{j}_2 \\ \hat{k}_2 \end{Bmatrix} = T_{\Lambda_1}^2 \begin{Bmatrix} \hat{i} \\ \hat{j} \\ \hat{k} \end{Bmatrix} \quad (6.1)$$

where

$$T_{\Lambda_1}^2 = \begin{bmatrix} \cos \Lambda_1^2 & \sin \Lambda_1^2 & 0 \\ -\sin \Lambda_1^2 & \cos \Lambda_1^2 & 0 \\ 0 & 0 & 1 \end{bmatrix} \quad (6.2)$$

and Λ_1^2 is positive for forward tip sweep. For segment 1, the transformation is given as

$$\begin{Bmatrix} \hat{i}_1 \\ \hat{j}_1 \\ \hat{k}_1 \end{Bmatrix} = T_{\Lambda_1}^1 \begin{Bmatrix} \hat{i} \\ \hat{j} \\ \hat{k} \end{Bmatrix} \quad (6.3)$$

where

$$T_{\Lambda_1}^1 = \begin{bmatrix} \cos \Lambda_1^1 & \sin \Lambda_1^1 & 0 \\ -\sin \Lambda_1^1 & \cos \Lambda_1^1 & 0 \\ 0 & 0 & 1 \end{bmatrix} \quad (6.4)$$

where Λ_1^1 is the sweep between the undeformed main blade coordinate system and the undeformed segment 1 coordinate system (positive forward).

Anhedral Transformation

The coordinate transformation, from the undeformed blade coordinate system to the undeformed segment 2 coordinate system, with an anhedral angle alone

(Λ_2^2 rotation about the negative \hat{j} -axis) is given by:

$$\begin{Bmatrix} \hat{i}_2 \\ \hat{j}_2 \\ \hat{k}_2 \end{Bmatrix} = T_{\Lambda_2}^2 \begin{Bmatrix} \hat{i} \\ \hat{j} \\ \hat{k} \end{Bmatrix} \quad (6.5)$$

where

$$T_{\Lambda_2}^2 = \begin{bmatrix} \cos \Lambda_2^2 & 0 & \sin \Lambda_2^2 \\ 0 & 1 & 0 \\ \sin \Lambda_2^2 & 0 & \cos \Lambda_2^2 \end{bmatrix} \quad (6.6)$$

and Λ_2^2 is negative for a droop (downward). For segment 1, the transformation is given as

$$\begin{Bmatrix} i_1 \\ j_1 \\ k_1 \end{Bmatrix} = T_{\Lambda_2}^1 \begin{Bmatrix} \hat{i} \\ \hat{j} \\ \hat{k} \end{Bmatrix} \quad (6.7)$$

where

$$T_{\Lambda_2}^1 = \begin{bmatrix} \cos \Lambda_2^1 & 0 & \sin \Lambda_2^1 \\ 0 & 1 & 0 \\ -\sin \Lambda_2^1 & 0 & \cos \Lambda_2^1 \end{bmatrix} \quad (6.8)$$

where Λ_2^1 is the anhedral angle between the undeformed main blade and the segment 1 coordinate system.

Pretwist Transformation

The coordinate transformation, from the undeformed main blade coordinate system to the undeformed segment 2 coordinate system with pretwist (Λ_3^2 rotation about the \hat{i} -axis), is given by:

$$\begin{Bmatrix} \hat{i}_2 \\ \hat{j}_2 \\ \hat{k}_2 \end{Bmatrix} = T_{\Lambda_3}^2 \begin{Bmatrix} \hat{i} \\ \hat{j} \\ \hat{k} \end{Bmatrix} \quad (6.9)$$

where

$$T_{\Lambda_3}^2 = \begin{bmatrix} 1 & 0 & 0 \\ 0 & \cos \Lambda_3^2 & \sin \Lambda_3^2 \\ 0 & -\sin \Lambda_3^2 & \cos \Lambda_3^2 \end{bmatrix} \quad (6.10)$$

and where Λ_3^2 is positive for nose up pitch. For segment 1, the transformation is given as

$$\begin{Bmatrix} \hat{i}_1 \\ \hat{j}_1 \\ \hat{k}_1 \end{Bmatrix} = \mathbf{T}_{\Lambda_3}^1 \begin{Bmatrix} \hat{i} \\ \hat{j} \\ \hat{k} \end{Bmatrix} \quad (6.11)$$

where

$$\mathbf{T}_{\Lambda_3}^1 = \begin{bmatrix} 1 & 0 & 0 \\ 0 & \cos \Lambda_3^1 & \sin \Lambda_3^1 \\ 0 & -\sin \Lambda_3^1 & \cos \Lambda_3^1 \end{bmatrix} \quad (6.12)$$

where Λ_3^1 is the pretwist angle between the undeformed main blade and the segment 1 coordinate system.

Transformation due to Sweep, Droop and Pretwist

Using Eqs.6.2, 6.6 and 6.10, the transformation between the undeformed blade coordinate system and segment coordinate 2 system with arbitrary sweep, followed by anhedral and then pretwist rotation is obtained as:

$$\begin{Bmatrix} \hat{i}_2 \\ \hat{j}_2 \\ \hat{k}_2 \end{Bmatrix} = \mathbf{T}_{\Lambda_3}^2 \cdot \mathbf{T}_{\Lambda_2}^2 \cdot \mathbf{T}_{\Lambda_1}^2 \begin{Bmatrix} \hat{i} \\ \hat{j} \\ \hat{k} \end{Bmatrix} = \mathbf{T}_{\Lambda}^2 \begin{Bmatrix} \hat{i} \\ \hat{j} \\ \hat{k} \end{Bmatrix} \quad (6.13)$$

where

$$\mathbf{T}_{\Lambda}^2 = \begin{bmatrix} C_1C_2 & S_1C_2 & S_2 \\ -S_1C_3 - C_1S_2S_3 & C_1C_3 - S_1S_2S_3 & C_2S_3 \\ S_1S_3 - C_1S_2C_3 & -C_1S_3 - S_1S_2C_3 & C_2C_3 \end{bmatrix}_2 \quad (6.14)$$

and where C_i and S_i represent $\cos \Lambda_i$ and $\sin \Lambda_i$, respectively ($i = 1$ to 3). The superscript 2 used in the above transformation matrix refers to the segment number to which the transformation applies. Relations between the segment 1 coordinate system and the undeformed blade coordinate system are obtained

using Eq. 6.4, 6.8 and 6.12 as

$$\begin{Bmatrix} \hat{i}_1 \\ \hat{j}_1 \\ \hat{k}_1 \end{Bmatrix} = \mathbf{T}_{A_3}^1 \cdot \mathbf{T}_{A_2}^1 \cdot \mathbf{T}_{A_1}^1 \begin{Bmatrix} \hat{i} \\ \hat{j} \\ \hat{k} \end{Bmatrix} - \mathbf{T}_A^1 \begin{Bmatrix} i \\ j \\ k \end{Bmatrix} \quad (6.15)$$

where

$$\mathbf{T}_A^1 = \begin{bmatrix} C_1C_2 & S_1C_2 & S_2 \\ -S_1C_3 + C_1S_2S_3 & C_1C_3 + S_1S_2S_3 & C_2S_3 \\ S_1S_3 + C_1S_2C_3 & -C_1S_3 + S_1S_2C_3 & C_2C_3 \end{bmatrix}_1 \quad (6.16)$$

The above transformation applies to segment 1 and the sweep, droop and pretwist used in Eq. 6.16 are the angles between the segment 1 and the main blade coordinate systems.

Transformation due to Pitch Control

Besides undergoing sweep, droop and pretwist rotations, the segment associated triad also undergoes pitch-control (θ_0) rotation with respect to the main blade coordinate system.

$$\begin{Bmatrix} \hat{i}_2 \\ \hat{j}_2 \\ \hat{k}_2 \end{Bmatrix} = \mathbf{T}_A^2 \cdot \mathbf{T}_\theta \begin{Bmatrix} \hat{i} \\ \hat{j} \\ \hat{k} \end{Bmatrix} = \mathbf{A}'_2 \begin{Bmatrix} \hat{i} \\ \hat{j} \\ \hat{k} \end{Bmatrix} \quad (6.17)$$

where

$$\mathbf{T}_\theta = \begin{bmatrix} 1 & 0 & 0 \\ 0 & \cos \theta_0 & \sin \theta_0 \\ 0 & -\sin \theta_0 & \cos \theta_0 \end{bmatrix} \quad (6.18)$$

This relation relates the undeformed segment 2 triad to the undeformed main blade reference triad. Note that the transformation is dependent on the blade sweep, droop and pretwist angle as well as *time varying blade pitch control*. The elements of the transformation matrix \mathbf{A}'_2 can be written as:

$$A'_{211} = A_{11}$$

$$\begin{aligned}
\Lambda'_{212} &= \Lambda_{12} \cos \theta_0 - \Lambda_{13} \sin \theta_0 \\
\Lambda'_{213} &= -\Lambda_{12} \sin \theta_0 + \Lambda_{13} \cos \theta_0 \\
\Lambda'_{221} &= -\Lambda_{21} \\
\Lambda'_{222} &= \Lambda_{22} \cos \theta_0 - \Lambda_{23} \sin \theta_0 \\
\Lambda'_{223} &= -\Lambda_{22} \sin \theta_0 + \Lambda_{23} \cos \theta_0 \\
\Lambda'_{231} &= -\Lambda_{31} \\
\Lambda'_{232} &= \Lambda_{32} \cos \theta_0 - \Lambda_{33} \sin \theta_0 \\
\Lambda'_{233} &= -\Lambda_{32} \sin \theta_0 + \Lambda_{33} \cos \theta_0
\end{aligned} \tag{6.19}$$

where Λ_{ij} are the elements of transformation \mathbf{T}_A^2 shown in Eq. 6.14. Similar relations can be derived for segment 1 leading to the transformation matrix $\mathbf{\Lambda}'_1$.

Intersegment Coordinate Transformation

The transformation between the undeformed segment 2 coordinate system and the undeformed main blade coordinate system is given as

$$\begin{Bmatrix} \hat{i}_2 \\ \hat{j}_2 \\ \hat{k}_2 \end{Bmatrix} = \mathbf{T}_A^2 \cdot \mathbf{T}_\theta \begin{Bmatrix} \hat{i} \\ \hat{j} \\ \hat{k} \end{Bmatrix} = \mathbf{\Lambda}'_2 \begin{Bmatrix} \hat{i} \\ \hat{j} \\ \hat{k} \end{Bmatrix} \tag{6.20}$$

Similarly, the undeformed segment 1 coordinate system and the undeformed main blade coordinate system are related by

$$\begin{Bmatrix} \hat{i}_1 \\ \hat{j}_1 \\ \hat{k}_1 \end{Bmatrix} = \mathbf{T}_A^1 \cdot \mathbf{T}_\theta \begin{Bmatrix} \hat{i} \\ \hat{j} \\ \hat{k} \end{Bmatrix} = \mathbf{\Lambda}'_1 \begin{Bmatrix} \hat{i} \\ \hat{j} \\ \hat{k} \end{Bmatrix} \tag{6.21}$$

The above two equations yield,

$$\begin{Bmatrix} \hat{i}_2 \\ \hat{j}_2 \\ \hat{k}_2 \end{Bmatrix} = \mathbf{T}_A^2 \cdot \mathbf{T}_\theta \cdot \mathbf{T}_\theta^T \cdot \mathbf{T}_A^{1T} \begin{Bmatrix} \hat{i}_1 \\ \hat{j}_1 \\ \hat{k}_1 \end{Bmatrix} = \mathbf{T}_s \begin{Bmatrix} \hat{i}_1 \\ \hat{j}_1 \\ \hat{k}_1 \end{Bmatrix} \quad (6.22)$$

where

$$\mathbf{T}_s = \mathbf{T}_A^2 \cdot \mathbf{T}_A^1 \quad (6.23)$$

The intersegment transformation matrix \mathbf{T}_s , which relates the undeformed segment 1 coordinate system to the undeformed segment 2 coordinate system, is independent of the pitch control θ_0 , due to the orthogonality of the \mathbf{T}_θ matrix.

6.2.2 Deformed Blade Geometry

The flexibility of rotor blades causes them to undergo elastic deflections about the undeformed position. To derive the blade equations, it is necessary to define the position vector of an arbitrary point on the deformed blade and to formulate transformations between the undeformed and deformed frame. For a segment undergoing deformations in the axial (u_e), lag (v), flap (w) and torsion (ϕ) directions, the transformation matrix between the deformed and undeformed frame attached to segment 2 can be defined as

$$\begin{Bmatrix} \xi_2 \\ \eta_2 \\ \zeta_2 \end{Bmatrix} = \mathbf{T}_2 \begin{Bmatrix} \hat{i}_2 \\ \hat{j}_2 \\ \hat{k}_2 \end{Bmatrix} \quad (6.24)$$

where

$$\mathbf{T}_2 = \begin{bmatrix} 1 - \frac{v_e'^2}{2} & \frac{w_e'^2}{2} & v_2' \\ -v_2' C_2 + w_2' S_2 & (1 - \frac{v_e'^2}{2}) C_2 - v_2' w_2' S_2 & S_2(1 - \frac{w_e'^2}{2}) \\ v_2' S_2 + w_2' C_2 & -(1 - \frac{v_e'^2}{2}) S_2 - v_2' w_2' C_2 & C_2(1 - \frac{w_e'^2}{2}) \end{bmatrix} \quad (6.25)$$

$$\begin{aligned} S_2 &= \sin \theta_2 \\ C_2 &= \cos \theta_2 \end{aligned} \quad (6.26)$$

and

$$\theta_2 = \theta_{t_2}(s_2) + \phi_2(s_2) - \int_0^{s_2} w'_2 v''_2 ds_2 - \theta_{t_2}(0) - \phi_2(0) + \theta_2(0) \quad (6.27)$$

Note that w_{t_2}, v_2, w_2 and ϕ_2 are deflections in segment 2, s_2 is the local coordinate along segment 2 and θ_{t_2} is the blade twist. In earlier formulations of the advanced geometry blade, the pitch control θ_0 was included in the \mathbf{T}_2 transformation matrix and the effects of time varying pitch control along the azimuthal direction were included in an approximate manner. In the new formulation presented here, the pitch control is included in the transformation between the blade reference frame and the undeformed frame, \mathbf{A}' (see Eq. 6.19). Therefore, for the formulation presented here, the transformation between the undeformed and deformed frames (\mathbf{T}_2) is independent of the pitch control.

For segment 1, the transformation between the undeformed and deformed frame is given as

$$\begin{Bmatrix} \dot{\xi}_1 \\ \dot{\eta}_1 \\ \dot{\zeta}_1 \end{Bmatrix} = \mathbf{T}_1 \begin{Bmatrix} \dot{i}_1 \\ \dot{j}_1 \\ \dot{k}_1 \end{Bmatrix} \quad (6.28)$$

where \mathbf{T}_1 is the same as \mathbf{T}_2 with subscript 2 replaced by 1 in Eq. 6.25.

For simplicity of notation, we define a shorthand for the undeformed and deformed coordinate systems. For example, for segment 2, U_2 are the deformations in the undeformed system and D_2 are the deformations in the deformed system.

Since the deformation variables for segment 1 and 2 must satisfy compatibility conditions at the junction, for the k th junction;

$$\begin{aligned} U_2 &= \mathbf{T}_s U_1 \\ D_{2k} &= \mathbf{T}_s D_{1k} \end{aligned} \quad (6.29)$$

where it is assumed that the built-in angle between the adjoining segments (and therefore \mathbf{T}_s) is retained after transformation. Between elements, there is a continuity of displacement for the elastic twist and axial, lag and flap deflections, and continuity of slope for flap and lag bending. The relation between the translational degrees of freedom between two elements are linear and is given as

$$\left\{ \begin{array}{c} u_{r2} \\ v_2 \\ w_2 \end{array} \right\}_k = \mathbf{T}_s \left\{ \begin{array}{c} u_{r1} \\ v_1 \\ w_1 \end{array} \right\}_k \quad (6.30)$$

The relations between the bending slopes and twist in segments 1 and 2 involve nonlinear transformations and is derived below. At the junction between segments 1 and 2 the transformation between the undeformed and deformed frames are

$$\begin{aligned} D_{2k} &= \mathbf{T}_{2k}(v'_{2k}, w'_{2k}, \theta_{2k}) U_{2k} \\ D_{1k} &= \mathbf{T}_{1k}(v'_{1k}, w'_{1k}, \theta_{1k}) U_{1k} \end{aligned} \quad (6.31)$$

Using Eq. 6.29 and Eq. 6.31, we obtain the following identity which relates the deformations in segments 1 and 2.

$$\begin{aligned} D_{2k} &= \mathbf{T}_s D_{1k} = \mathbf{T}_s \mathbf{T}_{1k} U_1 = \mathbf{T}_s \mathbf{T}_{1k} \mathbf{T}_s^T U_2 \\ &= \mathbf{T}_s \mathbf{T}_{1k} \mathbf{T}_s^T \mathbf{T}_{2k}^T D_{2k} \end{aligned} \quad (6.32)$$

or

$$\mathbf{T}_{2k} = \mathbf{T}_s \mathbf{T}_{ik} \mathbf{T}_s^T \quad (6.33)$$

The above equation represents the transformation between the variables (v_2^t, w_2^t, θ_2) and (v_1^t, w_1^t, θ_1) at the inter-segment junction. In terms of the deformations, the above equation can be written as

$$\begin{Bmatrix} \theta_2 \\ w_2^t \\ v_2^t \end{Bmatrix}_k = (\mathbf{T}_A^* + \bar{\mathbf{T}}^K) \cdot \begin{Bmatrix} \theta_1 \\ w_1^t \\ v_1^t \end{Bmatrix}_k = \mathbf{T}_{AR} \cdot \begin{Bmatrix} \theta_1 \\ w_1^t \\ v_1^t \end{Bmatrix}_k \quad (6.34)$$

where

$$\mathbf{T}_A^* = \begin{bmatrix} T_{11} & T_{12} & T_{13} \\ -T_{21} & T_{22} & -T_{23} \\ T_{31} & T_{32} & T_{33} \end{bmatrix}_s \quad (6.35)$$

The subscript s in the above transformation matrix implies that the elements are obtained from the intersegment transformation matrix, \mathbf{T}_s . The $\bar{\mathbf{T}}^K$ matrix is a nonlinear transformation since it depends on the segment deformations and is given as

$$\begin{aligned} \bar{\mathbf{T}}_{i1}^K &= a_{i1}\theta_1 + b_{i1}v_1^t \\ \bar{\mathbf{T}}_{i2}^K &= a_{i2}w_1^t + b_{i2}\theta_1 \\ \bar{\mathbf{T}}_{i3}^K &= a_{i3}v_1^t + b_{i3}w_1^t \end{aligned} \quad (6.36)$$

where $i = 1, 3$ and

$$\begin{aligned} a_{11} &= -(T_{s_{21}}T_{s_{32}} + T_{s_{23}}T_{s_{31}})/2 & b_{11} &= T_{s_{23}}T_{s_{31}} \\ a_{12} &= -(T_{s_{21}}T_{s_{31}} + T_{s_{23}}T_{s_{31}})/2 & b_{12} &= -T_{s_{22}}T_{s_{31}} \\ a_{13} &= -(T_{s_{21}}T_{s_{31}} + T_{s_{22}}T_{s_{32}})/2 & b_{13} &= T_{s_{23}}T_{s_{32}} \end{aligned}$$

$$\begin{aligned}
a_{21} &= -(T_{s_{12}} T_{s_{31}} + T_{s_{13}} T_{s_{32}})/2 & b_{21} &= T_{s_{13}} T_{s_{31}} \\
a_{22} &= -(T_{s_{12}} T_{s_{31}} + T_{s_{13}} T_{s_{33}})/2 & b_{22} &= -T_{s_{12}} T_{s_{31}} \\
a_{23} &= -(T_{s_{11}} T_{s_{31}} + T_{s_{12}} T_{s_{32}})/2 & b_{23} &= -T_{s_{13}} T_{s_{32}} \\
a_{31} &= -(T_{s_{12}} T_{s_{32}} + T_{s_{13}} T_{s_{31}})/2 & b_{31} &= T_{s_{13}} T_{s_{21}} \\
a_{32} &= -(T_{s_{12}} T_{s_{32}} + T_{s_{13}} T_{s_{32}})/2 & b_{32} &= -T_{s_{12}} T_{s_{21}} \\
a_{33} &= -(T_{s_{11}} T_{s_{31}} + T_{s_{12}} T_{s_{32}})/2 & b_{33} &= -T_{s_{13}} T_{s_{22}}
\end{aligned} \tag{6.37}$$

The relations given in Eq. 6.30 and Eq. 6.34 represent the intersegment compatibility relations.

Position Vector of an Arbitrary Point in the Deformed Blade

The key to derivation of the equations of motion is the determination of the position vector of an arbitrary point in the deformed frame with respect to the rotor hub. This is done as below:

Consider a typical segment; U_k denotes its undeformed state and D_k denotes its deformed state. The point P is a generic point on the elastic axis of U_k (see Fig. 6.1), and Q is an arbitrary point in the section normal to elastic axis at point P . P_1 and Q_1 are the positions occupied by the points in the deformed state D_k . The position vector of point Q_1 in the deformed segment cross-section is given by

$$\vec{r} = O\vec{Q}_1 = O\vec{A}_1 + \vec{A}_1\vec{A}_2 + \dots + \vec{A}_{k-1}\vec{A}_k + \vec{A}_k\vec{P} + \vec{P}\vec{P}_1 + \vec{P}_1\vec{Q}_1$$

Let $O\vec{A}_1 = l_0$, $\vec{A}_1\vec{A}_2 = l_1$, ..., $\vec{A}_{k-1}\vec{A}_k = l_{k-1}$. Also, let the vectors $\hat{i}, \hat{j}, \hat{k}$

referring to the main blade reference coordinate system be denoted as $\hat{i}_0, \hat{j}_0, \hat{k}_0$, respectively. Then,

$$\vec{r} = \sum_{p=0}^{k-1} l_p \hat{i}_p + s \hat{i}_k + \bar{x} \hat{i}_k + \bar{y} \hat{j}_k + \bar{z} \hat{k}_k \quad (6.38)$$

where subscript p refers to the p th segment inboard of the k th segment, and s is the distance of point P from the junction A_k and

$$\begin{aligned} \dot{x} &= u + u_e + \bar{u} - \lambda_T \phi' + v'(\bar{y} - v) + w'(\bar{z} - w) \\ \dot{y} &= v + \eta \cos \theta_T - \zeta \sin \theta_T \\ \dot{z} &= w + \eta \sin \theta_T + \zeta \cos \theta_T \end{aligned} \quad (6.39)$$

where

$$u = u_e + \bar{u} \quad (6.40)$$

and u_e, v, w and θ_T are degrees of freedom for the k th blade segment; u_e is the axial elastic displacement, v is the lag deflection, w is the flap deflection, and $\theta_T = \theta_2$ is given in Eq. 6.27. Radial shortening \bar{u} is experienced at the point $(s, 0, 0)$ on the elastic axis of the k th blade segment. Consider a p th blade segment inboard of the k th segment: its radial shortening with respect to the p th undeformed segment frame is given by

$$\bar{u}^p = -\frac{1}{2} \int_0^{l_p} (v_p'^2 + w_p'^2) ds_p \quad (6.41)$$

and radial shortening of the k th segment between locations 0 and s is given by

$$\bar{u} = -\frac{1}{2} \int_0^s (v_k'^2 + w_k'^2) ds_k \quad (6.42)$$

The net radial shortening at location s of the k th segment is obtained by summing the contributions from the inboard segments (Eq. 6.41) and the current segment (Eq. 6.42).

$$\bar{u}(s) = \tilde{u} + \sum_{p=0}^{k-1} T_{kp_{11}} u^p \quad (6.43)$$

where \mathbf{T}_{kp} is the transformation matrix relating the k th segment coordinate system to the p th segment coordinate system and is given by

$$\mathbf{T}_{kp} = \mathbf{T}_A^k \cdot \mathbf{T}_A^{pT} \quad (6.44)$$

The element $T_{kp_{11}}$ of the transformation matrix shown above projects the radial shortening of the p th element onto radial shortening of the k th element.

We now return to the derivation of the expression for the position vector given by Eq. 6.38. It is necessary to express the position vector in terms of one set of coordinates only; therefore, we need to find expressions for \hat{i}_p in terms of \hat{i}_k, \hat{j}_k and \hat{k}_k . Relative to the main blade reference triad $\hat{i}_0, \hat{j}_0, \hat{k}_0$ we can write the triads for the p th and k th segments as

$$\begin{Bmatrix} \hat{i}_p \\ \hat{j}_p \\ \hat{k}_p \end{Bmatrix} = \boldsymbol{\Lambda}'_p \begin{Bmatrix} \hat{i}_0 \\ \hat{j}_0 \\ \hat{k}_0 \end{Bmatrix} \quad (6.45)$$

$$\begin{Bmatrix} \hat{i}_k \\ \hat{j}_k \\ \hat{k}_k \end{Bmatrix} = \boldsymbol{\Lambda}'_k \begin{Bmatrix} \hat{i}_0 \\ \hat{j}_0 \\ \hat{k}_0 \end{Bmatrix} \quad (6.46)$$

Substituting $\hat{i}_0, \hat{j}_0, \hat{k}_0$ from Eq. 6.46 into Eq. 6.45 yields

$$\begin{Bmatrix} \hat{i}_p \\ \hat{j}_p \\ \hat{k}_p \end{Bmatrix} = \boldsymbol{\Lambda}'_p \boldsymbol{\Lambda}'_k {}^T \begin{Bmatrix} \hat{i}_k \\ \hat{j}_k \\ \hat{k}_k \end{Bmatrix} \quad (6.47)$$

from where we get

$$\hat{l}_p = T_{pk_1} \hat{i}_k + T_{pk_2} \hat{j}_k + T_{pk_3} \hat{k}_k \quad (6.48)$$

where the elements of the transformation T_{pk} are defined as

$$T_{pk_i} = \sum_{n=1}^3 \Lambda'_{p,n} \Lambda'_{k,n}, \quad i = 1, 3 \quad (6.49)$$

Substituting Eq. 6.48 in Eq. 6.38, we obtain the position vector for the k th segment as

$$\vec{r} = x_k \hat{i}_k + y_k \hat{j}_k + z_k \hat{k}_k \quad (6.50)$$

where

$$\begin{aligned} x_k &= s + \tilde{x} + L_1 \\ y_k &= \tilde{y} + L_2 \\ z_k &= \tilde{z} + L_3 \end{aligned} \quad (6.51)$$

and

$$\begin{aligned} L_1 &= \sum_{p=0}^{k-1} T_{pk_1} l_p \\ L_2 &= \sum_{p=0}^{k-1} T_{pk_2} l_p \\ L_3 &= \sum_{p=0}^{k-1} T_{pk_3} l_p \end{aligned} \quad (6.52)$$

are the projected lengths of the inboard segments on the k th segments. The expression for the position vector derived in this section is now used to formulate the governing equations of motion for an advanced geometry blade.

6.3 Equations of Motion

A finite element method based on Hamilton's principle is used to derive the equations of motion for the advanced geometry blade. The Hamilton's principle can be written as:

$$\int_{t_1}^{t_2} (\delta U + \delta T - \delta W) dt = 0 \quad (6.53)$$

where δU , δT and δW are the strain energy, kinetic energy and virtual work respectively, and are derived below.

6.3.1 Blade Strain Energy

The virtual strain energy is given by

$$\delta U = \int_0^R \int \int_A (\sigma_{xx} \delta \epsilon_{xx} + \sigma_{x\eta} \delta \epsilon_{x\eta} + \sigma_{x\zeta} \delta \epsilon_{x\zeta}) d\eta d\zeta dx \quad (6.54)$$

The advanced geometry blade is composed of slender isotropic beam-segments. Such a structure satisfies the uniaxial stress assumption ($\sigma_{yy} = \sigma_{zz} = 0$).

The stress-strain relations for an isotropic beam are:

$$\begin{aligned} \sigma_{xx} &= E \epsilon_{xx} \\ \sigma_{x\eta} &= G \epsilon_{x\eta} \\ \sigma_{x\zeta} &= G \epsilon_{x\zeta} \end{aligned} \quad (6.55)$$

where ϵ_{xx} is the axial stain and $\epsilon_{x\eta}$ and $\epsilon_{x\zeta}$ are shear strains. The strain-displacement relations are derived for moderate deflections and are given as

$$\epsilon_{xx} = u' + \frac{v'^2}{2} + \frac{w'^2}{2} + (\eta^2 + \zeta^2)(\theta'_0 \phi' + \frac{\dot{\phi}'^2}{2})$$

$$\begin{aligned}
&= v''(\eta \cos(\theta_2 + \phi) - \zeta \sin(\theta_2 + \phi)) \\
&\quad + w''(\eta \sin(\theta_2 + \phi) + \zeta \cos(\theta_2 + \phi)) \\
\epsilon_{x\eta} &= -(\zeta + \frac{\partial \lambda_T}{\partial \eta})\dot{\phi}' = -\dot{\zeta}\dot{\phi}' \\
\epsilon_{x\zeta} &= (\eta - \frac{\partial \lambda_T}{\partial \zeta})\dot{\phi}' = \dot{\eta}\dot{\phi}' \tag{6.56}
\end{aligned}$$

where λ_T is the cross-sectional warping function. Taking the variation of the strains and substituting Eq. 6.55 and Eq. 6.56 into Eq. 6.54 yields the virtual strain energy in terms of the blade section properties and displacements as:

$$\begin{aligned}
\frac{\delta U}{m_0 \Omega^2 R^3} &= \int_0^1 (U_{u_e'} \delta u_e' + U_{v''} \delta v'' + U_{w''} \delta w'' + U_{w'} \delta w' + U_{\phi} \delta \phi \\
&\quad + U_{\phi'} \delta \phi' + U_{\phi''} \delta \phi'') dx \tag{6.57}
\end{aligned}$$

where

$$\begin{aligned}
U_{u_e'} &= EA(u_e' + k_A^2 \theta_0' (\dot{\phi}' + u' v'') + k_A^2 \dot{\phi}'^2 / 2) \\
&= EAe_A(v''(\cos \theta_2 - \dot{\phi} \sin \theta_2) + w''(\sin \theta_2 + \dot{\phi} \cos \theta_2)) \\
U_{v''} &= v''(EI_z \cos^2 \theta_2 + EI_y \sin^2 \theta_2) + w''(EI_z - EI_y) \cos \theta_2 \sin \theta_2 \\
&= EAe_A u_e' (\cos \theta_2 - \dot{\phi} \sin \theta_2) - \dot{\phi}' E B_2 \theta_0' \cos \theta_2 \\
&\quad + w'' \phi(EI_z - EI_y) \cos 2\theta_2 - v'' \dot{\phi}(EI_z - EI_y) \sin 2\theta_2 \\
&\quad + (GJ + EB_1 \theta_0'^2) \dot{\phi}' w' + E A k_A^2 \theta_0' u' u_e' \\
U_{w''} &= (GJ + EB_1 \theta_0'^2) \dot{\phi}' v'' + E A k_A^2 \theta_0' v'' u_e' \\
U_{w'} &= w''(EI_y \cos^2 \theta_2 + EI_z \sin^2 \theta_2) + v''(EI_z - EI_y) \cos \theta_2 \sin \theta_2 \\
&= EAe_A u_e' (\sin \theta_2 + \dot{\phi} \cos \theta_2) - \dot{\phi}' E B_2 \theta_0' \sin \theta_2 \\
&\quad + w'' \phi(EI_z - EI_y) \sin 2\theta_2 + v'' \dot{\phi}(EI_z - EI_y) \cos 2\theta_2
\end{aligned}$$

$$\begin{aligned}
U_{\phi} &= w''^2(EI_z - EI_y) \sin \theta_2 \cos \theta_2 + v''w''(EI_z - EI_y) \cos 2\theta_2 \\
&= v''^2(EI_z - EI_y) \sin \theta_2 \cos \theta_2 \\
U_{\phi'} &= GJ(\dot{\phi}' + w'v'') + EB_1\theta_0'^2\dot{\phi}' + EAk_A^2(\theta_0' + \dot{\phi}')u'_c \\
&= EB_2\theta_0'(v'' \cos \theta_2 + w'' \sin \theta_2) \\
U_{\phi''} &= EC_1\dot{\phi}'' + EC_2(w'' \cos \theta_2 - v'' \sin \theta_2)
\end{aligned} \tag{6.58}$$

where

$$\begin{aligned}
EA &= \int \int_A E d\eta d\zeta & EAe_A &= \int \int_A E\eta d\eta d\zeta \\
EI_y &= \int \int_A EI_y^2 d\eta d\zeta & EI_z &= \int \int_A EI_z^2 d\eta d\zeta \\
GJ &= \int \int_A G(\eta^2 + \zeta^2) d\eta d\zeta & EAk_A^2 &= \int \int_A E(\eta^2 + \zeta^2) d\eta d\zeta \\
EB_1 &= \int \int_A E(\eta^2 + \zeta^2)^2 d\eta d\zeta & EB_2 &= \int \int_A E\eta(\eta^2 + \zeta^2)^2 d\eta d\zeta \\
EC_1 &= \int \int_A E\lambda_T^2 d\eta d\zeta & EC_2 &= \int \int_A E\zeta\lambda_T d\eta d\zeta
\end{aligned} \tag{6.59}$$

The axial, flap, lag and torsional stiffness are denoted by EA , EI_z , EI_y and GJ , respectively. EC_1 and EC_2 are terms related to cross-sectional warping. k_A is the radius of gyration. e_A is the offset of the tension-center from the elastic axis and EB_1 and EB_2 are other cross sectional constants which appear due to blade pitch.

6.3.2 Blade Kinetic Energy

The variation of kinetic energy is expressed as

$$\delta T = \int_0^R \int \int_A \rho \vec{V}_b \cdot \delta \vec{V}_b d\eta d\zeta dx \tag{6.60}$$

where \vec{V}_b is the velocity vector of an arbitrary point on the blade in the deformed frame. The velocity at the point Q_1 on the blade (see Fig. 1) with a position vector defined by r' and rotating with angular velocity $\vec{\omega}$ is defined as

$$\vec{V}_b = \frac{d\vec{r}'}{dt} = \frac{\partial \vec{r}'}{\partial t} + \vec{\omega} \times \vec{r}' \quad (6.61)$$

To derive an expression for the rotation vector ω , we need to relate the motion of the k th segment of the blade with the hub-fixed nonrotating system. For a blade rotating about the hub axis with rotational speed Ω and having a pitch rate of $\dot{\theta}_0$ about the undeformed main blade axis, the rotation vector can be written as

$$\vec{\omega} = \Omega \vec{K}_{NR} + \dot{\theta}_0 \hat{i} \quad (6.62)$$

where the subscript NR identifies the triad associated with the hub-fixed nonrotating frame. At this point we introduce the following transformations connecting the nonrotating frame to the blade reference frame,

$$\begin{Bmatrix} \hat{i}_{NR} \\ \hat{j}_{NR} \\ \hat{k}_{NR} \end{Bmatrix} = \mathbf{T}_{UR}^T \begin{Bmatrix} \hat{i} \\ \hat{j} \\ \hat{k} \end{Bmatrix} \quad (6.63)$$

where

$$\mathbf{T}_{UR} = \begin{bmatrix} \cos \beta_p \cos \psi & \cos \beta_p \sin \psi & \sin \beta_p \\ -\sin \psi & \cos \psi & 0 \\ -\sin \beta_p \cos \psi & -\sin \beta_p \sin \psi & \cos \beta_p \end{bmatrix} \quad (6.64)$$

From the above transformation we obtain,

$$K_{NR} = \sin \beta_p \hat{i} + \cos \beta_p \hat{k} \quad (6.65)$$

Also,

$$\begin{Bmatrix} \hat{i} \\ \hat{j} \\ \hat{k} \end{Bmatrix} = \mathbf{A}_k^T \begin{Bmatrix} \hat{i}_k \\ \hat{j}_k \\ \hat{k}_k \end{Bmatrix} \quad (6.66)$$

which yields

$$\dot{i} = \Lambda'_{11}\dot{i}_k + \Lambda'_{21}\dot{j}_k + \Lambda'_{31}\dot{k}_k \quad (6.67)$$

Substituting Eq. 6.65 and Eq. 6.67 into Eq. 6.62 yields

$$\omega = a_1\dot{i}_k + a_2\dot{j}_k + a_3\dot{k}_k \quad (6.68)$$

where

$$\begin{aligned} a_1 &= \Lambda'_{11} \sin \beta_p + \Lambda'_{21} \cos \beta_p + \Lambda'_{11} \dot{\theta}_0 \\ a_2 &= \Lambda'_{21} \sin \beta_p + \Lambda'_{23} \cos \beta_p + \Lambda'_{21} \dot{\theta}_0 \\ a_3 &= \Lambda'_{31} \sin \beta_p + \Lambda'_{33} \cos \beta_p + \Lambda'_{31} \dot{\theta}_0 \end{aligned} \quad (6.69)$$

Substituting Eq. 6.50 and Eq. 6.68 in Eq. 6.61, yields the blade velocity as

$$\vec{V}_b = V_1\dot{i}_k + V_2\dot{j}_k + V_3\dot{k}_k \quad (6.70)$$

where

$$\begin{aligned} V_1 &= \dot{x}_k + a_2 z_k - a_3 y_k \\ V_2 &= \dot{y}_k + a_3 x_k - a_1 z_k \\ V_3 &= \dot{z}_k + a_1 y_k - a_2 x_k \end{aligned} \quad (6.71)$$

Taking the virtual of the velocity in Eq. 6.71 yields

$$\begin{aligned} \delta V_1 &= \delta \dot{x}_k + a_2 \delta z_k - a_3 \delta y_k \\ \delta V_2 &= \delta \dot{y}_k + a_3 \delta x_k - a_1 \delta z_k \\ \delta V_3 &= \delta \dot{z}_k + a_1 \delta y_k - a_2 \delta x_k \end{aligned} \quad (6.72)$$

Substituting Eq. 6.72 and Eq. 6.71 into Eq. 6.60 and integrating by parts over time yields

$$\begin{aligned}
\int_{t_1}^{t_2} \int_0^R \int_A \rho \vec{V} \cdot \delta \vec{V} d\eta d\zeta dx dt = & (\dot{x}_k \delta x_k + \dot{x}_k a_2 \delta z_k \\
& - \dot{x}_k a_3 \delta y_k - a_2 \dot{z}_k \delta x_k - \dot{a}_2 z_k \delta x_k + a_2^2 z_k \delta z_k \\
& - a_2 a_3 z_k \delta y_k + a_3 \dot{y}_k \delta x_k + \dot{a}_3 y_k \delta x_k - a_2 a_3 y_k \delta z_k \\
& + a_3^2 y_k \delta y_k + a_1^2 z_k \delta z_k \\
& - \ddot{y}_k \delta y_k + a_3 \dot{y}_k \delta x_k - a_1 \dot{y}_k \delta z_k - a_3 \dot{x}_k \delta y_k \\
& - x_k \dot{a}_3 \delta y_k + a_3^2 x_k \delta x_k + a_1 a_2 x_k \delta y_k \\
& - \ddot{z}_k \delta z_k + a_1 \dot{z}_k \delta y_k - a_3 \dot{z}_k \delta x_k - a_1 \dot{y}_k \delta z_k \\
& - \dot{a}_1 y_k \delta z_k + a_1^2 y_k \delta y_k - a_1 a_2 y_k \delta x_k \\
& - a_2 \dot{x}_k \delta z_k + \dot{a}_2 x_k \delta z_k - a_1 a_2 x_k \delta y_k + a_2^2 x_k \delta x_k) \quad (6.73)
\end{aligned}$$

The integration by parts leads to new terms in the above equations containing \dot{a}_1 , \dot{a}_2 and \dot{a}_3 . These terms are obtained by differentiating Eq. 6.69 with respect to time and are given as

$$\begin{aligned}
\dot{a}_1 &= \dot{\Lambda}'_{12} \cos \beta_p \dot{\theta}_0 + \dot{\Lambda}'_{11} \ddot{\theta}_0 \\
\dot{a}_2 &= \dot{\Lambda}'_{22} \cos \beta_p \dot{\theta}_0 + \dot{\Lambda}'_{21} \ddot{\theta}_0 \\
\dot{a}_3 &= \dot{\Lambda}'_{32} \cos \beta_p \dot{\theta}_0 + \dot{\Lambda}'_{31} \ddot{\theta}_0 \quad (6.74)
\end{aligned}$$

Substituting expressions for x_k , y_k , z_k from Eq. 6.51 into the above equation, we obtain the following expression for the kinetic energy,

$$\delta T = \int_0^R (T_v \delta u + T_v \delta v + T_w \delta w + T_\phi \delta \hat{\phi} + T_{v'} \delta v' + T_{w'} \delta w') dx \quad (6.75)$$

where

$$\begin{aligned}
T_u &= -m\{\ddot{u} - 2(a_3\dot{v} - a_2\dot{w}) - (a_2^2 + a_3^2)(L_1 + s + u - v'e_g \cos \theta_2) \\
&\quad + a_1a_2(L_2 + v + e_g \cos \theta_2) + a_1a_3(L_3 + w + e_g \sin \theta_2) \\
&\quad - \dot{a}_3L_2 - \dot{a}_3v - \dot{a}_3e_g \cos \theta_2 + \dot{a}_3e_g \hat{\phi} \sin \theta_2\} \tag{6.76}
\end{aligned}$$

$$\begin{aligned}
T_v &= -m\{\ddot{v} - 2(a_1\dot{w} - a_3\dot{u}) - 2a_3e_g(\dot{v}' \cos \theta_2 + \dot{w}' \sin \theta_2) \\
&\quad - \dot{a}_1e_g \sin \theta_2 + a_1a_2(L_1 + s + u - v'e_g \cos \theta_2) \\
&\quad - (a_1^2 + a_3^2)(L_2 + v + e_g \cos \theta_2) + a_2a_3(L_3 + w + e_g \sin \theta_2) \\
&\quad - \dot{a}_3(L_1 + s) + \dot{a}_1L_3 - \dot{a}_3s - \dot{a}_3u + \dot{a}_1w \\
&\quad + \dot{a}_1e_g \hat{\phi} \cos \theta_2 + \dot{a}_3e_g v' \cos \theta_2 + \dot{a}_1e_g \sin \theta_2 + \dot{a}_3e_g w' \sin \theta_2\} \tag{6.77}
\end{aligned}$$

$$\begin{aligned}
T_w &= -m\{\ddot{w} - 2(a_2\dot{u} - a_1\dot{v}) - 2a_2e_g(\dot{v}' \cos \theta_2 + \dot{w}' \sin \theta_2) \\
&\quad + \dot{a}_1e_g \sin \theta_2 + a_1a_3(L_1 + s + u - v'e_g \cos \theta_2) \\
&\quad - (a_1^2 + a_2^2)(L_3 + w + e_g \sin \theta_2) + a_2a_3(L_2 + v + e_g \cos \theta_2) \\
&\quad - \dot{a}_3(L_1 + s) - \dot{a}_1L_2 - \dot{a}_2L_3 + \dot{a}_3u - \dot{a}_1v \\
&\quad - \dot{a}_2w - \dot{a}_1e_g \cos \theta_2 - \dot{a}_2\hat{\phi}e_g \cos \theta_2 + \dot{a}_3e_g v' \cos \theta_2 - \dot{a}_2e_g \sin \theta_2 \\
&\quad + \dot{a}_1e_g \hat{\phi} \sin \theta_2 + \dot{a}_3e_g w' \sin \theta_2\} \tag{6.78}
\end{aligned}$$

$$\begin{aligned}
T_{\hat{\phi}} &= -m\{k_m^2\hat{\phi} + e_g(\dot{v}' \cos \theta_2 - \dot{w}' \sin \theta_2) \\
&\quad - 2e_g \cos \theta_2(a_2\dot{u} + a_1\dot{v}) + 2e_g \sin \theta_2(a_1\dot{v} - a_3\dot{u})\}
\end{aligned}$$

$$\begin{aligned}
&= (a_1^2 + a_2^2)(L_3 \epsilon_g \cos \theta_2 + w \epsilon_g \cos \theta_2 + (k_{m3}^2 - k_{m1}^2) \cos \theta_2 \sin \theta_2) \\
&+ (a_1^2 + a_3^2)(L_2 \epsilon_g \sin \theta_2 + v \epsilon_g \sin \theta_2 + (k_{m2}^2 - k_{m1}^2) \cos \theta_2 \sin \theta_2) \\
&+ a_1 a_3 ((L_1 + s) \epsilon_g \cos \theta_2 + u \epsilon_g \cos \theta_2) \\
&- a_1 a_2 ((L_1 + s) \epsilon_g \sin \theta_2 + u \epsilon_g \sin \theta_2) \\
&+ a_2 a_3 (L_2 \epsilon_g \cos \theta_2 + v \epsilon_g \cos \theta_2 + k_{m3}^2) \\
&- a_2 a_3 (L_3 \epsilon_g \sin \theta_2 + w \epsilon_g \sin \theta_2 + k_{m4}^2) \\
&- w' \epsilon_g \cos \theta_2 [-(a_2^2 + a_3^2)(L_1 + s) + a_1 a_2 L_2 + a_1 a_3 L_3] \\
&- v' \epsilon_g \sin \theta_2 [-(a_2^2 + a_3^2)(L_1 + s) + a_1 a_3 L_3 - a_1 a_2 L_2] \\
&+ \dot{a}_2 k_{m1}^2 \cos \theta_2 + \dot{a}_1 k_{m2}^2 \cos \theta_2 \\
&- \dot{a}_2 k_{m2}^2 \cos \theta_2 \sin \theta_2 - \dot{a}_1 k_{m2}^2 \sin^2 \theta_2 \} \tag{6.79}
\end{aligned}$$

$$\begin{aligned}
T_{v'} &= -m \{ \ddot{u} \epsilon_g \cos \theta_2 - 2 \epsilon_g \cos \theta_2 (a_3 \dot{v} - a_2 \dot{w}) \\
&+ (a_2^2 + a_3^2)((L_1 + s) \epsilon_g \cos \theta_2 + u \epsilon_g \cos \theta_2) \\
&- a_1 a_2 (L_2 \epsilon_g \cos \theta_2 + v \epsilon_g \cos \theta_2) - a_1 a_3 (L_3 \epsilon_g \cos \theta_2 + w \epsilon_g \cos \theta_2) \\
&+ (k_{m1}^2 + k_{m2}^2) \dot{a}_3 \cos^2 \theta_2 \} \tag{6.80}
\end{aligned}$$

$$\begin{aligned}
T_{w'} &= -m \{ \ddot{u} \epsilon_g \sin \theta_2 - 2 \epsilon_g \sin \theta_2 (a_3 \dot{v} - a_2 \dot{w}) \\
&+ (a_2^2 + a_3^2)((L_1 + s) \epsilon_g \sin \theta_2 + u \epsilon_g \sin \theta_2) \\
&- a_1 a_2 (L_2 \epsilon_g \sin \theta_2 + v \epsilon_g \sin \theta_2) - a_1 a_3 (L_3 \epsilon_g \sin \theta_2 + w \epsilon_g \sin \theta_2) \\
&- \dot{a}_3 \cos \theta_2 (k_{m1}^2 \cos \theta_2 + k_{m2}^2 \sin \theta_2) \} \tag{6.81}
\end{aligned}$$

The sectional integrals are defined by

$$\begin{aligned}
m &= \iint_A \rho_s d\eta d\zeta \\
mc_g &= \iint_A \rho_s \eta d\eta d\zeta \\
mk_{m1}^2 &= \iint_A \rho_s \zeta^2 d\eta d\zeta \\
mk_{m2}^2 &= \iint_A \rho_s \eta^2 d\eta d\zeta \\
k_m^2 &= k_{m1}^2 + k_{m2}^2 \\
k_{m3}^2 &= k_{m1}^2 \sin^2 \theta_2 + k_{m2}^2 \cos^2 \theta_2 \\
k_{m1}^2 &= k_{m1}^2 \cos^2 \theta_2 + k_{m2}^2 \sin^2 \theta_2 \\
dk_m &= k_{m2}^2 - k_{m1}^2
\end{aligned}$$

In the above expressions, m is the blade mass per unit length; ρ_s is the blade structural density; c_g is the center-of-mass offset from the elastic axis for both the blade and tip, positive forward; mk_{m1}^2 and mk_{m2}^2 are the flapwise and chordwise mass moment of inertia per unit length; and k_m is the cross-section mass radius of gyration.

6.3.3 Blade Virtual Work

The virtual work δW can be expressed as:

$$\delta W = \int_0^R (L_u^A \delta u + L_v^A \delta v + L_w^A \delta w + M_\phi^A \delta \dot{\phi}) dx \quad (6.82)$$

where L_u^A , L_v^A , L_w^A and M_ϕ^A are the external aerodynamic loads distributed along the length of the blade in the axial, lead-lag, flap and torsion directions, re-

spectively. Calculation of the blade airloads requires information about the wind velocity seen by a blade. The blade section airloads are calculated in the blade deformed coordinate system, and then a transformation is used to convert these to the undeformed frame, consistent with the virtual work expression, Eq.(6.82).

6.4 Aerodynamic Modeling

Quasi-steady aerodynamic modeling is used to derive the blade section loads. The first step in the calculation of these loads is the derivation of the blade velocity at an arbitrary section on the blade.

6.4.1 Derivation of Blade Velocity

The resultant velocity seen at a blade section consists of the incoming velocity, the instantaneous blade motion, and the induced inflow. The general expression for the resultant blade velocity at a radial position x is given by

$$\vec{V} = -\vec{V}_w + \vec{V}_b \quad (6.83)$$

where \vec{V}_w is the wind velocity from the helicopter forward speed and the rotor inflow, and \vec{V}_b is the blade velocity relative to the hub fixed frame resulted from blade rotation and blade motions. The expression for the wind velocity is,

$$\vec{V}_w = (\mu\Omega R)I_{NR} - (\lambda\Omega R)K_{NR} \quad (6.84)$$

where $\mu = V \cos \alpha_s / \Omega R$ is the rotor advance ratio; V is the helicopter forward speed; λ is the rotor non-dimensional inflow; and ΩR is the rotor tip speed. The

\hat{I}_{NR} , \hat{J}_{NR} , and \hat{K}_{NR} are the unit vectors for the hub-fixed nonrotating coordinate system. The rotor inflow λ consists of two components and is expressed as

$$\lambda = (\mu \tan \alpha_s + \lambda_i) \approx \mu \alpha_s + \lambda_i \quad (6.85)$$

where $\mu \tan \alpha_s$ is the component of the forward flight velocity perpendicular to the hub plane, and λ_i is the nondimensional rotor induced inflow.

The velocity components in Eq.(6.84) are expressed in the nonrotating system. Two coordinate transformations are required to convert them into the undeformed swept segment coordinate system (i_k , j_k , k_k). These transformations are given in Eq. 6.63 and Eq. 6.66. After these transformations the air velocity due to the blade rotation, blade motion and the forward speed in the undeformed segment coordinate system is given by:

$$\vec{V} = \vec{V}_b + (\mu \Omega R) \hat{I}_{NR} + (\lambda \Omega R) \hat{K}_{NR} = U_x i_k + U_y j_k + U_z k_k \quad (6.86)$$

The blade velocity \vec{V}_b used in the above equations, has already been calculated during the derivation of the blade kinetic energy (Eq. 6.71). Since aerodynamic loads are calculated using the velocity component at 3/4 chord, these are expressed as:

$$\begin{aligned} U_x &= -\dot{v} + \eta_r(\dot{v}' \cos \theta_2 + \dot{w}' \sin \theta_2) + a_3(L_2 + v - \eta_r \cos \theta_2) \\ &\quad + a_2(L_3 + w + \eta_r \sin \theta_2) - (\lambda c_1 - \mu b_1) \end{aligned} \quad (6.87)$$

$$\begin{aligned} U_y &= -\dot{v} + \eta_r \dot{\theta}_2 \sin \theta_2 + a_1(L_3 + w + \eta_r \sin \theta_2) \\ &\quad + a_3((L_1 + s) + u + \eta_r(v' \cos \theta_2 + w' \sin \theta_2)) \end{aligned}$$

$$\begin{aligned}
& + (\lambda \epsilon_2 - \mu b_2) \\
& \quad (6.88)
\end{aligned}$$

$$\begin{aligned}
U_z &= -\dot{\eta}^r + \eta_r \dot{\theta}_2 \cos \theta_2 - u_1(L_2 + v + \eta_r \cos \theta_2) \\
& + a_3((L_1 + s) + u + \eta_r(v' \cos \theta_2 + w' \sin \theta_2)) \\
& - (\lambda \epsilon_3 - \mu b_3) \quad (6.89)
\end{aligned}$$

where,

$$\begin{aligned}
c_1 &= \Lambda'_{11} \sin \beta + \Lambda'_{13} \cos \beta \\
c_2 &= \Lambda'_{21} \sin \beta + \Lambda'_{23} \cos \beta \\
c_3 &= \Lambda'_{31} \sin \beta + \Lambda'_{33} \cos \beta \quad (6.90)
\end{aligned}$$

$$\begin{aligned}
b_1 &= \Lambda'_{11} \cos \beta_p \cos \psi + \Lambda'_{12} \sin \psi + \Lambda'_{13} \sin \beta_p \cos \psi \\
b_2 &= \Lambda'_{21} \cos \beta_p \cos \psi + \Lambda'_{22} \sin \psi + \Lambda'_{23} \sin \beta_p \cos \psi \\
b_3 &= \Lambda'_{31} \cos \beta_p \cos \psi + \Lambda'_{32} \sin \psi + \Lambda'_{33} \sin \beta_p \cos \psi
\end{aligned}$$

The air velocities in the deformed frame are calculated using the following relation:

$$\left\{ \begin{array}{l} -U_R \\ -U_T \\ -U_P \end{array} \right\} = \mathbf{T}_2 \left\{ \begin{array}{l} U_x \\ U_y \\ U_z \end{array} \right\} \quad (6.91)$$

where \mathbf{T}_2 is defined in Eq. 6.25. Then, the final blade velocity components, expressed in the rotating deformed frame are,

$$\hat{\mathbf{V}} = U_R \hat{i}_k + U_T \hat{j}_k + U_P \hat{k}_k \quad (6.92)$$

where

$$\begin{aligned}
\frac{U_R}{\Omega R} = & \dot{u} + (a_2 w - a_3 v) + \eta_r (\cos \theta_2 \dot{v}' + \sin \theta_2 \dot{w}') \\
& + \eta_r (a_2 \sin \theta_2 - a_3 \cos \theta_2) + \eta_r \dot{\phi} (a_2 \cos \theta_2 + a_3 \sin \theta_2) \\
& + (\alpha_3 + \lambda_i e_1 - \mu b_1) + (\alpha_1 + \lambda_i e_2 - \mu b_2 - a_1 \eta_r \sin \theta_2) v' \\
& + (\alpha_2 + \lambda_i e_3 - \mu b_3 + a_1 \eta_r \sin \theta_2) w' \tag{6.93}
\end{aligned}$$

$$\begin{aligned}
\frac{U_T}{\Omega R} = & \cos \theta_2 \dot{v} + \sin \theta_2 \dot{w} + \cos \theta_2 (a_3 u - a_1 w) + \sin \theta_2 (a_1 v - a_2 u) \\
& - \cos \theta_2 (\alpha_3 + \lambda_i e_1 - \mu b_1) v' - \sin \theta_2 (\alpha_3 + \lambda_i e_1 - \mu b_1) w' \\
& + (\alpha_3 + (\lambda_i e_2 - \mu b_2) \cos \theta_2 + (\lambda_i e_3 - \mu b_3) \sin \theta_2) \\
& + \dot{\phi} [\alpha_1 - (\lambda_i e_2 - \mu b_2) \sin \theta_2 + (\lambda_i e_3 - \mu b_3) \cos \theta_2] \tag{6.94}
\end{aligned}$$

$$\begin{aligned}
\frac{U_P}{\Omega R} = & \cos \theta_2 \dot{w} - \sin \theta_2 \dot{v} + \eta_r (\dot{\phi} + \dot{\theta}_2 + \alpha_1) \\
& + \cos \theta_2 (a_1 v - a_2 u) - \sin \theta_2 (a_3 u - a_1 w) \\
& + [(\alpha_3 + \lambda_i e_1 - \mu b_1) \sin \theta_2 + \eta_r a_2] v' \\
& + [-(\alpha_3 + \lambda_i e_1 - \mu b_1) \cos \theta_2 + \eta_r a_3] w' \\
& - (\alpha_3 + (\lambda_i e_2 - \mu b_2) \sin \theta_2 + (\lambda_i e_3 - \mu b_3) \cos \theta_2) \\
& + \dot{\phi} [-\alpha_1 - (\lambda_i e_2 - \mu b_2) \cos \theta_2 - (\lambda_i e_3 - \mu b_3) \sin \theta_2] \tag{6.95}
\end{aligned}$$

where a_1 , a_2 and a_3 are defined in Eq. 6.69, e_1 , e_2 and e_3 are defined in Eq. 6.90 and b_1 , b_2 and b_3 and α_1 , α_2 , α_3 , α_4 and α_5 are defined as follows:

$$\alpha_1 = a_3(L_1 + s) - a_1 L_3$$

$$\alpha_2 = a_1 L_2 - a_2(L_1 + s)$$

$$\begin{aligned}
\alpha_3 &= \alpha_2 L_3 + \alpha_3 L_2 \\
\alpha_4 &= -\alpha_1 \cos \theta_2 + \alpha_2 \sin \theta_2 \\
\alpha_5 &= -\alpha_1 \sin \theta_2 + \alpha_2 \cos \theta_2
\end{aligned} \tag{6.96}$$

6.4.2 Aerodynamic Loads

The circulatory forces per unit length are calculated using quasi-steady strip theory and are given by:

$$\begin{aligned}
\bar{L}_u &= D_u \\
\bar{L}_v &= L \sin \alpha - D \cos \alpha \\
\bar{L}_w &= -L \cos \alpha - D \sin \alpha \\
M_{\phi_c} &\approx M_{ac} - c_d \bar{L}_w
\end{aligned} \tag{6.97}$$

where

$$\begin{aligned}
L &= \frac{1}{2} \rho V^2 c C_l \\
D &= \frac{1}{2} \rho V^2 c C_d \\
M_{ac} &= \frac{1}{2} \rho V^2 c^2 C_{m_{ac}} \\
D_u &= -\frac{U_R}{U_T} D \\
V^2 &= U_I^2 + U_P^2
\end{aligned} \tag{6.98}$$

$$\begin{aligned}
C_l &= c_0 + c_1 \alpha \\
C_d &= d_0 + d_1 |\alpha| + d_2 \alpha^2 \\
C_{m_{ac}} &= f_0 + f_1 \alpha \\
\alpha &= \tan^{-1} \left(\frac{U_P}{U_T} \right) \approx \frac{U_P}{U_T}
\end{aligned}$$

Substituting Eq.(6.98) into Eq.(6.97) gives:

$$\begin{aligned}\overline{L}_{u_e} &= -\frac{1}{2}\rho c[d_0U_R U_T + d_1|U_P|U_R] \\ \overline{L}_{v_e} &= -\frac{1}{2}\rho c[-d_0U_T^2 + (c_0U_P - d_1|U_P|)U_T + (c_1 - d_2)U_P^2] \\ \overline{L}_{w_e} &= -\frac{1}{2}\rho c[c_0U_T^2 + (c_1 - d_0)U_P U_T - d_1|U_P|U_P] \\ M_{\phi_e} &= \frac{1}{2}\rho c^2[f_0U_T^2 + f_1U_P^2 + U_P U_T f_1] - c_d \overline{L}_{w_e}\end{aligned}\quad (6.99)$$

Compressibility effects are modeled using the Prandtl-Glauert correction factor: the section lift curve slope is modified as

$$c_1 = \frac{c_1|_{M=0}}{\beta} \quad (6.100)$$

where

$$\beta = \sqrt{1 - M^2} \quad (6.101)$$

The circulatory forces L_{u_e} , L_{v_e} and L_{w_e} acting on segment 2 in the undeformed frame are expressed as:

$$\begin{Bmatrix} L_{u_e} \\ L_{v_e} \\ L_{w_e} \end{Bmatrix} = \mathbf{T}_2^T \begin{Bmatrix} \overline{L}_{u_e} \\ \overline{L}_{v_e} \\ \overline{L}_{w_e} \end{Bmatrix} \quad (6.102)$$

The noncirculatory forces, $L_{w_{nc}}$ and $M_{\phi_{nc}}$ are obtained from thin airfoil theory,

$$\begin{aligned}L_{w_{nc}} &= -\frac{\pi\rho c^2}{4}[-\ddot{w} + U_{T_0}\dot{\theta}_1 + (\frac{c}{4} + c_d)\ddot{\theta}_1] \\ M_{\phi_{nc}} &= \frac{\pi\rho c^2}{4}[(\frac{c}{4} + c_d)\ddot{w} + (\frac{c}{2} + c_d)U_{T_0}\dot{\theta}_1]\end{aligned}\quad (6.103)$$

where U_{T_0} is the constant part of the tangential component of the aerodynamic velocity and $\theta_1 = \theta_2 + \dot{\phi}$. Total aerodynamic forces acting on the blade in the

undeformed frame are obtained from Eqs.(6.102) and (6.103):

$$\begin{aligned}
 L_u^A(x, \psi) &= L_{u_0} \\
 L_v^A(x, \psi) &= -L_{v_0} \\
 L_w^A(x, \psi) &= L_{w_0} + L_{w_{in}} \\
 M_\phi^A(x, \psi) &= -M_{\phi_0} + M_{\phi_{in}}
 \end{aligned} \tag{6.104}$$

These components are the motion-dependent airloads acting on a blade section. These aerodynamic section loads, in conjunction with the sectional inertial loads derived in the next section, are used for the calculation of the blade root loads and hub loads.

6.5 Inertial Loads

The velocity at any point on the blade with a position vector defined by \vec{r} and rotating with angular velocity $\vec{\omega}$ can be defined as

$$\frac{d\vec{r}}{dt} = \frac{\partial \vec{r}}{\partial t} + \vec{\omega} \times \vec{r} \tag{6.105}$$

Differentiating the above equation again, we obtain the acceleration

$$\frac{d^2\vec{r}}{dt^2} = \frac{\partial^2 \vec{r}}{\partial t^2} + 2\vec{\omega} \times \dot{\vec{r}} + \vec{\omega} \times \vec{\omega} \times \vec{r} + \ddot{\vec{\omega}} \times \vec{r} \tag{6.106}$$

It is important to note that in the formulation for an advanced geometry blade, $\ddot{\vec{\omega}}$ is nonzero due to time varying blade pitch control. For the k th segment of the advanced geometry blade, we have,

$$\vec{\omega} = a_1 \hat{i}_k + a_2 \hat{j}_k + a_3 \hat{k}_k \tag{6.107}$$

$$\dot{\vec{\omega}} = \dot{a}_1 \hat{i}_k + \dot{a}_2 \hat{j}_k + \dot{a}_3 \hat{k}_k \tag{6.108}$$

where a_1 , a_2 and a_3 are defined in Eq. 6.69 and \dot{a}_1 , \dot{a}_2 and \dot{a}_3 are defined in Eq. 6.74, respectively. The inertial forces and moments are calculated using the following definitions

$$M^I = - \int \int \rho_s \vec{s} \times \vec{a} d\eta d\zeta = M_u^I i_k + M_v^I j_k + M_w^I k_k \quad (6.109)$$

$$F^I = \int \int \rho_s \vec{a} d\eta d\zeta = L_u^I i_k + L_v^I j_k + L_w^I k_k \quad (6.110)$$

where

$$\begin{aligned} L_u^I &= -m(\ddot{u} + 2(a_2\dot{v} - a_3\dot{w}) - (a_2^2 + a_3^2)(L_1 + s + u) \\ &+ a_1a_2(L_2 + v) + a_1a_3(L_3 + w) - \dot{a}_3L_2 + \dot{a}_2L_3 - \dot{a}_3v + \dot{a}_2w \\ &+ c_g \cos \theta_2(-\ddot{v}' + 2\dot{\theta}_1a_2 + v'(a_2^2 + a_3^2) + a_1a_2) \\ &+ c_g \sin \theta_2(-\ddot{w}' + 2\dot{\theta}_1a_3 + w'(a_2^2 + a_3^2) + a_1a_3)) \end{aligned} \quad (6.111)$$

$$\begin{aligned} L_v^I &= -m(\ddot{v} + 2(a_3\dot{u} - a_1\dot{w} + a_1a_2(L_1 + s + u) - (a_1^2 + a_3^2)(L_2 + v) \\ &+ a_2a_3(L_3 + w) - c_g \cos \theta_2(2\dot{\theta}_2a_1 - 2a_3\dot{v}' - (a_1^2 + a_3^2) - a_1a_2v') \\ &- c_g \sin \theta_2(-\ddot{\theta}_2 + 2a_3\dot{v}' - a_2a_3 - a_1a_2w')) \\ &+ \dot{a}_3u - \dot{a}_1w + \dot{a}_3(L_1 + s) - \dot{a}_1L_3) \end{aligned} \quad (6.112)$$

$$\begin{aligned} L_w^I &= -m(\ddot{w} + 2(a_1\dot{v} - a_2\dot{u}) + a_1a_3(L_2 + v) - (a_1^2 + a_2^2)(L_3 + w) \\ &+ c_g \cos \theta_2(\dot{\theta}_2 + 2a_2\dot{v}' - a_2a_3 - a_1a_3v') \\ &+ c_g \sin \theta_2(-2\dot{\theta}_1a_1 + 2a_2\dot{v}' - (a_1^2 + a_2^2) - a_1a_3w') \\ &- \dot{a}_2(L_1 + s) + \dot{a}_1L_2 - \dot{a}_2u + \dot{a}_1v) \end{aligned}$$

(6.113)

$$\begin{aligned}
M_u^I &= -m((k_{m1}^2 + k_{m2}^2)\ddot{\theta}_2 - (k_{m2}^2 \sin^2 \theta_2 + k_{m1}^2 \cos^2 \theta_2)(2a_3\dot{w}' \\
&\quad - a_2a_3 + (a_2^2 + a_3^2)\phi - 2a_3\dot{\theta}_2v' + a_1a_2w') \\
&\quad + (k_{m2}^2 \cos^2 \theta_2 + k_{m1}^2 \sin^2 \theta_2)(2a_2\dot{\theta}_2w' + a_2a_3 \\
&\quad - (a_2^2 - a_3^2)\phi + a_1a_3v' + 2a_2\dot{v}') \\
&\quad - (k_{m2}^2 - k_{m1}^2)\sin \theta_2 \cos \theta_2(-2a_3\dot{v}' + 2a_2\dot{w}' + a_2^2 - a_3^2 - a_1a_2v' \\
&\quad + 4a_2a_3\phi + 2a_2\dot{\theta}_2v' + a_1a_3w' - 2a_3\dot{\theta}_2w' - 2a_2\dot{w}') \\
&\quad + e_q \cos \theta_2(a_2a_3v' + 2a_1\dot{v} - (a_1^2 - a_2^2)w' \\
&\quad + \ddot{w} - (a_1^2 - a_2^2)L_3 + a_1a_3(L_1 + s) \\
&\quad + a_2a_3L_2 + a_1^2L_2\dot{\phi} - a_1a_2\dot{\phi}(L_1 + s) - a_2a_3L_3\dot{\phi} + a_3^2L_2\phi) \\
&\quad + e_q \sin \theta_2(a_1^2v' + a_3^2v' - \ddot{v} - a_2a_3w' + 2a_1\dot{w}' \\
&\quad + a_1^2L_3 - a_1a_2(L_1 + s) - a_2a_3L_3 \\
&\quad - a_3^2L_3 + a_1^2L_3\dot{\phi} + a_2^2L_3\dot{\phi} - a_1a_3(L_1 + s)\dot{\phi} - a_2a_3L_2\ddot{\phi}) \\
&\quad + 2\dot{a}_1k_{m1}^2 \cos^2 \theta_2 + \dot{a}_1k_{m2}^2 \cos^2 \theta_2 + \dot{a}_1k_{m2}^2 \sin^2 \theta_2)
\end{aligned}$$

(6.114)

$$\begin{aligned}
M_v^I &= -m((k_{m2}^2 \sin^2 \theta_2 + k_{m1}^2 \cos^2 \theta_2)(a_1a_3 - a_1a_2\phi \\
&\quad + 2a_3\dot{\theta}_2 + 2a_2\dot{\theta}_2\phi - \ddot{w}' + \dot{\theta}_2v' + 2\dot{\theta}_2\dot{v}' - a_1^2w' + a_3^2w' - 2a_1\dot{\theta}_2w') \\
&\quad + (k_{m2}^2 \cos^2 \theta_2 + k_{m1}^2 \sin^2 \theta_2)(a_1a_2\dot{\phi} + 2a_2\phi\dot{\theta}_2 + a_2a_3v' - \dot{\theta}_2v') \\
&\quad - (k_{m2}^2 - k_{m1}^2)\sin \theta_2 \cos \theta_2(-a_1a_2 - 2a_1a_3\dot{\phi} \\
&\quad - 2a_2\dot{\theta}_2 - 4a_3\phi\dot{\theta}_2 + (a_1^2 - a_3^2)v' + 2a_1\dot{\theta}_2v' + \dot{v}' - a_2a_3w' + 2\dot{\theta}_2\dot{w}'))
\end{aligned}$$

$$\begin{aligned}
& + c_g \cos \theta_2 (a_1 a_2 L_2 \dot{\phi} - a_2^2 L_3 v' + a_1 a_3 v' (L_1 + s) + a_2 a_3 L_2 v') \\
& + c_g \sin \theta_2 (a_1 a_2 v - 2 a_3 \dot{v} + a_1 a_3 w + 2 a_2 \dot{w} + a_1 a_2 L_2 - a_2^2 (L_1 + s) \\
& + a_1 a_3 L_3 - a_3^2 (L_1 + s) - (a_1^2 + a_2^2) L_3 w' + a_1 a_3 (L_1 + s) w' + a_2 a_3 w' L_2) \\
& + (\dot{a}_2 + \dot{a}_3) k_{m1}^2 \cos^2 \theta_2 - \dot{a}_3 k_{m2}^2 \cos \theta_2 \sin \theta_2 + \dot{a}_2 k_{m2}^2 \sin^2 \theta_2
\end{aligned} \tag{6.115}$$

$$\begin{aligned}
M_w^T &= -m((k_{m2}^2 \cos^2 \theta_2 + k_{m1}^2 \sin^2 \theta_2)(-a_1 a_2 - a_1 a_3 \dot{\phi} \\
&\quad - 2 a_2 \dot{\theta}_2 - 2 a_3 \dot{\phi} \dot{\theta}_2 + (a_1^2 + a_2^2) v' + 2 a_1 \dot{\theta}_2 v' + \ddot{v}' + \ddot{\theta}_2 w' + 2 \dot{\theta}_2 \dot{v}') \\
&\quad + (k_{m2}^2 \sin^2 \theta_2 + k_{m1}^2 \cos^2 \theta_2)(a_1 a_3 \dot{\phi} + 2 a_3 \dot{\phi} \dot{\theta}_2 - a_2 a_3 w' + \ddot{\theta}_2 w')) \\
&= (k_{m2}^2 + k_{m1}^2) \sin \theta_2 \cos \theta_2 (a_1 a_3 - 2 a_1 a_2 \dot{\phi} + 2 a_3 \dot{\theta}_2 - 4 a_2 \dot{\phi} \dot{\theta}_2 + a_2 a_3 w' \\
&\quad + 2 \dot{\theta}_2 \dot{v}' - (a_1^2 + a_2^2) w' + 2 a_1 \dot{\theta}_2 w' - \ddot{v}') \\
&+ c_g \cos \theta_2 (-a_1 a_2 v + 2 a_3 \dot{v} - a_1 a_3 w - 2 a_2 \dot{w} - a_1 a_2 L_2 \\
&\quad + (a_2^2 L_3 + a_3^2 L_2) v') + c_g \sin \theta_2 (a_1 a_2 L_2 \dot{\phi} - a_2^2 (L_1 + s) \dot{\phi} \\
&\quad + a_1 a_3 L_3 \dot{\phi} - a_3^2 \dot{\phi} (L_1 + s)) \\
&+ a_1^2 L_2 w' - a_1 a_2 (L_1 + s) w' - a_2 a_3 L_3 w' + a_3^2 L_2 w' \\
&+ (\dot{a}_2 + \dot{a}_3) k_{m1}^2 \cos^2 \theta_2 + \dot{a}_3 k_{m2}^2 \cos^2 \theta_2 - \dot{a}_2 k_{m2}^2 \sin \theta_2 \cos \theta_2
\end{aligned} \tag{6.116}$$

These loads are dependent on the blade accelerations, \ddot{a} , \ddot{v} , \ddot{w} , and $\ddot{\phi}$, which can be directly calculated by differentiating the blade response twice as,

$$\ddot{\mathbf{q}}(v) = \Phi \ddot{\mathbf{H}}(s) \xi \tag{6.117}$$

Differentiation, however, reduces the order of the temporal shape functions. This can sometimes give a poor estimate for the inertial forces. The number of time elements or the order of the temporal shape functions can be increased to help alleviate this problem. Both of these approaches will, however, increase the computational time. An alternate method used here is to derive the acceleration terms, $\ddot{\mathbf{q}}$, directly from the equations of motion. The solution of the finite element in time equations yields values for \mathbf{q} and $\dot{\mathbf{q}}$, as well as for the mass, damping and stiffness matrices, and load vector, \mathbf{M} , \mathbf{C} , \mathbf{K} , and \mathbf{F} . Rearranging the governing matrix equations yields the following expression,

$$\ddot{\mathbf{q}}(\psi) = \mathbf{M}^{-1}(\mathbf{F}(\psi) - \mathbf{C}(\psi)\dot{\mathbf{q}}(\psi) - \mathbf{K}(\psi)\mathbf{q}(\psi)) \quad (6.118)$$

Although this adds some complexity to the formulation, it provides a better estimate of blade accelerations, and thus, inertial loads.

6.6 Hub Loads

The hub loads are calculated using a force summation method. For this, the motion induced aerodynamic and inertial loads are integrated along the blade span to obtain blade loads at the root, and then summed over the blade to obtain the rotor hub loads.

The calculation of steady hub loads is needed to trim the helicopter. The harmonics of the hub loads are responsible for vibration and dynamic stresses. There are six components of the hub loads in the nonrotating frame such as longitudinal (F_{xH}), lateral (F_{yH}), and vertical (F_{zH}) hub shear forces, and rolling

(M_{xH}) , pitching (M_{yH}), and yawing (M_{zH}) hub moments. The blade root loads are also composed of six components: radial (F_{xR}), chordwise (F_{yR}) and vertical (F_{zR}) shear forces and torsional (M_{xR}), flapwise (M_{yR}) and lagwise (M_{zR}) moments in the undeformed blade frame.

For calculation of blade loads, the inertial loads are added to the aerodynamic loads as follows:

$$L = L_u \hat{i} + L_v \hat{j} + L_w \hat{k} \quad (6.119)$$

$$M = M_u \hat{i} + M_v \hat{j} + M_w \hat{k} \quad (6.120)$$

where

$$L_u = L_u^A + L_u^I \quad (6.121)$$

$$L_v = L_v^A + L_v^I \quad (6.122)$$

$$L_w = L_w^A + L_w^I \quad (6.123)$$

$$M_u = M_u^A + M_u^I \quad (6.124)$$

$$M_v = M_v^A + M_v^I \quad (6.125)$$

$$M_w = M_w^A + M_w^I \quad (6.126)$$

At the blade root, the shear forces are obtained by integrating on the section forces over the length of the blade

$$\begin{Bmatrix} F_x \\ F_y \\ F_z \end{Bmatrix} = \int_0^1 \mathbf{\Lambda}_c'^T \begin{Bmatrix} L_u \\ L_v \\ L_w \end{Bmatrix} \quad (6.127)$$

and the blade root bending moments are obtained as

$$\begin{Bmatrix} M_x \\ M_y \\ M_z \end{Bmatrix} = \int_0^1 \mathbf{\Lambda}_c'^T \begin{Bmatrix} -L_v(L_3 + w) + L_w(L_2 + v) + M_u \\ L_u(L_3 + w) - L_w(L_1 + s + u) + M_v \\ -L_u(L_2 + v) + L_v(L_1 + s + u) + M_w \end{Bmatrix} \quad (6.128)$$

The rotor hub loads are obtained by summing load contributions from the individual blades. In the fixed frame, the hub loads are expressed as,

$$F_X^H(\psi) = \sum_{m=1}^{N_b} (F_x^m \cos \psi_m + F_y^m \sin \psi_m - F_z^m \cos \psi_m \beta_p) \quad (6.129)$$

$$F_Y^H(\psi) = \sum_{m=1}^{N_b} (F_x^m \sin \psi_m + F_y^m \cos \psi_m - F_z^m \sin \psi_m \beta_p) \quad (6.130)$$

$$F_Z^H(\psi) = \sum_{m=1}^{N_b} (F_z^m + F_x^m \beta_p) \quad (6.131)$$

$$M_X^H(\psi) = \sum_{m=1}^{N_b} (M_x^m \cos \psi_m + M_y^m \sin \psi_m - M_z^m \cos \psi_m \beta_p) \quad (6.132)$$

$$M_Y^H(\psi) = \sum_{m=1}^{N_b} (M_x^m \sin \psi_m + M_y^m \cos \psi_m - M_z^m \sin \psi_m \beta_p) \quad (6.133)$$

$$M_Z^H(\psi) = \sum_{m=1}^{N_b} (M_z^m + M_x^m \beta_p) \quad (6.134)$$

where F_x^m, F_y^m, F_z^m are the shear loads and M_x^m, M_y^m, M_z^m are the moments due to the m th blade and are obtained from Eqs. 6.127 and 6.128, respectively.

The blade root loads and hub loads are periodic over the rotor azimuth and Fourier analysis is used to identify the harmonic content of the loads. In general, a periodic function can always be expressed as a Fourier series:

$$f(\psi) = f_0 + \sum_{n=1}^{\infty} (f_{ne} \cos n\psi + f_{ns} \sin n\psi) \quad (6.135)$$

where

$$f_0 = \frac{1}{2\pi} \int_0^{2\pi} f(\psi) d\psi \quad (6.136)$$

$$f_{ne} = \frac{1}{\pi} \int_0^{2\pi} f(\psi) \cos n\psi d\psi \quad (6.137)$$

$$f_{ns} = \frac{1}{\pi} \int_0^{2\pi} f(\psi) \sin n\psi d\psi \quad (6.138)$$

$$f_n = \sqrt{f_{nc}^2 + f_{ns}^2} \quad (6.139)$$

The f_0 term is the steady component of the function. The subscript n indicates the n -th harmonic term, and f_n denotes the amplitude of the n per rev resultant component. In this equation, the function f can be the blade loads, hub loads or the response.

The higher harmonics are important for vibration analysis. The hub loads, therefore, are expanded in a Fourier series. The steady components are the rotor thrust, longitudinal and side forces, rolling and pitching moments, and the rotor shaft torque. For a tracked rotor, whose blades are identical structurally and aerodynamically, only harmonics equal to integer multiples of number of blades are transmitted to the body. Also, the harmonics of the bending and torsional moment at the blade root are a source of blade dynamic stresses.

6.7 Implementation of Advanced-tip Blade Formulation in UMARC

The analysis in UMARC is based on the finite element method. As such, all the mass, damping, stiffness and load matrices are calculated at the elemental level, and then assembled into the global matrices. Generic of this procedure is described in chapter 4.

For the implementation of advanced tip blade, two major steps are introduced in the code: one in the calculation of elemental matrices and the other in the assembly of elemental matrices. The input data-set contains the informa-

tion of tip sweep and anhedral angle, Λ_1 (positive for forward tip sweep) and Λ_2 (negative for tip droop), respectively.

Calculation of elemental matrices

The rotor blade is discretized into number of inboard blade and tip elements. For a tip element, the tip coordinate system (ACS) is defined according a given tip orientation (Λ_1 and Λ_2) (section 6.2). The elemental matrices (mass(M_e), damping(C_e), stiffness(K_e) and force (F_e)) of tip element are calculated in the tip coordinate system (based on an actual geometry of tip) using newly-derived kinetic energy expressions and aerodynamic loads expressions as derived in section 6.3 and 6.4.

Accordingly, these modifications are implemented in the structural routine (STRUCT) and aerodynamic routine (AEROMX). In case of rectangular blade ($\Lambda_1, \Lambda_2 = 0$), the tip coordinate system (ACS) naturally becomes an extension of the blade coordinate system. Also, the kinetic energy expressions and aerodynamic loads expressions of advanced tip become identical to those of rectangular blade. As a result, the elemental matrices (mass(M_e), damping(C_e), stiffness(K_e) and force (F_e)) of advanced tip element become those of rectangular tip element.

Subroutine SWEEP

This subroutine calculates the nonlinear transformation matrices with given

sweep and droop angles. The transformation matrices are used to convert elemental matrices to global matrices, or vice versa.

Subroutine STRUCT

For the advanced tip blade, this subroutine was modified to account for tip sweep and droop. For the specified sweep and droop angle for i th element, the structural elemental matrices (mass(\mathbf{M}_e), damping(\mathbf{C}_e), stiffness(\mathbf{K}_e) and force (\mathbf{F}_e)) of advanced tip element are calculated with respect to Tip Coordinate Systems (ACS) using Eqs. derived in Section 6.3. One of the reasons to calculate these elements in ACS (and complicates the procedure) is due to the fact that one can only obtain the consistent effect of tip sweep and droop by deriving the equations of motions about the actual geometry.

Subroutine AEROMX

For the advanced tip blade, this subroutine was also modified to account for tip sweep and droop.

For the specified sweep and droop angle for i th element, the variable constants due to tip sweep and droop are first determined using Eq.(6.69), Eq.(6.91), Eq.(6.96). Next, using these constants the blade velocity U_T , U_P and U_R are calculated wrt ACS. For this, Eq.(6.69)-(6.96) are used. Based on these information, the aerodynamic elemental matrices (mass(\mathbf{M}_e), damping(\mathbf{C}_e), stiffness(\mathbf{K}_e) and force (\mathbf{F}_e)) of advanced tip element are calculated.

Assembly of Blade and Tip Elements

After the elemental matrices (structural + aerodynamic) are calculated, one needs the transformation matrices in the assembly process in order to satisfy the compatibility conditions at the junction between blade and tip elements, as described in section 6.5.

The elemental mass, damping, stiffness and load matrices of the tip element are modified using nonlinear transformation relations. The mass(M_e), damping(C_e), stiffness(K_e) and force (F_e) of advanced tip element are transformed to modified mass(M_{Tip}), damping(C_{Tip}), stiffness(K_{Tip}) and force (F_{Tip}) matrices for assembly purpose.

In UMARC, these changes are implemented in the assembly routines (AS-BGMK, EVFRSW). In case of rectangular blade, all transformation matrices become unit matrices.

Note that these two modifications in UMARC due to advanced-tip are implemented in such a fashion that these are also valid for straight-tip element. Therefore, the user can specify any tip sweep and droop angle (Λ_1, Λ_2) in the input data-set. In addition, user also can specify the variable sweep and droop angles.

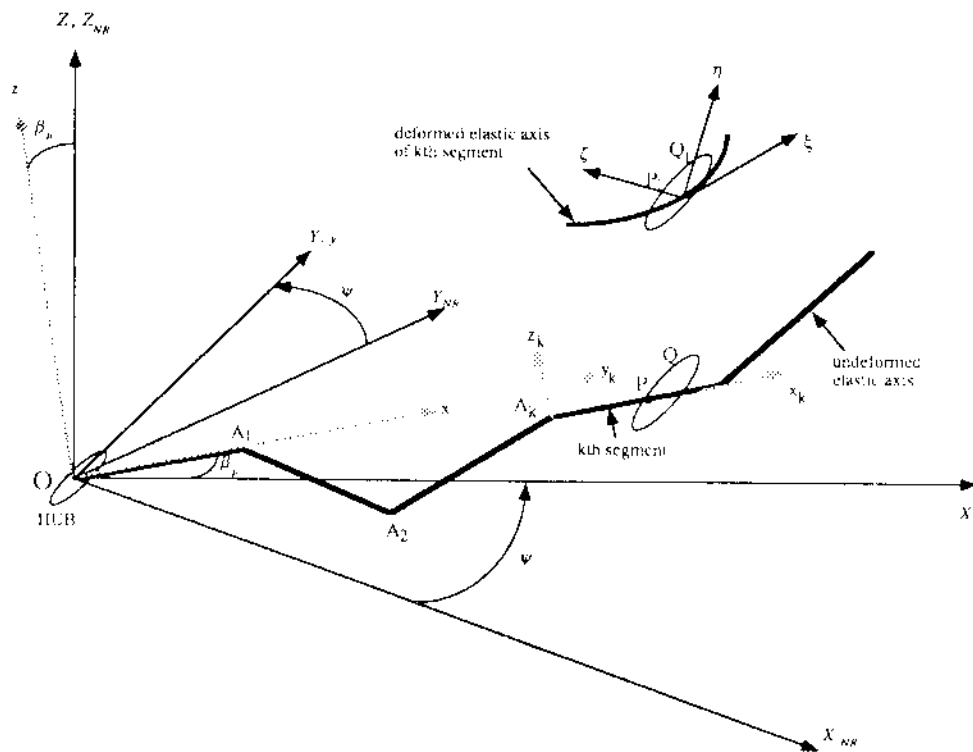


Figure 6.1: Coordinate systems used to define the blade geometry of the advanced geometry rotor

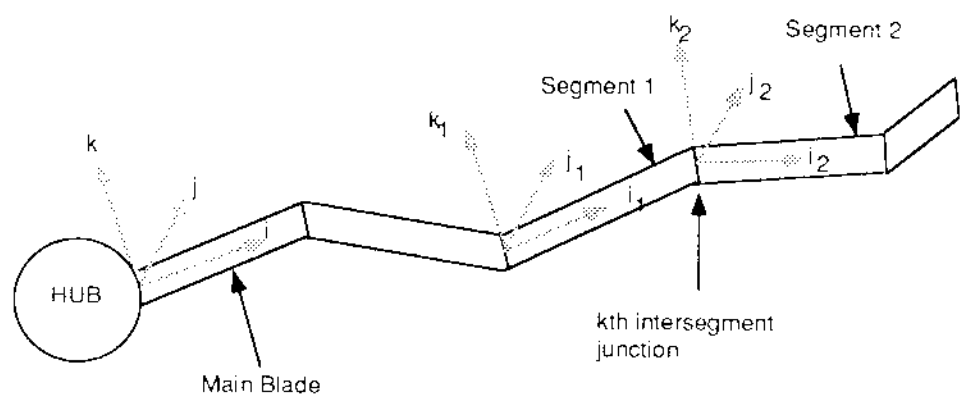


Figure 6.2: Definitions of the segment 1 and 2 and the intersegment junction

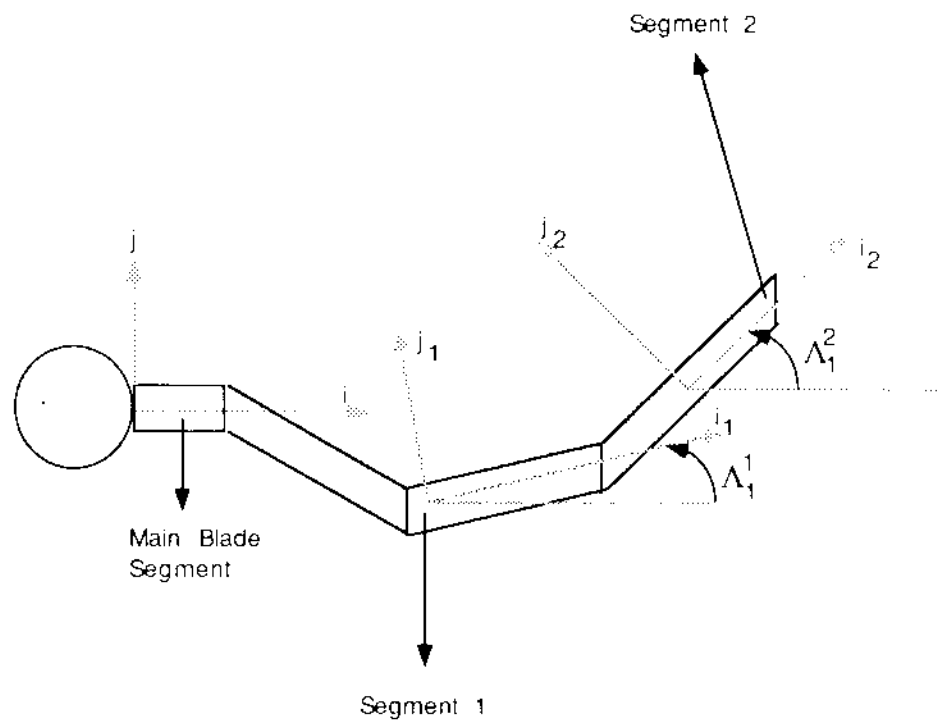


Figure 6.3: Definition of blade sweep at segments 1 and 2 (positive forward)

Bibliography

- [1] Bir, G., Chopra, I., "Aeromechanical Stability of Rotorcraft with Advanced Geometry Blades," Presented at the AIAA 34th Structures, Structural Dynamics and Materials Conference, La Jolla, Calif., Apr 1993.
- [2] Kim, K.C., "Dynamic Analysis of Advanced Tip Rotors including Three-Dimensional Aerodynamics", UMAERO Report No. 90-31, Also, Doctoral Dissertation, Department of Aerospace Engineering, University of Maryland, 1990.
- [3] Benquet, P. and Chopra, I., "Calculated Dynamic Response and Loads for an Advanced Tip Rotor in Forward Flight," *Proceedings of 15th European Rotorcraft Forum*, Amsterdam Netherlands, September 1989.

Chapter 7

BEARINGLESS ROTOR MODELING

Chapter 7

Bearingless Rotor Modeling

7.1 Introduction

The bearingless rotor is a specialized case of hingeless rotor wherein the pitch bearing, in addition to the flap and lag hinges, is eliminated. Pitch control from the pitch link to the main blade is transmitted via a torsionally stiff torque tube. This in turn twists a torsionally soft flexbeam, which functions effectively as a pitch bearing. The bearingless rotor is rapidly gaining acceptance as a design configuration for the future helicopters; it offers design simplicity, weight reduction, better maintenance, and more control power. However, these benefits cannot be realized without a good understanding of its dynamic loads and aeromechanical stability characteristics. The analysis of a bearingless rotor is more involved than that of a hingeless or an articulated rotor due to the multiple load paths near the blade root and nonlinear bending-torsion couplings due to large twisting of the flexbeam. To alleviate blade dynamic stresses, bearingless

rotors are designed as soft-inplane rotors. This makes these rotors susceptible to aeromechanical instabilities in air as well as on the ground.

In case of hingeless rotors, attempts have been made to analytically treat the blade as an equivalent-hinge, spring-restrained, rigid-blade model. Such modeling appears useful for approximate assessment of the response and stability problems. For bearingless rotors, such simplified models become less satisfactory – even for approximate analysis. This is because the torsion-bending couplings are very sensitive to pitch-control configuration parameters and can also vary significantly with changes in the operating conditions. All the important structural elements of the bearingless rotor need to be accurately modeled to capture the load redundancies and nonlinear couplings.

To date, several bearingless main rotor (BMR) configurations have evolved, each presenting unique modeling issues. As expected, the response loads and stability problems associated with each configuration are also unique. A key goal of UMARC is to accurately predict the response and stability characteristics of several bearingless rotor configurations. State-of-the-art finite element methodology is used to model the main structural elements of the bearingless rotor (e.g., blade, flexbeams and the torque tube). Typically, one BMR configuration differs from another the way its blade pitch change mechanism is designed and the way an optional snubber is used to alter the bending-torsion couplings. Figure 7.1 shows an advanced bearingless rotor configuration modeled in UMARC. As we shall see, through a proper selection and/or elimination of the various

configuration parameters, this configuration can model many bearingless rotor designs suggested in literature.

Analytical model of the bearingless rotor is described in Section 7.2. Hub kinematic equations, particularly those governing pitch-change mechanism and snubber action, are derived in section 7.3. Section 7.4 describes finite element modeling of the bearingless rotor blade using 15-dof beam elements discussed in Chapter 2. Adaptation of the BMR-related kinematic equations and boundary constraints to the finite element scheme is discussed in section 7.4.3. Section 7.5 describes modifications in the solution procedure dictated by the bearingless rotor configuration. Finally, section 7.6 discusses implementation of the bearingless rotor theory in the UMARC code.

7.2 Analytical Model

Analytical modeling of single-load-path blade, representing hingeless or articulated blade, was developed in Chapter 2. The modeling is extended here to include more complex bearingless blades which may have multiple load paths. Fig. 7.1 shows schematic of the bearingless blade analytical model. Only those components believed essential for characterizing the bearingless rotor dynamics are retained. As indicated in the introduction, a bearingless design eliminates

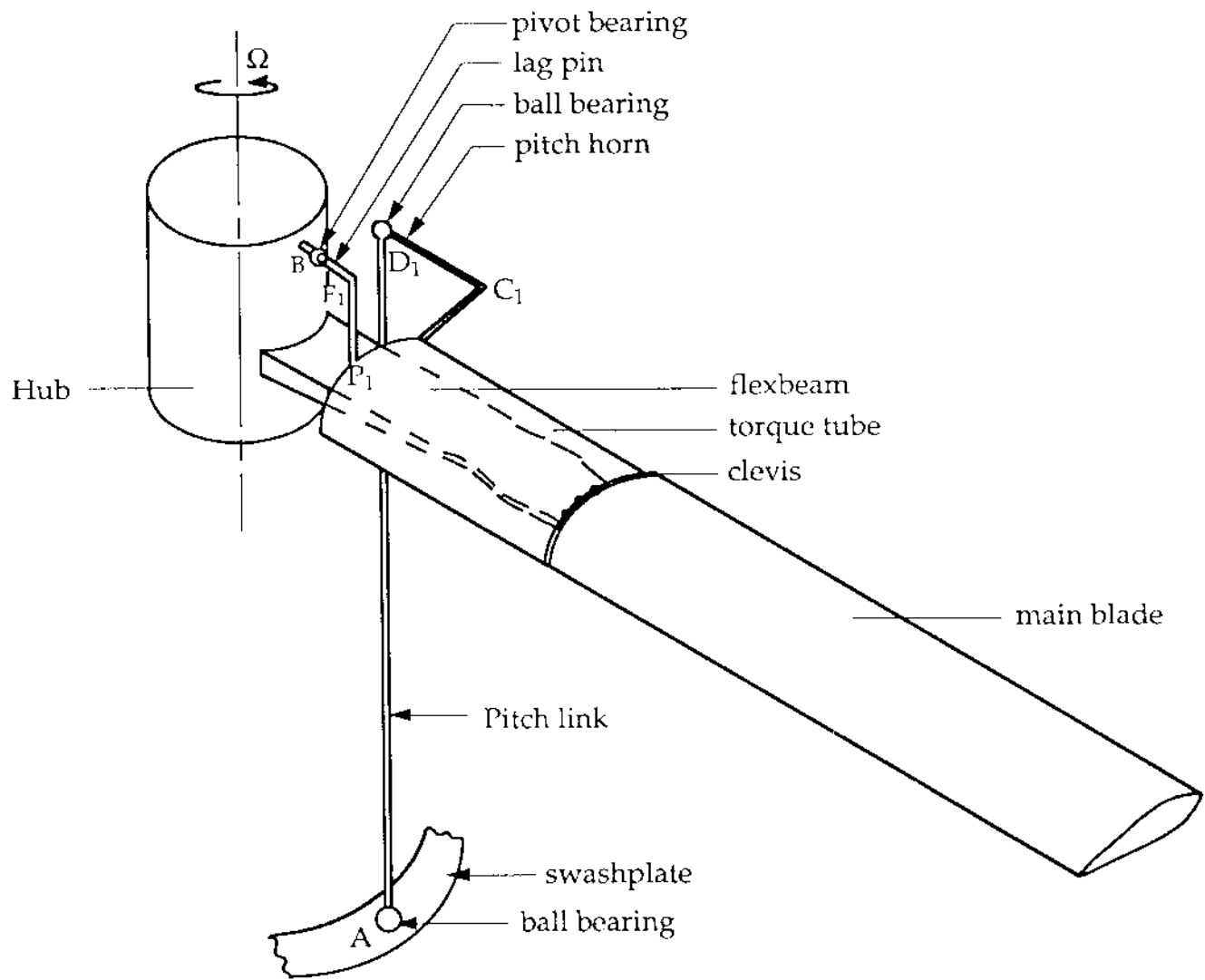


Fig 7.1: Schematic of the Bearingless Rotor Blade

the hinges and the pitch bearing as well. To facilitate pitch change, the bearingless blade has an elastic flexure consisting of flexbeams and a torque tube. The flexure extends from the hub to a rigid clevis where it is attached to the main blade. The inboard end of the torque tube is connected to a pitch link via a pitch horn, and the outboard end is attached to the clevis. The blade pitch is controlled by rotating the clevis attached to the inboard end of the blade via the torsionally-stiff torque tube.

The major structural load-carrying members of the bearingless rotor, viz. the blade, the torque tube and the flexbeams, are idealized as Euler-Bernoulli elastic beams undergoing flap bending w , lag bending v , elastic twist ϕ and axial deflection u . The inclusion of axial degree of freedom becomes essential for a multiple-load-path bearingless rotor configuration to properly model the flexure components. Each elastic beam member is discretized into a number of beam elements, with each element having fifteen degrees of freedom (described in Chapter 2). The pitch link can be modeled either as a rigid element or as a linear spring element to simulate the control stiffness. The pitch horn, joining the pitch link to the torque tube, has both radial and chordwise offsets. The rotor can have hub precone, prepitch of the blade relative to the flexure, variable sweep and variable blade twist.

The numerous pitch control designs suggested in literature can be reduced from the analytical model of Fig. 7.1. This requires a proper selection of the geometry and elastic properties of the pitch control elements. For example, if

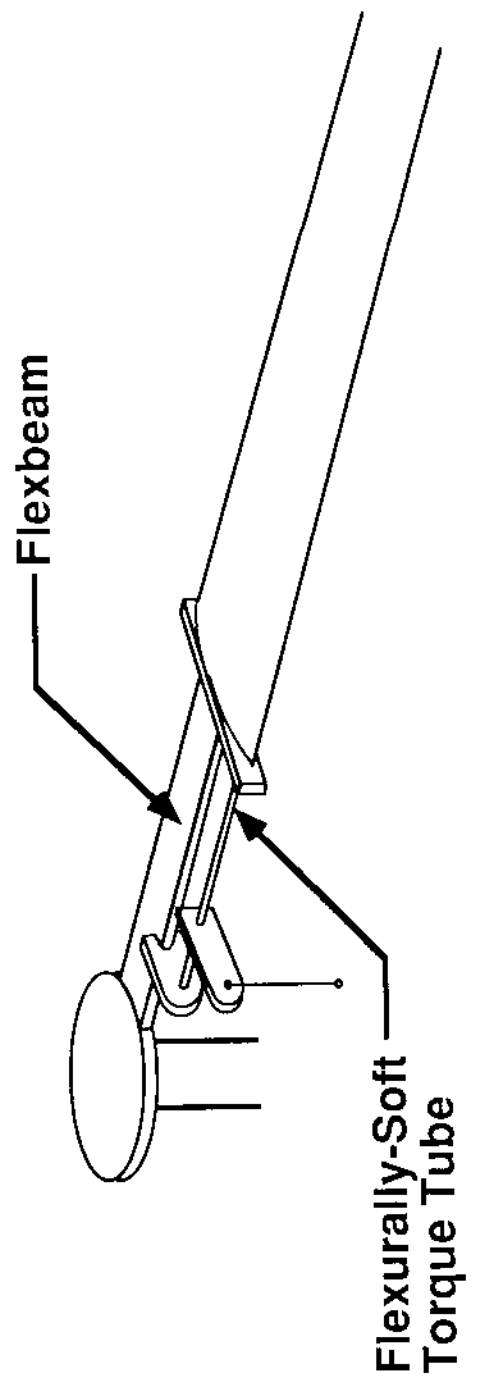


Fig. 7.2: Bearingless Blade with Flexible Torque Tube
(Case II of Ref. 2)

we wish to configure our analytical model to represent bearingless rotor blade shown in Fig 7.2 (which is configuration II of Ref.2), three simple modification are required (the user expresses the modification through easily understandable keywords described in Chapter 8). First, the lag pin is removed; this eliminates snubber action to be discussed shortly. Second, pitch arm length, a , is input as a negative parameter; this moves the pitch link to the trailing side of the blade. Third, flexural rigidity of the torque tube is reduced to simulate a flexurally-soft torque tube. It may be of interest to note that a flexurally-soft torque tube tends to eliminate the bending-torsion coupling; the bending-torsion coupling in fact is a complex function of the torque tube stiffness, pitch arm geometry, pitch link stiffness, and the operating conditions.

A cuff snubber offers a more effective way to control the bending-torsion coupling. In Fig 7.1, lag pin BF_1P_1 represents the cuff snubber; its vertical arm F_1P_1 is rigidly attached to the cuff at point P_1 , whereas its horizontal arm BF_1 freely slides through a pivot bearing B. The pivot bearing is a universal ball bearing allowing the lag pin a free angular motion in addition to the sliding motion. However, it restrains the vertical and lateral motions of the lag pin at point B. This, as we shall see in the next section, couples the blade lag motion with the pitch motion; the degree of coupling depends on the vertical and radial offsets of the cuff with respect to the snubber pivot point B, in addition to the chordwise offset of the pitch link from the blade elastic axis. Note that the pivot point B is fixed with respect to the blade rotating frame.

The usage of a snubber allows a favorable bending-torsion coupling without inducing undesirable bending moments in the flexbeams. For the configuration shown in Fig. 7.1, wherein the pitch link is at the leading edge side of the blade, a negative pitch-lag coupling results (i.e., lag back causes nose-up pitch motion).

7.3 Bearingless Rotor Hub Kinematics

Kinematics of the bearingless rotor hub is essentially governed by three sets of geometric constraints: (i) constraints at the inboard end of the torque tube which is attached to the lag pin and the pitch link; (ii) compatibility constraints at the clevis joining the flexure to the blade inboard end; and (iii) cantilevered constraints at the flexbeams inboard ends. We first derive constraint equations for the torque tube inboard end.

7.3.1 Kinematics Constraints due to Pitch Link and Lag Pin

Fig. 7.3 shows schematic of the rotor hub configuration in the deformed and the undeformed states. The orthogonal axes system x, y, z and associated unit vectors i, j, k are attached to the undeformed torque tube with origin P_1 at the inboard end and x axis directed along the elastic axis. The coordinate

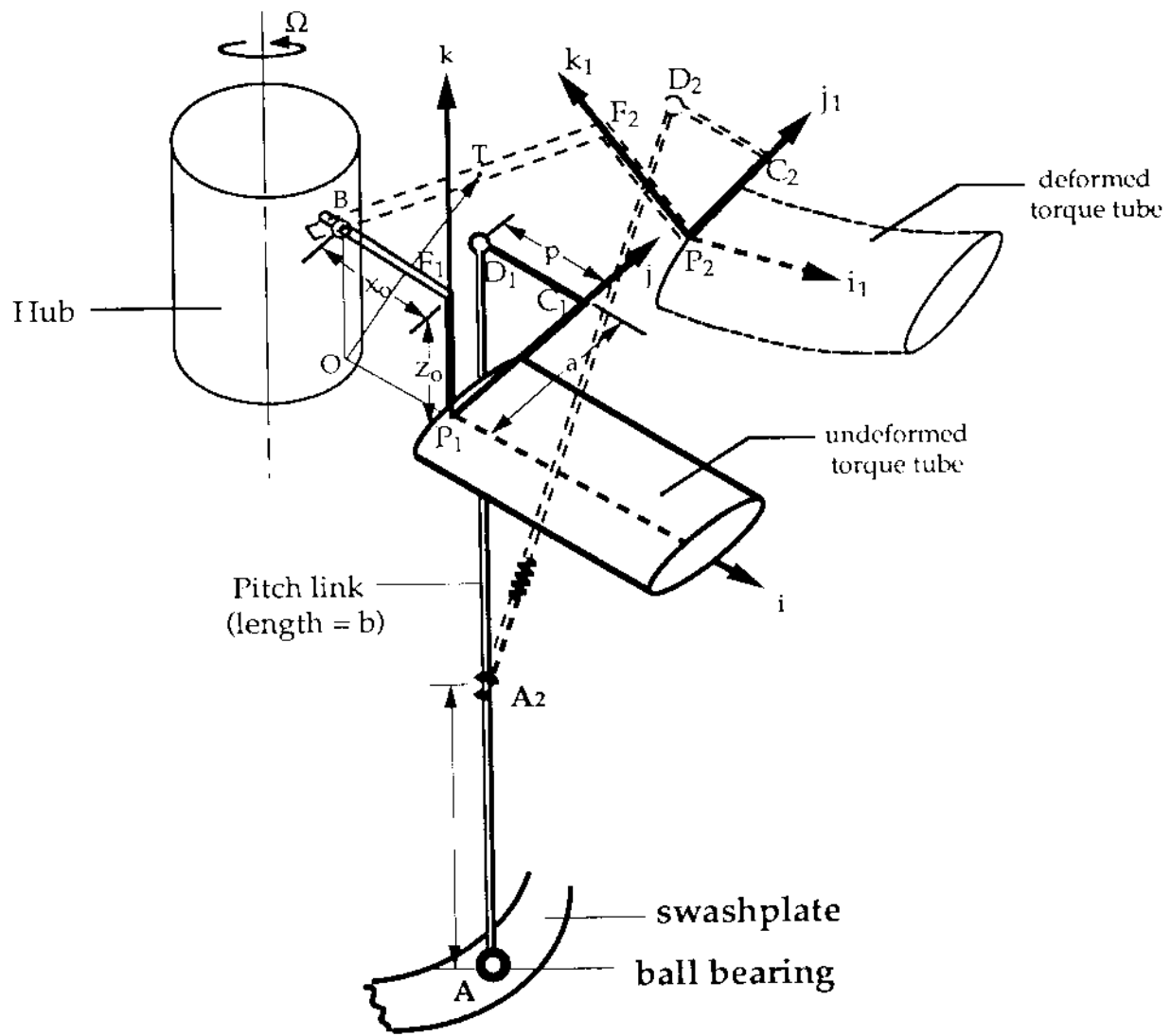


Fig 7.3 : Bearingless Rotor Hub Kinematics

axes x_1, y_1, z_1 and the associated unit vectors i_1, j_1, k_1 describe orientation of the inboard end of the torque end in the deformed state, with axis x_1 tangent to the elastic axis of the torque tube at point P_2 . In the undeformed state, the pitch horn is positioned at $P_1C_1D_1$, the pitch link is positioned at AD_1 with its lower end connected to swashplate via a ball bearing A and its upper end connected to the pitch horn via a ball bearing D_1 ; the lag pin is positioned at P_1F_1B with its vertical arm F_1P_1 rigidly attached to the torque tube and its horizontal arm F_1B passing through the pivot bearing B . When the bearingless rotor blade deforms, the pitch horn assumes the position $P_2C_2D_2$, the pitch link assumes the position A_2D_2 , and the lag pin assumes the position P_2F_2B . Note since the lag pin can slide through the pivot bearing B , arm length BF_1 need not equal length BF_2 . AA_2 represents the swashplate control deflection, and k_p represents the pitch link stiffness.

The position vector of the pitch link end D_2 with respect to its point of attachment to the displaced swashplate is given by

$$\begin{aligned}\overline{\mathbf{A}_2\mathbf{D}_2} &= \overline{\mathbf{O}\mathbf{D}_2} - \overline{\mathbf{O}\mathbf{A}} - \overline{\mathbf{A}\mathbf{A}_2} \\ &= \overline{\mathbf{O}\mathbf{P}_1} + \overline{\mathbf{P}_1\mathbf{P}_2} + \overline{\mathbf{P}_2\mathbf{C}_2} + \overline{\mathbf{C}_2\mathbf{D}_2} - \overline{\mathbf{O}\mathbf{A}} - \overline{\mathbf{A}\mathbf{A}_2}\end{aligned}\quad (7.1)$$

Now,

$$\overline{\mathbf{O}\mathbf{A}} = x_A i + y_A j - z_A k \quad (7.2)$$

where x_A, y_A, z_A are respectively the radial, chordwise and vertical offsets of

the pitch-link-to-swashplate attachment point A with respect to point O. Further, the undeformed axes unit vectors i, j, k are related to the deformed axes coordinates by the relation

$$\begin{bmatrix} i \\ j \\ k \end{bmatrix} = \mathbf{T}_{DU} \begin{bmatrix} i_1 \\ j_1 \\ k_1 \end{bmatrix} \quad (7.3)$$

where the transformation matrix \mathbf{T}_{DU} is derived in Section 2.1.2. Substitution of Eqns (7.2) and (7.3) in Eqn (7.1) yields

$$\begin{aligned} \overline{\mathbf{A}_2 D_2} &= (x_0 i + u i + v j + w k + a j_1 - p i_1) - (x_A i + y_A j - z_A k) - w_s k \\ &= (u + x_0 - x_A + a T_{21} - p T_{11}) i + (v - y_A + a T_{22} - p T_{12}) j \\ &\quad + (w + z_A + a T_{23} - p T_{13} - w_s) k \end{aligned} \quad (7.4)$$

where T_{11}, \dots, T_{13} are the elements of the transformation matrix \mathbf{T}_{DU} expressed in terms of the bending slopes u', v' and the blade rotation θ_1 (see Section 2.1.2). The remaining parameters are defined as follows

x_0 = *OP₁ = radial distance of the torque tube inboard end from*

pivot bearing B

a = *P₁C₁ = chordwise pitch arm length of the pitch horn,*

positive towards the leading

p = *C₁D₁ = spanwise pitch arm length of the pitch horn*

w_s = *AA₂ = vertical displacement of the swash plate at the pitch*

link attachment point

x_A = radial offset of the pitch link to swash plate attachment point, bearing A, with respect to point O

y_A = lateral offset of point A with respect to O

z_A = vertical offset of point A with respect to O positive downward

The square of length of the deformed pitch link is given by

$$\overline{\mathbf{A}_2 \mathbf{D}_2} \cdot \overline{\mathbf{A}_2 \mathbf{D}_2} = (b + w_p)^2 \quad (7.5)$$

where b is the length of the undeformed pitch link and w_p is the elastic elongation of the pitch link. Substitution of Eqn (7.4) in Eqn (7.5) and replacement of the matrix elements T_{11}, \dots, T_{13} by their equivalent expressions yields

$$\begin{aligned} b^2 + 2bw_p + w_p^2 &= [u + x_d - av' \cos \theta_1 - aw' \sin \theta_1 - p(1 - \frac{v'^2 + w'^2}{2})]^2 \\ &\quad + [v - y_A + a(\frac{(1 - \frac{v'^2}{2})(\cos \theta_1 - v'w' \sin \theta_1)}{2}) - pw']^2 \\ &\quad + \left[w + z_A + a(1 - \frac{w'^2}{2}) \sin \theta_1 - pw' - w_s \right]^2 \end{aligned} \quad (7.6)$$

where

$$x_d = x_0 - x_A \quad (7.7)$$

Substituting for the square of the pitch link length

$$b^2 = (x_d - p)^2 + (a - y_A)^2 + z_A^2 \quad (7.8)$$

in Eqn 7.6 and linearizing the resulting equation in terms of the deformation variables, we finally obtain

$$\begin{aligned} (a - y_A) v - (ax_d - py_A) v' + (z_A - w_s) (w - pw' + a\hat{\phi}) \\ = bw_p + (z_A w_s - \frac{w_s^2}{2}) \end{aligned} \quad (7.9)$$

Next, to derive the kinematic constraints imposed by the lag pin, consider an arbitrary point T on the horizontal arm BF_2 of the lag pin. Its position vector with respect to point O is

$$\begin{aligned} \bar{l} &= \overline{OT} \\ &= \overline{OF_2} + \overline{F_2T} \\ &= \overline{OP_1} + \overline{P_1P_2} + \overline{P_2F_2} + \overline{F_2T} \\ &= (x_0 + u)i + vj + wk + z_0k_1 + si_1 \\ &= (x_0 + u + z_o T_{31} + s T_{11})i + (v + z_0 T_{32} + s T_{12})j \\ &\quad + (w + z_0 T_{33} + s T_{13})k \end{aligned} \quad (7.10)$$

Since the arm F_2B must pass through the pivot bearing B, we should be able to find a scalar s for which $\bar{l} = \overline{OB} = z_0k$, i.e.,

$$z_0k = \text{right hand side of Eqn 7.10} \quad (7.11)$$

This is equivalent to the following three scalar equations

$$\begin{aligned}
x_0 + u + z_0 T_{31} + s T_{11} &= 0 \\
v + z_0 T_{32} + s T_{12} &= 0 \\
w + z_0 T_{33} + s T_{13} &= z_0
\end{aligned} \tag{7.12}$$

Elimination of s from the above equations, replacement of T_{11}, \dots, T_{13} in terms of the blade displacements, and subsequent linearization, yields the following two equations.

$$\begin{aligned}
-z_0 \phi + v &= v' x_0 \\
w &= w' x_o
\end{aligned} \tag{7.13}$$

Thus there is one kinematic constraint associated with the pitch link, Eqn. 7.9, and there are two boundary constraints associated with the lag pin, Eqns. 7.13. Equation 7.9 represents a boundary condition only if the pitch link is rigid, i.e., $w_p = 0$, in which case the equation represents equation of a spherical surface traced by end D_1 of the pitch link with its lower end A fixed. Equations 7.13 imply that the lag pin can freely slide through the pivot bearing but is restrained in the lateral and vertical directions.

We shall now adapt the kinematic constraints 7.9 and 7.13 to specialized cases of the bearingless rotor configuration exemplified by Fig. 7.1. For all these cases, it is assumed that the rotor controls are fixed. The boundary conditions are expressed in terms of the perturbation quantities.

Rigid Pitch Link Alone (No Lag Pin)

For this case, elastic elongation w_p is zero. Also, since the swashplate is fixed, $w_s = 0$. The kinematic equation 7.9 therefore simplifies to

$$(a - y_A) v - (ax_d - py_A) v' + (z_A)(w - pw' + a\dot{\phi}) = 0 \quad (7.14)$$

Further, if the pitch link is vertical, then

$$\begin{aligned} b &= z_A \\ a &= y_A \end{aligned} \quad (7.15)$$

and therefore,

$$x_d = x_0 - x_A = p \quad (7.16)$$

Because of the last two sets of equations, the boundary condition for the rigid vertical pitch link assumes the form

$$w - p w' + a \dot{\phi} = 0 \quad (7.17)$$

Any one of the three degrees of freedom appearing in the above equation can be taken as the dependent variable. In UMARC, the torsional degree of freedom $\dot{\phi}$ is selected as the dependent variable, and w, w' are selected as the independent variables. The dependent degree of freedom is eventually eliminated from the equations of motion.

Rigid Vertical Pitch Link with Lag Pin

For this case, Eqns. 7.13 and 7.14 apply. Since there are three boundary constraint equations, three dependent variables need to be selected. In UMARC, v , w , and $\hat{\phi}$ are selected as the dependent degrees of freedom. Using Eqns 7.13 and 7.14, these can be expressed in terms of the independent variables v' and w' as follows

$$\begin{aligned}\hat{\phi} &= -\frac{x_0 - p}{a} w' \\ w &= x_0 w' \\ v &= v' x_0 - z_0 \frac{x_0 - p}{a} w'\end{aligned}\tag{7.18}$$

Soft Vertical Pitch Link with Lag Pin

In this case, the boundary constraints associated only with the lag pin apply, i.e.,

$$\begin{aligned}w &= x_0 w' \\ v &= z_0 \hat{\phi} + x_0 v'\end{aligned}\tag{7.19}$$

The v' , w' , and $\hat{\phi}$ are the independent degrees of freedom. The dependent degrees of freedom, v and w , are eliminated from the equations of motion.

Note that, for all the cases considered, the axial deflection, u , is always an

independent degree of freedom at the torque tube end. For the case when there is no lag pin and the pitch link is soft, no boundary conditions apply at the torque tube inboard end.

7.3.2 Displacement Compatibility Conditions at the Clevis

As seen in Fig. 7.4, the inboard end of the main blade is attached to the flexure beams through a clevis. A rigid clevis, assumed in our analytical model, implies continuity of bending slopes between the main blade and the flexure beams, and constancy of the elastic offsets of beams at the clevis juncture. This assumption leads to the following compatibility relations:

$$\begin{aligned}
 u_k &= u_b - \eta_k v' \\
 v_k &= v_b \\
 v'_k &= v'_b \\
 w_k &= w_b + \eta_k (\theta_{cc} + \hat{\phi}_b) \\
 w'_k &= w'_b \\
 \hat{\phi}_k &= \hat{\phi}_b + \theta_{cc} \quad (\text{for the flexbeam}) \\
 \hat{\phi}_k &= \hat{\phi}_b \quad (\text{for the torque tube}) \tag{7.20}
 \end{aligned}$$

where u_k , v_k , w_k , and $\hat{\phi}_k$ are deflections of the k th flexure beam, and u_b , v_b , w_b , and $\hat{\phi}_b$ are deflections of the main blade at the clevis. The flexure beams are

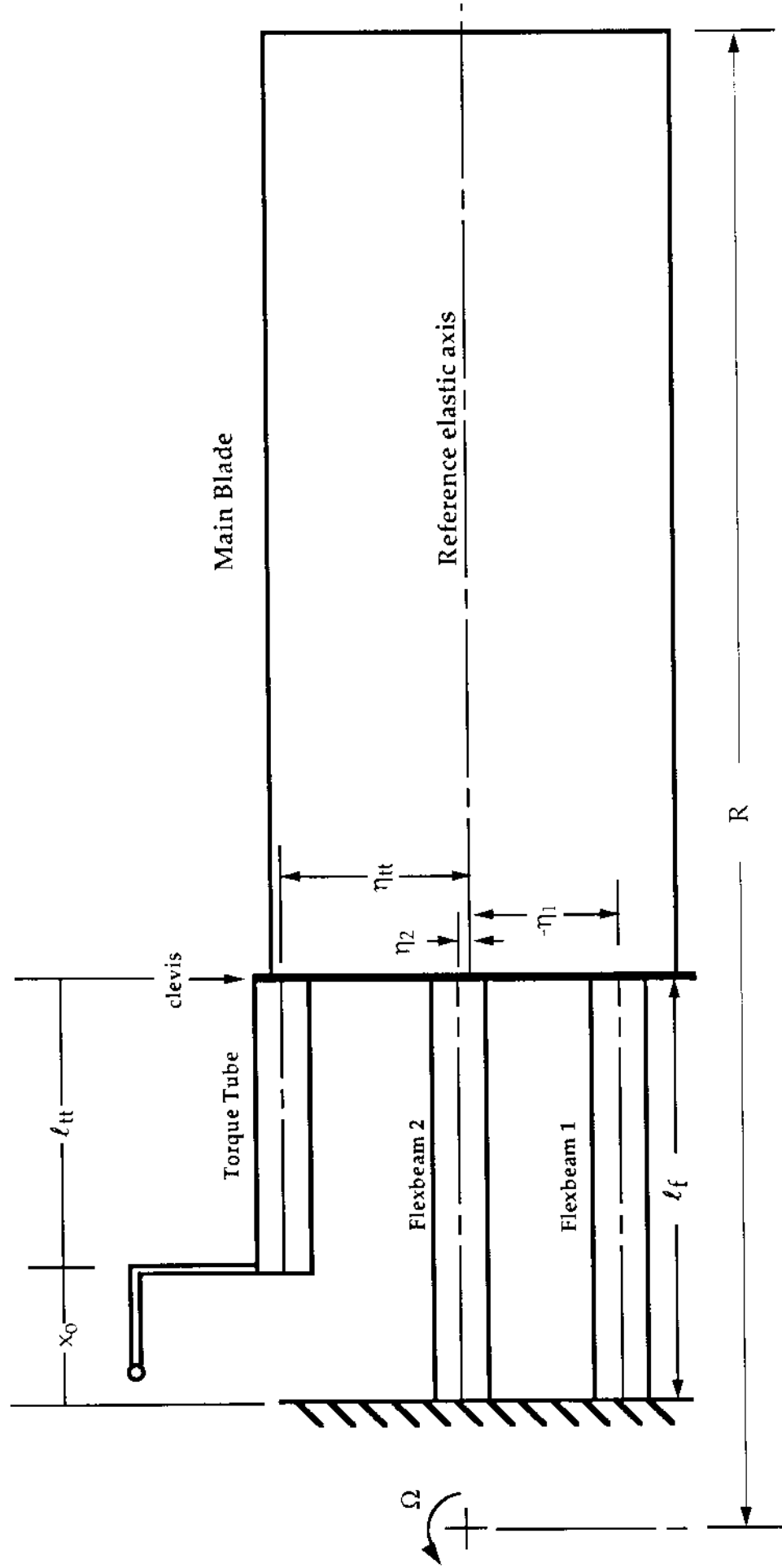


Fig 7.4: Analytical Model of the Bearingless Blade

θ_{cc} = pitch control

θ_{bf} = blade-to-flexbeam
built-in pitch

θ_{fh} = built-in pitch at the
flexbeam root

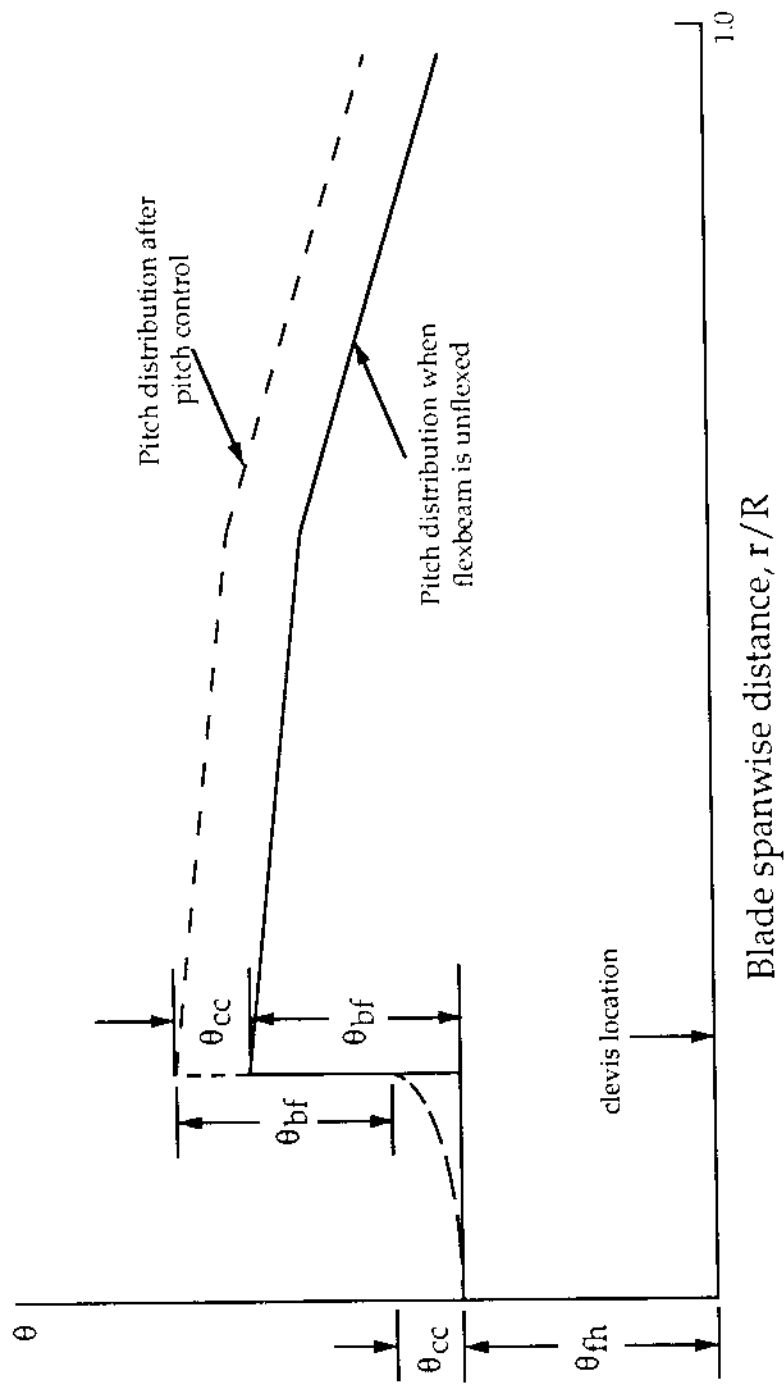


Fig. 7.5 : Pitch distribution along a bearingless blade

numbered 1,2,3, etc. with the last number reserved for the torque tube. The η_k is the offset of the k th flexure beam from the elastic axis of the main blade and is considered positive towards leading edge of the main blade. The angle θ_{cc} is the applied pitch control at the clevis (see Fig. 7.5).

Cantilevered Boundary Conditions

The cantilevered conditions at the flexbeam inboard end imply

$$\begin{aligned} u_k &= 0, \quad v_k = 0, \quad w_k = 0, \\ v'_k &= 0, \quad w'_k = 0, \quad \dot{\phi}_k = 0 \end{aligned} \tag{7.21}$$

where the subscript k refers to the k th flexbeam.

7.4 Finite Element Analysis

7.4.1 Formulation Using Hamilton's Principle

Equations of motion for the bearingless rotor are derived using Hamilton's variational principle:

$$\delta H = \int_{t_1}^{t_2} (\delta U - \delta T - \delta W) dt = 0 \tag{7.22}$$

The δU and δT are respectively the virtual variations of strain and kinetic energies, and δW is the virtual work done by the external forces. These virtual variations have contributions from the rotor and the fuselage (if included in the system). Contributions from the rotor can in turn be expressed as a sum of contributions from each blade. Therefore,

$$\begin{aligned}\delta U &= \delta U_R + \delta U_F = \sum_{b=1}^{N_b} \delta U_b + \delta U_F \\ \delta T &= \delta T_R + \delta T_F = \sum_{b=1}^{N_b} \delta T_b + \delta T_F \\ \delta W &= \delta W_R + \delta W_F = \sum_{b=1}^{N_b} \delta W_b + \delta W_F\end{aligned}\quad (7.23)$$

For a bearingless rotor , contributions to blade energy terms U_b , T_b , and W_b come from the main blade, the flexbeams and the torque tube. In addition, if the pitch link is flexible, its strain energy contribution is included in U_b . Thus,

$$U_b = U_{mb} + U_{tt} + \sum_{k=1}^{N_f} U_k + U_{pl} \quad (7.24)$$

where the subscripts mb , tt , k , pl refer respectively to the main blade, the torque tube, the k th flexbeam, and the pitch link. In Chapter 2, energy expressions are derived for an elastic beam. These expressions are equally applicable to the main blade, the torque tube , and the flexbeams, since all these are idealized as elastic beams. Energy expression for a soft pitch link will now be derived.

Energy Expression for Soft Pitch Link

If k_p is the pitch link stiffness and w_p is elastic deflection, then its strain energy is given by

$$\mathcal{U}_{pl} = \frac{1}{2}k_p w_p^2 \quad (7.25)$$

The variation in strain energy is therefore

$$\delta\mathcal{U}_{pl} = k_p w_p \delta w_p \quad (7.26)$$

Consider two bearingless rotor configurations: one without lag pin, and the other one with lag pin. The pitch link is assumed to be soft in both cases.

Bearingless rotor without lag pin

The kinematic motion of the pitch link is given by Eqn. 7.9. Assuming that the pitch link is vertical, i.e., $z_A = b$, $p = x_d = x_0 - x_A$, $a = y_A$, and that the swashplate displacement is small compared to the pitch link length, this equation reduces to the simple form

$$w_p = w - pw' + a\hat{\phi} \quad (7.27)$$

Substitution of Eqn. 7.27 in Eqn. 7.26 yields

$$\begin{aligned} \delta U_{pl} &= k_p (w - pw' + a\hat{\phi} - w_s) (\delta w - p\delta w' + a\delta\hat{\phi}) \\ &= k_p [w_s \delta w + w_s p \delta w' - w_s a \delta\hat{\phi} \\ &\quad + w \delta w - w p \delta w' + w a \delta\hat{\phi} - p w' \delta w + p^2 w' \delta w' \\ &\quad - p w' a \delta\hat{\phi} + a \hat{\phi} \delta w - a \hat{\phi} p \delta w' + a^2 \hat{\phi} \delta\hat{\phi}] \end{aligned} \quad (7.28)$$

The above equation is directly applicable to trim analyses only. For free vibration or stability analysis, when the swashplate is considered fixed and only perturbations in the blade motion are considered, the above expression simplifies to the form

$$\begin{aligned}\delta U_{pl} = & k_p [+w\delta w - wp\delta w' + wa\hat{\phi} - pw'\delta w + p^2 w'\delta w' \\ & - pw'a\hat{\phi} + a\hat{\phi}\delta w - a\hat{\phi}p\delta w' + a^2\hat{\phi}\delta\hat{\phi}] \end{aligned}\quad (7.29)$$

Note that in the above equation, w , w' , $\hat{\phi}$ refer to perturbed displacements, and δU_{pl} represents perturbation in the pitch link strain energy.

Bearingless rotor with lag pin

The presence of lag pin introduces additional constraints given by Eqns. 7.13. Substituting for w from Eqn. 7.13 in Eqn. 7.29, the energy expression for the pitch link becomes

$$\begin{aligned}\delta U_{pl} = & k_p [(x_0 - p)w' + a\hat{\phi} - w_s] (x_0 - p)\delta w' + a\delta\hat{\phi})] \\ = & k_p [-w_s(x_0 - p)\delta w' - w_s a\delta\hat{\phi} \\ & +(x_o - p)^2 w'\delta w' \\ & +(x_o - p)w'a\hat{\phi} + a\hat{\phi}(x_0 - p)\delta w' + a^2\hat{\phi}\delta\hat{\phi}] \end{aligned}\quad (7.30)$$

The above equation is applicable to trim analysis. For free vibration or stability analysis, assuming swashplate to be fixed and considering small per-

turbations in the blade motion, the above expression reduces to the form

$$\delta U_{PL} = k_p[(x_o - p)^2 w' \delta w' + (x_o - p) w' a \delta \hat{\phi} a \hat{\phi} (x_0 - p) \delta w' + a^2 \hat{\phi} \delta \hat{\phi}] \quad (7.31)$$

Again, note that w , w' , $\hat{\phi}$ in the above equation refer to perturbed displacements, and δU_{pl} represents perturbation in the pitch link strain energy.

7.4.2 Finite Element Modeling

Finite element modeling is used to discretize the spatial dependence of the equations of motion obtained from Hamilton's principle. The main blade, the flexbeams, and the torque tube is each divided into a number of beam elements. Each beam element consists of fifteen degrees of freedom [Ref.1]. As shown in Fig.7.6, these degrees of freedom are distributed over five nodes: two boundary nodes and two internal nodes. The element degrees of freedom allow consistent representation of the physical forces. For example, to properly represent the axial force distribution, which arises mainly from centrifugal acceleration of the blade, the axial strain distribution must be at least quadratic. This implies a cubic distribution of the axial displacement, i.e., four nodes for the axial degree of freedom, u .

Since the same beam element representation is used to model the main blade, the flexbeams, and the torque tube, the virtual energy expression, Eqn. 7.22,

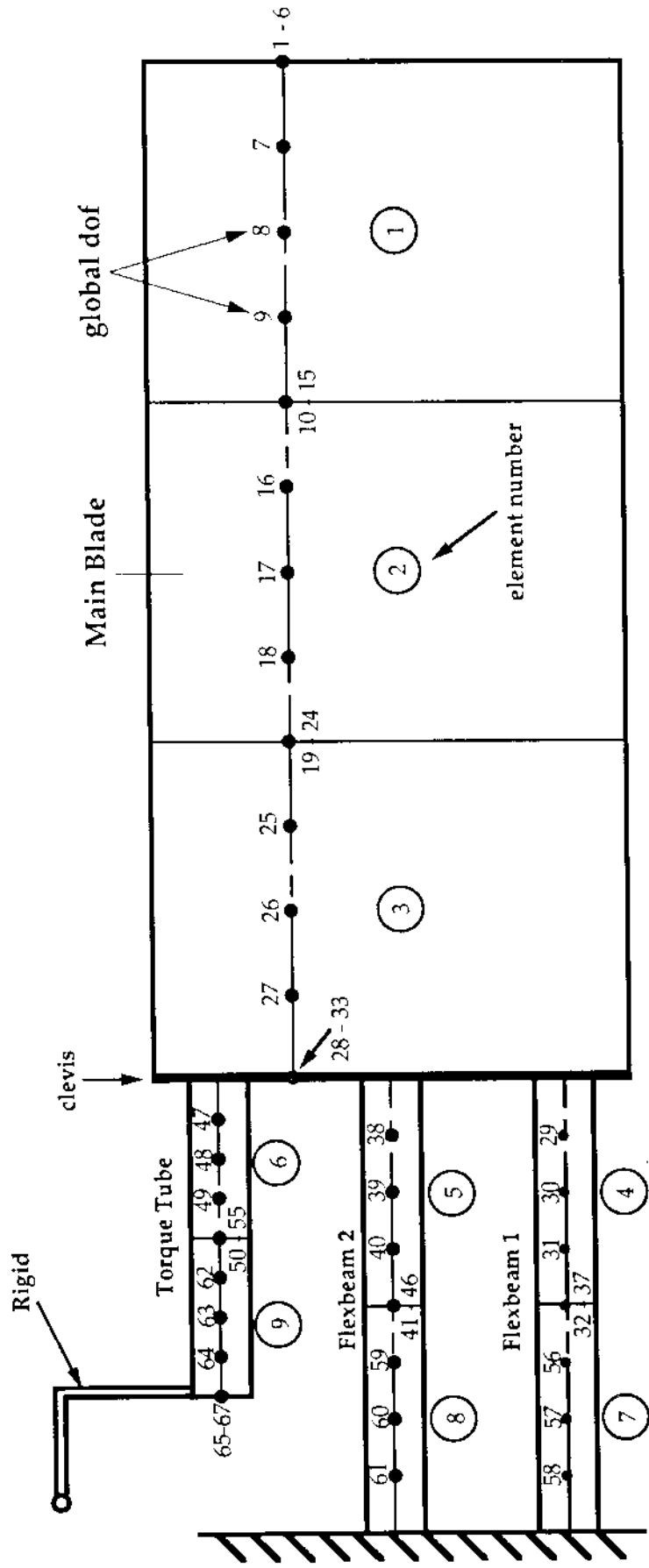


Fig 7.6 : Finite Element Modeling of Bearingless Blade

is discretized as

$$\delta H = \int_{t_1}^{t_2} \sum_{i=1}^N (\delta U_i - \delta T_i - \delta W_i) dt = 0 \quad (7.32)$$

where N is the total number of beam elements including those for the main blade and the flexure beams. Using the notation

$$\Delta_i = \delta U_i - \delta T_i - \delta W_i \quad (7.33)$$

and noting that the integral vanishes for all t_1 and t_2 , the equation of motion, Eqn 7.32, assumes the form

$$\sum_{i=1}^N \Delta_i = 0 \quad (7.34)$$

Following the approach described in section 2.3.2, the variation in element energy, Δ_i , can be expressed as

$$\begin{aligned} \Delta_i &= \delta \mathbf{q}_i^T (\mathbf{m}_{bi} \ddot{\mathbf{q}}_i + \mathbf{c}_{bi} \dot{\mathbf{q}}_i + \mathbf{k}_{bi} \mathbf{q}_i - \mathbf{f}_{bi} \\ &\quad + \mathbf{m}_{bF_i} \ddot{\mathbf{x}}_F + \mathbf{c}_{bF_i} \dot{\mathbf{x}}_F + \mathbf{k}_{bF_i} \mathbf{x}_F) \end{aligned} \quad (7.35)$$

where

$$\begin{aligned} \mathbf{q}_i^T &= (u_1, u_2, u_3, u_5, v_1, v'_1, v_2, v'_2, w_1, w'_1, w_2, w'_2, \hat{\phi}_1, \hat{\phi}_2, \hat{\phi}_3) \\ \mathbf{x}_F^T &= (x_F, y_F, z_F, \alpha_s, \phi_s) \end{aligned} \quad (7.36)$$

In Eqn. 7.35, \mathbf{m}_{bi} , \mathbf{c}_{bi} , \mathbf{k}_{bi} , \mathbf{f}_{bi} are blade element mass, damping, stiffness, and load matrices, respectively, and \mathbf{m}_{bF_i} , \mathbf{c}_{bF_i} , \mathbf{k}_{bF_i} are the blade-fuselage elemental mass, damping, and stiffness matrices, respectively. Expressions for

these elemental matrices are derived in Chapter 2 and the final expressions are provided in Eqns. 2.110-2.122. Note that kinematics modifications are applicable to only the inboard element of the torque tube; it is the only element directly attached to the pitch link and the lag pin.

Assembly of element matrices

The element matrices are assembled into global matrices by imposing displacement compatibility conditions at interelement boundaries. In general, the compatibility conditions imply the continuity of u, v, v', w, w' and $\dot{\phi}$ across the element boundaries. At the clevis, where the root element of the main blade joins with the outboard elements of the flexbeams and the torque tube, the displacement compatibility conditions are governed by Eqns. 7.20. The assembly process is mathematically indicated by substituting Eq 7.35 in Eqn 7.32. The result is

$$\begin{aligned}\delta\Pi = & \delta\mathbf{q}^T (\mathbf{M}_b \ddot{\mathbf{q}} + \mathbf{C}_b \dot{\mathbf{q}} + \mathbf{K}_b \mathbf{q} - \mathbf{Q}_b \\ & + \mathbf{M}_{bF} \ddot{\mathbf{x}}_F + \mathbf{C}_{bF} \dot{\mathbf{x}}_F + \mathbf{K}_{bF} \mathbf{x}_F) = \mathbf{0}\end{aligned}\quad (7.37)$$

where q denotes the global degrees of freedom vector obtained by assembling the elemental degree of freedom vectors, q_i . Since the virtual displacements, δq , are arbitrary, Eqn 7.37 leads to the nonlinear equation of motion

$$\mathbf{M}_b \ddot{\mathbf{q}} + \mathbf{C}_b \dot{\mathbf{q}} + \mathbf{K}_b \mathbf{q} + \mathbf{M}_{bF} \ddot{\mathbf{x}}_F + \mathbf{C}_{bF} \dot{\mathbf{x}}_F + \mathbf{K}_{bF} \mathbf{x}_F = \mathbf{Q}_b \quad (7.38)$$

Global Degrees of Freedom Numbering

An efficient numbering of the global degrees of freedom minimizes the bandwidth of global matrices. Fig.7.6 exemplifies the numbering scheme used in UMARC for a dual-flexbeam bearingless rotor blade. The bearingless blade is divided into a total of nine elements: three for the main blade, two each for the flexbeam, and two for the torque tube. The element numbers are identified by small circles around them. As seen in the figure, global degrees of freedom are assigned first to the main blade elements, proceeding from the tip element to the inboard element. Next, flexure elements directly attached to the main blade (i.e. elements 4, 6 and 8) are assigned global degrees of freedom, proceeding from element 4 to element 8. Rest of the flexure elements are assigned global degrees of freedom as shown in the figure. The reader can verify that this leads to minimum bandedness of the global matrices. Small dots on the elastic axes of the beams identify element nodes and the accompanying numbers indicate the global degrees of freedom numbering.

7.4.3 Application of the Kinematic Constraints

In section 7.3, we derived three sets of kinematic constraints: constraints imposed by the pitch link and the lag pin; displacement compatibility conditions at the clevis; and the cantilevered boundary conditions at inboard ends of the

flexbeam. We now discuss how these boundary constraints are accommodated in the finite element modeling.

Boundary Constraints at the Torque Tube End

Consider variation in elemental energy for the torque tube inboard element, Δ_i , given by

$$\begin{aligned}\Delta_i = & \delta \mathbf{q}_i^T (\mathbf{m}_{bi} \ddot{\mathbf{q}}_i + \mathbf{c}_{bi} \dot{\mathbf{q}}_i + \mathbf{k}_{bi} \mathbf{q}_i - \mathbf{f}_{bi} \\ & + \mathbf{m}_{bF,i} \ddot{\mathbf{x}}_F + \mathbf{c}_{bF,i} \dot{\mathbf{x}}_F + \mathbf{k}_{bF,i} \mathbf{x}_F)\end{aligned}\quad (7.39)$$

where \mathbf{q}_i and \mathbf{x}_F are defined by Eqns 7.37. As mentioned earlier, the element matrices \mathbf{m}_{bi}, \dots , etc., and the load vector, \mathbf{f}_{bi} , are modified by the boundary constraints at the torque tube end. For the case when the pitch link is rigid and the lag pin is present; the boundary conditions are governed by Eqns. 7.18. The three boundary conditions imply that, of the six element degrees of freedom at the torque tube inboard end, only three are independent. The six elemental degrees of freedom at the torque tube inboard are

$$\begin{aligned}q_1 &= u_1, \quad q_5 = v_1 \\ q_6 &= v'_1, \quad q_9 = w_1 \\ q_{10} &= w'_1, \quad q_{13} = \hat{\phi}_1\end{aligned}\quad (7.40)$$

Since the virtual displacements, by definition, must be compatible with the actual displacements, the above equations yield

$$\begin{aligned}\delta q_1 &= \delta u_1, \quad \delta q_5 = \delta v_1 \\ \delta q_6 &= \delta v'_1, \quad \delta q_9 = \delta w_1 \\ \delta q_{10} &= \delta w'_1, \quad \delta q_{13} = \delta \hat{\phi}_1\end{aligned}\tag{7.41}$$

In view of the boundary constraints 7.18, the elemental degrees of freedom q_5, q_9, q_{13} can be expressed as functions of the degrees of freedom q_6 and q_{10} :

$$\begin{aligned}q_5 &= x_0 v'_1 - \frac{z_0}{a} (x_0 - p) w'_1 \\ &= x_0 q_6 - \frac{z_0}{a} (x_0 - p) q_{10} \\ q_9 &= x_0 w'_1 \\ &= x_0 q_{10} \\ q_{13} &= \frac{p - x_0}{a} w'_1 \\ &= \frac{p - x_0}{a} q_{10}\end{aligned}\tag{7.42}$$

Similarly,

$$\begin{aligned}\delta q_5 &= x_0 \delta v'_1 - \frac{z_0}{a} (x_0 - p) \delta w'_1 \\ &= x_0 \delta q_6 - \frac{z_0}{a} (x_0 - p) \delta q_{10}\end{aligned}$$

$$\begin{aligned}
\delta q_9 &= x_0 \delta w'_1 \\
&= x_0 \delta q_{10} \\
\delta q_{13} &= \frac{p - x_0}{a} \delta w'_1 \\
&= \frac{p - x_0}{a} \delta q_{10}
\end{aligned} \tag{7.43}$$

To see how a typical element matrix appearing in Eqn 7.39 is modified by the kinematic constraints, consider the energy term associated with the blade element stiffness matrix, k_b , i.e., the term

$$\delta \mathbf{q}_i^T \mathbf{k}_{b_i} \mathbf{q}_i \tag{7.44}$$

Equations 7.42 imply that q_5 , q_9 and q_{13} are the dependent degrees of freedom. Now, by definition of the matrix multiplication, the virtual displacements δq_5 , δq_9 and δq_{13} are multipliers of the 5th, 9th and 13th rows of the matrix k_b . Similarly, the 5th, 9th, and 13th columns are multiplied by the actual displacements q_5 , q_9 and q_{13} . In view of Eqns. 7.43, the three aforementioned rows in fact are multiplied by the terms $(x_0 \delta q_6 - \frac{z_0}{a}(x_0 - p) \delta q_{10})$, $(x_0 \delta q_{10})$, and $(\frac{p-x_0}{a} \delta q_{10})$. The same numbered columns are similarly multiplied by terms $(x_0 q_6 - \frac{z_0}{a}(x_0 - p) q_{10})$, $(x_0 q_{10})$, and $(\frac{p-x_0}{a} q_{10})$. Performing these row and column operations, and then deleting rows and columns associated with dependent degrees of freedom q_5 , q_9 and q_{13} , we obtain the final modified matrix, $\bar{\mathbf{k}}_b$. In effect, the aforementioned operations are equivalent to performing the following three steps:

1. a) Obtain matrix \mathbf{k}'_{b_i} by applying the following row operations on matrix \mathbf{k}_{b_i}

$$\begin{aligned}\overline{R_6} &= R_6 + x_0 R_5 \\ \overline{R_{10}} &= R_{10} + x_0 R_9 - \frac{x_0 - p}{a} R_{13} - \frac{x_0 - p}{a} z_0 R_5\end{aligned}\quad (7.45)$$

where R_6 and R_{10} are respectively the 6th and 10th rows of the original matrix, \mathbf{k}_{b_i} .

2. b) Obtain matrix \mathbf{k}_{b_i}'' by applying the following column operations on matrix \mathbf{k}_{b_i}'

$$\begin{aligned}\overline{C_6} &= C_6 + x_0 C_5 \\ \overline{C_{10}} &= C_{10} + x_0 C_9 - \frac{x_0 - p}{a} C_{13} - \frac{x_0 - p}{a} z_0 C_5\end{aligned}\quad (7.46)$$

where C_6 and C_{10} are respectively the 6th and 10th columns of matrix, \mathbf{k}_{b_i}' , obtained in the previous step.

3. c) Delete the 5th, 9th, and 13th rows and columns from \mathbf{k}_{b_i}'' to obtain the final modified matrix, $\overline{\mathbf{k}_{b_i}}$.

The modified matrix, $\overline{\mathbf{k}_{b_i}}$, is related to the original matrix, \mathbf{k}_{b_i} by the relation

$$\delta \mathbf{q}_i^T \mathbf{k}_{b_i} \mathbf{q}_i = \delta \mathbf{q}_i^T \mathbf{k}_{b_i} \dot{\mathbf{q}}_i \quad (7.47)$$

The other blade element matrices, \mathbf{m}_{b_i} and \mathbf{c}_{b_i} , are modified similarly by subjecting them to operations (a) to (d). Note that the load vector, \mathbf{f}_{b_i} , is

premultiplied only by δq . Therefore, only the row operations are performed to yield the modified load vector, $\bar{\mathbf{f}}_{b_i}$.

The blade-fuselage matrices, as we notice in Eqn. 7.39, are premultiplied by $\delta \mathbf{q}^T$ and post-multiplied by \mathbf{x}_F and its time derivatives. Since the boundary constraints imposed by lag pin and pitch link operate only on the blade degrees of freedom, row operations only need to be carried out to yield the modified set of blade-fuselage matrices. Following similar reasoning, the blade-inflow matrices should also require row operations only. The fuselage-blade and fuselage-inflow matrices, since they are post-multiplied by the q or its derivatives, are modified using column operations.

Compatibility Conditions at the Clevis

Compatibility equations 7.20, before they can be applied to free vibration analysis, need to be written in terms of the perturbation displacements about a reference state. Using $u = u_0 + \Delta u$, etc., where Δ indicates perturbation quantity, the compatibility equations become

$$u_k = u_b - \eta_k v'$$

$$v_k = v_b$$

$$v'_k = v'_b$$

$$w_k = w_b + \eta_k \hat{\phi}_b$$

$$\begin{aligned} w'_k &= w'_b \\ \hat{\phi}_k &= \hat{\phi}_b \end{aligned} \quad (7.48)$$

For trim and stability analysis, modal approach is used; the compatibility conditions are implicitly embeded in the eigenvectors employed for modal analysis.

Flexbeam cantilevered boundary conditions

Implementation of the cantilevered boundary constraints is straightforward. Since $u, v, v', w, w', \hat{\phi}$ are all zero at the inboard ends of the flexbeams, the rows and columns corresponding to these degrees of freedom are eliminated from the element matrices during assembly.

7.4.4 Modeling of Snubber

A number of recent bearingless rotor designs are using an elastomeric snubber placed between the torque tube and the flexbeam. In general, it behaves as a nonlinear spring-damper. As a first approximation, it can be modelled as a combination of a 6-degree-of-freedom linear spring and a 6-degree-of-freedom linear damper. Spring behavior is represented by translational spring constants K_x, K_y, K_z and rotational spring constants $K_{\phi_x}, K_{\phi_y}, K_{\phi_z}$. Similarly, the damper properties are represented by translational viscous damping constants C_x, C_y, C_z and angular viscous damping constants $C_{\phi_x}, C_{\phi_y}, C_{\phi_z}$.

The elastic strain energy of the snubber is given by

$$\begin{aligned} U^s &= \frac{1}{2}[k_x(u_t - u_f)^2 + k_y(v_t - v_f)^2 + k_z(w_t - w_f)^2 \\ &\quad + k_{\phi_x}(\phi_t - \phi_f)^2 + k_{\phi_y}(w'_t - w'_f)^2 + k_{\phi_z}(v'_t - v'_f)^2] \end{aligned} \quad (7.49)$$

where quantities subscripted with t denote the torque tube degrees of freedom at the point of attachment to the snubber. Similarly, quantities subscripted with f denote the flexbeam degrees of freedom at the point of attachment to the snubber.

The variation in strain energy is obtained from Eq. (7.49) as

$$\begin{aligned} \delta U^s &= k_x(\delta u_t - \delta u_f)(u_t - u_f) + k_y(\delta v_t - \delta v_f)(v_t - v_f) + k_z(\delta w_t - \delta w_f)(w_t - w_f) \\ &\quad + k_{\phi_x}(\delta \phi_t - \delta \phi_f)(\phi_t - \phi_f) + k_{\phi_y}(\delta w'_t - \delta w'_f)(w'_t - w'_f) + k_{\phi_z}(\delta v'_t - \delta v'_f)(v'_t - v'_f) \end{aligned} \quad (7.50)$$

Since the snubber damping action is assumed to be governed by equivalent viscous constants, the snubber damping forces are given by

$$\left\{ \begin{array}{c} f_x \\ f_y \\ f_z \\ m_x \\ m_y \\ m_z \end{array} \right\} = \left[\begin{array}{cccccc} C_x & & & & & \\ & C_y & & & & \\ & & C_z & & & \\ & & & C_{\phi_x} & & \\ & & & & C_{\phi_y} & \\ & & & & & C_{\phi_z} \end{array} \right] \left\{ \begin{array}{c} \dot{u}_t - \dot{u}_f \\ \dot{v}_t - \dot{v}_f \\ \dot{w}_t - \dot{w}_f \\ \dot{\phi}_t - \dot{\phi}_f \\ \dot{w}'_t - \dot{w}'_f \\ \dot{v}'_t - \dot{v}'_f \end{array} \right\} \quad (7.51)$$

The virtual work done by the snubber damping forces is given by

$$\delta W^s = - \left\{ \begin{array}{c} \delta u_t - \delta u_f \\ \delta v_t - \delta v_f \\ \delta w_t - \delta w_f \\ \delta \phi_t - \delta \phi_f \\ \delta w'_t - \delta w'_f \\ \delta v'_t - \delta v'_f \end{array} \right\}^T \left\{ \begin{array}{c} f_x \\ f_y \\ f_z \\ m_x \\ m_y \\ m_z \end{array} \right\}$$

$$= - \left\{ \begin{array}{l} \delta u_t - \delta u_f \\ \delta v_t - \delta v_f \\ \delta w_t - \delta w_f \\ \delta \phi_t - \delta \phi_f \\ \delta w'_t - \delta w'_f \\ \delta v'_t - \delta v'_f \end{array} \right\}^T \left[\begin{array}{cccccc} C_x & & & & & \\ & C_y & & & & \\ & & C_z & & & \\ & & & C_{\phi_x} & & \\ & & & & C_{\phi_y} & \\ & & & & & C_{\phi_z} \end{array} \right] \left\{ \begin{array}{l} \dot{u}_t - \dot{u}_f \\ \dot{v}_t - \dot{v}_f \\ \dot{w}_t - \dot{w}_f \\ \dot{\phi}_t - \dot{\phi}_f \\ \dot{w}'_t - \dot{w}'_f \\ \dot{v}'_t - \dot{v}'_f \end{array} \right\} \quad (7.52)$$

The snubber elastic strain energy, U^s is added to the blade strain energy term U_b appearing in Eq. (7.23). Similarly, virtual work done by snubber damping forces, W^s , is added to the \mathcal{W}_b term.

7.5 Modifications in the Solution Procedure

In addition to the modeling differences discussed earlier, bearingless rotor analysis requires some more modifications in the solution procedure.

7.5.1 Centrifugal Force Computation

Finite element formulation developed in Chapter 2 indicates that centrifugal distribution in each blade element is required to formulate the stiffness matrix K . A multi-flexbeam configuration offers redundant load paths to the centrifugal force. For such a configuration, therefore, centrifugal force partitioning amongst the various flexbeams needs to be evaluated. In the earlier codes from which UMARC has evolved, a quasicoordinate was used to represent the axial degree

of freedom, which resulted in the bandedness of matrices. This necessitated computation of the *total* axial force to compute terms in the stiffness matrix. In the current version of UMARC, the physical elastic deflection represents the axial degree of freedom. This substantially enhances numerical stability. Also, only centrifugal component of the axial force is required to formulate stiffness matrix. The centrifugal force distribution is known a priori only over the outboard blade; it is unknown over the flexure members because of the multiple load paths. To obtain the initial estimate for linear solution, it is assumed that the centrifugal force in each of the flexbeams is the ratio of the tensile stiffness EA . At subsequent iterations, the centrifugal force is updated using the following relation obtained from Eqns. 2.37 of Chapter 2.

$$\begin{aligned}
 F_{CF}(x) = & EA[u' - e_A(v'' \cos \theta_0 + w'' \sin \theta_0) \\
 & + e_A(v'' \hat{\phi} \sin \theta_0 + w'' \hat{\phi} \cos \theta_0)] \\
 & + (EI_y + EI_z)\theta'_o \hat{\phi}' - \int_x^1 (2m\dot{v} - m\ddot{u} + L^A u) dx
 \end{aligned} \quad (7.53)$$

7.5.2 Trim Solution

As mentioned in the introduction, it is the pitch change mechanism which distinguishes a bearingless rotor blade from the conventional blade. This different pitch change mechanism requires changes in the coupled trim procedure (described in Chapter 4).

For a conventional blade, the pitch control can be uniquely defined in terms

of the blade pitch angle at any specific spanwise location on the blade. There is a direct geometric correspondence between this pitch angle and the swash plate displacement, w_s . However, for a bearingless blade, such a relationship cannot be established *a priori*. This is because the main blade pitch control setting depends on the flexbeam twist at the clevis junction, and the flexbeam twist has no direct geometric relationship to the swashplate deflection, w_s . The flexbeam in fact twists and as well as bends under the action of the pitch link force, F_P , and the blade centrifugal force acting at the outboard end of the flexbeam. If the swashplate displacement is a function of time, $w_s = w_s(\psi)$, the flexbeam will be subjected to dynamic forces as well.

This unique role played by the flexbeam in the bearingless rotor pitch change mechanism necessitates modifications in the coupled trim procedure. As explained in Chapter 4, coupled trim involves iteration between two main steps: computation of blade response due to specified controls, and update of controls to minimize residual forces on the vehicle. Accordingly, at each step of the trim procedure, the blade control is first specified. This is specified in terms of the pseudo-pitch-angle, θ_{75} , which has a direct geometric relation to the swashplate control, $w_s(\psi)$ as follows:

$$\theta_{75}(\psi) = a w_s(\psi) + \theta_{p_{75,P}} \quad (7.54)$$

where a is the pitch-horn chordwise offset and $\theta_{p_{75,P}}$ is the geometric pretwist of the 75% blade span relative to the point P on the blade attached to the pitch link. (Note that θ_{75} would be the actual pitch control at the blade 75% span

if the flexbeam functioned like a conventional pitch bearing). Blade response is calculated using this control. Next, vehicle forces are computed. Control, $\dot{\theta}_{75}$ (or, indirectly, control w_s), is updated to minimize the residual forces.

Consider the blade response equation

$$\mathbf{M}\ddot{\mathbf{q}} + \mathbf{C}\dot{\mathbf{q}} + \mathbf{K}\mathbf{q} = \mathbf{F}(\psi, \theta, \mathbf{q}, \dot{\mathbf{q}}) \quad (7.55)$$

where the displacement vector, \mathbf{q} , satisfies all the kinematic constraints (i.e. cantilevered boundary conditions, compatibility conditions and auxiliary conditions, such as due to lag pin). Now, the blade deflection must equal the prescribed deflection \mathbf{q}_p at a point P , where the control is prescribed. The blade response vector, \mathbf{q} , can thus be partitioned as

$$\mathbf{q} = \begin{Bmatrix} \mathbf{q}_R \\ \mathbf{q}_P \end{Bmatrix} \quad (7.56)$$

where q_p equals the swash plate control deflection, w_s , and \mathbf{q}_R is the vector of global degrees of freedom with the control degree of freedom suppressed. Eq. (7.51) can now be expressed as

$$\begin{aligned} & \begin{bmatrix} \mathbf{M}_R & \mathbf{M}_{RP} \\ \mathbf{M}_{PR} & \mathbf{M}_P \end{bmatrix} \begin{Bmatrix} \ddot{\mathbf{q}}_R \\ \ddot{\mathbf{q}}_P \end{Bmatrix} + \begin{bmatrix} \mathbf{C}_R & \mathbf{C}_{RP} \\ \mathbf{C}_{PR} & \mathbf{C}_P \end{bmatrix} \begin{Bmatrix} \dot{\mathbf{q}}_R \\ \dot{\mathbf{q}}_P \end{Bmatrix} \\ & + \begin{bmatrix} \mathbf{K}_R & \mathbf{K}_{RP} \\ \mathbf{K}_{PR} & \mathbf{K}_P \end{bmatrix} \begin{Bmatrix} \mathbf{q}_R \\ \mathbf{q}_P \end{Bmatrix} = \begin{Bmatrix} \mathbf{F}_R \\ \mathbf{F}_P \end{Bmatrix} \end{aligned} \quad (7.57)$$

or

$$\mathbf{M}_R \ddot{\mathbf{q}}_R + \mathbf{M}_{RP} \ddot{\mathbf{q}}_P + \mathbf{C}_R \dot{\mathbf{q}}_R + \mathbf{C}_{RP} \dot{\mathbf{q}}_P + \mathbf{K}_R \mathbf{q}_R + \mathbf{K}_{RP} \mathbf{q}_P = \mathbf{F}_R \quad (7.58)$$

$$\mathbf{M}_P \ddot{\mathbf{q}}_P + \mathbf{M}_{PR} \ddot{\mathbf{q}}_R + \mathbf{C}_P \dot{\mathbf{q}}_P + \mathbf{C}_{PR} \dot{\mathbf{q}}_R + \mathbf{K}_P \mathbf{q}_P + \mathbf{K}_{PR} \mathbf{q}_R = \mathbf{F}_P \quad (7.59)$$

Finite element equations (7.54) could be solved directly to yield blade response \mathbf{q}_R for a specified control displacement \mathbf{q}_P . Eq. (7.55) is required only if one is directly interested in the pitch link force \mathbf{F}_P . To allow solution of the blade response Eqs. (7.54) in the modal domain, the displacement vector \mathbf{q} is partitioned as follows

$$\mathbf{q} = \begin{pmatrix} \mathbf{q}_R \\ \mathbf{q}_P \end{pmatrix} = \begin{pmatrix} \mathbf{q}_s \\ \mathbf{q}_P \end{pmatrix} + \begin{pmatrix} \bar{\mathbf{q}} \\ \mathbf{0} \end{pmatrix} \quad (7.60)$$

where \mathbf{q}_P is the control deflection; \mathbf{q}_s is assumed blade displacement distribution such that it is compatible with the control deflection, \mathbf{q}_P , at the point P and satisfies all other kinematic constraints as well; $\bar{\mathbf{q}}$ is the unknown perturbation deflection such that $\mathbf{q}_s + \bar{\mathbf{q}}$ provides the actual blade deflection distribution. The perturbation displacement, $\bar{\mathbf{q}}$, also satisfies all the kinematic constraints and assumes a zero value at the control specification point P . The perturbation displacement vector, $\bar{\mathbf{q}}$, can thus be expressed in terms of the blade modes computed with the pitch link control fixed. Specification of assumed deflection \mathbf{q}_s used in UMARC is straightforward. For a given swashplate deflection, w_s , the flexbeam is assumed to be linearly twisted from a value of zero at the root to a value, $\bar{\theta}_0 = aw_s$, at the clevis. The rest of the blade is given a rigid pitch

rotation of $\bar{\theta}_0$. The assumed deflection satisfies all the kinematic constraints and is compatible with the swashplate control, w_s .

Substituting Eq. (7.56) in Eq. (7.54), we obtain

$$\mathbf{M}_R \ddot{\mathbf{q}} + \mathbf{C}_R \dot{\mathbf{q}} + \mathbf{K}_R \mathbf{q} = \mathbf{F}_R(q_s + \bar{q}) - \mathbf{F}_s - \mathbf{F}_{RP} \quad (7.61)$$

where \mathbf{F}_{RP} , the equivalent force due to the prescribed control, is given by

$$\mathbf{F}_{RP} = \mathbf{M}_{RP} \ddot{\mathbf{q}}_p + \mathbf{C}_{RP} \dot{\mathbf{q}}_p + \mathbf{K}_{RP} \mathbf{q}_p \quad (7.62)$$

and \mathbf{F}_s , the equivalent force due to the specified displacement distribution, is given by

$$\mathbf{F}_s = \mathbf{M}_R \ddot{\mathbf{q}}_s + \mathbf{C}_R \dot{\mathbf{q}}_s + \mathbf{K}_R \mathbf{q}_s \quad (7.63)$$

Eq. (7.57) is solved for $\bar{\mathbf{q}}$ by first transforming Eqs. (7.57) to the modal domain as described in Section 4.2.3 and then applying the finite element in time technique described in Section 4.3. The steady blade response is given by

$$\mathbf{q} = \begin{pmatrix} \mathbf{q}_s + \bar{\mathbf{q}} \\ \mathbf{q}_P \end{pmatrix} \quad (7.64)$$

The next step in the coupled trim procedure, i.e., update of controls, is accomplished using the Jacobian matrix, $J = [\partial F / \partial \bar{\theta}_{75}]$, computational procedure for which is described in Section 4.4.7. Here, F is the vector of vehicle residual forces and $\bar{\theta}_{75}$ represents the swash plate control via Eq. (7.50). The controls are updated as follows

$$\bar{\theta}_{75,i+1} = \bar{\theta}_{75,i} - \left[\frac{\partial \mathbf{F}}{\partial \bar{\theta}_{75}} \right]_{\bar{\theta}_{75}=\bar{\theta}_{75,i}}^{-1} \mathbf{F}(\bar{\theta}_{75,i}) \quad (7.65)$$

7.6 Implementation in UMARC

Input Required Exclusively for BMR Analysis

As discussed in chapter 8, the user inputs data either through keywords or user-defined routines. The keywords are translated by routine UMRINP into Fortran variables for use by executive part of the code. The keywords relevant to bearingless rotor configuration are listed in Table 8. Listed below are the corresponding FORTRAN input variable names.

- a) NCONF = rotor configuration type (should be 2 for BMR configuration)
- b) NSEG = number of beam segments (should equal no of flexbeams + one torque tube + one main blade)
- c) NPIN = flag for lag pin inclusion (=1 if lag pin is present; =0 otherwise)
- d) LNKSFT = flag indicating pitch link softness (=1 if pitch link is soft; =0 if it is rigid)
- e) NEFSI(I) = number of elements for segment I (where the first segment refers to main blade and the last segment number refers to the torque tube ; the intervening segment numbers refer to the flexbeam)
- f) NSELT = number of elements for the bearingless rotor blade (should equal $\sum_{I=1}^{NSEG} NEFSI(I)$)
- g) TTK = pitch link stiffness

h) TTA = pitch horn chordwise arm length = a

i) TTP = pitch horn spanwise length = p

j) TTZ = lag pin vertical arm length = z_0

k) TTB = pitch link length = b

l) TTX0 = lag pin horizontal arm length = x_0

Other input data, e.g., variable sweep, precone and droop, and elemental properties, are input in the same way as for other rotor types (see chapter 8).

BMR-related input and run-time data are shared amongst routines either via the subroutine arguments or via the common blocks CONF, SFTLNK, and LINK.

Listed below are routines which implement bearingless rotor related modeling and analysis modifications. It should be noted that four of these routines, viz. EXEC, BLDVIB, ASBGBM and ASBGM2, are used for all rotor configurations. Performance of these routines, relevant to BMR configuration only, will be described. The other routines are used only by the BMR configuration.

Detailed performance of each routine now follows.

SUBROUTINE EXEC

Its bearingless rotor related performance is as follows:

- a) Compute number of boundary conditions, NCON. If NCONF=2, i.e., if the rotor is of bearingless type,

$$NCON = 6 * NSEG - 11 + 2 * NPIN - LSFT$$

- b) Compute global degrees of freedom, NGD.

$$NGD = (NSELT+1) * 6 + NSELT * 3 - NCON$$

- c) Normalize the pitch link stiffness with respect to the operating rotor speed,

Ω :

$$TTK = TTK * \left(\frac{\Omega_{ref}}{\Omega}\right)^2$$

where Ω_{ref} is the nominal rotor speed used for normalizing the input value of the pitch link stiffness.

SUBROUTINE BLDVIB

This routine is called by EXEC to build the blade finite element model and compute its free vibration characteristics. Its bearingless rotor related performance steps are summarized below.

- a) Assign the number of elements for the main blade, i.e., segment 1, to NSEG1. For each of the NSEG1 number of elements, relate the elemental degrees of freedom to the global degrees of freedom using the connectivity

vector INDEG. Next, compute the centrifugal force, CFE(I), at the left-hand end of the elements, where I ranges from 1 to NSEG1. (These operations are performed in DO loop 40).

- b) Assign the number of elements for the torque tube to NSEG3. Compute CFTT, the centrifugal force contribution from the torque tube acting on the clevis in the outboard direction. Note that, for the torque tube, its centrifugal force distribution acts as a compressive load.
- c) Compute the centrifugal force , CFE(I), at the inboard ends of the flexbeam and torque tube elements. Relate element degrees of freedom to global degrees of freedom .

Next, impose the displacement compatibility conditions, Eqns 7.48, at the cuff, joining the main blade to the flexure elements. (These operations are performed in DO loop 8800).

Note: INDEG(n,l) = global degree of freedom corresponding to the nth elemental degree of freedom of the lth element.

- d) Impose cantilevered boundary constraints , Eqns 7.21, at the inboard ends of the flexbeams by setting the corresponding global degrees of freedom to zero. The zero numbering of the global degrees of freedom indicates to the assembly routine ASBGMK that the corresponding rows and columns in the global mass and stiffness matrices are to be ignored.
- e) If NSEG is greater or equal to 3 (BMR configuration), modify the global

connectivity vector in accordance with the boundary constraints, Eqns 7.17 to 7.19, associated with the pitch link and the lag pin.

- f) Compute and assemble the element mass and stiffness matrices. (These operations are performed in DO loop 100). As indicated in section 7.4.2, the last element number always refers to the inboard torque tube element. When the element loop control gets to the last element, number NSELT, and if the blade is bearingless type (NCONF=2), subroutine BMRMOD is called to modify the element matrices in accordance with the kinematic constraints associated with the pitch link and the lag pin. In addition, if the pitch link is soft (LSFT=1), the element stiffness matrix is augmented using Eqns 7.31.

SUBROUTINE ASBGBM

This routine is called by TRIM to compute the element matrices, structural and aerodynamic, in the space domain. Its bearingless rotor related function are as follows.

- a) For the last element, NSELT, and NCONF=2, call MODMAT to modify the element linear matrices EMP, ECP, EKP and also the nonlinear matrices DFX and DFXD. Call MODVEC to modify the load vector, EQP.
- b) For the inboard torque tube element (numbered NSELT), if the pitch link is soft, i.e., modify the normalized stiffness matrix, PK, to account for the pitch link stiffness (see equations 7.28). This is done as follows.

First, routine TWISTX is called to compute the geometric pitch, THX0, at the torque tube inboard end, assuming the main blade and the torque tube to be undeformed and set at pitch control angle, TH75. Geometry corresponding to undeformed pitch link is then used to compute the swashplate deflection, WSP(ψ). Eqns 7.28 are next applied to add the contribution of the pitch link stiffness, TTK, to the modal stiffness matrix, PK.

SUBROUTINE BMRMOD

This routine is called by BLDVIB and later by the stability routine STAB to modify the mass and stiffness matrices of the torque tube inboard element. As mentioned earlier, this is the only element directly influenced by the pitch link and lag pin kinematics. Further, if the pitch link is soft, the global stiffness matrix is also modified. Its performance is as follows.

- a) Assign the numbers 5, 6, 9, 10, 13, corresponding to the elemental degrees of freedom v, v', w, w' and $\dot{\phi}$, to the variables IV, IVP, IW, IWP, IPHI.
- b) Call routine MODMAT to modify element mass matrix, EM, and stiffness matrix, EK, required for free vibration analysis of the blade. The routine MODMAT functions as follows:

If NPIN=1 and LSFT=0, i.e., lag pin is present and the pitch link is rigid, use Eqns 7.18 to modify the element matrices.

If NPIN=1 and LSFT=1, i.e., lag pin is present and the pitch link is soft,

use Eqns 7.19.

If NPIN=0 and LSFT=0, i.e., lag pin is absent and the pitch link is rigid, use Eqns 7.17.

- c) If the pitch link is soft (LSFT=1), assign to JV, JVP, JW, JWP and JPHI the global degree of freedom numbers corresponding to the torque tube inboard node. If lag pin is present (NPIN=1), modify the global stiffness matrix using Eqns 7.30 of section 7.4.1. If lag pin is absent, use Eqns. 7.29 for the modification.

Bibliography

- [1] Sivaneri, N.T., "Finite Element Analysis for Bearingless Rotor Blade Aerelasticity", *Journal of the American Helicopter Society*, Vol. 20, No. 2, April 1984.
- [2] Hedges, D. H., "A Theoretical Technique for Analyzing Aeroelastic Stability of Bearingless Rotors", *AIAA Journal*, Vol. 17, No. 4, 1978.

Chapter 8

Composite Blade Modeling

Summary

UMARC has the modeling and analysis capability for free vibration, aeroelastic response and loads, aeroelastic stability, and aeromechanical stability of helicopters with elastically coupled composite rotor blades. The composite blade analysis is based on the recent work described in Refs. 8.1-8.5. Cross-section stiffness coefficients, including ply-induced elastic coupling parameters, can either be calculated for a laminated composite box-beam blade spar, or input directly by the user. The box-beam analysis, based on classical lamination theory, includes the nonclassical structural effects of transverse shear, torsion-related out-of-plane warping, and two-dimensional ply elasticity. Elastic couplings such as pitch-flap, pitch-lag, and extension-torsion are introduced through the anisotropy of the plies in the composite spar. For the aeroelastic and aeromechanical analysis, the composite blade is idealized as an elastic beam undergoing moderate deflections in flap and lag bending, elastic torsion, elastic axial deformation, and flap and lag transverse shear. A nineteen degree of freedom shear flexible beam element is introduced for the composite rotor blades. The structural model has been validated by correlation with experimental data and finite element solutions for static deflections of elastically coupled graphite-epoxy composite box-beams (refs. 8.1, 8.2, 8.5). The free vibration analysis has been validated by correlation with experimental data and finite element results for the in vacuo rotating natural frequencies of the composite box-beams (Refs. 8.3, 8.5).

Using the new aeroelastic and aeromechanical analysis, rotors with five different composite spar layups have recently been examined; a baseline composite blade with no ply-induced elastic couplings, three symmetric layup composite blades featuring negative pitch-flap elastic coupling, positive pitch-flap elastic coupling, and negative pitch-lag elastic coupling, and an anti-symmetric layup blade featuring extension-torsion and bending-shear elastic couplings. Results indicated that elastic couplings

introduced through the composite blade spar have a powerful effect on both shaft-fixed blade stability and rotor-body aeromechanical stability. The torsional response is also significantly affected by the composite couplings. Influence of composite couplings on blade and hub loads was measurable, but less pronounced.

Specialized analysis features for composite blades are reflected in the UMARC structural modeling, aerodynamic modeling, and trim/response analysis. The following chapter will describe the laminated composite beam model, as well as the composite blade-related modifications to UMARC.

8.1 Structural Modeling

Structural modeling is the primary aeroelastic discipline affected by elastically coupled composite rotor blades. The following sections describe the development of the composite blade structural model used in the aeroelastic and aeromechanical analysis. Emphasis is placed on modifications (to the analysis described in Chapters 2-5) related to *composite blade* analysis. The first section describes the formulation of a new laminated composite box-beam model. This analysis provides the foundation for the more comprehensive composite rotor blade analysis. In addition to the detailed formulation of the governing equations, the first section also includes discussions focused on the detailed modeling of cross-section warping and inplane elasticity and a summary of the relevant specialized forms of the governing differential equations. The second section addresses modifications to the helicopter model, including the vehicle kinematics and coordinate systems, blade deformation kinematics, and the nondimensionalization scheme. The third section describes modification to the formulation of the aeroelastic and aeromechanical analysis using Hamilton's Principle. Strain energy and kinetic energy expressions for the coupled composite rotor-fuselage

system are developed. The fourth and fifth sections of the following chapter focus on the finite element discretization of the blade and fuselage equations of motion. The description of the blade discretization includes a discussion on the selection of the shear flexible beam element used in the present analysis.

8.1.1 Laminated Composite Box-Beam Analysis

8.1.1.1 Formulation of Governing Equations

The box-beam geometry and coordinates are shown in Figure 8.1. The cross-section axis origin is at the center of the beam section. The deformation of the beam cross-section is described by stretching, bending, twisting, shearing, and warping. These assumptions yield displacements of the form

$$U = u(x) - \underline{\eta} \left(v'(x) - \underline{\gamma}_{x\eta}^0(x) \right) - \underline{\zeta} \left(w'(x) - \underline{\gamma}_{x\zeta}^0(x) \right) - \underline{\lambda} \underline{\phi}'(x) \quad (8.1a)$$

$$V = v(x) - \zeta \phi(x) \quad (8.1b)$$

$$W = w(x) + \eta \phi(x) \quad (8.1c)$$

The underlined terms arise due to shear deformation of the cross-section (commonly termed transverse shear). Figure 8.2a illustrates the combined bending and shearing deformations of a shear flexible beam. The double-underlined terms represent the warping of the cross-section. In this context, warping refers to the axial distortion of the cross-section due to torsional deformation. This is commonly referred to as torsion-related warping. Figure 8.2b shows the warping distribution for a box-beam section. Both torsion-related warping and shear deformation are among the specialized new features of the present aeroelastic rotor blade analysis.

In the present analysis, the thin-walled beam theory approach described by Megson [8.6] is modified to determine the shape of the warping deflections for a laminated composite box-beam. This shape, or warping function, is then transformed from contour form to two-dimensional cross-sectional form. This warping function is carried through the entire analysis, from the initial kinematic relations to the effective stiffnesses of the beam cross-section. This approach is particularly useful for studying the quantitative effects of warping on the elastic behavior of the box-beam structure. It is important to note that this is the only point in the analysis where the cross-section is treated on the contour level of thin-walled beam theory. The warping function is defined along the contour as

$$\lambda(s) = 2A \left(\frac{\delta_{os}}{\delta} - \frac{A_{os}}{A} \right) \quad (8.2a)$$

For the rectangular box-beam under consideration, the enclosed area of the cross-section is $A = cd$. Other contour parameters in Eqn. (8.2a) are defined as

$$\delta = \oint \frac{ds}{G(s)t(s)} \approx \frac{2d}{t_v G_v} + \frac{2c}{t_h G_h} \quad (8.2b)$$

and

$$\delta_{os} = \int_0^s \frac{ds}{G(s)t(s)} \quad (8.2c)$$

where A_{os} is the area swept out by a generator, with origin at the box-beam center, from $s = 0$ to $s = s$ on the contour. For the present box-beam cross-section, the assumed contour coordinates and resulting values for δ_{os} and A_{os} are given in Figure 8.3. At this point, an effective in-plane shear stiffness for each composite beam wall must be specified. For this purpose, each beam wall is considered to be a single laminated plate. For example, consider the vertical box-beam walls. Laminate stress

resultants N_{xx} , $N_{\zeta\zeta}$, and $N_{x\zeta}$ are related to laminate strains ε_{xx} , $\varepsilon_{\zeta\zeta}$, and $\varepsilon_{x\zeta}$ by the constitutive law

$$\begin{Bmatrix} N_{xx} \\ N_{\zeta\zeta} \\ N_{x\zeta} \end{Bmatrix} = \begin{bmatrix} A_{11} & A_{12} & A_{16} \\ A_{12} & A_{22} & A_{26} \\ A_{16} & A_{26} & A_{66} \end{bmatrix} \begin{Bmatrix} \varepsilon_{xx} \\ \varepsilon_{\zeta\zeta} \\ \varepsilon_{x\zeta} \end{Bmatrix} \quad (8.3a)$$

with

$$A_{ij} = \sum_{n=1}^{\text{\# of plies}} \bar{Q}_{ij}^{(n)} t_{\text{ply}}^{(n)} \quad (8.3b)$$

The elements of the ply stiffness matrix, $\bar{\mathbf{Q}}$, are defined in several texts discussing macromechanical behavior of composite plies [8.7, 8.8]. These stiffness coefficients are functions of ply orientation angle θ , as well as ply elastic moduli. For a single linearly elastic orthotropic composite ply, the constitutive relations are given by

$$\begin{Bmatrix} \sigma_L \\ \sigma_T \\ \sigma_{LT} \end{Bmatrix} = \mathbf{Q} \begin{Bmatrix} \varepsilon_L \\ \varepsilon_T \\ \varepsilon_{LT} \end{Bmatrix} \quad (8.4)$$

where ε_{LT} is the engineering shear strain and the ply stiffness matrix, \mathbf{Q} , is

$$\mathbf{Q} = \begin{bmatrix} Q_{11} & Q_{12} & 0 \\ Q_{12} & Q_{22} & 0 \\ 0 & 0 & Q_{66} \end{bmatrix} \quad (8.5a)$$

The nonzero elements of \mathbf{Q} are defined as

$$\begin{aligned} Q_{11} &= \frac{E_L}{1 - v_{LT} v_{TL}} & Q_{22} &= \frac{E_T}{1 - v_{LT} v_{TL}} \\ Q_{12} &= \frac{E_T v_{LT}}{1 - v_{LT} v_{TL}} & Q_{66} &= G_{LT} \end{aligned} \quad (8.5b)$$

with

$$E_T v_{LT} = E_L v_{TL} \quad (8.5c)$$

These ply stiffness coefficients are functions of the longitudinal (along fiber direction) ply modulus, E_L , transverse (perpendicular to fiber direction) modulus, E_T , major and minor ply Poisson's ratios, ν_{LT} and ν_{TL} , and ply shear modulus, G_{LT} . For an orthotropic ply oriented with the fibers at an angle, θ , with respect to the laminate axial direction (see Figure 8.1), the constitutive relation between ply stresses and ply strains in the laminate axis is

$$\begin{Bmatrix} \sigma_{xx} \\ \sigma_{yy} \\ \sigma_{xy} \end{Bmatrix} = \bar{\mathbf{Q}} \begin{Bmatrix} \varepsilon_{xx} \\ \varepsilon_{yy} \\ \varepsilon_{xy} \end{Bmatrix} \quad (8.6)$$

where ε_{xy} is the engineering shear strain and the ply stiffness matrix, $\bar{\mathbf{Q}}$, is defined as

$$\bar{\mathbf{Q}} = \begin{bmatrix} \bar{Q}_{11} & \bar{Q}_{12} & \bar{Q}_{16} \\ \bar{Q}_{12} & \bar{Q}_{22} & \bar{Q}_{26} \\ \bar{Q}_{16} & \bar{Q}_{26} & \bar{Q}_{66} \end{bmatrix} \quad (8.7)$$

The nonzero elements of $\bar{\mathbf{Q}}$ are given by

$$\bar{Q}_{11} = U_1 + U_2 \cos 2\theta + U_3 \cos 4\theta \quad (8.8a)$$

$$\bar{Q}_{22} = U_1 - U_2 \cos 2\theta + U_3 \cos 4\theta \quad (8.8b)$$

$$\bar{Q}_{12} = U_4 - U_3 \cos 4\theta \quad (8.8c)$$

$$\bar{Q}_{66} = U_5 - U_3 \cos 4\theta \quad (8.8d)$$

$$\bar{Q}_{16} = -\frac{1}{2} U_2 \sin 2\theta - U_3 \sin 4\theta \quad (8.8e)$$

$$\bar{Q}_{26} = -\frac{1}{2} U_2 \sin 2\theta + U_3 \sin 4\theta \quad (8.8f)$$

where U_1 , U_2 , U_3 , U_4 , and U_5 are ply elastic invariants defined as

$$U_1 = (3Q_{11} + 3Q_{22} + 2Q_{12} + 4Q_{66})/8 \quad (8.9a)$$

$$U_2 = (Q_{11} - Q_{22})/2 \quad (8.9b)$$

$$U_3 = (Q_{11} + Q_{22} - 2Q_{12} - 4Q_{66})/8 \quad (8.9c)$$

$$U_4 = (Q_{11} + Q_{22} + 6Q_{12} - 4Q_{66})/8 \quad (8.9d)$$

$$U_5 = (Q_{11} + Q_{22} - 2Q_{12} + 4Q_{66})/8 \quad (8.9e)$$

Note that the ply stiffness matrix $\bar{\mathbf{Q}}$ exhibits elastic couplings between stresses and strains in the axial directions and stresses and strains in the shear direction. These elastic coupling stiffness coefficients, \bar{Q}_{16} and \bar{Q}_{26} , are odd functions of ply orientation angle whereas the direct axial, \bar{Q}_{11} , transverse, \bar{Q}_{22} , shear, \bar{Q}_{66} , and inplane Poisson's coupling stiffnesses, \bar{Q}_{12} , are even functions of ply orientation angle.

If transverse in-plane stress resultant $N_{\zeta\zeta}$ is assumed small for beam structures, the laminate inplane stiffness matrix, \mathbf{A} (see Eqn. (8.3)), simplifies to

$$\mathbf{A}' = \begin{bmatrix} \left(A_{11} - \frac{(A_{12})^2}{A_{22}} \right) & \left(A_{16} - \frac{A_{12}A_{26}}{A_{22}} \right) \\ \left(A_{11} - \frac{A_{12}A_{26}}{A_{22}} \right) & \left(A_{66} - \frac{(A_{26})^2}{A_{22}} \right) \end{bmatrix} = \begin{bmatrix} A'_{11} & A'_{16} \\ A'_{16} & A'_{66} \end{bmatrix} \quad (8.10)$$

An effective in-plane shear stiffness for each vertical box-beam wall can now be defined by considering the shear strain, $\varepsilon_{x\zeta}$, which results from an applied shear force resultant $N_{x\zeta}$.

$$G_v = \frac{1}{t_v} \left(\frac{\varepsilon_{x\zeta}}{N_{x\zeta}} \right)^{-1} = \frac{1}{t_v} \left(A'_{66} - \frac{(A'_{16})^2}{A'_{11}} \right) \quad (8.11)$$

Similarly, an effective in-plane shear stiffness G_h is defined for each horizontal wall. This approach captures the effects of elastic coupling in the anisotropic plies in an approximate but practical manner. For relatively thin walled beams, the contour warping function $\lambda(s)$, can be simply transformed into the two-dimensional cross-sectional form

$$\lambda(\eta, \zeta) = \beta \eta \zeta \quad (8.12)$$

with β and α given by

$$\beta = -\frac{(1-\alpha)}{(1+\alpha)} \quad \text{and} \quad \alpha = \left(\frac{c}{d}\right) \left(\frac{t_v}{t_h}\right) \left(\frac{G_v}{G_h}\right)$$

Strain Displacement Relations and Two-Dimensional Ply Elasticity

Strains are determined by differentiating the displacement terms shown in Eqns. (8.1a-c). Since the walls of the box-beam are assumed to be relatively thin, only axial and in-plane shear strains are considered non-negligible. The resulting strain displacement relations are

$$\epsilon_{xx} = u' - \eta(v'' - \gamma_{x\eta}^{0'}) - \zeta(w'' - \gamma_{x\zeta}^{0'}) - \lambda\phi'' \quad (8.13)$$

$$\epsilon_{x\zeta} = \left(\eta - \frac{\partial \lambda}{\partial \zeta}\right)\phi' + \gamma_{x\zeta}^0 \quad (8.14)$$

in the vertical walls, and

$$\epsilon_{xx} = u' - \eta(v'' - \gamma_{x\eta}^{0'}) - \zeta(w'' - \gamma_{x\zeta}^{0'}) - \lambda\phi'' \quad (8.13)$$

$$\epsilon_{x\eta} = -\left(\zeta + \frac{\partial \lambda}{\partial \eta}\right)\phi' + \gamma_{x\eta}^0 \quad (8.15)$$

in the horizontal walls.

In classical beam theory, transverse in-plane normal strains, $\epsilon_{\zeta\zeta}$ and $\epsilon_{\eta\eta}$, will not enter the formulation. This is a natural consequence of the one-dimensional nature of beam theory. However, when the walls of the box-beam are made of laminated composite material plies, transverse in-plane normal stresses and strains (i.e., $\sigma_{\zeta\zeta}$ and $\epsilon_{\zeta\zeta}$ in the vertical walls and $\sigma_{\eta\eta}$ and $\epsilon_{\eta\eta}$ in the horizontal walls) can become more important. The anisotropic elastic characteristics of composite plies can result in highly two-dimensional elastic behavior. This becomes more apparent upon considering the stress-strain relationship for a single ply of composite material. For a ply in a vertical beam wall, these elastic constitutive relations are

$$\begin{Bmatrix} \sigma_{xx} \\ \sigma_{\zeta\zeta} \\ \sigma_{x\zeta} \end{Bmatrix} = \begin{Bmatrix} \bar{Q}_{11} & \bar{Q}_{12} & \bar{Q}_{16} \\ \bar{Q}_{12} & \bar{Q}_{22} & \bar{Q}_{26} \\ \bar{Q}_{16} & \bar{Q}_{26} & \bar{Q}_{66} \end{Bmatrix} \begin{Bmatrix} \epsilon_{xx} \\ \epsilon_{\zeta\zeta} \\ \epsilon_{x\zeta} \end{Bmatrix} \quad (8.16)$$

The specific manner in which the two-dimensional nature of the composite walls is captured by one-dimensional beam theory is another important issue in composite box-beam analysis. Elastic properties within the composite plies vary dramatically with ply orientation angle. For some composite designs, Poisson's effect can become significant, causing the plies to behave in a highly two-dimensional elastic manner. Since the walls of the composite box-beam are built up from laminated plies, mismatch of Poisson's effect between plies within a wall can cause in-plane stresses and strains to exist even if there are no in-plane applied loads. This behavior is similar in nature to the thermally induced strains and stresses which result from mismatch in ply thermal expansion coefficients. This issue is addressed in the present analysis by imposing the following conditions on the transverse in-plane normal stresses.

$$\iint_h \sigma_{\eta\eta} dA + \iint_v \sigma_{\zeta\zeta} dA = 0 \quad (8.17a)$$

$$\iint_h \sigma_{\eta\eta} \eta dA + \iint_v \sigma_{\zeta\zeta} \eta dA = 0 \quad (8.17b)$$

$$\iint_h \sigma_{\eta\eta} \zeta dA + \iint_v \sigma_{\zeta\zeta} \zeta dA = 0 \quad (8.17c)$$

This is roughly equivalent to setting the net in-plane force and in-plane bending moments to be zero. Transverse in-plane normal strains, $\epsilon_{\eta\eta}$ and $\epsilon_{\zeta\zeta}$, are determined to satisfy these conditions. For example, in the vertical walls, $\epsilon_{\zeta\zeta}$ is written in general form as a continuous function within the cross-section.

$$\epsilon_{\zeta\zeta} = au' + b(v'' - \gamma_{x\eta}'^0) + c(w'' - \gamma_{x\zeta}'^0) + d\phi' + e\phi'' + f\gamma_{x\eta}'^0 + g\gamma_{x\zeta}'^0 \quad (8.18)$$

The coefficients of the deformations are assumed to be linear functions within the cross-section. For example,

$$a = a_0 + a_1 \eta + a_2 \zeta \quad (8.19a)$$

$$b = b_0 + b_1 \eta + b_2 \zeta \quad (8.19b)$$

Expressions of identical linear form are assumed for the coefficients c, d, e, f , and g in Eqn. (8.18). Relations given in Eqns. (8.18) and (8.19) are substituted into Eqn. (8.16) and the constants a_0, a_1, a_2 , etc., are determined from the three conditions on the in-plane stresses. Once the in-plane strain function is fully determined in terms of elastic constants and cross-section geometry, $\varepsilon_{\zeta\zeta}$ are removed from the constitutive relations by substitution. A similar technique is used to define $\varepsilon_{\eta\eta}$ within the horizontal walls. This procedure is a more refined version of the procedure used previously during the determination of the effective in-plane shear moduli G_v and G_h .

Two other approaches to modeling two-dimensional inplane ply elasticity are also included in the present analysis.

Method 1

Based only on initial kinematic assumptions about the deformations of the beam

$$\text{Horizontal Walls:} \quad \varepsilon_{\eta\eta} = 0 \quad (8.20a)$$

$$\text{Vertical Walls:} \quad \varepsilon_{\zeta\zeta} = 0 \quad (8.20b)$$

and $\sigma_{\eta\eta}$ and $\sigma_{\zeta\zeta}$ have no effect on net cross-section forces and moments. This assumption is similar in nature to plane strain. This assumption was employed in the aeroelastic analyses of Hong and Chopra [8.9-8.11] and Panda and Chopra [8.12]. These conditions result in simplification of the ply elastic constitutive relations. For example, the constitutive relation for plies in the vertical walls reduces to

$$\begin{Bmatrix} \sigma_{xx} \\ \sigma_{x\zeta} \end{Bmatrix} = \begin{bmatrix} \bar{Q}_{11} & \bar{Q}_{16} \\ \bar{Q}_{16} & \bar{Q}_{66} \end{bmatrix} \begin{Bmatrix} \epsilon_{xx} \\ \epsilon_{x\zeta} \end{Bmatrix} \quad (8.21)$$

Method 2

The second method begins to address the transverse in-plane behavior. In this method

$$\text{Horizontal Walls: } \sigma_{\eta\eta} = 0 \quad (8.22a)$$

$$\text{Vertical Walls: } \sigma_{\zeta\zeta} = 0 \quad (8.22b)$$

and $\epsilon_{\eta\eta}$ and $\epsilon_{\zeta\zeta}$ are eliminated from the constitutive relations by substitution. For example, consider the vertical beam walls (Eqn. (8.16)) for which $\sigma_{\zeta\zeta} = 0$

$$\bar{Q}_{12}\epsilon_{xx} + \bar{Q}_{22}\epsilon_{\zeta\zeta} + \bar{Q}_{26}\epsilon_{x\zeta} = 0 \quad (8.23)$$

rearranging the above relation yields

$$\epsilon_{\zeta\zeta} = -\frac{1}{\bar{Q}_{22}}(\bar{Q}_{12}\epsilon_{xx} + \bar{Q}_{26}\epsilon_{x\zeta}) \quad (8.24)$$

Substitution of the above relation for $\epsilon_{\zeta\zeta}$ into Eqn. (8.16) for $\sigma_{\zeta\zeta}$ and $\sigma_{\xi\zeta}$ results in the modified ply constitutive relations. For example, the constitutive relation for plies in the vertical walls now reduces to,

$$\begin{Bmatrix} \sigma_{xx} \\ \sigma_{x\zeta} \end{Bmatrix} = \begin{bmatrix} \bar{Q}'_{11} & \bar{Q}'_{16} \\ \bar{Q}'_{16} & \bar{Q}'_{66} \end{bmatrix} \begin{Bmatrix} \epsilon_{xx} \\ \epsilon_{x\zeta} \end{Bmatrix} \quad (8.25)$$

with modified stiffness matrix \mathbf{Q}' defined as

$$\begin{bmatrix} \bar{Q}'_{11} & \bar{Q}'_{16} \\ \bar{Q}'_{16} & \bar{Q}'_{66} \end{bmatrix} = \begin{bmatrix} \left(\bar{Q}_{11} - \frac{(\bar{Q}_{12})^2}{\bar{Q}_{22}} \right) & \left(\bar{Q}_{16} - \frac{\bar{Q}_{12}\bar{Q}_{26}}{\bar{Q}_{22}} \right) \\ \left(\bar{Q}_{16} - \frac{\bar{Q}_{12}\bar{Q}_{26}}{\bar{Q}_{22}} \right) & \left(\bar{Q}_{66} - \frac{(\bar{Q}_{26})^2}{\bar{Q}_{22}} \right) \end{bmatrix} \quad (8.26)$$

This assumption is similar in nature to plane stress and is used in the finite element cross-sectional analyses developed by Kosmatka and Friedmann [8.13-8.15]. The

direct analytical contour method developed by Rehfield [8.16] is formulated in terms of the inplane, or membrane, stiffness matrix \mathbf{A} given in Eqn. (8.3). In this method, the transverse inplane stress resultant, N_{ss} is assumed to be zero and the effective laminate stiffness matrix reduces to a form similar to Eqn. (8.10).

Cross-Section Forces, Moments, and Elastic Constants

By substituting the strain-displacement relations into the stress-strain relations, the stresses within the beam walls can be related to the displacements of the beam cross-section. The net forces and moments acting over the cross-section can be related to the stresses in the beam walls by equilibrium as follows

$$F = \iint \sigma_{xx} dA \quad (8.27a)$$

$$Q_y = \iint \sigma_{x\eta} dA \quad (8.27b)$$

$$Q_z = \iint \sigma_{x\zeta} dA \quad (8.27c)$$

$$T = \iint \left[\left(\eta - \frac{\partial \lambda}{\partial \zeta} \right) \sigma_{x\zeta} - \left(\zeta + \frac{\partial \lambda}{\partial \eta} \right) \sigma_{x\eta} \right] dA + \frac{\partial}{\partial x} \left[\iint \lambda \sigma_{xx} dA \right] \quad (8.27d)$$

$$M_y = - \iint \sigma_{xx} \zeta dA \quad (8.27e)$$

$$M_z = - \iint \sigma_{xx} \eta dA \quad (8.27f)$$

All of these expressions are quite natural except for the cross-section torque T . As demonstrated by Brunelle [8.17], torsion-related out-of-plane warping affects the net torque on the section. This effect can have considerable influence on elastic couplings for composite box-beams. The second integral term in the torque expression would become important for determining warping restraint effects.

Since the stresses are known in terms of the displacements, the governing differential equations relating cross-sectional loads (forces and moments) to cross-sectional displacements (stretching, bending, twisting, shearing, and warping) are derived. In matrix form, this can be written as,

$$\mathbf{F} = \mathbf{K} \mathbf{x} \quad (8.28)$$

with \mathbf{F} and \mathbf{x} given by

$$\mathbf{F} = \begin{Bmatrix} F & Q_y & Q_z & T & M_y & M_z \end{Bmatrix}^T$$

and

$$\mathbf{x} = \begin{Bmatrix} u' & \gamma_{x\eta}^0 & \gamma_{x\zeta}^0 & \phi' & (w'' - \gamma_{x\zeta}^{00}) & (v'' - \gamma_{x\eta}^{00}) \end{Bmatrix}^T$$

The specific elements of \mathbf{K} which apply to the present analysis are given below

$$K_{11} = \iint_{h,v} \bar{Q}_{11} dA + a_0 \iint_{h,v} \bar{Q}_{12} dA \quad (8.29a)$$

$$K_{12} = \iint_h \bar{Q}_{16} dA + f_0 \iint_h \bar{Q}_{12} dA \quad (8.29b)$$

$$K_{13} = \iint_v \bar{Q}_{16} dA + g_0 \iint_v \bar{Q}_{12} dA \quad (8.29c)$$

$$K_{14} = -(1+\beta) \iint_h \bar{Q}_{16} \zeta dA + (1-\beta) \iint_v \bar{Q}_{16} \eta dA + d_0 \iint_{h,v} \bar{Q}_{12} dA \quad (8.29d)$$

$$K_{22} = \iint_h \bar{Q}_{66} dA + f_0 \iint_h \bar{Q}_{26} dA \quad (8.29e)$$

$$K_{25} = - \iint_h \bar{Q}_{16} \zeta dA - f_2 \iint_h \bar{Q}_{26} \zeta^2 dA \quad (8.29f)$$

$$K_{33} = \iint_v \bar{Q}_{66} dA + g_0 \iint_v \bar{Q}_{26} dA \quad (8.29g)$$

$$K_{36} = - \iint_v \bar{Q}_{16} \eta dA - g_1 \iint_v \bar{Q}_{12} \eta^2 dA \quad (8.29h)$$

$$\begin{aligned} K_{44} = & (1+\beta)^2 \iint_h \bar{Q}_{66} \zeta^2 dA + (1-\beta)^2 \iint_v \bar{Q}_{66} \eta^2 dA \\ & + d_0 \left[(1-\beta) \iint_v \bar{Q}_{26} \eta dA - (1+\beta) \iint_h \bar{Q}_{26} \zeta dA \right] \end{aligned}$$

$$+ d_1(1-\beta) \iint_v \bar{Q}_{26} \eta^2 \, dA - d_2(1+\beta) \iint_h \bar{Q}_{26} \zeta^2 \, dA \quad (8.29i)$$

$$K_{45} = (1+\beta) \iint_h \bar{Q}_{16} \zeta^2 \, dA - d_2 \iint_{h,v} \bar{Q}_{12} \zeta^2 \, dA \quad (8.29j)$$

$$K_{46} = -(1-\beta) \iint_v \bar{Q}_{16} \eta^2 \, dA - d_1 \iint_{h,v} \bar{Q}_{12} \eta^2 \, dA \quad (8.29k)$$

$$K_{55} = \iint_{h,v} \bar{Q}_{11} \zeta^2 \, dA - c_2 \iint_{h,v} \bar{Q}_{12} \zeta^2 \, dA \quad (8.29l)$$

$$K_{66} = \iint_{h,v} \bar{Q}_{11} \eta^2 \, dA - b_1 \iint_{h,v} \bar{Q}_{12} \eta^2 \, dA \quad (8.29m)$$

with coefficients defined as

$$a_0 = - \iint_{h,v} \bar{Q}_{12} \, dA / \iint_{h,v} \bar{Q}_{22} \, dA \quad (8.30a)$$

$$b_1 = \iint_{h,v} \bar{Q}_{12} \eta^2 \, dA / \iint_{h,v} \bar{Q}_{22} \eta^2 \, dA \quad (8.30b)$$

$$c_2 = \iint_{h,v} \bar{Q}_{12} \zeta^2 \, dA / \iint_{h,v} \bar{Q}_{22} \zeta^2 \, dA \quad (8.30c)$$

$$d_0 = \left[(1+\beta) \iint_h \bar{Q}_{26} \zeta \, dA - (1-\beta) \iint_v \bar{Q}_{26} \eta \, dA \right] / \iint_{h,v} \bar{Q}_{22} \, dA \quad (8.30d)$$

$$d_1 = -(1-\beta) \iint_v \bar{Q}_{26} \eta^2 \, dA / \iint_{h,v} \bar{Q}_{22} \eta^2 \, dA \quad (8.30e)$$

$$d_2 = (1+\beta) \iint_h \bar{Q}_{26} \zeta^2 \, dA / \iint_{h,v} \bar{Q}_{22} \zeta^2 \, dA \quad (8.30f)$$

$$f_0 = - \iint_h \bar{Q}_{26} \, dA / \iint_h \bar{Q}_{22} \, dA \quad (8.30g)$$

$$f_2 = - \iint_h \bar{Q}_{26} \zeta \, dA / \iint_h \bar{Q}_{22} \zeta^2 \, dA \quad (8.30h)$$

$$g_0 = - \iint_v \bar{Q}_{26} \, dA / \iint_v \bar{Q}_{22} \, dA \quad (8.30i)$$

$$g_1 = - \iint_v \bar{Q}_{26} \eta \, dA / \iint_v \bar{Q}_{22} \eta^2 \, dA \quad (8.30j)$$

From this set of governing equations, beam displacements can be determined if the applied forces and moments are known. The physical meaning of the previously derived beam stiffness coefficients is described below:

$K_{11} = EA$	= axial stiffness
$K_{22} = GA_y$	= lag shear stiffness
$K_{33} = GA_z$	= flap shear stiffness
$K_{44} = GJ$	= torsion stiffness
$K_{55} = EI_y$	= flap bending stiffness
$K_{66} = EI_z$	= lag bending stiffness
K_{12}	= extension-lag shear coupling stiffness
K_{13}	= extension-flap shear coupling stiffness
K_{14}	= extension-torsion coupling stiffness
K_{25}	= lag shear-flap bending coupling stiffness
K_{36}	= flap shear-lag bending coupling stiffness
K_{45}	= flap bending-torsion coupling stiffness
K_{46}	= lag bending-torsion coupling stiffness

It should be noted that additional elastic coupling constants would be present for box-beam sections with no material or geometric symmetry. For example, a box-beam with different ply orientation angles on the top and bottom wall laminates would exhibit extension-flap bending coupling (i.e. K_{15}).

The difference between Method 1, Method 2 and the method used in the present analysis can now be clarified by considering one of the resulting stiffness coefficients. For example, the axial stiffness of the box-beam as derived from Method 1, is given by

$$K_{11} = \iint_{h,v} \bar{Q}_{11} dA \quad (8.31)$$

Axial stiffness derived using Method 2 is given by

$$K_{11} = \iint_{h,v} \left[\bar{Q}_{11} - \frac{(\bar{Q}_{12})^2}{\bar{Q}_{22}} \right] dA \quad (8.32)$$

Axial stiffness derived using the present analysis method is given by

$$K_{11} = \iint_{h,v} \bar{Q}_{11} dA - \frac{\left(\iint_{h,v} \bar{Q}_{12} dA \right)^2}{\iint_{h,v} \bar{Q}_{22} dA} \quad (8.33)$$

Note the differences in the manner in which two-dimensional in-plane elastic behavior appears in the different expressions for axial stiffness. Quantitative differences between these methods are presented in Refs. 8.1, 8.2, and 8.5.

8.1.1.2 Special Forms of Governing Equations

The following section describes the force-deflection relationship for several pertinent coupled composite box-beam configurations. These configurations are of particular interest for potential applications to elastically tailored composite rotor blades.

Cross-Ply Layup

This configuration, consisting only of plies at $\theta = 0$ degree and $\theta = 90$ degree orientations, exhibits no elastic couplings. The governing differential equations, identical to those of an isotropic beam, are given by

$$\begin{Bmatrix} F \\ Q_y \\ Q_z \end{Bmatrix} = \begin{bmatrix} K_{11} & 0 & 0 \\ 0 & K_{22} & 0 \\ 0 & 0 & K_{33} \end{bmatrix} \begin{Bmatrix} u' \\ \gamma_{x\eta}^0 \\ \gamma_{x\zeta}^0 \end{Bmatrix} \quad (8.34)$$

and

$$\begin{Bmatrix} T \\ M_y \\ M_z \end{Bmatrix} = \begin{bmatrix} K_{44} & 0 & 0 \\ 0 & K_{55} & 0 \\ 0 & 0 & K_{66} \end{bmatrix} \begin{Bmatrix} \phi' \\ (w'' - \gamma_{x\zeta}^{(0)}) \\ (v'' - \gamma_{x\eta}^{(0)}) \end{Bmatrix} \quad (8.35)$$

Symmetric Layups

The ply orientations for three different types of symmetric layup box-beam are defined in Figures 8.5a-c. These configurations display bending-torsion coupling and extension-shear couplings. Elastic coupling between flap bending and torsion, K_{45} , arises from the top and bottom walls of the beam, whereas coupling between lag bending and torsion, K_{46} , arises from the side walls of the beam. Extension shear couplings, K_{12} and K_{13} are parasitic in nature and will accompany box-beam configurations designed to exhibit bending-torsion couplings. For example, extension-lag shear coupling, K_{12} , is generated by the horizontal top and bottom walls and will accompany flap bending-torsion coupling. The governing equations for symmetric layup box-beam configurations are

$$\begin{Bmatrix} F \\ Q_y \\ Q_z \end{Bmatrix} = \begin{bmatrix} K_{11} & K_{12} & K_{13} \\ K_{12} & K_{22} & 0 \\ K_{13} & 0 & K_{33} \end{bmatrix} \begin{Bmatrix} u' \\ \gamma_{x\eta}^{(0)} \\ \gamma_{x\zeta}^{(0)} \end{Bmatrix} \quad (8.36)$$

and

$$\begin{Bmatrix} T \\ M_y \\ M_z \end{Bmatrix} = \begin{bmatrix} K_{44} & K_{45} & K_{46} \\ K_{45} & K_{55} & 0 \\ K_{46} & 0 & K_{66} \end{bmatrix} \begin{Bmatrix} \phi' \\ (w'' - \gamma_{x\zeta}^{(0)}) \\ (v'' - \gamma_{x\eta}^{(0)}) \end{Bmatrix} \quad (8.37)$$

Note that the bending and torsion of the beam is not elastically coupled to the extension and shearing of the beam.

Antisymmetric Layups

The ply orientations for an antisymmetric layup beam are defined in Figure 8.6. This configuration displays extension-torsion coupling and bending-shear couplings. The bending-shear couplings are parasitic in nature and will be present (to some extent) in all box-beam designs featuring extension-torsion coupling. The governing differential equations for anti-symmetric layup box-beams are given by

$$\begin{Bmatrix} F \\ T \end{Bmatrix} = \begin{bmatrix} K_{11} & K_{14} \\ K_{14} & K_{44} \end{bmatrix} \begin{Bmatrix} u' \\ \phi' \end{Bmatrix} \quad (8.38a)$$

$$\begin{Bmatrix} Q_y \\ Q_z \\ M_y \\ M_z \end{Bmatrix} = \begin{bmatrix} K_{22} & 0 & K_{25} & 0 \\ 0 & K_{33} & 0 & K_{36} \\ K_{25} & 0 & K_{55} & 0 \\ 0 & K_{36} & 0 & K_{66} \end{bmatrix} \begin{Bmatrix} \gamma_{x\eta}^0 \\ \gamma_{x\zeta}^0 \\ (w'' - \gamma_{x\zeta}^{0'}) \\ (v'' - \gamma_{x\eta}^{0'}) \end{Bmatrix} \quad (8.38b)$$

Note that the extension and torsion of the beam is not elastically coupled to the bending and shearing of the beam.

8.1.2 The Helicopter Model

The helicopter is modeled as a rigid fuselage connected to a single main rotor with an arbitrary number, N_b , elastic blades. Each composite blade is assumed to be an elastic beam undergoing flap bending, lag bending, elastic twist and axial deflections, *as well as flap and lag transverse shear deflections*. The deflections are considered to be of moderate magnitude while strains are assumed to be small. Nonuniform blades having pretwist, precone, and chordwise offsets of blade center of gravity and aerodynamic center from the elastic axis can be accommodated. The primary structural component of the blade is a laminated composite box-beam spar. Elastic couplings arising from ply orientations within the walls of the composite spar are incorporated into the formulation. Stiffness coefficients and elastic coupling parameters can also be computed using more detailed analyses, and subsequently input into UMARC by the user. This feature allows for aeroelastic and aeromechanical analysis of many other composite spar configurations. The rigid body fuselage model is described in detail in Chapter 2.

8.1.2.1 Blade Deformation Kinematics and Coordinate Systems

In the composite blade analysis, both bending and transverse shearing deformations are considered. This model implies that the total translational lag and flap deflections, v and w , can be decomposed as shown below

$$\text{Lag: } v = v_b + v_s \quad (8.39)$$

$$\text{Flap: } w = w_b + w_s \quad (8.40)$$

where v_b and w_b are bending deflections and v_s and w_s are shearing deflections. The coordinate transformation between the undeformed and deformed blade coordinate systems is given by

$$\begin{Bmatrix} \hat{i}_\xi \\ \hat{j}_\eta \\ \hat{k}_\zeta \end{Bmatrix} = \mathbf{T}_{DU} \begin{Bmatrix} \hat{i} \\ \hat{j} \\ \hat{k} \end{Bmatrix} \quad (8.41)$$

The origin of the transformation matrix, \mathbf{T}_{DU} , is now described. Blade deformation can be described by a series of Euler angles as shown in Figure 2.10. In terms of these Euler angles, the transformation matrix between the deformed and undeformed blade coordinate systems is given by

$$\mathbf{T}_{DU} = \begin{bmatrix} \cos \bar{\theta} \cos \bar{\zeta} & \cos \bar{\theta} \sin \bar{\zeta} & \sin \bar{\theta} \\ -\sin \bar{\theta} \sin \bar{\beta} \cos \bar{\zeta} & \cos \bar{\theta} \cos \bar{\zeta} & \cos \bar{\beta} \sin \bar{\theta} \\ -\cos \bar{\theta} \sin \bar{\zeta} & -\sin \bar{\zeta} \sin \bar{\beta} \sin \bar{\theta} & \cos \bar{\beta} \cos \bar{\theta} \\ -\cos \bar{\theta} \sin \bar{\beta} \cos \bar{\zeta} & -\sin \bar{\theta} \cos \bar{\zeta} & \cos \bar{\beta} \cos \bar{\theta} \\ +\sin \bar{\theta} \sin \bar{\zeta} & -\sin \bar{\zeta} \sin \bar{\beta} \cos \bar{\theta} & \end{bmatrix} \quad (8.42)$$

The Euler angles, $\bar{\zeta}$, $\bar{\beta}$, and $\bar{\theta}$ can be approximately written in terms of blade deformations as

$$\begin{aligned} \cos \bar{\zeta} &= \frac{\sqrt{1-v'^2-w'^2}}{\sqrt{1-w'^2}} & \sin \bar{\zeta} &= \frac{v'}{\sqrt{1-w'^2}} \\ \cos \bar{\beta} &= \sqrt{1-w'^2} & \sin \bar{\beta} &= w' \\ \bar{\theta} &= \theta_1 \end{aligned} \quad (8.43)$$

where the *total* slopes, v' and w' , are given by

$$v' = v'_b + v'_s \quad (8.44a)$$

$$w' = w'_b + w'_s \quad (8.44b)$$

Substituting the above relations and simplifying to second order terms yields the transformation between deformed and undeformed blade positions

$$T_{DU} = \begin{bmatrix} 1 - \frac{v_b'^2}{2} - \frac{w_b'^2}{2} & v' & w' \\ -v' \cos \theta_1 - w' \sin \theta_1 & (1 - \frac{v_b'^2}{2}) \cos \theta_1 - v'_b w'_b \sin \theta_1 & (1 - \frac{w_b'^2}{2}) \sin \theta_1 \\ v' \sin \theta_1 - w' \cos \theta_1 & -(1 - \frac{v_b'^2}{2}) \sin \theta_1 - v'_b w'_b \cos \theta_1 & (1 - \frac{w_b'^2}{2}) \cos \theta_1 \end{bmatrix} \quad (8.45)$$

where total slopes, v' and w' , are previously defined above. This transformation matrix is similar to that which is derived in Ref. 8.18, however, the effects of transverse shear are modeled in the present transformation.

8.1.2.2 Nondimensionalization and Ordering Scheme

As discussed in Chapter 2, the entire formulation and all ensuing computations are carried out in nondimensional form.

In formulating Hamilton's principle, it is important to neglect higher order terms to simplify the analysis. Terms up to second order are retained in the analysis by introducing the nondimensional quantity ϵ , such that $\epsilon \ll 1$. Some third order terms related to elastic torsion are also retained in the energy expressions. The order of magnitude of the additional nondimensional quantities related to the composite rotor analysis is defined as follows:

$$\frac{EA}{m_0 \Omega^2 R^2}, \frac{GA_y}{m_0 \Omega^2 R^2}, \frac{GA_z}{m_0 \Omega^2 R^2} = O(\epsilon^{-2})$$

$$\frac{K_{12}}{m_0 \Omega^2 R^2}, \frac{K_{13}}{m_0 \Omega^2 R^2} = O(\epsilon^{-2})$$

$$\begin{aligned}
& \frac{K_{14}}{m_0 \Omega^2 R^3}, \frac{K_{25}}{m_0 \Omega^2 R^3}, \frac{K_{36}}{m_0 \Omega^2 R^3} = O(\varepsilon^{-1}) \\
& \frac{K_{45}}{m_0 \Omega^2 R^4}, \frac{K_{46}}{m_0 \Omega^2 R^4} = O(1) \\
& \frac{v_b}{R}, \frac{w_b}{R}, \phi, \beta_p, \frac{k_A}{R}, \frac{k_{m1}}{R}, \frac{k_{m2}}{R} = O(\varepsilon) \\
& \frac{u_e}{R}, \frac{v_s}{R}, \frac{w_s}{R}, \frac{d_0}{a}, \frac{f_l}{a} = O(\varepsilon^2)
\end{aligned} \tag{8.46}$$

where a is the lift curve slope and m_0 is a reference mass per unit length. For this analysis, the reference mass per unit length, m_0 , is defined as the mass per unit length of an equivalent *uniform* blade which has the same flap inertia as the actual (*i.e.* *nonuniform*) blade. Using this definition, m_0 can be written as

$$m_0 = \frac{3I_\beta}{R^3} \approx \frac{3 \int_0^R mr^2 dr}{R^3} \tag{8.47}$$

When applying the ordering scheme to the energy expressions, care must be taken to insure that the physics of the system is not violated. Symmetry in the structural stiffness matrix and mass matrix should be retained, and the antisymmetric damping matrix should reflect the gyroscopic couplings associated with Coriolis effects. The assumed orders of all other nondimensional quantities are defined in Chapter 2.

8.1.3 Formulation Using Hamilton's Principle

As described in Chapter 2, Hamilton's variational principle is used to derive the system equations of motion. The generalized Hamilton's principle, applicable to nonconservative systems, is expressed as

$$\delta \Pi = \int_{t_1}^{t_2} (\delta U - \delta T - \delta W) dt = 0 \tag{8.48}$$

where δU is the virtual variation of strain energy and δI is the virtual variation of kinetic energy. The δW is the virtual work done by external forces. These virtual variations have contributions from both the rotor and the fuselage (see Chapter 2). Elastically coupled composite rotor blades affect the strain energy of the blade. Consideration of shear deformations also results in modifications to the kinetic energy and virtual work expressions.

8.1.3.1 Blade Strain Energy, δU_b

Each rotor blade is considered to be a long slender *anisotropic* beam. The walls of the beam consist of laminated orthotropic composite plies. The corresponding relationship between ply stresses and classical engineering strains in the horizontal and vertical spar walls is given by

$$\text{Horizontal walls: } \begin{Bmatrix} \sigma_{xx} \\ \sigma_{\eta\eta} \\ \sigma_{x\eta} \end{Bmatrix} = \begin{bmatrix} \bar{Q}_{11} & \bar{Q}_{12} & \bar{Q}_{16} \\ \bar{Q}_{12} & \bar{Q}_{22} & \bar{Q}_{26} \\ \bar{Q}_{16} & \bar{Q}_{26} & \bar{Q}_{66} \end{bmatrix} \begin{Bmatrix} \epsilon_{xx} \\ \epsilon_{\eta\eta} \\ \epsilon_{x\eta} \end{Bmatrix} \quad (8.49a)$$

$$\text{Vertical walls: } \begin{Bmatrix} \sigma_{xx} \\ \sigma_{\zeta\zeta} \\ \sigma_{x\zeta} \end{Bmatrix} = \begin{bmatrix} \bar{Q}_{11} & \bar{Q}_{12} & \bar{Q}_{16} \\ \bar{Q}_{12} & \bar{Q}_{22} & \bar{Q}_{26} \\ \bar{Q}_{16} & \bar{Q}_{26} & \bar{Q}_{66} \end{bmatrix} \begin{Bmatrix} \epsilon_{xx} \\ \epsilon_{\zeta\zeta} \\ \epsilon_{x\zeta} \end{Bmatrix} \quad (8.49b)$$

where ϵ_{xx} is axial strain, and $\epsilon_{x\eta}$ and $\epsilon_{x\zeta}$ are engineering shear strains. For the relatively thin-walled box-beam spar, it is assumed $\epsilon_{x\zeta} = 0$ in horizontal spar walls and $\epsilon_{x\eta} = 0$ in vertical spar walls. As discussed in Section 8.1.1, treatment of two-dimensional inplane elasticity (i.e. $\sigma_{\eta\eta}$, $\sigma_{\zeta\zeta}$, $\epsilon_{\eta\eta}$, and $\epsilon_{\zeta\zeta}$) within the ply walls requires a modification to the constitutive equations. All of the effective beam stiffness coefficients can be obtained from the linear analysis as described in Section 8.1.1. For clarity, the strain energy formulation are carried out by neglecting the two-dimensional inplane elasticity. Beam stiffness coefficients are then calculated using the previously

derived cross-section integrals. Proceeding under these assumptions, the expression for strain energy of the *b*th blade, is given by

$$U_b = \frac{1}{2} \int_0^R \iint_A (\sigma_{xx}\varepsilon_{xx} + \sigma_{x\eta}\varepsilon_{x\eta} + \sigma_{x\zeta}\varepsilon_{x\zeta}) d\eta d\zeta dx \quad (8.50)$$

The expression for the variation of strain energy is given by

$$\delta U_b = \int_0^R \iint_A (\sigma_{xx}\delta\varepsilon_{xx} + \sigma_{x\eta}\delta\varepsilon_{x\eta} + \sigma_{x\zeta}\delta\varepsilon_{x\zeta}) d\eta d\zeta dx \quad (8.51)$$

Substituting the stress-strain relations into the variation of strain energy yields

$$\begin{aligned} \delta U_b = & \int_0^R \iint_h (\bar{Q}_{11}\varepsilon_{xx}\delta\varepsilon_{xx} + \bar{Q}_{16}\varepsilon_{x\eta}\delta\varepsilon_{x\eta}) d\eta d\zeta dx \\ & + \int_0^R \iint_v (\bar{Q}_{11}\varepsilon_{xx}\delta\varepsilon_{xx} + \bar{Q}_{16}\varepsilon_{x\zeta}\delta\varepsilon_{x\zeta}) d\eta d\zeta dx \end{aligned} \quad (8.52)$$

The next ingredient in the strain energy formulation is the strain displacement relations. The strain-displacement relations reflect the nonlinearities due to moderate deflections of the beam. Additional terms are also visible due to blade pitch, θ_0 . This pitch is generally due to combinations of elastic torsion, pretwist, and pitch control inputs.

$$\begin{aligned} \varepsilon_{xx} = & u'_e - \hat{\lambda}_T \phi'' + (\eta^2 + \zeta^2)(\theta'_0 \phi' + \frac{\phi'^2}{2}) \\ & - v''_b [\eta \cos(\theta_0 + \hat{\phi}) - \zeta \sin(\theta_0 + \hat{\phi})] \\ & - w''_b [\eta \sin(\theta_0 + \hat{\phi}) + \zeta \cos(\theta_0 + \hat{\phi})] \end{aligned} \quad (8.53)$$

$$\varepsilon_{x\eta} = -\left(\zeta + \frac{\partial \lambda_T}{\partial \eta}\right) \phi' + v'_s \cos(\theta_0 + \hat{\phi}) + w'_s \sin(\theta_0 + \hat{\phi}) \quad (8.54)$$

$$\varepsilon_{x\zeta} = \left(\eta - \frac{\partial \lambda_T}{\partial \zeta}\right) \phi' + w'_s \cos(\theta_0 + \hat{\phi}) - v'_s \sin(\theta_0 + \hat{\phi}) \quad (8.55)$$

noting the assumptions that $\varepsilon_{x\zeta} = 0$ in the horizontal spar walls and $\varepsilon_{x\eta} = 0$ in the vertical spar walls. The cross-sectional warping function, λ_T , is determined in closed form for the composite box-beam spar using Eqn. (8.12) (see section 8.1.1).

The variations in strains are given by

$$\begin{aligned}\delta\varepsilon_{xx} &= \delta u'_e + (\eta^2 + \zeta^2)(\theta'_0 + \phi')\delta\phi' - \lambda_T\delta\phi'' \\ &\quad - [\eta\cos(\theta_0 + \hat{\phi}) - \zeta\sin(\theta_0 + \hat{\phi})](\delta v''_b + w''_b\delta\phi) \\ &\quad - [\eta\sin(\theta_0 + \hat{\phi}) + \zeta\cos(\theta_0 + \hat{\phi})](\delta w''_b + v''_b\delta\phi)\end{aligned}\quad (8.56)$$

$$\begin{aligned}\delta\varepsilon_{x\eta} &= -\left(\zeta + \frac{\partial\lambda_T}{\partial\eta}\right)\delta\phi' + \cos(\theta_0 + \hat{\phi})(\delta v'_s + w'_s\delta\phi) \\ &\quad + \sin(\theta_0 + \hat{\phi})(\delta w'_s - v'_s\delta\phi)\end{aligned}\quad (8.57)$$

$$\begin{aligned}\delta\varepsilon_{x\zeta} &= \left(\eta - \frac{\partial\lambda_T}{\partial\zeta}\right)\delta\phi' + \cos(\theta_0 + \hat{\phi})(\delta w'_s - v'_s\delta\phi) \\ &\quad - \sin(\theta_0 + \hat{\phi})(\delta v'_s + w'_s\delta\phi)\end{aligned}\quad (8.58)$$

Variation of strain energy is determined using the stress-strain relations and strain-displacement relations given above. For small angles $\hat{\phi}$, the following trigonometric expansion can be used

$$\sin(\theta_0 + \hat{\phi}) = \sin\theta_0\cos\hat{\phi} + \sin\hat{\phi}\cos\theta_0 \approx \sin\theta_0 + \hat{\phi}\cos\theta_0 \quad (8.59)$$

$$\cos(\theta_0 + \hat{\phi}) = \cos\theta_0\cos\hat{\phi} - \sin\hat{\phi}\sin\theta_0 \approx \cos\theta_0 - \hat{\phi}\sin\theta_0 \quad (8.60)$$

The expression for variation of strain energy in nondimensional form is obtained retaining terms up to the second order in basic governing equations (i.e. $1 + \varepsilon^2 \approx 1$). In addition, some third order terms are also retained in the torsion equations. The strain energy variation can be written in terms of the variable $\hat{\phi}$ using the following relations (see Eqn. (2.7))

$$\hat{\phi}' = \phi' - w'v'' \approx \phi' - w'_b v''_b \quad (8.61a)$$

$$\delta\hat{\phi}' = \delta\phi' - w'_b\delta v''_b - v''_b\delta w'_b \quad (8.61b)$$

The axial deflection, u , is represented by two separate components; an elastic axial deflection, u_e , and a kinematic axial deflection due to foreshortening, u_F . Using this representation [8.19], the following relations are substituted into the strain energy expression,

$$u = u_e - u_F \quad (8.62a)$$

$$u = u_e - \frac{1}{2} \int_0^x (v'^2 + w'^2) dx \quad (8.62b)$$

$$u' = u'_e - \frac{1}{2} (v'^2 + w'^2) \quad (8.62c)$$

$$\dot{u} = \dot{u}_e - \int_0^x (v'\dot{v}' + w'\dot{w}') dx \quad (8.62d)$$

$$\delta u = \delta u_e - \int_0^x (v'\delta v' + w'\delta w') dx \quad (8.62e)$$

$$\delta u' = \delta u'_e - v'\delta v' - w'\delta w' \quad (8.62f)$$

recalling, $v' = v'_b + v'_s$ and $w' = w'_b + w'_s$, are the total lag and flap direction slopes. For the b th blade, the resulting expression is given by

$$\begin{aligned} \frac{\delta U_b}{m_0 \Omega^2 R^3} &= \int_0^1 (U_u \cdot \delta u'_e + U_{w'_b} \delta w'_b + U_{v''_b} \delta v''_b + U_{w''_b} \delta w''_b + U_{\hat{\phi}} \delta \hat{\phi} \\ &\quad + U_{\hat{\phi}'} \delta \hat{\phi}' + U_{\hat{\phi}''} \delta \hat{\phi}'' + U_{v'_s} \delta v'_s + U_{w'_s} \delta w'_s) dx \end{aligned} \quad (8.63)$$

where

$$\begin{aligned} U_u &= EA \left[u'_e + k_A^2 \theta'_0 (\hat{\phi}' + w'_b v''_b) + k_A^2 \frac{\hat{\phi}'^2}{2} \right] \\ &\quad - EA e_A \left[v''_b (\cos \theta_0 - \hat{\phi} \sin \theta_0) + w''_b (\sin \theta_0 + \hat{\phi} \cos \theta_0) \right] \\ &\quad + K_{14} (\hat{\phi}' + v''_b w'_b) \\ &\quad + K_{12} (v'_s \cos \theta_0 + w'_s \sin \theta_0) + K_{13} (w'_s \cos \theta_0 - v'_s \sin \theta_0) \end{aligned} \quad (8.64)$$

$$\begin{aligned}
U_{v_b''} = & v_b''(EI_z \cos^2 \theta_0 + EI_y \sin^2 \theta_0) + w_b''(EI_z - EI_y) \cos \theta_0 \sin \theta_0 \\
& - EAe_A u_e' (\cos \theta_0 - \hat{\phi} \sin \theta_0) - \hat{\phi}' EB_2 \theta_0' \cos \theta_0 \\
& + w_b'' \hat{\phi} (EI_z - EI_y) \cos 2\theta_0 - v_b'' \hat{\phi} (EI_z - EI_y) \sin 2\theta_0 \\
& + (GJ + EB_1 \theta_0'^2) \hat{\phi}' w_b' + EAk_A^2 \theta_0' w_b' u_e' \\
& - K_{45} (\hat{\phi}' \sin \theta_0 + \hat{\phi} \hat{\phi}' \cos \theta_0) + K_{46} (\hat{\phi}' \cos \theta_0 - \hat{\phi} \hat{\phi}' \sin \theta_0) \\
& + K_{14} u_e' w_b' + K_{45} (w_b' w_b'' \cos \theta_0 - 2v_b'' w_b' \sin \theta_0) \\
& + K_{46} (w_b' w_b'' \sin \theta_0 + 2v_b'' w_b' \cos \theta_0) \\
& + K_{25} (v_s' \sin \theta_0 \cos \theta_0 + w_s' \sin^2 \theta_0) + K_{36} (v_s' \sin \theta_0 \cos \theta_0 - w_s' \cos^2 \theta_0)
\end{aligned}$$

$$\begin{aligned}
U_{w_b'} = & (GJ + EB_1 \theta_0'^2) \hat{\phi}' v_b'' + EAk_A^2 \theta_0' v_b'' u_e' + K_{14} u_e' v_b'' \\
& + K_{45} (v_b'' w_b'' \cos \theta_0 - v_b'^2 \sin \theta_0) + K_{46} (v_b'^2 \cos \theta_0 + v_b'' w_b'' \sin \theta_0)
\end{aligned}$$

$$\begin{aligned}
U_{w_b''} = & w_b''(EI_y \cos^2 \theta_0 + EI_z \sin^2 \theta_0) + v_b''(EI_z - EI_y) \cos \theta_0 \sin \theta_0 \\
& - EAe_A u_e' (\sin \theta_0 + \hat{\phi} \cos \theta_0) - \hat{\phi}' EB_2 \theta_0' \sin \theta_0 \\
& + w_b'' \hat{\phi} (EI_z - EI_y) \sin 2\theta_0 + v_b'' \hat{\phi} (EI_z - EI_y) \cos 2\theta_0 \\
& + K_{45} (\hat{\phi}' \cos \theta_0 - \hat{\phi} \hat{\phi}' \sin \theta_0) + K_{46} (\hat{\phi}' \sin \theta_0 + \hat{\phi} \hat{\phi}' \cos \theta_0) \\
& + K_{45} v_b'' w_b' \cos \theta_0 + K_{46} v_b'' w_b' \sin \theta_0 \\
& - K_{25} (w_s' \sin \theta_0 \cos \theta_0 + v_s' \cos^2 \theta_0) - K_{36} (w_s' \sin \theta_0 \cos \theta_0 - v_s' \sin^2 \theta_0)
\end{aligned}$$

$$\begin{aligned}
U_{\hat{\phi}} = & w_b'^2 (EI_z - EI_y) \sin \theta_0 \cos \theta_0 + v_b'' w_b'' (EI_z - EI_y) \cos 2\theta_0 \\
& - v_b'^2 (EI_z - EI_y) \sin \theta_0 \cos \theta_0 \\
& - K_{45} (w_b'' \hat{\phi}' \sin \theta_0 + v_b'' \hat{\phi}' \cos \theta_0) + K_{46} (w_b'' \hat{\phi}' \cos \theta_0 - v_b'' \hat{\phi}' \sin \theta_0)
\end{aligned}$$

$$\begin{aligned}
U_{\hat{\phi}'} = & GJ (\hat{\phi}' + w_b' v_b'') + EB_1 \theta_0'^2 \hat{\phi}' + EAk_A^2 (\theta_0' + \hat{\phi}') u_e' \\
& - EB_2 \theta' (v_b'' \cos \theta_0 + w_b'' \sin \theta_0) + K_{14} u_e' \\
& + K_{45} (w_b'' \cos \theta_0 - v_b'' \sin \theta_0 - \hat{\phi} v_b'' \cos \theta_0 - \hat{\phi} w_b'' \sin \theta_0) \\
& + K_{46} (v_b'' \cos \theta_0 + w_b'' \sin \theta_0 + \hat{\phi} w_b'' \cos \theta_0 - \hat{\phi} v_b'' \sin \theta_0)
\end{aligned}$$

$$U_{\dot{\phi}''} = EC_1 \dot{\phi}'' + EC_2 (w_b'' \cos \theta_0 - v_b'' \sin \theta_0)$$

$$U_{v_s'} = GA_y \left(v_s' \cos^2 \theta_0 + w_s' \sin \theta_0 \cos \theta_0 \right) + GA_z \left(v_s' \sin^2 \theta_0 - w_s' \sin \theta_0 \cos \theta_0 \right)$$

$$\begin{aligned} &+ K_{12} u_e' \cos \theta_0 - K_{13} u_e' \sin \theta_0 \\ &+ K_{25} \left(v_b'' \sin \theta_0 \cos \theta_0 - w_b'' \cos^2 \theta_0 \right) + K_{36} \left(v_b'' \sin \theta_0 \cos \theta_0 + w_b'' \sin^2 \theta_0 \right) \end{aligned}$$

$$\begin{aligned} U_{w_s'} = GA_z \left(w_s' \cos^2 \theta_0 - v_s' \sin \theta_0 \cos \theta_0 \right) + GA_y \left(w_s' \sin^2 \theta_0 + v_s' \sin \theta_0 \cos \theta_0 \right) \\ &+ K_{12} u_e' \sin \theta_0 + K_{13} u_e' \cos \theta_0 \\ &+ K_{25} \left(v_b'' \sin^2 \theta_0 - w_b'' \sin \theta_0 \cos \theta_0 \right) - K_{36} \left(w_b'' \sin \theta_0 \cos \theta_0 + v_b'' \cos^2 \theta_0 \right) \end{aligned}$$

The section properties for the composite box-beam spar, EA , EI_y , ..., K_{46} , are defined in section 8.1.1. The axial (extensional) stiffness of the blade is EA . The tensile axis offset from the elastic axis is e_A (positive forward). The EI_y and EI_z are, respectively, the flap and lag bending stiffnesses, and GJ is the torsional stiffness. The EC_1 is the warping rigidity and EC_2 is another constant related to the warping of the beam section. Both EC_1 and EC_2 are related to the restraint of warping displacements; therefore, they are generally more important for open section beams. The k_A is the radius of gyration of the blade cross section, and EB_1 and EB_2 are other sectional constants which appear due to blade pitch. The $K_{12}, K_{13}, \dots, K_{46}$ are elastic coupling terms and are defined as in Section 8.1.1. Because of the assumed symmetry (geometric and material) of the blade cross section about the η axis, the following relationships hold:

$$K_{15} \approx \iint_{h,v} \bar{Q}_{11} \zeta dA = 0 \quad K_{17} \approx \iint_{h,v} \bar{Q}_{11} \lambda dA = 0$$

$$K_{56} \approx \iint_{h,v} \bar{Q}_{11} \eta \zeta dA = 0 \quad K_{67} \approx \iint_{h,v} \bar{Q}_{11} \lambda \eta dA = 0$$

$$K_{24} \approx \iint_h \bar{Q}_{66} \left(\zeta + \frac{\partial \lambda}{\partial \eta} \right) dA = 0$$

$$K_{26} \approx \iint_h \bar{Q}_{16} \eta dA = 0 \quad K_{27} \approx \iint_h \bar{Q}_{16} \lambda dA = 0$$

$$\begin{aligned}
K_{35} &\approx \iint_v \bar{Q}_{16} \zeta dA = 0 & K_{37} &\approx \iint_v \bar{Q}_{16} \lambda dA = 0 \\
K_{47} &\approx \iint_h \bar{Q}_{16} \left(\zeta + \frac{\partial \lambda}{\partial \eta} \right) \lambda dA - \iint_v \bar{Q}_{16} \left(\eta - \frac{\partial \lambda}{\partial \zeta} \right) \lambda dA = 0
\end{aligned} \tag{8.65}$$

Due to the assumed symmetry of the box-beam spar cross-section and ply layups (i.e. symmetric or anti-symmetric layups), the following relations also hold:

$$\begin{aligned}
K_{16} &= EAe_A \approx \iint_{h,v} \bar{Q}_{11} \eta dA = 0 \\
K_{34} &= GA_z e_A \approx \iint_v \bar{Q}_{66} \left(\eta - \frac{\partial \lambda}{\partial \zeta} \right) dA = 0
\end{aligned} \tag{8.66}$$

8.1.3.2 Blade Kinetic Energy, δT_b

The kinetic energy of the b th blade, δT_b , depends on the blade velocity. This velocity is generally due to: (1) blade motion relative to the hub, as well as (2) the motion of the hub itself. This relationship is expressed mathematically as

$$\vec{V} = \vec{V}_b + \vec{V}_f \tag{8.67}$$

where \vec{V}_b is the velocity of the blade relative to the hub and \vec{V}_f is the velocity (at the blade) induced by the motion of the fuselage. In the present analysis, the hub is assumed to be rigidly attached to the fuselage. Formulation of the blade kinetic energy for composite blades is identical to that for isotropic blades except for the shear deformations.

Blade Motion Induced Velocity, \vec{V}_b

A point $P(x,0,0)$ on the undeformed elastic axis moves to $P'(x+u,v,w)$ after deformation, and then the blade section undergoes a rotation θ_1 about the deformed elastic axis (see Figure 2.2b). The position vector, \vec{r} , of an arbitrary point on the blade

after deformation can be written as (x_1, y_1, z_1) in the undeformed blade coordinate system

$$\vec{r} = x_1 \hat{i} + y_1 \hat{j} + z_1 \hat{k} \quad (8.68)$$

where

$$\begin{aligned} x_1 &= x + u - \lambda_T \phi' - v'_b (y_1 - v) - w'_b (z_1 - w) \\ y_1 &= v_b + v_s + (y_1 - v) \\ z_1 &= w_b + w_s + (z_1 - w) \end{aligned} \quad (8.69)$$

The terms $(y_1 - v)$ and $(z_1 - w)$ are defined as

$$\begin{aligned} (y_1 - v) &= \eta \cos(\theta_0 + \hat{\phi}) - \zeta \sin(\theta_0 + \hat{\phi}) = \eta \cos \theta_1 - \zeta \sin \theta_1 \\ (z_1 - w) &= \eta \sin(\theta_0 + \hat{\phi}) + \zeta \cos(\theta_0 + \hat{\phi}) = \eta \sin \theta_1 + \zeta \cos \theta_1 \end{aligned} \quad (8.70)$$

Following the same procedure described in detail in Chapter 2, the blade kinetic energy variational is derived from the above expressions for the deflected blade position.

Variation in Kinetic Energy Without Fuselage (Hub) Motion

The kinetic energy of the *bth* blade is given by

$$T_b = \frac{1}{2} \int_0^R \iint_A \rho_s \vec{V} \cdot \vec{V} d\eta d\zeta dx \quad (8.71)$$

where \vec{V} is the total blade velocity and ρ_s is the mass density of the blade.

The variation of kinetic energy is given by

$$\delta T_b = \int_0^R \iint_A \rho_s \vec{V} \cdot \delta \vec{V} d\eta d\zeta dx \quad (8.72)$$

Without the contribution of fuselage motion induced velocity components, the total blade velocity, \vec{V} , equals only the velocity of the blade relative to the hub, \vec{V}_b . For this type of analysis, the variation in kinetic energy reduces to a significantly simpler form.

For the *bth* blade, the resulting kinetic energy expression is given by

$$\frac{\delta T}{m_0 \Omega^2 R^3} = \int_0^1 m (T_u \delta u_e + T_{v_b} \delta v_b + T_{w_b} \delta w_b + T_{v'_b} \delta v'_b + T_{w'_b} \delta w'_b + T_\phi \delta \phi + T_F + T_{v_s} \delta v_s + T_{w_s} \delta w_s) dx \quad (8.73)$$

where

$$T_u = x + u_e + 2(\dot{v}_b + \dot{v}_s) - \ddot{u}_e$$

$$\begin{aligned} T_{v_b} &= e_g (\cos \theta_0 + \ddot{\theta}_0 \sin \theta_0) + v_b + v_s - \hat{\phi} e_g \sin \theta_0 \\ &+ 2(\dot{w}_b + \dot{w}_s) \beta_p + 2\dot{v}' e_g \cos \theta_0 + 2\dot{w}' e_g \sin \theta_0 \\ &- \ddot{v}_b - \ddot{v}_s + \hat{\phi} e_g \sin \theta_0 - 2\dot{u}_e + 2 \int_0^x (v'_b \dot{v}'_b + w'_b \dot{w}'_b) d\xi \end{aligned}$$

$$\begin{aligned} T_{v_s} &= e_g (\cos \theta_0 + \ddot{\theta}_0 \sin \theta_0) + v_b + v_s - \hat{\phi} e_g \sin \theta_0 \\ &+ 2(\dot{w}_b + \dot{w}_s) \beta_p - \ddot{v}_b - \ddot{v}_s + \hat{\phi} e_g \sin \theta_0 - 2\dot{u}_e \end{aligned}$$

$$\begin{aligned} T_{v'_b} &= -e_g (x \cos \theta_0 - \hat{\phi} x \sin \theta_0 + 2\dot{v}_b \cos \theta_0) - k_{m2}^2 \ddot{v}'_b + k_{m1}^2 v'_b \\ T_{w_b} &= -x \beta_p - \ddot{\theta}_0 e_g \cos \theta_0 - 2(\dot{v}_b + \dot{v}_s) \beta_p \\ &- \ddot{w}_b - \ddot{w}_s - \hat{\phi} e_g \cos \theta_0 \end{aligned}$$

$$T_{w_s} = T_{w_b}$$

$$T_{w'_b} = -e_g (x \sin \theta_0 + \hat{\phi} x \cos \theta_0 + 2\dot{v}_b \sin \theta_0) - k_{m1}^2 \ddot{w}'_b + k_{m2}^2 w'_b$$

$$\begin{aligned} T_\phi &= -k_m^2 \hat{\phi} - (k_{m2}^2 - k_{m1}^2) \cos \theta_0 \sin \theta_0 - x \beta_p e_g \cos \theta_0 \\ &- (v_b + v_s) e_g \sin \theta_0 + v'_b x e_g \sin \theta_0 - w'_b x e_g \cos \theta_0 \\ &+ (\ddot{v}_b + \ddot{v}_s) e_g \sin \theta_0 - \hat{\phi} (k_{m2}^2 - k_{m1}^2) \cos 2\theta_0 \\ &- (\ddot{w}_b + \ddot{w}_s) e_g \cos \theta_0 - k_m^2 \ddot{\theta}_0 \end{aligned}$$

$$T_F = -(x + 2\dot{v}_b) \int_0^x (v'_b \delta v'_b + w'_b \delta w'_b) + (v'_s \delta v'_s + w'_s \delta w'_s)$$

$$+(v'_b \delta v'_s + w'_b \delta w'_s) + (v'_s \delta v'_b + w'_s \delta w'_b) d\xi$$

and the blade sectional integrals are defined as

$$\begin{aligned} m &= \iint_A \rho_s d\eta d\xi & mk_{m1}^2 &= \iint_A \rho_s \zeta^2 d\eta d\xi \\ me_g &= \iint_A \rho_s \eta d\eta d\xi & mk_{m2}^2 &= \iint_A \rho_s \eta^2 d\eta d\xi \\ && mk_m^2 &= mk_{m1}^2 + mk_{m2}^2 \end{aligned} \quad (8.74)$$

The blade mass per unit length, m , is nondimensionalized with respect to reference mass per unit length m_0 . The e_g is the blade center of gravity offset from the elastic axis (positive forward). The mk_{m1}^2 and mk_{m2}^2 are the flapwise and chordwise mass moments of inertia per unit blade length, respectively. The mk_m^2 is the torsional moment of inertia per unit length. Note that these are moments of inertia about the *elastic axis*. Since it is assumed that there is no offset in the thickness direction of the airfoil, additional blade sectional integrals related to the blade center of gravity offset can be defined as,

$$\begin{aligned} \iint_A \rho_s (y_1 - v) d\eta d\xi &= me_g \cos(\theta_0 + \hat{\phi}) \\ \iint_A \rho_s (z_1 - w) d\eta d\xi &= me_g \sin(\theta_0 + \hat{\phi}) \end{aligned} \quad (8.75a)$$

and the following relationships hold:

$$\begin{aligned} \iint_A \rho_s \zeta d\eta d\xi &= 0 \\ \iint_A \rho_s \eta \zeta d\eta d\xi &= 0 \end{aligned} \quad (8.75b)$$

As indicated by the foreshortening term, T_F (see Eqn. 8.73), the variation of kinetic energy, δT_b , results in the following *double integral* expression

$$-\int_0^1 mT_F dx = \int_0^1 m(x + 2\dot{v}) \left[\int_0^x (v' \delta v' + w' \delta w') d\xi \right] dx \quad (8.76a)$$

Integrating the above expression by parts yields the more convenient form,

$$\begin{aligned}
-\int_0^1 mT_F dx &= \int_0^1 (v' \delta v' + w' \delta w') \left[\int_x^1 m(x+2\dot{v}) d\xi \right] dx \\
&= \int_0^1 F_A (v' \delta v' + w' \delta w') dx + \int_0^1 (v' \delta v' + w' \delta w') \left[\int_x^1 2m\dot{v} d\xi \right] dx
\end{aligned} \tag{8.76b}$$

with the axial centrifugal force, F_A , defined as,

$$F_A(x) = \int_x^1 mx d\xi$$

The above expression reflects the "centrifugal stiffening" effect on the flap and lag equations, as well as the non-linear Coriolis damping effect. Anti-symmetric counterparts to the Coriolis damping terms are visible in the expression for T_v in Eqn. (8.73).

Variation in Kinetic Energy Including Fuselage Motion

The velocity and virtual velocity expressions including the fuselage motion are used to formulate the variation in kinetic energy for the b th blade as

$$\begin{aligned}
\delta T_b &= \int_0^R (T_u \delta u + T_v \delta v + T_w \delta w + T_{\dot{\phi}} \delta \dot{\phi} + T_{\ddot{\phi}} \delta \ddot{\phi} + T_{\dot{\psi}} \delta \dot{\psi} + T_{\ddot{\psi}} \delta \ddot{\psi} + T_F \\
&\quad + T_{x_F} \delta x_F + T_{y_F} \delta y_F + T_{z_F} \delta z_F + T_{\alpha_s} \delta \alpha_s + T_{\phi_s} \delta \phi_s) dx
\end{aligned} \tag{8.77}$$

where

$$T_u = m(x + 2\dot{v} - \ddot{u} - \ddot{x}_F \cos \psi - \ddot{y}_F \sin \psi + h\ddot{\alpha}_s \cos \psi - h\ddot{\phi}_s \sin \psi) \tag{8.78a}$$

$$\begin{aligned}
T_v &= m((v + e_g \cos \theta_0) + 2(\beta_p \dot{w} - \dot{u}) \\
&\quad + 2e_g(\dot{v} \cos \theta_0 + \dot{w} \sin \theta_0) - \ddot{v} + e_g(\ddot{\phi} + \ddot{\theta}_0) \sin \theta_0 \\
&\quad + \ddot{x}_F \sin \psi - \ddot{y}_F \cos \psi - h\ddot{\alpha}_s \sin \psi - h\ddot{\phi}_s \cos \psi)
\end{aligned}$$

$$\begin{aligned}
T_w &= m(-(\beta_p(x + 2\dot{v}) + \ddot{w} + e_g(\ddot{\phi} + \ddot{\theta}_0) \cos \theta_0 \\
&\quad - \ddot{z}_F - x\ddot{\alpha}_s \cos \psi + x\ddot{\phi}_s \sin \psi + 2x\dot{\alpha}_s \sin \psi + 2x\dot{\phi}_s \cos \psi \\
&\quad - x_{CG}\ddot{\alpha}_s + y_{CG}\ddot{\phi}_s)
\end{aligned}$$

$$T_{\dot{\phi}} = m((k_m^2 \ddot{\phi} + (k_{m_2}^2 - k_{m_1}^2) \cos \theta_0 \sin \theta_0)$$

$$\begin{aligned}
& + \hat{\phi}((k_{m_2}^2 - k_{m_1}^2)\cos\theta_0\sin\theta_0 + k_m^2\ddot{\theta}_0 \\
& + e_g x(w'\cos\theta_0 - v'\sin\theta_0) + e_g v\sin\theta_0 \\
& + e_g \beta_p x\cos\theta_0 - e_g (\ddot{v}\sin\theta_0 - \ddot{w}\cos\theta_0) \\
& - e_g (\ddot{x}_F \sin\psi\sin\theta_0 - \ddot{y}_F \cos\psi\sin\theta_0 + \ddot{z}_F \cos\theta_0 \\
& + (x\cos\psi\cos\theta_0 - h\sin\theta_0\sin\psi)\ddot{\alpha}_s \\
& + (-x\sin\psi\cos\theta_0 - h\sin\theta_0\cos\psi)\ddot{\phi}_s) \\
& - e_g \ddot{\alpha}_s x_{CG}\cos\theta_0 + e_g \ddot{\phi}_s y_{CG}\cos\theta_0)
\end{aligned}$$

$$\begin{aligned}
T_{v'} = & -me_g x \hat{\phi} \sin\theta_0 + me_g \cos\theta_0 (x + 2\dot{v} + \ddot{x}_F \cos\psi \\
& + \ddot{y}_F \sin\psi + \ddot{z}_F \beta_p - h\ddot{\alpha}_s \cos\psi + h\ddot{\phi}_s \sin\psi)
\end{aligned}$$

$$\begin{aligned}
T_{w'} = & me_g x \hat{\phi} \cos\theta_0 + me_g \sin\theta_0 (x + 2\dot{v} + \ddot{x}_F \cos\psi + \ddot{y}_F \sin\psi \\
& + \ddot{z}_F \beta_p - h\ddot{\alpha}_s \cos\psi + h\ddot{\phi}_s \sin\psi)
\end{aligned}$$

$$T_{x_F} = m(\ddot{v}\sin\psi + 2\dot{v}\cos\psi - v\sin\psi - \ddot{x}_F + h\ddot{\alpha}_s)$$

$$T_{y_F} = m(-\ddot{v}\cos\psi + 2\dot{v}\sin\psi + v\cos\psi - \ddot{y}_F - h\ddot{\phi}_s)$$

$$\begin{aligned}
T_{z_F} = & m(-\ddot{w} - \ddot{z}_F - \ddot{\alpha}_s x \cos\psi + \ddot{\phi}_s x \sin\psi - x_{CG} \ddot{\alpha}_s + y_{CG} \ddot{\phi}_s \\
& + 2\dot{\alpha}_s x \sin\psi + 2\dot{\phi}_s x \cos\psi + \alpha_s x \cos\psi - \phi_s x \sin\psi)
\end{aligned}$$

$$\begin{aligned}
T_{\alpha_s} = & m(-h^2 \ddot{\alpha}_s - x_{CG}^2 \ddot{\alpha}_s + h\ddot{x}_F + \ddot{\phi}_s x_{CG} y_{CG} \\
& - x_{CG} \ddot{w} - x_{CG} \ddot{z}_F - h x \cos\psi - \beta_p x^2 \cos\psi \\
& + h u \cos\psi - 2\dot{\alpha}_s x x_{CG} \cos\psi + 2\dot{\phi}_s x x_{CG} \cos\psi \\
& - 2h\dot{v} \cos\psi + \phi_s x y_{CG} \cos\psi + \ddot{\phi}_s x y_{CG} \cos\psi - x w \cos\psi \\
& - x \ddot{w} \cos\psi - x \ddot{z}_F \cos\psi - \dot{\alpha}_s x^2 \cos^2\psi + 2\dot{\phi}_s x^2 \cos^2\psi \\
& - 2h\dot{u} \sin\psi + 2\dot{\alpha}_s x x_{CG} \sin\psi - \phi_s x x_{CG} \sin\psi \\
& + \ddot{\phi}_s x x_{CG} \sin\psi + h v \sin\psi
\end{aligned}$$

$$-h\ddot{v}\sin\psi + 2\dot{\alpha}_s x^2 \cos\psi\sin\psi + \ddot{\phi}_s x^2 \cos\psi\sin\psi)$$

$$\begin{aligned} T_{\phi_s} = & m(-h^2 \ddot{\phi}_s + \ddot{\alpha}_s x_{CG} y_{CG} - \ddot{\phi}_s y_{CG}^2 - h\ddot{y}_F + y_{CG}\ddot{w} \\ & + y_{CG}\ddot{z}_F - 2h\dot{u}\cos\psi + h\cos\psi - h\dot{v}\cos\psi - x^2 \ddot{\phi}_s \sin^2\psi \\ & + \ddot{\alpha}_s xy_{CG}\cos\psi - 2\dot{\phi}_s xy_{CG}\cos\psi + h\dot{x}\sin\psi \\ & + \beta_p x^2 \sin\psi - h\dot{u}\sin\psi + \ddot{\alpha}_s xx_{CG}\sin\psi + 2h\dot{v}\sin\psi \\ & - 2\dot{\alpha}_s xy_{CG}\sin\psi - 2\ddot{\phi}_s xy_{CG}\sin\psi + xw\sin\psi \\ & + x\ddot{w}\sin\psi + x\ddot{z}_F\sin\psi + \ddot{\alpha}_s x^2 \cos\psi\sin\psi \\ & - 2\dot{\phi}_s x^2 \cos\psi\sin\psi - 2\dot{\alpha}_s x^2 \sin^2\psi) \end{aligned}$$

where the notation

$$\begin{aligned} v &= v_b + v_s & w &= w_b + w_s \\ \dot{v} &= \dot{v}_b + \dot{v}_s & \dot{w} &= \dot{w}_b + \dot{w}_s \\ \ddot{v} &= \ddot{v}_b + \ddot{v}_s & \ddot{w} &= \ddot{w}_b + \ddot{w}_s \\ v' &= v'_b & w' &= w'_b \end{aligned} \quad (8.78b)$$

is used for clarity.

8.1.3.3 Blade Virtual Work, δW_b

External aerodynamic forces on the rotor contribute to the virtual work of the system. For each degree of freedom there is a corresponding external force (or moment) due to aerodynamic loading. The general expression for the virtual work of the *bth* blade, δW_b , is given by

$$\delta W_b = \int_0^R (L_u^A \delta u + L_v^A (\delta v_b + \delta v_s) + L_w^A (\delta w_b + \delta w_s) + M_\phi^A \delta \phi) dx \quad (8.79)$$

where L_u^A , L_v^A , and L_w^A are the distributed airloads in the x , y , z directions respectively, and M_ϕ^A is the aerodynamic pitching moment about the undeformed elastic axis. Note

that the variational flap and lag deflections now consist of both bending and shearing

contributions. Many of the aerodynamic terms are motion dependent and thereby contribute to the element stiffness, damping, and mass matrices. Numerous additional nonlinear forces are also introduced in the virtual work expression. The method in which the aerodynamic forces and moments are computed is discussed in detail in Chapter 3.

8.1.4 Blade Equations of Motion

For the *bth* blade, the virtual energy expression in Eqn.(8.48) is written in the discretized form such that

$$\delta\Pi_b = \int_{\psi_i}^{\psi_f} \left[\sum_{i=1}^N (\delta U_i - \delta T_i - \delta W_i) \right]_b d\psi = 0 \quad (8.80)$$

Using the notation,

$$\Delta_i = \delta U_i - \delta T_i - \delta W_i \quad (8.81)$$

the virtual energy expression can also be written as

$$\delta II_b = \int_{\psi_i}^{\psi_f} \left[\sum_{i=1}^N \Delta_i \right]_b d\psi = 0 \quad (8.82)$$

where the subscript *i* denotes the *i*th beam element and the *N* is the total number of spatial finite elements in the blade. Applying the finite element method in space for this virtual energy expression yields the discretized equations of motion for the *bth* blade.

8.1.4.1 Finite Element Discretization in Space

The composite blade is discretized into a number of shear flexible beam finite elements (see Figure 8.7). Each beam element consists of *nineteen degrees of freedom*. These degrees of freedom are distributed over five element nodes (2 boundary nodes and 3 interior nodes). There are eight degrees of freedom at each element boundary node. These six degrees of freedom correspond to u , v_b , v'_b , w_b , w'_b , $\hat{\phi}$, v_s , and w_s . Recall

the subscript b denotes bending deflections and the subscript s denote shearing deflections. There are two internal nodes for axial (elastic) deflection u (the subscript "e" on the axial elastic deflection is dropped for notational convenience), and one internal node for elastic twist $\hat{\phi}$. Between elements there is continuity of displacement and slope for flap and lag bending deflections, and continuity of displacement for transverse shearing, elastic twist and axial deflections. This element insures physically consistent linear variations of bending moments and torsional moment, and quadratic variation of axial force within each element. Using the interpolating polynomials, the distribution of deflections over a beam element is expressed in terms of the elemental nodal displacements \mathbf{q}_i . For the i th beam element, the blade deflections, \mathbf{u}_i , are discretized as follows:

$$\mathbf{u}(s) = \mathbf{H}_s(s) \mathbf{q}_i \quad (8.83a)$$

or

$$\mathbf{u}(s) = \begin{bmatrix} u(s) \\ v_b(s) \\ w_b(s) \\ \hat{\phi}(s) \\ v_s(s) \\ w_s(s) \end{bmatrix} = \begin{bmatrix} \mathbf{H}_u & 0 & 0 & 0 & 0 & 0 \\ 0 & \mathbf{H}_{v_b} & 0 & 0 & 0 & 0 \\ 0 & 0 & \mathbf{H}_{w_b} & 0 & 0 & 0 \\ 0 & 0 & 0 & \mathbf{H}_{\hat{\phi}} & 0 & 0 \\ 0 & 0 & 0 & 0 & \mathbf{H}_{v_s} & 0 \\ 0 & 0 & 0 & 0 & 0 & \mathbf{H}_{w_s} \end{bmatrix} \mathbf{q}_i \quad (8.83b)$$

where the elemental nodal displacement vector is defined as

$$\mathbf{q}_i^T = [u_1, u_2, u_3, u_4, v_{b1}, v'_{b1}, v_{b2}, v'_{b2}, w_{b1}, w'_{b1}, w_{b2}, w'_{b2}, \hat{\phi}_1, \hat{\phi}_2, \hat{\phi}_3, v_{s1}, v_{s2}, w_{s1}, w_{s2}]$$

Note that each shear flexible element has nineteen degrees of freedom. The interpolating polynomials for the shape functions in Eqn.(8.83) are given as

$$\mathbf{H}_u^T = \begin{Bmatrix} H_{u1} \\ H_{u2} \\ H_{u3} \\ H_{u4} \end{Bmatrix} = \begin{Bmatrix} -4.5s^3 + 9s^2 - 5.5s + 1 \\ 13.5s^3 - 22.5s^2 + 9s \\ -13.5s^3 + 18s^2 - 4.5s \\ 4.5s^3 - 4.5s^2 + s \end{Bmatrix} \quad (8.84)$$

$$\mathbf{H}_{v_b}^T = \mathbf{H}_{w_b}^T = \begin{Bmatrix} H_{b1} \\ H_{b2} \\ H_{b3} \\ H_{b4} \end{Bmatrix} = \begin{Bmatrix} 2s^3 - 3s^2 + 1 \\ l_i(s^3 - 2s^2 + s) \\ -2s^3 + 3s^2 \\ l_i(s^3 - s^2) \end{Bmatrix} \quad (8.85)$$

$$\mathbf{H}_{\dot{\phi}}^T = \begin{Bmatrix} H_{\dot{\phi}1} \\ H_{\dot{\phi}2} \\ H_{\dot{\phi}3} \end{Bmatrix} = \begin{Bmatrix} 2s^2 - 3s + 1 \\ -4s^2 + 4s \\ 2s^2 - s \end{Bmatrix} \quad (8.86)$$

$$\mathbf{H}_{v_r}^T = \mathbf{H}_{w_s}^T = \begin{Bmatrix} H_{s1} \\ H_{s2} \end{Bmatrix} = \begin{Bmatrix} 1-s \\ s \end{Bmatrix} \quad (8.87)$$

where $s = x_i / \ell_i$ and ℓ_i is the length of the i th beam element. For lag and flap bending deflections, the interpolating polynomial is chosen from the family of Hermite polynomials, which allow continuity of displacement and slope. For elastic twist, elastic axial deflection, and transverse shear deflections, Lagrangian polynomials are used since these yield continuity of displacement.

On the Selection of the Shear Flexible Element

One of the distinguishing characteristics of the present investigation is the use of the previously described shear flexible finite element. Although shear flexible elements are commonly used in the *structural analysis* of composite beams, they are rarely (if ever) used in the *aeroelastic analysis* of rotor blades. Due to the long, slender physical geometry of helicopter blades, direct shear deformations are negligible and Bernoulli-

Euler elements have been sufficient for rotor aeroelasticity problems (e.g., Refs. 8.20, 8.21). The existence of bending-shear couplings in antisymmetric layup composite blades and extension-shear couplings in symmetric layup composite blades has directed interest towards shear flexible beam elements for aeroelastic analyses.

Shear flexible elements similar to the one used in the present study (previously described) have been used in several earlier investigations. Tessler and Dong [8.22] conducted a study comparing a hierarchy of shear flexible beam elements. Elements with different kinematic variables and interpolation polynomials were compared for nonrotating isotropic beam natural frequencies (hinged boundary conditions). The shear element with the same kinematic degrees of freedom and interpolating polynomials as the element selected for the present analysis demonstrated adequate performance in these test examples. The comparative study by Tessler and Dong also cited other earlier uses of the "present" beam element in the analysis of shear flexible beam structures [8.23, 8.24]. More recently, a similar shear flexible beam element was used by Nixon to investigate composite beams with extension-twist coupling [8.25]. This formulation also used separate kinematic variables for the bending deflection, w_b , and shearing deflection, w_s . Nixon's work showed successful correlations with experimental data for composite beams exhibiting dramatic bending-shearing couplings effects.

The use of separate kinematic variables for bending and shearing deflections is also appealing from a physical perspective. One of the objectives of the present research is to determine the quantitative importance of transverse shear effects for rotor dynamics analysis of coupled composite blades. The explicit "separation" of discretized bending and shearing deflections, w_b and w_s , helps clarify the role of transverse shear in the structural response.

The order of the shear deflection interpolating polynomials, or the number of shear-related degrees of freedom used in the beam element, is also selected based on both numerical and physical criteria. A linearly varying distribution of shear deflection within each element is assumed. The bending deflections are cubic within each element, with inter-element continuity of bending deflection and bending slope (rotation). The physical rationale for the relative orders of these polynomials can be understood from the governing differential equation for total flapwise deflection of an isotropic beam

$$w'' = \frac{Q'_z}{GA_z} + \frac{M_y}{EI_y} \quad (8.88)$$

When subjected to an applied tip force, P , in the flap direction, application of cantilevered boundary conditions, $w = 0$ and $w'_b = 0$, results in

$$w = w_s + w_b \quad (8.89a)$$

where

$$w(x) \propto \frac{a_s Px}{GA_z} + \frac{a_b Px^3}{EI_y} \quad (8.89b)$$

Note that the shearing contribution to the total deflection is linear and the bending contribution is cubic. The characteristic of shearing deflections being two polynomial orders lower than bending deflections is independent of the type of loading and the applied boundary conditions. The same fundamental behavior is also true for anti-symmetric layup beams with bending-shear elastic couplings. From a numerical point of view, the nineteen degree of freedom element used in the present analysis is free from detrimental locking phenomenon since *cubic* polynomials are used for bending interpolation polynomials. If *linear* bending and *linear* shearing polynomials had been used, the element would be susceptible to classical shear locking behavior for thin beams [8.26, 8.27].

8.1.4.2 Application of Blade Kinematic Boundary Conditions

Figure 8.8 shows the numbering scheme used for the shear flexible blade finite element global degrees of freedom. Element local degrees of freedom are described in Figure 8.7. Figure 8.8 also shows the application of boundary conditions for a hingeless composite rotor blade model.

For a hingeless rotor blade, the blade is assumed to be cantilevered at the blade root. This assumption implies that the response quantities u , v_b , v_b' , w_b , w_b' , v_s , w_s , and ϕ to be zero at the root. For an articulated rotor, the constraint on v_b' is relaxed at the lag hinge, and the constraint on w_b' is relaxed at the flap hinge. Geometric boundary conditions are enforced during the assembly of the element matrices (see Chapter 2).

8.1.5 Element Structural Matrices and Load Vector

8.1.5.1 Blade Matrices and Load Vector

The element mass, stiffness, and damping matrices can be partitioned to indicate contributions from axial deflection, flap bending, lag bending, and elastic torsion. Composite elastic coupling effects appear in the stiffness matrix and nonlinear load vector, while shear effects appear in mass, damping, and stiffness matrices. The *linear* mass, stiffness, and damping matrices can then be written as

$$[M_b]_i = \begin{bmatrix} [M_{uu}] & [M_{uv}] & [M_{uw}] & [M_{u\phi}] & [M_{uv_s}] & [M_{uw_s}] \\ [M_{vu}] & [M_{vv}] & [M_{vw}] & [M_{v\phi}] & [M_{vv_s}] & [M_{vw_s}] \\ [M_{wu}] & [M_{wv}] & [M_{ww}] & [M_{w\phi}] & [M_{wv_s}] & [M_{ww_s}] \\ [M_{\phi u}] & [M_{\phi v}] & [M_{\phi w}] & [M_{\phi\phi}] & [M_{\phi v_s}] & [M_{\phi w_s}] \\ [M_{v_s u}] & [M_{v_s v}] & [M_{v_s w}] & [M_{v_s \phi}] & [M_{v_s v_s}] & [M_{v_s w_s}] \\ [M_{w_s u}] & [M_{w_s v}] & [M_{w_s w}] & [M_{w_s \phi}] & [M_{w_s v_s}] & [M_{w_s w_s}] \end{bmatrix} \quad (8.90)$$

$$[C_b]_i = \begin{bmatrix} [C_{uu}] & [C_{uv}] & [C_{uw}] & [C_{u\phi}] & [C_{uv_s}] & [C_{uw_s}] \\ [C_{vu}] & [C_{vv}] & [C_{vw}] & [C_{v\phi}] & [C_{vv_s}] & [C_{vw_s}] \\ [C_{wu}] & [C_{wv}] & [C_{ww}] & [C_{w\phi}] & [C_{ww_s}] & [C_{ww_s}] \\ [C_{\phi u}] & [C_{\phi v}] & [C_{\phi w}] & [C_{\phi \phi}] & [C_{\phi v_s}] & [C_{\phi w_s}] \\ [C_{v_s u}] & [C_{v_s v}] & [C_{v_s w}] & [C_{v_s \phi}] & [C_{v_s v_s}] & [C_{v_s w_s}] \\ [C_{w_s u}] & [C_{w_s v}] & [C_{w_s w}] & [C_{w_s \phi}] & [C_{w_s v_s}] & [C_{w_s w_s}] \end{bmatrix} \quad (8.91)$$

$$[K_b]_i = \begin{bmatrix} [K_{uu}] & [K_{uv}] & [K_{uw}] & [K_{u\phi}] & [K_{uv_s}] & [K_{uw_s}] \\ [K_{vu}] & [K_{vv}] & [K_{vw}] & [K_{v\phi}] & [K_{vv_s}] & [K_{vw_s}] \\ [K_{wu}] & [K_{wv}] & [K_{ww}] & [K_{w\phi}] & [K_{ww_s}] & [K_{ww_s}] \\ [K_{\phi u}] & [K_{\phi v}] & [K_{\phi w}] & [K_{\phi \phi}] & [K_{\phi v_s}] & [K_{\phi w_s}] \\ [K_{v_s u}] & [K_{v_s v}] & [K_{v_s w}] & [K_{v_s \phi}] & [K_{v_s v_s}] & [K_{v_s w_s}] \\ [K_{w_s u}] & [K_{w_s v}] & [K_{w_s w}] & [K_{w_s \phi}] & [K_{w_s v_s}] & [K_{w_s w_s}] \end{bmatrix} \quad (8.92)$$

The element structural stiffness and mass matrices are symmetric (e.g. $[K_{uv}] = [K_{vu}]$, etc.). The linear mass matrix terms are defined as

$$\begin{aligned} [M_{uu}] &= \int_0^1 m H_u^T H_u \, ds & (8.93) \\ [M_{vv}] &= \int_0^1 m H^T H \, ds + \int_0^1 m k_{m2}^2 H'^T H' \, ds \\ [M_{ww}] &= \int_0^1 m H^T H \, ds + \int_0^1 m k_{m1}^2 H'^T H' \, ds \\ [M_{\phi\phi}] &= \int_0^1 m k_m^2 H_{\dot{\phi}}^T H_{\dot{\phi}} \, ds \\ [M_{v\phi}] &= - \int_0^1 m e_g \sin \theta_0 H^T H_{\dot{\phi}} \, ds \\ [M_{w\phi}] &= \int_0^1 m e_g \cos \theta_0 H^T H_{\dot{\phi}} \, ds \\ [M_{\phi v_s}] &= - \int_0^1 m e_g \sin \theta_0 H_{\dot{\phi}}^T H_s \, ds \\ [M_{\phi w_s}] &= \int_0^1 m e_g \cos \theta_0 H_{\dot{\phi}}^T H_s \, ds \\ [M_{v_s v_s}] &= \int_0^1 m H_s^T H_s \, ds \\ [M_{w_s w_s}] &= \int_0^1 m H_s^T H_s \, ds \\ [M_{ww_s}] &= \int_0^1 m H^T H_s \, ds \\ [M_{ww_s}] &= \int_0^1 m H^T H_s \, ds \end{aligned}$$

All other sub-matrices in Eqn. (8.90) are zero.

The linear damping matrix terms are defined as

$$\begin{aligned}
 [C_{uu}] &= -\int_0^1 2m\Omega \mathbf{H}'_u^T \mathbf{H} ds & (8.94) \\
 [C_{vv}] &= \int_0^1 2me_g\Omega \cos \theta_0 \mathbf{H}'^T \mathbf{H} ds - \int_0^1 2me_g\Omega \cos \theta_0 \mathbf{H}^T \mathbf{H}' ds \\
 [C_{vw}] &= -\int_0^1 2m\Omega \beta_p \mathbf{H}^T \mathbf{H} ds - \int_0^1 2me_g\Omega \sin \theta_0 \mathbf{H}^T \mathbf{H}' ds \\
 [C_{uv}] &= -\int_0^1 2m\Omega \mathbf{H}'_u^T \mathbf{H}_s ds \\
 [C_{vw_s}] &= -\int_0^1 2m\Omega \beta_p \mathbf{H}^T \mathbf{H}_s ds \\
 [C_{ww_s}] &= \int_0^1 2m\Omega \beta_p \mathbf{H}^T \mathbf{H}_s ds \\
 [C_{vu}] &= -[C_{uv}] \\
 [C_{wv}] &= -[C_{vw}] \\
 [C_{v,u}] &= -[C_{uv}] \\
 [C_{w,v}] &= -[C_{vw}] \\
 [C_{v,w}] &= -[C_{ww}]
 \end{aligned}$$

All other sub-matrices in Eqn. (8.91) are zero.

The linear stiffness matrix terms are defined as

$$\begin{aligned}
 [K_{uu}] &= \int_0^1 EA \mathbf{H}'_u^T \mathbf{H}'_u ds & (8.95) \\
 [K_{vv}] &= \int_0^1 F_A \mathbf{H}'^T \mathbf{H}' ds + \int_0^1 (EI_y \sin^2 \theta_0 + EI_z \cos^2 \theta_0) \mathbf{H}''^T \mathbf{H}'' ds - \int_0^1 m\Omega^2 \mathbf{H}^T \mathbf{H} ds \\
 [K_{ww}] &= \int_0^1 F_A \mathbf{H}'^T \mathbf{H}' ds + \int_0^1 (EI_z \sin^2 \theta_0 + EI_y \cos^2 \theta_0) \mathbf{H}''^T \mathbf{H}'' ds \\
 [K_{\phi\phi}] &= \int_0^1 m\Omega^2 (k_{m2}^2 - k_{m1}^2) \cos 2\theta_0 \mathbf{H}_{\hat{\phi}}^T \mathbf{H}_{\hat{\phi}} ds + \int_0^1 (GJ + EB_1 \theta_0'^2) \mathbf{H}'_{\hat{\phi}}^T \mathbf{H}'_{\hat{\phi}} ds \\
 &\quad + \int_0^1 EC_1 \mathbf{H}''_{\hat{\phi}}^T \mathbf{H}''_{\hat{\phi}} ds \\
 [K_{uv}] &= -\int_0^1 EAe_A \cos \theta_0 \mathbf{H}'_u^T \mathbf{H}'' ds \\
 [K_{uw}] &= -\int_0^1 EAe_A \sin \theta_0 \mathbf{H}'_u^T \mathbf{H}'' ds \\
 [K_{u\phi}] &= \int_0^1 EAk_A^2 \theta_0' \mathbf{H}'_u^T \mathbf{H}'_{\hat{\phi}} ds + \int_0^1 K_{14} \mathbf{H}'_u^T \mathbf{H}'_{\hat{\phi}} ds \\
 [K_{vw}] &= \int_0^1 (EI_z - EI_y) \sin \theta_0 \cos \theta_0 \mathbf{H}''^T \mathbf{H}'' ds
 \end{aligned}$$

$$\begin{aligned}
[K_{v\phi}] &= \int_0^1 m\Omega^2 e_g \sin \theta_0 \mathbf{H}^T \mathbf{H}'_{\dot{\phi}} ds - \int_0^1 xm\Omega^2 e_g \sin \theta_0 \mathbf{H}'^T \mathbf{H}'_{\dot{\phi}} ds \\
&\quad - \int_0^1 EB_2 \theta'_0 \cos \theta_0 \mathbf{H}''^T \mathbf{H}'_{\dot{\phi}} ds - \int_0^1 EC_2 \sin \theta_0 \mathbf{H}''^T \mathbf{H}''_{\dot{\phi}} ds \\
&\quad + \int_0^1 (K_{46} \cos \theta_0 - K_{45} \sin \theta_0) \mathbf{H}''^T \mathbf{H}'_{\dot{\phi}} ds \\
[K_{w\phi}] &= \int_0^1 xm\Omega^2 e_g \cos \theta_0 \mathbf{H}'^T \mathbf{H}'_{\dot{\phi}} ds - \int_0^1 EB_2 \theta'_0 \sin \theta_0 \mathbf{H}''^T \mathbf{H}'_{\dot{\phi}} ds \\
&\quad + \int_0^1 EC_2 \cos \theta_0 \mathbf{H}''^T \mathbf{H}''_{\dot{\phi}} ds \\
&\quad + \int_0^1 (K_{45} \cos \theta_0 + K_{46} \sin \theta_0) \mathbf{H}''^T \mathbf{H}'_{\dot{\phi}} ds \\
[K_{uv_s}] &= \int_0^1 (K_{12} \cos \theta_0 - K_{13} \sin \theta_0) \mathbf{H}'_u^T \mathbf{H}'_s ds \\
[K_{uw_s}] &= \int_0^1 (K_{13} \cos \theta_0 + K_{12} \sin \theta_0) \mathbf{H}'_u^T \mathbf{H}'_s ds \\
[K_{vv_s}] &= \int_0^1 (K_{25} + K_{36}) \sin \theta_0 \cos \theta_0 \mathbf{H}''^T \mathbf{H}'_s ds \\
&\quad - \int_0^1 m\Omega^2 \mathbf{H}^T \mathbf{H}_s ds + \int_0^1 F_A \mathbf{H}'^T \mathbf{H}'_s ds \\
[K_{ww_s}] &= \int_0^1 (K_{25} + K_{36}) \sin \theta_0 \cos \theta_0 \mathbf{H}''^T \mathbf{H}'_s ds + \int_0^1 F_A \mathbf{H}'^T \mathbf{H}'_s ds \\
[K_{vw_s}] &= \int_0^1 (K_{25} \sin^2 \theta_0 - K_{36} \cos^2 \theta_0) \mathbf{H}''^T \mathbf{H}'_s ds \\
[K_{wv_s}] &= \int_0^1 (K_{36} \sin^2 \theta_0 - K_{25} \cos^2 \theta_0) \mathbf{H}''^T \mathbf{H}'_s ds \\
[K_{v_z v_s}] &= \int_0^1 (GA_y \cos^2 \theta_0 + GA_z \sin^2 \theta_0) \mathbf{H}'_s^T \mathbf{H}'_s ds \\
&\quad - \int_0^1 m\Omega^2 \mathbf{H}^T \mathbf{H}_s ds + \int_0^1 F_A \mathbf{H}'_s^T \mathbf{H}'_s ds \\
[K_{v_z w_s}] &= \int_0^1 (GA_y - GA_z) \sin \theta_0 \cos \theta_0 \mathbf{H}'_s^T \mathbf{H}'_s ds \\
[K_{w_z w_s}] &= \int_0^1 (GA_z \cos^2 \theta_0 + GA_y \sin^2 \theta_0) \mathbf{H}'_s^T \mathbf{H}'_s ds + \int_0^1 F_A \mathbf{H}'_s^T \mathbf{H}'_s ds
\end{aligned}$$

All other sub-matrices in Eqn. (8.92) are zero.

The element force vector, \mathbf{F}_i , consists of contributions from the external virtual work, δW , as well as contributions from the variation in kinetic energy, δT . The force terms from the kinetic energy arise due to inertial forces on the blade (e.g. centrifugal force). This vector, like the element matrices, also contains linear and nonlinear terms. Recalling Eqn. (2.107), the elemental force vector can be written as

$$\mathbf{F}_i = (\mathbf{F}_0)_i + (\mathbf{F}_{NL})_i \quad (8.96)$$

The constant force vector terms are given below as

$$\{F_u\}_0 = \int_0^1 m\Omega^2 x \mathbf{H}_u^T ds \quad (8.97)$$

$$\{F_v\}_0 = \int_0^1 m(\Omega^2 e_g \cos \theta_0 + \ddot{\theta}_0 e_g \sin \theta_0) \mathbf{H}^T ds - \int_0^1 m\Omega^2 e_g \cos \theta_0 x \mathbf{H}'^T ds$$

$$\{F_w\}_0 = - \int_0^1 m\Omega^2 (\beta_{pc} x + \ddot{\theta}_0 e_g \sin \theta_0) \mathbf{H}^T ds - \int_0^1 m\Omega^2 e_g \sin \theta_0 x \mathbf{H}'^T ds$$

$$\{F_\phi\}_0 = - \int_0^1 m k_m^2 \ddot{\theta}_0 + m\Omega^2 (k_{m2}^2 - k_{m1}^2) \sin \theta_0 \cos \theta_0 \mathbf{H}_\phi^T ds$$

$$- \int_0^1 m\Omega^2 \beta_{pc} e_g \cos \theta_0 x \mathbf{H}_\phi^T ds$$

The nonlinear force vector terms are given below as

$$\begin{aligned} \{F_u\}_{NL} &= - \int_0^1 EA \left(e_A (v'' \hat{\phi} \sin \theta_0 - w'' \hat{\phi} \cos \theta_0) + k_A^2 \frac{\hat{\phi}'^2}{2} + k_A^2 \theta'_0 w' v'' \right) \mathbf{H}'^T ds \\ &\quad + \int_0^1 (K_{14} v'' w') \mathbf{H}_u^T ds \end{aligned} \quad (8.98)$$

$$\{F_v\}_{NL} = \int_0^1 \left((EI_z - EI_y) v'' \hat{\phi} \sin 2\theta_0 - (EI_z - EI_y) w'' \hat{\phi} \cos 2\theta_0 \right) \mathbf{H}''^T ds$$

$$- \int_0^1 EA e_A u'_e \hat{\phi}' \sin \theta_0 \mathbf{H}''^T ds - \int_0^1 (GJ \hat{\phi}' w' + EA k_A^2 \theta'_0 w' u'_e) \mathbf{H}''^T ds$$

$$+ \int_0^1 \left(2m \int_0^x (v' \dot{v}' + w' \dot{w}') d\xi \right) \mathbf{H}^T ds - \int_0^1 \left(2v' \int_x^1 m \dot{v} d\xi \right) \mathbf{H}'^T ds$$

$$+ \int_0^1 \left(K_{45} (w'' w' \cos \theta_0 - \hat{\phi} \hat{\phi}' \cos \theta_0 - 2v'' w' \sin \theta_0) \right) \mathbf{H}''^T ds$$

$$+ \int_0^1 \left(K_{46} (w'' w' \sin \theta_0 - \hat{\phi} \hat{\phi}' \sin \theta_0 + 2v'' w' \cos \theta_0) \right) \mathbf{H}''^T ds$$

$$+ \int_0^1 K_{14} (u'_e w') \mathbf{H}''^T ds$$

$$\{F_w\}_{NL} = - \int_0^1 \left((EI_z - EI_y) \cos 2\theta_0 v'' \hat{\phi} + (EI_z - EI_y) \sin 2\theta_0 w'' \hat{\phi} \right) \mathbf{H}''^T ds$$

$$+ \int_0^1 EA e_A u'_e \hat{\phi}' \cos \theta_0 \mathbf{H}''^T ds - \int_0^1 (GJ \hat{\phi}' v'' + EA k_A^2 \theta'_0 v'' u'_e) \mathbf{H}'^T ds$$

$$\begin{aligned}
& - \int_0^1 \left(2w' \int_x^1 m \dot{v} d\xi \right) \mathbf{H}'^T ds \\
& + \int_0^1 \left(K_{45}(v'' w' \cos \theta_0 - \hat{\phi} \hat{\phi}' \sin \theta_0) \right) \mathbf{H}''^T ds \\
& + \int_0^1 \left(K_{46}(v'' w' \sin \theta_0 + \hat{\phi} \hat{\phi}' \cos \theta_0) \right) \mathbf{H}''^T ds \\
& + \int_0^1 \left(K_{45}(v'' w'' \cos \theta_0 - v''^2 \sin \theta_0) \right) \mathbf{H}'^T ds \\
& + \int_0^1 \left(K_{46}(v'' w'' \sin \theta_0 + v''^2 \cos \theta_0) \right) \mathbf{H}'^T ds \\
& + \int_0^1 K_{14}(u'_e v'') \mathbf{H}'^T ds
\end{aligned}$$

$$\begin{aligned}
\{\mathbf{F}_\phi\}_{NL} = & - \int_0^1 \left((EI_z - EI_y) w''^2 \sin \theta_0 \cos \theta_0 + (EI_z - EI_y) v'' w'' \cos 2\theta_0 \right) \mathbf{H}_{\dot{\phi}}^T ds \\
& + \int_0^1 (EI_z - EI_y) v''^2 \sin \theta_0 \cos \theta_0 \mathbf{H}_{\dot{\phi}}^T ds - \int_0^1 \left(EAk_A^2 \hat{\phi}' u'_e + GJ w' v'' \right) \mathbf{H}_{\dot{\phi}}^T ds \\
& - \int_0^1 \left(K_{45}(\hat{\phi}' w'' \sin \theta_0 + \hat{\phi}' v'' \cos \theta_0) \right) \mathbf{H}_{\dot{\phi}}^T ds \\
& + \int_0^1 \left(K_{46}(\hat{\phi}' w'' \cos \theta_0 - \hat{\phi}' v'' \sin \theta_0) \right) \mathbf{H}_{\dot{\phi}}^T ds \\
& - \int_0^1 \left(K_{45}(\hat{\phi} w'' \sin \theta_0 + \hat{\phi} v'' \cos \theta_0) \right) \mathbf{H}_{\dot{\phi}}^T ds \\
& + \int_0^1 \left(K_{46}(\hat{\phi} w'' \cos \theta_0 - \hat{\phi} v'' \sin \theta_0) \right) \mathbf{H}_{\dot{\phi}}^T ds
\end{aligned}$$

In the above expressions, $v = v_b$ and $w = w_b$. The ordering scheme eliminates all nonlinear terms involving shear deformations. When evaluated at reference position, \mathbf{q}_0 , the nonlinear terms above are combined with the constant force terms, \mathbf{F}_0 (see Eqn. (2.109)). The partial derivative terms in the Taylor series approximation result in the displacement Jacobian matrix.

8.1.6 Summary

The preceding chapter has described the formulation of the structural modeling used for the aeroelastic and aeromechanical analysis of helicopters with elastically coupled composite blades. Combining Eqns. (2.161) and (2.168) yields the discretized form of the coupled (composite) rotor-fuselage equations

$$\begin{bmatrix} \mathbf{M}_b & \mathbf{M}_{bF} \\ \mathbf{M}_{Fb} & \mathbf{M}_{FF} \end{bmatrix} \begin{Bmatrix} \ddot{\mathbf{q}}_b \\ \ddot{\mathbf{x}}_F \end{Bmatrix} + \begin{bmatrix} \mathbf{C}_b & \mathbf{C}_{bF} \\ \mathbf{C}_{Fb} & \mathbf{C}_{FF} \end{bmatrix} \begin{Bmatrix} \dot{\mathbf{q}}_b \\ \dot{\mathbf{x}}_F \end{Bmatrix} + \begin{bmatrix} \mathbf{K}_b & \mathbf{K}_{bF} \\ \mathbf{K}_{Fb} & \mathbf{K}_{FF} \end{bmatrix} \begin{Bmatrix} \mathbf{q}_b \\ \mathbf{x}_F \end{Bmatrix} = \begin{Bmatrix} \mathbf{F}_b \\ \mathbf{F}_F \end{Bmatrix} \quad (8.99)$$

Elastic couplings introduced through the composite box-beam spar walls are reflected directly in the blade stiffness matrix, \mathbf{K}_b . Modifications related to the newly developed nineteen degree of freedom shear flexible element are reflected in all blade, blade-fuselage, and fuselage-blade matrices.

8.2 Aerodynamic Modeling

The following section describes the derivation of the resultant blade velocity components including blade transverse shear deflections. Details of the corresponding quasi-steady airloads expressions are presented in Chapter 2. The finite element discretization of the rotor-fuselage system virtual work is also covered in detail, with special attention given to modifications related to the shear flexible blade beam element.

8.2.1 Derivation of Resultant Air Velocity

The incident velocity at a specific blade station can be expressed a vector sum of three major components; the wind velocity, the blade velocity (due to motion of the blade relative to the shaft), and the velocity of the blade station due to the motion of the vehicle fuselage. The general expression for the resultant blade velocity, \vec{V} , at a radial station x , in the rotating undeformed reference frame is

$$\vec{V} = -\vec{V}_w + \vec{V}_b + \vec{V}_f \quad (8.100)$$

where \vec{V}_w is the wind velocity with contributions from the vehicle forward speed and rotor inflow, \vec{V}_b is the blade velocity due to blade rotation and elastic deflections, and \vec{V}_f is the blade station velocity due to fuselage motion.

Wind Velocity

The wind velocity is unchanged due to shear deformations of the blade. The expression for wind velocity is given in Chapter 3 - Aerodynamic Modeling.

Blade Velocity

The blade velocity in the rotating undeformed reference frame is given by

$$\vec{V}_b = \dot{\vec{r}} + \vec{\Omega} \times \vec{r} \quad (8.101)$$

where

$$\vec{r} = x_1 \hat{i} + y_1 \hat{j} + z_1 \hat{k} \quad (8.102a)$$

$$\dot{\vec{r}} = \dot{x}_1 \hat{i} + \dot{y}_1 \hat{j} + \dot{z}_1 \hat{k} + x_1 \dot{\hat{i}} + y_1 \dot{\hat{j}} + z_1 \dot{\hat{k}} \quad (8.102b)$$

$$\vec{\Omega} = \Omega \hat{K} \quad (8.102c)$$

and x_1 , y_1 , z_1 , and \dot{x}_1 , \dot{y}_1 , and \dot{z}_1 are defined in Chapter 2. The position vector from the hub center to a point (ξ, η, ζ) on the rotating deformed blade is \vec{r} . The velocity of the point with respect to the undeformed position is $\dot{\vec{r}}$. The blade angular rotation velocity vector can be transformed to the undeformed rotating frame using the transformation matrix \mathbf{T}_{UR} (defined in Chapter 2) and written as

$$\vec{\Omega} = \Omega \sin \beta_p \hat{i} + \Omega \cos \beta_p \hat{k} \quad (8.103)$$

Substituting Eqns. 3.11 and 3.12 into Eqn. (3.10) yields

$$\vec{V}_b = V_{b_x} \hat{i} + V_{b_y} \hat{j} + V_{b_z} \hat{k} \quad (8.104)$$

where

$$V_{b_x} = \dot{x}_1 - \Omega y_1 \cos \beta_p \quad (8.105a)$$

$$V_{b_y} = \dot{y}_1 + \Omega x_1 \cos \beta_p - \Omega z_1 \sin \beta_p \quad (8.105b)$$

$$V_{b_z} = \dot{z}_1 + \Omega y_1 \sin \beta_p \quad (8.105c)$$

Substitution of expressions for x_1 , y_1 , z_1 , and \dot{x}_1 , \dot{y}_1 , and \dot{z}_1 into the above results in the blade velocity expressions

$$\begin{aligned} V_{b_x} = & [\dot{u} - \lambda_T \dot{\phi}' - (\dot{v}'_b + w'_b \dot{\theta}_1)(\eta \cos \theta_1 - \zeta \sin \theta_1) \\ & - (\dot{w}'_b - v'_b \dot{\theta}_1)(\eta \sin \theta_1 - \zeta \cos \theta_1)] \\ & - \Omega(v_b + v_s + \eta \cos \theta_1 - \zeta \sin \theta_1) \cos \beta_p \end{aligned} \quad (8.106a)$$

$$\begin{aligned} V_{b_y} = & \dot{v}_b + \dot{v}_s - \dot{\theta}_1(\eta \sin \theta_1 + \zeta \cos \theta_1) \\ & + \Omega[x + u - \lambda_T \dot{\phi}' - v'_b(\eta \cos \theta_1 - \zeta \sin \theta_1) - w'_b(\eta \sin \theta_1 + \zeta \cos \theta_1)] \end{aligned}$$

$$-\Omega(w_b + w_s + \eta \sin \theta_1 + \zeta \cos \theta_1) \sin \beta_p \quad (8.106b)$$

$$\begin{aligned} V_{b_z} = & \dot{w}_b + \dot{w}_s + \dot{\theta}_1 (\eta \cos \theta_1 - \zeta \sin \theta_1) \\ & + \Omega(v_b + v_s + \eta \cos \theta_1 - \zeta \sin \theta_1) \sin \beta_p \end{aligned} \quad (8.106c)$$

where

$$\theta_1 = \theta_o + \hat{\phi}$$

The quasi-steady rotor blade aerodynamic loads are calculated using a blade section "strip" analysis based on the angle of attack at the section three-quarter chord location. At this chordwise location, ($\eta = \eta_r$, and $\zeta = 0$), and the velocity components simplify to

$$\begin{aligned} V_{b_x} = & \dot{u} - (\dot{v}'_b + w'_b \dot{\theta}_1) \eta_r \cos \theta_1 \\ & - (\dot{w}'_b - v'_b \dot{\theta}_1) \eta_r \sin \theta_1 - \Omega(v_b + v_s + \eta_r \cos \theta_1) \end{aligned} \quad (8.107a)$$

$$\begin{aligned} V_{b_y} = & \dot{v}_b + \dot{v}_s - \dot{\theta}_1 \eta_r \sin \theta_1 + \Omega[x + u - v'_b \eta_r \cos \theta_1 - w'_b \eta_r \sin \theta_1] \\ & - \Omega(w_b + \eta_r \sin \theta_1) \beta_p \end{aligned} \quad (8.107b)$$

$$V_{b_z} = \dot{w}_b + \dot{w}_s + \dot{\theta}_1 \eta_r \cos \theta_1 + \Omega \beta_p (v_b + \eta_r \cos \theta_1) \quad (8.107c)$$

Velocity of the Blade due to Fuselage Motion

For the coupled rotor-fuselage aeromechanical analysis, the velocity at the blade due to rigid body motion of the vehicle fuselage is required. The resulting velocity at the three-quarter chord on the blade station, \vec{V}_f , is given by

$$\vec{V}_f = \vec{V}_F + \vec{\omega}_f \times \vec{r}_F \quad (8.108)$$

where \vec{r}_F is the location of the three-quarter chord point on the blade with respect to the vehicle center of gravity, \vec{V}_F is the velocity of the fuselage center of gravity with respect to an inertial frame, and $\vec{\omega}_f$ is the angular velocity of the fuselage axis in the inertial frame. These components in the above velocity expression velocity are

$$\begin{aligned}\vec{r}_F = & (x_{CG}\hat{i}_F + y_{CG}\hat{j}_F + h\hat{k}_F) \\ & + ((x+u)\hat{i} + (v_b+v_s)\hat{j} + (w_b+w_s)\hat{k} + \eta_r\hat{j}_\eta)\end{aligned}\quad (8.109a)$$

$$\vec{V}_F = \dot{x}_F\hat{i}_I + \dot{y}_F\hat{j}_I + \dot{z}_F\hat{k}_I \quad (8.109b)$$

$$\vec{\omega}_f = -\dot{\phi}_s\hat{i}_I - \dot{\alpha}_s\hat{j}_I \quad (8.109c)$$

Substitution of the above relations into the velocity expression yields

$$\begin{aligned}\vec{V}_f = & (\dot{x}_F\hat{i}_I + \dot{y}_F\hat{j}_I + \dot{z}_F\hat{k}_I) \\ & + (-\dot{\phi}_s\hat{i}_I - \dot{\alpha}_s\hat{j}_I) \times [(x_{CG}\hat{i}_F + y_{CG}\hat{j}_F + h\hat{k}_F) \\ & + ((x+u)\hat{i} + (v_b+v_s)\hat{j} + (w_b+w_s)\hat{k} + \eta_r\hat{j}_\eta)]\end{aligned}\quad (8.110)$$

This velocity is transformed to the blade undeformed rotating frame using the following transformation relations

$$\begin{Bmatrix} \hat{i} \\ \hat{j} \\ \hat{k} \end{Bmatrix} = \mathbf{T}_{UR}\mathbf{T}_{RH}\mathbf{T}_{HI} \begin{Bmatrix} \hat{i}_I \\ \hat{j}_I \\ \hat{k}_I \end{Bmatrix} \quad (8.111a)$$

$$\begin{Bmatrix} \hat{i} \\ \hat{j} \\ \hat{k} \end{Bmatrix} = \mathbf{T}_{UR}\mathbf{T}_{RH} \begin{Bmatrix} \hat{i}_F \\ \hat{j}_F \\ \hat{k}_F \end{Bmatrix} \quad (8.111b)$$

$$\begin{Bmatrix} \hat{i} \\ \hat{j} \\ \hat{k} \end{Bmatrix} = \mathbf{T}_{DU} \begin{Bmatrix} \hat{i}_\xi \\ \hat{j}_\eta \\ \hat{k}_\zeta \end{Bmatrix} \quad (8.111c)$$

After application of these transformations, and the ordering scheme, the blade velocity due to fuselage motion is expressed as

$$\vec{V}_f = V_{fx}\hat{i} + V_{fy}\hat{j} + V_{fz}\hat{k} \quad (8.112)$$

with

$$V_{f_x} = (\dot{x}_F - h\dot{\alpha}_s)\cos\psi + (\dot{y}_F + h\dot{\phi}_s)\sin\psi \quad (8.113a)$$

$$V_{f_y} = -(\dot{x}_F - h\dot{\alpha}_s)\sin\psi + (\dot{y}_F + h\dot{\phi}_s)\cos\psi \quad (8.113b)$$

$$V_{f_z} = \dot{z}_F - \dot{\phi}_s x \sin\psi + \dot{\alpha}_s x \cos\psi + x_{CG} \dot{\alpha}_s - y_{CG} \dot{\phi}_s \quad (8.113c)$$

Resultant Velocity

The resultant blade velocity in the rotating undeformed reference frame is given by

$$\begin{aligned} \vec{V} &= U_x \hat{i} + U_y \hat{j} + U_z \hat{k} \\ &= (V_{b_x} - V_{w_x} + V_{f_x}) \hat{i} + (V_{b_y} - V_{w_y} + V_{f_y}) \hat{j} \\ &\quad + (V_{b_z} - V_{w_z} + V_{f_z}) \hat{k} \end{aligned} \quad (8.114)$$

where

$$\begin{aligned} U_x &= \dot{u} - (v'_b + w'_b \dot{\theta}_1) \eta_r \cos\theta_1 - (w'_b - v'_b \dot{\theta}_1) \eta_r \sin\theta_1 \\ &\quad - \Omega(v_b + v_s + \eta_r \cos\theta_1) \\ &\quad - \mu \Omega R \cos\psi + \lambda \Omega R \beta_p \\ &\quad + (\dot{x}_F - h\dot{\alpha}_s) \cos\psi + (\dot{y}_F + h\dot{\phi}_s) \sin\psi \end{aligned} \quad (8.115a)$$

$$\begin{aligned} U_y &= \dot{v}_b + \dot{v}_s - \dot{\theta}_1 \eta_r \sin\theta_1 + \Omega[x + u - v'_b \eta_r \cos\theta_1 - w'_b \eta_r \sin\theta_1] \\ &\quad - \Omega(w_b + \eta_r \sin\theta_1) \beta_p + \mu \Omega R \sin\psi \\ &\quad - (\dot{x}_F - h\dot{\alpha}_s) \sin\psi + (\dot{y}_F + h\dot{\phi}_s) \cos\psi \end{aligned} \quad (8.115b)$$

$$\begin{aligned} U_z &= \dot{w}_b + \dot{w}_s + \dot{\theta}_1 \eta_r \cos\theta_1 + \Omega \beta_p (v_b + \eta_r \cos\theta_1) \\ &\quad + \mu \Omega R \beta_p \cos\psi + \lambda \Omega R \\ &\quad + \dot{z}_F - \dot{\phi}_s x \sin\psi + \dot{\alpha}_s x \cos\psi + x_{CG} \dot{\alpha}_s - y_{CG} \dot{\phi}_s \end{aligned} \quad (8.115c)$$

The blade section loads are functions of the instantaneous resultant velocity and angle of attack (aerodynamic incidence angle) of the blade section. The resultant velocity and

corresponding angle of attack must be transformed to the deformed blade frame for the loads calculation using the transformation matrix T_{DU} (defined in Chapter 2)

$$\begin{Bmatrix} U_R \\ U_P \\ U_T \end{Bmatrix} = T_{DU} \begin{Bmatrix} U_x \\ U_y \\ U_z \end{Bmatrix} \quad (8.117)$$

The resultant velocity in the deformed blade frame is given by

$$\vec{V} = U_R \hat{i}_\xi + U_T \hat{j}_\eta + U_P \hat{k}_\zeta \quad (8.118)$$

with radial, tangential, and perpendicular velocity components, U_R , U_T , and U_P given in nondimensional form as

$$\begin{aligned} \frac{U_R}{\Omega R} = & \dot{u} - v + v'(x + \mu \sin \psi) - \mu \cos \psi (1 - \beta_p w') + \lambda (\beta_p + w') \\ & - \eta_r \cos \theta_0 (1 + \dot{v}') + \eta_r \sin \theta_0 (\dot{\phi} - \dot{w}') \\ & + v' \dot{v} + w' \dot{w} + \frac{1}{2} \mu \cos \psi (v'^2 + w'^2) \\ & + (\dot{x}_F - \dot{\alpha}_s h) \cos \psi + (\dot{y}_F + \dot{\phi}_s h) \sin \psi \end{aligned} \quad (8.119a)$$

$$\begin{aligned} \frac{U_T}{\Omega R} = & \cos \theta_0 (\dot{v} + u - w \beta_p + \dot{\phi} (\lambda + \dot{w}) + v' v \\ & + (x + \mu \sin \psi) (1 - \frac{v'^2}{2}) + \mu \cos \psi (v' + \dot{\phi} (\beta_p + w'))) \\ & + \sin \theta_0 (\dot{w} + \lambda + v (\beta_p + w') - \dot{\phi} \dot{v} \\ & - (x + \mu \sin \psi) (v' w' + \dot{\phi}) + \mu \cos \psi (w' + \beta_p - \dot{\phi} v')) \\ & - \cos \theta_0 ((\dot{x}_F - \dot{\alpha}_s h) \sin \psi - (\dot{y}_F + \dot{\phi}_s h) \cos \psi) \\ & + \sin \theta_0 (\dot{z}_F - \dot{\phi}_s x \sin \psi + \dot{\alpha}_s x \cos \psi + x_{CG} \dot{\alpha}_s - y_{CG} \dot{\phi}_s) \end{aligned} \quad (8.119b)$$

$$\begin{aligned} \frac{U_P}{\Omega R} = & \cos \theta_0 (\dot{w} + \lambda + v \beta_p + \mu \cos \psi (\beta_p + w' - \dot{\phi} v') + v w' \\ & - (x + \mu \sin \psi) (v' w' + \dot{\phi})) + \sin \theta_0 (-(\dot{v} + u) - v v' + w \beta_p \\ & - \dot{\phi} (\dot{w} + \lambda) - \mu \cos \psi (v' + \dot{\phi} (\beta_p + w')) - (x + \mu \sin \psi) (1 - \frac{v'^2}{2})) \end{aligned}$$

$$\begin{aligned}
& + \eta_r (\dot{\theta}_0 + \dot{\phi} + w' + \beta_p) \\
& + \sin \theta_0 ((\dot{x}_F - \dot{\alpha}_s h) \sin \psi - (\dot{y}_F + \dot{\phi}_s h) \cos \psi) \\
& + \cos \theta_0 (\dot{z}_F - \dot{\phi}_s x \sin \psi + \dot{\alpha}_s x \cos \psi + x_{CG} \dot{\alpha}_s - y_{CG} \dot{\phi}_s)
\end{aligned} \quad (8.119c)$$

where the following definitions pertaining to bending and shearing deflections are used for symbolic clarity

$$\begin{aligned}
w &= w_b + w_s & v &= v_b + v_s \\
\dot{w} &= \dot{w}_b + \dot{w}_s & \dot{v} &= \dot{v}_b + \dot{v}_s \\
w' &= w'_b + w'_s & v' &= v'_b + v'_s
\end{aligned} \quad (8.120)$$

Also recall that the ordering scheme eliminates all nonlinear terms involving the shear related deflections v_s and w_s .

8.2.2 Quasi-Steady Airloads Expressions

Two-dimensional strip theory is used to calculate the blade section aerodynamic loads. Once the *shear flexible* blade resultant velocity components have been formulated (as detailed in the previous section), the development of the quasi-steady airloads analysis for the composite rotor blade parallels the formulation for conventional isotropic blades. Details of the formulation relating to the quasi-steady airloads expressions, including modeling of both circulatory and noncirculatory section airloads, reversed flow effects, and compressibility corrections are provided in Chapter 2. For purposes of future reference, the total section airloads (resolved in the *blade rotating undeformed coordinate system*) are defined below as

$$L_w^A = (L_w^A)_C + (L_w^A)_{NC} \quad (8.121a)$$

$$L_v^A = (L_v^A)_C \quad (8.121b)$$

$$L_u^A = (L_u^A)_C \quad (8.121c)$$

$$M_{\phi}^A = \left(M_{\phi}^A\right)_C + \left(M_{\phi}^A\right)_{NC} \quad (8.121d)$$

where L_w^A , L_v^A , and L_u^A are the total section forces in the flapwise, lagwise, and radial directions respectively, and M_{ϕ}^A is the aerodynamic pitching moment about the blade section elastic axis.

8.2.3 Finite Element Discretization

As discussed in Chapter 2, the aeroelastic and aeromechanical analysis is formulated using a finite element discretization based on Hamilton's principle. For the coupled rotor-fuselage system, the external virtual work done by the aerodynamic forces can be expressed as

$$\delta W = \left(\sum_{m=1}^{N_b} \delta W_b \right) + \delta W_F \quad (8.122)$$

where δW_b is the virtual work done on the b th rotor blade and δW_F is the virtual work done on the fuselage. The external virtual work done on the b th blade is given by

$$\delta W_b = \int_0^R (L_u^A \delta u + L_v^A (\delta v_b + \delta v_s) + L_w^A (\delta w_b + \delta w_s) + M_{\phi}^A \delta \hat{\phi}) dx \quad (8.123)$$

where L_u^A , L_v^A , and L_w^A are the section airloads in the blade undeformed frame and M_{ϕ}^A is the sectional pitching moment about the undeformed elastic axis. The external virtual work done on the fuselage is given by

$$\begin{aligned} \delta W_F = & \int_0^R (F_x^A \delta x_F + F_y^A \delta y_F + F_z^A \delta z_F \\ & - M_{\alpha_s}^A \delta \alpha_s - M_{\phi_s}^A \delta \phi_s) dx \end{aligned} \quad (8.124)$$

where F_x^A , F_y^A , and F_z^A are the total fuselage aerodynamic forces and $M_{\alpha_s}^A$ and $M_{\phi_s}^A$ are the total aerodynamic pitch and roll moments about the vehicle center of gravity. The

negative sign on the pitch and roll moments reflects the nose-down and advancing-side down convention in the earlier definition of the vehicle angular rotations. These conventions are opposite those used in deriving the aerodynamic fuselage pitch and roll moments. In general, aerodynamic forces on the fuselage arise from two sources. The first source is the main rotor. Aerodynamic forces acting on the blades can be transmitted to the fuselage through the rotor hub. Aerodynamic forces generated directly by the fuselage also contribute to the external virtual work on the fuselage. In the present aeromechanical *stability* analysis, direct fuselage (perturbation) aerodynamic forces are neglected except for the contribution of the horizontal tail surface. Modeling of all steady fuselage forces is included in the vehicle trim analysis (discussed in Chapter 4).

In order to simplify the description of the finite element discretization, the following notation is defined

$$\begin{aligned}\mathbf{L}^A &= \begin{bmatrix} L_u^A & L_v^A & L_w^A & M_\phi^A & L_v^A & L_w^A \end{bmatrix}^T \\ \mathbf{u} &= \begin{bmatrix} u & v_b & w_b & \dot{\phi} & v_s & w_s \end{bmatrix}^T \\ \mathbf{F}_F^A &= \begin{bmatrix} F_x^A & F_y^A & F_z^A & -M_{\alpha_s}^A & -M_{\phi_s}^A \end{bmatrix}^T \\ \mathbf{x}_F &= \begin{bmatrix} x_F & y_F & z_F & \alpha_s & \phi_s \end{bmatrix}^T \\ \lambda &= \begin{bmatrix} \lambda_0 & \lambda_{1s} & \lambda_{1c} \end{bmatrix}^T\end{aligned}\tag{8.125}$$

Using this notation, the external virtual work on the blade and fuselage is written as

$$\delta W_b = \int_0^R \delta \mathbf{u}^T \mathbf{L}^A dr \tag{8.126}$$

$$\delta W_F = \int_0^R \delta \mathbf{x}_F^T \mathbf{F}_F^A dr \tag{8.127}$$

The aerodynamic forces can be symbolically expressed as

$$\mathbf{L}^A = (\mathbf{L}^A)_0 + (\mathbf{L}^A)_q + (\mathbf{L}^A)_{q^2} + (\mathbf{L}^A)_{x_F} + (\mathbf{L}^A)_\lambda \quad (8.128)$$

$$\mathbf{F}_F^A = \mathbf{F}_{FB}^A + \mathbf{F}_{FF}^A \quad (8.129)$$

where the subscripts 0, q , q^2 , x_F , and λ refer to constant, linear blade motion dependent, nonlinear blade motion dependent, fuselage motion dependent, and inflow components of the blade aerodynamic forces respectively. The vector, \mathbf{F}_{FB}^A , represents the contribution of the blade aerodynamic loads to the total fuselage external loads and \mathbf{F}_{FF}^A is the contribution of the direct fuselage aerodynamic loads to the fuselage load.

8.2.3.1 Discretization of the Blade Equations

Discretized Virtual Work

The *linear* terms in the blade force vector can be expressed as

$$(\mathbf{L}^A)_q + (\mathbf{L}^A)_{x_F} + (\mathbf{L}^A)_\lambda = (\mathbf{A}_u \mathbf{u} + \mathbf{A}_{u'} \mathbf{u}' + \mathbf{A}_{\dot{u}} \dot{\mathbf{u}} + \mathbf{A}_{\ddot{u}} \ddot{\mathbf{u}}) + (\mathbf{A}_{x_F} \mathbf{x}_F + \mathbf{A}_{\dot{x}_F} \dot{\mathbf{x}}_F) + (\mathbf{A}_\lambda \lambda) \quad (8.130)$$

where the displacement vector, \mathbf{u} , slope vector, \mathbf{u}' , velocity vector, $\dot{\mathbf{u}}$, and acceleration vector, $\ddot{\mathbf{u}}$, are given in discretized form as

$$\begin{aligned} \mathbf{u} &= \mathbf{H}_s \mathbf{q} \\ \mathbf{u}' &= \mathbf{H}'_s \mathbf{q} \\ \dot{\mathbf{u}} &= \mathbf{H}_s \dot{\mathbf{q}} \\ \ddot{\mathbf{u}} &= \mathbf{H}_s \ddot{\mathbf{q}} \end{aligned} \quad (8.131)$$

where the spatial shape function matrix, \mathbf{H}_s , is defined as

$$\mathbf{H}_s = \begin{bmatrix} H_v & 0 & 0 & 0 & 0 & 0 \\ 0 & H_{v_b} & 0 & 0 & 0 & 0 \\ 0 & 0 & H_{w_b} & 0 & 0 & 0 \\ 0 & 0 & 0 & H_{\dot{\phi}} & 0 & 0 \\ 0 & 0 & 0 & 0 & H_{v_s} & 0 \\ 0 & 0 & 0 & 0 & 0 & H_{w_s} \end{bmatrix} \quad (8.132)$$

and the elemental degree of freedom vector, \mathbf{q}_i , is defined as

$$\mathbf{q}_i^T = [u_1, u_2, u_3, u_4, v_{b1}, v'_{b1}, v_{b2}, v'_{b2}, w_{b1}, w'_{b1}, w_{b2}, w'_{b2}, \hat{\phi}_1, \hat{\phi}_2, \hat{\phi}_3, v_{s1}, v_{s2}, w_{s1}, w_{s2}]$$

Substitution of the discretized displacements and velocities above into the expression for blade virtual work (equation 3.34) yields the discretized virtual work as

$$\delta W_b = \sum_{i=1}^{N_e} [\delta W_b]_i \quad (8.133)$$

where

$$[\delta W_b]_i = \delta \mathbf{q}^T \left([M_b^A]_i \ddot{\mathbf{q}} + [C_b^A]_i \dot{\mathbf{q}} + [K_b^A]_i \mathbf{q} + [C_{bF}^A]_i \dot{\mathbf{x}}_F + [K_{bF}^A]_i \mathbf{x}_F \right. \\ \left. + [K_{b\lambda}^A]_i \lambda + [(Q_b^A)_0]_i + [(Q_b^A)_{q^2}]_i \right) \quad (8.134)$$

When combined with the structural kinetic and potential energy terms derived in Chapter 2, the above expression completes the governing *blade* equations for the coupled rotor-fuselage aeromechanical system.

8.2.3.2 Discretization of the Fuselage Equations

As previously discussed in this chapter, blade aerodynamic forces can be transmitted to the fuselage through the main rotor hub. The contribution of the blade force to the fuselage aerodynamic force is expressed as

$$\begin{Bmatrix} F_x^A \\ F_y^A \\ F_z^A \\ M_{\alpha_s}^A \\ M_{\phi_s}^A \end{Bmatrix} = \mathbf{T}_{FL} \begin{Bmatrix} L_u^A \\ L_v^A \\ L_w^A \\ M_\phi^A \end{Bmatrix} \quad (8.135)$$

or

$$\mathbf{F}_F^A = \mathbf{T}_{FL} \mathbf{L}^A \quad (8.136)$$

where the transformation matrix \mathbf{T}_{FL} is defined as

$$\mathbf{T}_{FL} = \begin{bmatrix} \cos\psi - \beta_p \alpha_s & -\sin\psi & -\beta_p \cos\psi - \alpha_s & 0 \\ \sin\psi + \beta_p \phi_s & \cos\psi & -\beta_p \sin\psi + \phi_s & 0 \\ \beta_p + \alpha_s \cos\psi - \phi_s \sin\psi & -\alpha_s \sin\psi - \phi_s \cos\psi & 1 - \alpha_s \beta_p \cos\psi + \phi_s \beta_p \sin\psi & 0 \\ -x_{CG} \beta_p + (w+h) \cos\psi & -(w+h) \sin\psi & v \sin\psi - (x+u) \cos\psi & (1 - \beta_p w') \sin\psi \\ +v \beta_p \sin\psi & -(x+u) \beta_p \sin\psi & -h \beta_p \cos\psi - x_{CG} & +v' \cos\psi \\ v \beta_p \cos\psi + y_{CG} \beta_p & -(w+h) \cos\psi & v \cos\psi + y_{CG} & (1 - \beta_p w') \cos\psi \\ -(h+w) \sin\psi & -(x+u) \beta_p & (u+x - \beta_p h) \sin\psi & -v' \sin\psi \end{bmatrix} \quad (8.137)$$

where the following definitions are again applied

$$\begin{aligned} w &= w_b + w_s & v &= v_b + v_s \\ w' &= w'_b + w'_s & v' &= v'_b + v'_s \end{aligned} \quad (8.138)$$

Since the transformation matrix, \mathbf{T}_{FL} , is central to the aeromechanical stability analysis, the derivation of this matrix is outlined in the following section.

8.3 Vehicle Trim and Response Analysis

In the present analysis, the vehicle trim equations and the blade response equations are solved simultaneously using a coupled trim procedure (see Chapter 4). This trim procedure is essential to the analysis of elastically coupled composite blades. The following section describes the modifications to the coupled trim procedure related to the shear flexible, elastically coupled composite blades.

8.3.1 Initial Controls Estimate

The aeroelastic trim analysis is nonlinear in nature. There is a complex nonlinear relationship between applied rotor controls and steady rotor forces. Due to moderate blade deflections, the blade response equations also contain both structural and aerodynamic nonlinearities. A reasonably accurate initial guess improves the efficiency and robustness of the nonlinear trim solution. This initial estimate is provided by a rigid flapping blade solution, combined with a five degree-of-freedom set of vehicle equilibrium equations (see Chapter 4).

Special Considerations for Elastically Twisted Composite Blades

The computation time required for the coupled trim solution is directly related to the proximity of the initial controls estimate to the final trim controls settings. For blades with significant magnitudes of static or dynamic elastic twist, the control pitch settings computed using a rigid blade estimate (no elastic twist) represent a poor initial starting point. Composite blades with elastic couplings often result in such conditions. In particular, blades with extension-torsion coupling experience several degrees of static elastic twist due to high centrifugal forces. For helicopter rotor blades examined in the present study, five to ten degrees elastic is common. For some future tilt-rotor applications, static elastic twist angles of twenty to forty degrees will occur. The initial "rigid blade" controls estimate of the collective pitch is adjusted to compensate for this steady elastic twist using the relation

$$\theta_{75} = (\theta_{75})_{\text{rigid}} - \phi_{75} \quad (8.139)$$

where ϕ_{75} is the elastic twist (positive nose up) at the three-quarter radial span location. An approximate expression for ϕ_{75} is calculated using the force-deformation relation

$$\begin{Bmatrix} F \\ T \end{Bmatrix} = \begin{bmatrix} EA & K_{14} \\ K_{14} & GJ \end{bmatrix} \begin{Bmatrix} u' \\ \phi' \end{Bmatrix} \quad (8.140)$$

with steady axial force, F , and torque, T , assumed to be

$$F \approx \frac{1}{2} m \Omega^2 (R^2 - r^2) \quad (8.141a)$$

$$T = 0 \quad (8.141b)$$

Using the above relations, and applying a root fixed constraint, the elastic twist at station r is given by

$$\phi(r) = \frac{-K_{14}m\Omega^2}{2(EAGJ - K_{14}^2)} \left[R^2r - \frac{r^3}{3} \right] \quad (8.142)$$

The elastic twist at the three-quarter radial span location, ϕ_{75} , reduces to

$$\phi_{75} = \frac{-K_{14}m\Omega^2}{2(EAGJ - K_{14}^2)} \left[0.75R^3 - \frac{(0.75R)^3}{3} \right] \quad (8.143)$$

In addition to reducing the trim solution time, this adjustment helps avoid numerical divergence of the trim scheme (sometimes induced by trim iterations resulting in large values of negative thrust).

8.3.2 Computation of Blade Loads

For each iteration during the coupled trim procedure, the blade loads must be calculated. The steady (time averaged around the azimuth) values of these blade loads combine in the fixed frame (at the hub) and are used in the evaluation of the vehicle equilibrium equations. In the present analysis, blade loads are calculated using the force summation technique. This method requires the calculation and spanwise integration of the blade inertia loads and blade aerodynamic loads. The blade loads generally consist of both motion dependent and non-motion dependent contributions. At each response calculation iteration the blade response is known; therefore the motion dependent loads can be evaluated directly.

The inertial loads can be determined solely from the blade motion. From Newton's Second Law, the sectional inertial force acting at blade station r is given by

$$\mathbf{F}^I = \iint \rho_s \vec{a} d\eta d\zeta \quad (8.144)$$

where $\mathbf{F}^I = [L_u^I, L_v^I, L_w^I]^T$, and L_u^I, L_v^I , and L_w^I are the section inertial forces acting in the x , y , and z directions in the blade undeformed reference frame, ρ_s is the blade mass density, and \vec{a} is the blade acceleration relative to an inertial reference frame. As derived in Chapter 2, the acceleration is

$$\begin{aligned} \vec{a} &= a_x \hat{i} + a_y \hat{j} + a_z \hat{k} \\ &= \ddot{\vec{r}} + \vec{\Omega} \times (\vec{\Omega} \times \vec{r}) + 2(\vec{\Omega} \times \dot{\vec{r}}) \end{aligned} \quad (8.145)$$

where $\ddot{\vec{r}}, \dot{\vec{r}}$ and \vec{r} are the blade acceleration, velocity, and displacement vectors in the rotating blade frame, and $\vec{\Omega}$ is the rotor rotational speed. The inertial component of the blade pitching moment about the deformed blade elastic axis is given by

$$\mathbf{M}^I = -\iint \mathbf{s} \times \vec{a} d\eta d\zeta = M_u^I \hat{i} + M_v^I \hat{j} + M_w^I \hat{k} \quad (8.146)$$

where the moment arm, \mathbf{s} , is given as

$$\mathbf{s} = -[v'(y_1 - v) + w'(z_1 - w)] \hat{i} + (y_1 - v) \hat{j} + (z_1 - w) \hat{k} \quad (8.147)$$

Using the above relations, the inertial section loads are given by

$$\begin{aligned} L_u^I &= -m[\ddot{u} - x - u - 2(\dot{v}_b + \dot{v}_s) + \beta_p(w_b + w_s) \\ &\quad + e_g(v'_b - \ddot{v}'_b)\cos\theta_1 + e_g(w'_b + \beta_p - \ddot{w}'_b + 2\dot{\theta}_1)\sin\theta_1] \end{aligned} \quad (8.148)$$

$$\begin{aligned} L_v^I &= -m[\ddot{v}_b - v_b + \ddot{v}_s - v_s + 2\dot{u} - 2\beta_p(\dot{w}_b + \dot{w}_s) \\ &\quad - e_g(1 + 2\dot{v}'_b)\cos\theta_1 - e_g(\ddot{\theta}_1 - \phi + 2\dot{w}'_b)\sin\theta_1 - 2v'_b\dot{v}_b] \\ &\quad - 2v''_b \int_x^1 m\dot{v}_b dx \end{aligned} \quad (8.149)$$

$$L_w^I = -m[(\ddot{w}_b + \ddot{w}_s) + \beta_p x + 2\beta_p(\dot{v}_b + \dot{v}_s) + e_g \ddot{\theta}_I \cos\theta_1] \\ - 2w_b'' \int_x^1 m\dot{v}_b dx \quad (8.150)$$

$$M_u^I = -m[k_m^2 \ddot{\theta}_I + (1 + 2\dot{v}_b' - 2\dot{\theta}_I)(k_{m2}^2 - k_{m1}^2) \cos\theta_1 \sin\theta_1 \\ + 2(\dot{w}_b + \dot{w}_s)(k_{m2}^2 \sin^2\theta_1 + k_{m1}^2 \cos^2\theta_1) \\ + (x\beta_p + 2(\dot{v}_b + \dot{v}_s) + \ddot{w}_b + \ddot{w}_s)e_g \cos\theta_1 \\ + (v_b + v_s - \ddot{v}_b - \ddot{v}_s)e_g \sin\theta_1] \quad (8.151)$$

$$M_v^I = -m[(v_b' + \beta_p - \ddot{v}_b')(k_{m2}^2 - k_{m1}^2) \cos\theta_1 \sin\theta_1 \\ + (w_b' - \ddot{w}_b' + 2\dot{\theta}_I)(k_{m2}^2 \sin^2\theta_1 + k_{m1}^2 \cos^2\theta_1) \\ - x\phi e_g \cos\theta_1 - (x + 2\dot{v}_b)e_g \sin\theta_1] \quad (8.152)$$

$$M_w^I = -m[(\ddot{w}_b' - w_b' - 2\dot{\theta}_1 - \beta_p)(k_{m2}^2 - k_{m1}^2) \cos\theta_1 \sin\theta_1 \\ + (\ddot{v}_b' - v_b')(k_{m2}^2 \sin^2\theta_1 + k_{m1}^2 \cos^2\theta_1) \\ + (x + 2\dot{v}_b)e_g \cos\theta_1 - x\phi e_g \sin\theta_1] \quad (8.153)$$

where

$$\dot{u} = \dot{u}_e - \int_0^x (v'\dot{v}' + w'\dot{w}') dx \quad (8.154a)$$

$$\ddot{u} \approx \ddot{u}_e \quad (8.154b)$$

$$L_u = L_u^A + L_u^I \quad (8.155)$$

$$L_v = L_v^A + L_v^I \quad (8.156)$$

$$L_w = L_w^A + L_w^I \quad (8.157)$$

$$M_u = M_\phi^A + M_u^I \quad (8.158)$$

$$M_v = v'M_\phi^A + M_v^I \quad (8.159)$$

$$M_w = w'M_\phi^A + M_w^I \quad (8.160)$$

The aerodynamic section loads are described in detail in Chapter 3. Once the section loads are known along the blade span, the force summation method is used to evaluate the blade root longitudinal, lateral, and vertical shear forces (F_x , F_y , and F_z), torsion moment (M_x), and flap and lag bending moments (M_y and M_z) in the rotating frame using the relations

$$\begin{Bmatrix} F_x \\ F_y \\ F_z \end{Bmatrix} = \int_0^R \begin{Bmatrix} L_u \\ L_v \\ L_w \end{Bmatrix} dr \quad (8.161)$$

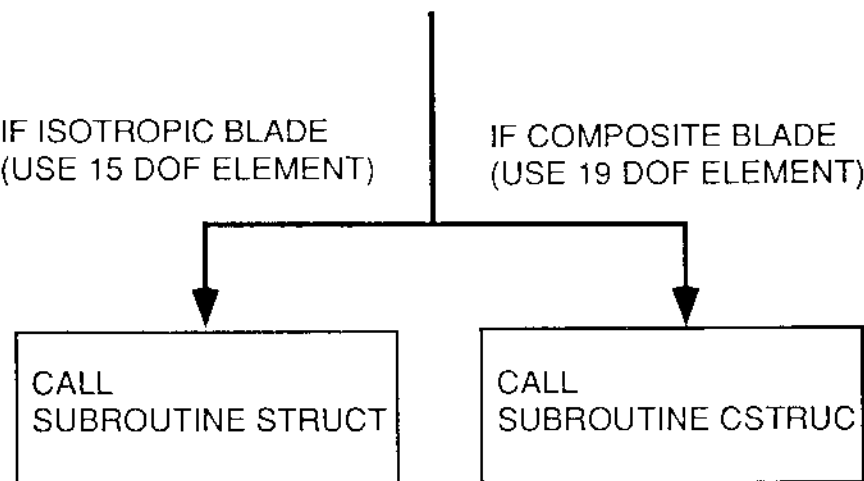
and

$$\begin{Bmatrix} M_x \\ M_y \\ M_z \end{Bmatrix} = \int_0^R \begin{Bmatrix} -L_v(w_b + w_s) + L_w(v_b + v_s) + M_u \\ L_u(w_b + w_s) - L_w(r + u) + M_v \\ -L_u(v_b + v_s) + L_v(r + u) + M_w \end{Bmatrix} dr \quad (8.162)$$

8.4 Composite Blade Model Implementation

Implementation Logic and Approach:

Integration of the composite blade analysis into UMARC involves two major aspects. The first aspect is the use of the nineteen degree of freedom shear flexible beam element. The second major aspect is the structural elastic coupling effects which can be introduced through the ply orientations in composite blade spar. This section describes the specific subroutines which are specifically affected by composite blade modeling. The diagram below shows the general decision logic used to integrate the composite analysis with the isotropic blade analysis



The current version of UMARC does not include bearingless composite blade modeling, or modeling for composite blades with advanced geometry tips. Composite blade stiffnesses and elastic couplings can only be calculated for a uniform box-beam blade spar in the current version of UMARC. However, these cross-section properties can be computed by the user externally and directly read into UMARC for aeroelastic

and aeromechanical analysis. The later option allows for analysis of nonuniform composite blades with more general cross-section geometries.

Additional SUBROUTINES:

The following subroutines have been added to UMARC specifically for composite rotor blade analysis.

CBPROP

Calculates elastic stiffness coefficients (EA , EI_y , etc.) and coupling parameters (K_{12} , K_{13} , etc.) for the laminated composite box-beam spar. This subroutine is called by UMRINP and returns the nondimensional stiffness coefficients. Input data is read from the file COMPBEAM.IN. The CBPROP routine also reads the reference mass per unit length, m_0 , blade radius, R , and reference rotational speed, Ω_0 . Specified values of nondimensional torsional inertia are also read by the CBPROP routine. This is usually required since the low material density of the composite box spar necessitates the use of nonstructural mass to obtain realistic levels of torsional inertia.

CSTRUC

Calculates the structural contributions to the elemental stiffness, damping, and mass matrices and load vector. This is the primary subroutine for the composite blade analysis. Inputs, outputs, and functionality are analogous to the isotropic counterpart, SUBROUTINE STRUCT.

AEROMC

This routine is the nineteen degree of freedom shear flexible element version of SUBROUTINE AEROMX. Aerodynamic contributions to the elemental stiffness,

damping, and mass matrices and load vector are calculated in SUBROUTINE AEROMC.

CHUBLD

This routine is the nineteen degree of freedom shear flexible element version of SUBROUTINE HUBLDS. In this routine, the force summation method is used to compute blade loads for the composite blade with shear flexible beam elements.

Modifications to Existing SUBROUTINES:

The following subroutines have been modified for composite rotor blade analysis.

EXEC

Input/output of composite blade structural finite element properties. The blade connectivity vector is assigned for either the fifteen degree of freedom Bernoulli-Euler beam element model or the nineteen degree of freedom shear flexible beam element model. Global and local degree of freedom parameters are also assigned in SUBROUTINE EXEC.

UMRINP

Input/output of composite blade structural finite element properties. This routine either calls SUBROUTINE CBPROP or directly reads the composite blade elemental structural properties.

BLDVIB

This routine builds the blade finite element model and computes the free vibration mode shapes and natural frequencies. For the composite blade, this subroutine calls SUBROUTINE CSTRU.

TRIM

This routine calls SUBROUTINE CHUBLD to compute blade loads for the composite rotor. Vehicle and blade response convergence is also checked in this routine. Output of the composite blade response (including shear deformations) is also a function of SUBROUTINE TRIM.

VTRIM

This routine calculated the initial controls estimate for the coupled trim procedure. For blades with extension-torsion coupling, the initial collective pitch setting is adjusted for elastic twist effects in SUBROUTINE VTRIM.

ASBGBM

This subroutine calls SUBROUTINE AEROMC and SUBROUTINE CSTRUC to compute the elemental matrices and load vector for the trim and response analysis.

STAB

After the blade response has been obtained, this subroutine recalculates the blade natural frequencies and mode shapes for subsequent use in the aeroelastic or aeromechanical stability analysis. For this free vibration analysis, the routine calls SUBROUTINE CSTRUC. This subroutine also calls SUBROUTINE AEROMC and SUBROUTINE CSTRUC to compute and assemble the elemental matrices for the stability analysis.

ASBGM2

This subroutine calls SUBROUTINE AEROMC and SUBROUTINE CSTRUC to compute the elemental matrices and load vector for the stability analysis.

Additional INCLUDE FILES:

The following files have been added to UMARC specifically for composite rotor blade analysis. These files contain either data statements or common blocks and are "included" in the UMARC program at compilation.

STRUCC

Common block containing the elastic coupling coefficients K_{12} , K_{13} , etc.

IVECBE

Data statement for connectivity vector of (15 DOF) Bernoulli-Euler beam elements.

IVECTS

Data statement for connectivity vector of (19 DOF) shear flexible beam elements.

ISWBE

Data statement for advanced geometry tip connectivity vector of (15 DOF) Bernoulli-Euler beam elements. Composite blades with advanced geometry tips are not included in the current version of UMARC. This data statement, included in SUBROUTINE SWEEP, is currently required only for compilation purposes.

ISWTS

Data statement for advanced geometry tip connectivity vector of (19 DOF) shear flexible beam elements. Composite blades with advanced geometry tips are not included in the current version of UMARC. This data statement, included in SUBROUTINE SWEEP, is currently required only for compilation purposes.

Modifications to existing INCLUDE FILES:

The following files have been modified for composite rotor blade analysis.

PARA

Primary file specifying parameters for array dimensions, and analysis option parameters.

STRUC

Common block containing the stiffness coefficients EA , EI_y , etc. This file is modified to include shear stiffnesses GA_y and GA_z .

Modifications to existing primary INPUT files:

The following new keywords are included for composite rotor analysis.

MATERIAL_TYPE:

This keyword is specified in the BLADE_PROPERTIES datablock. One of three options must be selected.

ISOTROPIC specifies conventional blade analysis. Bernoulli-Euler fifteen degree of freedom elements are used, and elemental elastic properties are input through the user specified primary input file.

COMPOSITE_CALC specifies composite blade analysis. Shear flexible nineteen degree of freedom elements are used, and elemental elastic properties are calculated for a uniform composite box-beam blade spar. Box-beam spar properties are specified in the data file COMPBEAM.IN.

COMPOSITE_READ specifies composite blade analysis. Shear flexible nineteen degree of freedom elements are used, and elemental elastic properties (including shear stiffnesses and elastic couplings) are input through the user specified primary input file.

GAY, GAZ, K12, K13, K14, K25, K36, K45, K46:

When the COMPOSITE READ option is selected for the MATERIAL_TYPE keyword, these additional input variables are required in the BLADE_PROPERTIES datablock.

Additional INPUT file:

compbeam.in

Composite box-beam spar properties are provided in this data file. Input includes spar size, ply elastic constants, ply orientation angles, and analysis option selectors for warping (NWARP) and two-dimensional inplane ply elasticity (NSTRES). This

Additional OUTPUT FILES:

The composite box-beam spar analysis (used when MATERIAL_TYPE = COMPOSITE_CALC) generates three additional files of output:

compbeam.out1

This file contains output related to box-beam geometry and ply orientation angles.

compbeam.out2

This file contains output related to box-beam ply elastic constants.

compbeam.out3

This file contains output related to box-beam cross-section properties.

Compilation and Execution Procedure

1. Change the following PARAMETERS in the PARA file:

MEDOF = 19

MBCS = 8

MGT = MSELT*11 + 8

2. Recompile the entire UMARC program using appropriate MAKEFILE

3. Specify MATERIAL_TYPE (one of the following options):

COMPOSITE_CALC: Provide the data file COMPBEAM.IN

COMPOSITE_READ: Provide shear stiffnesses and elastic
couplings in user specified main input file

4. Run UMARC program using standard command

References

- [8.1] Smith, E.C. and Chopra, I., "Formulation and Evaluation of an Analytical Model for Composite Box-Beams," *Proceedings of the 31st AIAA/ASME/ASCE/AHS/ASC Structures, Structural Dynamics and Materials Conference*, Long Beach, California, April 1990.
- [8.2] Smith, E.C. and Chopra, I., "Formulation and Evaluation of an Analytical Model for Composite Box-Beams," *Journal of the American Helicopter Society*, Vol 36, No. 3, July 1991.
- [8.3] Smith, E.C. and Chopra, I., "Aeroelastic Response and Blade Loads of a Composite Rotor in Forward Flight", *Proceedings of the 33rd AIAA/ASME/ASCE/AHS/ASC Structures, Structural Dynamics and Materials Conference*, AIAA Paper No. 92-2566,Dallas, Texas, April 13-15 1992.
- [8.4] Smith, E.C. and Chopra, I., "Aeromechanical Stability of Helicopters with Composite Rotor Blades in Forward Flight", *Proceedings of the 48th American Helicopter Society Annual Forum*, Phoenix, Arizona, June 3-5 1992.
- [8.5] Smith, E.C., "Aeroelastic Response and Aeromechanical Stability of Helicopters with Elastically Coupled Composite Rotor Blades," Doctoral Dissertation, Aerospace Engineering Department, University of Maryland, College Park, Maryland, 1992.
- [8.6] Megson, T. H. G., *Linear Analysis of Thin-Walled Elastic Structures*, John Wiley & Sons, New York, 1974, Chapter 5.
- [8.7] Jones, R. M., Mechanics of Composite Materials, Hemisphere Publishing Corporation, New York, 1975.
- [8.8] Agarwal, B. D., and Broutman, L. J., Analysis and Performance of Fiber Composites, John Wiley & Sons, 1980.

- [8.9] Hong, Chang-Ho and Chopra, I., "Aeroelastic Stability Analysis of a Composite Rotor Blade," *Journal of the American Helicopter Society*, Vol. 30, No. 2, April 1985.
- [8.10] Hong, Chang-Ho and Chopra, I., "Aeroelastic Stability Analysis of a Composite Bearingless Rotor Blade," *Journal of the American Helicopter Society*, Vol. 31, No. 4, October 1985.
- [8.11] Hong, Chang-Ho, "Aeroelastic Stability of Composite Rotor Blades," Ph.D. Dissertation, University of Maryland, College Park, Maryland, August 1985.
- [8.12] Panda, B. and Chopra, I., "Dynamics of Composite Rotor Blades in Forward Flight," *Vertica*, Vol. 11, (1/2), January 1987.
- [8.13] Kosmatka, J. B. and Friedmann, P. P., "Structural Dynamic Modeling of Advanced Composite Propellers By the Finite Element Method," *Proceedings of the 28th AIAA/ASME/ASCE/AHS Structures, Structural Dynamics and Materials Conference*, Monterey, California, April 1987.
- [8.14] Kosmatka, J. B. and Friedmann, P. P., "Vibration Analysis of Composite Turbopropellers Using a Nonlinear Beam-Type Finite Element Approach," *AIAA Journal*, Vol. 27, No. 11, November 1989.
- [8.15] Kosmatka, J.B., "Structural Dynmaic Modeling of Advanced Composite Propellers by the Finite Element Method," Ph.D. Dissertation, University of California at Los Angeles, Los Angeles, California, 1989.
- [8.16] Rehfield, L. W., "Design Analysis Methodology for Composite Rotor Blades," *Proceedings of the Seventh DoD/NASA Conference on Fibrous Composites in Structural Design*, AFWAL-TR-85-3094, Denver, Colorado, June 1985.
- [8.17] Brunelle, E. J., "Dynamical Torsion Theory of Rods Deduced From the Equations of Linear Elasticity," *AIAA Journal*, Vol. 10, No. 4, April 1971.

- [8.18] Hedges, D. H. and Dowell, E. H., "Nonlinear Equations of Motion For the Elastic Bending and Torsion of Twisted Non-Uniform Rotor Blades," *NASA TN D-7818*, December 1974.
- [8.19] Kaza, K.R., and Kvaternik, R.G., "Nonlinear Aeroelastic Equations for Combined Flapwise Bending, Chordwise Bending, Torsion, and Extension of Twisted Nonuniform Rotor Blades in Forward Flight," *NASA TM 74059*, August 1977.
- [8.20] Celi, R. and Friedmann, P.P., "Aeroelastic Modeling of Swept Tip Rotor Blades Using Finite Elements", *Journal of the American Helicopter Society*, Vol. 33, No. 2, April 1988.
- [8.21] Chopra, I. and Sivaneri, N.T., "Aeroelastic Stability of Rotor Blades Using Finite Element Analysis, NASA CR 166389, August 1982.
- [8.22] Tessler, A., and Dong, S.B., "On a Hierarchy of Conforming Timoshenko Beam Elements," *Computers & Structures*, Vol. 14, No. 3-4, 1981.
- [8.23] Archer, J.S., "Consistent Matrix Formulations for Structural Analysis Using Finite-Element Techniques, *AIAA Journal*, Vol. 3, No. 10, November 1965.
- [8.24] Davis, R., Henshell, R.D., and Warburton, G.B., "A Timoshenko Beam Element," *Journal of Sound and Vibration*, Vol. 22, No. 4, April 1972.
- [8.25] Nixon, M., "Analytical and Experimental Investigations of Extension-Twist Coupled Structures", M.S. Thesis, NASA Langley/George Washington University, 1989.
- [8.26] Bathe, K.J., Finite Element Procedures in Engineering Analysis, Prentice Hall, Inc., New Jersey, 1982.
- [8.27] Gallagher, R.H., Finite Element Analysis Fundamentals, Prentice Hall, Inc., New Jersey, 1975.

Compilation and Execution Procedure

1. Change the following PARAMETERS in the PARA file:

MEDOF = 19

MBCS = 8

MGT = MSELT*11 + 8

2. Recompile the entire UMARC program using appropriate MAKEFILE

3. Specify MATERIAL_TYPE (one of the following options):

COMPOSITE_CALC: Provide the data file COMPBEAM.IN

COMPOSITE_READ: Provide shear stiffnesses and elastic
couplings in user specified main input file

4. Run UMARC program using standard command

θ = Ply Orientation Angles

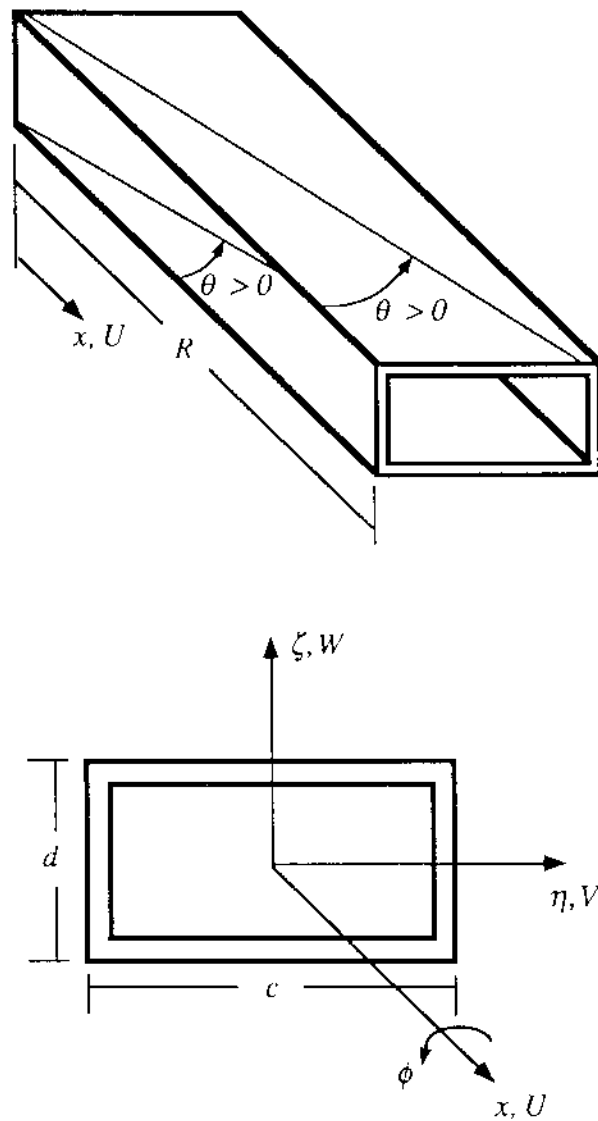


Figure 8.1 Box-beam dimensions and coordinate systems

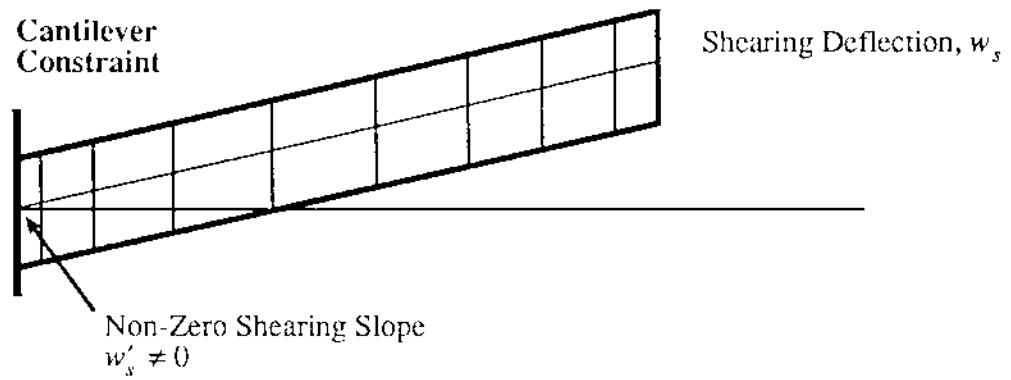
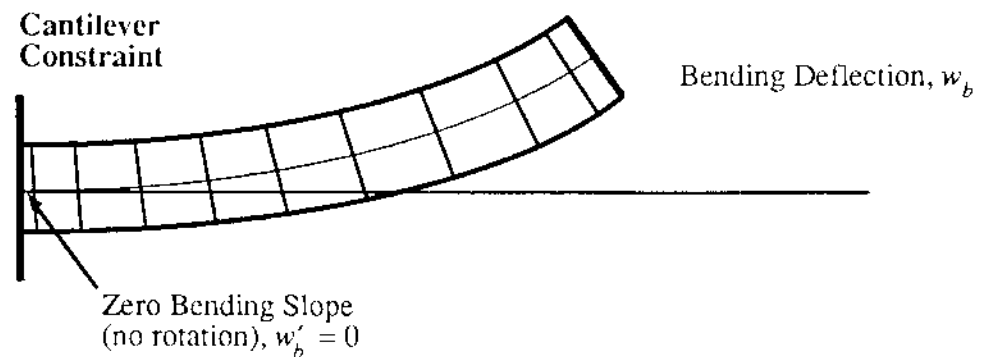
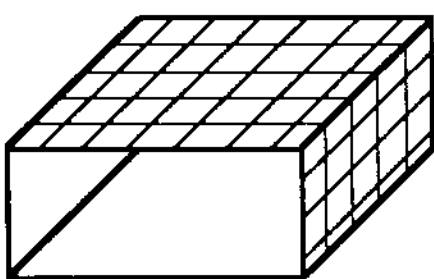
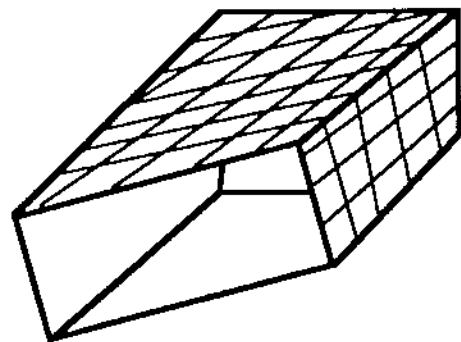


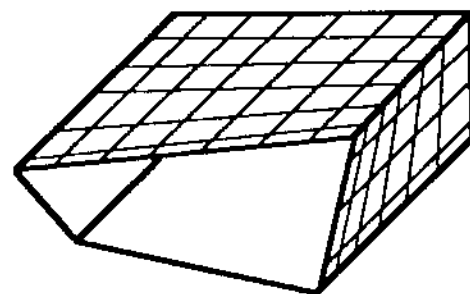
Figure 8.2a Beam bending and shearing deformations



Undeformed Cross-Section

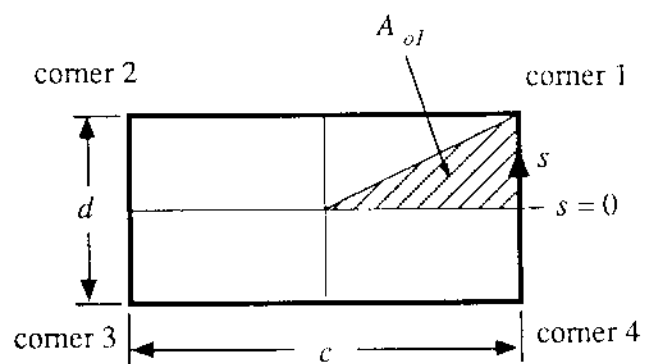


Cross-Section Rotation



Out-of-Plane
Torsion-Related Warping

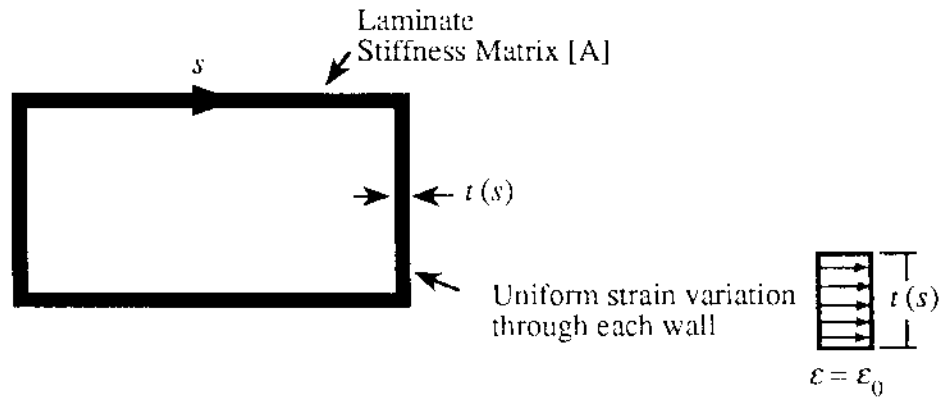
Figure 8.2b Torsional deformations of a box-beam section



Corner	δ_{os}	A_{os}
1	$\frac{d}{2G_v t_v}$	$cd/8$
2	$\frac{d}{2G_v t_v} + \frac{c}{G_h t_h}$	$3cd/8$
3	$\frac{3d}{2G_v t_v} + \frac{c}{G_h t_h}$	$5cd/8$
4	$\frac{3d}{2G_v t_v} + \frac{2c}{G_h t_h}$	$7cd/8$

Figure 8.3 Contour coordinates and warping parameters for box cross-section

Contour Analysis



2-D Section Analysis

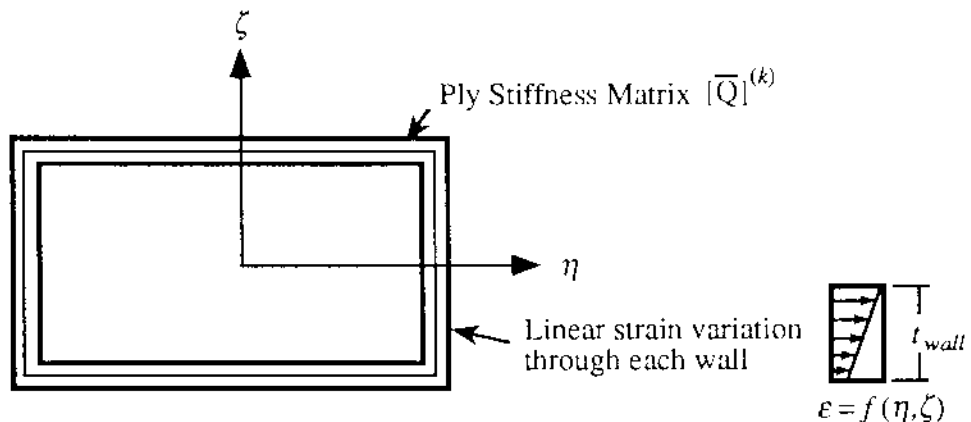
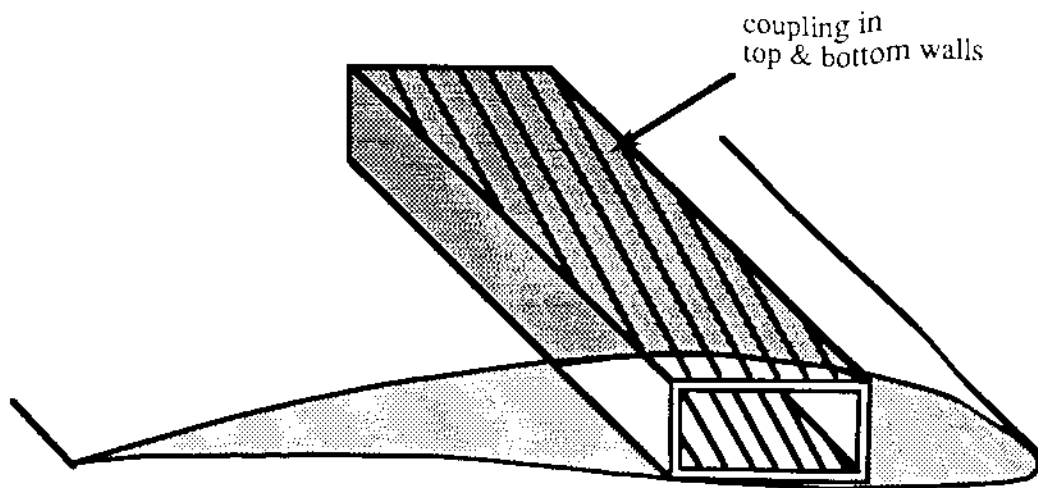


Figure 8.4 Two-dimensional and contour analysis features

Symmetric Layup Spar (Case A)

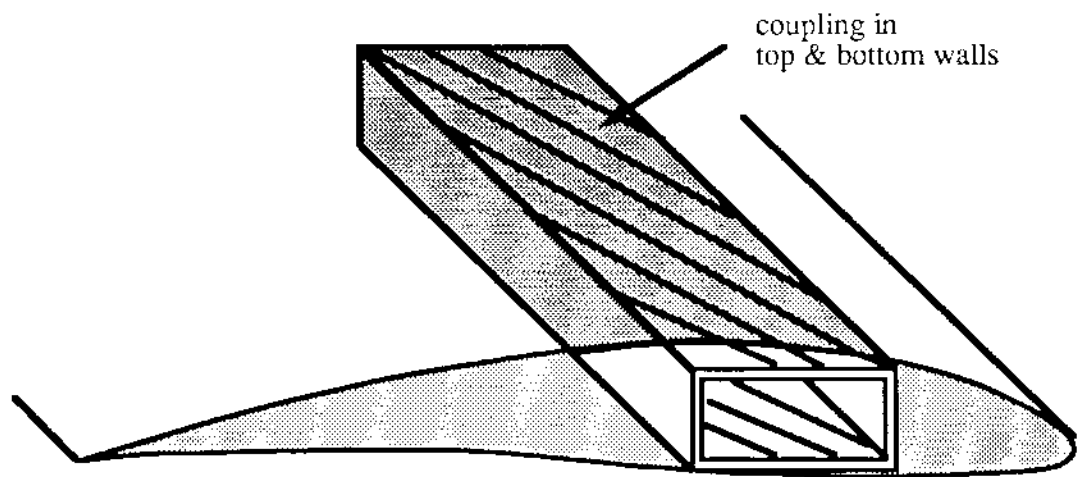


Negative Pitch-Flap Coupling: Flap Up → Pitch Up

Extension-Flap Shear Coupling: Tension → Shear Forward

Figure 8.5a Symmetric layup box-beam spar (*symmetric A*)

Symmetric Layup Spar (Case B)

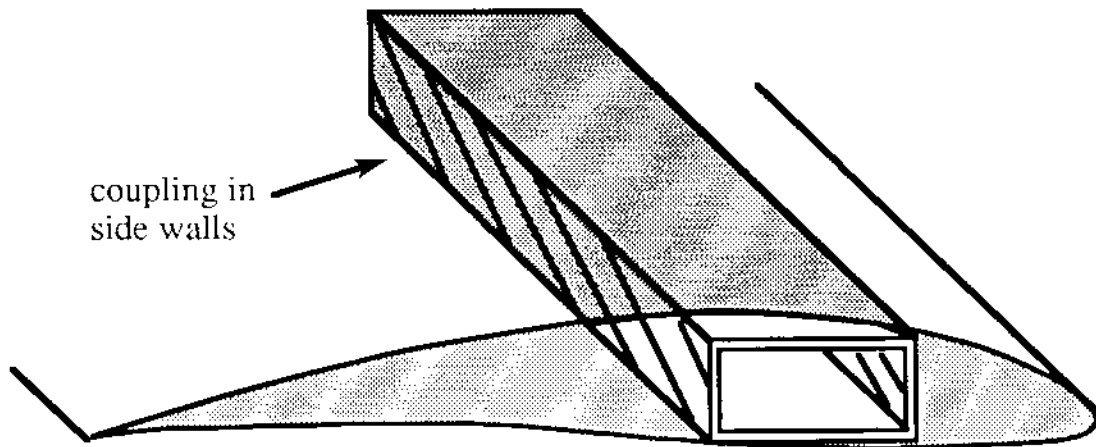


Positive Pitch-Flap Coupling: Flap Up → Pitch Down

Extension-Flap Shear Coupling: Tension → Shear Back

Figure 8.5b Symmetric layup box-beam spar (*symmetric B*)

Symmetric Layup Spar (Case C)

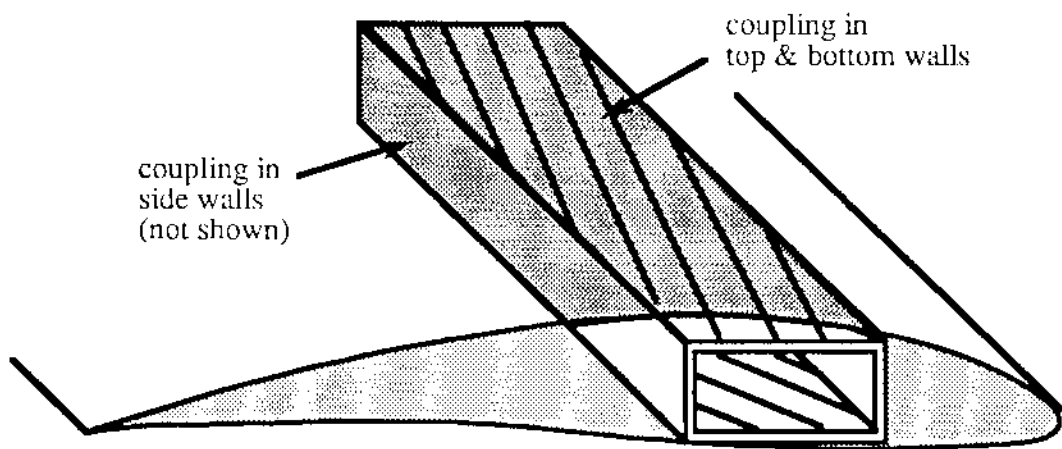


Negative Pitch-Lag Coupling: Lag Back → Pitch Up

Extension-Flap Shear Coupling: Tension → Shear Up

Figure 8.5c Symmetric layup box-beam spar (*symmetric C*)

Anti-symmetric Layup Spar



Extension-Torsion Coupling: Tension → Pitch Down

Bending- Shear Flap-Lag and Lag Flap Couplings

Figure 8.6 Anti-symmetric layup box-beam spar (*anti-symmetric*)

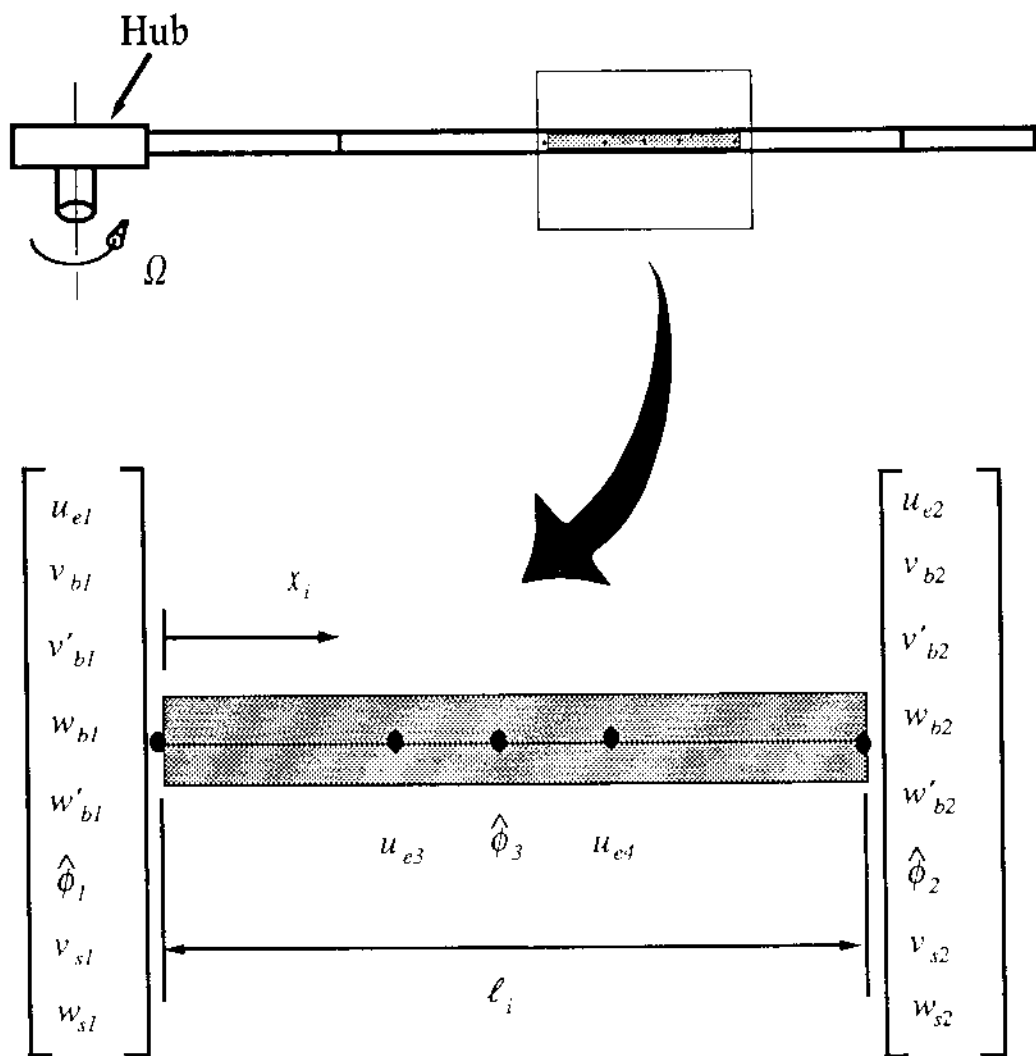
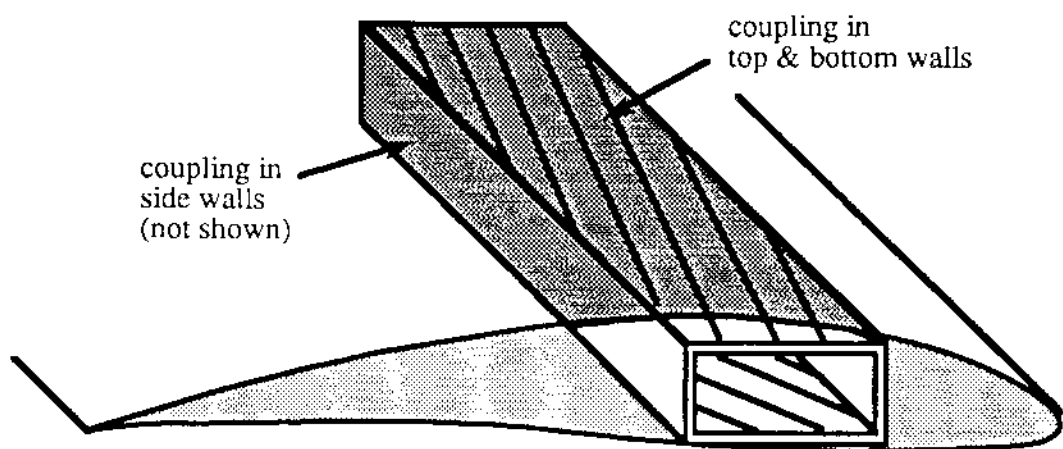


Figure 8.7 Nineteen Degree of Freedom Shear Flexible Beam Element Used for Rotor Blade

Anti-symmetric Layup Spar



Extension-Torsion Coupling: Tension → Pitch Down

Bending- Shear Flap-Lag and Lag Flap Couplings

Figure 8.6 Anti-symmetric layup box-beam spar (*anti-symmetric*)

Chapter 9

DISSIMILAR ROTOR BLADES

Chapter 9

Dissimilar Rotor Blades

Most aerelastic analyses of helicopter blades assume that the blades are identical. This assumption reduces the size of the problem to that of solving for the dynamics of just one blade. However, in reality, the blades may be dissimilar due to manufacturing differences, aging, or because of foreign object damage. These blade-to-blade dissimilarities can have a strong influence on the blade response, loads and aeromechanical stability. For an isotropic rotor (all blades identical), the periodicity of the coefficients of the equation is substantially reduced when the equations are transformed to the fixed reference frame. For example, for an isotropic rotor in hover, because of axial symmetry, all periodic coefficients cancel when the blade equations are transformed to the nonrotating frame. The coupled blade/imb equations can then be solved using techniques suitable for linear, constant coefficient differential equations. With dissimilar blades, the periodic coefficients do not cancel when the blade equations are transformed to the fixed frame, even in the case of hover. Therefore, the analysis of aeromechanical stability of a dissimilar rotor in hover or in ground resonance

always requires mathematical tools such as Floquet theory or time integration to solve the periodic coefficient equations.

The special features of the analysis for a rotor with dissimilar blades are discussed in this chapter [1]. This chapter is divided into three sections. Section 9.1 discusses the blade response and trim analysis for a dissimilar rotor and Section 9.2 discusses the stability analysis for a dissimilar rotor. Section 9.3 discusses the implementation of the dissimilar rotor in UMARC.

9.1 Blade Response and Trim Analysis

The details of the blade response and trim analysis for a rotor with identical blades are discussed in Chapter 4. The blade response for the m th blade can be obtained from the finite element in time equations given as (Eq. 4.41)

$$\mathbf{Q}_m^G + \mathbf{K}_{t_m}^G \Delta \boldsymbol{\xi}_m^{(i)} = 0 \quad (9.1)$$

where

$$\mathbf{Q}_{t_m}^G = \sum_{i=1}^{N_t} \int_{t_i}^{t_{i+1}} \mathbf{N}^T \mathbf{Q}_{t_m} d\psi \quad (9.2)$$

$$\mathbf{K}_{t_m}^G = \sum_{i=1}^{N_t} \int_{t_i}^{t_{i+1}} \mathbf{N}^T \mathbf{K}_{t_m} \mathbf{N} d\psi \quad (9.3)$$

and

$$\Delta \boldsymbol{\xi}^{(i)} = \sum_{i=1}^{N_t} \Delta \boldsymbol{\xi}_i \quad (9.4)$$

where \mathbf{Q}_i and \mathbf{K}_i are the load vector and the tangential stiffness matrix for the i th time finite element. \mathbf{N} is the time shape function. N_t are the number of time

finite elements spanning the azimuth and ξ is the blade response in temporal nodal coordinates.

For identical blades, all four blades have the same response and, therefore, only the response of one blade needs to be calculated. For dissimilar blades, the response of each blade may be different and must be calculated separately.

Once the blade response for each blade has been calculated, the blade loads of the m th blade at any blade section x_0 are calculated using (Eq. 4.77 and 4.78)

$$\begin{Bmatrix} F_x \\ F_y \\ F_z \end{Bmatrix}_m = \int_{x_0}^R \begin{Bmatrix} L_u \\ L_v \\ L_w \end{Bmatrix}_m dx \quad (9.5)$$

$$\begin{Bmatrix} M_x \\ M_y \\ M_z \end{Bmatrix}_m = \int_{x_0}^R \begin{Bmatrix} -L_v(w - w_0) + L_w(v - v_0) + M_u \\ L_u(w - w_0) - L_w(x + u - x_0 - u_0) + M_v \\ -L_u(r - v_0) + L_v(x + u - r_0 - u_0) + M_w \end{Bmatrix}_m dx \quad (9.6)$$

The longitudinal, lateral and vertical loads acting at any section x are given as L_u , L_v and L_w , respectively, and the torsion, flap and lag moment acting at any section x are given as M_u , M_v and M_w , respectively. These section loads are calculated using a force summation method. The loads at section x_0 are obtained by integrating over the blade span from x_0 to R : F_x , F_y and F_z are the longitudinal, lateral and vertical loads acting at the section x_0 , respectively. M_x , M_y and M_z are the torsional, flap and lag bending moments acting at the section x_0 , respectively.

For identical blades, the loads at any section are the same for each blade and are therefore calculated for one blade only. For dissimilar blades, however, the loads for each blade may be different and need to be calculated separately.

Note that these section loads are in the rotating frame and are directed along the undeformed blade axes. To compute the contribution of the blade loads to the hub loads (in the rotating frame), the spanwise integration is carried out from the hub center to the blade tip. For this case, Eqs. 9.5 and 9.6 assume the form:

$$\left\{ \begin{array}{c} F_x \\ F_y \\ F_z \end{array} \right\}_m = \int_0^R \left\{ \begin{array}{c} L_u \\ L_v \\ L_w \end{array} \right\}_m dx \quad (9.7)$$

$$\left\{ \begin{array}{c} M_r \\ M_g \\ M_s \end{array} \right\}_m = \int_0^R \left\{ \begin{array}{c} -L_v w + L_u v + M_u \\ L_u w - L_w (x + u) + M_v \\ -L_u v - L_r (x + u) + M_w \end{array} \right\}_m dx \quad (9.8)$$

The hub loads are needed to calculate the rotor forces T , H , V , M_{T_R} , M_{g_R} and M_{s_R} which are required for the vehicle trim. The rotor hub loads are obtained by summing load contributions from the individual blades. In the fixed frame, the hub loads are expressed as

$$F_X^H(\psi) = \sum_{m=1}^{N_b} (F_x^m \cos \psi_m - F_y^m \sin \psi_m + F_z^m \cos \psi_m \beta_p) \quad (9.9)$$

$$F_Y^H(\psi) = \sum_{m=1}^{N_b} (F_x^m \sin \psi_m + F_y^m \cos \psi_m - F_z^m \sin \psi_m \beta_p) \quad (9.10)$$

$$F_Z^H(\psi) = \sum_{m=1}^{N_b} (F_z^m + F_x^m \beta_p) \quad (9.11)$$

$$M_X^H(\psi) = \sum_{m=1}^{N_b} (M_r^m \cos \psi_m - M_g^m \sin \psi_m - M_s^m \cos \psi_m \beta_p) \quad (9.12)$$

$$M_Y^H(\psi) = \sum_{m=1}^{N_b} (M_r^m \sin \psi_m + M_g^m \cos \psi_m - M_s^m \sin \psi_m \beta_p) \quad (9.13)$$

$$M_Z^H(\psi) = \sum_{m=1}^{N_b} (M_s^m + M_g^m \beta_p) \quad (9.14)$$

where F_x^m , F_y^m , F_z^m are the shear loads and M_r^m , M_g^m , M_s^m are the moments due to the m th blade and are obtained from Eqs. 9.7 and 9.8.

For a tracked rotor (with identical blades) with N_b blades, only the N_b/rev forces and moments are transmitted by the rotor to the fuselage. The tracked rotor therefore acts as a filter for many harmonics. For dissimilar rotors, however, all harmonics of the forces are transmitted to the fuselage. This can lead to large 1/rev loads in the fixed frame for dissimilar blades.

The resulting steady hub loads are used for the six equilibrium equations of the helicopter (3 forces and 3 moment equations about the vehicle center of gravity), which are given as

$$F_1 = D_F \cos \theta_{FP} + H \cos \alpha_s - T \sin \alpha_s \quad (9.15)$$

$$F_2 = Y_F + Y \cos \alpha_s + T \sin \phi_s + T_h \quad (9.16)$$

$$F_3 = T \cos \alpha_s \cos \phi_s - D_F \sin \theta_{FP} + H \sin \alpha_s - Y \sin \phi_s - W - L_H \quad (9.17)$$

$$\begin{aligned} F_4 = M_{x_H} + M_{x_f} + Y_F(\bar{h} \cos \phi_s + y_{eq} \sin \phi_s) \\ + (W(\bar{h} \sin \phi_s - y_{eq} \cos \phi_s) + T_h(\bar{h} - z_H)) \end{aligned} \quad (9.18)$$

$$\begin{aligned} F_5 = M_{y_H} + M_{y_f} + W(\bar{h} \sin \phi_s + x_{eq} \cos \phi_s) \\ - D_F(\bar{h} \cos(\alpha_s + \theta_{FP}) + x_{eq} \sin(\alpha_s + \theta_{FP})) + L_H(x_H - r_{eq}) \end{aligned} \quad (9.19)$$

$$F_6 = M_{z_H} + M_{z_f} + T_h(x_H - x_{eq}) + D_F y_{eq} \cos \alpha_s - Y x_{eq} \cos \phi_s \quad (9.20)$$

A converged trim solution implies that the six vehicle equilibrium equations (shown above) are simultaneously satisfied, and that the blade response has converged.

9.2 Stability Analysis

The details of the stability analysis for a rotor with identical blades are discussed in Chapter 5. The linearized perturbation equations for the rotor/body system can be given as (Eq. 5.19)

$$\begin{aligned}
 & \left\{ \begin{array}{c} \delta q_1 \\ \delta q_2 \\ \vdots \\ \delta q_{N_b} \\ \delta x_F \end{array} \right\}^T \left(\begin{array}{ccccc} M_1 & 0 & \dots & 0 & M_{1F}(q_{1b}) \\ 0 & M_2 & \dots & 0 & M_{2F}(q_{2b}) \\ \vdots & \vdots & \ddots & \vdots & \vdots \\ 0 & 0 & \dots & M_{N_b} & M_{N_b F}(q_{N_bb}) \\ M_{F1} & M_{F2} & \dots & M_{FN_b} & M_{FF} \end{array} \right) \left\{ \begin{array}{c} \Delta \ddot{q}_1 \\ \Delta \ddot{q}_2 \\ \vdots \\ \Delta \ddot{q}_{N_b} \\ \Delta \ddot{x}_F \end{array} \right\} \\
 & + \left[\begin{array}{ccccc} C_1 & 0 & \dots & 0 & C_{1F}(q_{1b}) \\ 0 & C_2 & \dots & 0 & C_{2F}(q_{2b}) \\ \vdots & \vdots & \ddots & \vdots & \vdots \\ 0 & 0 & \dots & C_{N_b} & C_{N_b F}(q_{N_bb}) \\ C_{F1} & C_{F2} & \dots & C_{FN_b} & C_{FF} \end{array} \right] \left\{ \begin{array}{c} \Delta \dot{q}_1 \\ \Delta \dot{q}_2 \\ \vdots \\ \Delta \dot{q}_{N_b} \\ \Delta \dot{x}_F \end{array} \right\} \\
 & + \left[\begin{array}{ccccc} K_1 & 0 & \dots & 0 & K_{1F} & K_{1A} \\ 0 & K_2 & \dots & 0 & K_{2F} & K_{2A} \\ \vdots & \vdots & \ddots & \vdots & \vdots & \vdots \\ 0 & 0 & \dots & K_{N_b} & K_{N_b F} & K_{N_b A} \\ K_{F1} & K_{F2} & \dots & K_{FN_b} & K_{FF} & 0 \end{array} \right] \left\{ \begin{array}{c} \Delta q_1 \\ \Delta q_2 \\ \vdots \\ \Delta q_{N_b} \\ \Delta x_F \\ \Delta \lambda \end{array} \right\} \\
 & \quad \left. \left[\begin{array}{c} \Delta F_1(q_o \Delta q_1, q_o \Delta \dot{q}_1, \dot{q}_o \Delta q_1) \\ \Delta F_2(q_o \Delta q_2, q_o \Delta \dot{q}_2, \dot{q}_o \Delta q_2) \\ \vdots \\ \Delta F_{N_b}(q_o \Delta q_{N_b}, q_o \Delta \dot{q}_{N_b}, \dot{q}_o \Delta q_{N_b}) \\ \Delta F_F \end{array} \right] \right) \quad (9.24)
 \end{aligned}$$

where $\mathbf{q}_1, \mathbf{q}_2, \dots, \mathbf{q}_{N_b}$ are the displacement vectors for blades 1, 2, ..., N_b , respectively (\mathbf{q}_b refers to the displacement vector for the b th blade). Matrices \mathbf{M}_b , \mathbf{C}_b , and \mathbf{K}_b denote respectively the mass, damping, and stiffness matrices for the b th blade. \mathbf{M}_{bF} is the blade-fuselage coupled mass matrix which accounts for the effect of fuselage-induced inertia forces on the b th blade. Similarly, \mathbf{M}_{Fb} is the fuselage-blade coupled mass matrix which accounts for the effect of blade-

induced inertia forces on the fuselage. The coupled damping matrices \mathbf{C}_{bF} , \mathbf{C}_{Fb} and the coupled stiffness matrices \mathbf{K}_{bF} , \mathbf{K}_{Fb} can be similarly interpreted. The matrices \mathbf{M}_{FF} , \mathbf{C}_{FF} and \mathbf{K}_{FF} refer to the fuselage.

For identical blades, the blade response $\mathbf{q}_1, \mathbf{q}_2, \dots, \mathbf{q}_{N_b}$ are the same for each blade and the mass, stiffness and damping matrix for each blade differ only due to different azimuth location of the blade (v). For dissimilar blades, the blade response and matrices may be different for each blade because the blades have different mass and stiffness properties.

Combining the blade equations together gives the rotor equations and the complete set of linearized system equations becomes

$$\begin{bmatrix} \mathbf{M}_{RR} & \mathbf{M}_{RF} & 0 \\ \mathbf{M}_{FR} & \mathbf{M}_{FF} & 0 \\ 0 & 0 & 0 \end{bmatrix} \begin{Bmatrix} \Delta \ddot{\mathbf{q}}_R \\ \Delta \ddot{\mathbf{x}}_F \\ \Delta \ddot{\lambda} \end{Bmatrix} + \begin{bmatrix} \mathbf{C}_{RR} & \mathbf{C}_{RF} & 0 \\ \mathbf{C}_{FR} & \mathbf{C}_{FF} & 0 \\ \mathbf{C}_{\lambda R} & 0 & \mathbf{C}_{\lambda\lambda} \end{bmatrix} \begin{Bmatrix} \Delta \dot{\mathbf{q}}_R \\ \Delta \dot{\mathbf{x}}_F \\ \Delta \lambda \end{Bmatrix} - \begin{bmatrix} \mathbf{K}_{RR} & \mathbf{K}_{RF} & \mathbf{K}_{RA} \\ \mathbf{K}_{FR} & \mathbf{K}_{FF} & 0 \\ \mathbf{K}_{\lambda R} & 0 & \mathbf{K}_{\lambda\lambda} \end{bmatrix} \begin{Bmatrix} \Delta \mathbf{q}_R \\ \Delta \mathbf{x}_F \\ \Delta \lambda \end{Bmatrix} = 0 \quad (9.22)$$

These equations are normalized and converted to first order form as described in Section 5.2.4.1 and Section 5.2.4.2.

$$\dot{\mathbf{Y}} = \mathbf{A}(v)\mathbf{Y} \quad (9.23)$$

where \mathbf{Y} contains the lag, flap and torsion degrees of freedom for each of the N_b blades, as well as the rigid body degrees of freedom.

For a dissimilar rotor, even in the case of hover, periodic coefficients arise because of structural dissimilarities that make the rotor non-axisymmetric. Therefore, Floquet theory or direct numerical integration need to be used to solve the

periodic equations. The constant coefficient approach cannot be used when a rotor has dissimilarities.

9.3 Implementation

The implementation of the dissimilar blade rotor analysis is quite simple. For isotropic rotors, the blade frequency calculation, response analysis, trim analysis and stability analysis are conducted for one blade only. For dissimilar blades, the blade frequency calculation and response and trim analysis are conducted for each blade. The stability analysis incorporates the different contributions from each blade while forming the system matrix.

The current implementation of dissimilar blades in UMARC allows the following properties to vary for each blade at any spanwise finite element along the blade:

1. Flap stiffness EI_y (*EYFAC*)
2. Lag stiffness EI_z (*EZFAC*)
3. Torsion stiffness GI (*GJFAC*)
4. Mass m (*RMASEC*)
5. c_0 (*CZERO_DISS*)
6. d_0 (*DZERO_DISS*)

where c_0 and d_0 are lift and drag parameters defined in

$$C_l = c_0 + c_1 \alpha \quad (9.24)$$

$$C_d = d_0 + d_1 \alpha + d_2 \alpha^2 \quad (9.25)$$

and α is the angle of attack at an airfoil section along the bladespan. The terms in bracket (like $EIYFAC$) are the UMARC coefficients used to input the blade dissimilarity. These are defined for each blade and spatial finite element and have the dimensions: $EIYFAC(MBLADE, MSELT)$, where $MBLADE$ is the number of blades and $MSELT$ is the number of spatial finite elements.

To use the dissimilar blade option in UMARC, the following changes need to be made in the input file:

In the 'rotor-properties' section, put the option:

`! dissimilar blades`

and in the 'blade-properties' section, put the option:

```
! EIYFAC : 5
!          1   1   0.80
!          1   2   0.80
!          1   3   0.80
!          1   4   0.80
!          1   5   0.80
```

The first index (1) indicates the blade number and the second index (1,2,3,4,5) indicates the element numbers where the dissimilarity exists. The third term (0.80) indicates that the flap stiffness is reduced to 0.80 of its baseline value. Finally, the index 5 following the colon after $EIYFAC$ indicates the total number of elements with dissimilarities.

Bibliography

- [1] Wang, J., "Aeromechanical Stability of Helicopters with Dissimilar Blades," UMAERO Report No. 92-11. Also, Doctoral Dissertation, Department of Aerospace Engineering, University of Maryland, 1992.

Part 2

Users Manual

Chapter I

Users Manual

Chapter I

UMARC USER'S GUIDE

This chapter describes the input subsystem for UMARC and explains how to compile and execute UMARC on the IBM mainframe and Sun workstation. Section I.1 describes the input data file, Section I.2 briefly describes user defined input routines, Section I.3 explains how to compile and execute UMARC, and Section I.4 discusses the UMARC input routines.

The input subsystem is illustrated in the data flow diagram in Section I.5. The user provided input data are read from the input data file and are checked for errors and inconsistencies. If the data are valid, they are written in a formatted form to a temporary data file defined by unit 8. This temporary data file is then read by the executive portion of the code (EXEC). This allows usage of the original UMARC input scheme, if required.

I.1 INPUT DATA FILE

This file provides a direct interface between the user and the UMARC executive code. The user directly enters data into this file in the form of numeric input (describing structural properties, aerodynamic properties and operating conditions), indicators (to indicate users of modelling, analysis and output options), flags (to set limits on the various iteration

loops) and convergence criteria. Input in the data file is identified by UMARC through READ statements and does not require compilation.

I.1.1 Description

Typical input data files are presented in Section I.6. As shown in the examples, all of the input in a data file is grouped into data blocks. A data block consists of related data. For example, all the data pertaining to the blade are grouped in the data block named BLADE_PROPERTIES.

The first entry in a data block indicates the data block name (e.g., ROTOR_PROPERTIES, BLADE_PROPERTIES, ANALYSIS_OPTIONS, etc.). An example of a data block is shown below. The input formatting is dynamic, i.e., input to a data block can be entered in any arbitrary sequence. Should there be a mistyped entry or a data conflict, an error message is issued indicating the problem and, if possible, suggesting a remedy. If UMARC detects a missing data item from the data block, it supplies either a default value for that entry or issues an error message telling the user to supply missing data. If UMARC supplies a default value, the user is informed of this action.

Example : Data Block

```
*=====
  ROTOR_PROPERTIES
*=====
! ROTOR_TYPE   : BMR   SINGLE_FLEXBEAM   RIGID_PITCH_LINK
! ROTOR_NAME  : ITR
! NO_OF_BLADES = 4
! LOCK_NUMBER = 5
```

Each data item in the data file is represented by an entry name or keyword. Keywords are selected to suggest the nature of the input and are usually different from the FORTRAN variable name used in the code. For example, the keyword for the number of blades is NO_OF_BLADES and the corresponding FORTRAN variable is NBLADE. There may not be any direct correspondence between the entry names and the FORTRAN variables. For example, if the keyword for the rotor type is

```
ROTOR_TYPE : BMR SINGLE_FLEXBEAM LAG_PIN SOFT_PITCH_LINK
```

then UMARC understands that three rotor blade segments are to be used (main blade + one flexbeam + torque tube) and the executive variable NSEG is set to 3. In addition, because the number of boundary conditions for this blade type is eight, the executive variable NBC is set to 8.

I.1.2 Dynamic Formatting

Dynamic formatting makes the input scheme user friendly. The input data need not follow any sequence or format. The beginning of a data block is indicated if the first character in a line is not '*' or '!'. The subsequent lines must have '!' in the first column to indicate continuation of data. Any line with '*' in the first column is considered a comment line. Blank lines are allowed and are not considered part of the data. After each keyword, the data can be entered in a free format, separated by a single delimiter, a group of delimiters, or with blanks. Valid delimiters include the following set: { * ! : ; ' " , = }. Also, the data can begin and end anywhere after the keyword and can continue on subsequent lines.

I.1.3 Data Dictionary

The data dictionary (Table I-1) in Section I.8 explains the data items associated with each data block. There are seven columns in the table. The first column gives the keyword and the second column gives the associated FORTRAN variable in the code. The type of the

data item is provided in column 3. The data item can be a real variable, integer variable or character variable. Column 4 shows the dimensions a particular data item is assigned in the code. Column 5 lists the default values, if any, for a particular data item. The next column provides typical values for the various data items. Column 7 shows the allowable range for a particular data variable. It should be noted that all the numeric data entries are nondimensional. Table I-2 in Section I.8 explains the nondimensionalization of important input variables.

I.2 USER-DEFINED ROUTINES

Sometimes it is expedient to read data directly from user defined routines, e.g., aerodynamic properties and twist distribution along the span. Though these can be read using the input scheme, the nature of the complex aerodynamic data and twist distributions make user defined routines simpler to implement. A typical user defined routine is TWISTX. TWISTX calculates the twist and twist rate along the span of the blade for the ITR-BMR rotor.

I.3. COMPIILATION AND EXECUTION OF UMARC

Section I.3.1 presents the FORTRAN files necessary to run UMARC. Sections I.3.2 and I.3.3 describe the steps necessary to compile and execute UMARC, respectively, on the IBM mainframe. Section I.3.4 contains listings of the command macros required for compilation and execution on IBM. Sections I.3.5 and I.3.6 explain steps required to compile and execute UMARC, respectively, on SUN. Structure charts for the entire code are provided in Section I.5. A sample output file may be found in Section I.7.

I.3.1 UMARC Source Code Files

UMARC subroutines are contained in the following FORTRAN source code files:

UMRINP

UM1

UM2

UM3

UM4

BLDVIB

TRIM

STAB

AEROMX

ASBGBM

MATH

UTILS

WAKES

CBEAM

The following files contain the PARAMETER and COMMON statements which are included in UMARC via INCLUDE statements :

PARA

THPLNK

LINK

SFTLNK

LINUNS

DFQ2

STRUC

AEROD

CPLTRM

GAUSS

BASIC

RADSHR

MODE

FLOW

DAMP

SWEPT

STRUCC

IVECBE

IVECTS

ISWBE

ISWTS

Notes:

1. The users on the IBM system must terminate the source file names with a blank followed by FORTRAN to indicate to the system that the source files are written in the Fortran language.

Examples: UMI FORTRAN

WAKES FORTRAN

Users on the Sun system must terminate the source file names with '.f' to indicate to the system that the source files are written in the Fortran language.

Examples: um1.f

wakes.f

2. The users on the IBM system must terminate the INCLUDE file names with a blank followed by COPY.

Examples: PARA COPY

AEROD COPY

Users on the Sun system may leave the INCLUDE file names as they appear in the list. The user must however ensure that the case of alphabetic characters used in naming these files matches that of the source codes. Thus, if the source codes are written in lower case, the INCLUDE file names will also be in lower case.

Examples: para

aerod

Dimension statements in UMARC have been parameterized to i) optimize memory requirement, ii) facilitate understanding and debugging of the code, and iii) aid future enhancements of the program. All the dimension parameters are included in the PARA file and these must match the associated FORTRAN variables which are assigned values through keywords in the input data file. Therefore, after setting up the input file, the parameters in the PARA file should be assigned values as follows before compiling.

PARAMETER	VARIABLE	RELATED KEYWORD
LSFT	LNKSFT	SOFT_PITCH_LINK
MSELT	NSELT	NO_SPACE_ELEMENTS
MTELT	NTELT	NO_TIME_ELEMENTS
MSECT	LSECT	(NODES_PER_TIME_ELEM) - 1
MBLADE	NBLADE	NO_BLADES
MHUB	NHUB	NO_HUB_DOF Note: if NO_HUB_DOF is set to 0 in the input data file, MHUB must be set to 5 in PARA COPY
IFUS	INDFUS	=1 if NO_HUB_DOF > 0 = 0 if NO_HUB_DOF = 0
IDYNFL	IDYN	DYNAMIC_INFLOW
MMODET	NFLAP+NLAG+NTORSN +NAXIAL	NO_FLAP_MODES + NO_LAG_MODES + NO_TORSION_MODES + NO_AXIAL_MODES
MMODES	NFLAP+NLAG+NTORSN	NO_FLAP_MODES + NO_LAG_MODES + NO_TORSION_MODES

In addition, parameter MBCS (in PARA file) must be defined as follows:

ROTOR TYPE	MBCS
BMR with pin	9 - LSFT
BMR without pin	7 - LSFT
Articulated	4 - LSFT
Hingeless (Isotropic)	6 - LSFT
Hingeless (Composite)	8 - LSFT

I.3.2 Compiling UMARC (for IBM users only)

There are five steps required to compile UMARC. First, UMRINP is compiled with an option to inform the compiler that the maximum character length is 7200. Second, the MAC executive file is invoked from FILELIST to activate the INCLUDE statements. Third, the FORTV executive file is invoked from FILELIST to compile UMARC1, UMARC2, UMARC3, EIGENS, MATH and UTILS. Fourth, the GL executive file is executed to include FORTRAN system libraries. Then the WAKES file is compiled. The actual commands issued are summarized below:

1. FORTVS UMRINP (CHARLEN(7200))
2. MAC
3. FORTV
4. GL
5. FORTVS WAKES

Notes:

1. If changes are made to an INCLUDE (COPY) file then only the following steps need to be performed:

MAC

FORTV

2. If changes are made to a source code file only, then only that file needs to be compiled again, not all of the files. This is done as follows:

GL

FORTVS <filename>

I.3.3 Executing UMARC (for IBM users only)

There are five basic steps required to execute UMARC. First, 12 megabytes of memory must be allocated. Second, the IPL CMS command must be issued to return to system commands. Third, the RNRT executive file is invoked to define the I/O data files and link and run UMARC. Then memory is reset back to 2 megabytes and the IPL CMS command is once again executed. The actual commands issued are summarized below:

1. ST12
2. IPL CMS
3. RNRT
4. ST2
5. IPL CMS

Notes:

1. Data file names can be changed by editing the RNRT EXEC file and modifying the FILEDEF statements.

2. To run the code with a modified version of a source code file with a different name, the LOAD statement can be modified in RNRT EXEC.

Example: modified version of UMARC1 with name MUMARC1

LOAD UMRINP MUMARC1(rest of line same)

I.3.4 Command Macros

MAC EXEC :

```
/* */  
" DISCARD UMLIB MACLIB A "  
" MACLIB GEN UMLIB PARA DFQ2 STRUC AEROD CPLTRM GAUSS "  
" MACLIB ADD UMLIB BASIC RADSHR LINUNS MODE FLOW "  
" MACLIB ADD DAMP LINK SFTLINK "
```

FORTV EXEC:

```
/* */  
" GLOBAL MACLIB UMLIB "  
" FORTVS UMARC1 "  
" DISCARD UMARC1 LISTING A "  
" GLOBAL MACLIB UMLIB "  
" FORTVS UMARC2 "  
" DISCARD UMARC2 LISTING A "  
" GLOBAL MACLIB UMLIB "  
" FORTVS UMARC3 "  
" DISCARD UMARC3 LISTING A "  
" GLOBAL MACLIB UMLIB "  
" FORTVS UTILS "  
" DISCARD UTILS LISTING A "  
" GLOBAL MACLIB UMLIB "  
" FORTVS MATH "  
" DISCARD MATH LISTING A "
```

GL EXEC:

```
/* */  
" GLOBAL MACLIB UMLIB "
```

ST12 EXEC :

```
/* */  
" DEFINE STORAGE 12M "
```

ST2 EXEC :

```
/* */  
" DEFINE STORAGE 2M "
```

RNRT EXEC :

```
/* */  
" FILEDEF 5 DISK BMR DATA A (PERM "  
" FILEDEF 8 DISK TEMPINP DATA A (PERM "  
" FILEDEF 9 DISK UMARC OUTPUT A (PERM "  
" GLOBAL TXTLIB VLNKMLIB VFORTLIB CMSLIB IMSLD "  
" LOAD UMRINP UMARC1 UMARC2 UMARC3 WAKES UTILS MATH (START "  
" LOAD UMRINP UMARC1 UMARC2 UMARC3 WAKES UTILS MATH (START "
```

1.3.5 Compiling UMARC (for Sun users only)

Before compiling UMARC on the Sun workstation, the user must ensure the following:

1. All the Fortran source files listed in Section I.3.1 terminate with ".f" (e.g., umrinp.f).
2. All the INCLUDE statements in the source files have the following format:

```
include ' file name '
```

Example: include ' para '

3. All the alphabetic characters appearing in the source files, include files and data files have the same case (upper case or lower case). For example, you wish all files to be in the lower case format and one of the files, say MATH.F, has alphabetic entries in upper case. Then, the following UNIX command may be used to transform contents of math.f file to lower case:

```
tr A-Z a-z < MATH.F > math.f
```

The user may compile all the source files individually and then link them into a single executable. Alternatively, he or she may use the macro 'makefile' provide on the next page to perform both compilation and linking with a single command:

```
make -f makefile
```

92/08/07
14:54:36

makefile

```

makefile

# Identify compiled versions of source codes to be linked into
# an executable
um3.o: um3.c thplink sftlink dfq2 struc aeroe optitm gauss basic radsh\ 
linus mode flow link swept para vecbe ivects struc lswbe lswts\ 
f77 -g -c S*.f

um4.o: um4.c thplink sftlink dfq2 struc aeroe optitm gauss basic radsh\ 
linus mode flow link swept para vecbe ivects struc lswbe lswts\ 
f77 -g -c S*.f

utilis.o: utilis.f thplink sftlink dfq2 struc aeroe optitm gauss basic radsh\ 
linus mode flow link swept para vecbe ivects struc lswbe lswts\ 
f77 -g -c S*.f

wakes.o: wakes.f thplink sftlink dfq2 struc aeroe optitm gauss basic radsh\ 
linus mode flow link swept para vecbe ivects struc lswbe lswts\ 
f77 -g -c S*.f

math.o: math.f thplink dfq2 struc aeroe optitm gauss basic radsh\ 
linus mode flow link swept para vecbe ivects struc lswbe lswts\ 
f77 -g -c S*.f

stab.o: stab.f thplink sftlink dfq2 struc aeroe optitm gauss basic radsh\ 
linus mode flow link swept para vecbe ivects struc lswbe lswts\ 
f77 -g -c S*.f

stab.o: stab.f thplink sftlink dfq2 struc aeroe optitm gauss basic radsh\ 
linus mode flow link swept para vecbe ivects struc lswbe lswts\ 
f77 -g -c S*.f

trim.o: trim.f thplink sftlink dfq2 struc aeroe optitm gauss basic radsh\ 
linus mode flow link swept para vecbe ivects struc lswbe lswts\ 
f77 -g -c S*.f

asbgm.o: asbgm.f thplink sftlink dfq2 struc aeroe optitm gauss basic radsh\ 
linus mode flow link swept para vecbe ivects struc lswbe lswts\ 
f77 -g -c S*.f

aeromx.o: aeromx.f thplink sftlink dfq2 struc aeroe optitm gauss basic radsh\ 
linus mode flow link swept para vecbe ivects struc lswbe lswts\ 
f77 -g -c S*.f

hubd.o: hubd.f thplink sftlink dfq2 struc aeroe optitm gauss basic radsh\ 
linus mode flow link swept para vecbe ivects struc lswbe lswts\ 
f77 -g -c S*.f

umb.o: umb.f thplink sftlink dfq2 struc aeroe optitm gauss basic radsh\ 
linus mode flow link swept para vecbe ivects struc lswbe lswts\ 
f77 -g -c S*.f

```

Comments have been inserted in the macro file (identified by # signs) to explain its performance. The main advantage is that the compilation is automated; only those files are compiled which have been changed (edited). In case the para file is changed, all the source files are automatically recompiled. After compilation, the object files are linked into a single executable named 'um'.

I.3.6 Executing UMARC (for Sun users)

The execution of UMARC can be initiated by issuing the following command:

```
um < input_data_file > output_file &
```

where `input_data_file` is the input data file name. The specification of `output_file` is optional. If `output_file` name is supplied, the run-time terminal output, which normally would be directed to the screen, is instead stored in this file. The usage of ampersand, `&`, is also optional; it directs the computer to carry out execution in the background. Here are some examples of the execution command:

Examples: `um < gaz.data`

`um < bo105.data > bo105.output`

`um < bmr.data > bmr.out &`

I.4 DESCRIPTION OF UMARC INPUT ROUTINES

The UMARC main program (EXEC) invokes the routines UMRINP, UINP2, and UINP3 to read input from the data file. UMRINP, UINP2, and UINP3 call several subroutines (see Structure Chart in Section I.5). These subroutines provide the interface between the user and the code. Brief descriptions of these subroutines follow in Section I.4.1 through Section I.4.6. Section I.4.7 presents the actual FORTRAN statements used to read the various input data and Section I.4.8 describes how to add or delete input variables in UMARC.

I.4.1 Subroutine DINPUT

Function :

This routine reads each data block as a line of characters. It skips blank lines and all lines whose first character positions are '*'. It identifies the start of the block if the first character is not '*' or '!'. If the first character positions is '!', it understands the data is continuing and does not go beyond the last continuation line. It fills up all the delimiter positions with blanks. Then it separates all the substrings, and identifies their first and last character positions.

If there is an error while reading the data block an error code is returned. A maximum of 100 lines with a field width of 72 characters are allowed in each data block. This 100 line limitation is due to the character length definition of DATA. Currently a character length of 7200 is used. This can be changed in the subroutines UMRINP, UINP2 and UINP3 and all the subroutines called by them. In addition, the compile command for the input routines must be modified for the IBM.

Parent routines:	UMRINP, UINP2, and UINP3
Call Statement :	CALL DINPUT(IER)
Internal Variables:	DATA, IB(400),IE(0:400) CHARACTER*7200 DATA, IER*6
IER:	= 'NODATA' if no data is found = 'EXE100' if number of input data lines exceed 100
DATA :	the input data in each block is stored here
IB(i):	first character position of the substring number i
IE(i):	last character position of the substring number i

I.4.2 Subroutine DATCHK

Function :

This routine is used to check if a keyword is present in the data block. If the keyword is present it returns an error code of ' ' for IER. If the keyword is not present it returns an error code of 'NOTAVL' for IER. This information is suitably used by the calling routine.

Parent routines: UMRINP, UINP2, and UINP3

Call Statement: CALL DATCHK(IER,'keyword')

keyword: the keyword to be checked for its presence

I.4.3 Subroutine DATCHR

Function :

This routine is used to read character variables for the keyword. It goes inside the data block and looks for the keyword. If it is present it reads the next substring for this keyword. Otherwise an error code of 'NOTAVL' is returned. If the keyword is found, and is the last one for the data block, but there is no data it returns an error code of 'NOVALU'. To determine if no data was available for a keyword other than the last, verification checks on the data returned to the parent routine must be made.

Parent routines: UMRINP UINP2, and UINP3

Call Statement: CALL DATCHR(IER,'keyword',CHRVAR)

CHRVAR: the data immediately after the keyword is stored in this
 character variable

I.4.4 Subroutine DATCHD

Function :

This subroutine performs the same basic function as DATCHR only it is used to read multiple strings of character data for an array of character strings.

Parent routines:	UMRINP, UINP2, and UINP3
Call Statement:	CALL DATCHD(IER,'keyword',ND,CHRVAR)
ND:	# of character values connected with the keyword (dimension)
CHRVAR:	the data immediately after the keyword is stored in this character string array (of size ND)

I.4.5 Subroutine DATFLO

Function :

This routine is used to read floating point variables for the keyword. It goes inside the data block and looks for the keyword. If it is present it reads the next available substrings and stores them in the supplied real variable. If the dimension is more than one, it reads the data in the next 'dimension' number of substrings. If the keyword is not found an error is returned. If the keyword is present but no data is present or data of the wrong type is present, an error code of 'NOVALU' is returned.

Parent routines:	UMRINP, UINP2, and UINP3
Call Statement:	CALL DATFLO(IER,'keyword',ND,RV)
ND:	# of real values connected with the keyword (dimension)
RV:	the data after the keyword stored in this variable (of size ND)

I.4.6 Subroutine DATINT

Function :

This does the same job as DATFLO but for integers.

Parent routine: UMRINP, UINP2, and UINP3

Call Statement: CALL DATINT(IER,'keyword',ND,IV)

I.4.7 FORTRAN Implementation Details

Specific examples are provided below to explain how the input scheme is implemented in UMARC. The statements that follow are found in UMRINP, UINP2 and UINP3. The actual FORTRAN statements are listed on the left hand side and explanatory comments are listed on the right hand side. Note that reading an integer variable is performed in the same way as a real variable, only using DATINT instead of DATFLO. Similarly, reading a character array is implemented in the same way as reading a character variable, only with DATCHD instead of DATCHR. Specific examples can be found in the UMRINP, UINP2 and UINP3 subroutines and should be used as a reference for adding or deleting input variables (Section I.4.8). Note that the input is echoed as output in the UMARC output file, unit 9.

Reading a Data Block

```
CALL INPUT(IER)
IF (IER .EQ. 'NODATA') THEN
  WRITE (9,200)
  GOTO 99
END IF

IF (IER .EQ. 'EXED100') THEN
  WRITE (9,201)
  GOTO 99
END IF
```

reads the data block
if IER=NODATA (no data available),
job will be terminated through control
99.

if # of input data lines exceed 100,
job will be terminated through control
99.

Reading a Real Variable with Default Option

```
CALL DATFLO(IER,'CG_HUB_OFFSET_X',1,XCG)
IF (IER .EQ. 'NOTAVL') THEN
  XCG = 0.0
  CHR30 = 'CG_HUB_OFFSET_X'
  WRITE (9,204) CHR30,XCG
END IF

IF (IER .EQ. 'NOVALU') THEN
  WRITE (9,203) 'CG_HUB_OFFSET_X'
  IERROR = IERROR + 1
END IF

CHR30 = 'CG_HUB_OFFSET_X'
IF (IER .NE. 'NOTAVL') WRITE (9,207) CHR30,XCG
```

reads XCG after the keyword CG_HUB_OFFSET_X. 1 is the dimension.
if IER=NOTAVL (not available) then XCG is given a default value of 0.0.

if IER=NOVALU (no data or unidentified data after the keyword), error message is issued and the error count is increased by 1.

Reading a Real Variable without Default Option

```
CALL DATFLO(IER,'CT/SIGMA',1,CTSIG)
IF (IER .EQ. 'NOTAVL') THEN
  WRITE (9,202) 'CT/SIGMA'
  IERROR = IERROR + 1
END IF

IF (IER .EQ. 'NOVALU') THEN
  WRITE (9,203) 'CT/SIGMA'
  IERROR = IERROR + 1
END IF

CHR30 = 'CT/SIGMA'
WRITE (9,207) CHR30, CTSIG
```

reads CTSIG after the keyword CT/SIGMA. 1 is the dimension.
if IER=NOTAVL (not available), error message is issued and the error count is increased by 1.

if IER=NOVALU (no data or unidentified data after the keyword), error message is issued and the error count is increased by 1.

Reading a Character Variable With Default Option

```
CALL DATCHR(IER,'COUPLED_TRIM_SCHEME',SCHEME))
IF (IER .EQ. 'NOTAVL') THEN
  SCHEME = 'MARQ_NEWTON'
  CHR30 = 'COUPLED_TRIM_SCHEME'
  WRITE(9,215) CHR30, SCHEME
END IF

IF (IER .EQ. 'NOVALU') THEN
  WRITE (9,203) 'COUPLED_TRIM_SCHEME'
  IERROR = IERROR + 1
ENDIF
```

reads character variable SCHEME after the keyword COUPLED_TRIM_SCHEME.
if keyword is not found then SCHEME is assigned default value MARQ_NEWTON.

if no data found after the keyword, error message is issued and error count increased by 1.

```

IF SCHEME = 'MARQ_NEWTON' THEN
  ITSCHM = 0
ELSE IF SCHEME = 'NEWTON' THEN
  ITSCHM = 1
ELSE
  ITSCHM = 0
END IF

IF (IER .NE. NOTAVL) THEN
  CHR30 = 'COUPLED_TRIM_SCHEME'
  WRITE (9,206) CHR30, SCHEME
END IF

```

assign the flag ITSCHM a value based on the character input. if the input is not a valid string, then assign the default value of 0 to ITSCHM.

Reading a Character Variable Without Default Option

```

CALL DATCHR(IER,'COUPLED_TRIM_SCHEME',SCHEME))

IF (IER .EQ. NOTAVL) THEN
  WRITE (9,202) 'COUPLED_TRIM_SCHEME'
  IERROR = IERROR + 1
END IF

IF (IER.EQ.'NOVALU') THEN
  WRITE (9,203) 'COUPLED_TRIM_SCHEME'
  IERROR = IERROR + 1
ENDIF

IF SCHEME = 'MARQ_NEWTON' THEN
  ITSCHM = 0
ELSE IF SCHEME = 'NEWTON' THEN
  ITSCHM = 1
ELSE
  WRITE (9,203) 'COUPLED_TRIM_SCHEME'
  IERROR = IERROR + 1
END IF

CHR30 = 'COUPLED_TRIM_SCHEME'
WRITE(9,206) CHR30, SCHEME

```

reads character variable SCHEME after the keyword COUPLED_TRIM_SCHEME. if IER=NOTAVL (not available) error message is issued and error count increased by 1.

if no data found after the keyword, error message is issued and error count increased by 1.

assign the flag ITSCHM a value based on the character input. if the input is not a valid string, then error message is issued and error count is increased by 1.

Checking if a Keyword is Present

CALL DATCHK(IER,'LINEAR_INFLOW') IF(IER .NE. 'NOTAVL') INCODE=1	looks for the keyword 'LINEAR_INFLOW'. if IER is not equal to NOTAVL (not available), INCODE=1. In the program INCODE=1 means linear inflow.
--	--

I.4.8 Adding/Deleting Input Variables

Input data are obtained from the input data file via the subroutines UMRINP, UINP2, and UINP3. They are written to the temporary data file in UINP3. They are read from the temporary data file in the routine EXEC. This section discusses how to add or delete input variables in UMARC.

UMRINP reads input variables related to: title, rotor properties, blade properties, fuselage properties, and tail properties. UINP2 reads input variables related to: airfoil properties, flight condition and aerodynamics. UINP3 reads input variables related to: trim analysis, stability analysis, and output options. Variables should be added in the section of code where related variables are processed (e.g., a variable relating to trim convergence criteria would be added in the trim analysis section of UINP3). To add or delete input variables, the following steps must be taken:

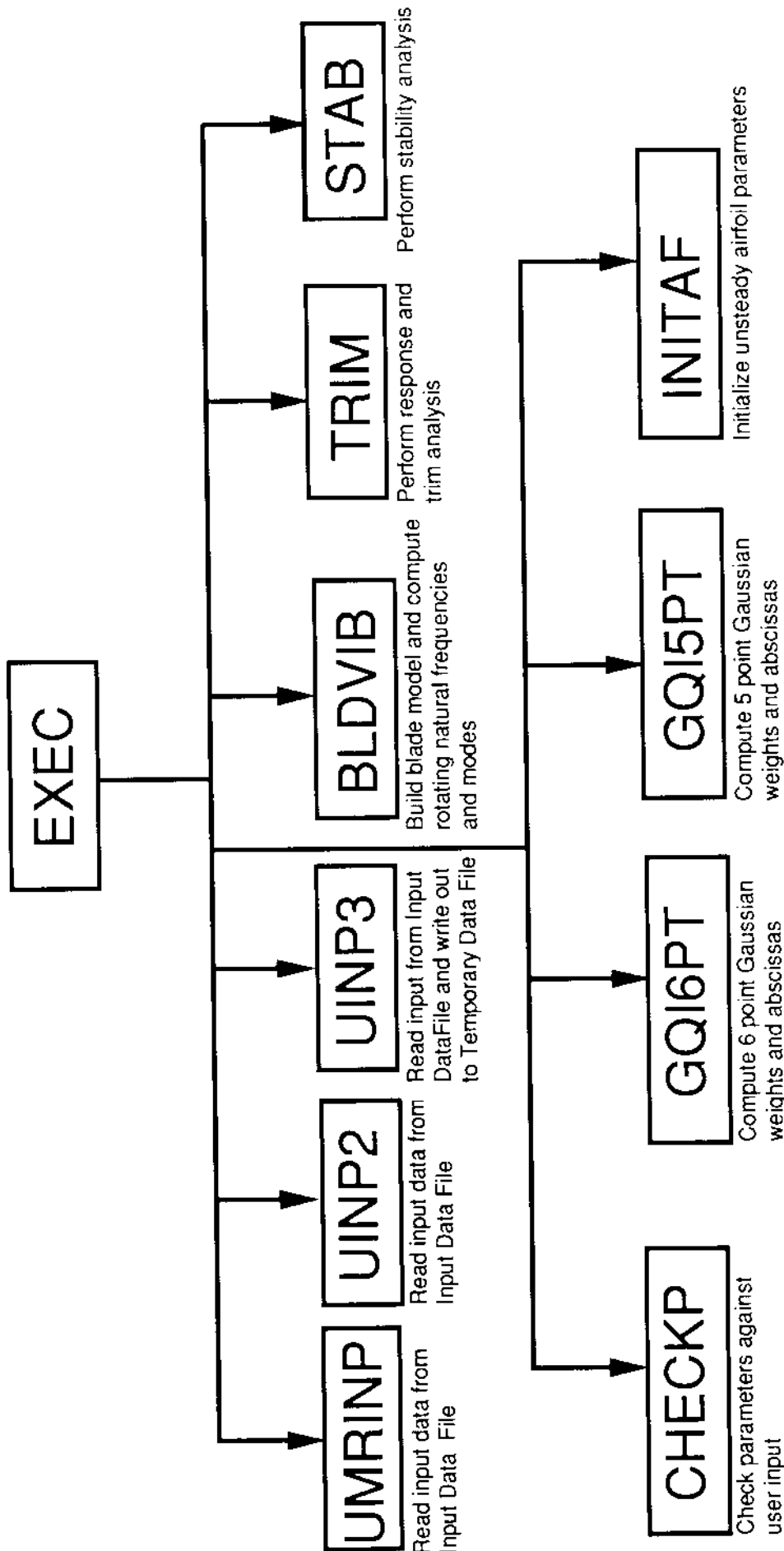
1. Add (delete) FORTRAN code for the input variables as described in Section I.4.7 in the appropriate section of UMRINP, UINP2, or UINP3. All new variables must be included in a new COMMON block in UMRINP, UINP2, and UINP3. This is how data is shared between the three routines for purposes of writing to the temporary data file in UINP3. If variables are deleted, then delete them from the COMMON blocks they are contained in (in all three routines.)

2. In UINP3, add (delete) WRITE statements (to the temporary data file) corresponding to the new (deleted) input variables. This block of code appears at the end of UINP3. Note that additional variables can be written out in one or more WRITE statements at the user's discretion.

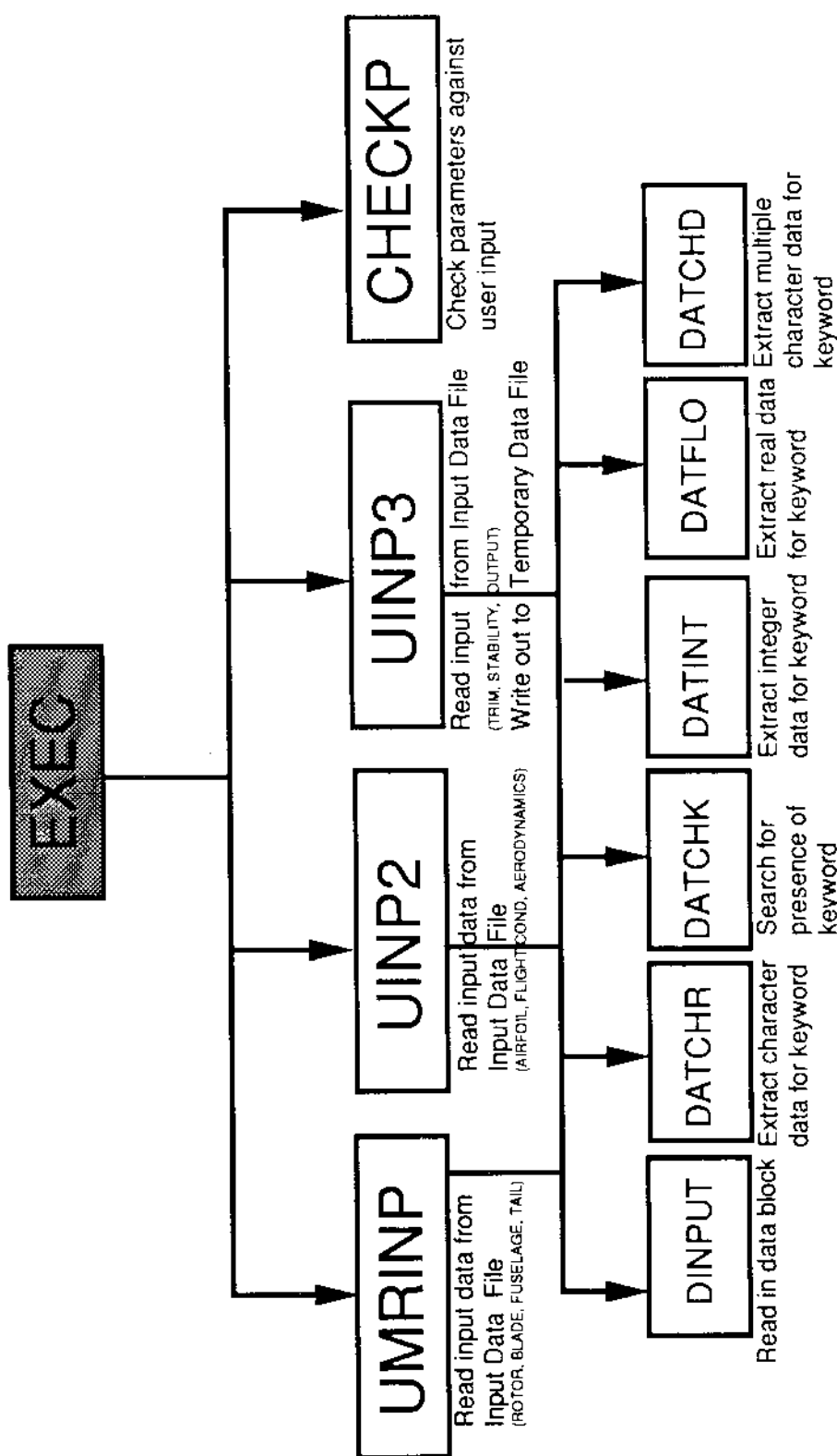
3. In EXEC, add (delete) READ statements (from the temporary data file) corresponding to the new (deleted) variables. The READs must be added in the same order as the WRITEs.

I.5 UMARC STRUCTURE CHARTS

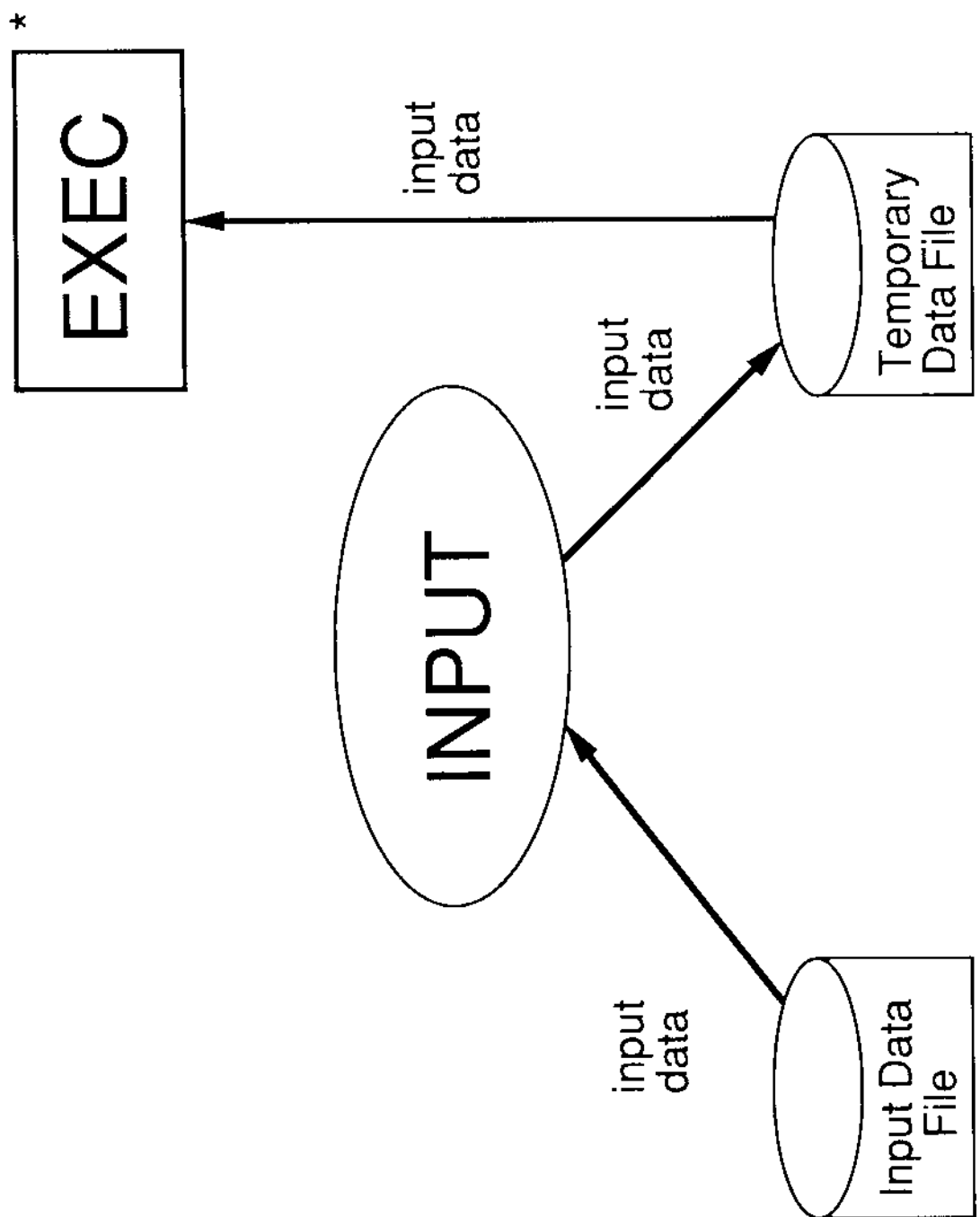
This section presents structure charts depicting the static organization of UMARC. In addition, the function of each subroutine is indicated.



EXEC STRUCTURE CHART (FIRST LEVEL ONLY)

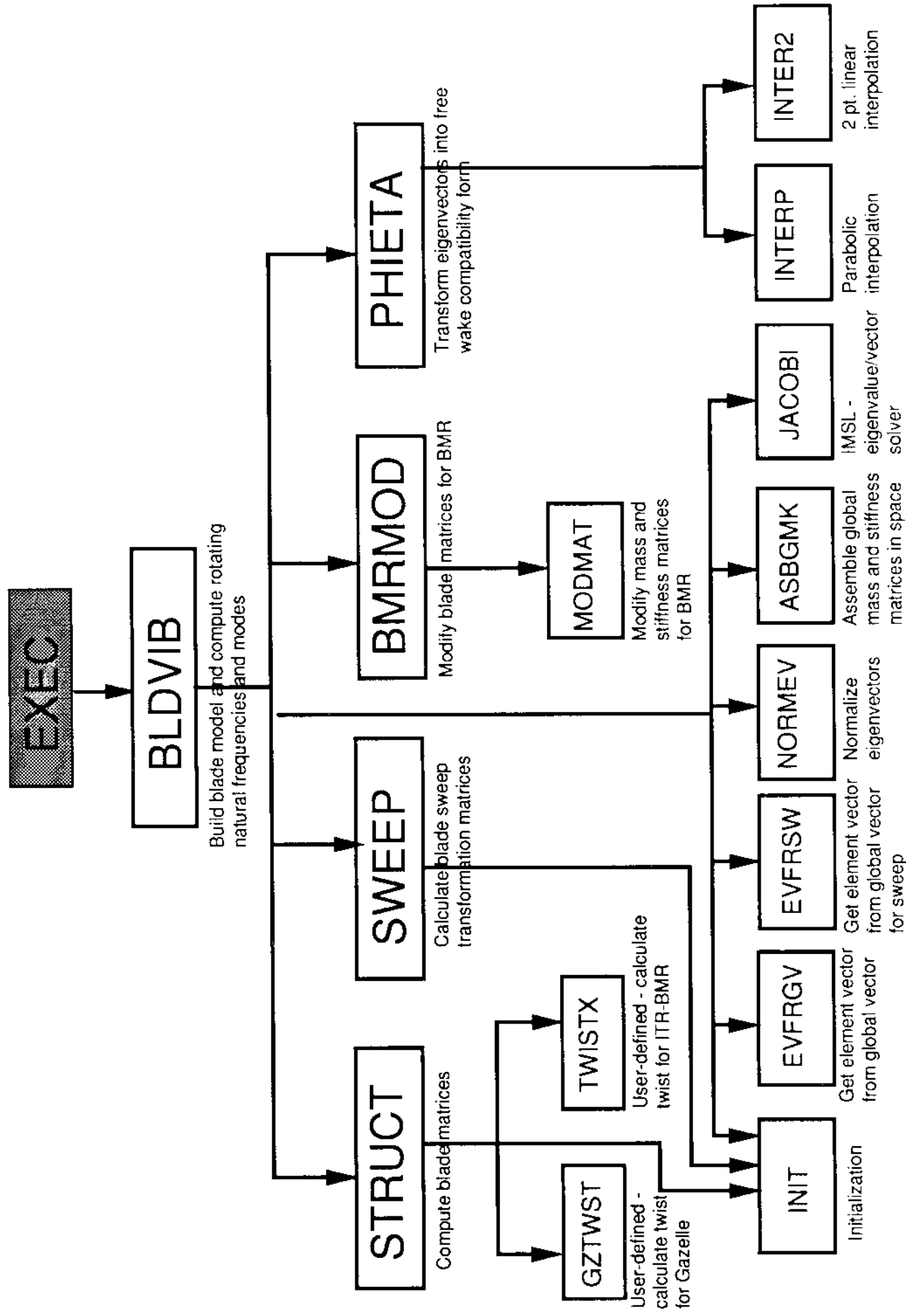


INPUT SUBSYSTEM STRUCTURE CHART

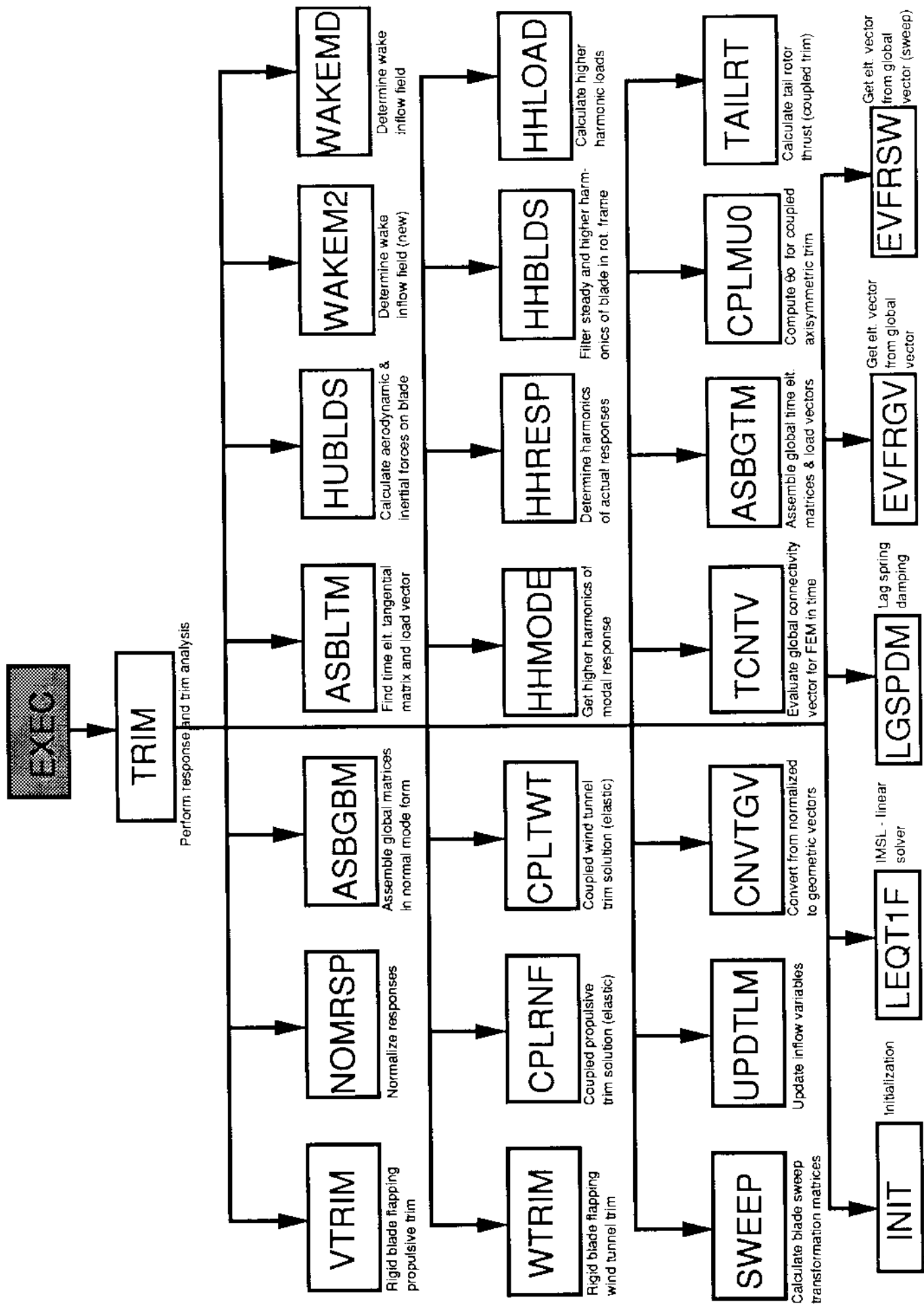


* User-Defined routines are not shown

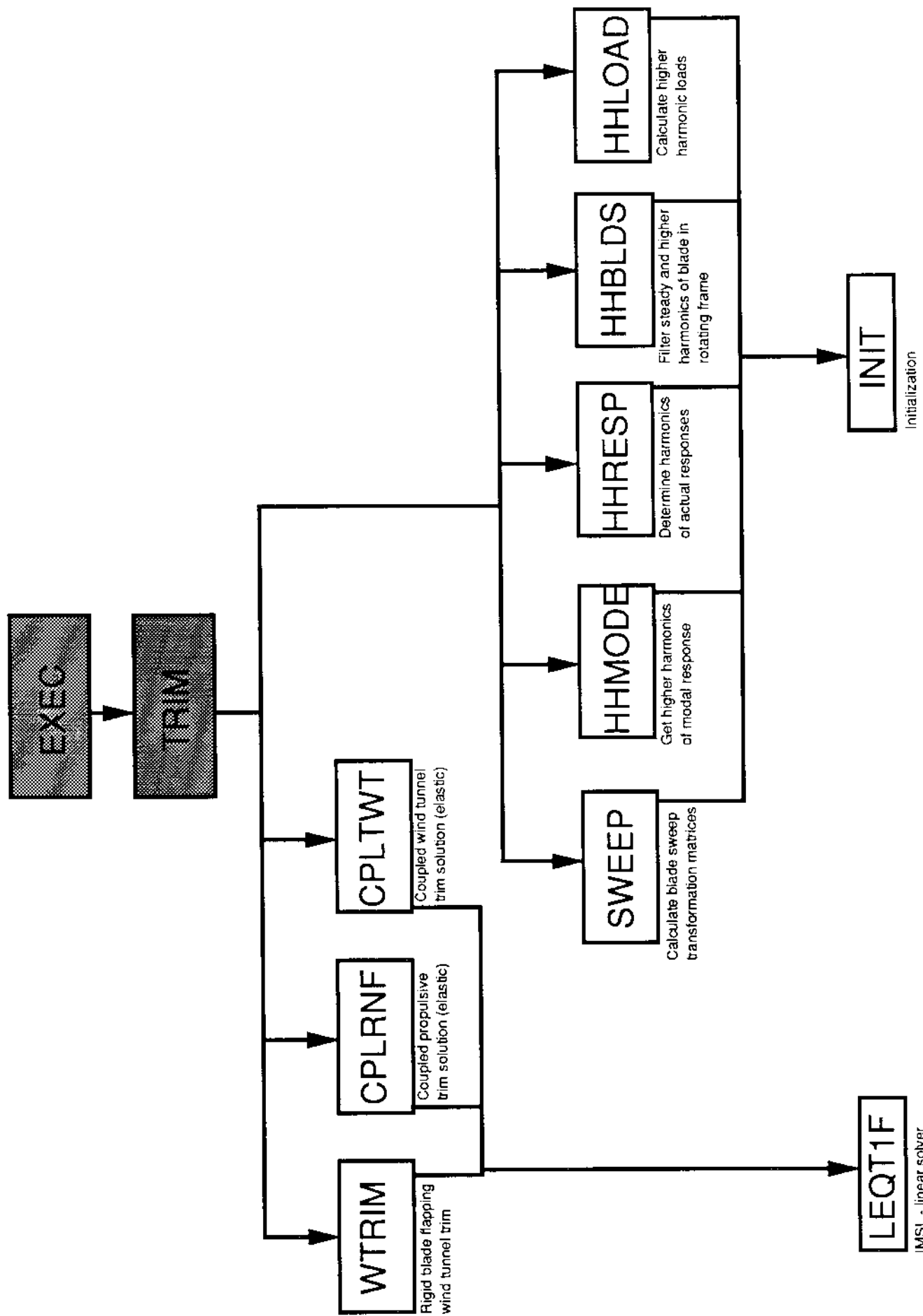
Data Flow Diagram for Input Subsystem



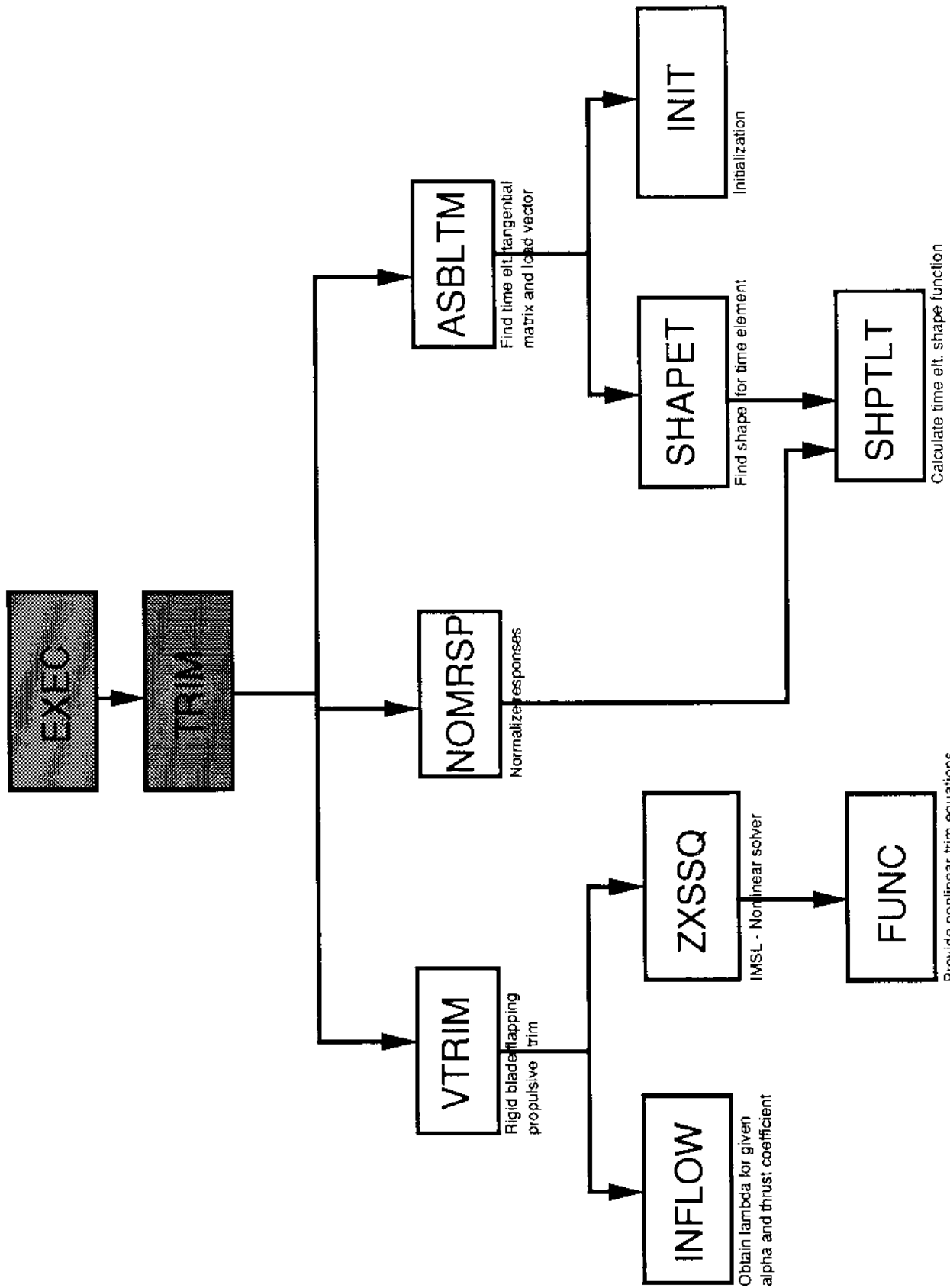
BLDVIB STRUCTURE CHART



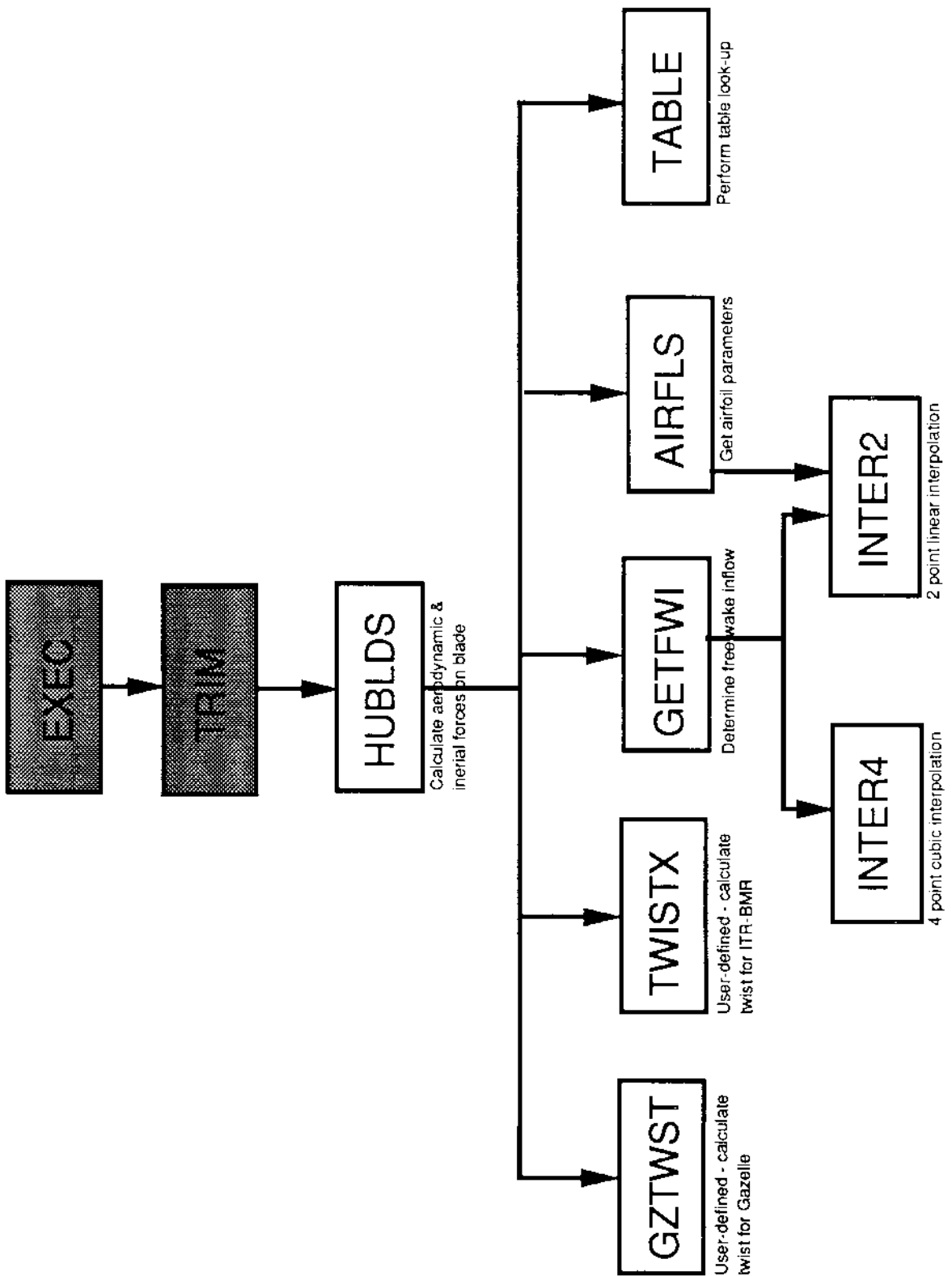
TRIM STRUCTURE CHART -- LEVEL ONE



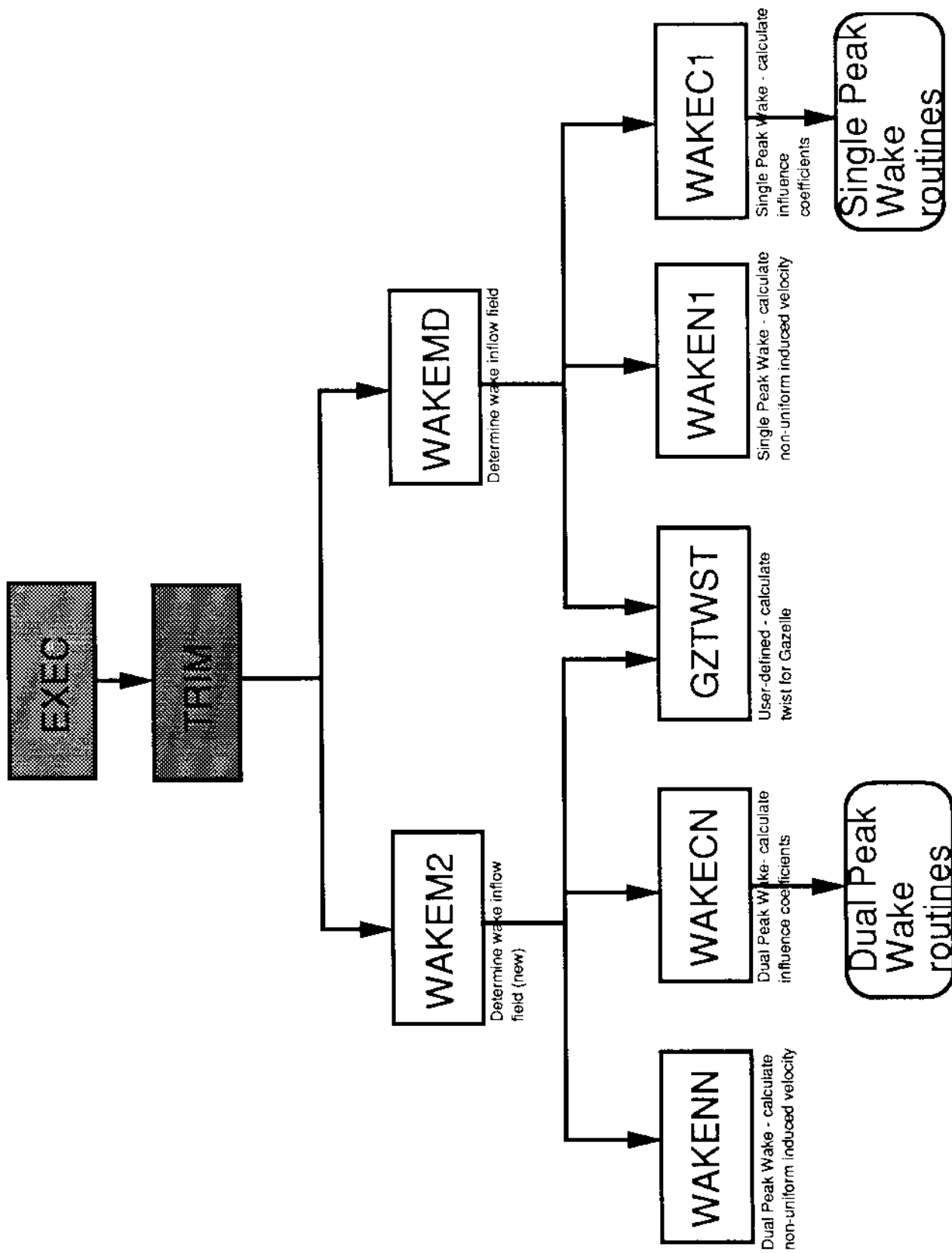
TRIM SUBROUTINES: STRUCTURE CHART (1 of 5)



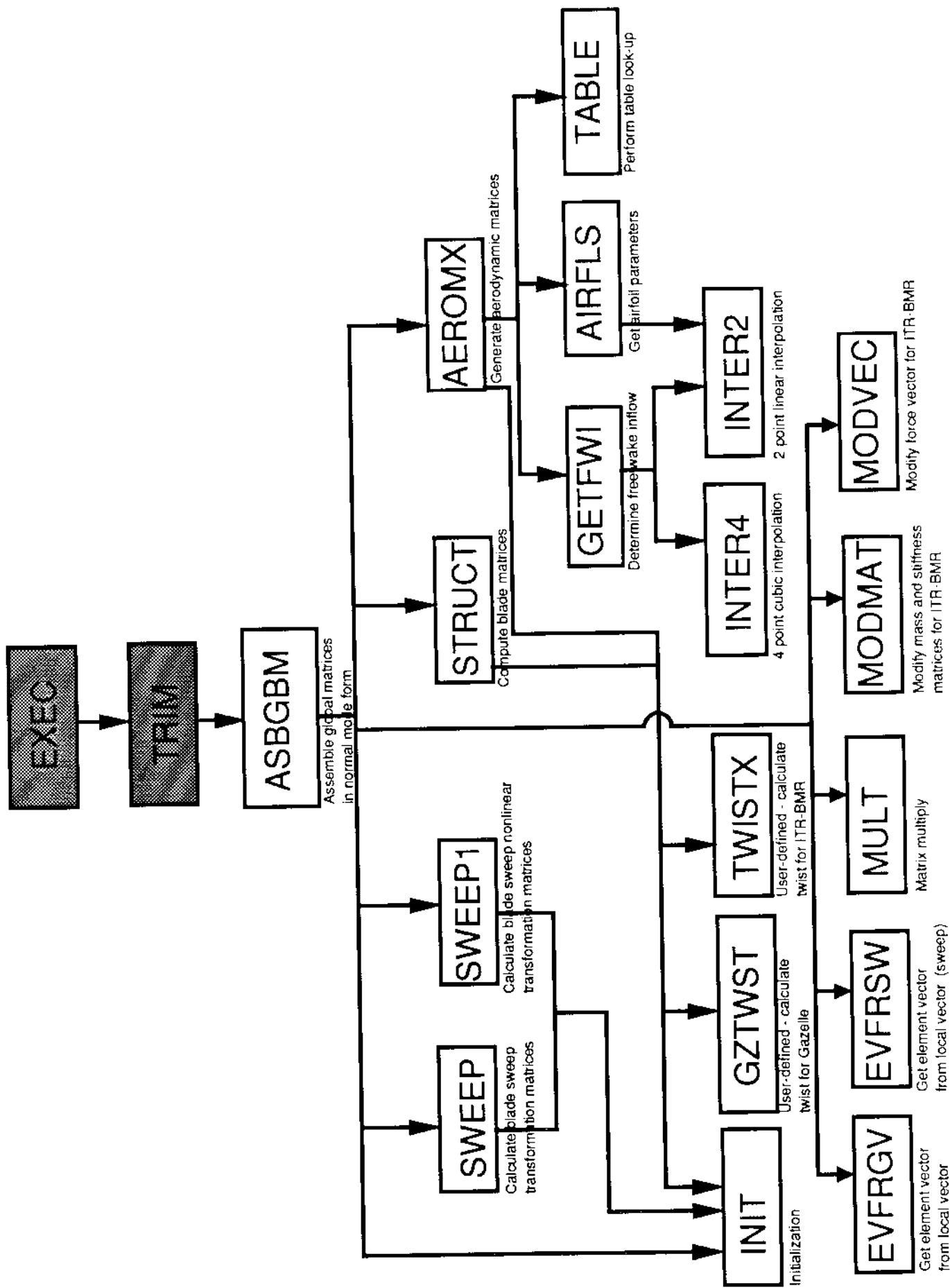
TRIM SUBROUTINES: STRUCTURE CHART (2 of 5)



TRIM SUBROUTINES: STRUCTURE CHART (3 of 5)

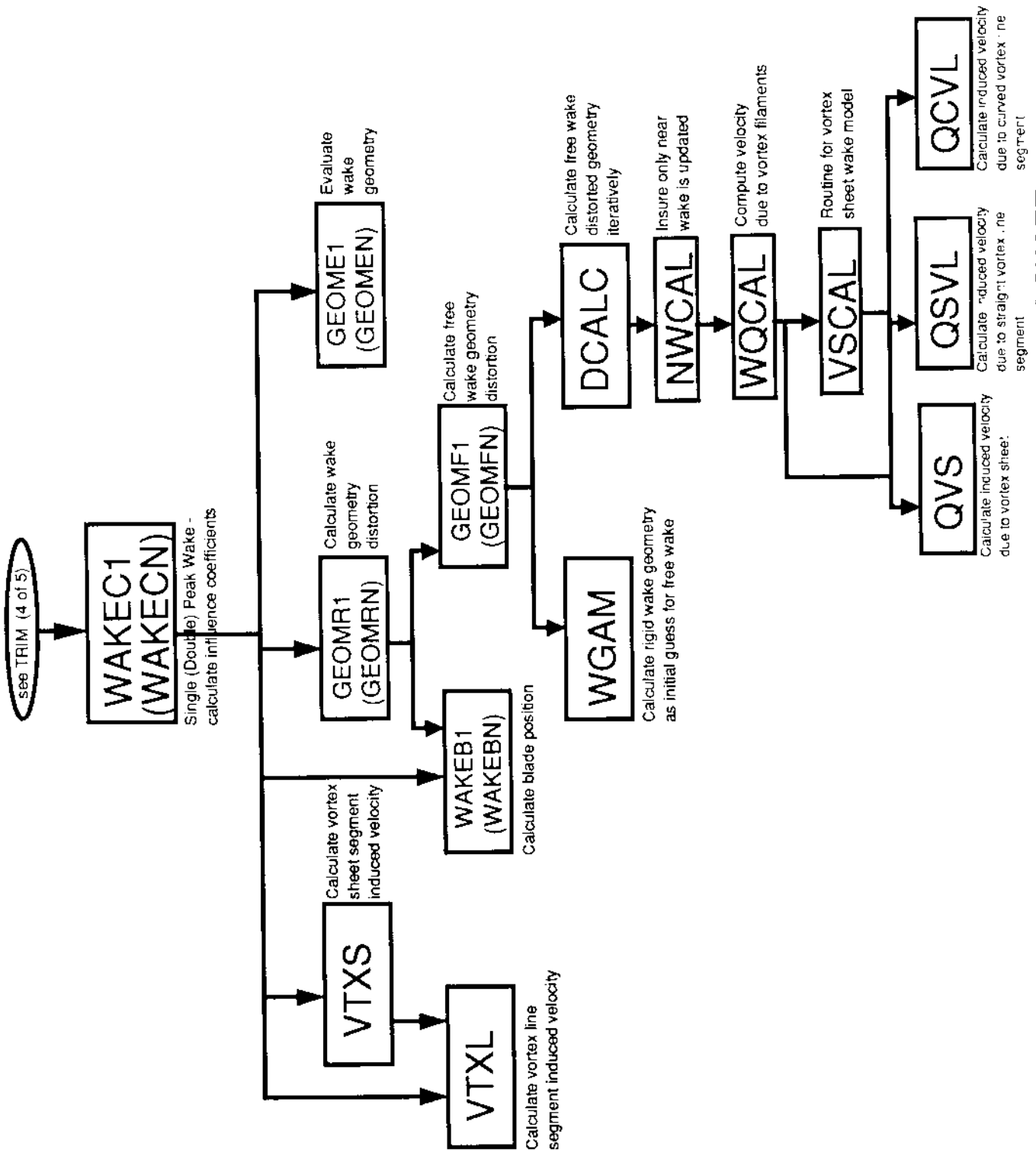


TRIM SUBROUTINES: STRUCTURE CHART (4 of 5)

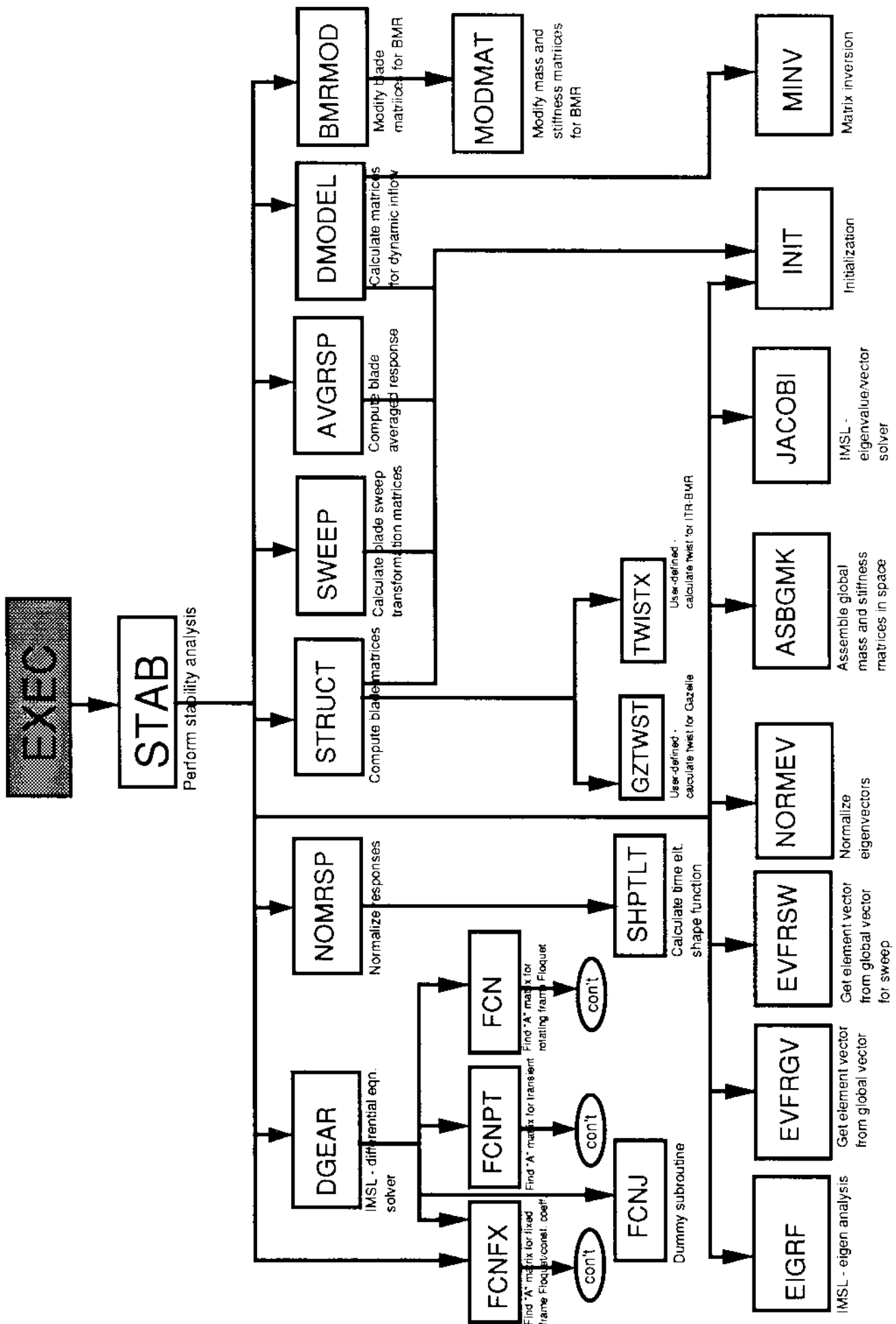


TRIM SUBROUTINES: STRUCTURE CHART (5 of 5)

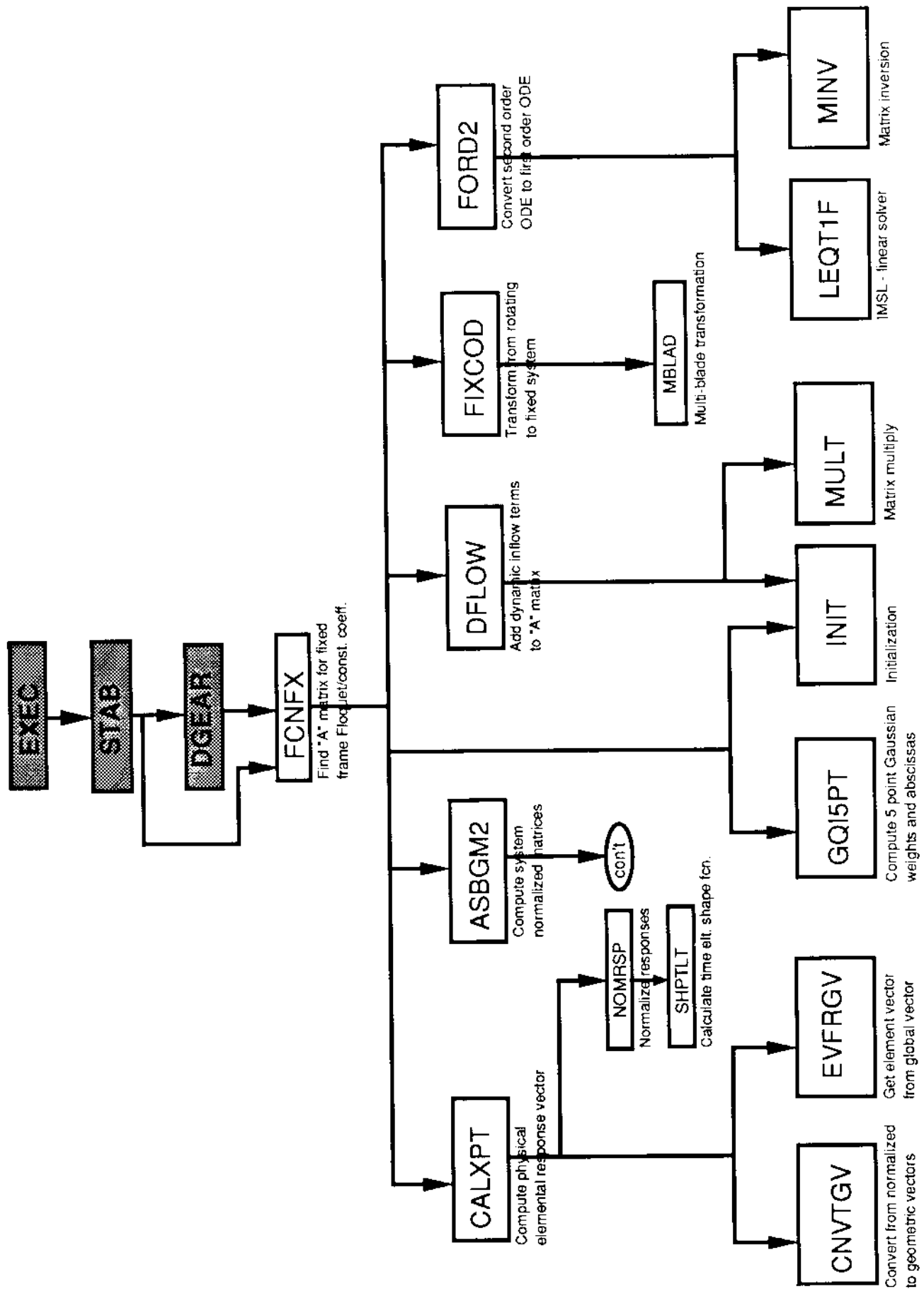
SINGLE (DUAL) PEAK WAKE ROUTINES STRUCTURE CHART

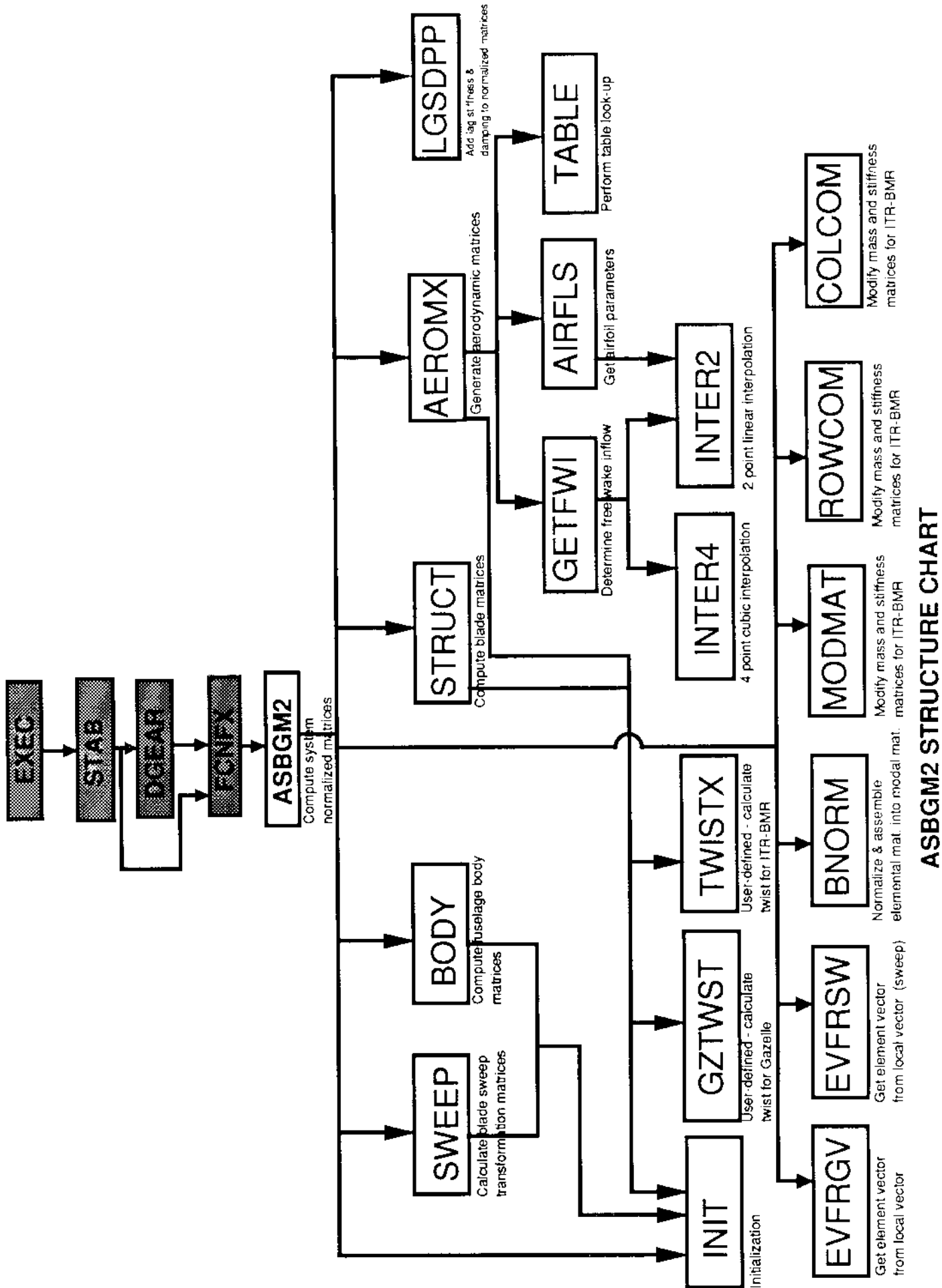


STABILITY STRUCTURE CHART

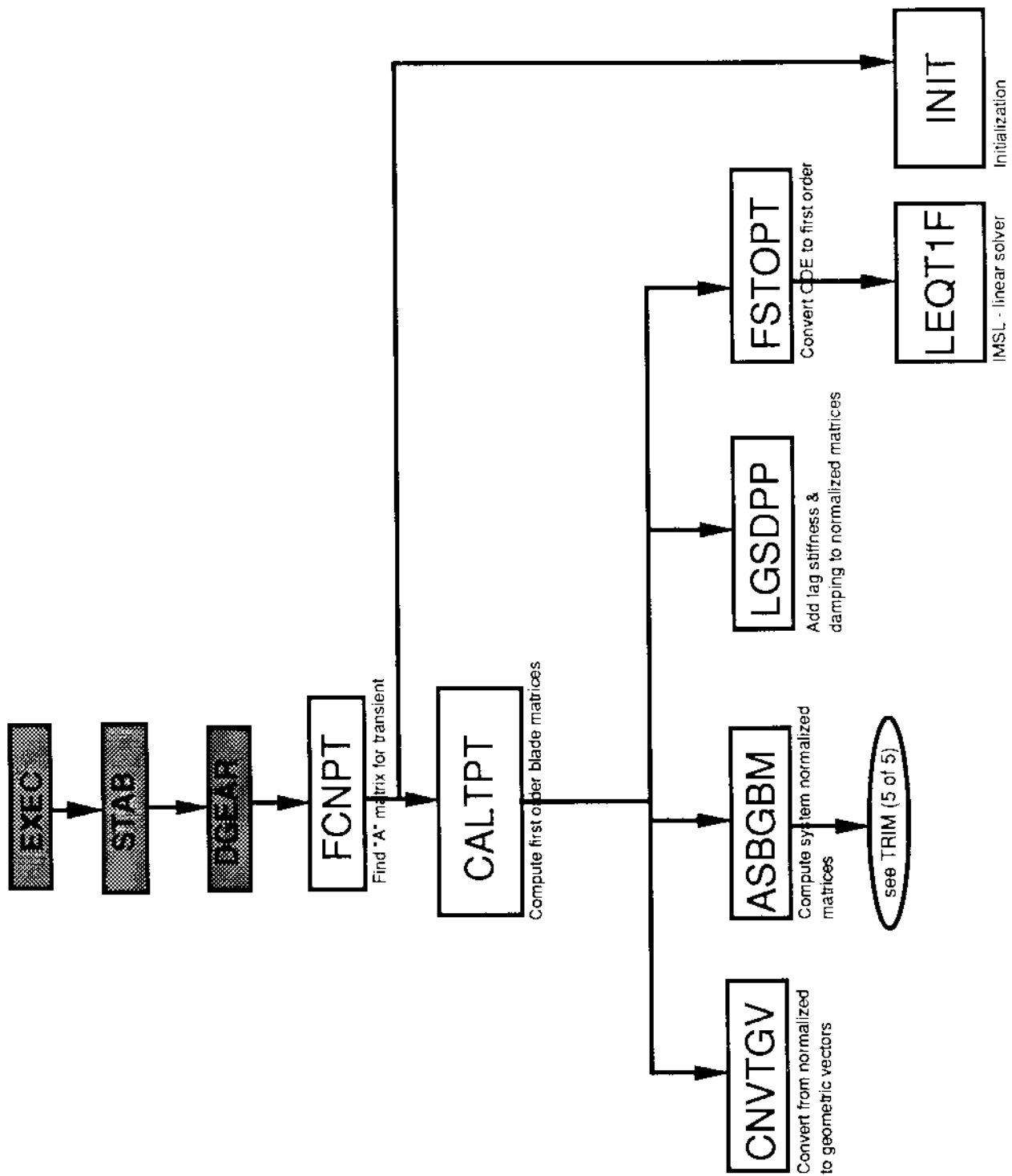


FCNFX STRUCTURE CHART

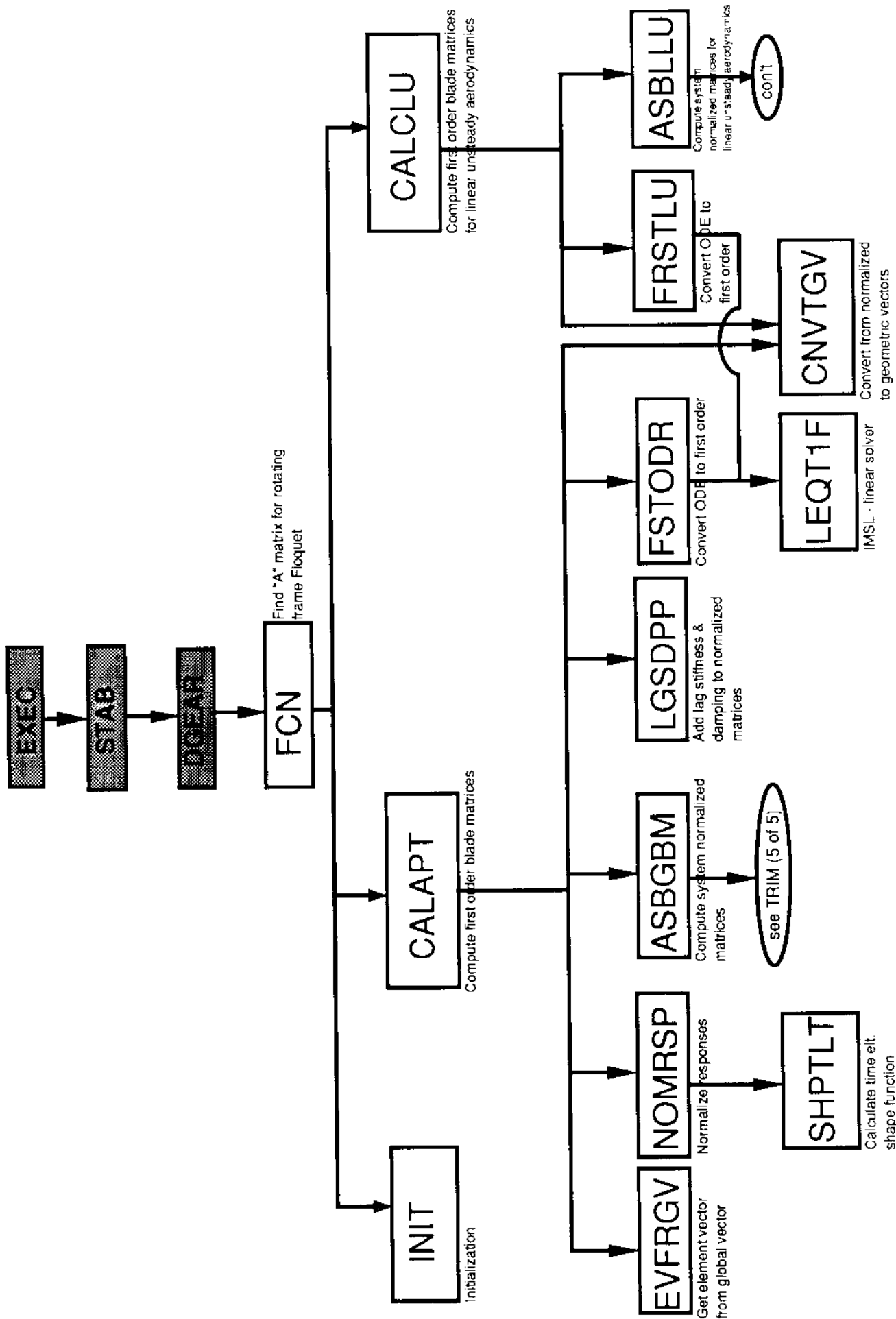




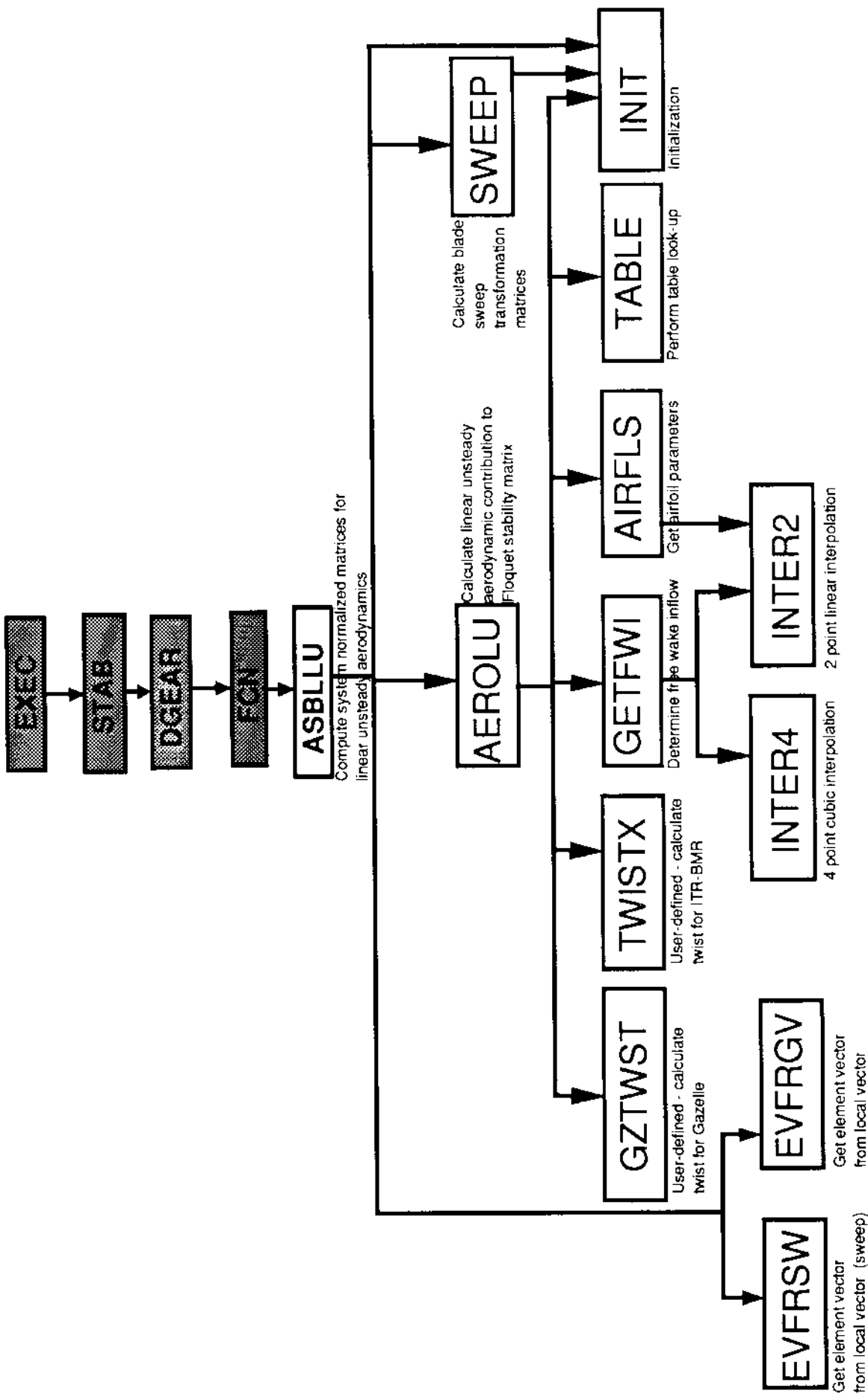
FCNPT STRUCTURE CHART



FCN STRUCTURE CHART



ASBLLU STRUCTURE CHART



I.6 INPUT DATA FILES

This section presents typical input data files for UMARC.

Sample Input:

Articulated Rotor

93/03/31
12:07:29

articulated-composite.wake.input

```
=====
* INPUT data for articulated rotor
* =====

    cg below hub           = 0.28
    cg_hub_offset_x        = 0.334
    cg_hub_offset_y        = 0.0
    root_cut(%)            = 21.4

    blade_properties

    material_type = composite_c.a.c
    twist(deg)   = -9.53
    lag_spring_constant = 0.05
    pitch_spring_constant = 0.0002
    no_space_elements = 7

    sweep_flag     = 0
    sweep_angle    = 0.0  0.3  0.3  0.0  0.3  0.0  0.0
    droop_angle    = 0.0  0.3  0.3  0.0  0.3  0.0  0.0
    twist_angle    = 0.0  0.3  0.3  0.0  0.3  0.0  0.0

    element_length : 0.128/68 0.113/636 0.113/636
                     0.189/394 0.166/667 0.166/667
    chord          : 0.2827 0.2827 0.2827
                     0.2827 0.2827 0.2827
    cfa              : 0.002166 0.032/66 0.032/354
                     0.032543 0.035/630 0.036/68C
    etz              : 0.355561 0.266/269 0.258/286 0.263/294
                     0.367/803 0.202/1639 0.235/343
    gjt              : 0.302166 0.032/66 0.032166 0.302166
                     0.033/296 0.035/839
    ea               : SC_J 50.0 50.0 50.0
                     SC_J 50.0 50.0
    eba              : 0.0 0.0 0.0 0.0 0.0 0.0 0.0
                     0.3 0.3 0.3 0.3 0.3 0.3 0.3
    ebb              : 0.0 0.0 0.0 0.0 0.0 0.0 0.0
                     0.3 0.3 0.3 0.3 0.3 0.3 0.3
    eci              : 0.0 0.0 0.0 0.0 0.0 0.0 0.0
                     0.3 0.3 0.3 0.3 0.3 0.3 0.3
    ec2              : 0.0 0.0 0.0 0.0 0.0 0.0 0.0
                     0.3 0.3 0.3 0.3 0.3 0.3 0.3
    offset_cgfea : 0.3459 0.0339 -0.2744 -0.0737
                     -0.3737 -0.592 -0.0339

=====

    offset_tatea : 0.0 0.0 0.0 0.0 0.0 0.0 0.0
                     0.0133 0.0133 0.00363 0.00363
    offset_aftlea : 0.0 0.0 0.0 0.0 0.0 0.0 0.0
                     0.0073 0.0073 0.00303 0.00303
    element_mass  : 1.3195 1.793 1.215 5.750
                     0.5198 1.215 0.2240 0.5775
    sq_km2       : 0.00077 0.000429 0.000355 0.000355
                     0.000386 0.000355 0.00028 0.00028
    sq_km       : 0.00 0.00 0.00 0.00
                     0.00 0.00 0.00 0.00
    =====

    offset_properties

    no_hub_dof = 3
    body_seg   : 1 2 3 4 5
    effective_x_mass
    effective_y_mass
    effective_z_mass
    fuselage_pitch_inertia = 5.472
    fuselage_rci_inertia = 2.1143

    fuselage_x_damper = 0.0
    fuselage_y_damper = 0.0
    fuselage_z_damper = 0.0
    fuselage_pitch_damper = 0.0
    fuselage_roll_damper = 0.0
    fuselage_x_spring = 0.0
    fuselage_y_spring = 0.0
    fuselage_z_spring = 0.0
    fuselage_pitch_spring = 0.0
    fuselage_roll_spring = 0.0
    body_roll_moment_coeff = 0.0
    body_side_force_coeff = 0.0
    parasite_drag_area = 0.0
    =====

    tail_properties

    gear_ratio_tail_rot  = 5.618
    solidify_tail_rot   = 0.217
    rad_ratio_tail_rot  = 0.1856
    rg_tail_rot_offset_x = -1.2386
    tail_above_cg      = 3.489
    tail_twistdeg_tail_rot = 0.0
    c_tail_rot          = 5.7
    tail_rear_table_locX: on
    tail_rear_table_locY: on
    tail_rear_table_locZ: on
    tail_offset_table : on
    * Files used are .c files, and .obj files.
    area_ratio_tail_hor = 3.0
    cg_tail_hor_offset_x = 1.0
    c_tail_hor           = 4.5
    cc_tail_hor          = 3.0
    =====

    airfoil_properties
```

93/03/31
12:07:29

articulated-composite.wake.input

```
2

: airfoil = myairfoil
: table_lock_up = off no_aerofoils =
: airfoil_starting_locations = .0
: cl_table_names test
: cd_table_names notab
: cr_table_names notab
: ref_wt_ft_curve_slope = 6.00
: czero = 0.1055 c1 = 6.00 dzero = 0.0074 d1 = 0.003
: d2 = 0.2101 crac = -0.0057 f1 = 0.0762
: le_reccv_fact = 0.97
: *-----*
: flight_condition
: advance_ratio = 0.11 density_ratio = 1.0
: vector_speed_ratio = 1.0 flight_angle = 0.0
: l_ip_mach = 0.615
: *-----*
: aerodynamics
: sing_peak_pres_wake
: wake_iter_ra = 9
: *-----*
: trim_analysis
: coupled_ic
: alpha_s = 2.93 phi_s = -1.29 theta_75 = 5.74
: theta_1c = 2.46 theta_1s = 1.33 theta_0_c_hat = 4.48
: nl_struct_aero
: first_flap_freq_per_rev = 1.3228
: coupled_trim_scheme = mard_newton
: delta_controls(4) = 5
: conv_crit = active
: resp_conv_crit = 0.012 tlim_ccnv_crit = 0.0001
: rc_max_iter = 50
: es_aero_damp = 40.00 us_aero_damp = 40.00
: *-----*
: rco_time_elements = 5
: (ss_change_mteit)
: nodes_per_time_elem = 5
: (ss_change_msect = nodes-1)
: for 6 and 5
: no flap_modes = 2
: flap_mode_seq = 2 3
: flap_mode_damping = 0.3 0.3
: no lag_modes = 2
: lag_mode_seq = 1 5
```


Sample Input:

Hingeless Rotor

```

ttitle : bo-105 data
        (ref 1: agard ls-179, rotocraft system id, pp 9-1 to 9-50)
        (ref 2: rasa sr-3144, a compilation and analysis of
        helicopter handling qualities data)

rotor : fuselage + dynamic inflow
coupled trim in forward flight
aeromechanical stability : 5 fuselage dof
dynamic lift/no
quasi steady aero
floquet approach in fixed frame

input_data non_dimensional:
* ref: mass = 1. ref_toler_speed = 1. rcto: radius = 1.

rotor_properties
material_type : hingeless
motor_name : myotor
no_blades = 4 solidity = C.07
lock_no = 5.2 ct/sigma
cg_below_hub = 0.2 cg_hub_offset_x = C.0
cg_hub_offset_x = 0.0 cg_hub_offset_y = C.0

blade_properties
material_type = tsctrcc
twist(deg) = 0.0 precone(deg) = 0.0
foot_cut(%) = 0.0 no_space_elements = 5

e1y : -31.08 -0.1308 -0.0108 -0.0108 -0.0108
e1z : -0.3268 -0.0268 -0.0268 -0.0268 -0.0268
g1 : .30615 -.00015 -.00015 -.00015 -.00015
ea : 47.959 47.959 47.959 47.959 47.959
eb1 : 0.0 0.0 0.0 0.0 0.0
eb2 : 0.0 0.0 0.0 0.0 0.0
ec1 : 0.0 0.0 0.0 0.0 0.0
ec2 : 0.0 0.0 0.0 0.0 0.0

offset_cgxa : 0.0 0.0 0.0 0.0 0.0
offset_takea : 0.0 0.0 0.0 0.0 0.0
offset_actxa : 0.0 0.0 0.0 0.0 0.0

element_passes : 1.0 1.0 1.0 1.0 1.0
sq_kr1 : .000174 .000174 .000174 .000174 .000174
sq_kr2 : .000610 .000610 .000610 .000610 .000610

----- fuselage properties -----
no_hub_dof = 5
body_seg = 1 2 3 4 5
effective_x_mass = 77.24
effective_y_mass = 77.24
effective_z_mass = 77.24
fuselage_pitch_inertia = 7.432
fuselage_rci_inertia = 2.739
fuselage_x_damper = 0.0
fuselage_y_damper = 0.0
fuselage_z_damper = 0.0
fuselage_pitch_damper = 0.0
fuselage_roll_damper = 0.0
fuselage_x_spring = 0.0
fuselage_y_spring = 0.0
fuselage_z_spring = 0.0
fuselage_pitch_spring = 0.0
fuselage_roll_spring = 0.0

----- tail properties -----
body_roll_moment_coeff = C.0 body_pitch_moment_coeff = 0.0
body_sides_force_coeff = C.0 parasite_drag_area = C.31
* note: tail properties are only typical values *

tail : tail properties
solidity_tail_rot = 0.12
gear_ratio_tail_rot = 5.3
rad_ratio_tail_rot = 0.2
twistdeg_tail_rot = 0.0
cg_tail_rot_offset_x = 1.2
tail_rot_above_cg = 0.2
cg_tail_rot = 0.2
cg_tail_hori = 6.0
ec_tail_hori = 0.2

----- airfoil properties -----
table_lok_3D : off no_airfoils = 1
airfoil_starting_locations = .0
ct_table_names_list,
cd_table_names_list,
cm_table_names_list

ref_lift_curve_slope = 6.00
czero = 0.00 c1 = 6.00 dzero = C.3063 f1 = 0.000
c2 = 0.20 cmac = 0.000 le_recov_fact = 0.97

```

flight condition

```

: advance_ratio = 0.2 density_ratio = 1.0
: rotor_speed_ratio = 1.0 flight_angle 0.0
: r-p_mach = 0.65

```

aerodynamics

```

: drees_linear_inflow
: bsw_linear_inflow
: uniform_inflow
: reverse_inflow

```

trim_analysts

```

: coupled_rb
: rnl_struct_aero
: no_time_elements = 4
: nodes_per_time_elem = 4

```

```

: no_tdep_modes = 3
: flap_mode_seq = 2 3 6
: flap_mode_damping = 0. 0. 0.

```

```

: no_lag_modes = 2
: lag_mode_seq = 1 4
: lag_mode_damping = 0. 0.

```

```

: no_torsion_modes = 1
: torsion_mode_seq = 5
: torsion_mode_damping = 0. 0.

```

```

: no_axial_modes = 0
: axial_mode_seq = 0
: axial_mode_damping = 0.0

```

```

: conv_crit : active
: first_flap_freq_per_rev = 1.145
: delta_crit(0.5) = 5
: trim_conv_crit = -0.031
: resp_conv_crit = -0.05
: coupled_trim_scheme = mact_newton
: no_max_iter = 40
: qg_aero_damp = 1.00
: alpha_s_wt = 0.0
: theta_0_wt = 0.0

```

stability_analysts

```

: fix_qs_flag no_qs_locations = 24
: dynamic_inflow

```

```

: output_options print_control = 4

```

high load control = 0

Sample Input:

Bearingless Rotor

```

* input data for bmr rotor
*   g_s_dif      feb 9, 1992
*   g_s_dif      feb 9, 1992
*-----*
*-----* title : bmr rotor ( rigid pitch link & lag pin )
*-----* air_resn : rotor + 2-deg body + dynamic inflow
*-----* wind_tunnel : trim in hover
*-----* input_data : non_dimensional
*-----* ref_mass = 1. ref_rotor_speed = 1. rotor_radius = 1.
*-----* rotor_properties
*-----* rotor_type : bmr single_flexbeam rigid_pitch_link
*-----* rotor_name : ltr
*-----* ro blades      4 solidity      0.1079
*-----* lock_nc       5.673 ct/sigma     0.09
*-----* cg_below_hub  0.2969
*-----* lag_pin
*-----* cg_hub_offset_x 0.0 cg_hub_offset_y 0.0
*-----* body_roll_moment_coeff 0.0 body_pitch_moment_coeff 0.0
*-----* parasite_drag_area 0.01
*-----* body_side_force_coeff 0.0
*-----* no_elem_in_flexbeam_i = 2 no_elm_1rf_torque_type = 2
*-----* blade_properties
*-----* material_type = isotropic
*-----* twist(deg)      0.0 precone(deg)    4.25
*-----* lag_spring_constant 0.3 lag_damper_constant 0.3
*-----* defl3d_constant 0.3 pitch_spring_constant 0.0
*-----* root_cutfail    25 no_space_elements 6
*-----* no_elm_in_flexbeam_i = 2
*-----* element_length : 0.25 0.5625 0.2417 0.1215 0.3417 0.3868
*-----* chord : 0.0776 0.0847 0.094 0.0265 0.0263
*-----* e_xy : 0.03306 0.003756 0.002250 0.001532 0.00543;
*-----* e_zz : 0.0312924 0.05367 0.06443 0.05367 0.010733 0.00915;
*-----* g4 : 0.022817 0.003381 0.003357 0.006716 0.003381
*-----* ea : 0.006162 0.113 0.4428 0.221 0.072 0.094 0.0265 0.0263
*-----* e_b2 : 0.0 0.0 0.0 0.0 0.0 0.0 0.0 0.0 0.0
*-----* e_b1 : 0.0 0.0 0.0 0.0 0.0 0.0 0.0 0.0 0.0
*-----* e_b2 : 0.0 0.0 0.0 0.0 0.0 0.0 0.0 0.0 0.0
*-----* fuselage_properties
*-----* no_hub_dcf = 2
*-----* body_sea : 4.5 effective_x_mass 64.78
*-----* effective_x_mass 86.1
*-----* effective_y_mass 64.78
*-----* effective_z_mass 64.78
*-----* fuselage_pitch_inertia = 4.58
*-----* fuselage_roll_inertia = 2.05
*-----* fuselage_x_damper 0.0
*-----* fuselage_y_damper 0.0
*-----* fuselage_z_damper 0.0
*-----* fuselage_lPitch_damper 0.5
*-----* fuselage_rPitch_damper 0.5
*-----* fuselage_rRoll_damper 0.315
*-----* fuselage_ePitch_damper 0.446
*-----* fuselage_x_spring 0.0
*-----* fuselage_y_spring 0.0
*-----* fuselage_z_spring 0.0
*-----* fuselage_pitch_spring 0.0
*-----* fuselage_roll_spring 0.0
*-----* fuselage_rPitch_spring 0.82
*-----* fuselage_rRoll_spring 1.82
*-----* tail_properties
*-----* solidity_tail_rot 0.15
*-----* gear_ratio_tail_rot 5.3
*-----* lead_ratio_tail_rot 0.2
*-----* twist(deg)_tail_rot 0.2
*-----* cg_tail_rot_offset_x 1.2
*-----* tail_rot_above_cg 0.2969
*-----* cl_tail_rot 6.20
*-----* tail_rotor_table_tail_up : off
*-----* cg_tail_hor_offset_x 0.95
*-----* hor_tail_area 0.0
*-----* CG_tail_hor 6.0
*-----* EC_tail_hor 0.2

```

```

airfoil_properties
table_lock_up = off
airfoil_starting_locations = 0
c1_table_names Test
cd_table_names rotab
cm_table_names rotab
ref_lift_curve_slope = 6.00
czer = 0.115 cl = 6.00
d2 = 0.10 cmac = -0.006 d1 = 0.005
re_recov_fact = 2.97
flight_condition
advance_ratio = 0. density_ratio = 1.0
motor_speed_ratio = 1.00
tip_mach = 0.229 flight_angle = 0.0
aerodynamics
dress_linear_inflow
uniform_inflow
reverse_flow
trim_analysis
coupled_wt
nl_struct_aero
no_time_elements = 1
nodes_per_time_elem = 4
no_flap_modes = 2
flap_mode_seq = 2 3 6
flap_mode_damping = 0. 0. 0.
no_lag_modes = 2
lag_mode_scy = 1 5
lag_mode_damping = 0.0 0.0
lag_mode_damping = 0.015
no_torsion_modes = 2
torsion_mode_seq = 4 8
torsion_mode_damping = 0.3 0.0
no_axial_modes = 0
axial_mode_seq = 1
axial_mode_damping = 0.0
conv_crit      active
first_flap_freq_per_rev = 1.0C7
delta_controls(4) = 2
trim_conv_crit = .0005
res_conv_crit = .005
coupled_trim_gmbr = mrg_newton
no_max_iter = 50
qs_aero_damp = .

```

I.7 OUTPUT DATA FILE

This section presents a typical output file for UMARC.

Sample Output:

Articulated Rotor

93/03/29
13:51:36

articulated-composite.wake.output

```
-----  
-----  
-----  
-----  
-----
```

Input data

```
-----  
-----  
-----  
-----
```

rotor_name : sh2

articulated : 1

flap_lag_coincide : 4

no_blades : 5

solidity : 0.07253

lock_no : 5

ct./sigma : 0.280033

cg_below_hub : 0.224033

cg_hub_offset_x : 0.0330033

blade properties

twist (deg) : -9.53200

precone (deg) : 0.00300

root cut (%) : 21.46000

no_space_elements : ?

no_ele_in_segments : ?

material_type : composite_calc

lag_spring_constant : 0.03200

lag_damper_constant : 0.027903

delta3_constant : 3.000033 (default)

pitch_spring_constant : 3.0000203

blade element properties

ele_no	length	mass	e1_x	e1_y	e1_z
1	2.120188	1.039530	0.028345	0.323198	
2	2.113636	1.790339	0.038345	0.323198	
3	2.115636	0.924030	0.358345	0.323198	
4	2.189394	0.570330	0.358345	0.323198	
5	2.182394	0.519830	0.338345	0.323198	
6	2.166667	1.270530	0.338345	0.323198	
7	0.67235	5.775630	0.338345	0.323198	

ele_no	sg1	sg2	east_a	eg
1	0.0038C2		378.094	0.000000
2	0.0038C2		378.094	0.000000
3	0.0038C2		378.094	0.000000
4	0.0038C2		378.094	0.000000
5	0.0038C2		378.094	0.000000
6	0.003802		378.094	0.000000
7	3.003802		378.094	0.000000

```
blade element properties
```

ele_no	sg1	sg2	chord	ed
1	3.003100	0.100400	0.037700	0.013330
2	3.003100	0.000400	0.087700	0.036330
3	3.003100	0.100400	0.087700	0.359230
4	3.003100	0.000400	0.087700	0.333330
5	3.003100	0.100400	0.087700	0.533330
6	3.003100	0.000400	0.087700	0.573330
7	3.003100	0.100400	0.087700	0.030000

93/03/29
13:51:36

articulated-composite.wake.output

```

1 1 50.426816 25.677459 0.030083
1 2 50.426816 25.677459 0.030083
1 3 50.426816 25.677459 0.030083
1 4 50.426816 25.677459 0.030083
1 5 50.426816 25.677459 0.030083
1 6 50.426816 25.677459 0.030083
1 7 50.426816 25.677459 0.030083

effective_x_mass = 56.000000
effective_y_mass = 56.000000
effective_z_mass = 56.000000
fuselage_flight_inertia = 5.712000
fuselage_foil_inertia = 2.114300
fuselage_x_damper = 0.000000
fuselage_y_damper = 0.000000
fuselage_z_damper = 0.000000
fuselage_pitch_damper = 0.000000
fuselage_roll_damper = 0.000000
fuselage_x_spring = 0.000000
fuselage_y_spring = 0.000000
fuselage_z_spring = 0.000000
fuselage_cg_spring = 0.000000
body_roll_moment_coeff = 0.000000
body_pitch_moment_coeff = 0.000000
body_side_force_coeff = 0.000000
parasite_drag_area = 0.310000

tail_properties
-----
rad_ratio_tail_fct = 0.195600
solidity_tail_fct = 0.411700
gear_ratio_tail_fct = 5.618000
twist_deg_tail_rot = 0.000000
cg_tail_rot_offset_x = 1.238600
cg_tail_rot_above_cg = 0.148900
cl_tail_rot = 5.700300
hor_tai_area = 0.000000 (default)
hor_tai_area = 0.000000
cg_tai_for_offset_x = 2.000000
cg_tai_bar = 4.500000
cc_tai_bar = 0.000000

airfoil_properties
-----
ref_lift_curve_slope = 6.000000
czer_c = 0.105500
c1_c = 6.000000
dzero = 0.007400
d1_c = 0.000000
d2_c = 0.000000
wmac = 0.210100
f1_c = -0.005700
je_recoy_fact = 0.076200
c = 0.970000
flight_conditions
-----
advance_ratio = 0.110000
rotor_speed_ratio = 1.000000
density_ratio = 1.000000
flight_angle = 0.500000

fuselage_properties
-----
no_hub_dof = 0
hub_seq = 0

```

93/03/29
13:51:36

articulated-composite.wake.output

t_ip_mach = 2.613850
tip_mach_latt_rcf = 2.64126;

aerodynamics

* sing peak_free_wake

wake_iter_no = 9

* trim analysis

* analysis option

* coupled_aero

* coupled_1d

* no_time_elements

* nodes_per_time_elem = 5

* conv_crit

* coupled_trim_scheme

* delta_controls(1)

* trim_conv_crit = 5.000000

* resp_conv_crit = 0.000000

* gs_aero_damp = 0.000000

* no_max_iter = 50

* first_flap_freq_per_rev = 1.022600

* no_flap_modes

* flap_mode_seq

* flap_mode_damping

* no_lag_modes

* lag_mode_seq

* lag_mode_damping

* no_torsion_modes

* torsion_mode_seq

* torsion_mode_damping

* no_axial_modes

* axial_mode_seq

* axial_mode_damping

* ttheta_r

* ttheta_c

* ttheta_s

* alpha_s

* phi_s

* theta_o_tail

* theta_o_rail

* stability analysis

* print_control
* huc_lead_control

* 4
* 3

input data as read in from temporary data file

analysis of unknown helicopter ???:???

(data = 7)

* no_spatial_elements = 7
* no_of_response_modes = 5
* no_of_iterations = 50
* no_of_stability_modes = 5
* u-s damping factor = 0.000
* q-s damping factor = 0.000
* no_bades = 4
* lndnl = 1
* revf = 3
* rnb = 5
* idyn = 0
* istab = 0
* incde = 0
* lcpit = 3
* indus = 0
* trwke = 1
* tip_mach_number = 0.615
* free wake: engaged at iteration # 9

element number = 1

* ely = 0.008345 elb1 = 0.000004 eg = 0.345900 skm1 = 0.000100
* elz = 0.02198 elb2 = 0.000003 ed = 0.033300 skm2 = 0.000400
* g1 = 0.003802 elc1 = 0.000000 ea = 0.000000 rmas = 1.0395
* eac = 378.39 elc2 = 0.000000 el = 0.128788 cor = 0.382700

element number = 2

* ely = 0.008345 elb1 = 0.000004 eg = 0.000000 skm1 = 0.000100
* elz = 0.02198 elb2 = 0.000000 ed = 0.036300 skm2 = 0.000400
* g1 = 0.003802 elc1 = 0.000000 ea = 0.000000 rmas = 1.3903
* eac = 378.09 elc2 = 0.000000 el = 0.136316 cor = 0.382700
* g2y = 50.43 gaz = 25.58
* k12 = 33.668962 k13 = -7.144318 k14 = 0.000000
* k23 = 0.000000 k26 = 0.000000
* k45 = 0.001268 k46 = -0.001269

element number = 3

* ely = 0.008345 elb1 = 0.000004 eg = -0.274400 skm1 = 0.000100
* elz = 0.02198 elb2 = 0.000003 ed = 0.059200 skm2 = 0.000400
* g1 = 0.003802 elc1 = 0.000000 ea = 0.000000 rmas = 0.9245
* eac = 378.09 elc2 = 0.000000 el = 0.136316 cor = 0.082703

93/03/29
13:51:36

articulated-composite.wake.output

gaz = 50.43 gaz = 25.68
k13 = 33.668962 k13 = 17.144318 k14 = 0.300000
k36 = 0.000330 k36 = 0.300000
k46 = 0.031268 k46 = -0.302269

element number = 4
eiy = 0.008345 eb1 = 0.000004 eg = -0.073700 skml = 0.300000
eiz = 0.023198 eb2 = 0.000000 ed = 0.000000 skm2 = 0.000000
qj = 0.003802 ec1 = 0.000000 ea = 0.000000 rmas = 0.000000
eac = 378.09 ec2 = 0.000000 el = 0.189394 cor = 0.000000

gaz = 50.43 qaz = 25.68
k12 = 33.668962 k13 = 17.144318 k14 = 0.000000
k25 = 0.000000 k36 = 0.000000
k46 = -0.301269

element number = 5
eiy = 0.008345 eb1 = 0.000004 eg = -0.073700 skml = 0.300000
eiz = 0.023198 eb2 = 0.000000 ed = 0.000000 skm2 = 0.000000
qj = 0.033802 ec1 = 0.000000 ea = 0.000000 rmas = 0.000000
eac = 378.09 ec2 = 0.000000 el = 0.189394 cor = 0.000000

gaz = 50.43 gaz = 25.68
k12 = 33.668962 k13 = 17.144318 k14 = 0.000000
k25 = 0.000000 k36 = 0.000000
k46 = -0.301269

element number = 6
eiy = 0.008345 eb1 = 0.000004 eg = -0.059230 skml = 0.300000
eiz = 0.023198 eb2 = 0.000000 ed = 0.007300 skm2 = 0.000000
qj = 0.033802 ec1 = 0.000000 ea = 0.000000 rmas = 0.000000
eac = 378.09 ec2 = 0.000000 el = 0.166667 cor = 0.000000

gaz = 50.43 qaz = 25.68
k12 = 33.668962 k13 = 17.144318 k14 = 0.300000
k25 = 0.000000 k36 = 0.000000
k46 = -0.301269

element number = 7
eiy = 0.008345 eb1 = 0.000004 eg = -0.033350 skml = 0.300000
eiz = 0.023198 eb2 = 0.000000 ed = 0.000000 skm2 = 0.300000
qj = 0.033802 ec1 = 0.000000 ea = 0.000000 rmas = 0.000000
eac = 378.09 ec2 = 0.000000 el = 0.067235 cor = 0.000000

gaz = 50.43 qaz = 25.68
k12 = 33.668962 k13 = 17.144318 k14 = 0.000000
k25 = 0.000000 k36 = 0.000000
k46 = -0.301269
lag spring = 0.000000 lag damper = 0.027900
delta-3, p.b. = 0.000000 pitch link stiffness = 0.3000200

advance ratio = 0.100000
dc = 5.073300 d0 = 0.125500 cl = 6.070000
dc = 0.007400 d1 = 0.050000 d2 = 0.210000

drstx = 1.000000 htp = 0.000000 sigma = 0.105200
crac = -0.005700 fl = 0.076200 slc = 6.000000
lwtw = -0.166337 cl/sigma = 0.072500

heat = 0.2800
cnrf = 0.6500
cyf = 0.0000
hfp = 0.0000
etaun = 0.9700

sigmat = 0.2417
ratios = 0.1856
tdept = 0.6413
xtfr = 1.0000
atratn = 4.5000
ctht = 0.0000

lw: 0
dqqr1(t) = 0.3000000000000000
dqqr2(t) = 0.3000000000000000

global dof corresponding to local dof

spatial element # 1 2 3 4 5 6 7
local dof 1 12 23 34 45 56 67 0
local dof 2 11 22 33 44 55 66 77
local dof 3 10 20 31 42 53 64 75
local dof 4 1 12 23 34 45 56 67
local dof 5 13 24 35 46 57 68 0
local dof 6 14 25 36 47 58 69 79
local dof 7 2 13 24 35 46 57 68
local dof 8 3 14 25 36 47 58 69
local dof 9 15 26 37 48 59 70 0
local dof 10 16 27 38 49 60 71 78
local dof 11 17 28 39 50 61 72 0
local dof 12 18 29 40 51 62 73 0
local dof 13 19 30 41 52 63 74 0
local dof 14 20 31 42 53 64 75 0
local dof 15 6 17 28 39 50 61 72 0
local dof 16 18 29 40 51 62 73 0
local dof 17 19 30 41 52 63 74 0
local dof 18 20 31 42 53 64 75 0
local dof 19 21 32 43 54 65 76 0

x coordinate of loc. end cf element
1 0.0712120000
2 0.1557600000
3 0.6439400000
4 0.4554600000
5 0.2651520000
6 0.9848500000
7 0.3125000000

ef.ap = 0.03125
ef.ajq = 0.03125

930329
135136

articulated-composite.wake.output

```

eigenvalue( 74) = 0.255744
frequency = 0.030000
eigenvector:
1.3 -0.030007 15
1.6 0.306947 18
1.9 -0.030002 21
2.2 0.030000 23
2.5 -0.030043 24
2.8 -0.030043 26
3.1 0.030043 27
3.4 0.030000 32
3.7 0.186669 38
4.0 0.000000 41
4.3 -0.300108 44
4.6 0.300010 47
4.9 0.304945 50
5.2 -0.030003 53
5.5 0.030003 56
5.8 -0.030003 59
6.1 0.030010 62
6.4 0.030006 65
6.7 0.030000 68
7.0 0.030000 69
7.3 0.023223 71
7.6 0.030000 74
7.9 0.030010 77
8.2 0.030024 78

mode = 1 response mode sequence = 1
mode = 2 response mode sequence = 2
mode = 3 response mode sequence = 3
mode = 4 response mode sequence = 4
mode = 5 response mode sequence = 5
mode = undeformed blade
modes used for trim response
free vibration exciting frequencies 6 mode shapes

```

```

eigenvalue( 75) = 0.303348
frequency = 0.033000
eigenvector:
1.3 -0.030006 15
1.6 -0.030015 18
1.9 0.030000 21
2.2 0.030000 23
2.5 0.030000 24
2.8 0.030000 26
3.1 0.030000 27
3.4 0.030000 32
3.7 0.030000 36
4.0 -0.030003 39
4.3 -0.000003 42
4.6 0.000000 45
4.9 -0.030007 48
5.2 0.030000 51
5.5 -0.030014 54
5.8 0.030000 57
6.1 0.030000 60
6.4 0.030000 63
6.7 0.030000 66
7.0 0.030008 69
7.3 0.031223 72
7.6 0.030005 75
7.9 0.030000 78
8.2 -0.030003 79

eigenvalue( 76) = 0.34247303
frequency = 0.34247303
eigenvector:
1.3 -0.030006 15
1.6 -0.030015 18
1.9 0.030000 21
2.2 0.030000 24
2.5 0.030000 27
2.8 0.030000 30
3.1 0.030000 33
3.4 0.030000 36
3.7 0.030000 39
4.0 0.049234 41
4.3 -0.030003 44
4.6 0.030000 47
4.9 0.030000 50
5.2 -0.030027 53
5.5 0.030003 56
5.8 -0.030013 59
6.1 0.030000 62
6.4 0.030012 65
6.7 -0.030007 68
7.0 0.017219 71
7.3 -0.030035 74
7.6 -0.012233 77
7.9 -0.011243 79

eigenvalue( 77) = 0.1177880D+02
frequency = 0.1177880D+02
eigenvector:
1.3 -0.030006 15
1.6 -0.030015 18
1.9 0.030000 21
2.2 0.030000 24
2.5 0.030000 27
2.8 0.030000 30
3.1 0.030000 33
3.4 0.030000 36
3.7 0.030000 39
4.0 0.049234 41
4.3 -0.030003 44
4.6 0.030000 47
4.9 0.030000 50
5.2 -0.030027 53
5.5 0.030003 56
5.8 -0.030013 59
6.1 0.030000 62
6.4 0.030012 65
6.7 -0.030007 68
7.0 0.017219 71
7.3 -0.030035 74
7.6 -0.012233 77
7.9 -0.011243 79

eigenvalue( 78) = 0.1545670D+01
frequency = 0.1545670D+01
eigenvector:
1.3 -0.030004 15
1.6 0.000000 18
1.9 0.295284 21
2.2 0.030002 24
2.5 0.030001 26
2.8 0.030001 29
3.1 0.030001 32
3.4 0.030000 35
3.7 0.030000 38
4.0 0.030000 41
4.3 -0.030003 44
4.6 0.030000 47
4.9 0.030000 50
5.2 -0.030027 53
5.5 0.030003 56
5.8 -0.030013 59
6.1 0.030000 62
6.4 0.030012 65
6.7 -0.030007 68
7.0 0.017219 71
7.3 -0.030035 74
7.6 -0.012233 77
7.9 -0.011243 79

eigenvalue( 79) = 0.2208820D+00
frequency = 0.2208820D+00
eigenvector:
1.3 0.000000 15
1.6 0.000245 18
1.9 0.000005 21
2.2 0.000000 24
2.5 0.000000 27
2.8 0.000000 30
3.1 0.000001 33
3.4 0.000001 36
3.7 0.000001 39
4.0 0.049266 41
4.3 -0.030003 44
4.6 0.000000 47
4.9 0.000000 50
5.2 -0.030027 53
5.5 0.000003 56
5.8 -0.030013 59
6.1 0.000000 62
6.4 0.000002 65
6.7 -0.030007 68
7.0 0.017219 71
7.3 -0.030035 74
7.6 -0.012233 77
7.9 -0.011243 79

```

93.0329

13.5136

articulated-composite.wake.output

6

```

13   2.321683          14
     2.309064          15
     -2.309064          16
     -2.330029          17
     2.330029          18
     2.325121          19
     2.325121          20
     0.225130          21
     0.225130          22
     0.287790          23
     0.287790          24
     0.350028          25
     0.350028          26
     0.265977          27
     0.265977          28
     0.280032          29
     0.280032          30
     0.280032          31
     0.280032          32
     0.280032          33
     0.280032          34
     -0.003232         35
     -0.003232         36
     -0.003232         37
     -0.003306         38
     -0.003306         39
     0.003280         40
     0.003280         41
     0.194309         42
     0.194309         43
     -0.546359         44
     -0.546359         45
     0.027879         46
     0.027879         47
     0.036286         48
     0.036286         49
     0.036286         50
     0.036286         51
     0.036286         52
     0.036286         53
     0.036286         54
     0.036286         55
     0.036286         56
     0.036286         57
     0.036286         58
     0.036286         59
     0.036286         60
     0.036286         61
     0.036286         62
     0.036286         63
     0.036286         64
     0.036286         65
     0.036286         66
     0.036286         67
     0.036286         68
     0.036286         69
     0.036286         70
     0.036286         71
     0.036286         72
     0.036286         73
     0.036286         74
     0.036286         75
     0.036286         76
     0.036286         77
     0.036286         78
     -0.196594         79
  
```

```

eigenvector( 75 ) = C.246083D+C2
frequency = 0.496068D+01
  
```

```

eigenvector;
  
```

```

1   0.000008          1
     0.000458          2
     -0.000458          3
     0.000458          4
     -0.000458          5
     0.000458          6
     -0.000458          7
     0.000458          8
     -0.000458          9
     0.000458          10
     -0.000458          11
     0.000458          12
     -0.000458          13
     0.000458          14
     -0.000458          15
     0.000458          16
     -0.000458          17
     0.000458          18
     -0.000458          19
     0.000458          20
     -0.000458          21
     0.000458          22
     -0.000458          23
     0.000458          24
     -0.000458          25
     0.000458          26
     -0.000458          27
     0.000458          28
     -0.000458          29
     0.000458          30
     -0.000458          31
     0.000458          32
     -0.000458          33
     0.000458          34
     -0.000458          35
     0.000458          36
     -0.000458          37
     0.000458          38
     -0.000458          39
     0.000458          40
     -0.000458          41
     0.000458          42
     -0.000458          43
     0.000458          44
     -0.000458          45
     0.000458          46
     -0.000458          47
     0.000458          48
     -0.000458          49
     0.000458          50
     -0.000458          51
     0.000458          52
     -0.000458          53
     0.000458          54
     -0.000458          55
     0.000458          56
     -0.000458          57
     0.000458          58
     -0.000458          59
     0.000458          60
     -0.000458          61
     0.000458          62
     -0.000458          63
     0.000458          64
     -0.000458          65
     0.000458          66
     -0.000458          67
     0.000458          68
     -0.000458          69
     0.000458          70
     -0.000458          71
     0.000458          72
     -0.000458          73
     0.000458          74
     -0.000458          75
     0.000458          76
     -0.000458          77
     0.000458          78
     -0.000458          79
  
```

```

=====
=====
```

```

flap;      0.00052
           1   0.00052
           2   0.00052
           3   0.00052
           4   0.00052
           5   0.00052
           6   0.00052
           7   0.00052
           8   0.00052
           9   0.00052
           10  0.00052
           11  0.00052
           12  0.00052
           13  0.00052
           14  0.00052
           15  0.00052
           16  0.00052
           17  0.00052
           18  0.00052
           19  0.00052
           20  0.00052
           21  0.00052
           22  0.00052
           23  0.00052
           24  0.00052
           25  0.00052
           26  0.00052
           27  0.00052
           28  0.00052
           29  0.00052
           30  0.00052
           31  0.00052
           32  0.00052
           33  0.00052
           34  0.00052
           35  0.00052
           36  0.00052
           37  0.00052
           38  0.00052
           39  0.00052
           40  0.00052
           41  0.00052
           42  0.00052
           43  0.00052
           44  0.00052
           45  0.00052
           46  0.00052
           47  0.00052
           48  0.00052
           49  0.00052
           50  0.00052
           51  0.00052
           52  0.00052
           53  0.00052
           54  0.00052
           55  0.00052
           56  0.00052
           57  0.00052
           58  0.00052
           59  0.00052
           60  0.00052
           61  0.00052
           62  0.00052
           63  0.00052
           64  0.00052
           65  0.00052
           66  0.00052
           67  0.00052
           68  0.00052
           69  0.00052
           70  0.00052
           71  0.00052
           72  0.00052
           73  0.00052
           74  0.00052
           75  0.00052
           76  0.00052
           77  0.00052
           78  0.00052
           79  0.00052
  
```

```

=====
=====
```

wake mode shapes
etar, eta, etat:

nonlinear solution for large angles
rigid flap propulsive trim solution

93/03/29
13:51:36

articulated-composite.wake.output

```

all angles in degrees

advance ratio= 0.11303

b0 = 1.926C7 b1c = -2.78599 b2s = -0.21984
thetaic = 5.83286 thetaic' = -0.13433 thetaic'' = 0.74247
alpha = 3.94635 phi = 0.33121

lambda = 0.84012 lambda0 = 0.83267 lamday = 0.83000
lambda_max = 0.83000 lamday_max = 0.83000
thrust coefficient = 0.3076;

tail: rotor collective = 4.0937

theta0 = 5.74000
thetaic = 2.66000
thetaic's = 1.33000
totali = 4.48000
alphas = 2.93000
phis = -1.29000

total uniform inflow: lambda = 0.04015
lambda_max = 0.30000
lamday = 0.30000
lamday_max = 0.30000

time uniform inflow: lambda = 0.03000
lambda_max = 0.03000

```

```

local dof 9 9 29 49 69 89
local dof 10 10 30 50 70 90
local dof 11 11 31 51 71 91
local dof 12 12 32 52 72 92
local dof 13 13 33 53 73 93
local dof 14 14 34 54 74 94
local dof 15 15 35 55 75 95
local dof 16 16 36 56 76 96
local dof 17 17 37 57 77 97
local dof 18 18 38 58 78 98
local dof 19 19 39 59 79 99
local dof 20 20 40 60 80 100
local dof 21 21 41 61 81 101
local dof 22 22 42 62 82 102
local dof 23 23 43 63 83 103
local dof 24 24 44 64 84 104
local dof 25 25 45 65 85 105

```

```

lag harmonics
-----+
zero harm = -0.259452
1st cos = 0.301196 1st sin = 0.301052
2nd cos = -0.333351 2nd sin = 0.330551
3rd cos = -0.330620 3rd sin = 0.330330
4th cos = 0.330399 4th sin = -0.330333
5th cos = 0.330300 5th sin = 0.330330

```

```

flap harmonics
-----+
zero harm = 0.030932
1st cos = -0.338980 1st sin = 0.032567
2nd cos = -0.030110 2nd sin = 0.030110
3rd cos = -0.030229 3rd sin = -0.030229
4th cos = 0.030306 4th sin = 0.030301
5th cos = 0.030303 5th sin = 0.030303

```

```

torsion harmonics
-----+
zero harm = -0.334904
1st cos = 0.003837 1st sin = 0.002191
2nd cos = -0.003236 2nd sin = -0.003077
3rd cos = -0.003222 3rd sin = -0.003025
4th cos = 0.003237 4th sin = -0.003017
5th cos = -0.003221 5th sin = -0.003003

```

```

vehicle equilibrium residuals
x: for r2; y for z for roll: pitch: yaw: roll: pitch: yaw
0.032456 -0.322140 0.019340 0.003392 -0.000464 -0.000901

```

```

initial controls used for response (deg)
alphas phis thc thic this
2.93 -0.29 5.74 2.46 1.33

```

```

time finite element model description
(response)
global time dof corresponding to local time dof

```

```

time element # 1 2 3 4 5
local dof 1 1 2 2 41 61 81
local dof 2 2 22 42 62 82
local dof 3 3 23 43 63 83
local dof 4 4 24 44 64 84
local dof 5 5 25 45 65 85
local dof 6 6 26 46 66 86
local dof 7 7 27 47 67 87
local dof 8 8 28 48 68 88

```

```

response convergence function = 1.0000000
step convergence function = 0.01973e-25

```


93/03/29
13:51:36

articulated-composite.wake.output

9

Jacobian evaluation -- control perturbation # 4

Lag harmonics

```
zero harm = -0.060262; 1st sin = 0.001969
1st cos = 0.301266 2nd sin = 0.000364
2nd cos = -0.300041 3rd sin = 0.000301
3rd cos = -0.000021; 4th sin = -0.000003
4th cos = -0.000001; 5th sin = 0.000000
5th cos = 0.000000
```

Flap harmonics

```
zero harm = 0.030765 1st sin = 0.032428
1st cos = -0.030886 2nd sin = 0.033168
2nd cos = -0.000221; 3rd sin = -0.000223
3rd cos = -0.000006; 4th sin = 0.000001
4th cos = 0.000001; 5th sin = 0.000000
```

Torsion harmonics

```
zero harm = -0.000989 1st sin = 0.002269
1st cos = 0.000925 2nd sin = -0.000047
2nd cos = -0.000021; 3rd sin = -0.000024
3rd cos = -0.000026 4th sin = -0.000018
4th cos = 0.000036; 5th sin = -0.000001
5th cos = -0.000002
```

Vehicle equilibrium residuals

#1: x for t2: z for

#3: z for t4: roll m

#5: pitch m

#6: yaw m

-0.0003465 -0.0003465 -0.0003465

Perturbed controls for Jacobian (deg)

alpha_s phi_s theta_s thic

2.93 -1.29 5.74 2.46

Jacobian evaluation -- control perturbation # 5

Lag harmonics

```
zero harm = -0.060202 1st sin = 0.001993
1st cos = 0.301190 2nd sin = 0.000257
2nd cos = -0.300258 3rd sin = 0.000205
3rd cos = -0.000023 4th sin = -0.000003
4th cos = 0.000003 5th sin = 0.000000
5th cos = 0.000000
```

Flap harmonics

```
zero harm = 0.030894 1st sin = 0.002294
1st cos = -0.030857 2nd sin = -0.000266
2nd cos = -0.000022 3rd sin = -0.000025
3rd cos = -0.000007 4th sin = -0.000017
4th cos = 0.000001 5th sin = -0.000002
5th cos = 0.000000
```

Perturbed controls for Jacobian (deg)

alpha_s phi_s theta_s thic

2.93 -1.29 5.74 2.46

Torsion harmonics

```
zero harm = -0.060262; 1st sin = 0.001969
1st cos = 0.301266 2nd sin = 0.000364
2nd cos = -0.300041 3rd sin = 0.000301
3rd cos = -0.000021; 4th sin = -0.000003
4th cos = -0.000001; 5th sin = 0.000000
5th cos = 0.000000
```

Vehicle equilibrium residuals

#1: x for t2: y for

#3: z for

#4: roll m

#5: pitch m

#6: yaw m

-0.0002700 -0.0002700 -0.0002700

Perturbed controls for Jacobian (deg)

alpha_s phi_s theta_s thic

2.93 -1.29 5.74 2.46

Jacobian evaluation -- control perturbation # 6

Lag harmonics

```
zero harm = -0.060262; 1st sin = 0.001969
1st cos = 0.301266 2nd sin = 0.000364
2nd cos = -0.300041 3rd sin = 0.000301
3rd cos = -0.000021; 4th sin = -0.000003
4th cos = -0.000001; 5th sin = 0.000000
5th cos = 0.000000
```

Flap harmonics

```
zero harm = 0.030894 1st sin = 0.002294
1st cos = -0.030857 2nd sin = -0.000266
2nd cos = -0.000022 3rd sin = -0.000025
3rd cos = -0.000007 4th sin = -0.000017
4th cos = 0.000001 5th sin = -0.000002
5th cos = 0.000000
```

Torsion harmonics

```
zero harm = -0.060202 1st sin = 0.001993
1st cos = 0.301190 2nd sin = 0.000257
2nd cos = -0.300258 3rd sin = 0.000205
3rd cos = -0.000023 4th sin = -0.000003
4th cos = 0.000003 5th sin = 0.000000
5th cos = 0.000000
```

Perturbed controls for Jacobian (deg)

alpha_s phi_s theta_s thic

2.93 -1.29 5.74 2.46

Jacobian evaluation -- control perturbation # 7

Lag harmonics

```
zero harm = 0.030894 1st sin = 0.002294
1st cos = -0.030857 2nd sin = -0.000266
2nd cos = -0.000022 3rd sin = -0.000025
3rd cos = -0.000007 4th sin = -0.000017
4th cos = 0.000001 5th sin = -0.000002
5th cos = 0.000000
```

93/03/29

13:51:36

articulated-composite.wake.output

```
alphaE phis t0:0 this 0.004904
2.93 -1.29 5.74 2.46 1.33
```

```
t0:011
4.79
```

```
updated lambda: 0.031069
total lambda: 0.031069
induced lambda > alpha, alx, alv : 0.025439 0.000000 0.000000
```

```
coupled trim -- iteration # 1
lag harmonics
zero harm = -0.059452
1st cos = 0.001196 1st sin = 0.001952
2nd cos = -0.000551 2nd sin = -0.003251
3rd cos = -0.000220 3rd sin = 0.000000
4th cos = 0.000000 4th sin = -0.000003
5th cos = 0.000000 5th sin = 0.000000

flap harmonics
zero harm = 0.030833
1st cos = -0.038980 1st sin = 0.03567
2nd cos = -0.000279 2nd sin = -0.000170
3rd cos = -0.000066 3rd sin = -0.000229
4th cos = 0.000001 4th sin = 0.000000
5th cos = 0.000000 5th sin = 0.000000

torsion harmonics
zero harm = -0.004904
1st cos = 0.000857 1st sin = 0.002197
2nd cos = -0.000266 2nd sin = -0.000057
3rd cos = -0.000022 3rd sin = -0.000025
4th cos = 0.000007 4th sin = -0.000017
5th cos = -0.000001 5th sin = -0.000000

current coupled-trim controls (deg)
lambda = 0.046161
alpha phis t0:0 this 0.004904
2.93 -1.29 5.74 2.46 1.33
```

```
response convergence function = 0.30000000
trim convergence function = 0.01973825
coupled trim -- iteration # 2
lag harmonics
zero harm = -0.040818
1st cos = -0.001299 1st sin = -0.001461
2nd cos = 0.000845 2nd sin = 0.000216
3rd cos = 0.000000 3rd sin = 0.000006
4th cos = -0.000001 4th sin = 0.000001
5th cos = 0.000000 5th sin = 0.000000

flap harmonics
zero harm = 0.036477
1st cos = -0.046382 1st sin = 0.036197
2nd cos = -0.000039 2nd sin = 0.0000137
3rd cos = 0.000000 3rd sin = -0.000015
4th cos = 0.000002 4th sin = 0.000000
5th cos = 0.000000 5th sin = 0.000000

torsion harmonics
zero harm = -0.002456
1st cos = 0.000078 1st sin = 0.000000
2nd cos = 0.000024 2nd sin = -0.000011
3rd cos = 0.000002 3rd sin = 0.000007
4th cos = -0.000001 4th sin = -0.000001
5th cos = 0.000000 5th sin = -0.000000

circulation distribution for free wake:
most: size gamma x = 0.45 0.68 0.85 0.91 0.97
1: 0.012887 0.009171 0.012458 0.012887 0.012561 0.011948
2: 0.012349 0.009338 0.012289 0.012349 0.011869 0.011377
3: 0.012157 0.009004 0.012157 0.011851 0.011211 0.010224
4: 0.012062 0.008254 0.012062 0.011486 0.010609 0.009444
5: 0.012035 0.0013594 0.012035 0.011310 0.010130 0.008798
6: 0.012133 0.0013929 0.012133 0.011893 0.010893 0.008316
7: 0.012257 0.001241 0.012257 0.011888 0.010849 0.008200
8: 0.012518 0.001105 0.012518 0.011493 0.010940 0.008370
9: 0.012819 0.0011438 0.012819 0.011438 0.010304 0.008718
10: 0.013119 0.0011760 0.013119 0.011689 0.010793 0.009347
11: 0.013393 0.0011697 0.013393 0.011697 0.011367 0.010349
```


93.03.29

13.51.36

articulated-composite.wake.output

```

16   0.02020   0.057455   0.215335   0.218975   0.220426   0.C156.3
17   0.02425   0.051562   0.011430   0.01198   0.024725   0.C21303
18   0.026927   0.057761   0.011638   0.010811   0.025322   0.C26927
19   0.03133   0.036680   0.019591   0.01874   0.024496   0.C31133
20   0.021168   0.026935   0.0306930   0.030250   0.010390   0.C21168
21   0.020913   0.019185   0.030778   0.030751   0.020649   0.C20913
22   0.013159   0.016756   0.013159   0.013189   0.01044   0.008898
23   0.016754   0.013155   0.016754   0.015982   0.010798   0.013563
24   0.C1913   0.014920   0.01943   0.019421   0.017317   0.013352

vehicle equilibrium residuals:
fl: x for f2: y for f3: z for f4: roll m f5: pitch m f6: yaw m
-C.000012 -0.000065 -0.000065 -0.000065 -0.000065 -0.000065
          -0.000065 -0.000065 -0.000065 -0.000065 -0.000065 -0.000065

current coupled-trim controls (deg)
lambda = 0.C38486
alpha = 2.98
beta = -0.6;
psi = 7.62
roll = 3.99
pitch = 2.87
yaw = 5.25

updated lambda:
tctai_lambda = 2.038406
induced_alpha = 0.032687
induced_beta = 0.030000
induced_gamma = 0.030000
psi = 0.91
roll = 0.85
pitch = 0.91
yaw = 0.91

updated ct / sigma = 0.072404

induced velocity, (deg,vinr3(z,r,R,psi))
x = radial station
y = axial
z = azimuthal

x = 0.45   C.68   0.85   0.91   0.91
y = 0.3524   -0.3759   -0.1037   -0.1104   -0.1149
      -0.3196   -0.3730   -0.0985   -0.1085   -0.1231
      -0.30477   -0.3718   -0.0957   -0.1039   -0.1100
      -0.0486   -0.1449   -0.1006   -0.1099   -0.1121
      -0.0523   -0.0523   -0.05856   -0.1227   -0.1308
      -0.05227   -0.05227   -0.1329   -0.1434   -0.1702
      -0.0691   -0.0691   -0.1851   -0.1229   -0.1229
      -0.0684   -0.0684   -0.38592   -0.0315   -0.0318
      -0.0663   -0.0663   -0.38592   -0.0315   -0.0318
      -0.0436   -0.0436   -0.238   -0.0267   -0.0353
      -0.0420   -0.0420   -0.0533   -0.0238   -0.0238
      -0.0444   -0.0444   -0.0111   -0.0221   -0.0146
      -0.0459   -0.0459   -0.0244   -0.0275   -0.0172
      -0.0388   -0.0388   -0.0320   -0.0366   -0.0366
      -0.0466   -0.0466   -0.0298   -0.0327   -0.0194
      -0.0398   -0.0398   -0.0119;   -0.0138   -0.0141
      -0.0386   -0.0386   -0.0619   -0.0305   -0.0329
      -0.0359   -0.0359   -0.0416   -0.0070   -0.0044
      -0.0446   -0.0446   -0.0446   -0.0139   -0.0197
      -0.0446   -0.0446   -0.0446   -0.0139   -0.0197
      -0.0528   -0.0528   -0.0825   -0.1173   -0.1352
      -0.0519   -0.0519   -0.0777   -0.0999   -0.1047
      -0.0515   -0.0515   -0.0747   -0.0953   -0.1032
      -0.0534   -0.0534   -0.0756   -0.0989   -0.1066
          -0.0566   -0.0566   -0.0989   -0.1197

updated ct / sigma = 0.072404

induced velocity, (deg,vinr3(z,r,R,psi))
x = radial station
y = axial
z = azimuthal

x = 0.45   C.68   0.85   0.91   0.91
y = 0.3524   -0.3759   -0.1037   -0.1104   -0.1149
      -0.3196   -0.3730   -0.0985   -0.1085   -0.1231
      -0.30477   -0.3718   -0.0957   -0.1039   -0.1100
      -0.0486   -0.1449   -0.1006   -0.1099   -0.1121
      -0.0523   -0.0523   -0.05856   -0.1227   -0.1308
      -0.05227   -0.05227   -0.1329   -0.1434   -0.1702
      -0.0691   -0.0691   -0.1851   -0.1229   -0.1229
      -0.0684   -0.0684   -0.38592   -0.0315   -0.0318
      -0.0663   -0.0663   -0.38592   -0.0315   -0.0318
      -0.0436   -0.0436   -0.238   -0.0267   -0.0353
      -0.0420   -0.0420   -0.0533   -0.0238   -0.0238
      -0.0444   -0.0444   -0.0111   -0.0221   -0.0146
      -0.0459   -0.0459   -0.0244   -0.0275   -0.0172
      -0.0388   -0.0388   -0.0320   -0.0366   -0.0366
      -0.0466   -0.0466   -0.0298   -0.0327   -0.0194
      -0.0398   -0.0398   -0.0119;   -0.0138   -0.0141
      -0.0386   -0.0386   -0.0619   -0.0305   -0.0329
      -0.0359   -0.0359   -0.0416   -0.0070   -0.0044
      -0.0446   -0.0446   -0.0446   -0.0139   -0.0197
      -0.0446   -0.0446   -0.0446   -0.0139   -0.0197
      -0.0528   -0.0528   -0.0825   -0.1173   -0.1352
      -0.0519   -0.0519   -0.0777   -0.0999   -0.1047
      -0.0515   -0.0515   -0.0747   -0.0953   -0.1032
      -0.0534   -0.0534   -0.0756   -0.0989   -0.1066
          -0.0566   -0.0566   -0.0989   -0.1197

response convergence function = 0.0009734;
trim convergence function = 0.00036749

```

93/03/29

13:51:36

articulated-composite.wake.output

198.00	-0.0000005	-0.0211422	12.	0.00553386	-0.0042333	0.3816263	0.0022057
216.00	-0.0036002	-0.019443	90.	0.0068559	-0.0034944	0.3893821	0.0022794
234.00	0.0355031	0.013885	108.	0.002688	0.0038202	0.3853485	-0.0023475
252.00	0.0250032	0.013945	116.	0.000116	-0.0035018	0.3765168	-0.0020771
270.00	0.0250031	0.008384	126.	0.002827	-0.0055974	0.3750298	-0.0024362
288.00	0.0250032	0.0092918	144.	0.005586	-0.0023333	0.3843662	-0.0014641
306.00	0.0250033	0.0145639	162.	0.0068559	-0.0034944	0.3862623	-0.0043969
324.00	-0.0000003	-0.0128667	180.	0.0068559	-0.0034944	0.3890271	0.0022794
342.00	-0.0000001	-0.0028116	198.	0.002688	0.0038202	0.3853485	-0.0028056
			216.	0.000116	-0.0035018	0.3765168	-0.0020771
			234.	0.002827	-0.0055974	0.3750298	-0.0024362
			252.	0.005586	-0.0023333	0.3843662	-0.0014641
			270.	0.0068559	-0.0034944	0.3890271	0.0022794
			288.	0.002688	0.0038202	0.3853485	-0.0028056
			306.	0.000116	-0.0035018	0.3765168	-0.0020771
			324.	0.002827	-0.0055974	0.3750298	-0.0024362
			342.	0.005586	-0.0023333	0.3843662	-0.0014641
						0.0043969	-0.0043969

elastic twist distribution:

1.0000	0.007132	zero harm = 0.003582	1st sin = 0.000000	magnitude/zero harmonic fz
0.9356	0.007235	1st cos = 0.000000	2nd sin = 0.000000	0.000000
0.8712	0.006935	2nd cos = 0.000000	3rd sin = 0.000000	0.000000
0.8144	0.006521	3rd cos = 0.000000	4th sin = 0.000000	0.000000
0.7576	0.005900	4th cos = 0.000000	5th sin = 0.000000	0.000000
0.7008	0.005671	5th cos = 0.000000	6th sin = 0.000000	0.000000
0.6439	0.004044	hub mx harmonics:		
0.5492	0.001866	zero harm = -0.002621	1st sin = 0.000000	magnitude/zero harmonic fz
0.4545	-0.000575	1st cos = 0.000000	2nd sin = 0.000000	0.000000
0.3598	-0.003219	2nd cos = 0.000000	3rd sin = 0.000000	0.000000
0.2652	-0.005980	3rd cos = 0.000000	4th sin = 0.000000	0.000000
0.1818	-0.007583	4th cos = 0.000000	5th sin = 0.000000	0.000000
0.0985	-0.003864	5th cos = 0.000000	6th sin = 0.000000	0.000000
0.0649	-0.002956			

blade root forces & moments (rotating frame)

deg	f_xr	f_yr	f_zr	m_xr	m_yr	m_zr	mag	hub mx harmonics:
0.	-0.032447	-0.042207	0.3000197	3.0004444	-0.0012389	zero harm = 0.002621	0.000000	zero harm = 0.000000
18.	-0.0315682	-0.0191983	0.2998889	3.0003724	-0.0003965	1st cos = 0.000000	0.000000	1st sin = 0.000000
36.	-0.0305389	-0.0032981	0.0000053	0.0003108	-0.0009433	2nd cos = 0.000000	0.000000	2nd sin = 0.000000
54.	-0.0322770	0.0068612	-0.0000095	-0.0002144	-0.0012387	3rd cos = 0.000000	0.000000	3rd sin = 0.000000
72.	-0.0316443	-0.0392277	0.0072233	-0.0000000	-0.0000000	4th cos = 0.000000	0.000000	4th sin = 0.000000
90.	-0.0374699	0.0232930	-0.0000000	-0.0000000	-0.0000000	5th cos = 0.000000	0.000000	5th sin = 0.000000
108.	0.5194184	-0.0152901	0.0220533	-0.00000404	-0.0000000	6th cos = 0.000000	0.000000	6th sin = 0.000000
126.	-0.517978	-0.031267	0.0215655	0.00015551	-0.0000000	1st cos = 0.000000	0.000000	1st sin = 0.000000
144.	-0.516906	-0.0339173	0.0309106	0.0003957	-0.0000000	2nd cos = 0.000000	0.000000	2nd sin = 0.000000
162.	-0.5172392	-0.0360709	0.0463915	-0.0000000	-0.0000000	3rd cos = 0.000000	0.000000	3rd sin = 0.000000
180.	-0.5174075	-0.0387339	0.0571468	-0.0000000	-0.0000000	4th cos = 0.000000	0.000000	4th sin = 0.000000
198.	-0.5233119	-0.0366004	0.0561518	-0.0000000	-0.0000000	5th cos = 0.000000	0.000000	5th sin = 0.000000
216.	-0.5231548	-0.0349303	0.0463031	-0.0000000	-0.0000000	6th cos = 0.000000	0.000000	6th sin = 0.000000
234.	-0.52223381	-0.0340065	0.0344162	0.0000000	-0.0000000	1st cos = 0.000000	0.000000	1st sin = 0.000000
252.	-0.523251	-0.0350274	0.0298579	0.0000000	-0.0000000	2nd cos = 0.000000	0.000000	2nd sin = 0.000000
270.	0.5244642	-0.0150561	0.0228575	-0.0000000	-0.0000000	3rd cos = 0.000000	0.000000	3rd sin = 0.000000
288.	-0.5256062	-0.0332282	0.0192937	-0.0000000	-0.0000000	4th cos = 0.000000	0.000000	4th sin = 0.000000
306.	0.5252042	-0.0313651	0.0122315	-0.0000000	-0.0000000	5th cos = 0.000000	0.000000	5th sin = 0.000000
324.	-0.5244577	-0.0314515	0.0294939	-0.0000000	-0.0000000	6th cos = 0.000000	0.000000	6th sin = 0.000000
342.	-0.52229195	-0.0318417	-0.0378713	-0.0000000	-0.0000000	1st cos = 0.000000	0.000000	1st sin = 0.000000
						2nd cos = 0.000000	0.000000	2nd sin = 0.000000
						3rd cos = 0.000000	0.000000	3rd sin = 0.000000
						4th cos = 0.000000	0.000000	4th sin = 0.000000
						5th cos = 0.000000	0.000000	5th sin = 0.000000
						6th cos = 0.000000	0.000000	6th sin = 0.000000
						hub my harmonics:		
						zero harm = 0.000000		
						1st cos = 0.000000		
						2nd cos = 0.000000		
						3rd cos = 0.000000		
						4th cos = 0.000000		
						5th cos = 0.000000		
						6th cos = 0.000000		

hub loads in nonrotating frame

deg	f_xh	f_yh	f_zh	f_2h	f_3h	f_4h	f_5h	f_6h
0.	0.0068559	-0.00004944	0.0000000	0.0000000	-0.0000000	-0.0000000	-0.0000000	-0.0000000
18.	0.0026388	0.0000000	0.0000000	0.0000000	-0.0000000	-0.0000000	-0.0000000	-0.0000000
36.	0.0000016	-0.0000000	0.0000000	0.0000000	-0.0000000	-0.0000000	-0.0000000	-0.0000000
54.	0.0026827	-0.0005974	0.0000000	0.0000000	-0.0000000	-0.0000000	-0.0000000	-0.0000000

93/03/29
13:31:36

articulated-composite.wake.output

```

5th cos = 0.000000      5th sin = 0.000000
6th cos = 0.000000      6th sin = 0.000000

hub mz harmonics:
zero harm = -0.04279
1st cos = 0.000000      magnitude/zero harmonic mz
1st cos = 0.000000      0.000000
2nd cos = 0.000000      0.000000
2nd cos = 0.000000      0.000000
3rd cos = 0.000000      0.000000
3rd cos = 0.000000      0.000000
4th cos = -0.000237    3rd sin = 0.000000
4th cos = 0.000046     4th sin = 0.000000
5th cos = 0.000000      5th sin = 0.000000
5th cos = 0.000000      0.000000
6th cos = 0.000000      6th sin = 0.000000

**** rotating blade load harmonics ****
(loads by force summation i)

```

```

hub fx harmonics:
zero harm = 0.521066      magnitude/zero harmonic fz
1st cos = 0.001451      1st sin = -0.003069
2nd cos = -0.005679     2nd sin = 0.000160
3rd cos = 0.000534     3rd sin = -0.000050
4th cos = -0.000123    4th sin = 0.000046
5th cos = 0.000066     5th sin = 0.000000
6th cos = -0.000318    6th sin = -0.000265

**** rotating blade load harmonics ****
(loads by total summation i)

```

```

hub fy harmonics:
zero harm = -0.000340      magnitude/zero harmonic fz
1st cos = 0.002308      1st sin = 0.000340
2nd cos = 0.000101      2nd sin = -0.000286
3rd cos = 0.000516      3rd sin = 0.000155
4th cos = -0.000893     4th sin = 0.000074
5th cos = -0.000300     5th sin = -0.000336
6th cos = 0.000422      6th sin = -0.000061

**** rotating blade load harmonics ****
(loads by force summation i)

```

```

hub fz harmonics:
zero harm = -0.004566      magnitude/zero harmonic fz
1st cos = 0.001451      1st sin = 0.000340
2nd cos = -0.000286     2nd sin = -0.000160
3rd cos = 0.000050      3rd sin = -0.000050
4th cos = -0.000015     4th sin = 0.000000
5th cos = 0.000000      5th sin = 0.000000
6th cos = -0.000000     6th sin = -0.000000

**** rotating blade load harmonics ****
(loads by total summation i)

```

```

hub mx harmonics:
zero harm = 0.021870      magnitude/zero harmonic mz
1st cos = -0.000416     1st sin = -0.003668
2nd cos = 0.000416     2nd sin = 0.002036
3rd cos = -0.000354    3rd sin = -0.003399
4th cos = 0.000210     4th sin = 0.000466
5th cos = -0.000181    5th sin = 0.000285
6th cos = -0.000140    6th sin = -0.000325
6th cos = -0.000385    6th sin = 0.000270

**** rotating blade load harmonics ****
(loads by force summation i)

```

```

hub my harmonics:
zero harm = -0.000043      magnitude/zero harmonic mz
1st cos = 0.000008      1st sin = 0.000000
2nd cos = -0.000013     2nd sin = -0.000013
3rd cos = 0.000020      3rd sin = 0.000020
4th cos = -0.000012     4th sin = -0.000012
5th cos = 0.000014      5th sin = 0.000014
6th cos = 0.000002      6th sin = 0.000002

**** rotating blade load harmonics ****
(loads by total summation i)

```

```

hub mx harmonics:
zero harm = -0.000043      magnitude/zero harmonic mz
1st cos = 0.000008      1st sin = 0.000000
2nd cos = -0.000013     2nd sin = -0.000013
3rd cos = 0.000020      3rd sin = 0.000020
4th cos = -0.000012     4th sin = -0.000012
5th cos = 0.000014      5th sin = 0.000014
6th cos = 0.000002      6th sin = 0.000002

**** rotating blade load harmonics ****
(loads by force summation i)

```

```

hub my harmonics:
zero harm = -0.000043      magnitude/zero harmonic mz
1st cos = 0.000008      1st sin = 0.000000
2nd cos = -0.000013     2nd sin = -0.000013
3rd cos = 0.000020      3rd sin = 0.000020
4th cos = -0.000012     4th sin = -0.000012
5th cos = 0.000014      5th sin = 0.000014
6th cos = 0.000002      6th sin = 0.000002

**** rotating blade load harmonics ****
(loads by total summation i)

```

93/03/29
13:51:36

articulated-composite.wake.output

hub mz harmonics:
zero harm = -0.301283
1st cos = 0.000052
2nd cos = 0.000037
3rd cos = 0.000030
4th cos = -0.000055
5th cos = 0.000006
6th cos = 0.000000

			magnitude/zero harmonic mz
1st sin	=	-0.000045	-0.063516
2nd sin	=	-0.000008	-0.009616
3rd sin	=	0.000025	-0.036017
4th sin	=	0.000019	-0.054311
5th sin	=	-0.000001	-0.001311
6th sin	=	0.000005	-0.000491

15
16

Sample Output:

Hingeless Rotor

```

title    bo-ics data
        (ref 1 agard ls-78 rototraft system id pp 9-, to 9-50)
        (ref 2 nasa cr-544 a compilation and analysis of
        helicopter handling qualities data )
rotor + fuselage + dynamic inflow
        coupled trim in forward flight.

aeromechanical stability   5 fuselage dof
dynamic inflow
quasi-steady aero
        floquet approach in fixed frame

```

```

input_data

```

```

title    bo-ics data
        (ref 1 agard ls-78 rototraft system id pp 9-, to 9-50)
        (ref 2 nasa cr-544 a compilation and analysis of
        helicopter handling qualities data )
rotor + fuselage + dynamic inflow
        coupled trim in forward flight.

aeromechanical stability   5 fuselage dof
dynamic inflow
quasi-steady aero
        floquet approach in fixed frame

```

```

input_data

```

```

rotor_name      : myrotor
rotor_type      : hingeless
no_blades      : 4
solidity       : 0.07000
lock_no        : 5.20000
ct/sigma       : 0.07000
cg_below_hub   : 0.20000
cg_hub_offset_x: 0.00000
cg_hub_offset_y: 0.00000

blade_properties

```

```

twist(deg)      : 0.03000
precone(deg)   : 0.00000
root_cut(%)    : 0.00000
no_spare_elements: 5
no_elem_in_segments: 5
material_type  : isotropic

```

```

blade element properties

```

University of Maryland advanced rotor code

ele.no	length	mass	el-y	el-z
1	0.230000	1.000000	0.310800	0.326800
2	0.230000	1.000000	0.310800	0.326800
3	0.230000	1.000000	0.310800	0.326800
4	0.230000	1.000000	0.310800	0.326800
5	0.190000	1.000000	0.310800	0.326800

ele.no	g;	ea	east	eg
1	0.006150	47.959	0.000000	0.000000
2	0.006150	47.959	0.000000	0.000000
3	0.006150	47.959	0.000000	0.000000
4	0.006150	47.959	0.000000	0.000000
5	0.006150	47.959	0.000000	0.000000

ele.no	el1	el2	el3	el4
1	0.0000D+00	0.0000D+00	0.0000D+00	0.0000D+00
2	0.0000D+00	0.0000D+00	0.0000D+00	0.0000D+00
3	0.0000D+00	0.0000D+00	0.0000D+00	0.0000D+00
4	0.0000D+00	0.0000D+00	0.0000D+00	0.0000D+00
5	0.0000D+00	0.0000D+00	0.0000D+00	0.0000D+00

ele.no	sk1	sk2	chord	ed
1	0.000174	0.000610	0.05500	0.000000
2	0.000174	0.000610	0.05500	0.000000
3	0.000174	0.000610	0.05500	0.000000
4	0.000174	0.000610	0.05500	0.000000
5	0.000174	0.000610	0.05500	0.000000

ele.no	le_swp	swdeg	ddeg
1	0	0.000000	0.000000
2	0	0.000000	0.000000

b0105.output

Wed Mar 31 11:39:35 1993

2

```
#-----#
#-----# 0.000000 0.300000 0.300000 0.300000
#-----# 1 3 0 0.000000 0.300000 0.300000 0.300000
#-----# 1 4 3 0 0.000000 0.300000 0.300000 0.300000
#-----# 1 5 0 0 0.000000 0.300000 0.300000 0.300000
#-----#
```

```
fuselage_properties
-----#
  effective_x_mass = 77.240000
  effective_y_mass = 77.240000
  effective_z_mass = 77.240000
  fuselage_pitch_inertia = 2.739000
  fuselage_roll_inertia = 0.000000
  fuselage_x_damper = 0.000000
  fuselage_y_damper = 0.000000
  fuselage_z_damper = 0.000000
  fuselage_pitch_damper = 0.000000
  fuselage_roll_damper = 0.000000
  fuselage_x_spring = 0.000000
  fuselage_y_spring = 0.000000
  fuselage_z_spring = 0.000000
  fuselage_pitch_spring = 0.000000
  fuselage_roll_spring = 0.000000
  body_roll_moment_coeff = 0.000000
  body_pitch_moment_coeff = 0.000000
  body_side_force_coeff = 0.000000
  parasite_drag_area = 0.000000
  tail_properties
-----#
  rad_ratio_tail_rot = 0.200000
  solidity_tail_rot = 0.120000
  gear_ratio_tail_rot = 5.000000
  twist(deg)tail_rot = 0.000000
  cg_tail_rot_offset_x = -0.200000
  tail_rot_above_cg = 0.200000
  c1_tail_rot = 0.000000
  hor_tail_area = 0.010000
  cg_tail_hor_offset_x = 0.950000
  cg_tail_hor = 0.300000
  cg_tail_hor = 0.200000
  airfoil_properties
-----#
  ref_lift_curve_slope = 6.000000
  c0 = 6.000000
  c1 = 0.000000
  c2 = 0.000000
  c3 = 0.000000
  c4 = 0.000000
  stability_analysis
-----#
  analysis option
```

```

analysis option : fix_qs_flop

no_psi_locations : 24
f_loquet_integration_by : dgear method

tol_for_dgear = 0.000150 (default)
output options :
-----  

print_control:
hub_load_control:  

no_spatial_elements = 5  

no_time_elements = 4  

no_of_stability_modes = 6  

no_of_unsteady_aero_iterations = 99  

nC = 4C  

qs_damping_factor = 1.000 u-s damping factor = 0.033  

lockin = 0 irani = 1 no. blades = 4  

luncl = 0 apert = 4 brev = 5 nhub = 1  

lunimp = 0 atsch = 0 lartic = 3 dyn = 1  

lunmom = 0 impac = 0 stab = 4 incode = 1  

lusep = 0 lcptr = 1 irafus = 1 lsfwke = 0  

lvertx = 0 ltrny = 1 tip mach number = 0.650  

element number = 1
element number = 2
element number = 3
element number = 4
element number = 5
element number = 6
element number = 7
element number = 8
element number = 9
element number = 10
element number = 11
element number = 12
element number = 13
element number = 14
element number = 15
element number = 16
element number = 17
element number = 18
element number = 19
element number = 20
element number = 21
element number = 22
element number = 23
element number = 24
eiy = 0.010800 ebl = 0.300000 eq = 0.000000 skml = 0.000174
eiz = 0.226800 ebl = 0.300000 eq = 0.000000 skml = 0.000610
gj = 0.006150 ebl = 0.300000 eq = 0.000000 skml = 1.0550
eac = 47.96 ec1 = 0.000330 e1 = 0.200000 eq = 0.055000
eiy = 0.010800 ebl = 0.300000 eq = 0.000000 skml = 0.000174
eiz = 0.226800 ebl = 0.300000 eq = 0.000000 skml = 0.000610
gj = 0.006150 ebl = 0.300000 eq = 0.000000 skml = 1.0550
eac = 47.96 ec1 = 0.000330 e1 = 0.200000 eq = 0.055000
-----  

advance_ratio = 0.250000
gamma = 5.250000 cc = 0.000000 cl = 6.300000
dc = 0.006000 dl = 0.000000 cd = 0.250000
density = 1.000000 bkg = 0.000000 sigma = 0.010000
cmac = 0.000000 cl = 0.000000 sic = 6.000000
thtw = 0.000000 ct/sigma = 0.070000
tbar = 0.2000 xcg = 0.0000 ycg = 0.0000
cmxf = 0.0000 emyf = 0.0000 fbya = 0.0100
cyf = 0.0000 thfp = 0.0000 etau = 0.9000
-----  

sigmat = 0.1200 gratio = 5.0000 twail = 0.0000
rtrat = 0.2000 xlrt = 1.2000 ztrt = 0.2500
tipre = 0.6500 clt = 6.0000
xtriz = 0.9500 aratt = 0.0110
ccht = 6.0000
cort = 0.2000
lrot = 0
sig2(1) = 0.000 0.000 0.000 0.000 0.000
sig2p(1) = 0.000 0.000 0.000 0.000 0.000
bodys = 1. 2. 3. 4. 5.
mass = 77.24000 77.24000 77.24000 77.24000 2.73900
cdamp = 0.30000 0.30000 0.30000 0.30000 0.00000
spring = 0.30000 0.30000 0.30000 0.30000 0.00000
global dof corresponding to local dof
spatial element mode: description
(Connectivity and geometry)
global: element 1 2 3 4
spatial: element 1 2 3
-----  


```

```

local dof 1 10 19 28 37 0 0.00000 26 0.30530 27
local dof 2 9 18 27 36 45 0.36634 28 0.81735 30
local dof 3 7 16 25 34 43 0.30030 29 0.30030 31
local dof 4 1 12 19 28 37 0.00000 30 0.20030 32
local dof 5 12 20 29 38 47 0.00000 31 0.24541 33
local dof 6 22 21 30 39 48 0.00000 32 0.30030 34
local dof 7 11 20 29 38 47 0.00000 33 0.30030 35
local dof 8 3 12 21 30 39 0.00000 34 0.30030 36
local dof 9 13 22 31 40 49 0.00000 35 0.30030 37
local dof 10 14 23 32 41 50 0.00000 36 0.30030 38
local dof 11 4 13 22 31 40 0.00000 37 0.30030 39
local dof 12 5 14 23 32 41 0.00000 38 0.30030 40
local dof 13 15 24 33 42 51 0.00000 39 0.30030 41
local dof 14 8 17 26 35 44 0.00000 40 0.30030 42
local dof 15 6 15 24 33 42 0.00000 41 0.30030 43
eigenvalue( 44 ) = 0.131279C+CI frequency = 0.114574D-31
eigenvector:
 1  0.00000  2  0.00000  3  0.00000
 2  0.349127  5  0.431583  6  0.30030
 3  0.00000  8  0.00000  9  0.30030
 4  0.00000 11  0.00000 12  0.30030
 5  0.00000 13  0.429554 15  0.30030
 6  0.00000 14  0.262944 17  0.30030
 7  0.00000 16  0.00000 18  0.30030
 8  0.00000 19  0.00000 21  0.30030
 9  0.178263 23  0.415336 24  0.30030
10  0.00000 25  0.00000 27  0.30030
11  0.00000 26  0.00000 28  0.30030
12  0.00000 29  0.00000 30  0.30030
13  0.098191 32  0.382355 33  0.30030
14  0.00000 34  0.00000 35  0.30030
15  0.00000 36  0.00000 37  0.30030
16  0.00000 38  0.281736 42  0.30030
17  0.00000 40  0.030199 43  0.30030
18  0.00000 41  0.00000 44  0.30030
eigenvalue( 43 ) = 0.123350C+CI frequency = 0.35212E+C1
eigenvector:
 1  0.00000  2  0.00000  3  0.00000
 2  -0.141463  5  0.673936  6  0.00000
 3  0.00000  8  0.00000  9  0.00000
 4  0.00000 11  0.00000 12  0.00000
 5  -0.011418 14  0.586417 15  0.00000
 6  0.00000 17  0.00000 18  0.00000
 7  0.00000 20  0.00000 21  0.00000
 8  0.00000 22  0.075293 23  0.00000
 9  0.00000 25  0.00000 26  0.00000
10  0.00000 28  0.00000 29  0.00000
11  0.084593 32  0.337717 33  0.00000
12  0.00000 34  0.00000 35  0.00000
13  0.00000 37  0.00000 38  0.00000
14  0.00000 40  0.035411 41  0.295261
15  0.00000 43  0.00000 44  0.00000
eigenvalue( 42 ) = 0.197773C+CI frequency = 0.444719D+01
eigenvector:
 1  0.00000  2  0.00000  3  0.00000
 2  0.00000  5  0.00000  6  0.00000
 3  0.00000  8  0.00000  9  0.00000
 4  0.00000 11  0.00000 12  0.00000
 5  0.00000 14  0.00000 15  0.00000
 6  0.00000 17  0.00000 18  0.00000
 7  0.00000 20  0.00000 21  0.00000
 8  0.00000 22  0.00000 23  0.00000
 9  0.00000 25  0.00000 26  0.00000
10  0.00000 28  0.00000 29  0.00000
11  0.00000 31  0.00000 32  0.00000
12  0.00000 34  0.00000 35  0.00000
13  0.00000 37  0.00000 38  0.00000
14  0.00000 40  0.00000 41  0.00000
15  0.00000 43  0.00000 44  0.00000
eigenvalue( 41 ) = 0.55328D+C0 frequency = 0.743786D+00
eigenvector:
 1  0.00000  2  0.345191  3  0.451258
 2  0.00000  5  0.00000  6  0.00000
 3  0.00000  8  0.00000  9  0.00000
 4  0.00000 11  0.255127 12  0.447620
 5  0.00000 14  0.00000 15  0.00000
 6  0.00000 17  0.00000 18  0.00000
 7  0.00000 20  0.361387 21  0.405471
 8  0.00000 23  0.00000 24  0.00000
 9  0.00000 26  0.00000 27  0.00000
10  0.00000 28  0.00000 29  0.00000
11  0.00000 31  0.00000 32  0.00000
12  0.00000 34  0.00000 35  0.00000
13  0.00000 37  0.00000 38  0.00000
14  0.00000 40  0.00000 41  0.00000
15  0.00000 43  0.00000 44  0.00000

```

b0105.output

Wed Mar 31 11:39:35 1993

5

```
37) 0.230000C 38) 0.035343 39) 0.304719
45) 0.230000C 41) 0.035300 42) 0.035333
43) 0.230000C 44) 0.035300 45) 0.035333
```

```
eigenvalue( 41) = 0.230397D+02
eigenvector:
```

```
1) 0.000000 2) 0.000000 3) 0.000000
4) 0.000000 5) 0.000000 6) 0.430144
7) 0.000000 8) 0.000000 9) 0.000000
10) 0.000000 11) 0.000000 12) 0.000000
13) 0.000000 14) 0.000000 15) 0.509231
16) 0.000000 17) 0.31364 18) 0.035300
19) 0.000000 20) 0.035300 21) 0.035300
22) 0.035300 23) 0.035300 24) 0.344724
25) 0.035300 26) 0.299242 27) 0.035300
28) 0.035300 29) 0.000000 30) 0.035300
31) 0.035300 32) 0.000000 33) 0.246093
34) 0.035300 35) 0.186632 36) 0.035300
37) 0.035300 38) 0.000000 39) 0.035300
40) 0.035300 41) 0.202389 42) 0.122388
43) 0.035300 44) 0.61836 45) 0.035300
```

```
eigenvalue( 40) = 0.631033D+02
eigenvector:
```

```
1) 0.000000 2) 0.000000 3) 0.000000
4) 0.386975 5) 0.79745 6) 0.300000
7) 0.290000 8) 0.035300 9) 0.035300
10) 0.000000 11) 0.035300 12) 0.000000
13) -0.038226 14) 0.399956 15) 0.000000
15) 0.000000 16) 0.035300 18) 0.000000
16) 0.000000 17) 0.035300 21) 0.000000
19) 0.035300 20) 0.035300 24) 0.361924
22) -0.036428 23) 0.035300 27) 0.000000
25) 0.035300 26) 0.000000 30) 0.000000
28) 0.000000 29) 0.035300 33) 0.048427
31) 0.048395 32) 0.000000 36) 0.035300
34) 0.000000 35) 0.000000 39) 0.035300
37) 0.035300 38) 0.000000 42) 0.295571
40) 0.046313 41) 0.000000 45) 0.000000
43) 0.000000 44) 0.000000
```

```
frequency = 0.453079D+01
time element # 1 frequency = 0.794357D+01
```

```
tire element # 1 time element # 1
```

```
local dof 1 local dof 1 1 1 2 2 3 3 4 4
local dof 2 local dof 2 2 2 2 2 2 2 2 2
local dof 3 local dof 3 3 3 3 3 3 3 3 3
local dof 4 local dof 4 4 4 4 4 4 4 4 4
local dof 5 local dof 5 5 5 5 5 5 5 5 5
local dof 6 local dof 6 6 6 6 6 6 6 6 6
local dof 7 local dof 7 7 7 7 7 7 7 7 7
local dof 8 local dof 8 8 8 8 8 8 8 8 8
local dof 9 local dof 9 9 9 9 9 9 9 9 9
local dof 10 local dof 10 10 10 10 10 10 10 10 10
local dof 11 local dof 11 11 11 11 11 11 11 11 11
local dof 12 local dof 12 12 12 12 12 12 12 12 12
local dof 13 local dof 13 13 13 13 13 13 13 13 13
local dof 14 local dof 14 14 14 14 14 14 14 14 14
local dof 15 local dof 15 15 15 15 15 15 15 15 15
local dof 16 local dof 16 16 16 16 16 16 16 16 16
local dof 17 local dof 17 17 17 17 17 17 17 17 17
local dof 18 local dof 18 18 18 18 18 18 18 18 18
local dof 19 local dof 19 19 19 19 19 19 19 19 19
local dof 20 local dof 20 20 20 20 20 20 20 20 20
local dof 21 local dof 21 21 21 21 21 21 21 21 21
local dof 22 local dof 22 22 22 22 22 22 22 22 22
local dof 23 local dof 23 23 23 23 23 23 23 23 23
local dof 24 local dof 24 24 24 24 24 24 24 24 24
```

```
rigid flap propulsive trim solution
```

```
nonlinear solution for large angles
ail angles in degrees
```

```
advance ratio= 0.20000
```

```
b0 = 1.81489 blc = 0.00716 bis = -0.03904
beta0 = 5.674.3 beta1c = -1.19533 the1als = -2.12584
alpha = 2.44230 phi = 0.5754
```

```
lag harmonics
```

```
zero harm = -0.3003763
1st cos = 0.002711
2nd sin = 0.000002
3rd cos = 0.000001
4th cos = 0.000003
5th cos = 0.000003
```

```
flap harmonics
zero harm = 0.335119
1st cos = -0.001838
2nd sin = 0.000007
3rd sin = 0.000007
4th sin = 0.000007
5th sin = -0.000007
```

bol05.output

Wed Mar 31 11:39:35 1993 6

```

2nd cos = -0.302054 2nd sin = 0.300074
3rd cos = 0.300018 3rd sin = -0.300079
4th cos = 0.300010 4th sin = -0.300097
5th cos = -0.300037 5th sin = -0.300012

```

torsion harmonics

```
zero harm = -0.003921
```

```

1st cos = 0.302331 1st sin = -0.000507
2nd cos = 0.300016 2nd sin = 0.300184
3rd cos = 0.300036 3rd sin = 0.300011
4th cos = 0.300005 4th sin = 0.300004
5th cos = 0.300005 5th sin = -0.300001

```

```
vehicle equilibrium residuals
```

```

f1: x for f2: y for f3: z for f4: roll m f5: pitch m f6: yaw m
0.000994 0.000947 -0.017418 -0.000982 0.002066 0.000338
initial controls used for response (deg)
alphas phis th0 this thic -2.72
2.44 0.57 5.67 1.20 2.68

```

```
response convergence function = 1.0000000
trim convergence function = 0.01795554
```

```
jacobian evaluation -- control perturbation # 1
```

lag harmonics

```

zero harm = -0.3035763
1st cos = 0.002711 1st sin = -0.001358
2nd cos = 0.000302 2nd sin = 0.000017
3rd cos = 0.000001 3rd sin = 0.000007
4th cos = 0.000003 4th sin = 0.000006
5th cos = 0.000003 5th sin = -0.000001

```

```
jacobian evaluation -- control perturbation # 2
```

slap harmonics

```

zero harm = -0.3035763
1st cos = 0.002711 1st sin = -0.001358
2nd cos = 0.000302 2nd sin = 0.000017
3rd cos = 0.000001 3rd sin = 0.000007
4th cos = 0.000003 4th sin = 0.000006
5th cos = 0.000003 5th sin = -0.000001

```

```
vehicle equilibrium residuals
```

```

f1: x for f2: y for f3: z for f4: roll m f5: pitch m f6: yaw m
0.000994 0.000947 -0.017418 -0.000982 0.002066 0.000338

```

```
jacobian evaluation -- control perturbation # 3
```

```

lag harmonics
zero harm = -0.3035921
1st cos = 0.002331 1st sin = -0.002507
2nd cos = 0.0003016 2nd sin = 0.300084
3rd cos = -0.000006 3rd sin = 0.500001
4th cos = 0.000005 4th sin = 0.000004
5th cos = 0.000005 5th sin = -0.000001

```

```
vehicle equilibrium residuals
```

```

f1: pitch m f2: roll m f3: yaw m
0.000338 0.300274 0.000338

```

```
lag harmonics
```

```

zero harm = -0.3036178
1st cos = 0.002287 1st sin = -0.001231
2nd cos = -0.000005 2nd sin = 0.000030
3rd cos = -0.000001 3rd sin = 0.000009

```

bol05.output

Wed Mar 31 11:39:35 1993

7

```

4th cos = 0.00003      4th sin = 0.00005      4th sin = 0.00004
5th cos = 0.00003      5th cos = 0.00005      5th sin = -0.00001
5th sin = -0.00001
=====
flap harmonics
=====
zero harm = 0.00000
1st cos = -0.000045CS
2nd cos = -0.000213
3rd cos = 0.000077
4th cos = 0.000010
5th cos = -0.000009
=====
```

torsion harmonics

```

zero harm = -0.00439
1st cos = 0.002373
2nd cos = 0.000223
3rd cos = -0.000055
4th cos = 0.000006
5th cos = 0.000005
=====
vehicle equilibrium residuals
f1: x for f2: y for f3: z for f4: roll m f5: pitch m f6: yaw m
0.001090 0.002987 -0.001494 -0.001046 0.002600 0.00073
=====
```

perturbed controls for Jacobian (deg)

```

alphas   phis   thc   ths   thail   total
2.44    0.57    1.20   2.68   -2.72    2.68
=====
```

jacobian evaluation -- control perturbation # 5

```

lag harmonics
=====
zero harm = -0.00585
1st cos = 0.002860
2nd cos = 0.000200
3rd cos = -0.000015
4th cos = 0.000006
5th cos = 0.000003
=====
```

jacobian evaluation -- control perturbation # 4

```

lag harmonics
=====
zero harm = -0.005772
1st cos = 0.002866
2nd cos = 0.000206
3rd cos = 0.000011
4th cos = 0.000003
5th cos = 0.000003
=====
```

jacobian evaluation -- control perturbation # 3

```

lag harmonics
=====
zero harm = 0.005128
1st cos = -0.001523
2nd cos = -0.000207
3rd cos = 0.000019
4th cos = 0.000002
5th cos = -0.000003
=====
```

jacobian evaluation -- control perturbation # 2

```

lag harmonics
=====
zero harm = -0.003918
1st cos = 0.002223
2nd cos = 0.000011
3rd cos = -0.000036
=====
```

```

4th cos = 0.000005      4th sin = 0.000004
5th cos = 0.000005      5th sin = -0.000001
=====
```

flap harmonics

```

=====
zero harm = 0.00000
1st cos = -0.000045CS
2nd cos = -0.000213
3rd cos = 0.000077
4th cos = 0.000010
5th cos = -0.000009
=====
```

torsion harmonics

```

=====
zero harm = -0.00585
1st cos = 0.002860
2nd cos = 0.000200
3rd cos = -0.000015
4th cos = 0.000006
5th cos = 0.000003
=====
vehicle equilibrium residuals
f1: x for f2: y for f3: z for f4: roll m f5: pitch m f6: yaw m
0.001090 0.002987 -0.001494 -0.001046 0.002600 0.00073
=====
```

perturbed controls for Jacobian (deg)

```

alphas   phis   thc   ths   thail   total
2.44    0.57    1.20   2.68   -2.72    2.68
=====
```

jacobian evaluation -- control perturbation # 5

```

lag harmonics
=====
zero harm = -0.005587
1st cos = 0.002860
2nd cos = 0.000200
3rd cos = -0.000015
4th cos = 0.000006
5th cos = 0.000003
=====
```

jacobian evaluation -- control perturbation # 4

```

lag harmonics
=====
zero harm = -0.005271
1st cos = 0.002859
2nd cos = 0.000201
3rd cos = -0.000016
4th cos = 0.000007
5th cos = 0.000004
=====
```

jacobian evaluation -- control perturbation # 3

```

lag harmonics
=====
zero harm = -0.004988
1st cos = 0.002859
2nd cos = 0.000201
3rd cos = -0.000016
4th cos = 0.000007
5th cos = 0.000004
=====
```

jacobian evaluation -- control perturbation # 2

```

lag harmonics
=====
zero harm = -0.004694
1st cos = 0.002859
2nd cos = 0.000201
3rd cos = -0.000016
4th cos = 0.000007
5th cos = 0.000004
=====
```

jacobian evaluation -- control perturbation # 1

```

lag harmonics
=====
zero harm = -0.004351
1st cos = 0.002859
2nd cos = 0.000201
3rd cos = -0.000016
4th cos = 0.000007
5th cos = 0.000004
=====
```

bo105.output

8

Wed Mar 31 11:39:35 1993

```

zero harm = -0.005763          3rd cos = 0.000301          3rd sin = 0.000001
1st cos = 0.000271           1st sin = -0.000358          4th cos = 0.000003
2nd cos = 0.000002           2nd sin = 0.000007          4th sin = 0.000006
3rd cos = 0.000001           3rd sin = -0.000007          5th sin = -0.000001
4th cos = 0.000003           4th sin = 0.000006
5th cos = 0.000003           5th sin = -0.000002

flap harmonics
=====
zero harm = 0.0035119          3rd cos = 0.000301          3rd sin = 0.000001
1st cos = -0.001838          4th cos = 0.000003          4th sin = 0.000006
2nd cos = -0.002054          5th cos = 0.000003          5th sin = -0.000001
3rd cos = 0.00018          4th cos = 0.0000018          4th sin = -0.0000078
4th cos = 0.000018          5th cos = -0.000007          5th sin = -0.0000027
5th cos = -0.000007          5th sin = -0.0000017

torsion harmonics
=====
zero harm = -0.003921          1st cos = 0.000301          1st sin = -0.000507
1st cos = 0.0002301          2nd cos = 0.0002016          2nd sin = 0.0000184
2nd cos = 0.0000016          3rd cos = -0.000006          3rd sin = 0.0000011
3rd cos = -0.000006          4th cos = 0.000005          4th sin = 0.000004
4th cos = 0.000005          5th cos = 0.000005          5th sin = -0.000001
5th cos = 0.000005          5th sin = -0.0000010

vehicle equilibrium residuals
=====
f1: x for f2: y for f3: z for f4: roll m f5: pitch m f6: yaw m
0.000394 0.003316 -0.017478 -0.000982 0.002096 0.0003493

perturbed controls for jacobian (deg)
alphas      this      total
phys      rho      this      this      this      this
2.44      0.57      1.23      -2.72      2.81

updated lambda:
total lambda = 0.018349
induced lambda -> alGalks.a.y = 0.009819
0.012999 -0.003927

updated sigma / sigma =
0.056342

vehicle Jacobian matrix:
=====
-0.265; 0.0000 0.0193 -0.0255 0.0990 0.3364
0.2600 0.0651 0.0002 -0.049 -0.0217 0.0554
-0.2442 -0.0004 1.2063 0.0033 0.4153 0.0003
0.3000 0.0162 -0.0129 0.2461 0.0486 0.0006
0.3669 0.0030 0.1019 -0.0528 0.1693 0.0003
0.3000 0.0002 -0.0333 -0.0093 0.0331 0.0665

coupled trim -- iteration 4
=====
coupled trim -- iteration 4 ?
=====
lag harmonics
=====
zero harm = -0.005624          1st cos = 0.0003000          1st sin = -0.000500
1st cos = 0.0003330          2nd cos = -0.0000011          2nd sin = -0.0000075
2nd cos = 0.0000022          3rd cos = 0.0000022          3rd sin = 0.0000098
3rd cos = 0.0000033          4th cos = 0.0000033          4th sin = 0.0000036
4th cos = 0.0000033          5th cos = 0.0000033          5th sin = -0.0000031

flap harmonics
=====
```

```

zero harm = 0.037206      St: cos = -0.000007      5th sin = -0.000008
1st cos = -0.002611      1st sin = -0.003751
2nd cos = -0.002210      2nd sin = -0.003081
3rd cos = 0.000211       3rd sin = -0.000368
4th cos = 0.000229       4th sin = -0.000209
5th cos = -0.000206      5th sin = -0.000208

torsion harmonics
-----
zero harm = -0.003445      zero harm = -0.003445
1st cos = 0.001984       1st sin = -0.003320
2nd cos = 0.000622       2nd sin = 0.000200
3rd cos = 0.000115       3rd sin = -0.000028
4th cos = 0.000219       4th sin = 0.000144
5th cos = 0.000033       5th sin = -0.000031

zero harm = -0.001695      vehicle equilibrium residuals
1st cos = 0.001966       f1: x for f3: z for f4: roll m f5: pitch m f6: yaw r
2nd cos = 0.000255       1st sin = -0.000329
3rd cos = 0.000110       2nd sin = 0.000325
4th cos = 0.000210       3rd sin = -0.000077
5th cos = 0.000246       4th sin = 0.000112
St: cos = 0.000033       5th sin = -0.000033

vehicle equilibrium residuals
f1: x for f2: y for f3: z for f4: roll m f5: pitch m f6: yaw r
2.44 0.57 -0.002725 -0.000332 0.002212 0.000147
total 2.61

current coupled-trim controls (deg)
lambda = 0.019044      updated lambda:
alpha = 0.0101532       total 0.016492
beta = 0.57              induced lambda => al0,ax,ay = 0.010630
phi = 0.244               0.012698 -0.004252

updated ct / sigma = 0.064001
=====
coupled trim - iteration # 1
=====
lag harmonics
-----
zero harm = -0.005746      flap harmonics
1st cos = 0.003552       1st sin = -0.001713      1st harm = -0.001787
2nd cos = -0.000614      2nd sin = -0.000377      1st cos = 0.005921
3rd cos = 0.000202       3rd sin = 0.000067      2nd sin = -0.002396
4th cos = 0.000204       4th sin = 0.000011      3rd sin = 0.000000
5th cos = 0.000003       5th sin = -0.000001      4th sin = 0.000009
St: cos = 0.000008       5th sin = -0.000001      5th sin = -0.000005

zero harm = 0.037587      torsion harmonics
1st cos = -0.003266      1st sin = -0.003713
2nd cos = -0.002145      2nd sin = 0.000813
3rd cos = 0.000324      3rd sin = -0.000088
4th cos = 0.000008      4th sin = -0.000008

```

bol05.output10
Wed Mar 31 11:39:35 1993

vehicle equilibrium residuals
 f1: x for f2: y for f3: z for f4: roll m f5: pitch m f6: yaw m
 1st cos = 0.302335 1st sin = -0.280396 1st cos = 0.300396 1st sin = -0.280396
 2nd cos = -0.300146 2nd sin = 0.280262 2nd cos = -0.300007 2nd sin = -0.280003
 3rd cos = 0.300026 3rd sin = 0.280003 3rd cos = 0.300007 3rd sin = -0.280004
 4th cos = 0.300034 4th sin = 0.280010 4th cos = 0.300009 4th sin = -0.280004
 5th cos = 0.300003 5th sin = -0.280002 5th cos = 0.300003 5th sin = -0.280003

vehicle equilibrium residuals
 f1: x for f2: y for f3: z for f4: roll m f5: pitch m f6: yaw m
 -0.300003 -0.300011 -0.300024 -0.300004 -0.300009 -0.300004 -0.300003

current coupled-trim controls (deg)
 lambda = 0.019287 alpha = 0.004966
 phi's total = 2.95
 1.38 -0.78 -0.98

updated lambda:
 total lambda = 0.019322 induced lambda -> alC,alx,aly = 0.019316
 1.98 -0.78 6.65

updated sigma / sigma = 0.37278

response convergence function = 0.001908C0
 trim convergence function = 0.000099C1

response and hub loads corresponding to converged solution

trim controls (degrees):

alpha-shaft = 1.9775
 phi-shaft = -0.7710
 thetaC 2 75deg 6.6536
 theta-x 2 2.1232
 theta-z 2 -3.6480
 thetaC (tail) = 2.9446

ct tail motor = 0.0043

non-linear steady-state solution (blade tip response)

coupled trim -- iteration # 12

-aq harmonics

zero harm = -0.007400 1st sin = -0.001118
 1st cos = 0.025931 2nd sin = -0.000097
 2nd cos = 0.025067 3rd sin = 0.000053
 3rd cos = 0.025011 4th sin = 0.000059
 4th cos = 0.025005 5th sin = -0.000001
 5th cos = 0.025006

ps1 (deg) *axial-e** *lag** v/r w/z p1: (rad)

90.00 0.000000 -0.0013836 0.3495758
 0.000000 -0.0023591 0.049987
 22.50 0.000000 -0.0041095 0.2504220
 45.00 0.000000 -0.0022961 0.001184
 67.50 0.000000 -0.0034573 0.348303
 90.00 0.000000 -0.0044662
 112.50 0.000000 -0.0105670 0.2446169
 135.00 0.000000 -0.0122776 0.2396223
 157.50 0.000000 -0.0132085 0.0357310
 180.00 0.000000 -0.0132688 0.3456744
 202.50 0.000000 -0.0124734 0.0339635
 225.00 0.000000 -0.0108873 0.036323
 247.50 0.000000 -0.0087605 0.0404713
 270.00 0.000000 -0.0036660 0.0441722

t-ap harmonics

zero harm = 0.343891 1st sin = 0.301936
 1st cos = 0.307958 2nd sin = -0.303362 2nd cos = -0.302322
 2nd cos = 0.300049 3rd sin = -0.303008 3rd cos = 0.300049
 4th cos = 0.300010 4th sin = -0.303009 4th cos = 0.300010
 5th cos = 0.300003 5th sin = -0.303005 5th cos = 0.300003

zero harm = -0.004255 1st sin = -0.303394
 1st cos = 0.302336 2nd sin = 0.303282 2nd cos = -0.300146
 2nd cos = 0.300026 3rd sin = 0.000003 3rd cos = 0.300026
 4th cos = 0.300034 4th sin = 0.000011 4th cos = 0.300034
 5th cos = 0.300003 5th sin = -0.303002 5th cos = 0.300003

bo105.output

11 Wed Mar 31 11:39:35 1993

	f_{xz}	f_{yz}	f_{zx}	f_{zy}
292.50	5.000000	-9.0240699	2.0469365	-0.0331186
315.00	6.000000	-9.02123435	2.0485667	-0.0326464
337.50	6.000000	-9.0313770	2.0492056	-0.0322652

blade root forces & moments (rotating frame)

deg	f_{xz}	f_{yz}	f_{zx}	f_{zy}	m_{xr}	m_{yr}	m_{zr}
0.	2.4966150	-0.0033211	0.0225423	-0.0003469	-0.0339851	-0.0322958	0.0000000
22.	3.4948836	-0.0037934	0.0232901	-0.0003456	-0.0339864	-0.0300574	0.0000000
45.	3.4936639	-0.0036563	0.0241444	-0.0003437	-0.0330617	-0.0303238	0.0000000
68.	3.4931142	-0.0036068	0.0243763	-0.0003024	-0.0330915	-0.0307885	0.0000000
90.	3.4933647	-0.0052343	0.0233255	-0.00030435	-0.0339504	-0.0312069	0.0000000
112.	3.4943181	-0.0036333	0.0213324	-0.00030492	-0.0336647	-0.0316753	0.0000000
135.	3.4957302	-0.0032285	0.0190358	-0.0000572	-0.0333079	-0.0311947	0.0000000
158.	3.4974656	-0.0022055	0.0166988	-0.0000529	-0.0329713	-0.0302724	0.0000000
180.	3.4993214	-0.0082236	0.0156186	-0.0000524	-0.0309056	-0.02020337	0.0000000
202.	3.5012726	-0.0075424	0.0155157	-0.0003084	-0.0307374	-0.01801817	0.0000000
225.	3.5025148	-0.0069494	0.0166248	-0.0003039	-0.0329475	-0.0014124	0.0000000
248.	3.5032213	-0.0044238	0.0185295	-0.0003238	-0.0333182	-0.0009349	0.0000000
270.	3.5033315	-0.0033862	0.0207613	-0.0003481	-0.0337524	-0.0004559	0.0000000
292.	3.5023342	-0.00315202	0.0222633	-0.0003498	-0.0340551	-0.0000254	0.0000000
315.	3.50208917	-0.00304463	0.0226840	-0.0003511	-0.0341327	-0.0002678	0.0000000
338.	3.4989802	0.0002209	0.0225569	-0.0000554	-0.0340769	-0.0004076	0.0000000

hub loads in nonrotating frame

deg	f_{xh}	f_{yh}	f_{zh}	m_{xt}	m_{yt}	m_{zt}
0.	-0.3003585	-0.0018043	0.082476	0.0002135	-0.0012245	-0.0034567
22.	-0.3006846	-0.0016550	0.0824015	0.0002135	-0.0012959	-0.0034452
45.	-0.3005003	-0.0012052	0.0824571	0.0002155	-0.0013688	-0.0034157
68.	-0.3002783	-0.0012170	0.0823596	0.0003035	-0.0013159	-0.0034086
90.	-0.300335956	-0.0012434	0.0822478	0.0002135	-0.0012245	-0.0034567
112.	-0.30036846	-0.0012650	0.08224515	0.0002135	-0.0012959	-0.0034454
135.	-0.30035000	-0.0011852	0.0824571	0.0002155	-0.0013688	-0.0034157
158.	-0.30032783	-0.0011759	0.0823586	0.0003035	-0.0013159	-0.0034086
180.	-0.300235986	-0.0010843	0.0824798	0.0002135	-0.0012245	-0.00334567
202.	-0.30036846	-0.0010650	0.08244515	0.0002135	-0.0012959	-0.00334454
225.	-0.30035200	-0.0010552	0.0824571	0.0002155	-0.0013688	-0.00334157
248.	-0.3002783	-0.0011709	0.0823586	0.0003035	-0.0013159	-0.0034086
270.	-0.3003586	-0.00118043	0.0822478	0.0002135	-0.0012245	-0.0034567
292.	-0.30036846	-0.00116550	0.08242405	0.0000336	-0.0012959	-0.0034454
315.	-0.30035000	-0.0011852	0.0824571	0.0002155	-0.0013688	-0.0034157
338.	-0.3002783	-0.0012170	0.0823586	0.0003035	-0.0013159	-0.0034086

hub ± 2 harmonics:

	zero harm	1st sin	2nd sin	3rd sin	4th sin	5th sin	6th sin
zero harm	0.000000	0.000000	0.000000	0.000000	0.000000	0.000000	0.000000
1st cos	0.000000	0.000000	0.000000	0.000000	0.000000	0.000000	0.000000
2nd cos	0.000000	0.000000	0.000000	0.000000	0.000000	0.000000	0.000000
3rd cos	0.000000	0.000000	0.000000	0.000000	0.000000	0.000000	0.000000
4th cos	0.000000	0.000000	0.000000	0.000000	0.000000	0.000000	0.000000
5th cos	0.000000	0.000000	0.000000	0.000000	0.000000	0.000000	0.000000
6th cos	0.000000	0.000000	0.000000	0.000000	0.000000	0.000000	0.000000

magnitude/zero harmonic fz

hub ± 2 harmonics:

	zero harm	1st sin	2nd sin	3rd sin	4th sin	5th sin	6th sin
zero harm	0.000000	0.000000	0.000000	0.000000	0.000000	0.000000	0.000000
1st cos	0.000000	0.000000	0.000000	0.000000	0.000000	0.000000	0.000000
2nd cos	0.000000	0.000000	0.000000	0.000000	0.000000	0.000000	0.000000
3rd cos	0.000000	0.000000	0.000000	0.000000	0.000000	0.000000	0.000000
4th cos	0.000000	0.000000	0.000000	0.000000	0.000000	0.000000	0.000000
5th cos	0.000000	0.000000	0.000000	0.000000	0.000000	0.000000	0.000000
6th cos	0.000000	0.000000	0.000000	0.000000	0.000000	0.000000	0.000000

magnitude/zero harmonic fz

hub ± 2 harmonics:

	zero harm	1st sin	2nd sin	3rd sin	4th sin	5th sin	6th sin
zero harm	0.000000	0.000000	0.000000	0.000000	0.000000	0.000000	0.000000
1st cos	0.000000	0.000000	0.000000	0.000000	0.000000	0.000000	0.000000
2nd cos	0.000000	0.000000	0.000000	0.000000	0.000000	0.000000	0.000000
3rd cos	0.000000	0.000000	0.000000	0.000000	0.000000	0.000000	0.000000
4th cos	0.000000	0.000000	0.000000	0.000000	0.000000	0.000000	0.000000
5th cos	0.000000	0.000000	0.000000	0.000000	0.000000	0.000000	0.000000
6th cos	0.000000	0.000000	0.000000	0.000000	0.000000	0.000000	0.000000

magnitude/zero harmonic fz

hub ± 4 harmonics:

	zero harm	1st sin	2nd sin	3rd sin	4th sin	5th sin	6th sin
zero harm	0.000000	0.000000	0.000000	0.000000	0.000000	0.000000	0.000000
1st cos	0.000000	0.000000	0.000000	0.000000	0.000000	0.000000	0.000000
2nd cos	0.000000	0.000000	0.000000	0.000000	0.000000	0.000000	0.000000
3rd cos	0.000000	0.000000	0.000000	0.000000	0.000000	0.000000	0.000000
4th cos	0.000000	0.000000	0.000000	0.000000	0.000000	0.000000	0.000000
5th cos	0.000000	0.000000	0.000000	0.000000	0.000000	0.000000	0.000000
6th cos	0.000000	0.000000	0.000000	0.000000	0.000000	0.000000	0.000000

magnitude/zero harmonic fz

hub ± 4 harmonics:

	zero harm	1st sin	2nd sin	3rd sin	4th sin	5th sin	6th sin
zero harm	0.000000	0.000000	0.000000	0.000000	0.000000	0.000000	0.000000
1st cos	0.000000	0.000000	0.000000	0.000000	0.000000	0.000000	0.000000
2nd cos	0.000000	0.000000	0.000000	0.000000	0.000000	0.000000	0.000000
3rd cos	0.000000	0.000000	0.000000	0.000000	0.000000	0.000000	0.000000
4th cos	0.000000	0.000000	0.000000	0.000000	0.000000	0.000000	0.000000
5th cos	0.000000	0.000000	0.000000	0.000000	0.000000	0.000000	0.000000
6th cos	0.000000	0.000000	0.000000	0.000000	0.000000	0.000000	0.000000

magnitude/zero harmonic fz

bol05.output

12
Wed Mar 31 11:39:35 1993

```

3rd cos = 0.0000044
3rd sin = -0.0000055
4th cos = -0.0000022
4th sin = 0.0000032
5th cos = 0.0000011
5th sin = -0.0000033
6th cos = 0.0000015
6th sin = -0.0000002

```

```

4: h cos = -0.0000016
4: h sin = -0.0000025
5: h cos = 0.0000001
5: h sin = -0.000002
6: h cos = 0.0000000
6: h sin = -0.000002

```

```

hub fx harmonics:
zero harm = 0.0000052
1st cos = -0.0000051
1st sin = 0.0000029
2nd cos = -0.0000055
2nd sin = 0.0000033
3rd cos = 0.0000001
3rd sin = -0.0000001
4th cos = 0.0000016
4th sin = -0.0000015
5th cos = 0.0000015
5th sin = -0.0000014
6th cos = -0.0000022
6th sin = -0.0000033

```

```

hub mx harmonics:
zero harm = -0.0000025
1st cos = 0.0000012
1st sin = -0.0000073
2nd cos = -0.0000004
2nd sin = 0.0000003
3rd cos = 0.0000001
3rd sin = -0.0000001
4th cos = 0.0000005
4th sin = -0.0000005
5th cos = 0.0000005
5th sin = -0.0000005
6th cos = 0.0000000
6th sin = -0.0000000

```

```

magnitude/zero harmonic fz
1st sin = 0.0001329
2nd sin = -0.000233
3rd sin = 0.000028
4th sin = 0.000292
5th sin = 0.000297
6th sin = -0.0000159

```

```

hub my harmonics:
zero harm = -0.0000012
1st cos = -0.0000052
1st sin = -0.0000002
2nd cos = 0.0000040
2nd sin = 0.0000012
3rd cos = 0.0000019
3rd sin = 0.0000001
4th cos = 0.0000001
4th sin = 0.0000002
5th cos = -0.0000003
5th sin = 0.0000003
6th cos = 0.0000001
6th sin = 0.0000000

```

```

magnitude/zero harmonic mz
1st sin = -0.0000102
2nd sin = 0.0000112
3rd sin = 0.0000001
4th sin = 0.0000002
5th sin = 0.0000003
6th sin = 0.0000002

```

```

hub mx harmonics:
zero harm = -0.0000025
1st cos = 0.0000019
1st sin = -0.0000073
2nd cos = -0.0000004
2nd sin = 0.0000003
3rd cos = 0.0000001
3rd sin = -0.0000001
4th cos = 0.0000005
4th sin = -0.0000005
5th cos = 0.0000005
5th sin = -0.0000005
6th cos = 0.0000000
6th sin = -0.0000000

```

```

magnitude/zero harmonic mz
1st sin = -0.0000102
2nd sin = 0.0000112
3rd sin = 0.0000001
4th sin = 0.0000002
5th sin = 0.0000003
6th sin = 0.0000002

```

```

hub my harmonics:
zero harm = -0.0000025
1st cos = 0.0000019
1st sin = -0.0000073
2nd cos = -0.0000004
2nd sin = 0.0000003
3rd cos = 0.0000001
3rd sin = -0.0000001
4th cos = 0.0000005
4th sin = -0.0000005
5th cos = 0.0000005
5th sin = -0.0000005
6th cos = 0.0000000
6th sin = -0.0000000

```

```

magnitude/zero harmonic mz
1st sin = -0.0000102
2nd sin = 0.0000112
3rd sin = 0.0000001
4th sin = 0.0000002
5th sin = 0.0000003
6th sin = 0.0000002

```

*** rotating blade load harmonics ***
(leads by modal summation)

```

hub fx harmonics:
zero harm = 0.49820;
1st cos = -0.0000039
2nd cos = -0.0000036
3rd cos = 0.0000029
4th cos = -0.0000038
5th cos = 0.0000019
6th cos = -0.0000029

```

```

magnitude/zero harmonic fz
1st sin = -0.0000049
2nd sin = -0.00000103
3rd sin = -0.0000037
4th sin = 0.0000044
5th sin = -0.0000052
6th sin = 0.0000039

```

```

hub my harmonics:
zero harm = -0.0000006
1st cos = 0.0000003
2nd cos = 0.0000005
3rd cos = 0.0000001
4th cos = -0.0000008
5th cos = 0.0000000
6th cos = -0.0000002

```

```

magnitude/zero harmonic mz
1st sin = -0.0000004
2nd sin = 0.0000003
3rd sin = -0.0000001
4th sin = -0.0000004
5th sin = 0.0000000
6th sin = -0.0000002

```

```

hub fx harmonics:
zero harm = -0.0000006
1st cos = 0.0000003
2nd cos = 0.0000005
3rd cos = 0.0000001

```

```

magnitude/zero harmonic fz
1st sin = -0.0000004
2nd sin = 0.0000003
3rd sin = -0.0000001
4th sin = -0.0000004
5th sin = 0.0000000
6th sin = -0.0000002

```

```

hub my harmonics:
zero harm = -0.0000006
1st cos = 0.0000003
2nd cos = 0.0000005
3rd cos = 0.0000001

```

```

magnitude/zero harmonic mz
1st sin = -0.0000004
2nd sin = 0.0000003
3rd sin = -0.0000001
4th sin = -0.0000004
5th sin = 0.0000000
6th sin = -0.0000002

```

=====
free vibration rotating frequencies & mode shapes

mode = 1 stability mode sequence = 1

mode = ? stability mode sequence = 2

mode = 3 stability mode sequence = 3

--- deformed blade

--- modes used for stability analysis

```

mode = 4 stability mode sequence = 4
eigenvalue( 4 ) = C.548624D+00 frequency = C.740691D-00
eigenvector:
1 0.300000 2 -0.343969 3 -5.449229
4 -0.011682 5 -0.01168 6 -0.030518
7 C.030000 8 -C.030351 9 0.000000
10 0.000000 11 0.25425 12 0.445605
13 -0.000000 14 -0.01180 15 -0.030330
16 0.000000 17 -0.029857 18 0.423842
19 0.000000 20 0.166698 21 -0.028948
22 -0.00684 23 -0.011517 24 -0.028948
25 0.000000 26 -0.021558 27 0.000000
28 0.000000 29 0.08754 30 -0.367072
31 -0.004165 32 -0.012744 33 -0.023384
34 0.000000 35 -0.02216 36 0.000000
37 0.000000 38 0.024559 39 0.242209
40 -C.001529 41 -0.012745 42 -C.017276
43 0.000000 44 -0.010610 45 0.000000
frequency = C.442899D+00

mode = 5 stability mode sequence = 5
eigenvalue( 42 ) = C.196159D+02 frequency = C.442899D+00
eigenvector:
1 2 -0.090002 2 -0.042146
4 -0.030542 5 -0.02711 6
7 0.000002 6 0.402979 9
10 0.000002 11 -0.032927 12
13 -0.003736 14 -0.034443 15
16 0.000002 17 0.364244 18
19 0.000002 20 0.038627 21
22 0.003108 23 -0.00980 24
25 0.000002 26 0.281747 27
28 0.000001 29 0.026592 30
31 0.003440 32 0.005997 33
34 0.000001 35 0.17554 36
37 0.000001 38 0.010771 39
40 0.001385 41 0.01954 42
43 0.003000 44 0.054893 45
frequency = C.000000

mode = 6 stability mode sequence = 6
eigenvalue( 41 ) = C.208651D+02 frequency = C.456783D+01
eigenvector:
1 2 -0.000002 2 -0.007044
4 0.00868 5 0.304129
7 0.000002 6 0.423549
10 0.000002 9 0.29682 12
13 0.000002 11 0.003666 15
16 0.000002 14 0.07244
19 0.000002 17 0.380631 18
22 0.000002 20 -0.003919 21
25 0.000001 23 0.011680 24
28 0.000002 26 0.299342 27
31 0.000002 29 -0.04421 30
34 0.000002 32 -0.000897 33
37 0.000001 35 0.07385 36
40 0.000001 38 -0.011779 39
43 0.000001 41 -0.01984 42
frequency = C.456783D+01

mode = 7 stability mode sequence = 7
eigenvalue( 44 ) = C.1311686D+01 frequency = C.1114155D+01
eigenvector:
1 2 0.013832 3 0.021216
4 C.431592 5 0.000000
7 0.000000 9 -C.000550
10 0.000000 11 0.000000
13 0.0262582 14 0.000500
16 0.000000 17 0.000000
19 0.000000 20 0.000000
22 0.1177917 23 0.415160
25 0.000000 26 0.000000
28 0.000000 29 0.213139
31 0.597914 32 0.379514
34 0.300000 35 -0.300000
37 0.000000 38 0.000000
40 0.030000 41 0.280775
43 0.000000 44 0.000000
frequency = C.1114155D+01

mode = 8 stability mode sequence = 8
eigenvalue( 43 ) = 0.1123205D-02 frequency = 0.3513076D+C1
eigenvector:
1 2 0.000000 3 0.000000
4 -0.142288 5 0.668008
7 0.300000 8 0.300000
10 0.000000 11 0.000000
13 -0.011379 14 -0.581531
16 0.000000 15 -0.306605
19 0.000000 17 -0.000000
22 0.000000 18 0.280991
25 0.000000 19 -0.307495
28 0.000000 20 0.000000
31 0.000000 21 0.000000
34 0.000000 22 0.000000
37 0.000000 23 0.000000
40 0.000000 24 0.000000
43 0.000000 25 0.000000
frequency = 0.3513076D+C1

mode = 9 stability mode sequence = 9
eigenvalue( 42 ) = 0.3513076D+C2 frequency = 0.3513076D+C2
eigenvector:
1 2 0.000000 3 0.000000
4 -0.000000 5 0.000000
7 0.000000 8 0.000000
10 0.000000 9 0.000000
13 0.000000 10 0.000000
16 0.000000 11 0.000000
19 0.000000 12 0.000000
22 0.000000 13 0.000000
25 0.000000 14 0.000000
28 0.000000 15 0.000000
31 0.000000 16 0.000000
34 0.000000 17 0.000000
37 0.000000 18 0.000000
40 0.000000 19 0.000000
43 0.000000 20 0.000000
frequency = 0.3513076D+C2

```

	alpha	frequency	
1	0.0000000	0.000000	-C.312751
2	0.0000000	0.000000	-0.312751
3	0.0000000	0.CC00000	-C.04891
4	0.0004377	0.010236	0.0000000
5	0.0004377	0.010236	-0.454530
6	-0.000472	0.006995	-0.498014
7	-0.000472	0.006995	-0.498014
8	-0.017504	0.0000000	-0.498014
9	-0.00527	C.206332	-0.498014
10	-0.00527	C.206332	-0.498014
11	-0.00511	C.255594	-0.498014
12	-0.00511	-0.255594	-0.498014
13	-0.002627	0.254285	-0.498014
14	-0.002627	-0.254285	-0.498014
15	-0.00654	0.256796	-0.498014
16	-0.00654	-0.256796	-0.498014
17	-0.003237	0.475b40	-0.498014
18	-0.003237	-0.475b40	-0.498014
19	-0.00706	0.453238	-0.498014
20	-0.00706	-0.453238	-0.498014
21	-0.00432	0.453363	-0.498014
22	-0.00432	-0.453363	-0.498014
23	-0.008310	0.462770	-0.498014
24	-0.008310	-0.462770	-0.498014
25	-0.116318	C.117591	-0.498014
26	-0.116318	-0.117591	-0.498014
27	-0.209994	0.238066	-0.498014
28	-0.209994	-0.238066	-0.498014
29	-0.250234	0.113975	-0.498014
30	-0.250234	-0.113975	-0.498014
31	-0.264386	0.C91106	-0.498014
32	-0.264386	-0.C91106	-0.498014
33	-0.271141	0.1C2028	-0.498014
34	-0.271141	-0.1C2028	-0.498014
35	-0.264882	0.123475	-0.498014
36	-0.264882	-0.123475	-0.498014
37	-0.316558	0.043667	-0.498014
38	-0.316558	-0.043667	-0.498014
39	-0.356601	0.015838	-0.498014
40	-0.386836	0.0000000	-0.498014
41	-0.418128	0.46829	-0.498014
42	-0.418128	-0.46829	-0.498014
43	-0.223170	0.467830	-0.498014
44	-0.223170	-0.467830	-0.498014
45	-0.224643	0.464829	-0.498014
46	-0.224643	-0.464829	-0.498014
47	-0.228264	0.465829	-0.498014
48	-0.228264	-0.465829	-0.498014
49	-0.231006	0.465962	-0.498014
50	-0.231006	-0.465962	-0.498014
51	-0.319899	0.464364	-0.498014
52	-0.319899	-0.464364	-0.498014
53	-0.316559	0.451725	-0.498014
54	-0.316559	-0.451725	-0.498014
55	-0.315351	0.452847	-0.498014
56	-0.315351	-0.452847	-0.498014

Sample Output:

Bearingless Rotor

bmr.output

Wed Mar 31 12:11:19 1993

1

```

diss Joule   numm      memm      aa      rr rr    cccc
 0.0 0.0    energy   energy   aaaa   rr rr    cc cc
 0.0 0.0    enm   nm   nm   nm   nm   nm   nm   nm
 0.0 0.0    rr rr    mm mm    aa aa    rr rr    cc cc
 0.0 0.0    mm mm    mm mm    aa aa    rr rr    cccc
 0.0 0.0    mm mm    mm mm    aa aa    rr rr    cccc

University of maryland advanced rotor code

```

```

pl_axial_length      = 0.034700
pl_height            = 0.070000
pl_height            = 0.010400
-p_axial_length     = 0.034700

blade element properties

```

ele_no	length	mass	elx	ely	elz
1	0.25300	0.879653	0.001006	0.053612	
2	0.562500	0.879653	0.001756	0.064003	
3	0.041700	0.100303	0.00153	0.005367	
4	0.12500	0.440000	0.001502	0.010733	
5	0.041700	0.395603	0.005431	0.009451	
6	0.088800	0.561600	0.001282	0.013681	

```

title    bmr_rotor    ( rigid pitch link & lag ptm )

air resn.    rotor    2-dof body + dynamic inflow

wind tunnel trim in hover

```

```

input_data
non_dimensions

```

```

motor properties

```

```

motor_name
motor_type
bmr_configuration
bmr_configuration
snubber
pitch_link
no_blades
solidity
lock_no
ct/sigma
cg_below_hub
cg_hub_offset_x
cg_hub_offset_y

```

ele_no	el1	el2	elata	eq
1	0.322817	113.443	0.000000	0.000000
2	0.330381	122.387	0.000000	0.000000
3	0.330257	184.515	0.000000	0.000000
4	0.338676	365.224	0.000000	0.000000
5	0.333381	275.132	0.000000	0.000000
6	0.039762	304.655	0.000000	0.000000

ele_no	skew	skew	chord	ed
1	0.000000	0.200000	0.077603	0.000000
2	0.300000	0.200558	0.084700	0.000000
3	0.200000	0.000000	0.018700	0.000000
4	0.300000	0.000024	0.019400	0.000000
5	0.200000	0.000033	0.026500	0.000000
6	0.300000	0.000087	0.026300	0.000000

```

blade properties

```

```

twist(deg)
precone(deg)
root_cut(W)
no_space_elements
no_elm_in_flexbeam
no_elm_in_torque_tube
no_elm_in_segments
material_type
pc_chord_length

```

```

set_list_curve_slope = 6.00000
zero_c1 = 0.13500
c1_drag = 6.00000
d1_drag = 0.00850
d1 = 0.009300
d2 = 0.10000
d3_drag = -0.00600
cmac = 0.00000
fl = 0.00000
de_recov_fact = 0.97000
clp_mach_tail_rot = 0.22900

flight_condition = -----
advance_ratio = 0.30000
rotor_speed_ratio = 1.30000
density_zat_0 = 1.00000
flight_angle = 0.30000
clp_mach_tail_rot = 0.22900
c1 = 0.22900

fuselage_properties = -----
no_hub_dof = 2
body_seq = 4 5
effective_x_mass = 64.78000
effective_y_mass = 64.78000
effective_z_mass = 64.78000
fuselage_pitch_inertia = 4.58300
fuselage_roll_inertia = 2.15300
fuselage_x_damper = 0.00000
fuselage_y_damper = 0.00000
fuselage_z_damper = 0.00000
fuselage_pitch_damper = 0.00000
fuselage_roll_damper = 0.00000
fuselage_x_spring = 0.00000
fuselage_y_spring = 0.00000
fuselage_z_spring = 0.00000
fuselage_pitch_spring = 0.00000
fuselage_roll_spring = 0.00000
body_roll_moment_coeff = 0.00000
body_pitch_moment_coeff = 0.00000
body_side_force_coeff = 0.00000
parasite_drag_area = 3.01300

tail_properties = -----
radiatio_tail_rot = 0.20000
solidity_tail_cr = 0.15000
gear_ratio_tail_rot = 5.00000
twist_deg_tail_rot = 0.00000
cg_tail_rot_offset_x = 1.20000
cg_tail_rot_above_cg = 0.296900
cl_tail_rot = 6.330000
hor_tail_area = 0.330000
cg_tail_hor_offset_x = 0.950000
cl_tail_hor = 6.330000
cg_tail_hor = 0.200000

airfoil_properties = -----

```

bear.output

Wed Mar 31 12:11:19 1993 3

```

alpha_s_wt      = 0.0CCCC00
theta_0_wt     = 6.0CCCC00
stability_analysis
=====

analysis option   : dynamic inflow
output options
=====
analysis option   : fix_q5_const.
print_control    : 4
hub_load_control= 0
no_psi_locations = 2

element number = 3
e1y = 0.003756 e11 = 0.000000 eg = 0.000000 sk1 = 0.000000
e1z = 0.064000 e12 = 0.000000 ed = 0.000000 sk2 = 0.00558
q1 = 0.00381 e11 = 0.000000 ea = 0.000000 rms = 0.8797
eac = 122.19 e12 = 0.000000 el = 0.000000 cor = 0.084100
=====

element number = 4
e1y = 0.001505 eb1 = 0.000000 eg = 0.000000 sk1 = 0.000000
e1z = 0.053567 eb2 = 0.000000 ed = 0.000000 sk2 = 0.000030
q1 = 0.00057 e11 = 0.000000 ea = 0.000000 rms = 0.1100
eac = 184.51 e12 = 0.000000 el = 0.04790 cor = 0.016100
=====

element number = 5
e1y = 0.001592 eb1 = 0.000000 eg = 0.000000 sk1 = 0.000000
e1z = 0.010733 eb2 = 0.000000 ed = 0.000000 sk2 = 0.000034
q1 = 0.000616 e11 = 0.000000 ea = 0.000000 rms = 0.4400
eac = 365.22 e12 = 0.000000 el = 0.12500 cor = 0.019400
=====

element number = 6
e1y = 0.005431 eb1 = 0.000000 eg = 0.000000 sk1 = 0.000000
e1z = 0.009151 eb2 = 0.000000 ed = 0.000000 sk2 = 0.000053
q1 = 0.003391 e11 = 0.000000 ea = 0.000000 rms = 0.3956
eac = 275.13 e12 = 0.000000 el = 0.341720 cor = 0.265000
=====

element number = 7
e1y = 0.001282 eb1 = 0.000000 eg = 0.000000 sk1 = 0.000000
e1z = 0.013681 eb2 = 0.000000 ed = 0.000000 sk2 = 0.000087
q1 = 0.006762 e11 = 0.000000 ea = 0.000000 rms = 0.5516
eac = 304.66 e12 = 0.000000 el = 0.366800 cor = 0.223000
=====

advance ratio = 0.000000
gamma = 5.673000 c1 = 6.000000 cl = 0.000000
dc = 0.008500 d1 = 0.000000 bl = 0.100000
=====
density = 1.000000 b1p = 0.374776 sigma = 0.107900
cmac = -0.000000 f1 = 0.000000 sic = 6.000000
ct/sigma = 0.000000 thw = 0.000000
=====
hbay = 0.2969 xcg = 0.0000 ycg = 0.0000
cmxf = 0.0000 cmvf = 0.0000 rbya = 0.0000
cyf = 0.0000 cmfp = 0.0000 etach = 0.9100
=====
stimat = 0.1559 qratio = 5.0000 twall = 0.0000
x1rt = 0.2030 x1rt = 1.2000 zclrt = 0.2969
ratio = 0.2290 cit = 6.0000 arattn = 0.0000
t1mt = 0.9500 chnt = 6.0000
x1hz = 0.0000 cint = 0.0000
c1ht = 0.2030
=====
dr32t(1) = 0.000 0.000 0.000 0.000 0.000
dr4rp(1) = 0.000 0.000 0.000 0.000 0.000
ibody = 4 5
=====
```


5
bmr.output Wed Mar 31 12:11:19 1993

3.7	0.000023	38	0.00000	3.9
4.0	0.000065	41	0.00000	4.2
4.3	-0.027397	44	-0.25096	4.5
4.6	0.000039	47	0.00000	4.8
4.9	0.000023	50	0.00000	5.1

$$\text{frequency}_{CV} = 0.483183D+01$$

$$\text{eigenvalue}(4) = 0.3301930 \cdot e^{0.5746240 \cdot i}$$

1. *Leucosia* (L.) *leucostoma* (L.) *leucostoma* (L.) *leucostoma* (L.) *leucostoma* (L.)

$\sigma_{112345678}$	$\sigma_{12345678}$	$\sigma_{12345679}$	$\sigma_{12345689}$	$\sigma_{12345789}$	$\sigma_{12346789}$	$\sigma_{13456789}$
0.0030000	-0.2035764	-0.3074760				
-0.0023755	+0.2095064	0.3000000				
0.2000000	0.2000000	-0.2034146				
-0.0046570	-0.2052329	-0.2015311				
-0.3000912	0.0000000	0.0000000				
-0.3028690	-0.0030481	-0.00363340				

bmr.output

7

```

Wed Mar 31 12:11:19 1993

wind tunnel control settings
  alpha   phis   trc   ths
  6.00    0.00    6.00    0.00

updated lambda:
total lambda = 0.055198
induced lambda => alfa,x,ay = 0.347998  0.000300  0.000000

updated ct / sigma = 0.042103
response convergence function 1.5000000

=====
===== iteration # 2 =====
===== azimuth = 0.0 deg =====

azimuth = 185.0 deg

  0.0003000 -0.0051997 -0.0075253 -0.0032973 -0.0051997 -0.0075253 -0.0032973
  -0.0007590 -0.0109765 -0.0139765 -0.0109765 -0.0060000 -0.0060000 -0.0060000
  0.0003000 0.0063000 0.0063000 0.0063000 -0.003455 -0.003455 -0.003455
  -0.0065039 0.0000000 -0.0000000 -0.0000000 -0.0000000 -0.0000000 -0.0000000
  -0.0034396 -0.0050553 -0.0079141 -0.0015788 -0.0000000 -0.0000000 -0.0000000
  0.0000000 -0.0009457 0.0000000 0.0000000 -0.0000000 -0.0000000 -0.0000000
  -0.0000808 -0.0025854 -0.0032754 -0.0039467 -0.0000000 -0.0000000 -0.0000000
  -0.0000121 0.0000000 -0.0001562 0.0000000 0.0000000 0.0000000 0.0000000
  0.0000000 -0.0019211 0.0000000 0.0000000 0.0000000 0.0000000 0.0000000
  -0.0001906 -0.0022327 -0.0034710 -0.0034710 0.0000000 0.0000000 0.0000000
  -0.0000804 0.0000000 -0.0004027 0.0000000 0.0000000 0.0000000 0.0000000
  0.0000000 -0.0019471 0.0000000 0.0000000 0.0000000 0.0000000 0.0000000
  azimuth = 270.0 deg

  0.0000000 -0.0051997 -0.0075253 -0.0032973 -0.0051997 -0.0075253 -0.0032973
  -0.0007590 0.0000000 -0.0000000 -0.0000000 -0.0000000 -0.0000000 -0.0000000
  0.0000000 0.0063000 0.0063000 0.0063000 -0.003455 -0.003455 -0.003455
  -0.0065039 0.0000000 -0.0000000 -0.0000000 -0.0000000 -0.0000000 -0.0000000
  -0.0034396 -0.0050553 -0.0079141 -0.0015788 -0.0000000 -0.0000000 -0.0000000
  0.0000000 -0.0009457 0.0000000 0.0000000 -0.0000000 -0.0000000 -0.0000000
  -0.0000808 -0.0025854 -0.0032754 -0.0039467 -0.0000000 -0.0000000 -0.0000000
  -0.0000121 0.0000000 -0.0001562 0.0000000 0.0000000 0.0000000 0.0000000
  0.0000000 -0.0019211 0.0000000 0.0000000 0.0000000 0.0000000 0.0000000
  -0.0001906 -0.0022327 -0.0034710 -0.0034710 0.0000000 0.0000000 0.0000000
  -0.0000804 0.0000000 -0.0004027 0.0000000 0.0000000 0.0000000 0.0000000
  0.0000000 -0.0019471 0.0000000 0.0000000 0.0000000 0.0000000 0.0000000
  azimuth = 270.0 deg

  0.0000000 -0.0051997 -0.0075253 -0.0032973 -0.0051997 -0.0075253 -0.0032973
  -0.0007590 0.0000000 -0.0000000 -0.0000000 -0.0000000 -0.0000000 -0.0000000
  0.0000000 0.0063000 0.0063000 0.0063000 -0.003455 -0.003455 -0.003455
  -0.0065039 0.0000000 -0.0000000 -0.0000000 -0.0000000 -0.0000000 -0.0000000
  -0.0034396 -0.0050553 -0.0079141 -0.0015788 -0.0000000 -0.0000000 -0.0000000
  0.0000000 -0.0009457 0.0000000 0.0000000 -0.0000000 -0.0000000 -0.0000000
  -0.0000808 -0.0025854 -0.0032754 -0.0039467 -0.0000000 -0.0000000 -0.0000000
  -0.0000121 0.0000000 -0.0001562 0.0000000 0.0000000 0.0000000 0.0000000
  0.0000000 -0.0019211 0.0000000 0.0000000 0.0000000 0.0000000 0.0000000
  -0.0001906 -0.0022327 -0.0034710 -0.0034710 0.0000000 0.0000000 0.0000000
  -0.0000804 0.0000000 -0.0004027 0.0000000 0.0000000 0.0000000 0.0000000
  0.0000000 -0.0019471 0.0000000 0.0000000 0.0000000 0.0000000 0.0000000
  azimuth = 270.0 deg

```



```

-0.0038165      -0.0346779      -0.0353836      -0.0015757      torsion harmonics
0.0030000      -0.0009436      0.0000000      0.0002000      zero harm = -0.010957
-0.0002016      -0.0029427      -0.0013018      -0.0364977      1st sin = 0.000000
0.0003114      0.0000000      -0.0001559      0.0000000      2nd sin = 0.000000
0.0002000      -0.001894       0.0000000      0.0000000      3rd sin = 0.000000
-0.0002197      -0.0025278      -0.0032458      0.0000000      4th sin = 0.000000
-0.0000035      0.0000000      -0.0034018      -0.0000000      5th sin = 0.000000
azimuth = 270.0 deg

-0.0000035      0.0000000      -0.0000000      0.0000000      1st harmonic flapping residuals (deg)
beta 1c      beta 1s      beta 2c      beta 2s      beta 3c      beta 3s
0.3000      0.3000      0.3000      0.3000      0.3000      0.3000
wind tunnel control settings
alphas      phis      rho      this
0.00      0.00      6.00      0.00
azimuth = 270.0 deg

0.0000000      -0.0055773      -0.0079216      -0.0276399      updated lambda:
-0.0178762      -0.009315       0.0000000      -0.0106544      total lambda = 0.055023
0.0000000      0.0000000      -0.0036234      -0.0075273      induced Lambda -> a[3,d1x,alv] = 0.047846
-0.0228428      -0.0222957      -0.0097800      0.0000000      0.0000000      0.0000000
-0.0064891      0.0060000      0.0000000      -0.0003504      response convergence function = 0.10991263
-0.0038305      -0.0046779      -0.00563836     * * * * *
0.0000000      -0.0039436      0.0000000      -0.0015752      response calculation -- iteration # 4
-0.0002076      -0.0024217      -0.0030618      -0.00364977      azimuth = 0.0 deg
-0.0003114      0.0000000      -0.0001559      0.0000000      0.0000000      0.0000000
0.0000000      -0.001894       0.0000000      0.0000000      0.0000000      -0.0075630      -0.0301122
-0.0002192      -0.0025228      -0.0032458      -0.0334642      -0.0205520      -0.0109777      0.0000000      -0.0106798
-0.0000035      0.0000000      -0.0034018      0.0000000      0.0000000      0.0000000      -0.0033704      -0.0071661
0.0000000      -0.0015084      -0.0239813      -0.0246444      -0.0249774      -0.0098033      0.0000000
lag harmonics
zero harm = -0.0235577      1st sin = 0.000000      1st sin = 0.000000
1st cos = 0.000000      2nd sin = 0.000000      2nd sin = 0.000000
2nd cos = 0.000000      3rd sin = 0.000000      3rd sin = 0.000000
3rd cos = 0.000000      4th sin = 0.000000      4th sin = 0.000000
4th cos = 0.000000      5th sin = 0.000000      5th sin = 0.000000
5th cos = 0.000000

lap harmonics
zero harm = -0.027640      1st sin = 0.000000      1st sin = 0.000000
1st cos = 0.000000      2nd sin = 0.000000      2nd sin = 0.000000
2nd cos = 0.000000      3rd sin = 0.000000      3rd sin = 0.000000
3rd cos = 0.000000      4th sin = 0.000000      4th sin = 0.000000
4th cos = 0.000000      5th sin = 0.000000      5th sin = 0.000000
5th cos = 0.000000
azimuth = 90.0 deg

```

beer.output Wed Mar 31 12:11:19 1993

1

bmr.output Wed Mar 31 12:11:19 1993

11

updated st / sigma = 0.038803

response convergence function = 0.09365167

===== response calculation -- iteration # 5 =====

azimuth = 0.0 deg

0.3000000	-0.0053999	-0.3017369	-0.3289588	0.0000000	azimuth = 180.0 deg	-0.0004667	-0.0247954
-0.3193641	-0.0109701	-0.3036453	-0.3036453	0.0000000	-0.0033998	-0.0289588	
0.0000000	0.0000000	0.0000000	0.0000000	0.0000000	-0.0109701	-0.0006725	
-0.3238043	-0.0237268	-0.0200633	-0.0200633	-0.0000000	-0.0034924	-0.0073379	
-0.0065601	0.0300000	0.0003301	0.0003301	-0.0000000	-0.0237268	0.0000000	
-0.0036453	-0.0046607	-0.015779	-0.015779	0.0000000	0.0000000	-0.0003301	
0.0000000	-0.3009452	0.0000000	0.0000000	-0.0000000	-0.0048407	-0.0015779	
-0.3001949	-0.0027730	-0.0370651	-0.0370651	0.0000000	-0.0093452	0.0000000	
-0.033125	0.0000000	-0.0015611	-0.0015611	-0.0000000	-0.0097966	0.0000000	
0.3000000	-0.3011914	0.0000000	0.0000000	0.0000000	-0.0014267	-0.0247954	
-0.0000056	-0.0021855	-0.0303578	-0.0345866	0.0000000	-0.0053998	-0.0289588	
-0.0028049	0.0000000	-0.0004025	0.0000000	-0.0109701	0.0000000	-0.0109701	
0.0000000	-0.3014567	-0.0247954	0.0000000	0.0000000	-0.0034924	-0.0073379	
azimuth = 90.0 deg							
0.0000000	-0.0053998	-0.0071369	-0.0289588	0.0000000	-0.0237268	0.0000000	
-0.6193041	-0.0109701	0.0000000	-0.0109701	-0.0000000	0.0000000	-0.0003301	
0.0000000	0.0000000	-0.0014924	-0.0014924	-0.0000000	-0.0048407	-0.0015779	
-0.3238043	-0.0237268	-0.0370651	-0.0370651	-0.0000000	-0.0093452	0.0000000	
-0.0065601	0.0000000	0.0000000	0.0000000	-0.0000000	-0.0027730	-0.0037751	
-0.0036453	-0.0048407	-0.0366416	-0.0366416	0.0000000	-0.0000000	0.0000000	
-0.3000000	-0.2604552	0.0000000	0.0000000	-0.0000000	-0.0031951	-0.0345566	
-0.0000000	-0.3021949	-0.02031680	-0.0377651	-0.0000000	-0.0000000	-0.0000000	
-0.0028049	0.0000000	-0.0015611	0.0000000	-0.0000000	-0.0014267	-0.0247954	
0.0000000	-0.0011914	0.0000000	0.0000000	0.0000000	0.0000000	0.0000000	
-0.0002855	-0.3033578	-0.0345866	0.0000000	-0.0053998	-0.0289588	0.0000000	
-0.0000000	-0.3011914	0.0000000	0.0000000	-0.0014267	-0.0247954	0.0000000	
0.0000000	-0.0000000	-0.0004025	0.0000000	-0.0109701	0.0000000	-0.0109701	
-0.0000000	-0.0021855	-0.0303578	-0.0345866	0.0000000	-0.0053998	-0.0289588	
0.0000000	-0.0000000	-0.0015611	-0.0015611	0.0000000	-0.0000000	0.0000000	
-0.0000000	-0.3014567	-0.0247954	0.0000000	-0.0034924	-0.0073379	0.0000000	
azimuth = 180.0 deg							
0.0000000	-0.0053998	-0.0071369	-0.0289588	0.0000000	-0.0237268	0.0000000	
-0.6193041	-0.0109701	0.0000000	-0.0109701	-0.0000000	0.0000000	-0.0003301	
0.0000000	0.0000000	-0.0014924	-0.0014924	-0.0000000	-0.0048407	-0.0015779	
-0.3238043	-0.0237268	-0.0370651	-0.0370651	-0.0000000	-0.0093452	0.0000000	
-0.0065601	0.0000000	0.0000000	0.0000000	-0.0000000	-0.0027730	-0.0037751	
-0.0036453	-0.0048407	-0.0366416	-0.0366416	0.0000000	-0.0000000	0.0000000	
-0.3000000	-0.2604552	0.0000000	0.0000000	-0.0000000	-0.0031951	-0.0345566	
-0.0000000	-0.3021949	-0.02031680	-0.0377651	-0.0000000	-0.0000000	-0.0000000	
0.0000000	-0.0011914	0.0000000	0.0000000	-0.0014267	-0.0247954	0.0000000	
-0.0002855	-0.3033578	-0.0345866	0.0000000	-0.0053998	-0.0289588	0.0000000	
-0.0000000	-0.0000000	-0.0015611	0.0000000	-0.0000000	-0.0000000	0.0000000	
0.0000000	-0.0011914	0.0000000	0.0000000	-0.0014267	-0.0247954	0.0000000	
-0.0002855	-0.3033578	-0.0345866	0.0000000	-0.0053998	-0.0289588	0.0000000	
-0.0000000	-0.0000000	-0.0015611	0.0000000	-0.0000000	-0.0000000	0.0000000	

lag harmonics -----

zero harm = -0.005400
1st cos = 0.000000 1st sin = 0.000000
2nd cos = 0.000000 2nd sin = 0.000000

bmr.output

13

Wed Mar 31 12:11:19 1993

```
zero harm = -0.005404
1st cos = 0.000000
2nd cos = 0.000000
3rd cos = 0.000000
4th cos = 0.000000
5th cos = 0.000000

-lag harmonics
zero harm = -0.010965
1st cos = 0.000000
2nd cos = 0.000000
3rd cos = 0.000000
4th cos = 0.000000
5th cos = 0.000000

-torsion harmonics
zero harm = -0.028929
1st cos = 0.000000
2nd cos = 0.000000
3rd cos = 0.000000
4th cos = 0.000000
5th cos = 0.000000

1st harmonic f-appng residuals (deg)
1st cos = 0.000000
2nd cos = 0.000000
3rd cos = 0.000000
4th cos = 0.000000
5th cos = 0.000000

2nd harmonic f-appng residuals (deg)
1st cos = 0.000000
2nd cos = 0.000000
3rd cos = 0.000000
4th cos = 0.000000
5th cos = 0.000000

3rd harmonic f-appng residuals (deg)
1st cos = 0.000000
2nd cos = 0.000000
3rd cos = 0.000000
4th cos = 0.000000
5th cos = 0.000000

4th harmonic f-appng residuals (deg)
1st cos = 0.000000
2nd cos = 0.000000
3rd cos = 0.000000
4th cos = 0.000000
5th cos = 0.000000

5th harmonic f-appng residuals (deg)
1st cos = 0.000000
2nd cos = 0.000000
3rd cos = 0.000000
4th cos = 0.000000
5th cos = 0.000000

blade root forces & moments (rotating frame)
de4 = f_xx f_yy f_zz m_xx m_yy m_zz
```

```
zero harm = -0.0345595
1st cos = 0.000000
2nd cos = 0.000000
3rd cos = 0.000000
4th cos = 0.000000
5th cos = 0.000000

wind tunnel control settings
alpha_s 0.00
alpha_t 0.00
phi_s 0.00
phi_t 0.00
beta_ls 0.000000
beta_ts 0.000000
beta_ls 0.000000
beta_ts 0.000000

updated lambda:
total lambda = 0.003785
induced lambda => alfa,alfa,y = 0.046766
0.003000 0.003000

updated st / sigma = 0.040038
response convergence function = 0.00119932

response and hub loads corresponding to converged solution
trim controls (degrees):
alpha-shaft 0.0000
phi-shaft 0.0000
theta0 @ 75%r = 6.5000
theta_a/c = 0.0000
theta_a/s = 0.0000
theta_a/tail = 0.0000
```

```
zero harm = -0.003036
1st cos = 0.000000
2nd cos = 0.000000
3rd cos = 0.000000
4th cos = 0.000000
5th cos = 0.000000

wind tunnel control settings
alpha_s 0.000000
alpha_t 0.000000
phi_s 0.000000
phi_t 0.000000
beta_ls 0.000000
beta_ts 0.000000
beta_ls 0.000000
beta_ts 0.000000

updated lambda:
total lambda = 0.00373425
induced lambda => alfa,alfa,y = 0.046766
0.003000 0.003000

updated st / sigma = 0.040038
response convergence function = 0.00119932

response and hub loads corresponding to converged solution
trim controls (degrees):
alpha-shaft 0.0000
phi-shaft 0.0000
theta0 @ 75%r = 6.5000
theta_a/c = 0.0000
theta_a/s = 0.0000
theta_a/tail = 0.0000
```

```
zero harm = -0.0034908
1st cos = 0.000000
2nd cos = 0.000000
3rd cos = 0.000000
4th cos = 0.000000
5th cos = 0.000000

wind tunnel control settings
alpha_s 0.000000
alpha_t 0.000000
phi_s 0.000000
phi_t 0.000000
beta_ls 0.000000
beta_ts 0.000000
beta_ls 0.000000
beta_ts 0.000000

updated lambda:
total lambda = 0.00373425
induced lambda => alfa,alfa,y = 0.046766
0.003000 0.003000

updated st / sigma = 0.040038
response convergence function = 0.00119932

response and hub loads corresponding to converged solution
trim controls (degrees):
alpha-shaft 0.0000
phi-shaft 0.0000
theta0 @ 75%r = 6.5000
theta_a/c = 0.0000
theta_a/s = 0.0000
theta_a/tail = 0.0000
```

```
zero harm = -0.0034908
1st cos = 0.000000
2nd cos = 0.000000
3rd cos = 0.000000
4th cos = 0.000000
5th cos = 0.000000

wind tunnel control settings
alpha_s 0.000000
alpha_t 0.000000
phi_s 0.000000
phi_t 0.000000
beta_ls 0.000000
beta_ts 0.000000
beta_ls 0.000000
beta_ts 0.000000

updated lambda:
total lambda = 0.00373425
induced lambda => alfa,alfa,y = 0.046766
0.003000 0.003000
```

bmr.output Wed Mar 31 12:11:19 1993 14

2

Wed Mar 31 12:11:19 1993

2

卷之三

		Magnitude/zero harmonic fz
1st harm	sin	0.000000
1st cos	0.000000	0.000000
2nd harm	sin	0.000000
2nd cos	0.000000	0.000000
3rd harm	sin	0.000000
3rd cos	0.000000	0.000000
4th harm	sin	0.000000
4th cos	0.000000	0.000000
5th harm	sin	0.000000
5th cos	0.000000	0.000000
6th harm	sin	0.000000
6th cos	0.000000	0.000000

sub fz harmonics:		magnitude/zero harmonic fz
zero harm	= 0.051105	
1st cos	= 0.000000	0.000000
1st sin	= 0.000000	0.000000
2nd cos	= 0.000000	0.000000
2nd sin	= 0.000000	0.000000
3rd cos	= 0.000000	0.000000
3rd sin	= 0.000000	0.000000
4th cos	= 0.000000	0.000000
4th sin	= 0.000000	0.000000
5th cos	= 0.000000	0.000000
5th sin	= 0.000000	0.000000
6th cos	= 0.000000	0.000000
6th sin	= 0.000000	0.000000

卷之三

hub mx harmonics:

hub my harmonics:		magnitude/zero harmonic m z
zero harm =	0.000000	
1st cos =	0.000000	1st sin = 0.000000
2nd cos =	0.000000	2nd sin = 0.000000
3rd cos =	0.000000	3rd sin = 0.000000
4th cos =	0.000000	4th sin = 0.000000
5th cos =	0.000000	5th sin = 0.000000
6th cos =	0.000000	6th sin = 0.000000
hub my harmonics:		magnitude/zero harmonic m z
zero harm =	0.000000	0.000000
1st cos =	0.000000	1st sin = 0.000000
2nd cos =	0.000000	0.000000
3rd cos =	0.000000	0.000000
4th cos =	0.000000	0.000000
5th cos =	0.000000	0.000000
6th cos =	0.000000	0.000000

hub mz harmonics:		magnitude/zero harmonic mz
zero harm	= -0.003878	
1st cos	= 0.000000	1st sin = 0.000000
2nd cos	= 0.000000	2nd sin = 0.000000
3rd cos	= 0.000000	3rd sin = 0.000000
4th cos	= 0.000000	4th sin = -0.100000
5th cos	= 0.000000	5th sin = 0.000000
6th cos	= 0.000000	6th sin = -0.000000

**** rotating blade load harmonics ****
(loads by force summation)

hub fx harmonics:		magnitude/zero harmonic fz
zero harm =	0.438330	
1st cos =	0.000000	1st sin = 0.000000
2nd cos =	0.000000	2nd sin = 0.000000
3rd cos =	0.000000	3rd sin = 0.000000
4th cos =	0.000000	4th sin = 0.000000
5th cos =	0.000000	5th sin = 0.000000
6th cos =	0.000000	6th sin = 0.000000

hub fy harmonics:		magnitude/zero harmonic fz
zero harm =	-0.003011	
1st cos =	0.000000	1st sin = 0.000000
2nd cos =	0.000000	2nd sin = 0.000000
3rd cos =	0.000000	3rd sin = 0.000000
4th cos =	0.000000	4th sin = 0.000000
5th cos =	0.000000	5th sin = 0.000000
6th cos =	0.000000	6th sin = 0.000000

hub fz harmonics:		magnitude/zero harmonic fz
zero harm	= -0.019738	
1st cos	= 0.000000	1st sin = 0.000000
2nd cos	= 0.000000	2nd sin = 0.000000
3rd cos	= 0.000000	3rd sin = 0.000000
4th cos	= 0.000000	4th sin = 0.000000
5th cos	= 0.000000	5th sin = 0.000000
6th cos	= 0.000000	6th sin = 0.000000

bmr.output

Wed Mar 31 12:11:19 1993 15

```

1st cos = 0.000000      1st sin = 0.000000      2nd cos = 0.000000      2nd sin = 0.000000
2nd cos = 0.000000      2nd sin = 0.000000      3rd cos = 0.000000      3rd sin = 0.000000
3rd cos = 0.000000      3rd sin = 0.000000      4th cos = 0.000000      4th sin = 0.000000
4th cos = 0.000000      4th sin = 0.000000      5th cos = 0.000000      5th sin = 0.000000
5th cos = 0.000000      5th sin = 0.000000      6th cos = 0.000000      6th sin = 0.000000
6th cos = 0.000000      6th sin = 0.000000

```

hub my harmonics:

```

zero harm = -0.001782      1st sin = 0.000000      2nd cos = 0.000000      2nd sin = 0.000000
1st cos = -0.000000      2nd sin = 0.000000      3rd cos = 0.000000      3rd sin = 0.000000
2nd cos = -0.000000      3rd sin = 0.000000      4th cos = 0.000000      4th sin = 0.000000
3rd cos = -0.000000      4th sin = 0.000000      5th cos = 0.000000      5th sin = 0.000000
4th cos = 0.000000      5th sin = 0.000000      6th cos = 0.000000      6th sin = 0.000000
5th cos = 0.000000      6th sin = 0.000000

```

hub mz harmonics:

```

zero harm = 0.001666      1st sin = 0.000000      2nd cos = 0.000000      2nd sin = 0.000000
1st cos = 0.000000      2nd sin = 0.000000      3rd cos = 0.000000      3rd sin = 0.000000
2nd cos = -0.000000      3rd sin = 0.000000      4th cos = 0.000000      4th sin = 0.000000
3rd cos = -0.000000      4th sin = 0.000000      5th cos = 0.000000      5th sin = 0.000000
4th cos = 0.000000      5th sin = 0.000000      6th cos = 0.000000      6th sin = 0.000000
5th cos = 0.000000      6th sin = 0.000000

```

hub fx harmonics:

```

zero harm = 0.437334      1st sin = 0.000000      2nd cos = 0.000000      2nd sin = 0.000000
1st cos = 0.000000      2nd sin = 0.000000      3rd cos = 0.000000      3rd sin = 0.000000
2nd cos = 0.000000      3rd sin = 0.000000      4th cos = 0.000000      4th sin = 0.000000
3rd cos = 0.000000      4th sin = 0.000000      5th cos = 0.000000      5th sin = 0.000000
4th cos = 0.000000      5th sin = 0.000000      6th cos = 0.000000      6th sin = 0.000000
5th cos = 0.000000      6th sin = 0.000000

```

*** rotating blade load harmonics ***

(loads by mode: summation)

hub fy harmonics:

```

zero harm = -0.001619      1st sin = 0.000000      2nd cos = 0.000000      2nd sin = 0.000000
1st cos = 0.000000      2nd sin = 0.000000      3rd cos = 0.000000      3rd sin = 0.000000
2nd cos = 0.000000      3rd sin = 0.000000      4th cos = 0.000000      4th sin = 0.000000
3rd cos = 0.000000      4th sin = 0.000000      5th cos = 0.000000      5th sin = 0.000000
4th cos = 0.000000      5th sin = 0.000000      6th cos = 0.000000      6th sin = 0.000000
5th cos = 0.000000      6th sin = 0.000000

```

hub fz harmonics:

```

zero harm = -0.001619      1st sin = 0.000000      2nd cos = 0.000000      2nd sin = 0.000000
1st cos = 0.000000      2nd sin = 0.000000      3rd cos = 0.000000      3rd sin = 0.000000
2nd cos = 0.000000      3rd sin = 0.000000      4th cos = 0.000000      4th sin = 0.000000
3rd cos = 0.000000      4th sin = 0.000000      5th cos = 0.000000      5th sin = 0.000000
4th cos = 0.000000      5th sin = 0.000000      6th cos = 0.000000      6th sin = 0.000000
5th cos = 0.000000      6th sin = 0.000000

```

hub sz harmonics:

```

zero harm = -0.001888      1st sin = 0.000000      2nd cos = 0.000000      2nd sin = 0.000000
1st cos = 0.000000      2nd sin = 0.000000      3rd cos = 0.000000      3rd sin = 0.000000
2nd cos = 0.000000      3rd sin = 0.000000      4th cos = 0.000000      4th sin = 0.000000
3rd cos = 0.000000      4th sin = 0.000000      5th cos = 0.000000      5th sin = 0.000000
4th cos = 0.000000      5th sin = 0.000000      6th cos = 0.000000      6th sin = 0.000000
5th cos = 0.000000      6th sin = 0.000000

```

hub mx harmonics:

```

zero harm = -0.000273      1st sin = 0.000000      2nd cos = 0.000000      2nd sin = 0.000000
1st cos = 0.000000      2nd sin = 0.000000      3rd cos = 0.000000      3rd sin = 0.000000
2nd cos = 0.000000      3rd sin = 0.000000      4th cos = 0.000000      4th sin = 0.000000
3rd cos = 0.000000      4th sin = 0.000000      5th cos = 0.000000      5th sin = 0.000000
4th cos = 0.000000      5th sin = 0.000000      6th cos = 0.000000      6th sin = 0.000000
5th cos = 0.000000      6th sin = 0.000000

```

free vibration rotating frequencies & mode shapes

```

---- deformed blade
---- modes used for stability analysis

```

```

mode = 1 stability mode sequence = 1
mode = 2 stability mode sequence = 2
mode = 3 stability mode sequence = 3
mode = 4 stability mode sequence = 4
mode = 5 stability mode sequence = 5

```

```

eigenvale( 51) = 0.4867095e+00   frequency = 0.697645e+00
eigenvctr:

```

1	0.000000	2	-0.393958
4	0.019531	5	0.019215
7	0.003000	8	0.01538
10	0.000000	11	-0.277342
13	0.014746	14	0.018940
16	0.000000	17	-0.00399
19	0.003000	20	-0.037363
22	0.003319	23	0.019152
25	0.000000	26	-0.028155

bmr.output

Wed Mar 31 12:11:19 1993

16

28	0.003330	29	-0.023141	30	-3.31251	22	-0.301172	27	0.081392
31	0.002295	32	0.023579	33	-0.349211	25	0.000055	26	0.000030
34	0.005230	35	-0.045910	36	0.003100	28	0.000030	27	0.004688
37	0.003000	38	-0.003249	39	0.000050	31	-0.000038	32	0.000384
40	0.002293	41	-0.024654	42	-0.257650	34	0.000000	35	0.000434
43	0.002373	44	0.026903	45	-0.007762	37	0.000000	38	0.008788
46	0.005093	47	-0.004657	48	0.002330	40	0.000000	41	0.000418
49	0.000062	50	-0.180441	51	0.016810	43	-0.000037	44	-0.001116
						46	0.000030	47	0.002073
						49	0.000000	50	0.000318
							51		0.000219
<hr/>									
eigenvalue(50) = 0.1152250+0.0			frequency = 0.1373435+0.0		eigenvector:	elgenvalue(47) = 0.3308215+0.0		frequency = 0.5051700-0.1	
1	0.000000	2	0.021843	3	0.028126	1	0.000033	2	0.383692
4	0.381159	5	0.920641	6	0.003319	4	0.000000	5	0.318363
7	0.000000	8	0.034351	9	0.000000	7	0.000000	8	0.349550
10	0.000000	11	0.014696	12	0.028125	10	0.000000	11	0.304703
13	0.274563	14	0.424028	15	0.003273	13	0.000000	14	0.315150
16	0.300000	17	0.322856	18	0.000000	16	0.000000	17	0.309378
19	0.000000	20	0.301055	21	0.01873	19	0.000000	20	0.300391
22	0.045298	23	0.352095	24	0.001973	22	0.000000	23	0.205112
25	0.000000	26	0.010665	27	0.000000	25	0.000000	26	0.033654
28	0.000000	29	0.004934	30	0.011563	28	0.017440	29	0.074350
31	0.029517	32	0.353018	33	0.017615	31	0.000000	32	0.030652
34	0.000000	35	0.073770	36	0.000000	34	0.000000	35	0.278398
37	0.000000	38	0.002110	39	0.000000	37	0.000000	38	-0.028194
40	0.000000	41	0.005664	42	0.005443	40	0.000000	41	0.000000
43	0.031110	44	0.329471	45	0.000008	43	0.000000	44	0.000000
46	0.000000	47	0.004643	48	0.000000	46	0.000000	47	0.022470
49	0.000000	50	0.004299	51	0.225861	49	0.000000	50	0.000000
						51	0.000000		0.134389
<hr/>									
eigenvalue(49) = 0.8430762+0.0			frequency = 0.2903573+0.0		eigenvector:	elgenvalue(48) = 0.2311433+0.0		frequency = 0.4807745+0.0	
1	0.000000	2	-0.014425	3	-0.368563	1	0.000000	2	0.000000
4	0.141865	5	0.679932	6	0.010454	4	0.000000	5	0.766768
7	0.000000	8	0.01392	9	0.000000	7	-0.049059	8	-6.766768
10	0.000000	11	0.013358	12	-0.050039	10	0.000000	11	5.598960
13	-0.014437	14	0.489996	15	0.010350	13	0.000000	14	-0.826502
16	0.000000	17	0.012266	18	0.000000	16	0.026846	17	-0.926502
19	0.000000	20	0.033992	21	0.000000	19	-0.007333	20	-0.242408
22	-0.037810	23	-0.258494	24	0.003160	22	0.000000	23	4.758197
25	0.000000	26	-0.023434	27	0.000000	25	0.000000	26	-0.242408
28	0.000000	29	0.026660	30	0.031430	28	0.000000	29	5.736116
31	-0.0225102	32	-0.297478	33	-0.007333	31	0.000000	32	-0.242335
34	0.000000	35	-0.07655	36	0.000000	34	0.000000	35	-0.735909
37	0.000000	38	0.002470	39	0.000000	37	0.000000	38	-0.313909
40	0.000000	41	0.002887	42	0.000000	40	0.000000	41	4.601280
43	-0.0227235	44	-0.249438	45	0.0001763	43	0.000000	44	-0.736116
46	0.000000	47	0.00069	48	0.000000	46	0.000000	47	5.735909
49	0.000000	50	0.022834	51	-0.214330	49	0.000000	50	-0.307872
						51	0.000000		-0.761394
<hr/>									
eigenvalue(48) = 0.2311433+0.0			frequency = 0.4807745+0.0		eigenvector:	elgenvalue(47) = 0.3308215+0.0		frequency = 0.5051700-0.1	
1	0.000004	2	-0.02445	3	-0.011768	1	-0.000004	2	0.000000
4	-0.000004	5	0.548496	6	0.563637	4	0.000004	5	-3.594279
7	0.000004	8	0.000000	9	0.000000	7	-0.000000	8	-4.591923
10	0.000004	11	-0.000000	12	-0.008604	10	-0.340249	11	-2.828260
13	0.000231	14	-0.001364	15	0.50382	13	-0.140249	14	-2.828260
16	0.000003	17	0.334599	18	0.000000	16	-0.007872	17	1.762394
19	0.000000	20	0.000581	21	0.000420	19	-0.000000	20	-0.000000

Wed Mar 31 12:11:19 1993

24	-0.380641	1.897190
25	-0.380641	-1.897190
26	-0.394639	1.928829
27	-0.394639	-1.928829
28	-0.339713	2.827306
29	-0.339713	-2.827306
30	-1.138C03	0.153087
31	-1.138C03	-0.153087
32	-0.875979	0.000000
33	-0.CC1555	2.293145
34	-0.CC1555	-2.293145
35	-0.107216	0.168664
36	-0.107216	-0.168664
37	0.000000	0.000000
38	-0.033714	0.393390
39	-0.033714	-0.393390
40	-0.337639	0.873011
41	-0.337639	-0.873011
42	-0.400830	0.960397
43	-0.400830	-0.960397
44	-0.012020	0.699449
45	-0.012020	-0.699449
46	-0.010018	0.701336
47	-0.010018	-0.701336

const coeff: stability completed

I.8 DATA DICTIONARY

This section presents Table I-1, the Input Data Dictionary and Table I-2, Nondimensionalization of Important Input Variables.

Table I.1 Input Data Dictionary

Definitions :
 Data Block : A block of related input data
 KEYWORD : entry name appearing in the input file (entered by the user)
 ASSOCIATED VARIABLE : Fortran executive variable in (UMARC) associated with the keyword.

* : used only in UMRINP

. Data Block : TITLE

(should be the first keyword if title is given)

KEYWORD	ASSOCIATED VARIABLE	TYPE	DIMENSION	DEFAULT (IF ANY)	TYPICAL VALUE	ALLOWABLE RANGE
TITLE	--	CHAR	--	no TITLE	--	20 lines

. Data Block : INPUT_DATA

(should be the first keyword)

KEYWORD	ASSOCIATED VARIABLE	TYPE	DIMENSION	DEFAULT (IF ANY)	TYPICAL VALUE	ALLOWABLE RANGE
NON_DIMENSIONAL	--	CHAR	--	--	--	--
DIMENSIONAL	--	CHAR	--	--	--	--

DIMENSIONAL should be followed by :

REF_MASS	--	REAL	1	--	--	--
REF_ROTOR_SPEED	--	REAL	1	--	--	--
ROTOR_RADIUS	--	REAL	1	--	--	--

• Data Block : ROTOR PROPERTIES

(should be the first keyword)

KEYWORD	ASSOCIATED VARIABLE	TYPE	DIMENSION	DEFAULT (IF ANY)	TYPICAL VALUE	ALLOWABLE RANGE
ROTOR_NAME	ROTNAM*	CHR	1	--	MYROTOR	--
if ROTNAM = 'GAZELLE' = 'BO105' = 'TRR' = 'MYROTOR' = 'SH2'	IDATA=1 IDATA=0 IDATA=8 IDATA=9 IDATA=7	INTEG INTEG INTEG INTEG INTEG				
ROTOR_TYPE	ROTOR*	CHR	1	--	HINGELESS	--
if ROTOR = 'ARTICULATED' = 'HINGELESS' = 'BMR'	NCONF=0 NCONF=0 NCONF=2	INTEG INTEG INTEG				
<u>ARTICULATED rotor should be followed by one of :</u>						
FLAP	IARTIC=1	INTEG	--	--	--	--
FLAP_LAG	IARTIC=2	INTEG	--	--	--	--
FLAP_LAG_DELTA3	IARTIC=3	INTEG	--	--	--	--
FLAP_LAG_COINCIDE	IARTIC=4	INTEG	--	--	--	--
<u>BMR rotor should be followed by one of :</u>						
SINGLE_FLEXBEAM	NSEQ=3	INTEG	--	--	--	--
TWIN_FLEXBEAM	NSEQ=4	INTEG	--	--	--	--
<u>additional data for ARTICULATED rotor :</u>						
LAG_SPRING_CONSTANT	SPRLAG	REAL	1	--	--	--
LAG_DAMPER	DMPLAG	REAL	1	--	--	--
DELTA3_CONSTANT	DEL3PB	REAL	1	--	--	--

```

PITCH_SPRING_CONSTANT      SPRPBR      REAL      1      -
-
additional_data_for_BMR_rotor_i:
SOFT_PITCH_LINK    ---->   LNKSFT =1      -      -
LAG_PIN           ---->   NPIN=1      -      -
SNUBBER          ---->   ISNUB=1      -      -
-
for all types of rotors:
NO_BLADES        NBLADE     INTEG     1      -
SOLIDITY         SIGMA      REAL      1      -
LOCK_NO          GAMA       REAL      1      -
CT/SIGMA        CTSG       REAL      1      -
CG_BELOW_HUB    HBAR       REAL      1      0.0
CG_HUB_OFFSET_X XCG        REAL      1      0.0
CG_HUB_OFFSET_Y YCG        REAL      1      0.0
-
LNKSFT = 0      -      -
NPIN = 0       -      -
ISNUB = 0       -      -
-
4      -
0.07
5.0
0.07
0.2
-
-
0 or 1
0 or 1
0 or 1

```

• Data Block : BLADE PROPERTIES

(should be the first keyword)

KEYWORD	ASSOCIATED VARIABLE	TYPE	DIMENSION	DEFAULT (IF ANY)	TYPICAL VALUE	ALLOWABLE RANGE
TWIST(DEG)	TWIST	REAL	1	0.0	-8.0	--
PRECONE(DEG)	BTP	REAL	1	0.0	5.0	--
ROOT_CUT(%)	RROOT	REAL	1	0.0	2.0	--
NO_SPACE_ELEMENTS	NSELT	INTEG	1	5	5	--
MATERIAL_TYPE	BMTYPE	CHAR	14	ISOTROPIC	--	--
if MATERIAL_TYPE = TSOTROPIC = COMPOSITE_CALC = COMPOSITE_READ						
15 DOF elements used, properties read from main data file 19 DOF elements used, box-beam spar properties calculated based on COMPBEAM.JN data 19 DOF elements used, properties read from main data file						
for_BMR_rotor:						
NO_ELEM_IN_FLEXBEAM_1	NEFS(2)	INTEG	1	--	--	--
NO_ELEM_IN_FLEXBEAM_2 (for twin flex beams)	NEFS(3)	INTEG	1	--	--	--
NO_ELEM_IN_TORQUE_TUBE	NEFS(4)	INTEG	1	--	--	--
for_all_types_of_rotors:						
ELEMENT_LENGTH	EL	REAL	NSELT	(1.0-RRROT)/NSELT	0.2	--
CHORD	COR	REAL	NSELT	--	--	--
ELEMENT_MASS	RMAS	REAL	NSELT	1.0	--	--
OFFSET_TA&EA	EA	REAL	NSELT	--	--	--

OFFSET _CG&EA	BG	REAL	NSELT	-
OFFSET _AC&EA	ED	REAL	NSELT	-
GJ	GJ	REAL	NSELT	-
EY	EY	REAL	NELT	-
EZ	EZ	REAL	NSELT	-
EA	EAC	REAL	NSELT	-
EB1	EB1	REAL	NSELT	-
EB2	EB2	REAL	NSELT	-
EC1	EC1	REAL	NSELT	-
EC2	EC2	REAL	NSELT	-
GAY	GAY	REAL	NSELT	-
GAZ	GAZ	REAL	NSELT	-
K12	K12	REAL	NSELT	-
K13	K13	REAL	NSELT	-
K14	K12	REAL	NSELT	-
K25	K13	REAL	NSELT	-
K36	K12	REAL	NSELT	-
K45	K13	REAL	NSELT	-
K46	K12	REAL	NSELT	-

For COMPOSITE rotors (COMPOSITE READ option):

SQ_KA	SKA	REAL	NSELT	-
SQ_KM1	SKM1	REAL	NSELT	-
SQ_KM2	SKM2	REAL	NSELT	-
SWEEP_FLAG	IELSWP	INTEG	NSELT	0
SWEEP_ANGLE (degrees)	SWDEG	REAL	NSELT	0.0
DROOP_ANGLE (degrees)	DRDEG	REAL	NSELT	0.0

note : (1) sweep angle is negative for swept back tip
 (2) droop angle is negative for droop down

for_HINGELESS or BMR rotor:

PL_STIFFNESS (if PITCH_LINK is SOFT)	TTX	REAL	1	-
PL_CHORD_LENGTH	TTA	REAL	1	-
PL_AXIAL_LENGTH	TTP	REAL	1	-
PL_HEIGHT	TTB	REAL	1	-

for_BMR_rotor_if_there_is_LAG_PIN:

LP_AXIAL_LENGTH	TTX0	REAL	1	-
LP_HEIGHT	TTZ	REAL	1	-

• Data Block : FUSELAGE_PROPERTIES

(should be the first keyword)

KEYWORD	ASSOCIATED VARIABLE	TYPE	DIMENSION	DEFAULT (IF ANY)	TYPICAL VALUE	ALLOWABLE RANGE
NO_HUB_DOF	NHUB if NHUB > 0 INDFUS = 1 if NHUB ≤ 0 INDFUS = 0	INTEG	1	5	5	--
BODY_SEQ	IBODY	INTEG	NHUB	--	--	--
EFFECTIVE_X_MASS	HMX*	REAL	1	0.0	--	--
EFFECTIVE_Y_MASS	HMY*	REAL	1	0.0	--	--
EFFECTIVE_Z_MASS	HMZ*	REAL	1	0.0	--	--
FUSELAGE_PITCH_INERTIA	HIVH*	REAL	1	0.0	--	--
FUSELAGE_ROLL_INERTIA	HIXH*	REAL	1	0.0	--	--
EFFECTIVE_X_DAMPER	HCX*	REAL	1	0.0	--	--
EFFECTIVE_Y_DAMPER	HCY*	REAL	1	0.0	--	--
EFFECTIVE_Z_DAMPER	HCZ*	REAL	1	0.0	--	--
FUSELAGE_PITCH_DAMPER	HCALPS*	REAL	1	0.0	--	--
FUSELAGE_ROLL_DAMPER	HCPHIS*	REAL	1	0.0	--	--

EFFECTIVE_X_SPRING	HKX*	REAL	1	0.0	--
EFFECTIVE_Y_SPRING	HKY*	REAL	1	0.0	--
EFFECTIVE_Z_SPRING	HKZ*	REAL	1	0.0	--
FUSELAGE_PITCH_SPRING	HKALPS*	REAL	1	0.0	--
FUSELAGE_ROLL_SPRING	HKPHIS*	REAL	1	0.0	--
BODY_ROLL_MOMENT_COEFF	CMXF	REAL	1	0.0	--
BODY_PITCH_MOMENT_COEFF	CMYF	REAL	1	0.0	--
PARASITE_DRAG_AREA	FBYA	REAL	1	0.0	0.01
BODY_SIDE_FORCE_COEFF	CYF	REAL	1	0.0	--

* : used only in UMRIMP

In_UMARC

```

BMASS = ( HMX, HMY, HMZ, HIYH, HIXH )
BDAMP = ( HCX, HCY, HCZ, HCALPS, HCPHIS )
BSPRNG = ( HCX, HCY, HCZ, HCALPS, HCPHIS )

```

. Data Block : TAIL_PROPERTIES

(TAIL be the first keyword)

KEYWORD	ASSOCIATED VARIABLE	TYPE	DIMENSION	DEFAULT (IF ANY)	TYPICAL VALUE	ALLOWABLE RANGE
RAD_RATIO_TAIL_ROT	RRATIO	REAL	--	0.2	--	--
SOLIDITY_TAIL_ROT	SIGMAT	REAL	--	0.15	--	--
GEAR_RATIO_TAIL_ROT	GRATIO	REAL	--	5.0	--	--
TWIST(DEG)_TAIL_ROT	TWTAIL	REAL	--	0.0	--	--
CG_TAIL_ROT_OFFSET_X	XTLRT	REAL	--	1.0	--	--
TAIL_ROT_ABOVE_CG	ZTLRT	REAL	--	0.0	--	--
C1_TAIL_ROT	C1T	REAL	--	6.28	--	--
TAIL_ROTOR_TABLE_LOOK_UP	ITRTAB	INTEG	--	0	--	0 or 1
AREA_RATIO_TAIL_HOR	ARATH	REAL	--	0.0	--	--
CG_TAIL_HOR_OFFSET_X	XTLHZ	REAL	--	1.0	--	--
C1_TAIL_HOR	C1TH	REAL	--	6.28	--	--
C0_TAIL_HOR	COTH	REAL	--	0.0	--	--

. Data Block : AIRFOIL_PROPERTIES

(should be the first keyword)

KEYWORD	ASSOCIATED VARIABLE	TYPE	DIMENSION	DEFAULT (IF ANY)	TYPICAL VALUE	ALLOWABLE RANGE
NO_AIRFOILS	NARFL	INTEG	1	1	--	--
AIRFOIL_NAMES	ARFL	CHAR	NARFL	--	--	--
AIRFOIL_STARTING_LOCATIONS	XAF	REAL	NARFL	--	--	--
TABLE_LOOK_UP	TAB	CHAR	1	OFF	--	--
 if TABLE_LOOK_UP = ON:						
CL_TABLE_NAMES	CLTAB	CHAR	NARFL	--	--	--
CD_TABLE_NAMES	CDTAB	CHAR	NARFL	--	--	--
CM_TABLE_NAMES	CMTAB	CHAR	NARFL	--	--	--
(preparation of table look up data file is explained at the end)						
REF_LIFT_CURVE_SLOPE	SLC	REAL	1	6.0	6.0	--
CZERO	C0	REAL	1	0.0	0.0	--
C1	C1	REAL	1	6.28	6.28	--
DZERO	D0	REAL	1	0.01	0.01	--
D2	D2	REAL	1	0.0	0.0	--
CMAC	CMAC	REAL	1	0.0	--	--

F1	F1	REAL	1	0.0	--
LE_RECV_FACT	ETAUN	REAL	1	0.95	--

Note :

$$C_L = CO + C1 * \alpha$$

$$C_D = DO + D2 * \alpha^2$$

$$C_M = CMAC + F1 * \alpha$$

Data Preparation for Table Look Up

Example Input :

```
NO_AIRFOILS = 2
CL_TABLE NAMES = CLITAB, CL2TAB
CD_TABLE NAMES = CDITAB, CD2TAB
CM_TABLE NAMES = CMITAB, CM2TAB
```

Table Preparations :

1. Open data files in the following names:

- (i). FILE CLITAB
- (ii). FILE CL2TAB
- (iii). FILE CDITAB
- (iv). FILE CD2TAB
- (v). FILE CM1TAB
- (vi). FILE CM2TAB

2. Data arrangement in a typical file:

NALFAS, NMACHS
ANG11, ANG12, ANG21, ANG22, ANG31, ANG32, ANG41, ANG42, ANG51, ANG52

(five pairs of most preferable range of angle of attacks)

MACHNO(1),.....	MACHNO(NMACHS)
ANGLE(1),.....	CL(1),.....
ANGLE(2),.....	'CL(NMACHS)
ANGLE(3),.....	'CL(NMACHS)
	'CL(NMACHS)
	'CL(NMACHS)
	'CL(NMACHS)

ANGLE(NALFAS),	CL(1),.....	'CL(NMACHS)

Important Note : NALFAS, NMACHS and ANG11, ANG12,.....,ANG52 are the same for all the coefficients (CL, CD, and CM). They can be different for different airfoils. There is no built in facility to check for the relevance or sufficient size of input data file. Therefore the user must check the data in the temporary output file defined by unit 17, which has been created just for checking.

Example CL table.

9,6 -2.0,3.0		(NALFAS, NMACHS)		9 pairs of preferable angle of attach range)		
		-4.0,-2.0	3.0,4.0	0.0,0.0	0.0,0.0	0.6
		0.0	0.3	0.4	0.5	0.65 (mach numbers)
(ang. of attack)		(CL values)		(CL values)		
-4.0	-435	-435	-452	-48	-545	.59
-3.0	-325	-325	-337	-355	-4051	.445
-2.0	-215	-215	-222	-230	-265	.305
-1.0	-1075	-1075	-111	-115	-1325	.165
0.0	0.0	0.0	0.0	0.0	0.0	0.0
1.0	1075	1075	.111	.115	.1325	.165
2.0	215	215	.222	.230	.265	.305
3.0	325	325	.337	.355	.4051	.445
4.0	435	435	.452	.48	.545	.59

• Data Block : FLIGHT CONDITION

(should be the first keyword)

KEYWORD	ASSOCIATED VARIABLE	TYPE	DIMENSION	DEFAULT (IF ANY)	TYPICAL VALUE	ALLOWABLE RANGE
ADVANCE_RATIO	AMU	REAL	1	0.0	0.3	--
ROTOR_SPEED_RATIO	OMEGAR	REAL	1	1.0	1.0	--
DENSITY_RATIO	DNSTY	REAL	1	1.0	1.0	--
FLIGHT_ANGLE	THFP	REAL	1	0.0	0.0	--
TIP_MACH	TIPM	REAL	1	--	0.6	--

• Data Block : AERODYNAMICS

(should be the first keyword)

KEYWORD	ASSOCIATED VARIABLE	TYPE	DIMENSION	DEFAULT (IF ANY)	TYPICAL VALUE	ALLOWABLE RANGE
REVERSE_FLOW	IREVF=1	--	--	--	--	--
L_CIRC_US	IUNCIR=1	--	--	--	--	--
L_IMPUL_US	IUNIMP=1	--	--	--	--	--
L_US_DRAG	IUNDRG=1	--	--	--	--	--
L_US_PM	IUNMOM=1	--	--	--	--	--
NL_US_TE_SEP	ITSESEP=1	--	--	--	--	--
DYN_STALL	IVORTX=1	--	--	--	--	--
UNIFORM_INFLOW	INCODE=0	--	--	--	--	--
DREES_LINEAR_INFLOW	INCODE=1	--	--	--	--	--
B&W_LINEAR_INFLOW	INCODE=2	--	--	--	--	--
SING_PEAK_FREE_WAKE	IFRWKE=1 INEWKKE=0 LEVEL =2	--	--	--	--	--
SING_PEAK_PRES_WAKE	IFRWKE=1 INEWKKE=0 LEVEL =1	--	--	--	--	--
DUAL_PEAK_FREE_WAKE	IFRWKE=1 INEWKKE=1 LEVEL =2	--	--	--	--	--

DUAL_PEAK_PRES_WAKE

IFRWKE=1
INNEWKE=1
LEVEL =1

WAKE_ITTER_NO

ITTERFW
INTEG

1

. Data Block : TRIM ANALYSIS

(should be the first keyword)

KEYWORD	ASSOCIATED VARIABLE	TYPE	DIMENSION	DEFAULT (IF ANY)	TYPICAL VALUE	ALLOWABLE RANGE
NL_STRUCT_AERO	INDNL=1	--	--	--	--	--
UNCOUPLED_RB	ICPLTR=0	--	--	--	--	--
COUPLED_RB	=1	--	--	--	--	--
UNCOUPLED_IC	=2	--	--	--	--	--
COUPLED_IC	=3	--	--	--	--	--
HOVER_COUPLED_RB	=11	--	--	--	--	--
COUPLED_WT	=12	--	--	--	--	--
NO_TIME_ELEMENTS NODES_PER_TIME_ELEM	NTLT NNTE	INTEG INTEG	1 1	6	--	--
NO_FLAP_MODES FLAP_MODE_SEQ FLAP_MODE_DAMPING	NFLAP FMODES FDAMP	INTEG INTEG REAL	1 1 1	NFLAP NFLAP NFLAP	--	--
NO_LAG_MODES LAG_MODE_SEQ LAG_MODE_DAMPING	NLAG LMODES LDAMP	INTEG INTEG REAL	1 1 1	NLAG NLAG NLAG	--	--
NO_TORSION_MODES TORSION_MODE_SEQ TORSION_MODE_DAMPING	NTORSN TMODES TDAMP	INTEG INTEG REAL	1 1 1	NTORSN NTORSN NTORSN	--	--

```

NO_AXIAL_MODES          NAXIAL      1
AXIAL_MODE_SEQ          TMODES     NAXIAL
AXIAL_MODE_DAMPING      ADAMP      NAXIAL
                           -        -
FIRST_FLAP_FREQ         F1FREQ    REAL
                           -        -
OS_AERO_DAMP            XJFCT1   REAL
US_AERO_DAMP            XJFCT2   REAL
                           -        -
NO_QS_JTER_BEFORE_US   ITERUN    1
NO_MAX_JTER             NITER     1
                           -        -
                           -        -
CONV_CRIT               CONCRI   CHAR
                           -        -
if CONCRI = 'ACTIVE'    ITRMCV   = 1
if CONCRI = 'NOT_ACTIVE' ITRMCV   = 0
                           -        -
                           -        -
DELTA_CONTROLS(%)       DELCON   REAL
                           -        -
                           -        -
TRIM_CONV_CRIT          CNVCRT   REAL
RESP_CONV_CRIT          RESCNV   REAL
WT_CONV_CRIT            WTCNV    REAL
                           -        -
                           -        -
COUPLED_TRIM_SCHEME    SCHEME   CHAR
                           -        -
if SCHEME = 'NEWTON'    ITSCHM   = 1
if SCHEME = 'MARQ_NEWTON' ITSCHM   = 0
                           -        -
                           -        -
THETA_75    (deg)      TH75     REAL
                           -        -
                           -        -

```

I-2 ≤ ICPLTR ≤ 9:

THETA_JC	(deg)	THJC	REAL	1
THETA_IS	(deg)	THIS	REAL	1
ALPHA_S	(deg)	ALPS	REAL	1
PHI_S	(deg)	PHIS	REAL	1
THETA_O_TAIL	(deg)	TOTL	REAL	1
<u>I_ICPLTR = 12</u>				
ALPHA_S_WT	(deg)	ALPHWT	REAL	1
THETA_O_WT	(deg)	THOWT	REAL	1

• Data Block : STABILITY ANALYSIS

(should be the first keyword)

KEYWORD	ASSOCIATED VARIABLE	TYPE	DIMENSION	DEFAULT (IF ANY)	TYPICAL VALUE	ALLOWABLE RANGE
DYNAMIC_INFLOW	IDYN=1	--	--	not included	--	--
ROT_QS_FLOQ	IROT=1 ISTAB = 4 if IDYN = 1 or INDFUS = 1 ISTAB = 1 if IDYN = 0 and INDFUS = 0	--	--	--	--	--
FIX_QS_CONST	ISTAB=3	--	--	--	--	--
NO_PSI_LOCATIONS <small>(only for FIX_QS_CONST)</small>	NPSICC	INTEG	1	--	--	--
FIX_QS_FLOQ	ISTAB=4	--	--	not included	--	--
ROT_US_FLOQ	ISTAB=5	--	--	--	--	--
TRANS_PB_LUS	ISTAB=6	--	--	--	--	--
TRANS_PB_NLUS	ISTAB=7	--	--	--	--	--
DGEAR_METHOD	IRUNGE=0	--	--	0	--	--
RUNGE_KUTTA_METHOD	IRUNGE=1	--	--	0	--	--
TOl_FOR_DGEAR <small>(only for DGEAR_METHOD)</small>	TOl	REAL	1	.1*10.4	--	--

NO_INTEGRATION_POINTS
(only for RUNGE_KUTTA method)

60

1

--

1

--

--

. Data Block : OUTPUT OPTIONS

(should be the first keyword)

KEYWORD	ASSOCIATED VARIABLE	TYPE	DIMENSION	DEFAULT (IF ANY)	TYPICAL VALUE	ALLOWABLE RANGE
PRINT_CONTROL	IPRINT	INTEG	1	--	--	--
HUB_LOAD_CONTROL	ICKOUT	INTEG	1	--	--	--
PRINT CONTROLS:						
PRINT NOTHING				IPRINT =0		
PRINT EVERYTHING (EXCEPT=6)						=1
PRINT INPUT/TRIM / DISPLACEMENTS/ WAKE INFLOW/HUB LOADS / BLADE STABILITY RESULTS / CIRCULATION						=2
PRINT MODE SEQUENCES / GLOBAL_LOCAL DOFS/EIGENVALUES AND EIGEN VECTORS (RESPONSE ONLY)						=3

RESPONSE AND STABILITY	=4
PRINT SPATIAL ELEMENT (BANDED) MATRICES, MODALIZED & COMBINED (ELEM =1 TIME PT = 1)	=5
PRINT GLOBAL FEM/T MATRICES	=6
PRINT GLOBAL MASS AND STIFFNESS MATRICES FOR RESPONSE AND STABILITY NORMAL MODE CALCULATION	=7
PRINT TRANSITION MATRIX/CONSTANT COEFFICIENT MATRIX AND CORRESPONDING EIGENVALUES/VECTORS	=8
PRINT RESPONSE'S STRUCTURAL AND AERO EM, EC, EK, AND PERTURBATIONS STRUCTURAL AND AERO EM,EC,EK, WHEN IPRINT=9, PROGRAM AUTOMATICALLY SETS ISTAB=3	=9
PRINT FIXCOD MATRICES	=10
HUB LOAD CONTROLS:	
HUB LOADS CALCULATED AT 15-deg STEPS NO CHECK OUTPUT	ICKOUT=0
HUB LOADS CALCULATED AT 5-deg STEPS CHECK OUTPUT AT ITERATION # N	ICKOUT=N

Table 1.2 Nondimensionalization of Important Input Variables

KEYWORD	MEANING	ASSOCIATED VARIABLE	NON DIMENSIONAL EQUIVALENT
LAG_SPRING_CONSTANT	--	SPRLAG	$K_\zeta / m_o \Omega_o^2 R^3$
LAG_DAMPER	--	DMPLAG	$C_\zeta / m_o \Omega_o R^3$
DELTA3_CONSTANT	$K_p \beta$	DEL3PB	$\kappa p \beta$
PITCH_LINK_CONSTANT	SPRING_STIFFNESS	SPRPBR	$K / m_o \Omega_o^2 R^3$
CG_BELOW_HUB	--	HBAR	h/R
CG_HUB_OFFSET_X	--	XCG	X_{CG}/R
CG_HUB_OFFSET_Y	--	YCG	Y_{CG}/R
BODY_ROLL_MOMENT_COEFF	--	CMXF	$M_{XF} / \rho_o A (\Omega_o R)^2 R$
BODY_PITCH_MOMENT_COEFF	--	CMYF	$M_{YF} / \rho_o A (\Omega_o R)^2 R$
PARASITE_DRAG_AREA	--	FBYA	f/A
BODY_SIDE_FORCE_COEFF	--	CYF	$Y_F / \rho_o A (\Omega_o R)^2$
LOCK_NO	--	GAMA	$\rho a c R^4 / I_b$

ELEMENT_LENGTH	--	EL	L_i / R
CHORD	--	COR	c / R
ELEMENT_MASS	element mass per unit length	RMAS	m / m_0
OFFSET_TA&EA	distance of tensile center ahead of elastic axis	EA	e_A / c
OFFSET_CG&EA	distance of CG ahead of elastic axis	BG	e_G / c
OFFSET_AC&EA	distance of aero. centre aft of e.a	ED	e_d / c
EA	axial stiffness	EAC	$EAC / m_0 \Omega_0^2 R^2$
GJ	torsional stiffness	GJ	$GJ / m_0 \Omega_0^2 R^4$
EY	bending stiffness w.r.to Y-axis	EIY	$EI_Y / m_0 \Omega_0^2 R^4$
EZ	bending stiffness w.r.to Z-axis	EIZ	$EI_Z / m_0 \Omega_0^2 R^4$
EB1	--	EB1	$EB1 / m_0 \Omega_0^2 R^6$
EB2	--	EB2	$EB2 / m_0 \Omega_0^2 R^5$
EC1	--	EC1	$EC1 / m_0 \Omega_0^2 R^6$
EC2	--	EC2	$EC2 / m_0 \Omega_0^2 R^5$
SQ_KA	radius of gyration square (elastic)	SKA	κ_A^2 / R^2
SQ_KM1	radius of gyration square (mass)	SKM1	κ_{m1}^2 / R^2

SQ_KM2	radius of gyration square (mass)	SKM2	$\kappa m_2^2 / R^2$
PL_STIFFNESS	--	TK	$K / m_o \Omega_o^2 R$
PL_CHORD_LENGTH	--	TA	L_{CPL} / R
PL_AXIAL_LENGTH	--	TP	L_{APL} / R
PL_HEIGHT	--	TB	H_{PL} / R
LP_AXIAL_LENGTH	--	TXO	L_{ALP} / R
LP_HEIGHT	--	TZ	H_{LP} / R
DENSITY_RATIO	--	DNSTY	ρ / ρ_o
EFFECTIVE_X_MASS	--	BMASS(1)	$M_X / m_o R$
EFFECTIVE_Y_MASS	--	BMASS(2)	$M_Y / m_o R$
EFFECTIVE_Z_MASS	--	BMASS(3)	$M_Z / m_o R$
FUSELAGE_ROLL_INERTIA	--	BMASS(4)	$I_\phi / m_o R^3$
FUSELAGE_PITCH_INERTIA	--	BMASS(5)	$I_\alpha / m_o R^3$
FUSELAGE_X_DAMPER	--	BDAMP(1)	$2\xi \omega_X / \Omega_o$
FUSELAGE_Y_DAMPER	--	BDAMP(2)	$2\xi \omega_Y / \Omega_o$
FUSELAGE_Z_DAMPER	--	BDAMP(3)	$2\xi \omega_Z / \Omega_o$
FUSELAGE_ROLL_DAMPER	--	BDAMP(4)	$2\xi \omega_\phi / \Omega_o$

FUSELAGE_PITCH_DAMPER	--	$2\zeta \omega_d / \Omega_0$
FUSELAGE_X_SPRING	--	BSPRNG(1)
FUSELAGE_Y_SPRING	--	BSPRNG(2)
FUSELAGE_Z_SPRING	--	BSPRNG(3)
FUSELAGE_ROLL_SPRING	--	BSPRNG(4)
FUSELAGE_PITCH_SPRING	--	BSPRNG(5)
RAD_RATIO_TAIL_ROT	--	R_u / R
GEAR_RATIO_TAIL_ROT	--	Ω_u / Ω
CG_TAIL_ROT_OFFSET_X	--	x_u / R
TAIL_ROT_ABOVE_CG	--	z_u / R
AREA_RATIO_TAIL_HOR	--	S_h / A
CG_TAIL_HOR_OFFSET_X	--	x_{ht} / R
MODAL_DAMPING	--	$2\zeta \omega_b / \Omega_0$
(for FLAP,LAG,TORSION and AXIAL modes)		
FIRST_FLAP_FREQ	--	ω_1 / Ω_0
DFQZT,DFQ2P	--	
F1FREQ	--	

THETA_75	pitch at 75% radius	TH75	θ_{75}
THETA_JC	lateral cyclic pitch	TH1C	θ_{1C}
THETA_IS	longitudinal cyclic pitch	TH1S	θ_{1S}
ALPHA_S	longitudinal shaft angle	A1PS	α_S
PHI_S	lateral shaft angle	PHIS	ϕ_S
THETA_O_TAIL	tail rotor collective pitch	TOTL	θ_{OT}
ALPHA_S_WT	ALPHA_S for wind tunnel trim	ALPHWT	α_{SWT}
THETA_O_WT	collective pitch for wind tunnel trim	THOWT	θ_{OWT}

Reference Parameters Used for Nondimensionalization

m_0 = Reference mass

Ω_0 = Reference rotational speed

R = Radius of the rotor

ρ_0 = Sea level air density

A = Area of the rotor = πR^2

c_0 = Reference chord length

For this analysis, the reference mass per unit length, m_0 , is defined as the mass per unit length of an equivalent *uniform* blade which has the same flap inertia as the actual (*i.e. nonuniform*) blade. Using this definition, m_0 can be written as

$$m_0 = \frac{3I_\beta}{R^3} \approx \frac{3 \int_0^R mr^2 dr}{R^3}$$

Blade Sectional Constants

$$mk_{m1}^2 = \iint_A \rho_s \zeta^2 d\eta d\zeta \quad EI_y = \iint_A E \zeta^2 d\eta d\zeta$$

$$mk_{m2}^2 = \iint_A \rho_s \eta^2 d\eta d\zeta \quad EI_z = \iint_A E \eta^2 d\eta d\zeta$$

$$EAk_A^2 = \iint_A E(\eta^2 + \zeta^2) d\eta d\zeta \quad GJ = \iint_A G(\hat{\eta}^2 + \hat{\zeta}^2) d\eta d\zeta$$

$$EB_1 = \iint_A E(\eta^2 + \zeta^2)^2 d\eta d\zeta \quad EC_1 = \iint_A E \lambda^2 d\eta d\zeta$$

$$EB_2 = \iint_A E\eta(\eta^2 + \zeta^2)^2 d\eta d\zeta \quad EC_2 = \iint_A E \zeta \lambda d\eta d\zeta$$

I.9 IMPORTANT NOTES

- 1) If the input to UMARC is nondimensional, the user must identify this by the keyword 'non_dimensional'. For dimensional input, user must supply the keyword 'dimensional'. In the later case, ensure that all the dimensional data items are in consistent units. The user must also supply the blade reference mass per unit length, m_0 , reference rotor speed, Ω_0 , and the rotor radius, R .
- 2) The UMARC code always operates on nondimesional data. If the user input is dimensional, the code nondimensionalizes it before initiating analysis. Nondimension-alization of the input data is explained in Table I.2. The user must ensure that the reference mass, m_0 , used in the nondimensionalization procedure and the input Lock number satisfy the following relation:

$$\gamma = \frac{3\rho acR}{m_0}$$

- 3) The rotor related data are entered via the data block 'rotor_properties' (see Table I.1). The user must supply the rotor name at the beginning of this data block. The rotor name sets the flag IDATA to a particular value depending on the rotor name (see Table I.1). The code uses this flag to obtain unsteady aerodynamic parameters and blade twist distribution appropriate to the selected rotor. If MYROTOR is used for rotor name, IDATA is set to a value 9. This flag value directs the code to use NACA 0012 airfoil (default selection). It also directs the code to use the input linear twist distribution (input) to compute blade pretwist at any section. Should the user wish to use a different airfoil, he or she must indicate this in the subroutine AIRFLS when IDATA=9. Similarly, to use specific blade twist distribution, the user must direct calls to a user-supplied routine when IDATA=9. This user-supplied routine must yield the correct blade pretwist at any blade section.

Chapter II

Validation Studies

Chapter II

Validation Studies

Representative ITR configurations from Reference 1 are selected to correlate predicted results from UMARC with experimental data. The experimental data sets were generated by the Army Aeroflightdynamics Directorate at Ames as part of the Integrated Technology Rotor (ITR) program. Validation studies are first carried out for an isolated rotor in hover and the correlation results are discussed in Section II.1. Section II.1.1 considers a hingeless isolated rotor and Section II.1.2 considers a bearingless isolated rotor. Next, aeromechanical stability correlation studies are conducted for two hingeless configurations. First hingeless configuration considers vacuum conditions and results are presented in Section II.2.1. Second hingeless configuration considers hover condition and results are presented in Section II.2.2.

Each section provides the structural and aerodynamic properties of the rotor configuration along with the finite element discretization used for calculations. Quasisteady aerodynamics and dynamic inflow modeling are used in all the studies.

II.1 Isolated Rotor Aeroelastic Stability

II.1.1 Hingeless Model Rotor Aeroelastic Stability

Correlation in Hover

Theoretical prediction of aeroelastic stability of isolated hingeless rotors (shaft fixed) using UMARC is compared with experimental data of Ref. II.2 (contained in Ref. II.1). The correlation is performed for a torsionally soft rotor, first with a soft flexure and then with a stiff flexure. For each configuration, three subcases are studied: rotor with zero precone and zero droop, rotor with 5 degrees precone, and rotor with -5 degrees droop outboard of the flexure.

The properties of the model rotor are shown in Table II.1. Figure II.1 shows a schematic of the finite element model discretization used for the analysis by UMARC. Tables II.2 and Table II.3 show the model blade nondimensional finite element properties used as input to UMARC for the soft and the stiff flexures respectively. Since the blade mass and stiffness properties are uniform from the 9.5% radius location to the tip, only two elements are used for this part. Table II.4 shows the correlation for the nonrotating natural frequencies (in Hz) for the rotor blade with soft flexure. Table II.5 shows the correlation for the nonrotating natural frequencies (in Hz) for the rotor blade with stiff flexure. It is noted that the nonrotating frequencies given by UMARC show close agreement with the experimental values. For the stiff flexure blade, the flexure stiffness was slightly modified to match the fundamental nonrotating frequencies. For the soft flexure blade, no such modification was necessary. Tables II.6 and II.7 show the correlation for the rotating frequencies of the soft-flexure and stiff-flexure blades respectively.

Six normal modes were used for the aeroelastic analysis. These included two flap, two lag and two torsion modes. It was observed that inclusion of the second flap and the second lag mode improved the correlation with data.

Figure II.2 shows results of the aeroelastic analysis. For the model rotor with zero precone and droop, the correlation is very good at low collective pitch. However, the correlation deteriorates with increasing collective pitch. For the model rotor with a precone of 5 degree and no droop, the correlation is good throughout the collective sweep. For the model rotor with droop of 5 degrees and no precone the correlation is good for small collective angles only. The likely cause for the deterioration of the correlation for higher collective angles may be the limitation of the attached flow aerodynamic model in that region.

In conclusion, it is seen that the correlation is very good for the blade with precone and satisfactory for the other two blade settings (droop only and zero-droop zero-precone).

Table II.1 Model Rotor Properties

Main Rotor:

Number of Blades	2
Rotor Diameter, ft	6.309
Nominal Rotational Speed Ω_0 , RPM	1000
Nominal Tip Mach Number	0.35
Airfoil	NACA 0012
c_0, c_1	0.0 , 6.00
d_0, d_1, d_2	0.01 , 0.0, 0.0
C_{mac}	0.0
c/R	0.0898
Solidity, σ	0.0572
Lock Number, γ	6.34
Reference Mass per unit length, slug/in	0.0184
Aerodynamic root cutout, x_{root}/R	0.0095
Lag Damping (lag mode 1), $C_\zeta/m_0\Omega_0$	0.0196

**Table II.2 Model Rotor Nondimensional Finite Element Properties
(Soft Flexure)**

Element	ℓ_i/R	m/m_0	$\frac{EI_y}{m_0\Omega^2R^4}$	$\frac{EI_z}{m_0\Omega^2R^4}$	$\frac{GJ}{m_0\Omega^2R^4}$	$\frac{EA}{m_0\Omega^2R^2}$	$\frac{k_{m1}^2}{R^2}$	$\frac{k_{m2}^2}{R^2}$
1	0.4513	1.0489	0.00549	0.1119	0.00165	47.95	0.00004	0.000644
2	0.4523	1.0489	0.00549	0.1119	0.00165	47.95	0.00004	0.000644
3	0.0396	8.5869	2.46220	20.4159	2.25517	47.95	0.00006	0.000906
4	0.0125	31.4130	24.2193	24.2193	18.4274	47.95	0.00009	0.000600
5	0.0244	6.8423	0.15015	0.18559	0.00030	47.95	0.00000	0.002500

**Table II.3 Model Rotor Nondimensional Finite Element Properties
(Stiff Flexure)**

Element	ℓ_i/R	m/m_0	$\frac{EI_y}{m_0\Omega^2R^4}$	$\frac{EI_z}{m_0\Omega^2R^4}$	$\frac{GJ}{m_0\Omega^2R^4}$	$\frac{EA}{m_0\Omega^2R^2}$	$\frac{k_{m1}^2}{R^2}$	$\frac{k_{m2}^2}{R^2}$
1	0.4513	1.0489	0.00549	0.1119	0.00165	47.95	0.00004	0.000644
2	0.4523	1.0489	0.00549	0.1119	0.00165	47.95	0.00004	0.000644
3	0.0396	8.5869	2.46220	20.4159	2.25517	47.95	0.00006	0.000906
4	0.0125	31.4130	24.2193	24.2193	18.4274	47.95	0.00009	0.000600
5	0.0244	6.8423	2.15789	1.88879	0.00556	47.95	0.00000	0.002500

Table II.4 Nonrotating Natural Frequencies (Hz) of Model Hingeless Rotor Blades ($\theta_0 = 0$ deg) with Soft Flexure

Mode	Experiment	UMARC (15 DOF)
Flap 1	5.19	5.17
Flap 2	32.50	32.621
Lag 1	22.02	22.517
Torsion 1	38.38	37.38

Table II.5 Nonrotating Natural Frequencies (Hz) of Model Hingeless Rotor Blades ($\theta_0 = 0$ deg) with Stiff Flexure

Mode	Experiment	UMARC (15 DOF)
Flap 1	5.25	5.15
Flap 2	32.75	32.67
Lag 1	23.76	23.34
Torsion 1	44.73	44.67

Table II.6 Rotating Natural Frequencies (/ rev) of Model Hingeless Rotor Blades ($\theta_0 = 0$ deg) for Soft Flexure

Mode	Experiment	UMARC (15 DOF)
Flap 1	1.15	1.17
Lag 1	1.38	1.46
Torsion 1	2.56	2.45

Table II.7 Rotating Natural Frequencies (/ rev) of Model Hingeless Rotor Blades ($\theta_0 = 0$ deg) for Stiff Flexure

Mode	Experiment	UMARC (15 DOF)
Flap 1	1.15	1.18
Lag 1	1.50	1.51
Torsion 1	2.85	2.86

II.1.2 Validation of Aeroelastic Stability Analysis for a Bearingless Rotor

UMARC capability to analyze bearingless rotor stability is checked with experimental data of Ref II.3 (contained in Ref. II.1). The experimental attempt, described in this reference, examined the aeroelastic stability of a small-scale bearingless model rotor in hover. The 5.88-ft diameter model rotor included flap, lead-lag, and torsional degrees of freedom, but no body degrees of freedom (hub fixed). Three cases of pitch control configuration were tested. Figure II.3 shows these cases schematically. The first case examined a configuration with a single pitch link at the leading edge, the second case examined a configuration with a single pitch link at the trailing edge, and the third case investigated a configuration with one pitch link at the leading edge to provide pitch control and another pitch link at the trailing edge to simulate shear restraint. The model rotor properties are summarized in Table II.8. For each test case, the blade pitch angle was set by manually adjusting the pitch link and swashplate combination, prior to test run, such that the flap bending moment induced in the flexbeam was zero.

For finite element analysis by UMARC, the bearingless blade was divided into seven elements as shown in Fig. II.4. There are three elements for the main blade, two elements for the flexbeam (numbered 4 and 5), and two elements for the torque tube (numbered 6 and 7). The blade finite element properties are presented in nondimensionalized form in Table II.9. Table II.10 compares nonrotating frequency measurements with calculations for the three cases. Nonrotating frequencies calculated by UMARC show close agreement with the experimental data. This indicates that UMARC modeling could quite accurately capture the structural behavior of the model rotor.

For aeroelastic stability analysis, five modes (two flap modes, two lag modes and one torsion mode) were used. Quasisteady aerodynamics was used for airload computations. A simple 3-state dynamic inflow model was used to account for the unsteady inflow effects. It was observed that inclusion of second flap and second lag modes improved correlation with the experimental data.

Figures II.5 to II.7 present aeroelastic stability correlations for cases 1 to 3 respectively. For each case, blade lag damping is plotted against the blade pitch angle setting. For Case 1, the agreement between the data and the calculated values is good over the blade pitch range of -2° to 4° . The predicted damping value is minimum at blade pitch setting of about 0.7° , whereas the data shows that this occurs at an angle just below 2° . For Case 2, UMARC overpredicts lag damping at negative pitch settings and underpredicts it at positive pitch settings. The agreement is poor. UMARC also predicts pitch-flap flutter over the pitch setting range of -4° to 4° (Fig. II.6b). This range is wider than that encountered during the experimental attempt. Though the experiment could not quantify the pitch-flutter range, it was estimated to be little wider than the range 0° to 2° . For Case 3, the correlation is good for blade pitch settings up to 2° . The discrepancy between data and predicted values widens as the pitch setting is increased further. A probable cause of this deterioration of correlation can be the limitation of quasisteady aerodynamics at higher blade pitch angles.

Table II.8 BMR Model Rotor Properties

Rotor type	BMR
Number of blades	2
Rotor diameter, in	35.445
Chord, in	1.65
Number of flexbeams per blade	1
Pitch link spanwise location from hub center, in	3.6
Pitch link chordwise offset from blade pitch axis, in	1.447
Nominal rotational speed Ω_0 , RPM	1100
Nominal tip Mach number	0.304
Airfoil	NACA 23012
c_0, c_1	0.15 , 5.73
d_0, d_2	0.0079 , 1.7
C_{mac}	-0.012
Solidity, σ	0.0296
Lock number, γ	5.40
Precone angle, deg	0
Blade pretwist, deg	0
Reference mass per unit length, slug/in	2.5621E-4
Aerodynamic root cutout, x_{root} / R	0.102
Lag damping (lag mode), $C_\zeta / m_0 \Omega_0$	0.0146

Table II.9. Finite Element Properties of the Model Rotor Blade
(presented in nondimensionalized form)

Element	ℓ_i/R	m/m_0	$\frac{EI_y}{m_0\Omega^2 R^4}$	$\frac{EI_z}{m_0\Omega^2 R^4}$	$\frac{GJ}{m_0\Omega^2 R^4}$	$\frac{EA}{m_0\Omega^2 R^2}$	$\frac{k_{m1}^2}{R^2}$	$\frac{k_{m2}^2}{R^2}$
1	0.50	0.702	0.0055	0.1488	0.0029	113.5	0.0000	0.000091
2	0.234	0.702	0.0055	0.1488	0.0029	113.5	0.0000	0.000091
3	0.0684	26.29	0.2621	0.4321	0.2904	184.5	0.0000	0.000347
4	0.1126	0.979	.00157	0.00616	.000205	365.3	0.0000	0.000097
5	0.0454	75.42	8.064	4.910	16.61	275.1	0.0000	0.000214
6	0.0509	11.25	4.473	4.495	1.664	304.7	0.0000	0.000521
7	0.0509	11.25	4.473	4.495	1.664	350.0	0.0000	0.000521

Table II.10. Comparison of Measured and Predicted Nonrotating Frequencies (Hz)
(Case 1: Pitch Link at the Leading Edge)

Mode	Experiment	UMARC
Flap 1	4.84	4.83
Flap 2	--	25.87
Lag 1	10.97	11.02
Torsion 1	39.69	42.96

Table II.11. Comparison of Measured and Predicted Nonrotating Frequencies (Hz)
(Case 2: Pitch Link at the Trailing Edge)

Mode	Experiment	UMARC
Flap 1	4.88	4.86
Flap 2	24.81	24.98
Lag 1	10.95	11.00
Torsion 1	40.56	42.07

Table II.12. Comparison of Measured and Predicted Nonrotating Frequencies (Hz)
(Case 3: Pitch Links at Leading and Trailing Edges)

Mode	Experiment	UMARC
Flap 1	6.05	6.03
Flap 2	24.81	26.5
Lag 1	10.80	11.04
Torsion 1	173.0	181.2

II.2 Rotor-Fuselage Aeromechanical Stability

II.2.1 Hingeless Model Rotor Correlation Under Simulated Vacuum Conditions

Theoretical predictions of coupled rotor/body stability of hingeless rotors calculated using UMARC are correlated with experimental data [II.4]. In the experiment, the vacuum condition was simulated by using tantalum rods instead of blades. These rods eliminated all the major aerodynamic effects and were connected to the hub through flap and lag flexures. These rods were stiff in bending, torsion and axial directions. Hence, only the first flap and lag bending modes (which are mainly due to the elastic properties of the flexure) are used for the stability analysis. Figure II.8 shows the blade finite element model used for the analysis.

The rotor is mounted on a gimbal through pitch and roll springs. For Case 1, the gimbal is very stiff in pitch direction and essentially provides only roll motion alone. For Case 2, the gimbal provides both pitch and roll degrees of freedom.

The properties of the model rotor and support are given in Table II.13. The blade element properties are given in Table II.14. Table II.15 shows the comparison for nonrotating frequencies of the blade and for the support coupled to the rotor. The blade inboard of the flap flexure is not used for idealization. The support springs are slightly modified to match the coupled nonrotating body frequencies.

The blades is of circular cross section. Hence it does not generate any lift or pitching moment. The only aerodynamic force experienced by the blade is the drag force. Constant coefficient stability analysis was carried out and the results are given in Fig.II.9. Figure II.9a shows the correlation for modal frequencies and Fig. II.9b shows the correlation for

regressing lag mode damping for Case 1. The correlation between UMARC and experiment is excellent for this case. Fig. II.9c shows the correlation for modal frequencies and Fig. II.9d shows the correlation for regressing lag mode damping for Case 2. The correlation again is excellent. In both cases UMARC captures the peak value of the lag mode damping.

Table II.13 Hingeless Model Rotor and Support Properties

Main Rotor	
Number of Blades	3
Radius, in	14.963
Nominal Rotational Speed Ω_0 , RPM	700
Nominal Tip Mach Number	0.25
Airfoil	Circular Cross Section
c_0, c_1	0.0, 0.0
d_0, d_1, d_2	1.00, 0.0, 0.0
C_{mac}	0.0
c/R	0.033146
Solidity, σ	0.0318
Precone, β_p	0.0
Lock Number, γ	0.0182
Reference Mass per unit length, slug/in	0.00383362
Hub Length, x_{hub}/R	0.2079
Aerodynamic root cutout, x_{root}/R	0.2079
Lag Damping (lag mode 1), $C_\xi/m_0\Omega_0$	0.001905
Flap Damping (flap mode 2), $C_\beta/m_0\Omega_0$	0.0
Support	
Pitch Inertia, I_α/m_0R^3	4.1342
Roll Inertia, I_ϕ/m_0R^3	1.4578
Pitch Damping, $C_\alpha/m_0\Omega_0 = 2\zeta\omega_\alpha/\Omega_0$	0.013269
Roll Damping, $C_\phi/m_0\Omega_0 = 2\zeta\omega_\phi/\Omega_0$	0.013114
Support Roll Spring, $K_\phi/m_0\Omega_0^2R^3$	0.2
Case 1	
Support Pitch Spring, $K_\alpha/m_0\Omega_0^2R^3$	22.14238
Case 2	
Support Pitch Spring, $K_\alpha/m_0\Omega_0^2R^3$	0.34
Long., Lat. CG offsets, $x_{CG}/R, y_{CG}/R$	0.0, 0.0
CG Below Hub, h/R	0.63411

Table II.14 Model Rotor Nondimensional Finite Element Properties

Element	ℓ/R	m/m_0	$\frac{EI_y}{m_0\Omega^2R^4}$	$\frac{EI_z}{m_0\Omega^2R^4}$	$\frac{GJ}{m_0\Omega^2R^4}$	$\frac{EA}{m_0\Omega^2R^2}$	$\frac{k_{m1}^2}{R^2}$	$\frac{k_{m2}^2}{R^2}$
1	0.12751	0.9559	1.07001	1.07001	0.78537	31568	0.000134	0.000134
2	0.12751	0.9559	1.07001	1.07001	0.78537	31568	0.000134	0.000134
3	0.12751	0.9559	1.07001	1.07001	0.78537	31568	0.000134	0.000134
4	0.12751	0.9559	1.07001	1.07001	0.78537	31568	0.000134	0.000134
5	0.12751	0.9559	1.07001	1.07001	0.78537	31568	0.000134	0.000134
6	0.12282	1.8970	16.59574	19.74191	14.5930	62648	0.001543	0.001543
7	0.00902	0.6909	0.00033	0.13037	0.06450	22816	0.000552	0.000552
8	0.01504	0.4296	0.00033	0.00060	0.01348	14188	0.000273	0.000273
9	0.00762	0.6653	0.00033	0.12625	0.06246	21970	0.000540	0.000540

Table II.15 Nonrotating Natural Frequencies (Hz) of Model Hingeless Isolated Rotor Blades ($\theta_0 = 0$ deg) and Support (with rotor)

Mode	Experiment	UMARC (15 DOF)
Flap 1	3.01	3.05
Lag 1	6.39	6.01
Pitch	2.58	2.58
Roll	2.55	2.55

II.2.2 Hingeless Model Rotor Correlation

Validation of the aeromechanical stability analysis is carried out by correlation with experimental data. Experimental data from Ref. II.5 (contained in Ref. II.1) and Ref. II.6 for the coupled rotor-body stability of a soft-inplane hingeless rotor model in hover is used for the correlation. The three rotor blades have inboard flexure attached to uniform main blades. The present correlation study addresses Configuration 1 as designated in Refs. II.5 and II.6. For this configuration, the flexure is a nonmatched stiffness design with the nonrotating lag frequency approximately twice the nonrotating flap frequency. The support has only rigid body pitch and roll degrees of freedom. The resulting coupled rotor-body stability phenomenon is most representative of a ground resonance condition.

The rotor and support properties used in the analysis are given in Table II.16. A schematic of the finite element model discretization is shown in Figure II.10. The finite element model consists of eight *fifteen degree of freedom* Bernoulli-Euler type beam elements. The individual element properties are shown in Table II.17. It should be noted that flexure flap and lag element stiffnesses are increased by 16% and 25% respectively to match the fundamental nonrotating natural frequencies. In Ref. II.6, the author also notes that the given flexure stiffnesses are too low. The given torsion stiffnesses yielded a fundamental torsion frequency approximately 50% lower than the measured experimental value. The torsion stiffnesses of all elements were increased 419% to again match the experimental data. This large discrepancy is not a major concern since the blade were designed to be very rigid torsionally. Support stiffnesses in pitch and roll were also slightly reduced to match nonrotating coupled body natural frequencies (13% in pitch and 8% in roll). These initial adjustments are considered reasonable given the uncertainty in the measurement of the corresponding experimental values (see Ref. II.6). All element axial stiffnesses were estimated since no data was provided. The resulting nonrotating blade and coupled support

natural frequencies are given in Table II.18. Six normal modes (two flap, two lag, and two torsion) are used for the blade response solution. Dynamic inflow is included in all aeromechanical stability calculations.

Figure II.11 shows the variation in coupled rotor and body frequencies as the rotor rotational speed is increased from 0 to 950 RPM. Correlation between analysis and experiment is excellent. For the same rotor speed variation, Figures II.12-II.14 show the decay rates for the rotor regressive (low frequency cyclic) lag mode, body pitch mode, and body roll mode respectively. Correlation between analysis and experiment is again very satisfactory. The results illustrated in Figures II.11-II.14 are for the rotor in a zero collective pitch condition. The variation in regressive lag mode decay rate with rotor rotational speed at a blade collective pitch of nine degrees is shown in Figure II.15. The general trend of the variation is captured by the analysis. Note the two separate minima in the decay rate corresponding to the regions where the rotor regressive lag frequency is proximate to the body pitch and body roll frequencies.

Variation in rotor regressive lag decay rate with collective pitch setting is shown in Figures II.16a-e for rotor rotational speeds of 650 RPM, 720 RPM, 760 RPM, 820 RPM, and 900 RPM respectively. Correlation between analysis and experiment is excellent for low and moderate collective pitch settings. For rotor speeds below 900 RPM, the analytical results begin to deviate from the experimental data at high collective pitch settings. Limitations of the attached flow aerodynamic model is the most likely cause for the discrepancies at high collective pitch. The variation of body pitch and body roll mode decay rates with collective pitch at a rotor speed of 650 RPM is shown in Figures II.17a and II.17b . Correlation between analysis and experiment is excellent for the body pitch mode and satisfactory for the body roll mode.

Table II.16 Model Rotor and Support Properties

Main Rotor	
Number of Blades	3
Radius, in	31.92
Nominal Rotational Speed Ω_0 , RPM	1000
Nominal Tip Mach Number	0.25
Airfoil	NACA 23012
c_0, c_I	0.15, 5.73
d_0, d_I, d_2	0.0079, 0.0, 1.7
C_{mac}	-0.012
c/R	0.0517
Solidity, σ	0.0493
Precone, β_p	0.0
Lock Number, γ	7.37
Reference Mass per unit length, slug/in	0.000169
Hub Length, x_{hub}/R	0.09745
Aerodynamic root cutout, x_{root}/R	0.1856
Lag Damping (lag mode 1), $C_\zeta/m_0\Omega_0$	0.00418
Flap Damping (flap mode 2), $C_\beta/m_0\Omega_0$	0.0189
Support	
Pitch Inertia, I_α/m_0R^3	11.782
Roll Inertia, I_ϕ/m_0R^3	3.499
Pitch Damping, $C_\alpha/m_0\Omega_0 = 2\zeta\omega_\alpha/\Omega_0$	0.007129
Roll Damping, $C_\phi/m_0\Omega_0 = 2\zeta\omega_\phi/\Omega_0$	0.004137
Support Pitch Spring, $K_\alpha/m_0\Omega_0^2R^3$	0.125
Support Roll Spring, $K_\phi/m_0\Omega_0^2R^3$	0.180
Long., Lat. CG offsets, $x_{CG}/R, y_{CG}/R$	0.0, 0.0
CG Below Hub, h/R	0.2967

Table H.17 Model Rotor Nondimensional Finite Element Properties

Element	ℓ_i/R	m/m_0	$\frac{EI_y}{m_0\Omega^2 R^4}$	$\frac{EI_z}{m_0\Omega^2 R^4}$	$\frac{GJ}{m_0\Omega^2 R^4}$	$\frac{EA}{m_0\Omega^2 R^2}$	$\frac{k_{m1}^2}{R^2}$	$\frac{k_{m2}^2}{R^2}$
1	0.27148	1.3926	0.01422	0.3848	0.03136	5000	0.0	0.000157
2	0.27148	1.3926	0.01422	0.3848	0.03136	5000	0.0	0.000157
3	0.27148	1.3926	0.01422	0.3848	0.03136	5000	0.0	0.000157
4	0.05329	21.199	6.269	8.970	14.51	75000	0.001976	0.001976
5	0.01989	24.625	0.0900	2.108	1.125	88000	0.002775	0.002775
6	0.00432	15.606	0.0002026	0.08242	0.1712	20000	0.001827	0.001827
7	0.00705	9.742	0.0002026	0.0004054	0.03031	30000	0.006798	0.006798
8	0.00357	17.06	0.0002026	0.08586	0.1714	60000	0.001533	0.001533

Table II.18 Nonrotating Natural Frequencies (Hz) of Model Hingeless Rotor Blades ($\theta_0 = 0$ deg) and Support (with rotor)

Mode	Experiment (Ref. 5)	UMARC (15 DOF)
Flap 1	3.14	3.14
Flap 2	32.2	32.6
Flap 3	96.0	95.3
Lag 1	6.70	6.71
Lag 2	150	163
Lag 3	357	369
Torsion 1	342	342
Pitch	1.59	1.60
Roll	3.96	3.96

References

- II.1 McNulty, M.J. and Bousman, W.G. (editors), *Integrated Technology Rotor Methodology Assessment Workshop*, Proceeding of a Workshop Sponsored by NASA Ames Research Center and the U.S. Army, June 21-22, 1983, NASA CP-10007.
- II.2 Sharpe, D.L., "A Comparison of Theory and Experiment for Aeroelastic Stability of a Hingeless Rotor Model in Hover", *Integrated Technology Rotor Methodology Assessment Workshop*, June 21-22, 1983, NASA CP-10007.
- II.3 Dawson, S., "A Comparison of Theory and Experiment for the Aeroelastic Stability of a Bearingless Model Rotor in Hover", *Integrated Technology Rotor Methodology Assessment Workshop*, June 21-22, 1983, NASA CP-10007.
- II.4 Bousman, W.G., "A Comparison of Theory and Experiment for Coupled Rotor-Body Stability of a Hingeless Rotor Model in Hover Under Simulated Vacuum Conditions", *Integrated Technology Rotor Methodology Assessment Workshop*, NASA CP-10007.
- II.5 Bousman, W.G., "A Comparison of Theory and Experiment for Coupled Rotor-Body Stability of a Hingeless Rotor Model in Hover", *Integrated Technology Rotor Methodology Assessment Workshop*, NASA CP-10007.
- II.6 Bousman, W.G., "An Experimental Investigation of the Effects of Aeroelastic Couplings on Aeromechanical Stability of a Hingeless Rotor Helicopter", *Journal of the American Helicopter Society*, Vol. 26, No. 1, January 1981, pp. 46-54.

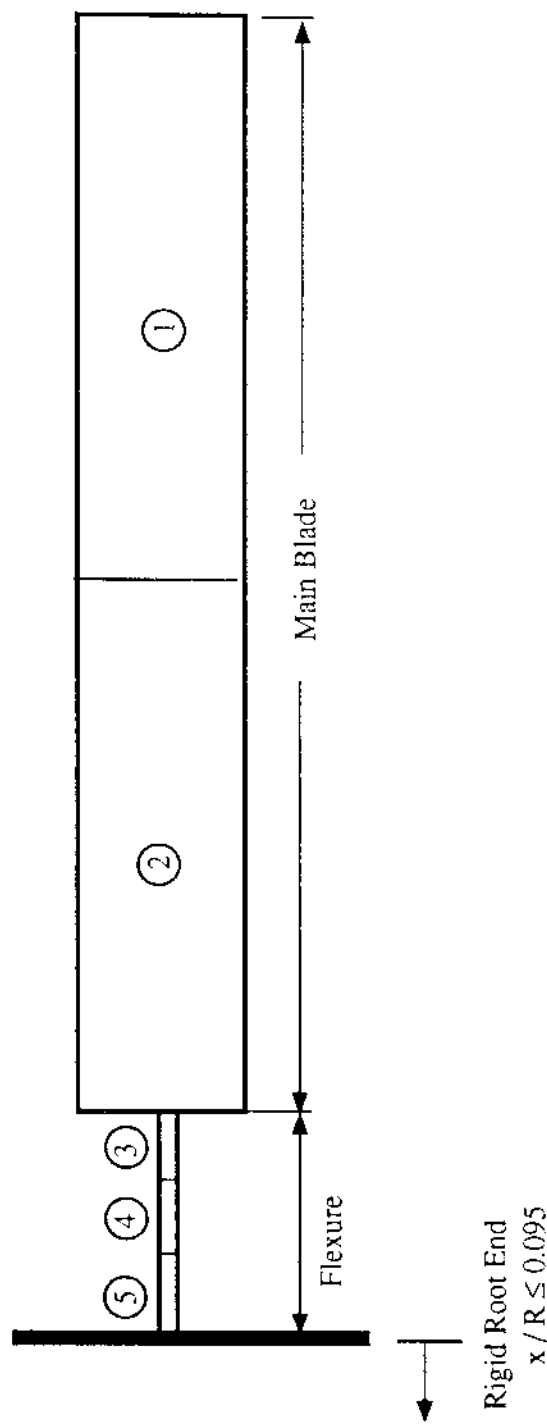


Figure II.1 Schematic of Model Rotor Blade Finite Element Discretization

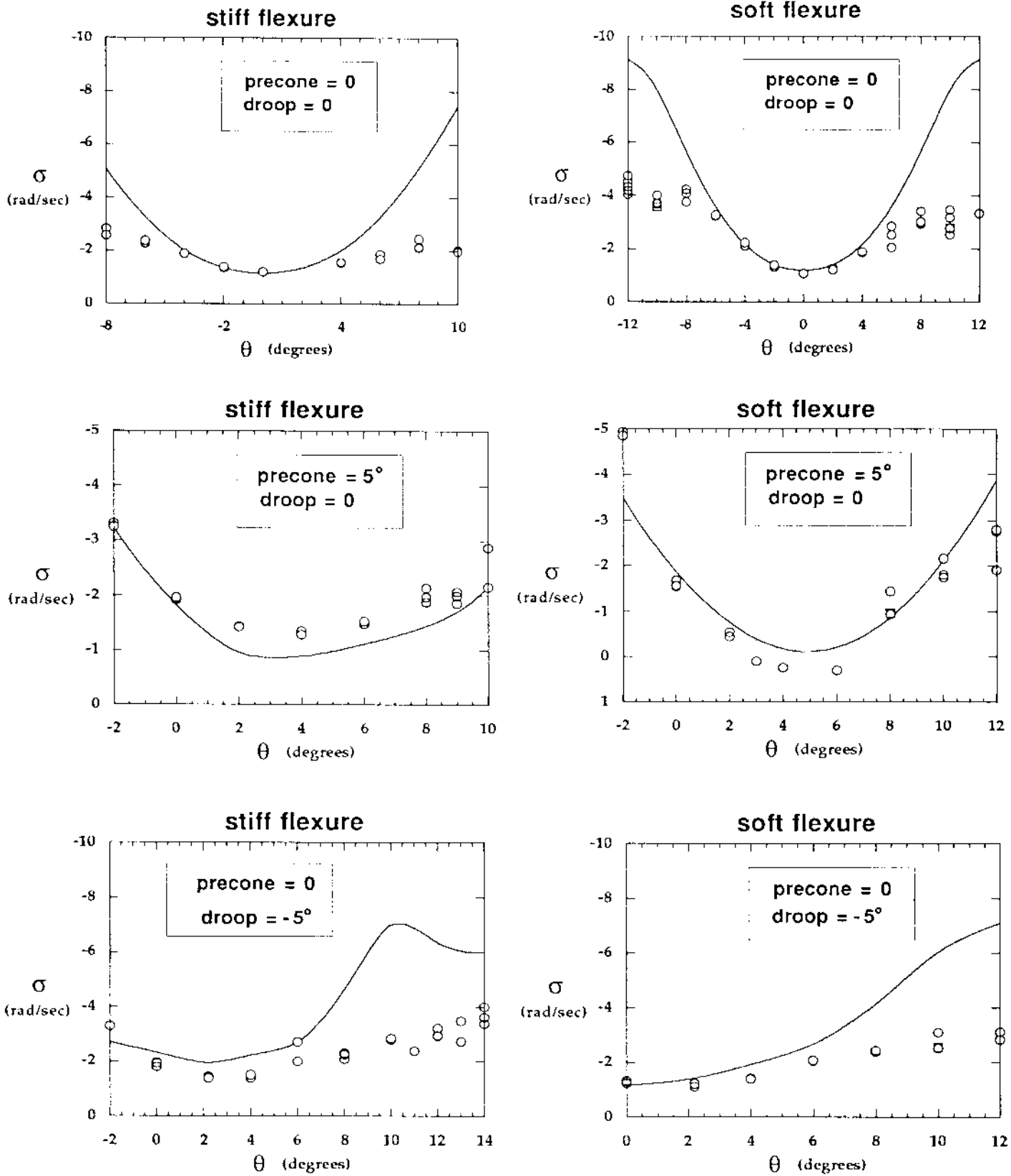


Fig. II.2 Variation of Lag Mode Damping with Collective Pitch for Hingeless Rotor

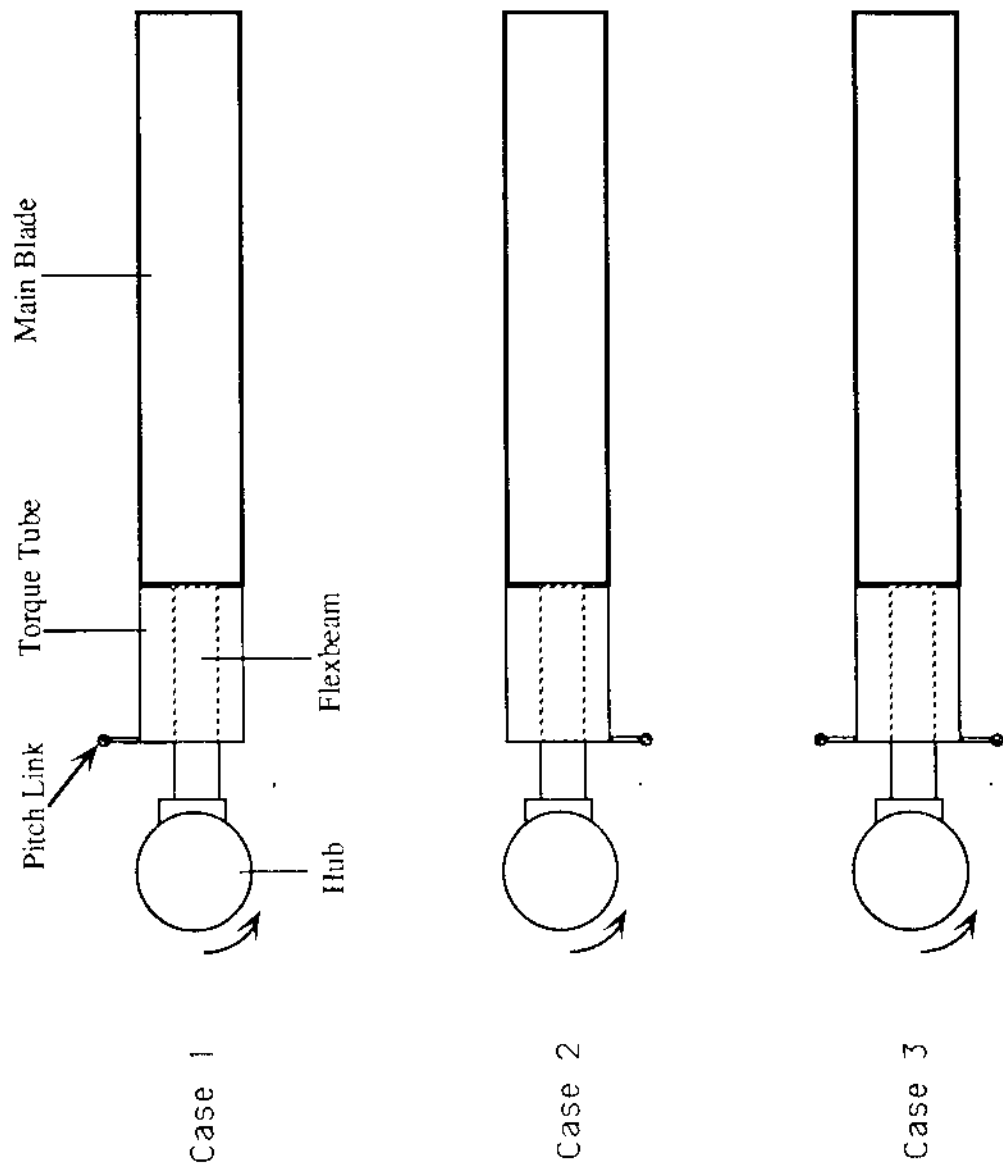


Figure II.3: Bearingless Model Rotor Control Configurations

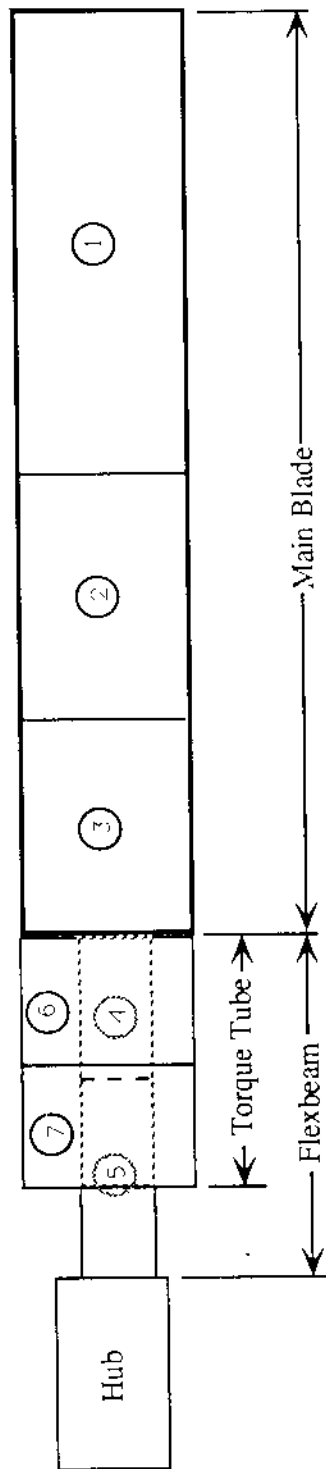


Figure II.4: Schematic of BMR Blade Finite Element Discretization

CASE 1

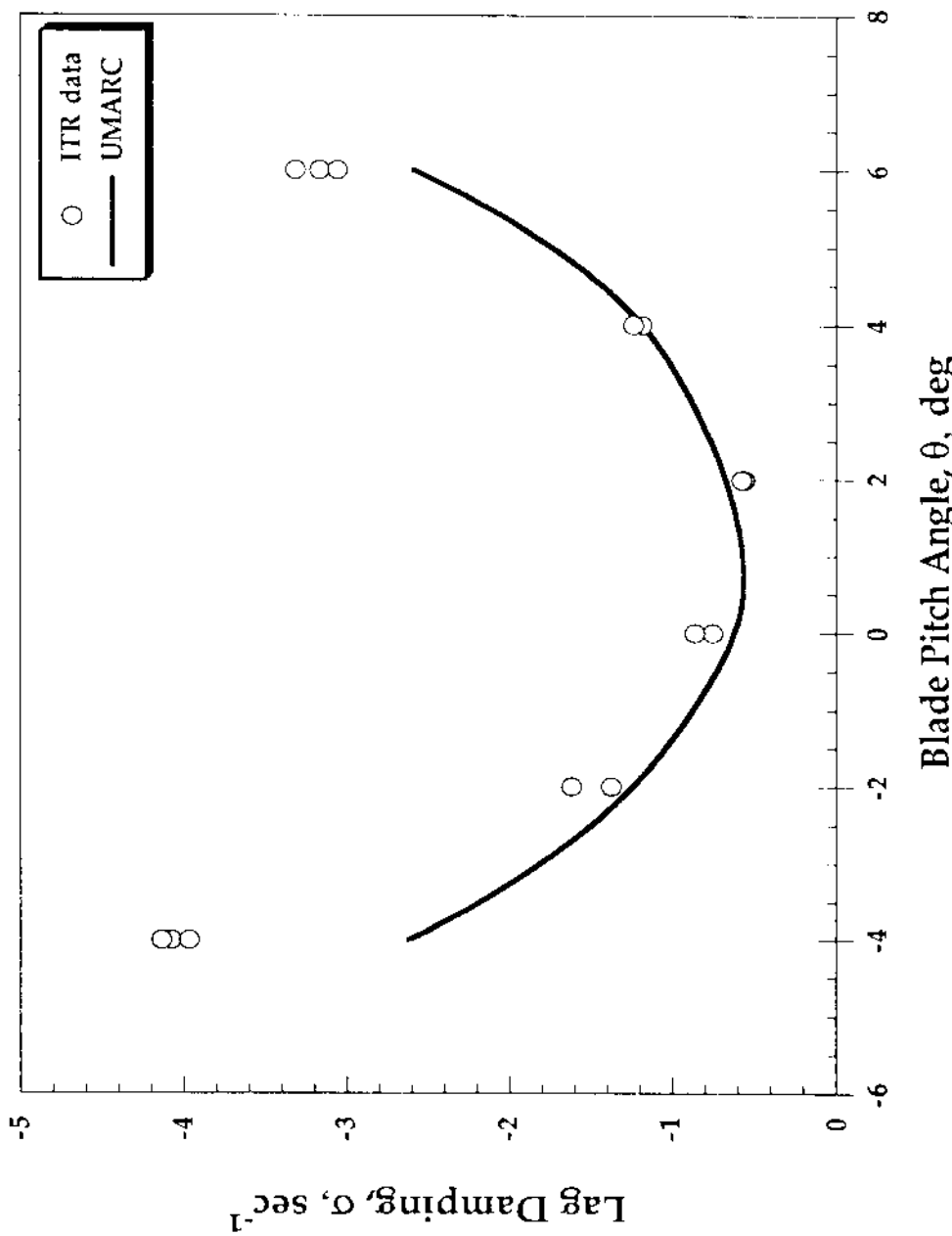


Fig. II.5 Lag damping comparison for Case 1

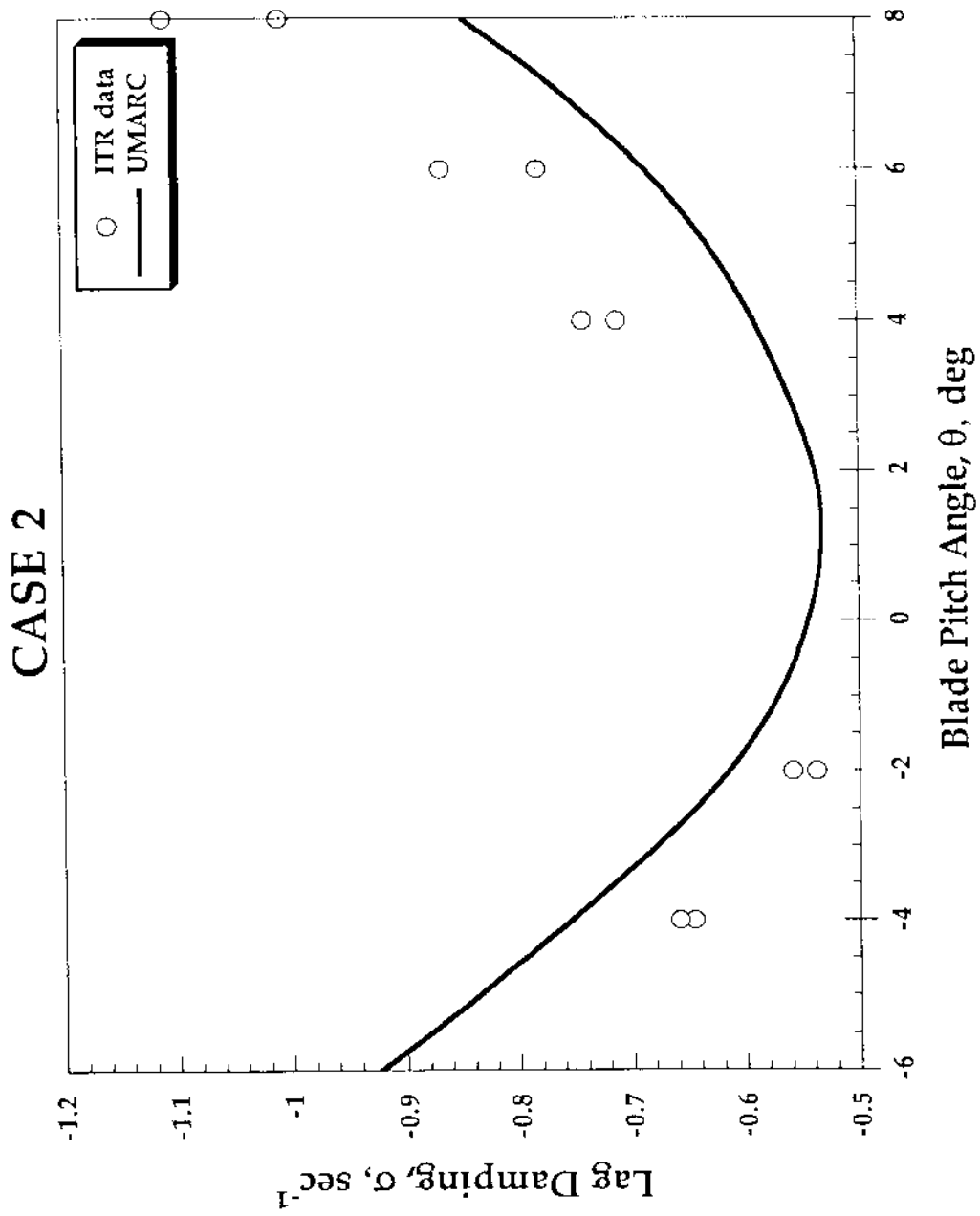


Fig. II.6a Lag damping comparison for Case 2

CASE 2

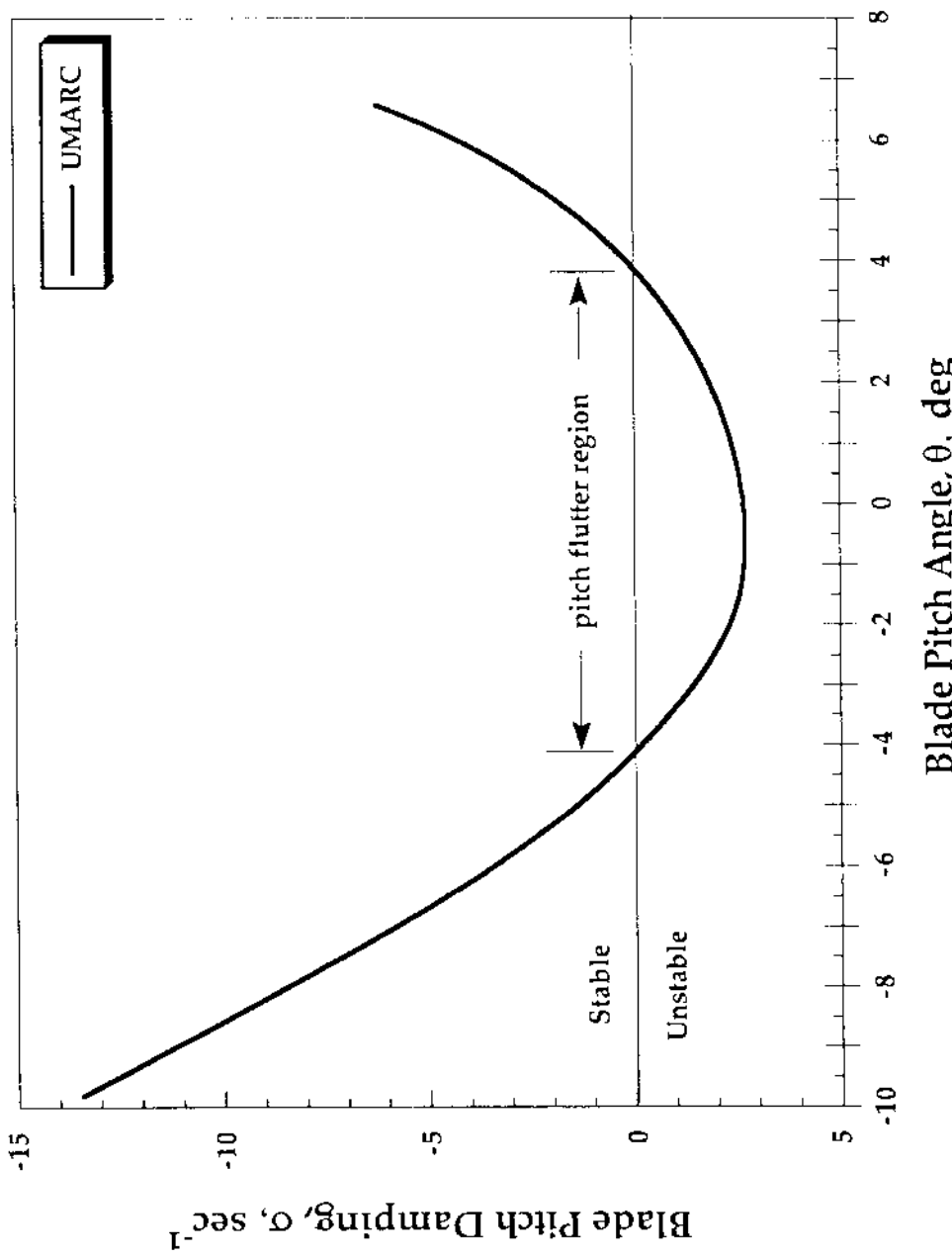


Fig. II.6b Variation of Pitch Damping with Blade Pitch Setting (Case 2)

CASE 3

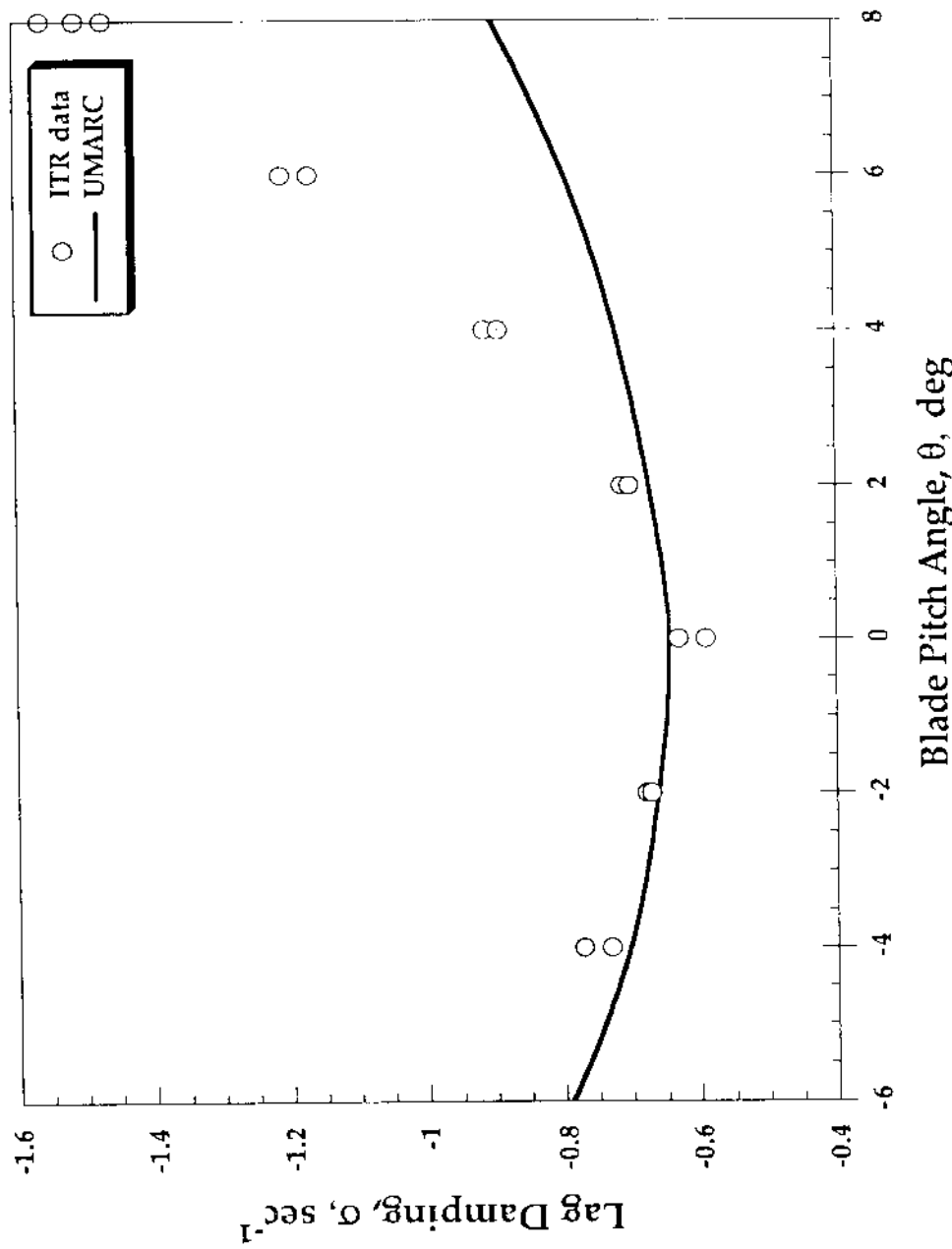


Fig. II.7 Lag damping comparison for Case 3

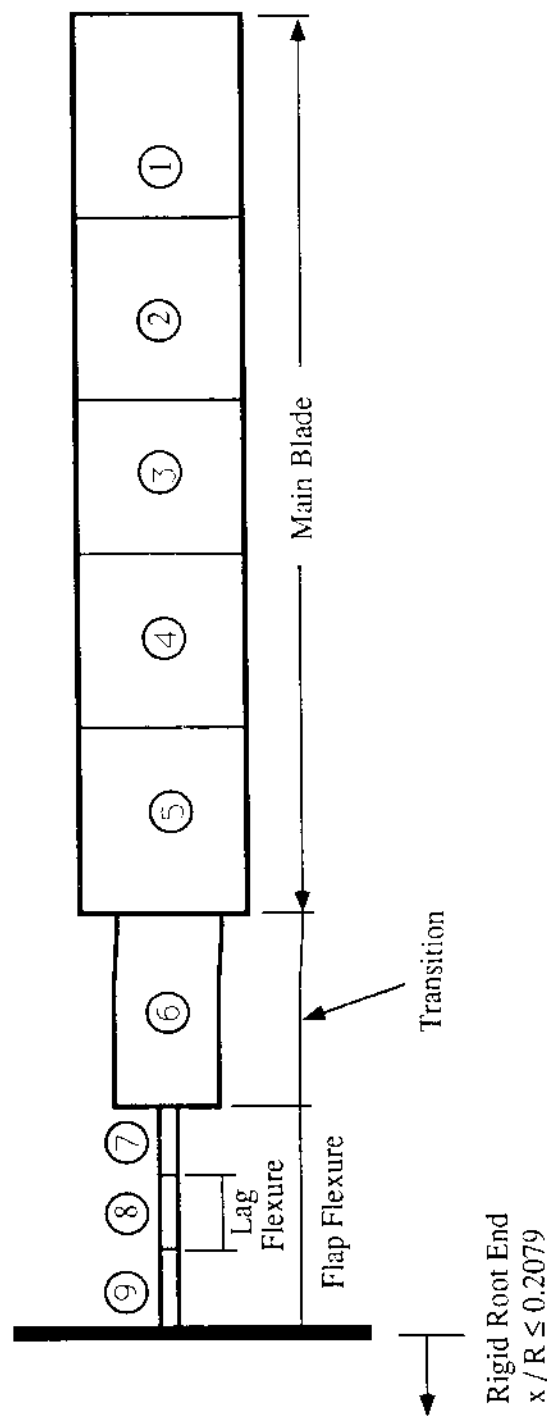
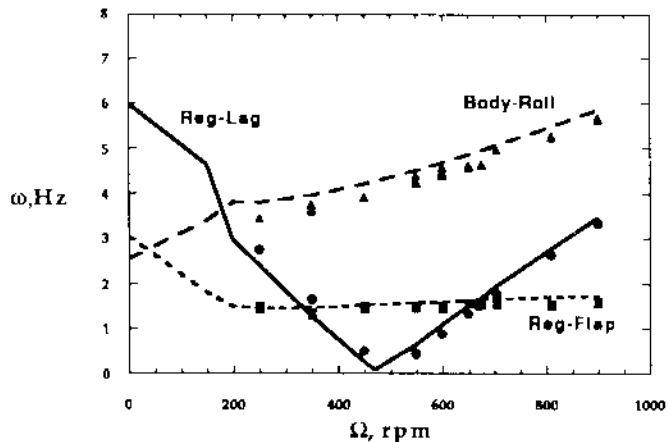


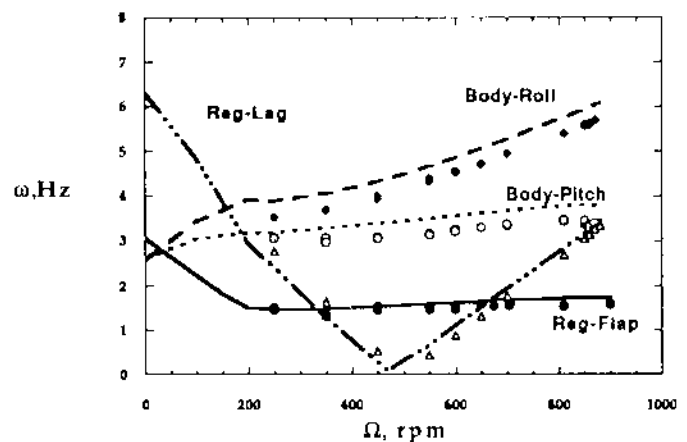
Figure II.8 Schematic of Model Rotor Blade Finite Element Discretization

Body Roll Only

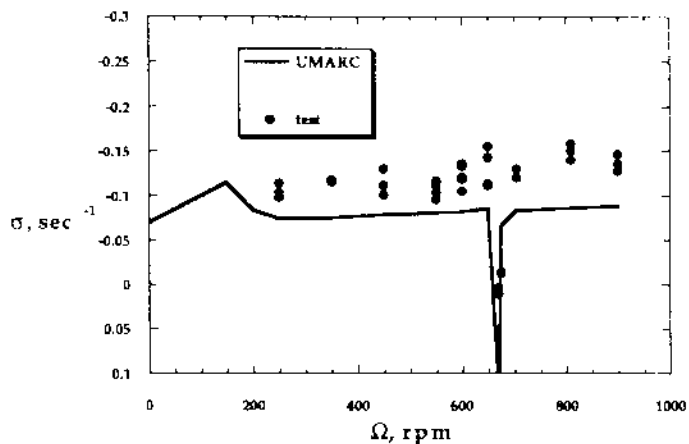


(a) Modal Frequencies for Case 1

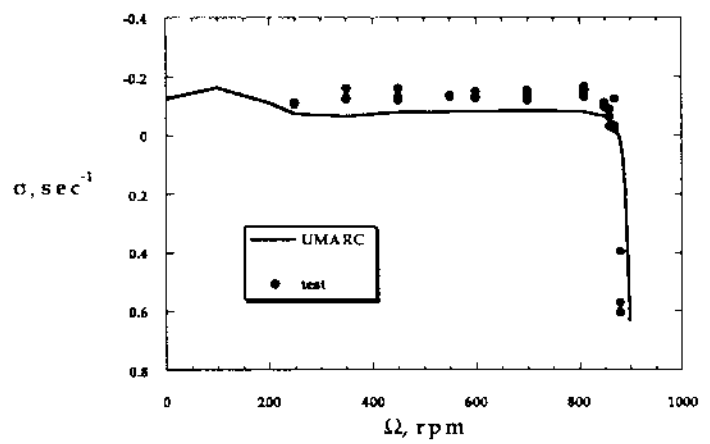
Body Pitch and Roll



(c) Modal Frequencies for Case 2



(b) Lead-Lag Damping for Case 1



(d) Lead-Lag Damping for Case 2

Figure II.9 Correlation of Modal Frequencies and Lead-Lag Mode Damping

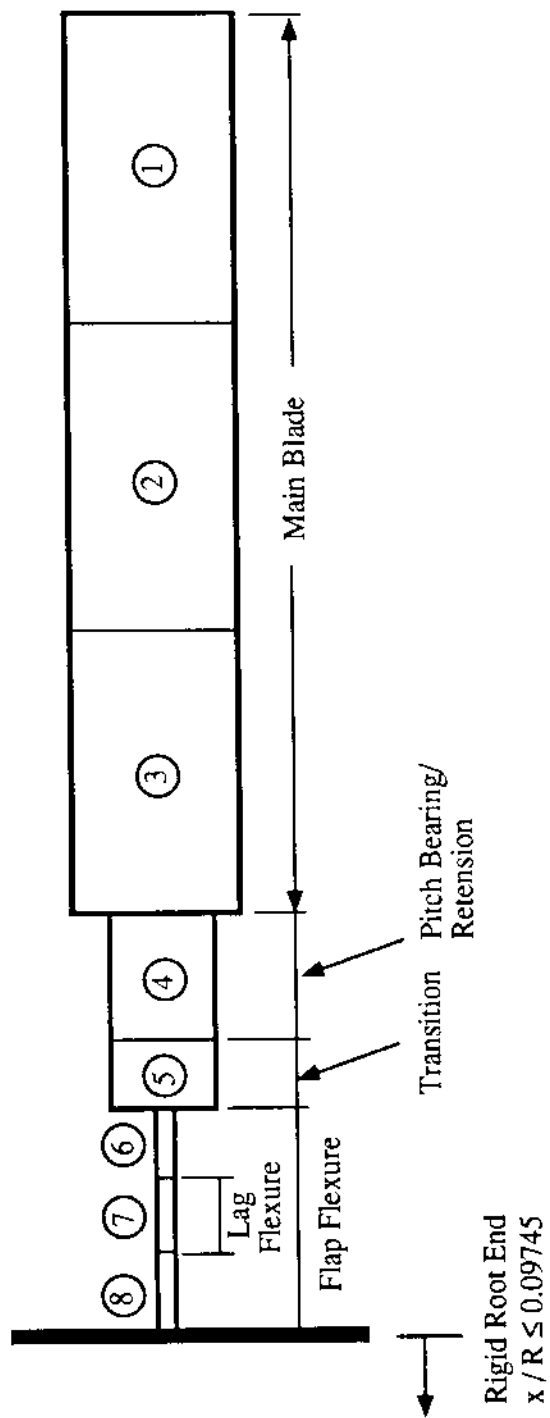


Figure II.10 Schematic of Model Rotor Blade Finite Element Discretization

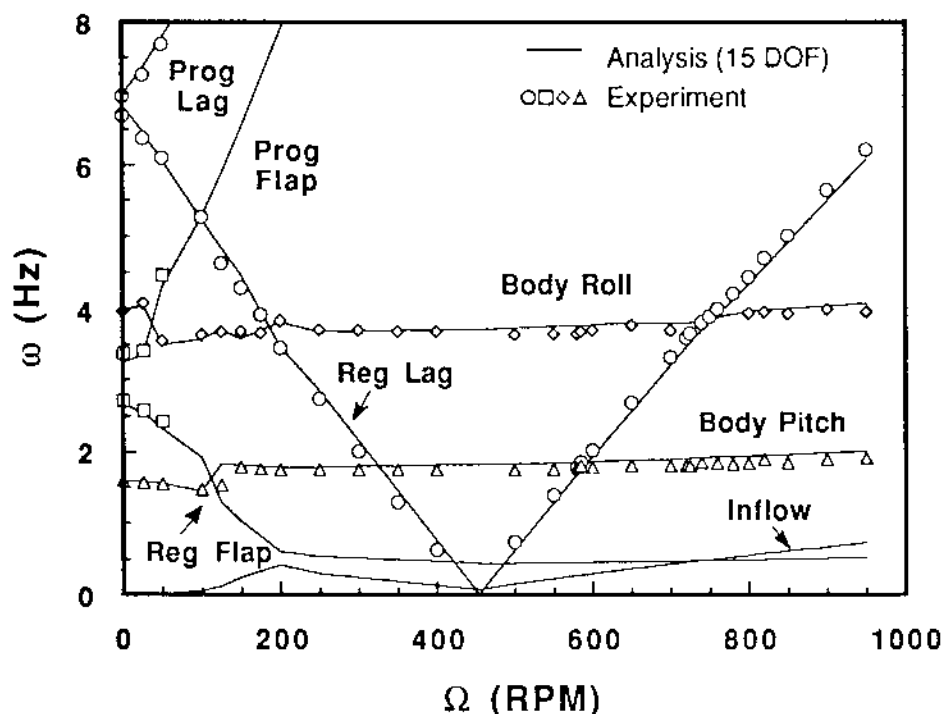


Figure II.11 Modal Frequency Variations with Rotor Rotational Speed
(Rotor Collective Pitch, $\theta_0 = 0$ degrees)

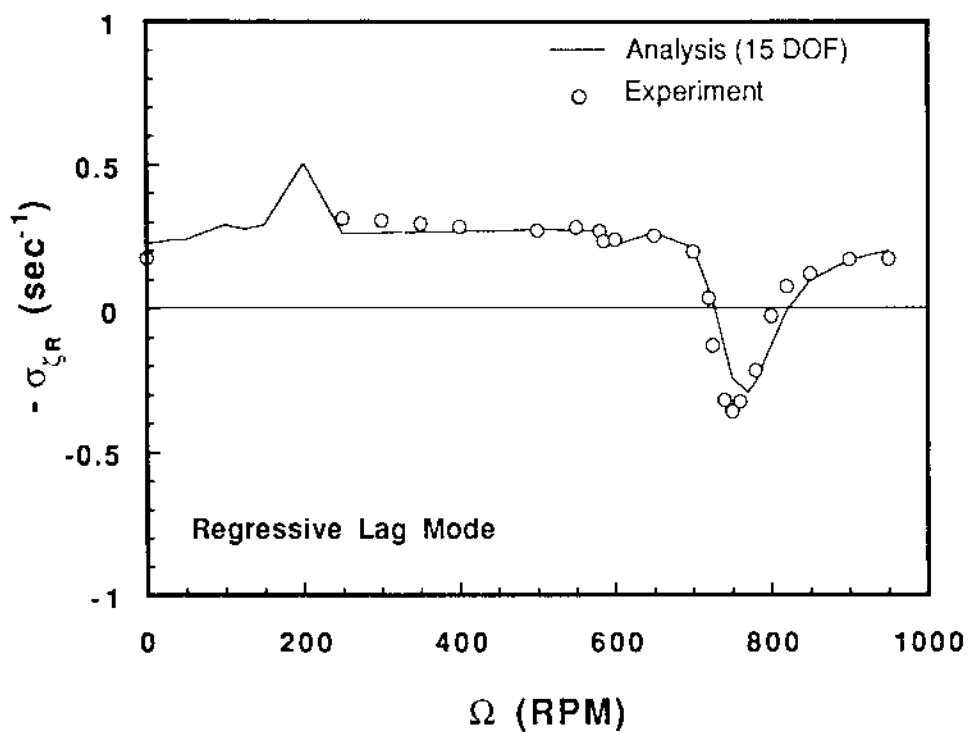


Figure II.12 Regressive Lag Mode Damping Variation with Rotor Rotational Speed
(Rotor Collective Pitch, $\theta_0 = 0$ degrees)

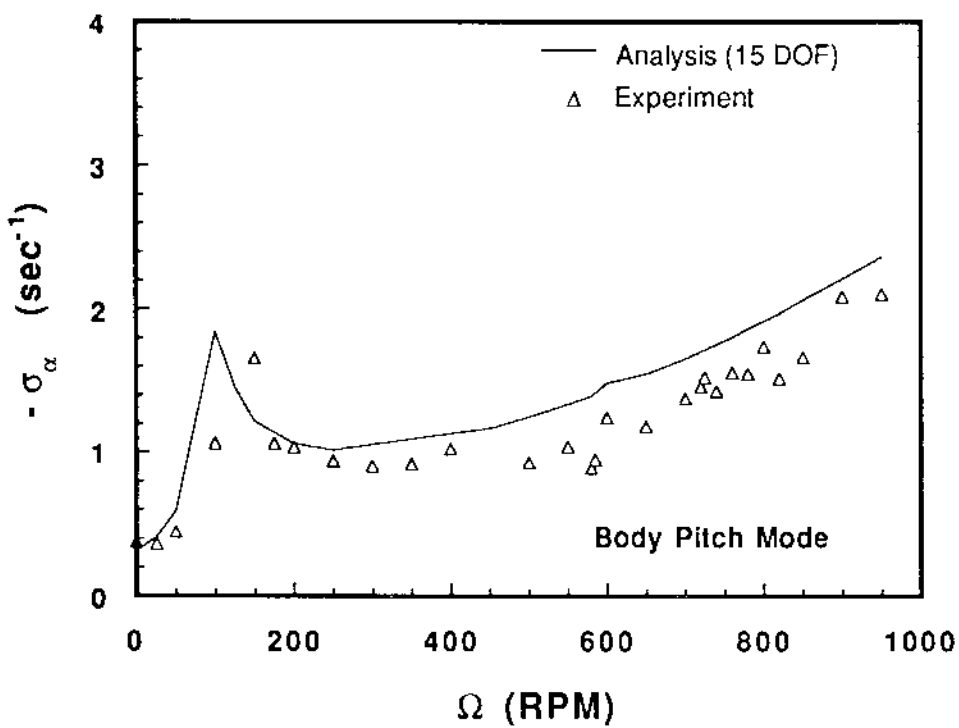


Figure II.13 Body Pitch Mode Damping Variation with Rotor Rotational Speed
(Rotor Collective Pitch, $\theta_0 = 0$ degrees)

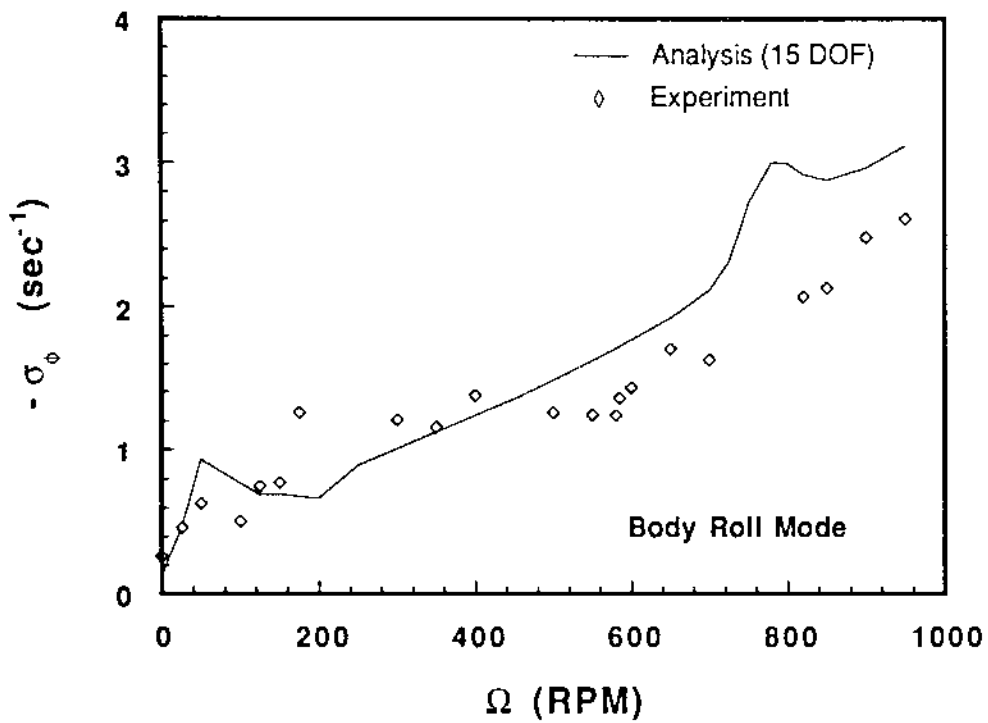


Figure II.14 Body Roll Mode Damping Variation with Rotor Rotational Speed
(Rotor Collective Pitch, $\theta_0 = 0$ degrees)

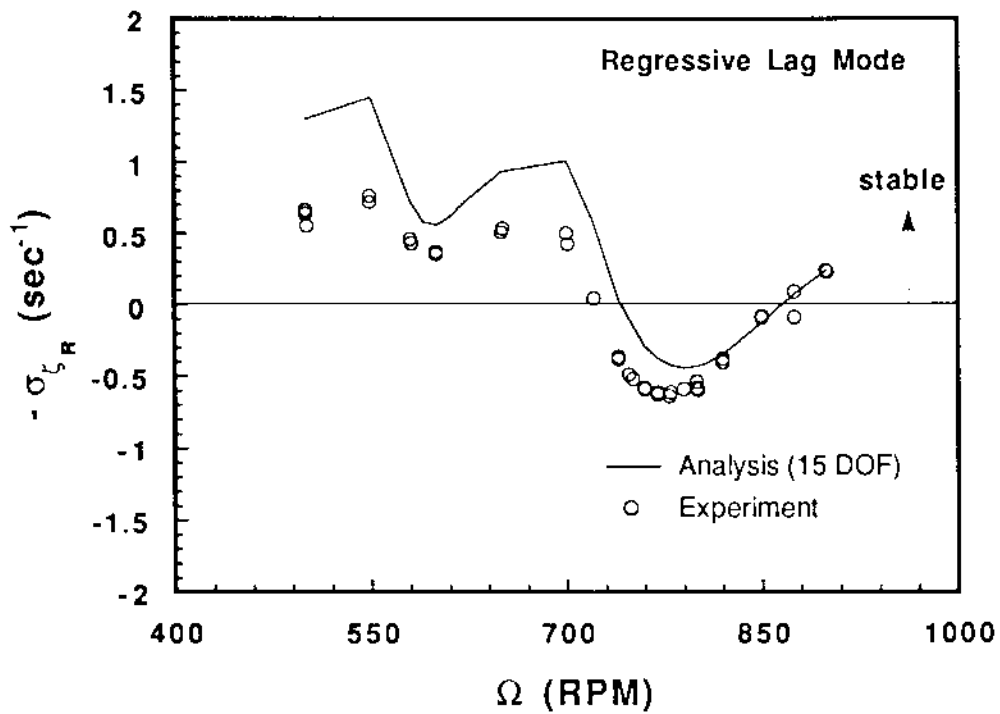


Figure II.15 Regressive Lag Mode Damping Variation with Rotor Rotational Speed
(Rotor Collective Pitch, $\theta_0 = 9$ degrees)

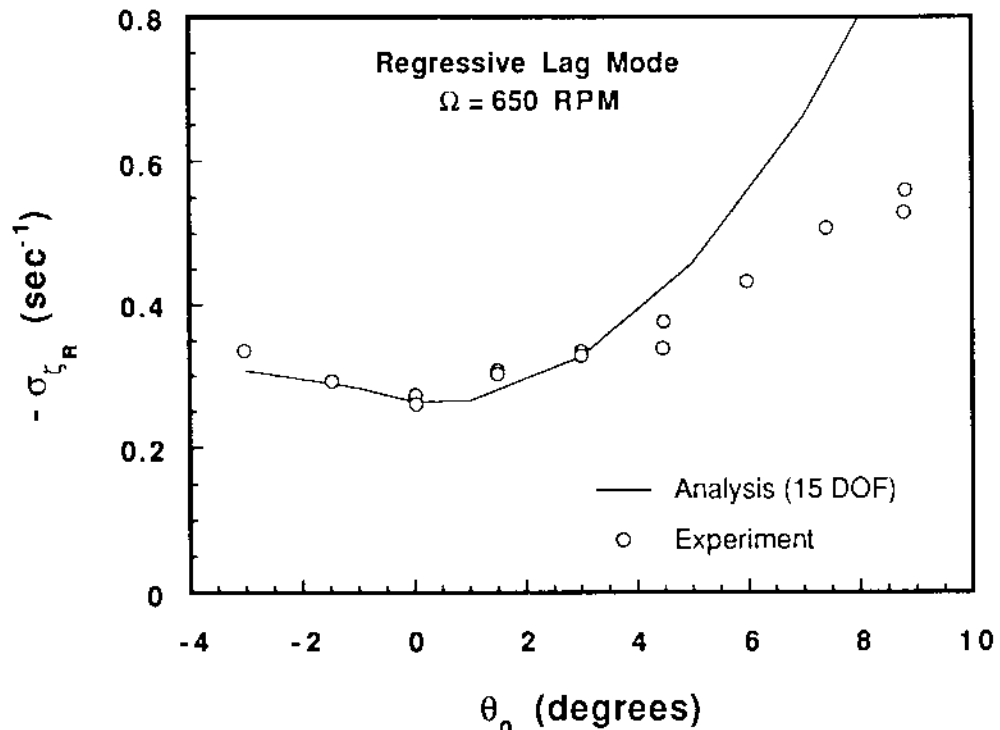


Figure II.16a Regressive Lag Mode Damping Variation with Rotor Collective Pitch
(Rotor Rotational Speed, $\Omega = 650$ RPM)

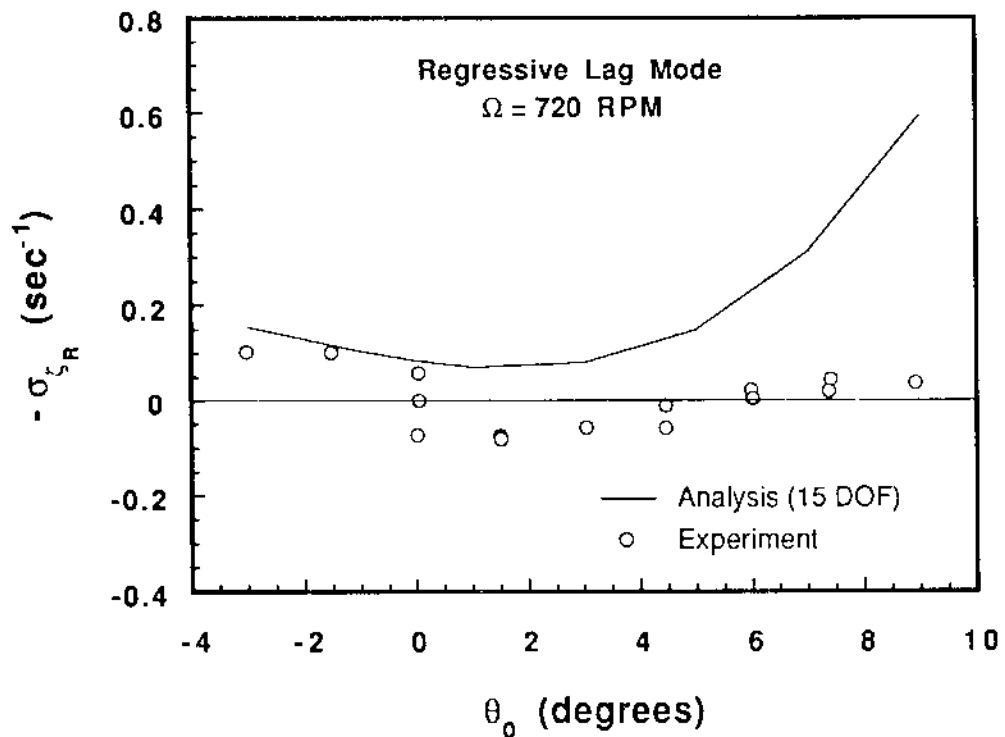


Figure II.16b Regressive Lag Mode Damping Variation with Rotor Collective Pitch
(Rotor Rotational Speed, $\Omega = 720$ RPM)

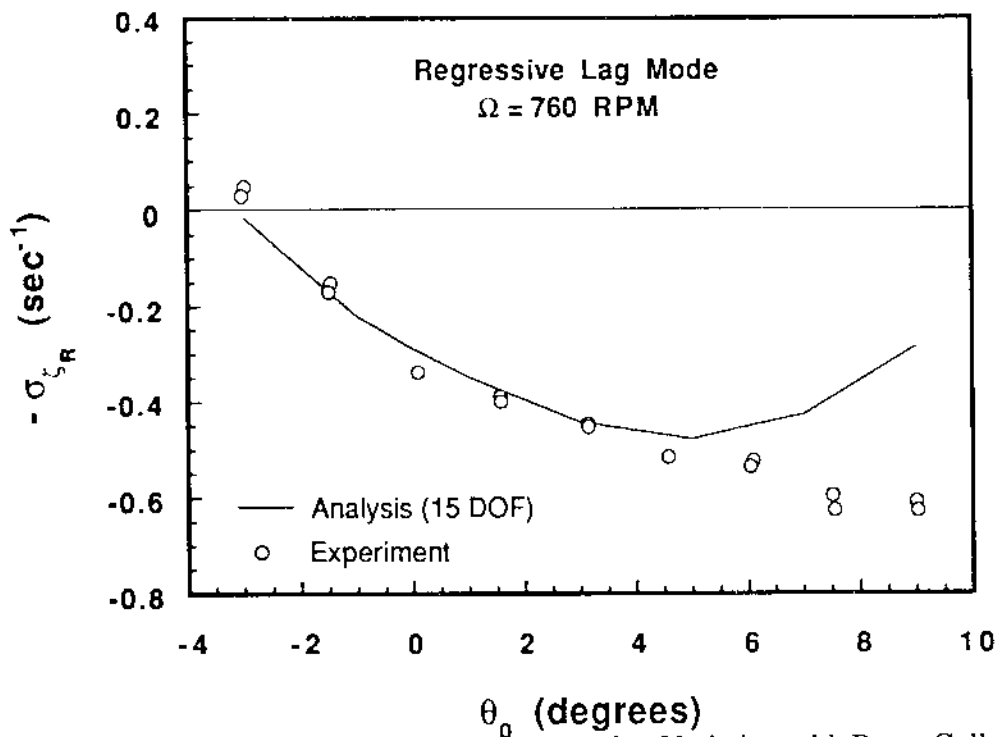


Figure II.16c Regressive Lag Mode Damping Variation with Rotor Collective Pitch
(Rotor Rotational Speed, $\Omega = 760$ RPM)

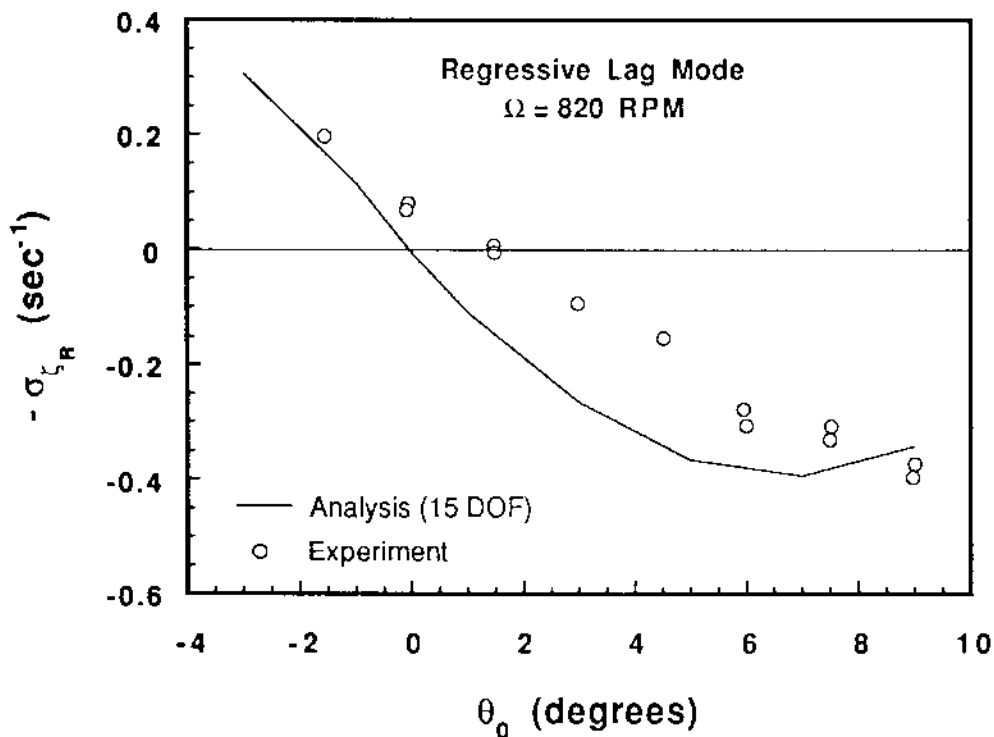


Figure II.16d Regressive Lag Mode Damping Variation with Rotor Collective Pitch
(Rotor Rotational Speed, $\Omega = 820$ RPM)

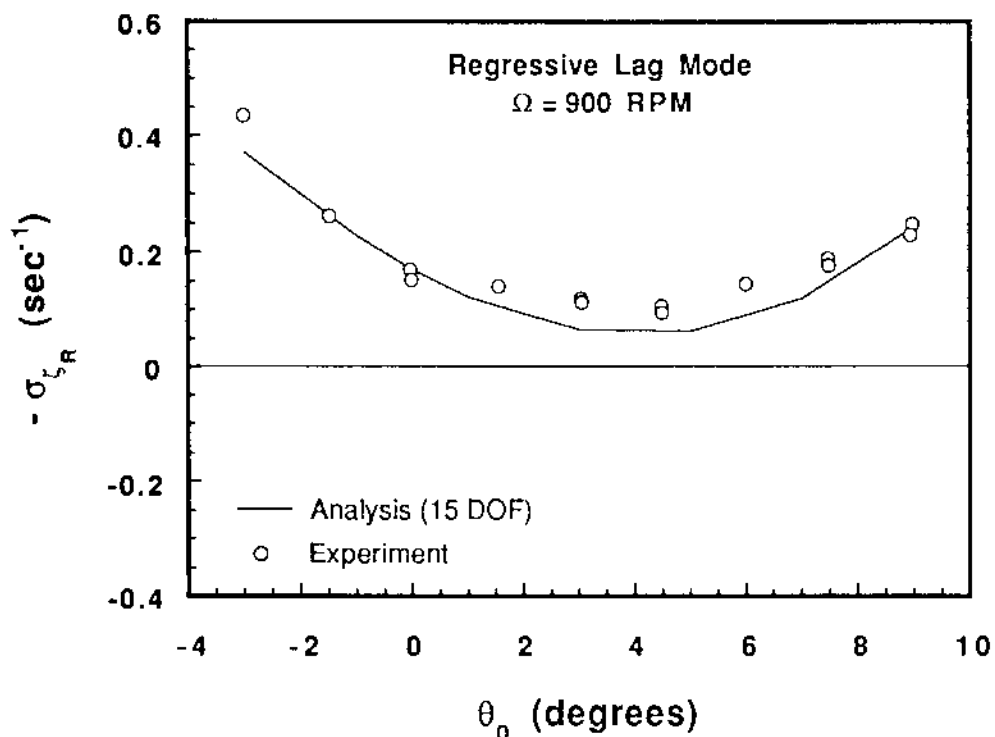


Figure II.16e Regressive Lag Mode Damping Variation with Rotor Collective Pitch
(Rotor Rotational Speed, $\Omega = 900$ RPM)

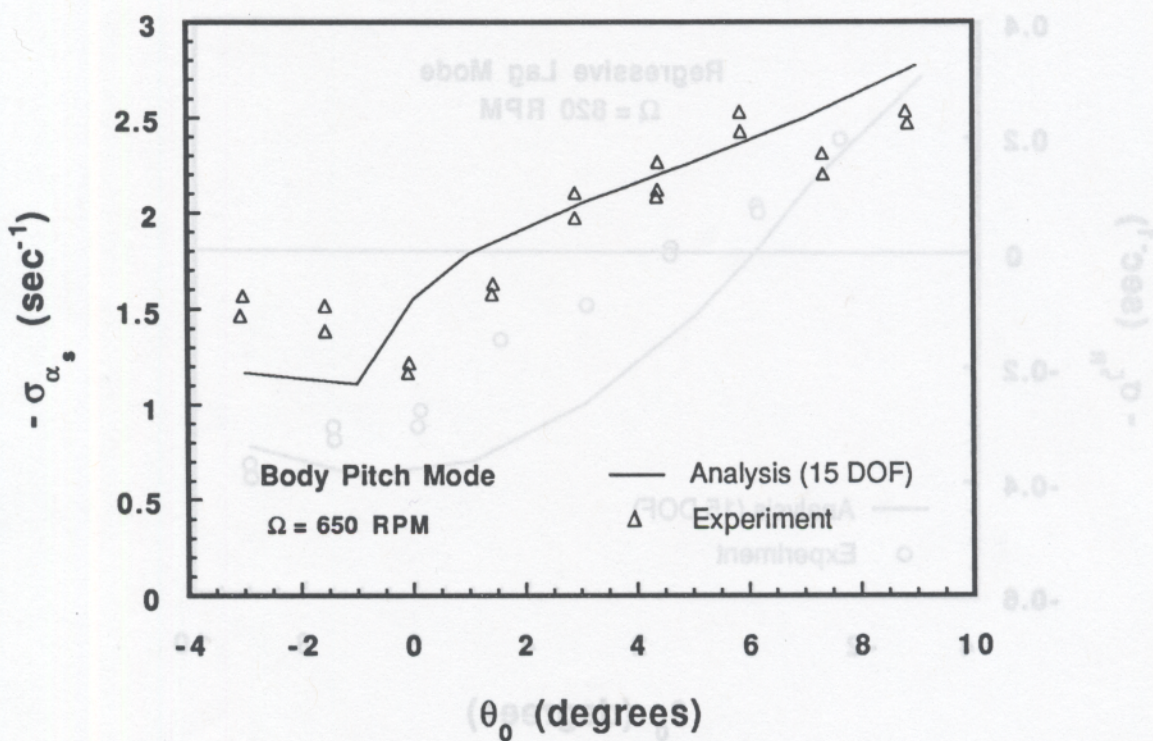


Figure II.17a Body Pitch Mode Damping Variation with Rotor Collective Pitch
(Rotor Rotational Speed, $\Omega = 650 \text{ RPM}$)

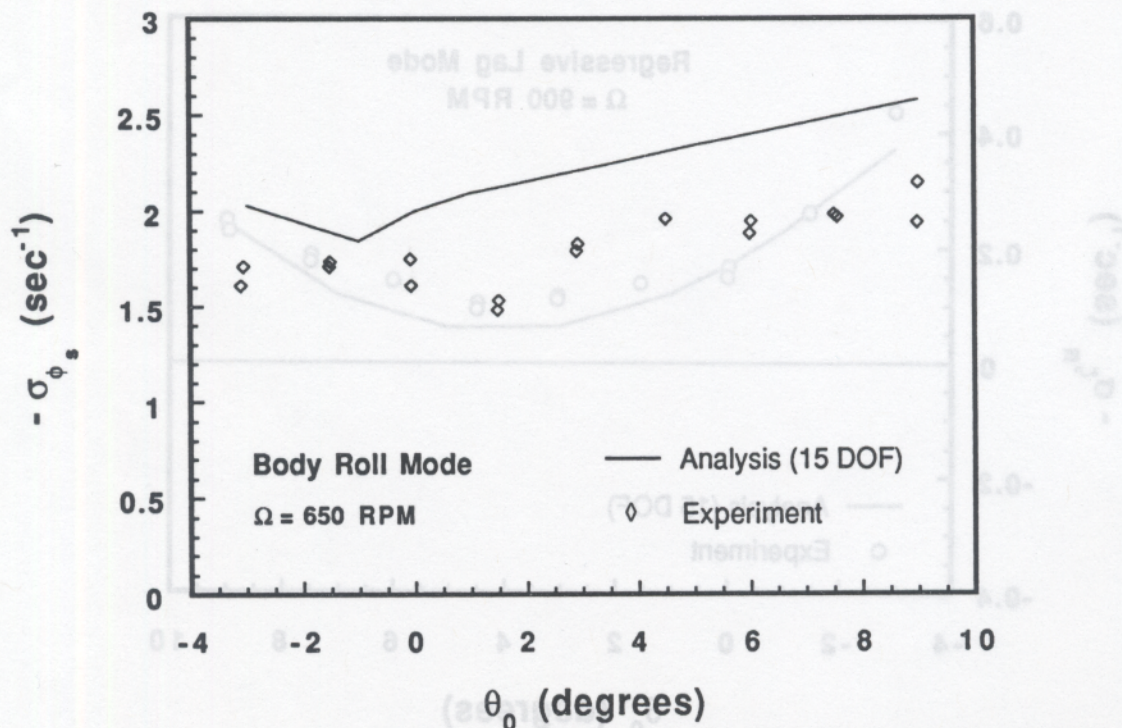


Figure 17b. Body Roll Mode Damping Variation with Rotor Collective Pitch
(Rotor Rotational Speed, $\Omega = 650 \text{ RPM}$)



